CRANFIELD UNIVERSITY

SARAH QURESHI

CONTRAIL-FREE AERO-ENGINES

School of Aerospace Transport and Manufacturing
AEROSPACE PROPULSION

DOCTOR OF PHILOSOPHY
Academic Year: 2016

Supervisor: Dr. Pericles Pilidis
August 2016

CRANFIELD UNIVERSITY

School of Aerospace Transport and Manufacturing
AEROSPACE PROPULSION

PhD

Academic Year 2016

SARAH QURESHI

CONTRAIL-FREE AERO-ENGINES

Supervisor: Dr. Pericles Pilidis
August 2016

ABSTRACT

This thesis presents a contrail-free aero-engine designed to reduce the aviation induced global warming through the development of a condensation and containment mechanism for the exhaust water vapour content of an aero-engine. This mechanism intends to eliminate the source of contrail formation.

A pressure-based turbomachinery defined as the water expeller is developed and introduced as a modular attachment to a standard aero-engine. It employs the use of centrifugal compression to generate pressure in the exhaust gas leading to a phase change that precipitates out the water content of the core exhaust gases. The water produced is drained out of the device and collected within the engine. The heat dissipated by water during condensation is absorbed by the remaining combustion gases.

The design of the centrifugal water expeller is derived from a patented invention and evolved into a practical system. The theory of centrifugal extraction is explained and the underlying physics is established. This proceeds with a thermodynamic analysis whereby data for mechanical design is computed and advanced towards a prototype ready engineering model inclusive of structural design and structural analysis. The power requirements of this system are determined using thermodynamic data. In the preliminary design, the inclusion of the water expelling device results in a thirty percent increase in the length of the engine which has a likelihood of being reduced through optimization.

The initial design parameters of the system are obtained from the performance analysis of a standard high-bypass three-spool turbofan engine and the study of atmospheric science and water physics. The design of the condensation device is validated through the study of the thermo-chemistry of the exhaust gases and a simple heat transfer analysis. The inter-gaseous exchange of energy at the molecular level during the process of condensation is also quantified.

The performance of the standard engine with the integration of the centrifugal water expeller is analysed and progressed towards the performance evaluation of a standard wide body large aircraft with four contrail-free engines on board. Initial estimates indicate an increase in the weight of the engine by twenty five percent with the installation of the centrifugal water expeller onto the engines. This is merely a two percent increase in the overall weight of the aircraft. The integration of the mechanical device with the aero-engine results in an environmentally favourable engine-aircraft configuration with a three percent thrust penalty which is recognized as the acceptable trade-off for environmental benefits.

Dedicated to the most beautiful chapter of my life; my daughter Ayat Mehrunnisa

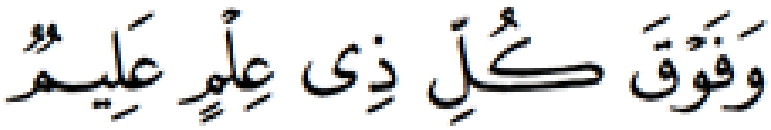

And beyond the knowledge of all possessors of knowledge, lies the knowledge of (Allah), the All-knowing (Al- Quran12:76)

ACKNOWLEDGEMENTS

This research project has had a significant involvement from a number of individuals to whom I feel forever indebted. I owe my gratitude to the following:

Professor Pericles Pilidis, my supervisor, for his never-ending support and encouragement towards my work, as well as for being a source of intellectual motivation and reassurance to conduct the research to its completion.

Mr. Masood Latif Qureshi, the inventor of the centrifugal water expeller, for his consent to use his patent freely for this research project and for his extensive scientific contribution towards the development of the contrail-free aero-engine.

Dr. Rumana Qureshi for her valuable technical assistance on the subject of Thermochemistry of Combustion Gases.

Mr. Fernando Lartategui Atela, for his active participation in the preparation of the chapters on Engine Performance and Aircraft Performance.

Professor. Riti Singh for bringing the research on contrail prevention at Cranfield University to its present level that provided the essential groundwork for the launch of this project.

The Propulsion Centre at the School of Aerospace for the grant of the research funding towards this project and Cranfield University for providing the resources and the environment conducive to study.

My parents, Rumana and Masood for the wonderful upbringing that made most of what I am today and imparted in me the confidence to take up challenges in life.

My sister, Zahra Qureshi for her inspiring presence in my life.

My husband, Asim Naseer for his unlimited patience and unconditional support towards the pursuit of my interests.

All my family and friends, both at home and at Cranfield, who facilitated this academic journey.

Sarah Qureshi
Cranfield, 14 August 2016

TABLE OF CONTENTS

LIST OF FIGURES

LIST OF TABLES

LIST OF EQUATIONS

LIST OF ABBREVIATIONS

Intrec	Intercooled-Recuperated
TET	Turbine Entry Temperature
SFC	Specific Fuel Consumption
DP	Design Point
OD	Off-Design Point
LPC	Low Pressure Compressor
IPC	Intermediate Pressure Compressor
HPC	High Pressure Compressor
LPT	Low Pressure Turbine
IPT	Intermediate Pressure Turbine
HPT	High Pressure Turbine
LPS	Low Power Shaft
IPS	Intermediate Power Shaft
HPS	High Power Shaft
IC	Intercooler
REC	Recuperator
CC	Combustor
CD	Compression Device
CN	Convergent Nozzle
BPN	Bypass Nozzle
RF	Radiative Forcing
CO_2	Carbon-Di-Oxide
N_2	Nitrogen
H_2O	Water
Vib Temp	Vibrational Temperature
RPM	Revolutions Per Minute
FEM	Finite Element Method
SVP	Saturated Vapour Pressure

1 INTRODUCTION

This project falls under the category of environmental studies for civil aircraft with an investigation into the global warming and global cooling potential of the aero-gas turbine power plants that are extensively used in aviation because of their exceptional power to weight characteristics. The investigation will encompass a comparative assessment of traditional and novel prime mover cycles including the performance of the engine and the environmental analysis of the system. The originality of work lies in the technical and environmental innovation of gas turbines that is based on current and novel engine cycles for an advanced airframe application in a wide range of operations.

The research addresses the various aspects of the environmental impact of aviation and highlights the importance of contrail mitigation. It establishes credibility for a specific contrail avoidance strategy and the multi-dimensional benefits associated with it. The key aspects ascertained by this research are:

1. Contrail elimination reduces the radiative forcing of cloud cover in the atmosphere and hence prevents global warming due to contrails.

2. Condensation and containment of the aero-engine exhaust gas water vapour within the engine prevent the release of a greenhouse gas into the upper atmosphere which would again reduce global warming.

3. Nitrogen acts as a carrier for the energy of the greenhouse combustion gases; carbon-di-oxide and water into the atmosphere and thereby reduces the global warming contribution of these gases. Nitrogen is not a green-house gas and hence does not have a role to play in the phenomenon of global warming.

The research intent of this project is to explore techniques to extract water from the exhaust emissions within the engine and the desired research outcome is to prevent aviation induced global warming through contrail avoidance and water recycling in the atmosphere. However, the benefits of this invention are multi-folds. Since water is condensed, collected and contained within the engine, it can be utilized on board by various aircraft systems, released as rainfall at lower altitudes to induce cooling or brought down to the Earth. This also prevents water from playing its role as a green- house gas in the atmosphere irrespective of contrail formation. All this is additional to the basic purpose of contrail prevention.

Contrails are primarily artificially induced cirrus clouds that are created by the atmospheric condensation of the supersaturated vapour that is present in the exhaust emissions of the aero-engines. They are visible in the atmosphere as a

trailing line of vapour behind the aircraft. Contrail formation mostly occurs during cruise flight conditions when the hot exhaust emissions of the aero-engine that contain water vapour as a combustion by-product are released into the cold atmosphere at high altitudes. The super saturated water vapour creates aviation induced cirrus clouds at high altitudes that affect the earth's infra-red signature(Burkhardt and Kärcher, 2011).

In the wider context of the environmental impact of aviation, contrails created through aero emissions upset the atmospheric balance and disturb the earth's radiation budget either by reflecting sunlight back to space or by trapping the infra-red radiation emitted by the earth's surface.(Weihs et al., 2015) Contrails released during aircraft flight constitute a considerable proportion of the aviation's contribution to global warming. Recent studies indicate that the global warming potential of contrails is much greater than that of carbon-di-oxide (Lee, D.S. Clare, P.E. Haywood, J. Kärcher, B. Lunnon, R.W. Pilling, I. and Slingo,A. 2000). Hence a reduction in the water footprint is equally important as that in the CO_2 footprint. According to IPCC contrails cover 0.1% of the Earth's surface. This is likely to rise to 0.5 % by 2050. The radiative effect of contrails is said to vary around 10mW/m^2. IPCC projects the contrail cover to grow faster than aviation fuel consumption in the future, mainly due to increased propulsive efficiency. Contrail avoidance therefore remains the current focus of many aero engine researchers and various technologies are reflected upon to achieve this target. The technologies involved to address the issue have been discussed at length in the Literature Review in Chapter 2.

In the first stage of the research, various available state of the art methods are evaluated and analysed to determine the best possible approach towards condensing the water vapour within an exhaust engine. Studies are carried out to determine the most viable mechanism for condensing the water vapour of the exhaust gases at the most lucrative design point in order to avoid contrail formation. A patent by (Taylor, Noppel and Singh, 2007) laid the foundation of this research. The underlying concept of condensing water within the engine was adopted from this patent.

A recent patent (Qureshi, 2016a) is selected that describes a unique gas turbine heat exchanger, whereby the heat dissipation requirement of the core exhaust gas is considerably reduced. This works on the concept of separating the water vapour and carbon dioxide centrifugally by achieving the desired condensation pressure within the device leading to a phase change, and then presenting only the water vapour for further cooling using the cold bypass flow. The water vapour is subjected to centrifugal forces in order to compress the water and further assist in its precipitation within the centrifugal vessel. The hot carbon dioxide and nitrogen gases pass through un-cooled.

This concept is adopted by the author and is developed from the basic physics towards a complete engineering solution. It concludes by providing a modular attachment to an existing engine. The device evolved out of this concept is termed as the centrifugal water expeller. The patent by (Qureshi, 2016a) is freely used to derive the concept design and is such appended to the thesis for reference in Appendix 3.

The mechanism claimed above is designed as an add-on attachment to an existing engine. Once integrated into the engine, the modified engine is termed as the contrail-free engine. Its functionality involves the condensation and containment of the contrail forming water vapour within the engine while releasing a cleaner exhaust into the atmosphere. This add-on device also acts as a means of capturing and harnessing water out of exhaust emissions and the water thus produced is retained within.

This is a unique pressure based condensation system devised for airborne applications as compared to the conventional temperature based heat exchangers designed for land based application. The manufacture of this device is similar to the production of the other components of the aero-engine and it maintains the simplicity of the gas turbine design by employing a turbo-machinery mechanism with no complicated flow paths.

It serves to benefit the global environment by eliminating contrails in the upper atmosphere, preventing the exhaust of water vapor as a green-house gas into the environment, creating water for in-flight use as well acting as a resource for artificial rainfall and induced cooling. Not only does the technology reduce the aviation industry's contribution to global warming, but it also signifies a positive contribution by the aviation industry towards meeting the global challenge of water scarcity.

The technology has a potential to redefine the design of the future generation of contrail free civil aero-engines that can conform to environmental regulations. The design of this device and the technology involved in its development are synergistic with the current technology employed by the aero-engine manufacturers. Hence this device can be easily incorporated within the existing framework of aero-engine design.

A multidisciplinary approach is adopted to address the underlying technology in the development of the contrail-free engine. The methodology is presented according to the chronological order of the research topics undertaken whereas thesis chapters are organised to highlight the original contribution to the research field. The research outline can be summarized as follows:

1. Literature review of the techniques of contrail prevention and the selection of the concept of moisture extraction from exhaust emissions for further development. (Chapter 2)

2. Performance analysis of a three spool conventional turbofan engine and the intercooled-recuperated turbofan engine using the commercial software “GasTurb”. Engine specifications and aircraft specifications have been derived from the Rolls-Royce Trent 900 engine and the Airbus A380-800 aircraft published data respectively. The remaining inputs required are either intelligent assumptions, or determined through iterations. (Chapter 6)

3. Preliminary study of the heat exchange mechanism between the core exhaust flow and the bypass stream with an investigation into the present-day heat exchanger arrangements. (Chapter 8)

4. Study of Atmospheric Science and Water Physics to determine the condensation design point for achieving a phase change in water(Chapter 8)

5. Establishing the design philosophy of the water extraction system and the use of data obtained from the above analyses to define the design specifications of the centrifugal water expeller. All Data is tabulated using Excel spreadsheets. (Chapter 3)

6. Assessment of the standard centrifugal compressor as a compression condensation mechanism. (Chapter 8)

7. Thermal design of the centrifugal water expeller and calculating the power requirements of the centrifugal water expeller. (Chapter 4)

8. Mechanical design of the centrifugal water expeller with component modelling according to size and dimensions. The CAD software “Pro-E Creo” is used for mechanical modelling (Chapter 4)

9. Structural analysis of the centrifugal water expeller using the “Pro-Mechanica” software. The weight of the device is also estimated based on the requirement of structural strength using the same application. (Chapter 4)

10. Analysis of the intermolecular energy transfer among the components of the combustion gases for design validation using the commercial software “Gaussian”. (Chapter 5)

11. Integration of the centrifugal water expeller into the conventional engine to build the contrail-free engine and to determine the change in weight and dimensions of the engine as well as the exhaust nozzle characteristics. (Chapter 4)

12. Engine performance analysis with the centrifugal water expeller attached to the conventional engine to form the contrail-free engine. The analysis was conducted using the in-house engine performance software “TurboMatch”. (Chapter 6)

13. Performance analysis for a conventional multi-engine aircraft replacing one test engine with the contrail-free engine. The analysis was conducted using the in-house aircraft software “Hermes”. (Chapter 7)

14. Proposals for future directions to be followed in order to promote the research to the next level of technology. (Chapter 10)

Design Scheme (Chapter 3 and Chapter 4)

The research involves the design of a pressure based water expeller that is developed from the basic concepts of moisture condensation presented in prior art (Qureshi, 2016a) and (Qureshi, 2016b). The details of the design are presented, whereby the centrifugal force generated in a rotating vessel is used to create sufficient pressure to induce condensation within the engine. It employs the use of centrifugal compression to generate pressure in the exhaust gas leading to a phase change. These ideas employ the use of the centrifugal force generated by the rotation of the exhaust gases. Mechanisms are devised whereby the centrifugal effect is created in a rotating vessel. The centrifugal force generated results in a change in the pressure and temperature of the gas. This change is exploited in order to achieve a pre-determined design point temperature and pressure whereby the condensation of water vapour can occur. Hence condensation is achieved through the centrifugal action.

The underlying theory is examined followed by a mathematical model that is advanced towards the development of a mechanical prototype. A complete thermodynamic analysis is performed on the model to determine the variation of pressure due to the centrifugal effect in order to determine the various parameters of thermal design and also to evaluate the functionality of the equipment to effectively execute the condensation mechanism for the water

vapour present in the exhaust gases of the engine. Data and specifications for mechanical design are computed subsequently. The power requirement of this system is determined using thermodynamic data. Power losses associated with the integration of this system into the engine are identified and the thrust compensation provided by this mechanism is evaluated. Mechanical design data is used to generate the 3D CAD model of the water expeller with an engineering perspective. This compression based condensation device is designed with the intent to be integrated with the contemporary aero-engine as an add-on attachment. It is meant to be placed in the engine in between the last turbine and the core nozzle in order to create the contrail-free aero-engine. The water produced through this mechanism is meant to be collected and contained within the engine and later released into the environment as appropriate. This specification is also an inherent part of the moisture extraction system design.

According to the emission index of water, 1.25 kg of water is produced for every 1 kg of kerosene fuel burn. The water vapour constitutes 2.25 % of the core exhaust mass flow. The fuel burn rate for a long haul cruise flight using the Trent 900 baseline engine is 1.0715 kg/s (A1.2). Hence the amount of water produced is 1.34 Kg/s. This amounts to 38592 kg of water produced per engine for an average transatlantic flight of 8 hours on an A380 baseline aircraft. This shall aggregate to 154368 kg for four engines installed on an A380-800 baseline aircraft. The water produced replaces an equal amount of fuel by volume since water happens to be denser than kerosene.

However, it can be argued that carrying water aboard during cruise flight can result in additional fuel burn and hence an increase in CO_2 emission. A recent study by Atela (2016) investigated this effect and concluded that for a similar engine-aircraft configuration the fuel burn and CO_2 emissions increase by 17%. Nevertheless, since the radiative forcing of CO_2 is less than that of water, there is a 40 % decrease in the overall radiative forcing of exhaust emissions. Our study of thermochemistry also proves that CO_2 is de-excited during the condensation of water and therefore its contribution to global warming in this state is reduced as compared to the original conditions of the exhaust plume.

Engine Performance (Chapter 6 and Chapter 7)

The design point parameters for initial assessment of the system are obtained from the performance analysis of a three spool turbofan engine and the study of atmospheric science and water physics. Engine and aircraft base line parameters are derived from the Trent 900 engine and the A380 aircraft published data respectively. Design point is established at the cruise condition and standard engine performance analysis has been conducted using the engine simulation software “TurboMatch”.

The formation of contrails mostly occurs at design point cruise conditions and the engine also operates at that condition for the longest time. Therefore this operating condition remains one with the greatest interest with reference to contrail formation where this mechanism comes into action. The performance of the engine with the additional functionality of the centrifugal water expeller is evaluated at cruise. Even though this system is to be optimized for cruise operations; nevertheless it would have an impact on the off-design performance of the engine as well since it is a fixed attachment and cannot be bypassed during off-design operations. (Exhaust throughput methods have been suggested in the chapter on Future Work). Although the formation of contrails is not a continuous process, nevertheless, the mechanism for centrifugal extraction is a continuous one. This necessitated the off-design performance analysis of this concept engine. The impact of the modified engine on the performance of the aircraft is assessed in order to evaluate the performance of an on-board contrail-free engine. The contrail free engine is 30 % longer and 30 % heavier than the standard engine on average. The impact of the change in the dimensions of the engine on the crucial aircraft parameters is investigated using the in-house aircraft performance software “Hermes”.

Thermochemistry (Chapter 5)

The design of the condensation device is validated through the study of the thermo-chemistry of the exhaust gas. Combustion gases are analysed at the molecular level to determine the condensation behaviour of the water vapour in the presence of the other exhaust gases. The inter-gaseous exchange of energy at the molecular level during the process of condensation is also quantified. Molecular mechanics is discussed for the exchange, release and absorption of thermal energy at the exhaust temperature and pressure. Inferences are made regarding the intermolecular and inter-gaseous transfer of heat energy. This analysis is carried out to establish the strength and credibility of the hypothesis regarding the inter-gaseous exchange of energy as well as to verify the occurrence of condensation of the water vapour contained in the exhaust. The non-condensable exhaust gases, carbon-di-oxide and nitrogen; act as a heat sink and the latent heat of water is absorbed by them. This phenomenon is correlated with the change in the properties and condition of the non-condensable exhaust gases when they rotate through the condensation device before being released into the atmosphere.

The energy transition among combustion gases is associated to the environmental impact of releasing a water free aero-engine exhaust emission into the atmosphere. It is established that by employing this device into an aero-engine, the environmental impact of the emission gases can be significantly reduced primarily by preventing the formation of contrails and secondly by

transferring the latent heat of water to nitrogen which happens to be a non-greenhouse gas in contrast to water and carbon-di-oxide; hence reducing the greenhouse impact of water in the atmosphere.

Mechanical Model (Chapter 4)

The philosophy of mechanical design is established and an overview is provided of the various components which support the design. A detailed description of the assembly of the device is illustrated with figures which provide an overview of the design schematics. (Chapter 3)

The mechanism for the collection of water is also devised. The mechanical design provides details of the stator, the rotor, the vessel shell, the water drain, the shaft and the shaft bearings. An assembly of the various fitting and details of the collection mechanism are provided. A design for the rotating vessel seal that contains the water is also proposed.

Basic turbine performance is discussed for the rotor and the stator that are coupled to a vessel shell to complete the design structure. This assembly of components is meant to be integrated to the core of the engine. Specifications are defined for the rotor and the stator mechanical design. A thermal analysis is carried out for the vessel shell. The direction of gas flow is crucial therefore the stator and the rotor are designed indigenously inclusive of blade design.

Data is computed for the vessel to determine the pressure that is generated within and defines the rotational behavior of the gas for condensation to occur at the defined condensation design point. This is achieved by employing the vortex energy equation in order to model condensation of water vapor within the engine. Critical value calculations for temperature, pressure, and velocity are carried out with respect to the available data in order to ensure that the design by no means results in sonic values of the gas flow. The critical air angles are also derived. The blades for the rotor and stator are designed by specifying the air angles. The blade angles are then determined accordingly. This is because the direction and angle of the deflecting gas flow is the fundamental criterion of this design. It is ensured that the gas angles defined must be safely able to avoid the critical gas angles whereby sonic velocity can be reached. Once air angles are defined, the blade angles are calculated accordingly.

A preliminary structural investigation is performed for the model using the finite element method in order to determine whether the vessel can sustain the high pressures involved. Since the centrifugal water expeller is virtually a rotating pressure vessel where high pressures are involved, a basic static and modal analysis is formulated that defines material selection for prototyping and manufacturing.

The condensation device is meant to be integrated within the engine as an add-on attachment. It is meant to be placed in the engine in between the last turbine and the core nozzle. The position of the attachment in the engine is illustrated in Figure 1-1 with reference to the overall engine schematics. The notations used for the schematics have been described in the List of Abbreviations. The invisible contrail-less exhaust exiting an aircraft during flight is illustrated in Figure 1-2.

Background Study (Chapter 8)

Some contextual studies are carried out prior to the selection of the water condensation design proposed in order to establish the strength and credibility of the hypothesis of condensing the aero-engine exhaust water vapour. This is initiated with a heat transfer analysis for a heat exchange mechanism that can condense the gaseous water content of the core exhaust of an aero-engine into liquid water. The model consists of a simple parallel flow heat exchange mechanism, whereby the bypass flow of the engine is used to cool the core exhaust through un-mixed convective flow. The results confirm that the magnitudes of the thermodynamic requirements are excessive, and the calculations for the amount of cooling required, with the help of the bypass flow for condensation does not work out into practical figures. The capacity of the bypass flow to cool the core exhaust, unmixed, in a simple heat exchanger is much less than the amount of heat transfer required.

The analysis of a centrifugal compressor based on existing design parameters has also been performed for preliminary design investigation of a compression based condensation device. Calculations are carried out for a standard aero-engine centrifugal compressor in-order to determine whether this type of a centrifugal compression device can be used to condense the water vapour present in the exhaust emissions. It is inferred that the centrifugal compressor does not fulfil the requirements of a water vapour condensation apparatus.

A basic study of the water physics and atmospheric science is executed in order to determine the behaviour of the water vapour when released into the atmosphere through the exhaust of an aero-engine. This is further linked with the change in the properties and condition of the water vapour as it undergoes condensation as well as the change in the state of the remaining exhaust gases when they rotate through the condensation device before being released into the atmosphere.

Future Directions (Chapter 10)

This concludes the research with the design of the water condenser completed to the level where it validates the concept applied with solid mathematical

evidence and provides a basis for proceeding towards the development of a physical prototype. Several future directions have appeared during the course of this research. The conclusion is supplemented with proposals for future directions.

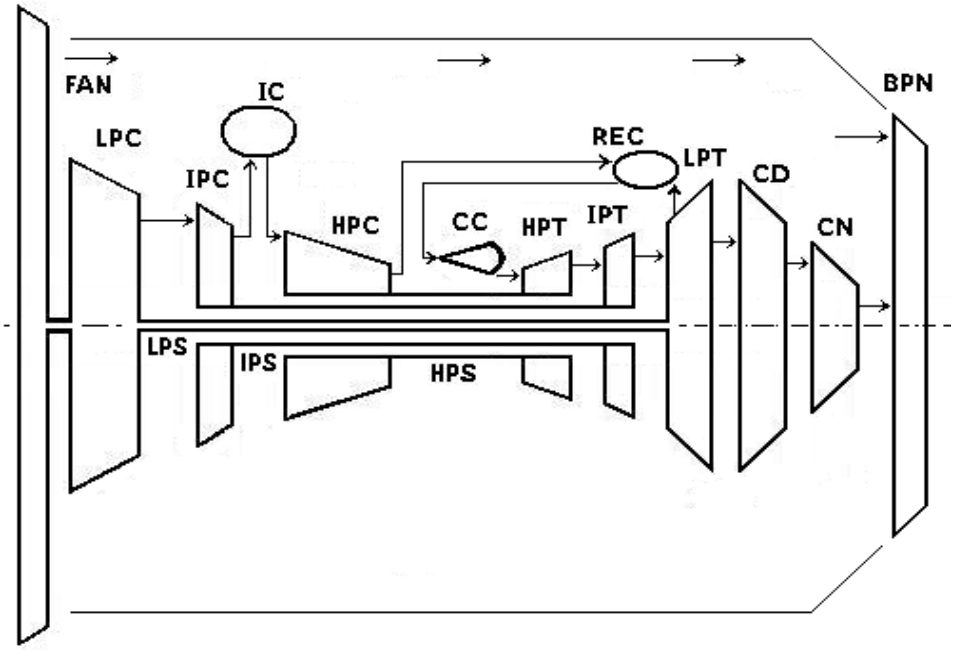

Figure 1-1 : **The Intercooled Recuperated Engine Schematics with the Compression Device**

Figure 1-2 : The Centrifugal Water Expeller Integrated into the Core Engine

(Courtesy: Airbus for A380 Photograph)

2 LITERATURE REVIEW

There have been two parallel types of studies regarding atmospheric moisture. One branch aims to create artificial rain, and the other aims to reduce the formation of cirrus clouds. Our survey focuses on available literature that describes the different methods used by other researchers to curtail the formation of contrail induced cirrus clouds.

Artificial rain is created through induced condensation by introducing nucleation into the moisture laden clouds. This phenomenon is known as cloud seeding. However, some of the methods used to achieve both of the above aims could be common. For example, the process of induced condensation is also used in the prevention of contrails. The reduction of contrail formation uses two types of techniques, one is to induce condensation under controlled conditions, and the other is to prevent condensation altogether by the dispersion of moisture to an un-condensable state. The techniques suggested in the available literature are summarized in the block diagram shown below.

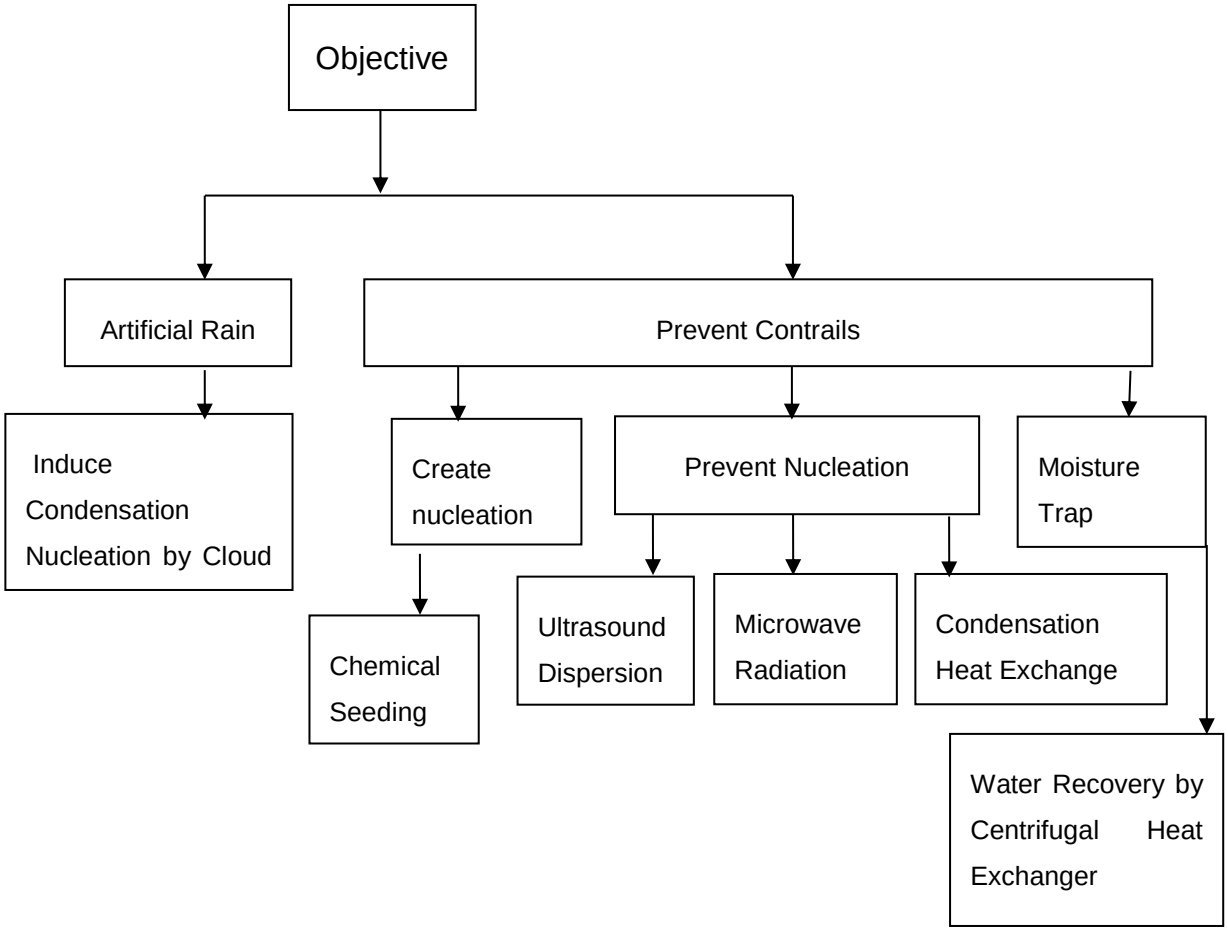

Bright (2011) describes a method and apparatus to convert the water vapour in the exhaust of an aero engine into ice crystals that are large enough to fall through the atmosphere. This is achieved by the process of artificial seeding. Seed ice crystals are introduced into the exhaust plume (outside the engine) for water vapour to condense onto the crystals. Seeds are either created by irradiating the air using electromagnetic radiation, or by applying an electric potential. Seeds can also be mechanically produced by super cooling compressed air through expansion to a temperature below the dew point of water, and then introducing water into it, which then freezes into ice and acts as seed. He also claims that the size of the seed ought to be of the order of 1000μm so as to allow preferential condensation, because other smaller condensation nuclei are also present in the atmosphere. The large size of the particle enables it to fall under the effect of gravity. The particle falls to either an altitude of un-saturation and sublimes, or falls all the way to the ground. The claim however, does not mention any particular method to control the size of the crystal. Bright (2011) does not quantify the power required for the electromagnetic radiation, which would be a reasonable fraction of the power output of the engine. Neither does he quantify the amount of water to be carried aloft the aircraft for creating and dispersing the ice crystals. The quantity of water required for ice dispersion would be a function of the water emitted by the engine's combustion, and thus be a reasonable amount of fuel burnt. This would be a severe penalty on the payload.

Anderson (1970) suggests injecting a non-corrosive alcoholic solution into the exhaust plume of an engine to create hyper nucleation in order to condense the water into micro-particles that are not perceivable by the naked eye. The chemical constituents of the solution and a method of preparing the solution have been claimed. The main objective is to hide the contrails rather than prevent their formation. This method involves carrying aloft chemicals and their subsequent release into the atmosphere. This involves an additional operational cost. He does not quantify the amount of these chemicals as a function of the quantity of the water exhaust of the engine.

Singh (1992) suggests a method similar to Anderson (1970), using the almost the same chemicals that act as a nucleating agent and a freezing point depressant. He also claims non corrosiveness of his method. However, chemical methods cannot be applied in an environmental context because the introduction of chemicals into the atmosphere can prove otherwise.

Noppel, Singh and Taylor (2008) claim a method for contrail suppression and suggest an apparatus that comprises an ultrasound generator directing the waves at the exhaust gases of an aero engine in order to directly disintegrate the water vapour into extremely small particles that are not capable of forming

contrails. An assembly is claimed which comprises an ultrasound generator, a waveguide, a contrail detector and a modulator. The modulator controls the amplitude and frequency of the ultrasound wave according to the plume content and the atmospheric conditions. They claim that the power required by the ultrasound generator to be of the order of 50 KW which is an infinitesimal amount compared to the power of the engine.

Noppel, Singh and Taylor (2008) claim another method for contrail suppression and suggest another apparatus that generates microwaves instead of ultrasound waves. The microwaves are directed towards the exhaust plume, and impart additional thermal energy such that the ice crystals evaporate, and contrails are not formed.

Another patent claim by Noppel, Singh and Taylor (2007), refers to a standard three-spool intercooled recuperated turbofan engine that comprises of the basic components that include three compressors driven by three turbines, a combustor, an exhaust nozzle, an intercooler, a recuperator and a bypass duct. The additional components proposed for design innovation are a dehumidifier and an exhaust mixer. The dehumidifier is positioned between the intercooler and the recuperator whereas the mixer is placed before the exhaust nozzle. The dehumidifier is claimed to condense the water vapour present in the exhaust before releasing it into the atmosphere as a liquid through the water condenser. The mixer just mixes the various airflows before the final exhaust. The design claims that contrails can be avoided if water is extracted from the exhaust emissions by condensing it as a liquid within the engine using an additional heat exchanger as a water condenser. The patent above also implies that this condenser would provide optimum performance if integrated with a standard intercooled recuperated turbofan engine. Liquefied water can then be separately released into the atmosphere whereby it would precipitate to the ground and should also be partly injected into the combustor for enhanced thermal performance and reduced NOx emissions. The final part of the patent claims that if the dehumidified core exhaust plume is mixed with the bypass stream before being released into the atmosphere, it would achieve a temperature that is not conducive to the formation of contrails. An extensive study was carried out to investigate the design claims as well as to evaluate the practical viability of the design and its limitations.

The designs of conventional heat exchangers do not consider the excessive weight penalty to provide an extremely large surface area for heat transfer, as most heat exchangers are used for ground based applications. However, ground based engines do not require contrail suppression. The prime objective of our research remains contrail suppression.

Nelson (1992) describes a system for detecting contrails that is carried aloft an aircraft. A laser beam is directed onto a volume of contrails. The beam scatters back towards a detector on the aircraft. The scattered radiation is analysed to indicate the formation of contrails behind an aircraft. This apparatus can be used along with one of the contrail prevention techniques discussed so far to engage the system for contrail prevention only in that flight segment which results in the formation of contrails.

Schumann (2000) discusses the influence of propulsion efficiency on contrail formation. He concludes that higher propulsion efficiency results in contrails at higher temperature over a large range of flight altitude. A comparison has been drawn for lower CO_2 emission with increased propulsive efficiency and higher contrail formation. The engine modelling has been carried out by varying the overall efficiency and contrail prediction has been conducted using the Applemann criterion as well as on board experimental measurements. He indicates that the propulsive efficiency is a function of the engine aircraft operation in a particular condition, due to the balancing effect of the thrust and the drag during cruise operation. He also highlights the fact that high bypass ratio results in a higher overall propulsive efficiency.

Haglind (2008) also suggests contrail avoidance through reduced propulsive efficiency. He achieved it by using variable guide vanes with the fan to reduce propulsive efficiency and increase the TET by operating on a higher power setting. It is probable that the change in the geometry of the fan changes the intake mass flow as well as the fan pressure ratio which in turn reduces the efficiency.

Filippone (2010) suggests that the minimum altitude for contrail formation is 8.8 km. Contrails can be avoided by flying lower or higher. However, he debates that flying lower is not a practical prospect in terms of the manufacturing complexities involved as well as increased fuel consumption. Lower altitudes are also more prone to weather conditions. The author carried out a detailed analysis of various performance parameters and concludes on the limited availability of real time contrail data. Suggestions are made for variable aircraft geometry to maintain optimum performance at different altitudes. Changing altitude is more efficient for long haul than short haul flights due to landing and take-off fuel consumption. Williams, Noland and Toumi (2002) also suggest restricting cruise altitude. They conclude that this shall increases CO_2 by 4% and change the average journey time by 1min.

Out of the numerous literature survey conducted, two very relevant patents were considered to further the cause of contrail suppression. Namely Qureshi (2016a) and Qureshi (2016b) These patents described contrail suppression by the extraction of water using a centrifugal method for customized compression.

They facilitated the separation of the water vapour from the other exhaust gases so that preferential cooling can occur. Qureshi (2016a) and Qureshi (2016b) claim that the exhaust gases are introduced into a centrifugal vessel. The water vapour in the exhaust is denser than the CO_2 at the exhaust temperature. In the vessel, the denser vapour is thrown out wards towards the circumference due to the centrifugal force. As a consequence, the rarer CO_2 would be forced towards the centre of the centrifugal vessel. The centrifugal force would compress the vapour particles closer to each other, and thus enable them to coalesce. The exterior of the vessel is subjected to the cold bypass flow, directly cooling the vapour at its periphery. If sufficient pressure is generated by the centrifugal vessel, and simultaneously heat is lost to the surroundings, the water moves down the phase diagram into a region where the water can exist in the liquid state. The CO_2 and N_2 do not lose their heat, and exit the nozzle uncooled. This reduces the overall amount of cooling required, since only the water needs to be cooled. The centrifugal mechanism only exposes the water to the cooler surface of the vessel and thus enhances the heat transfer rate. A further phase shift is created by piping this high-pressure high-temperature water through the leading edges of the aircraft for de-icing, and thus bringing the temperature to a comfortable level, such that it can be stored and brought back to Earth. It is of interest to mention that the volume of water produced by burning kerosene is equal the volume of fuel carried abroad. It has been claimed that some pre-cooling of the exhaust gas is required before presenting it to the centrifugal vessel. Due to the presence of certain combustion by products like SO_2, Soot particles, etc., acting as nucleation centres, the water vapour already has a certain amount of precipitation, thus the centrifugal forces bring the moisture together. The inventor suggests that It might also help to inject some additional nucleation centres to expedite the condensation in the centrifugal vessel.

In the latter method claimed by Qureshi (2016b) , the linear exhaust gas flow is rotated by stators deflecting the gas into a static chamber, and the rotation of the exhaust gas creates the centrifugal effect discussed at length. The dehumidified gas is then again deflected to exit as linear flow. Here the chamber or vessel in which the centrifugal effect is created is a static vessel, and the gas is flowing and rotating inside. The separated liquid flows around the static vessel. It was assumed that this might cause a boundary layer separation. This mechanism is driven by the LPT shaft as an external load.

In the former patent Qureshi (2016a), the separation mechanism is different. Here the exhaust gas introduced is first deflected by stators, as described earlier, and introduced into a vessel to continue rotating, creating the centrifugal effect as before, however, here the vessel is also rotating with the same angular velocity as the gases. The liquid here is not flowing on the surface of the vessel, but is in firm contact with the vessel, and no boundary layer separation takes

place. The liquid and vessel move together as one. The residual gases rotate along the central axis and are straightened out by stators to exit into the atmosphere as linear thrust. In the latter method, the gas is similarly deflected by stator foils to rotate inside a vessel; however, the vessel also rotates along with the gas. The centrifugal effect created is the same, thus separating the components of the gas, and the separated water also rotates along the periphery. After this literature survey, it was decided to develop our contrail suppression system along the lines of Qureshi (2016a). The first mechanism Qureshi (2016b) was simpler to build, since it has no moving parts and is thus more reliable. The second system has moving parts, and requires a challenging sealing system. However it shows more promise in achieving the extraction of water, because no boundary layer separation would take place between the liquid and the internal surface of the vessel.

Water comprises of 2.25% of the exhaust gas constituents Once water is separated it is easier to cool rather than within a mixture of non-condensable gases which results in excessive magnitudes of heat being released and unwanted loss of energy. Separation of the water from the remaining gases results in a reduction in the amount of heat loss required for condensation to only 2.25% of the existing requirement excluding the requirement of latent heat loss which is specific to water vapour alone. All mechanisms assume that the low power turbine expands to ambient and that the initial temperature is below the critical point of water. No phase change is possible beyond the critical point temperature. The excess power derived by expanding the low power turbine to ambient is used to compensate for the thrust loss from the core and is also used to provide power to drive the condensation device attached to the engine.

The heat dissipated by water during condensation is absorbed by the nitrogen present in the exhaust emission which is a highly promising aspect of employing this condensation device; unlike carbon-di-oxide and water, nitrogen does not contribute to the green-house effect. This mechanism enables to avoid the weight and size penalty, complicated flow paths and duct losses of the conventional heat exchangers as well. Besides it provides the additional benefits of exploiting the full potential of water by obtaining it as a recovered product rather than merely managing it as a waste commodity. This is the first attempt to condense water within the engine as well as to collect it within the aircraft during cruise flight. It seeks to eliminate the contrails at source within the engine as compared to other methods of contrail prevention that mitigate the contrails after their release into the atmosphere. It also serves to reduce the green-house effect of water and carbon-di-oxide in the atmosphere as well as create water. This technology addresses environmental concerns only whereby the economic penalty of condensing and carrying water aboard an aircraft is willingly accepted.

3 THEORY OF CENTRIFUGAL WATER EXTRACTION

3.1 INTRODUCTION

The centrifugal moisture extraction system works on the coagulation of water vapour and its collection, as opposed to the other systems in the literature that work on the dispersal of water vapour in the contrail. The mechanism is engineered as an arrangement of stator and rotor components and is developed into a turbomachinery that can be attached to an existing aero-engine.

The concept employs the use of the centrifugal force generated by the rotation of the exhaust gases. A mechanism is devised whereby the centrifugal effect is created in a rotating vessel and the force thus generated results in a change in the pressure and temperature of the exhaust gas input into it. This change is exploited in order to achieve a pre-determined design point temperature and pressure whereby the condensation of water vapour can occur. Hence condensation is achieved through the centrifugal action.

In the exhaust gases of a turbine engine, the water molecule is the lightest in the presence of other main species like CO_2 and N_2. If at least 4 molecules of H_2O coalesce, then a particle is formed that is heavier than the other two particles. First and foremost the water molecule needs to be formed into water vapour, and favourable conditions of temperature and pressure need to be created to achieve this. Water undergoes a phase change when subjected to a certain pressure at a given temperature. These conditions are such that CO_2 and N_2 continue to remain in the molecular, gaseous state, while, more and more molecules of H_2O coalesce to form even larger particles. The water vapour can then be separated from the other gases using the centrifugal method. The residual thermal energy in the exhaust gas is of a magnitude that equals the absorption capacity of the entire bypass airflow. If the bypass flow needs to act as the cold stream, an enormous amount of flow would need to pass through a very large heat exchanger. For any heat exchanger to achieve this would compromise the entire propulsion of the bypass airflow, thus rendering excessive losses and flow complications. However, the thermal energy in the water vapour is only a fraction of the total thermal energy of the remaining exhaust gases. Thus, if the water can be separated from the exhaust gas, then only the water needs to be subject to cooling, while, the rest of the gases can be allowed to exit the system un-cooled, and into the atmosphere.

When a mixture of gases having different densities are introduced into a cylinder and the gases are made to rotate in a circular manner, the denser gas collects at the periphery of the cylinder while the rarer gases are squeezed inwards. Hypothetically, consider a number of concentric cylinders of gases

rotating around a single axis. The density of the gases in these hypothetical cylinders varies from the densest gas in the outermost cylinder to the rarest gas in the innermost cylinder. This concept is illustrated in Figure 3-1

Work has been carried out in parallel over three different concepts of moisture extracting centrifugal systems for separating water from the other exhaust gases. All the three concepts involve centrifugal compression leading to a phase change in water and condensation on the walls of the centrifugal vessel. The phenomenon leads to complete separation of water and not just enrichment whereby the water is condensed and collected. The aim is to form liquid water within the engine that is well suited to storage and disposal.

The behaviour of a fluid under centrifugal force can be worked out from the vortex energy equation. The objective is to move the state point on the water phase diagram onto a favourable region where water exists in a liquid state. The relationships governing the behaviour of compressible gases under the centrifugal effect are obtained and the minimal temperature and pressure required to achieve condensation is determined. This then enables us to proceed with the mechanical design.

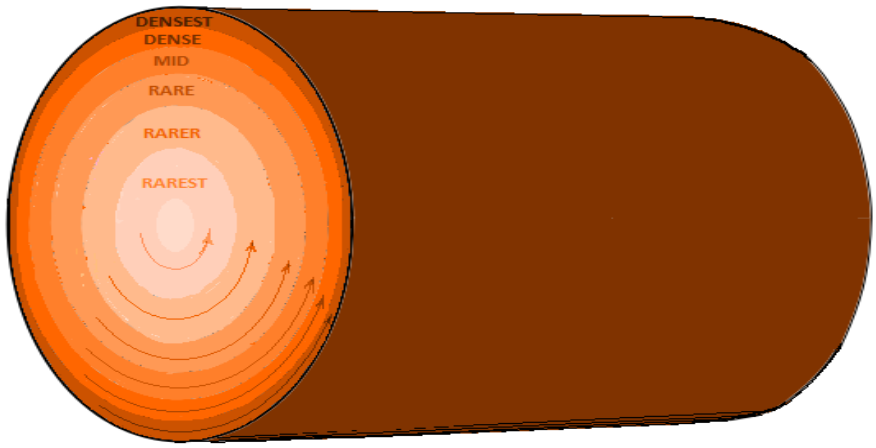

Figure 3-1: Density Variation in the Radial Direction in a Rotating Mixture of Gases in a Cylinder

Due to viscosity and other factors, this does not happen perfectly. In practice, the outermost cylinder of rotating gases contains an above-average ratio of denser gases, while the inner most cylinder of rotating gases contains a below-average ratio, and a gradual variation in-between. The gas in the outermost

cylinder would be richer in the denser gas, and the innermost cylinder would be richer in the rarer gas. This phenomenon is therefore called enrichment.

When rotating two gases with almost similar densities, complete separation is not practically possible. Due to temperature and velocity differences, there is diffusion of gases, and some re-mixing also takes place. However, the net effect is that the centrifugal effect prevails. When passing the richer gas through a number of such stages, the needed gas can get richer and richer, but the asymptote would meet at infinity.

In the context of the application, when the gases are subjected to centrifugal compression, water molecules undergo a phase change and coalesce to form liquid water which is denser than the other combustion species that retain their molecular state. This makes the separation of water possible through this mechanism.

3.1.1 COMBUSTION PRODUCTS

In the perspective of our centrifugal system, we discuss the physical properties of the products of combustion, and their application to the centrifugal system. The products of combustion in the turbine engine are mostly H_2O, CO_2, N_2 and un-used O_2. Their molecular weights are:

Molecule	Relative Molecular Weight
H_2O	18
N_2	28
O_2	32
CO_2	44
$C_{12}H_{26}$	170

Table 3-1: Relative Molecular Weight of the Combustion Gases in the Exhaust

H_2O is the lightest, and as such, if passed through a spinning cylinder, would spin towards the centre. The heavier molecules would likewise spin towards the periphery. A centrifugal system based on this method is proposed for discussion only. However, it remains impractical because as the temperature drops or pressure increases, and some water molecules coalesce to form water vapour, they get heavier and move outwards and thus reverse the centrifugal effect. This is like operating in two physical states of water. A comfortable system would be where we can operate in a single, or a narrow band, of water state.

Among the three combustion gases, the behaviour of water vapour is unique and anomalous. Unlike CO_2 and N_2, water tends to undergo a phase change at a relatively lower pressure whereas the other two combustion products still remain in their gaseous form. It is also inclined to shift towards the liquid state from the gaseous state on the introduction of a slight disturbance; it tends to nucleate over microscopic particles of the order of less than a micron and then coalesce to form water droplets of the order of 100 microns. This facilitates the coagulation of water molecules in the system and makes it the heaviest specie amongst the three gases.

In this chapter, we proceed under the pre-condition that all or most of the water is in the vapour form, and all the other species in the exhaust are in their molecular state. Thus, preceding with the pre-condition that water is in the form of nano-droplets, within a mixture of all the other exhaust gases, they are all made to move in a circular manner. The water droplets move in an ever expanding outward spiral and eventually collide with the outer walls of the centrifugal vessel. The cylindrical walls of the centrifugal vessel we shall henceforth call the shell. The water droplets move through the other gases, to land on the inner walls of the shell. The initial temperature of the mixture would be at the previously decided operating point of water on the phase diagram.

In a relative manner, this behaves like rain drops reaching the ground through the atmosphere. The viscosity of the atmosphere is the retarding force on the rain drop during its descent due to the gravity of the Earth. This analogy of rainfall is being used here to show what is happening inside the centrifugal shell. The centrifugal force is creating the artificial G force inside the shell. Consider the analogy of a rotating toroid as a space station. The radius of the toroid and its angular velocity are kept such as to create a centrifugal force equal to the gravity of the Earth i.e. =1G, so that humans in the space station can be comfortable. Since the engine is already within the Earth’s gravitational field, the artificial gravity created in the centrifugal shell (for a particle to travel upwards at 1G) should at least be more than 2G.

Here again, the viscosity of the exhaust gases would be the retarding force on the nano-droplet on its travel radially outwards. This would determine the minimum number of revolutions that the mixture gas would require for the water droplet in the innermost orbit to travel to the outermost orbit.

The exterior surface of the shell is exposed to the cold bypass airflow, and thus would be cooler than the exhaust temperature. The water droplet landing on the shell would cool and further coalesce to form a larger droplet. This would be partly helped by the silver coating on the inside of the shell, as well as the temperature drop. Droplet formation is better than film formation on a condensation surface, and a property of silver surface is that it encourages

droplet formation of water vapour instead of film formation. Thus, if the inner surface of the shell is coated with silver it would help to form droplets on the surface.

The drop has to flow away to clear the surface so that further condensation can take place. This is done by gradually increasing the diameter of the shell, as a portion of a cone spreading outwards. The drops on the inner surface of the shell, due to the centrifugal force, move out towards the larger diameter. Thus, a fresh condensation surface is continuously being created. The volume increases, and acts as a diffuser, increasing the pressure, and thus, pushing the working point on the phase diagram towards a favourable region. Further working is done to evaluate these conditions.

The rotating gases in the expanding cone first reach the largest diameter and then, the shell is shaped as a reducing cone, and the surface is now tapering towards the centre. The reducing spiral only brings the lighter gases inwards, leaving behind the water in a ring at the widest diameter.

The water is drained out through different possible mechanisms, and the rest of the gases escape through the exit nozzle. Preferably, the spiralling gases could be made to straighten out, thus exiting the centrifugal vessel in a linear manner, with whatever residual energy leftover for generating thrust. Most of the moisture has been collected in the expanding cone and has dropped into the canal where it remains until drained out. The residual moisture if any appears in the contractive cone. The entire concept is illustrated in Figure 3-2 and Figure 3-3

According to the above discussion, we would like to force the issue, and first ensure that the water is no longer in the two states (molecular gas and vapour), but only in the vapour state. We have to first create conditions whereby a number of water molecules coalesce, and achieve a size and particle weight slightly heavier than the heaviest molecule in the exhaust gas. This nano-droplet would then behave as a heavier molecule. It can then be assumed that the water can now behave as very dense gas. This state of the water molecule is achieved by generating centrifugal compression within the vessel that results in condensation.

3.2 MECHANICAL DESIGNS FOR THE CENTRIFUGAL WATER EXTRACTOR

A number of mechanical methods can be employed to rotate the exhaust gases and extract water. Many configurations were designed and some of those have been described here for interest. Some of their advantages and disadvantages have been highlighted. The design finally selected for further development is

discussed at length. Three designs are mentioned below as described by (Qureshi, 2016b) and (Qureshi, 2016a)

1. Centrifugal water extractor with a static swirl generator and a rotating shell.
2. Centrifugal water extractor with a rotating impeller and expeller in a static shell.
3. Centrifugal water extractor with a static impeller and shell and no moving parts.

One would expect that any mechanical design with the minimum moving parts would have been selected, but the advantages of a rotating shell allows an improvement over the static shell, and is a truly centrifugal system. Rotation of the shell prevents the formation of the boundary layer and eliminates the losses due to the viscous effect. In addition it also generates the centrifugal force which is required for moisture extraction.

3.2.1 DESIGN PRESUMPTIONS

The design of the moisture extraction system is based on the following presumptions:

1. The size and mass of the droplet formed is specified.
2. The droplet moves radially outwards as it undergoes a single rotation.
3. The droplet formed is moving in a viscous fluid.
4. The radial viscosity component is considered. The angular viscosity component is constant and hence can be ignored.
5. The remainder volume of the vessel is occupied by nitrogen and carbon-di-oxide once condensation has occurred and all the water has condensed..
6. The water produced is immediately removed so that the system maintains a single phase configuration.
7. All gases are moving axially and radially in a cylinder. The angular component remains constant.

3.3 DESIGN SKETCHES

The three-dimensional figures are illustrated to explain the various design concepts that are modelled using the CAD software Pro-Engineer. The models are displayed in the side-view (which refers to the engine lengthwise) and the three-dimensional isometric view in order to provide a clear visual understanding of the conceptual design. All drawings are modelled to scale by utilizing the engine size (Trent 900 baseline specifications) as a reference

dimension. Exterior surfaces have been represented translucent in order to make the interior components of the assembly visible.

3.3.1 STATIC SWIRL GENERATOR WITH A ROTATING SHELL

The most feasible proposal appears to be that of the static swirl generator and a rotating shell for a centrifugal force generator where the outer vessel rotates at a low speed so that the shear forces at the periphery are negated and frictional losses are minimized. This prevents the loss of momentum due to the viscous boundary layer. The remaining mechanism and functionality are common to all designs. Figure 3-5 and Figure 3-6 thus illustrate the design that is evolved for development and practical implementation. It consists of the static swirl generator with a rotating shell. The outer vessel is rotated to overcome the viscous drag. As discussed above, the boundary layer separation can tend to prevent the droplets landing on the surface. The solution to this problem is to rotate the shell at a velocity equal to the surface velocity of the gases such that the surface of the shell has zero relative velocity.

The exhaust gas flow enters the water extractor by passing through stator vanes. The stator vane aerofoils are shaped so as to deflect the gas flow and create a swirl. In this case, the linear flow of the exhaust is deflected to rotate in a circular manner. It can be seen in Figure 3-4 that the blades are initially aligned with the incidence of the core flow. The aerofoil is then twisted in a direction to create a swirl of the gases. This part is rigidly fixed after the low power turbine station. Assuming that this swirling motion allows the gas to maintain its inertia and angular momentum as it enters the centrifugal vessel, the gas imparts its energy to another turbine rotor which rotates the shell as a single body.

This energy transfer reduces the temperature of the exhaust gases. The rotating shell and gases create their own centrifugal force that is exerted on the moisture droplets. These moisture droplets then travel radially outwards at a minimal gravitational force greater than two and land on the inner walls of the shell .The shell is also rotating at the same surface velocity as that of the exhaust gases.

In-order to synchronize the two velocities, the turbine rotor has been introduced at the entrance of the centrifugal shell immediately after the stator. The turbine and the shell are coupled and rotate together on a common shaft. The shaft would be running freely and the energy for rotating it would be generated by the gas flow in the turbine. In other words, the deflected gas flow from the stator is rotating the turbine. This also has a thermodynamic influence. Mechanical energy is being drawn by the turbine thus reducing the temperature of the exhaust gas. In a simplified version it can be assumed that the turbine is

absorbing energy as well as giving a rotational motion to the gas. The droplets landing on the shell would be relatively normal to the surface of the shell and there would be no boundary layer since the gas is static with the shell because they are both rotating with the same speed.

As described earlier, the inner surface is coated with silver, encouraging droplet formation and these droplets are travelling outwards into the collector. The droplets coalesce and get larger as they move along the shell and the diameter of the shell cone gets larger and these droplets fall and collect into the trough. The gases continue their circular motion unguided and the cone now tapers inwards, leaving the water behind. Only the lighter gases can then come towards the centre of rotation.

Here again, any residual vapour would also go the surface of the rotating cone and due to the artificial gravitational effect, it also slides into the collector. The remaining exhaust gases exit the centrifugal shell spirally. Another set of stator vanes would deflect out the spiral rotation into a linear motion and thus the exhaust gases would exit the centrifugal shell linearly retaining certain residual thrust. Details of the mechanism are outlined in the concept sketch is provided in Figure 3-4.

Figure 3-5 and Figure 3-6 indicate that the shell contains a hollow inner core. Both the inner core and the outer vessel rotate together. The core compensates for the change in volume due to the conical expansion of the outer vessel which would otherwise result in the expansion of the gas. The hollow inner core tends to minimize the volume of the gas at the largest diameter of the vessel where condensation and extraction of water is meant to take place.

This completes the mechanical concept design. The design objectives defined for this concept and the design presumptions laid shall be addressed in the chapters that follow. A complete mathematical model is developed and data is computed to convert this concept into a practically implementable form. The other two concepts listed are also patented by the same inventor and are discussed in the sections that follow since they provide the foundation over which this model evolved. They are explained only to highlight the background of this design and no further working is carried out on them.

3.3.2 ROTATING IMPELLER AND EXPELLER IN A STATIC SHELL

Figure 3-7 and Figure 3-8 illustrate the mechanical conceptual design of the centrifugal water extractor. The mechanism consists of an impeller, a collector vessel and an expeller assembled together. The impeller and expeller are rotating on the low power shaft of the engine whereas the collector vessel is rigidly fixed. An axial flow of exhaust gases is introduced into a rotating impeller,

which compresses the gases. The flow rotates and is pushed forward. Due to the centrifugal force, the heavier water vapour is thrown towards the periphery of the vessel. The lighter carbon-di-oxide and nitrogen forms the core gas which escapes through the centre of the vessel into the atmosphere. The downward taper of the vessel compresses the gas towards the widest part where there is an increase in the volume and hence this region of the vessel acts as a diffuser. This diffuser further increases the pressure of the gas and retards the velocity. There occurs a net increase in the pressure of the gas due to the centrifugal compression in the impeller followed by the rise in static pressure in the diffuser. The rotating exhaust gas in the diffuser experiences a force due to the centrifugal effect, and the water nano-droplets (being heavier than the molecular CO_2 and the molecular N_2) are forced tangentially towards the circumferential wall of the shell. The device is enveloped by the bypass flow.

Exposure to the bypass air at the periphery results in the cooling of the gas that is thrown at the walls of the vessel. As compression progresses in the impeller with a loss of heat to the surroundings, a phase change in the exhaust water vapour is initiated and condensation occurs. The phase change can start prior to reaching the widest diameter once sufficient pressure is generated at the given temperature. The pressure compresses the gas, and results in shifting the operating point towards the liquid phase. Water droplets trickle and slide down the walls of the vessel and collect at the base of the collector. As condensation occurs, the remaining gas rarefies and exits at the core. The lining of the shell is coated with silver, aiding condensation.

The water droplets in the circular flow of the exhaust gases tend to move the droplets into a larger circumference, until they drop into the canal. The water in the canal flows circumferentially into a drain at the bottom. A collection mechanism is also provided on the outer vessel to collect and contain the water condensed. The collector vessel surrounds both the impeller and the expeller. The droplets are drained out from the collector for adequate disposal.

Efficient compression can only be achieved with a minimum possible mechanical clearance between the impeller and the collector vessel. Since the expeller is rotating on the same shaft as the impeller, it helps the remnant water vapour being thrown radially outwards to be deposited on the collector. The impeller and expeller rotate on the engine’s low pressure shaft while the outer vessel is stationary. The dimensions of the device conform to the engine length and diameter scale.

3.3.3 STATIC IMPELLER IN A STATIC SHELL

The exhaust gas rotates when passing through stator vanes. It is thrown towards the periphery of the vessel due the centrifugal force generated through

rotation. The gas that hits the walls is cooled by the bypass air surrounding the vessel. The pressure generated due to the centrifugal forces causes a phase change. Both the inner core and the outer vessel remain stationary. No power is required to drive the centrifugal water extractor.

Figure 3-9 Illustrates a static swirl generator which consists of a static spiral enclosed in a rigid shell. The design intent is to avoid any moving parts since a fixed geometry has its inherent advantages. In this configuration, the exhaust gas exiting at the low power turbine station is input into the spiral channel. The axial flow of the gas is deflected by the concentric spiralling channels which appear as spiralling walls on the shaft. The gas deflects at its entry into the impeller and starts rotating around the shaft. It is contained by the outer shell during rotation. At the widest diameter of the impeller, the gases in the individual channels mix and rotate to move in a circular manner. The centrifugal force induced in to the gas compresses the vapour to condense in the collector. Cooling fins attached to the collector vessel are shown in Figure 3-10

The remaining exhaust gases continue rotating and exit in a spiralling manner out into the atmosphere. The gas is deflected to move in a circular configuration and the centrifugal extraction of water takes place. The water in the collector is drained out. The advantage of this system is that no shaft energy is required to rotate the impeller. However, there exists a certain loss of core thrust when the linear exhaust vector is deflected into a circular vector. At the exit of the centrifugal shell, stator vanes could be added to straighten the exiting exhaust gases if it is practically found to be necessary. A possible drawback might be the frictional losses due to the spiralling walls of the deflector. Since the entire system is static including the outer shell, there would be a boundary layer separation which can prevent the moisture coming into contact with the shell since the vapour and gases are all moving together. These issues have been addressed in the other concept design by introducing a rotating shell.

This completes the conceptual design of the various mechanisms proposed for the condensation of the water vapour content of the exhaust emissions of an aero-engine. Advancement shall now be made towards a qualitative assessment of a centrifugal water expeller that is based on the concept of a static swirl generator with a rotating shell as detailed. A complete thermodynamic analysis supported by mechanical design and for the selected mechanism is presented in Chapter 4.

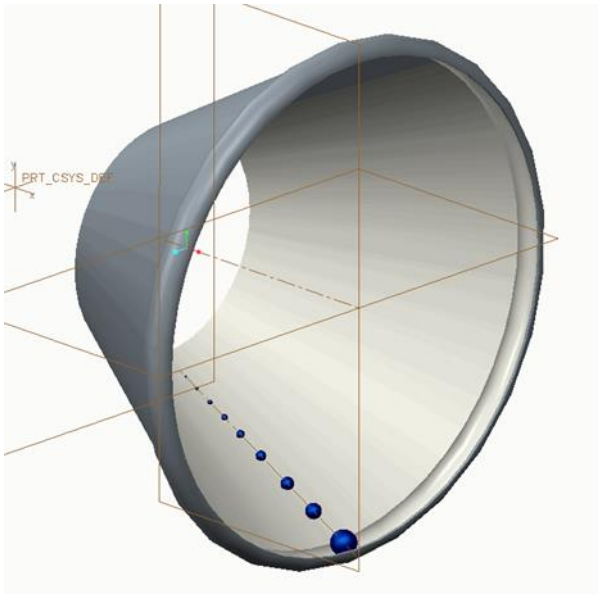

Figure 3-2: Condensation and Growth of Water Droplets in a Single Sided Spinning Cone

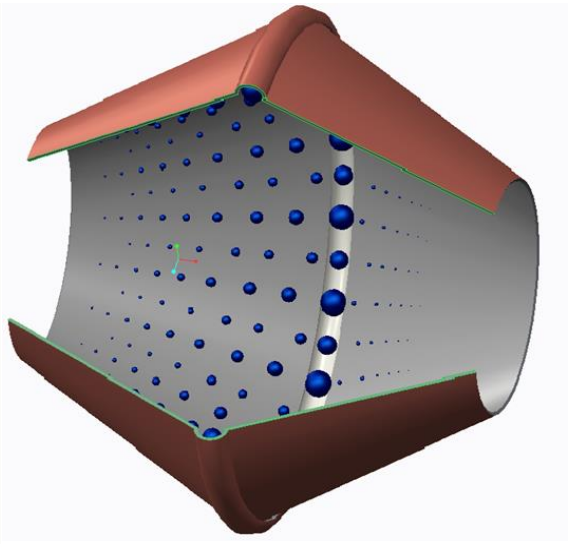

Figure 3-3: Condensation and Growth of Water Droplets in a Dual Sided Spinning Cone

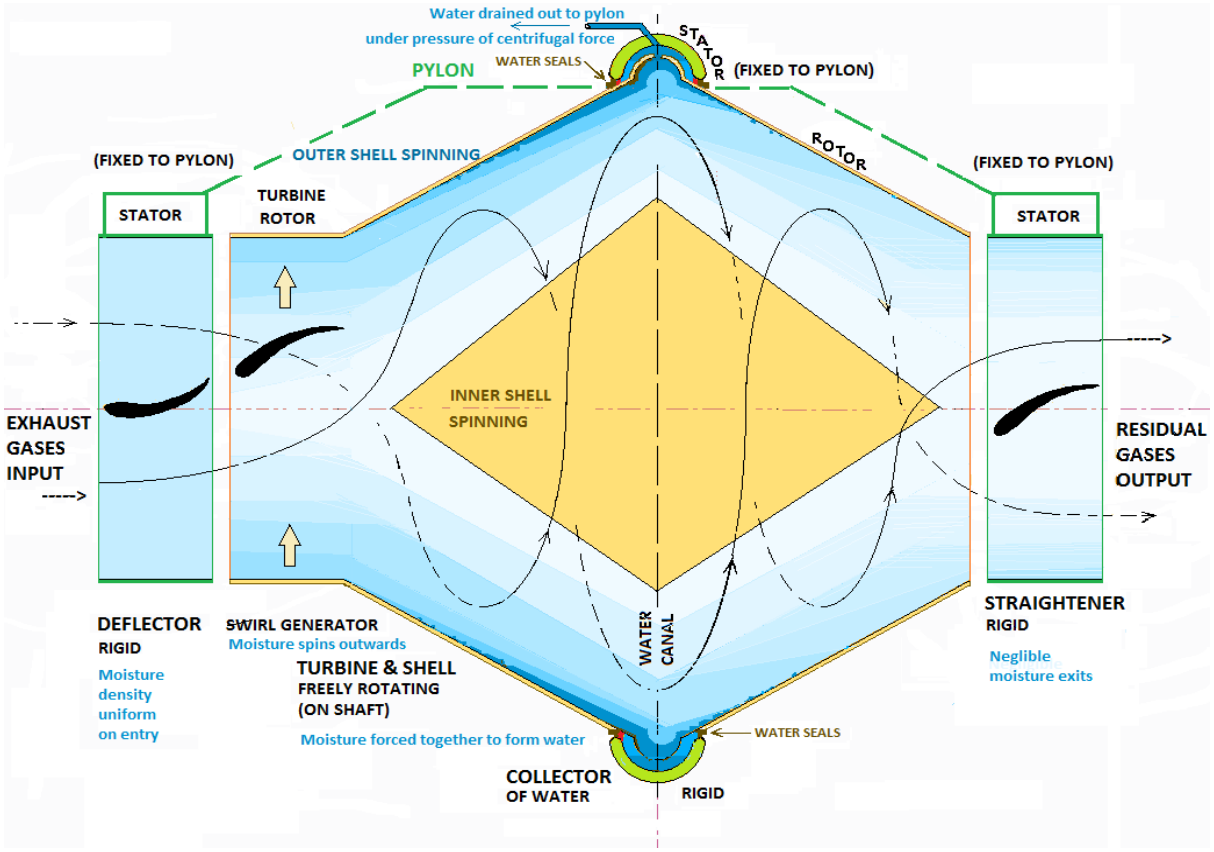

Figure 3-4 : Concept Sketch for the Centrifugal Swirl Generator

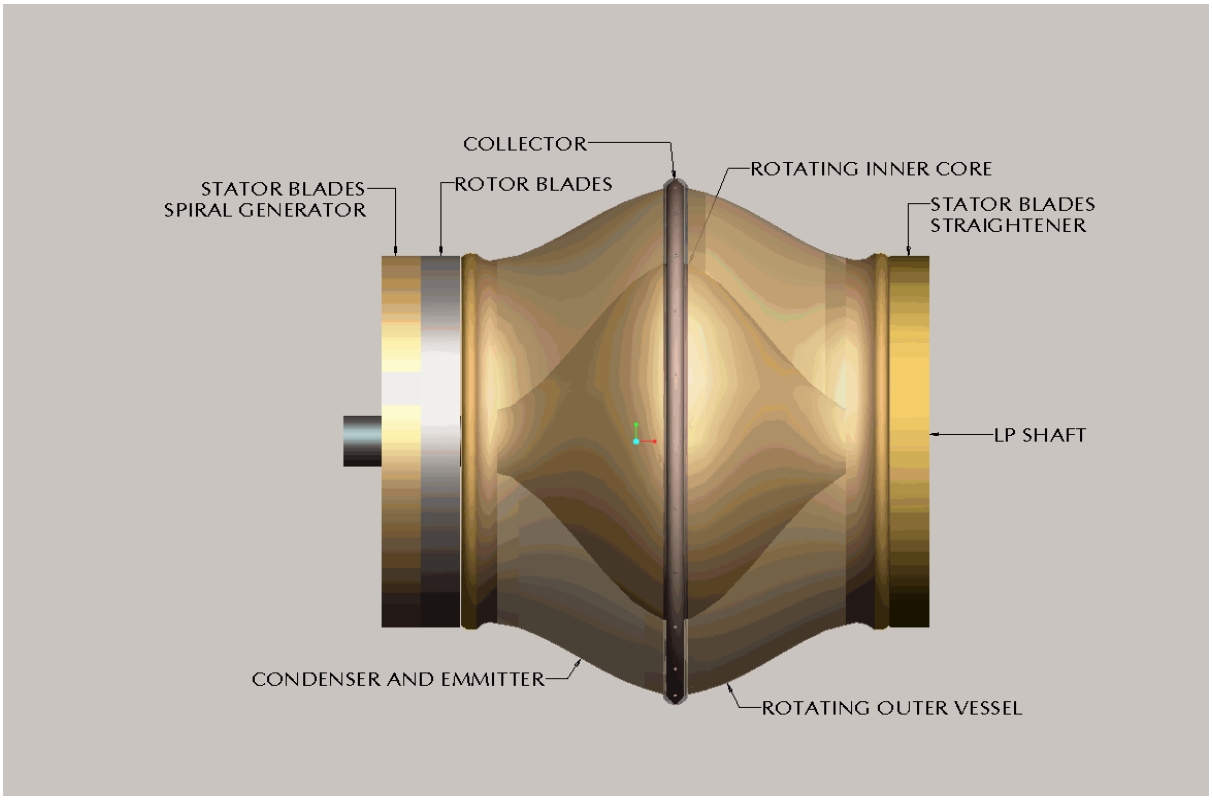

Figure 3-5: Side View of the Static Swirl Generator with a Rotating Shell

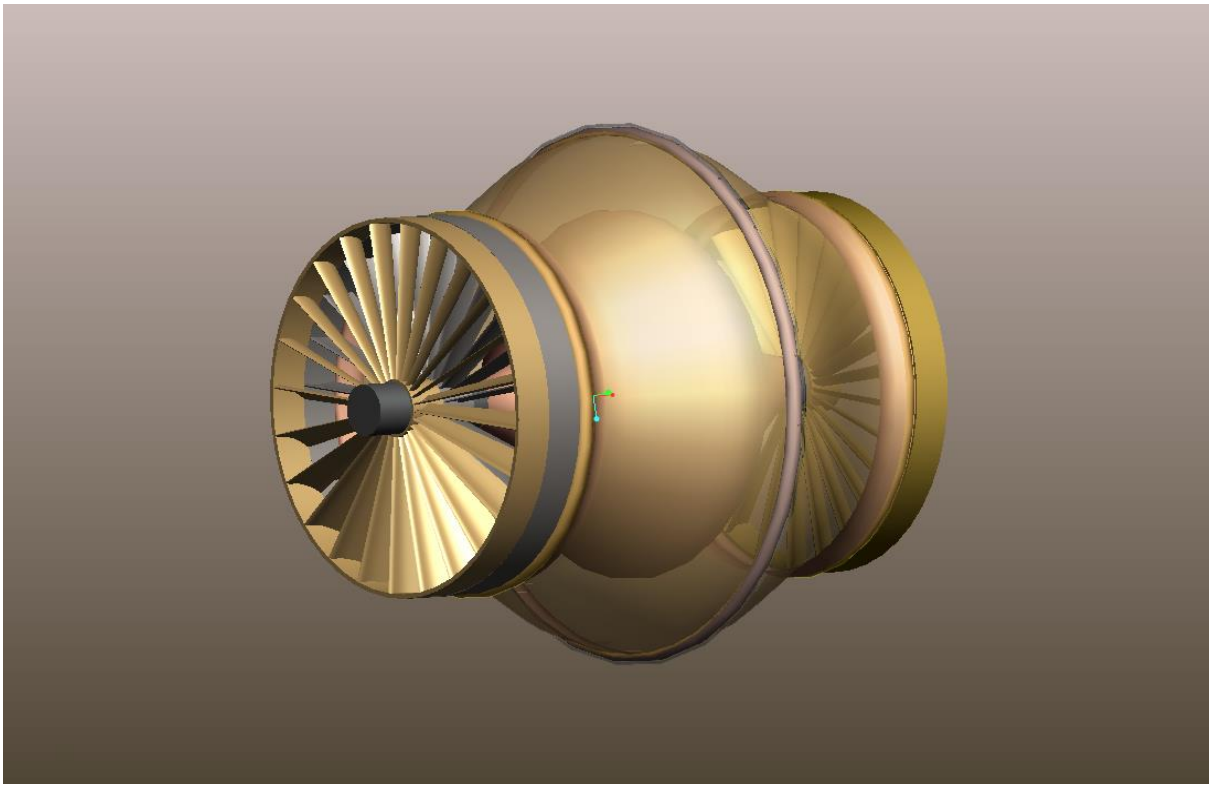

Figure 3-6: Isometric View of the Static Swirl Generator with a Rotating Shell

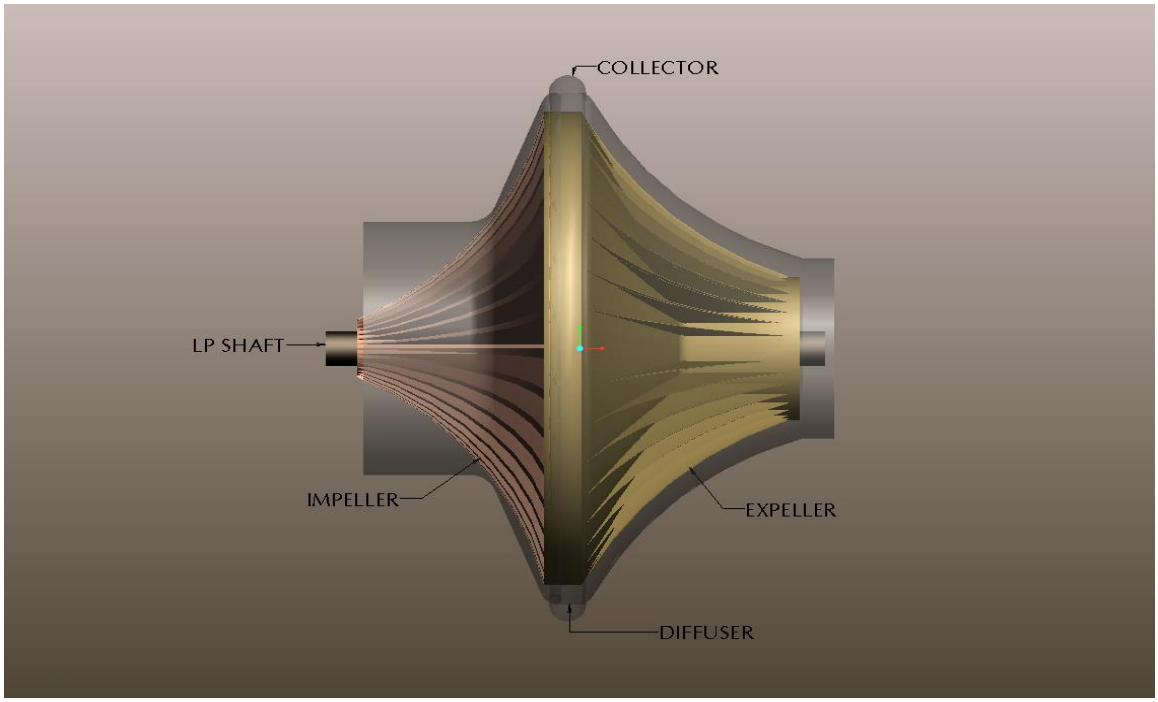

Figure 3-7: Rotating Impeller and Expeller in a Static Shell- -Side View

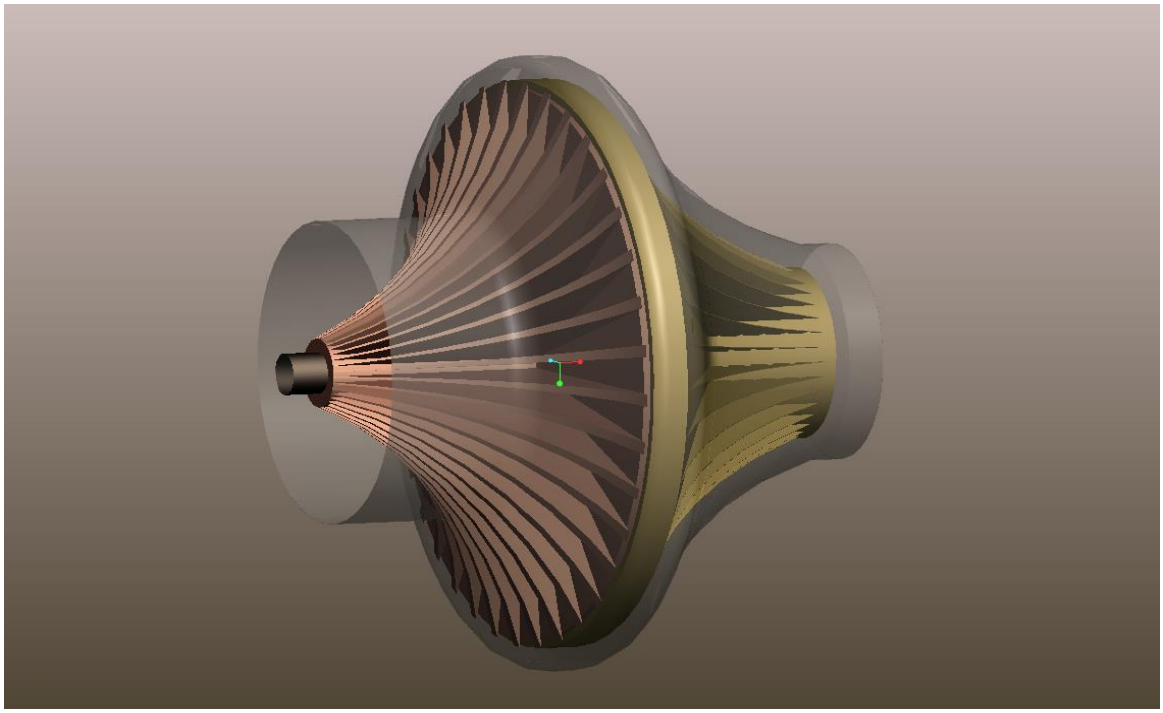

Figure 3-8: Rotating Impeller and Expeller in a Static Shell- -Isometric View

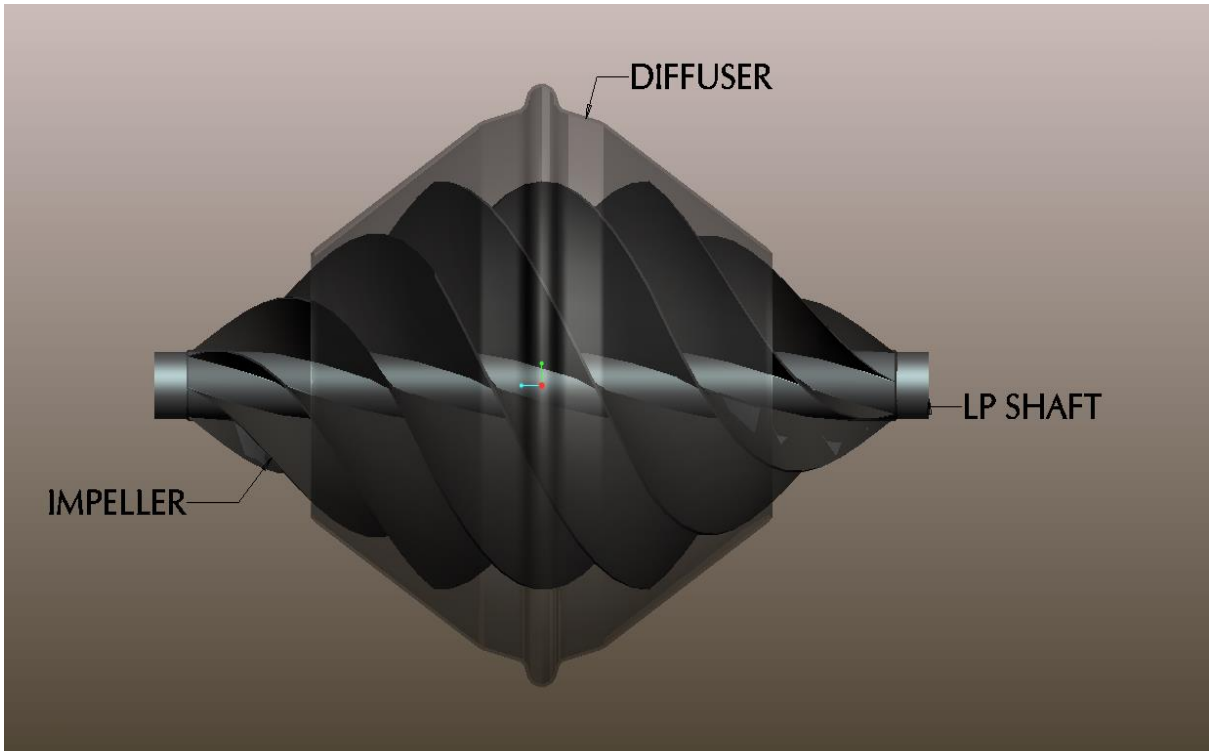

Figure 3-9: Static Impeller in a Static Shell-Side View

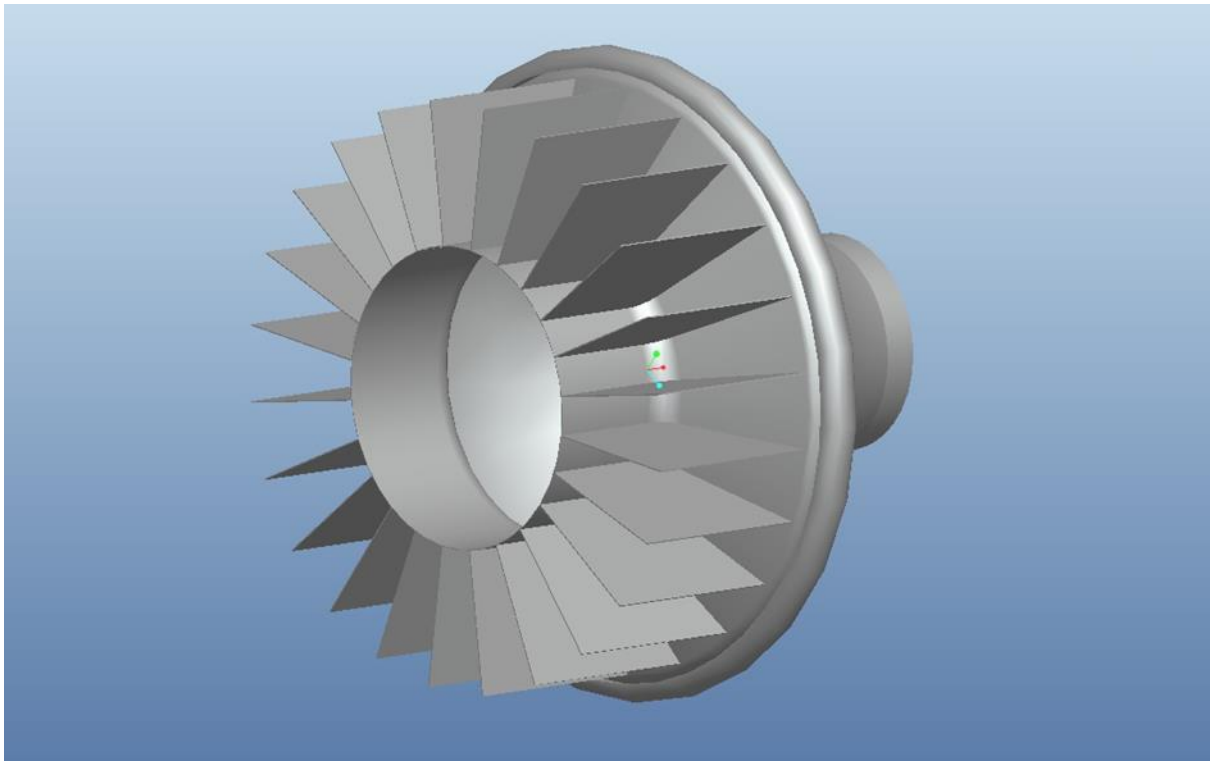

Figure 3-10 : The Static Shell with Cooling Fins Attached

4 THE CENTRIFUGAL WATER EXPELLER

4.1 INTRODUCTION

The centrifugal water expeller is an arrangement of a stator, leading to a rotor turbine that is coupled to a centrifugal vessel shell, and an exhaust stator. Exhaust gas that exits from the low power turbine enters the stator in the axial direction where it undergoes a change of direction. This gas then impinges on the rotor blades and rotates the turbine. The rotation of the turbine results in the rotation of the centrifugal vessel that is coupled to the turbine. Simultaneously, while passing through the stator and the rotor, the exhaust gas undergoes subsequent deflection and a whirl component is induced which allows the gas to rotate at a tangential velocity. Once introduced into the centrifugal vessel, the rotating gas continues to rotate within it due its own inertia and also due to the rotation of the centrifugal vessel and hence is thrown radially outwards at the walls of the vessel. As a result, a contained vortex is formed and the behaviour of the gas within the vessel is governed by the vortex energy equation.(Saravanamuttoo, 2008)

$$\frac{1}{\rho}\frac{dp}{dr} = \frac{C_w^2}{r}$$

Equation 4-1 : The Vortex Energy Equation

Where ρ denotes the density of the exhaust gas, p denotes the static pressure of the gas, r denotes the radius of the vessel and C_w denotes the whirl velocity of the gas. This equation is also known as the radial equilibrium equation.

Pressure varies radially and also as a function of the whirl velocity. Integrating the equation above and applying our limits to the radius of the vessel determines the variation of the static pressure with the whirl velocity. The pressure generated by the rotating vortex acts as a pressure ratio over the existing pressure. The gas continues to rotate and there is a build-up of pressure in the axial direction since the pressure increases after every successive rotation cycle of the gas. After several rotations of the gas at its existing temperature, the static pressure increases until it reaches the saturated vapour pressure of water. Once that pressure is achieved, condensation of the water vapour contained within the exhaust gas is initiated. Condensation occurs and droplets are formed, the latent heat released by water vapour is absorbed by the other two exhaust gases. The condensed water is thrown at the walls of

the vessels where it is collected and drained whereas the other two gases exit the vessel through the stator after absorbing the latent heat of water. This sketches our concept of moisture extraction.

In contrast to a heat exchanger where the entire thermal energy of the exhaust gases is meant to be lost in order to condense water, the losses with this approach are minimized; the energy lost by water is gained by the other gases and they contribute to the thrust with a lost percentage. Selective further cooling of water prevents the entire gas from losing its thermal energy.

4.2 DESIGN SCHEME

The engineering design procedure has been summarised in Figure 4-1 in order to elaborate the design sequence; starting from basic performance data of the standard engine leading to a complete mechanical model of the centrifugal water expeller. The flow path is sequential inclusive of two iterative processes.

The design of the centrifugal system was initiated by determining the prerequisite inlet conditions. As discussed earlier this device is meant to be attached in between the low power turbine station and the core nozzle. The outlet conditions at the low power turbine station are the inlet conditions for the device. Outlet conditions for the low power turbine station (LPT) were determined by the performance analysis of a standard three spool high bypass turbofan engine.

One can only proceed with the complete design if you are able to achieve a temperature below the critical temperature of water at the rotor exit. Secondly the pressure generated in the vessel must be greater than the saturated vapour pressure of water. If these two conditions are not met, then the performance of the engine needs to be optimised as has been indicated in the flow diagram in Figure 4-1.

4.3 DESIGN CALCULATIONS

The inlet conditions for the device are given in Table 4-1 as defined by the exit conditions of the LP turbine of a standard three spool turbofan engine. The outlet conditions at the low power turbine station are input into the stator. Once the inlet conditions are specified, other specifications are also defined. These are given in Table 4-2. Figure 4-2 illustrates the air angles and blade angles specified in Table 4-2 whereas Figure 4-3 illustrates the sectional drawing indicating the dimension of the stator, the rotor and the vessel shell as tabulated in Table 4-2. A quarter section has been shown since the assembly is symmetrical about the horizontal axis. The vessel shell is also symmetrical about the vertical axis with only a stator attached to it at the exit side.

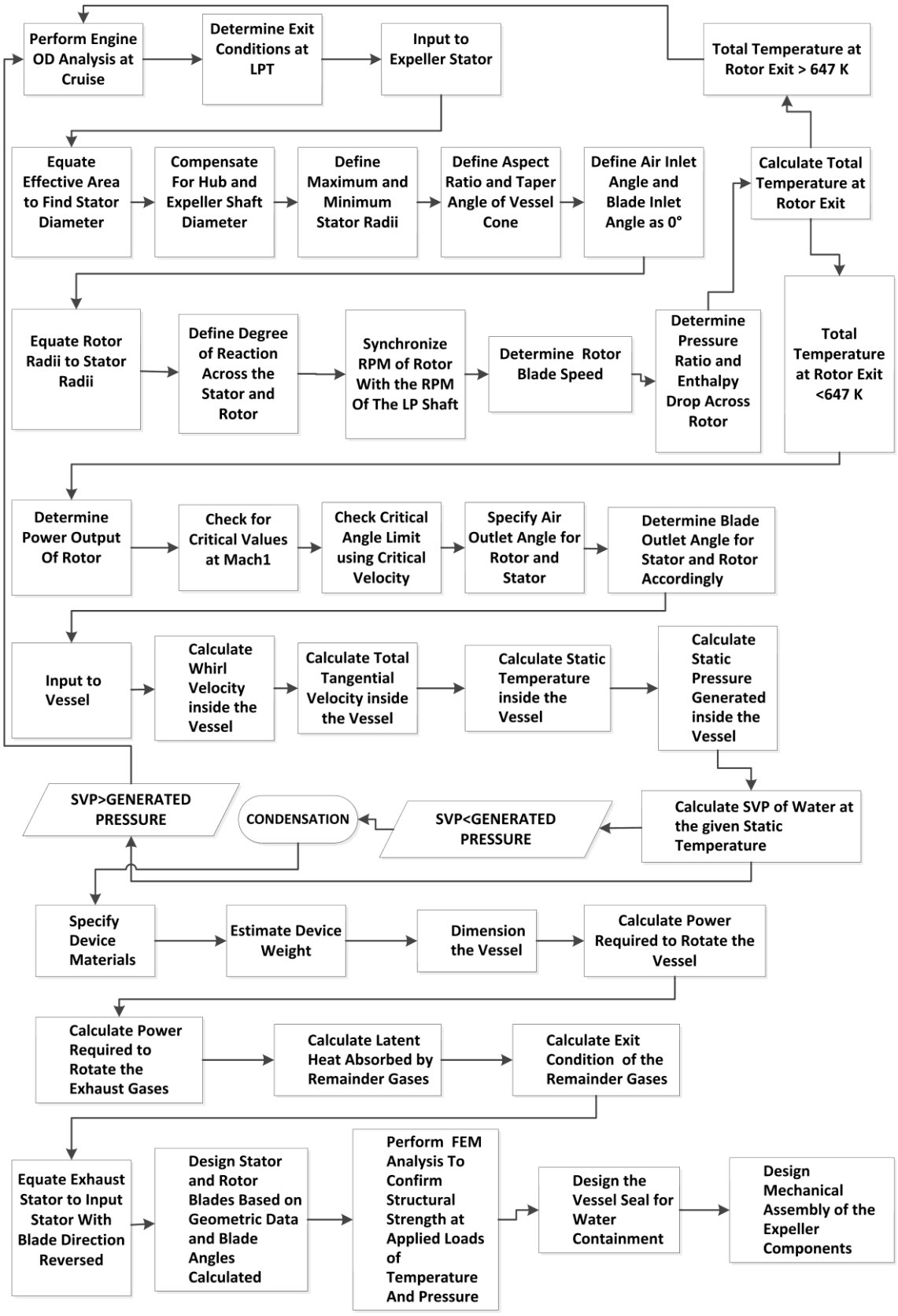

Figure 4-1: The Centrifugal Water Expeller Design Flow Diagram

Parameters	symbol	Value	units
Axial Velocity (LPT exit)	Ca	153	m/sec
Inlet Temperature (LPT exit)	T_{07}	687	°K
Inlet Pressure (LPT exit)	P_{07}	48539	Pa
Inlet effective Area (LPT exit)	A_{07}	3.53	m^2
Specific Heat Capacity	Cp	1148	J/Kg/K
Gas Constant	*R*	287	J/kg/K
Mass Flow Rate	m	57	Kg/sec
Gamma Gas	γ	1.33	
Ambient Pressure	P_{amb}	23835	Pascal
Ambient Temperature	T_{amb}	218	°K
Cruise Altitude	Alt	10670	m

Table 4-1: Inlet Conditions for the Centrifugal Water Expeller Defined from the Outlet Conditions at Engine LPT Station

Design Specifications	symbol	Value	units
Air Inlet Angle	α_1	0	degrees
Blade Inlet Angle	β_1	0	degrees
Turbine Efficiency	ηt	0.9	
Reaction (Stator Impulse)	Λ	1	
Effective Inlet Radius	re (r_{max} - r_{min})	1.0075	m
Effective Inlet Area	Ae	3.53	m^2
Turbine Rotational Speed	N	50	rev/sec

Table 4-2: Design Specifications of the Centrifugal Water Expeller

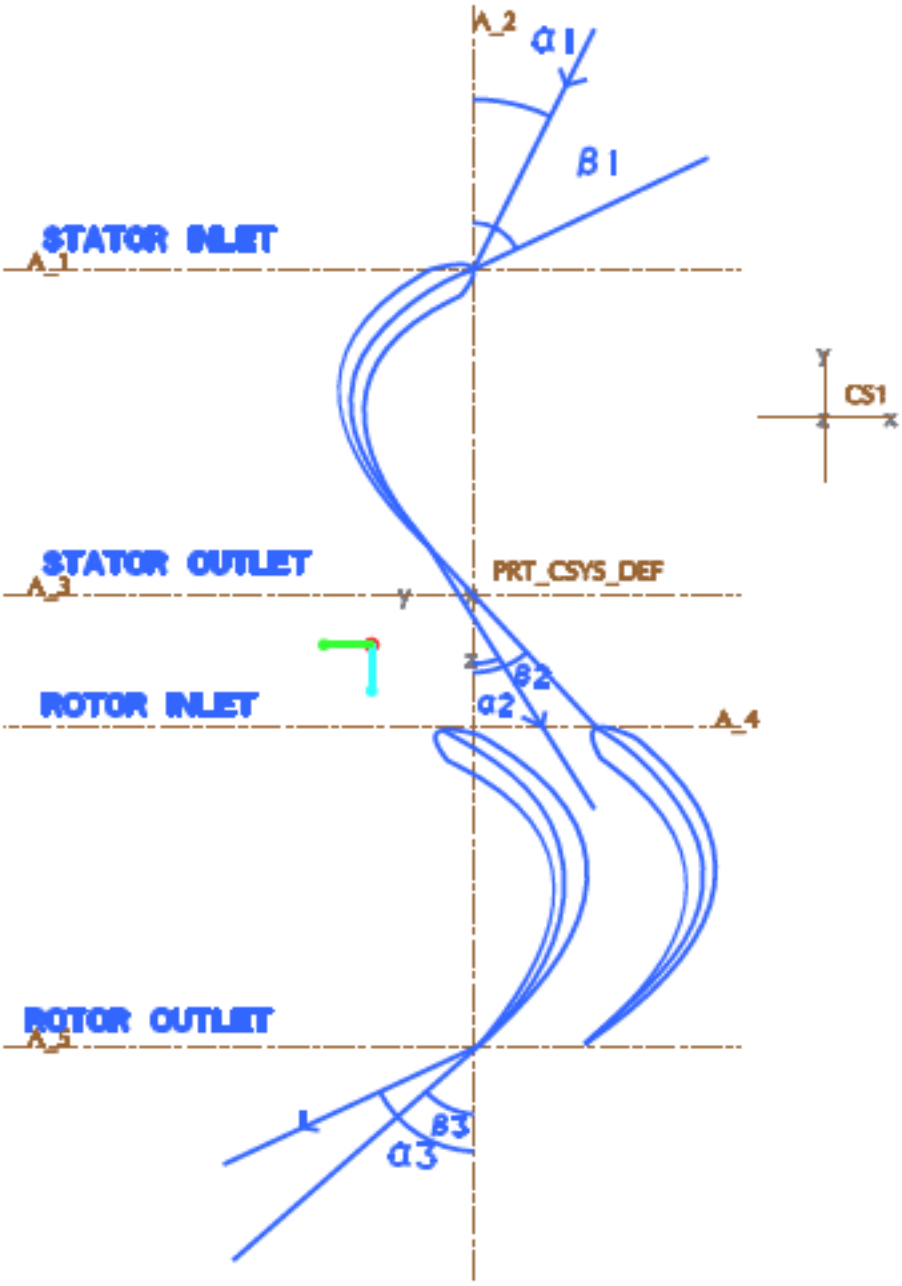

Figure 4-2: Blade Sectional Drawing Indicating Air Angles α and Blade Angles β

As indicated by Figure 4-2 for both the rotor blades and the stator blades, the air angles indicate the angle that the incoming air velocity makes with the vertical section of the blades. Similarly the blade angles indicate the angles that the camber line of the blade profile makes with the vertical. The gas flows from the stator inlet to the stator outlet, and then enters the rotor inlet and exits at the rotor outlet before entering the vessel shell. Although for simplicity of design, the gas is made to enter the stator axially at zero air angle, nevertheless the angles have been exaggerated in the diagram for clarity of illustration. The stator outlet air angle is the rotor inlet air angle.

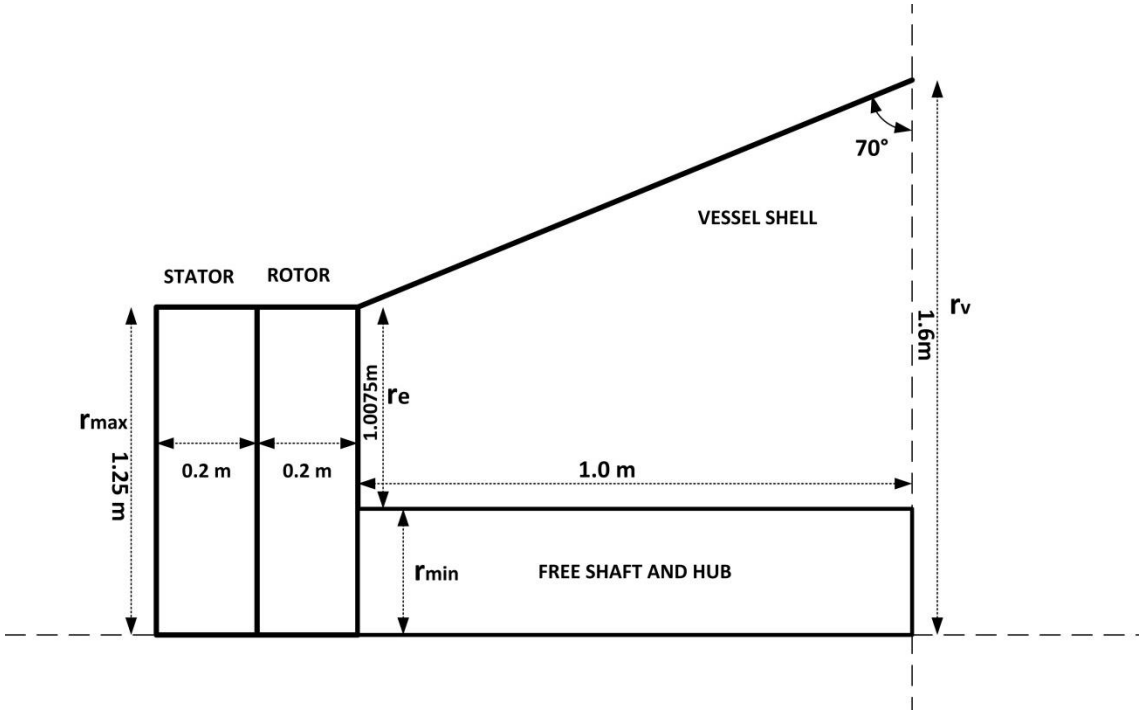

Figure 4-3: Centrifugal Expeller Section Indicating Device Dimensions and Radii

The inlet effective area for the expeller is maintained as that of the low power turbine station so that the inlet velocity and density of the exhaust gas remain unchanged. Compensation is provided for the shaft and hub and hence the effective radius is taken as 1.0075 m for an effective inlet area of 3.53 m^2. The turbine is designed as a stator impulse turbine with a degree of reaction of 1 since no static pressure change is desired across the stator and the entire pressure drop of this single stage turbine occurs through the rotor. The rotational speed of the centrifugal vessel is fixed at 50 revolutions per second in order to synchronize it with the LP shaft speed. The turbine efficiency is assumed to be 0.9 as for a standard turbine. Air inlet angle to the first stator is assumed to be zero and the blade inlet angle is also designed to be zero. The specific heat capacity of the combustion gas is taken as 1148 J/Kg/K. Even though there exists a possibility that a pre-whirl might exist in the exhaust gas exiting from the last turbine nevertheless, the gas is assumed to be axial before entering the stator of the centrifugal expeller. This assumption is made to maintain the simplicity of the initial design. In further analyses, an input whirl can possibly make the stator component redundant and result in weight saving.

Air exiting the LP turbine of the engine possesses a certain amount of kinetic energy that is utilized in jet propulsion for generating thrust. For that very purpose, the last turbine is not designed to expand to ambient and there exists a pressure ratio between the LP outlet total pressure and the ambient static pressure. In a standard configuration, this defines the nozzle pressure ratio.

This pressure ratio is used to drive the turbine rotor that is coupled to the centrifugal shell. As mentioned earlier, no pressure change occurs across the stator. The gas is deflected at a predefined angle which is determined by the stator exit air angle α_2. For the available pressure ratio and the assumed value of turbine efficiency, the turbine output power amounts to 5.7 MWatts. The power is consumed in generating a torque to rotate the centrifugal shell at 50 revolutions per second.

The expansion in the expeller's turbine rotor reduces the total pressure to 25156 Pascal and the temperature to 595 Kelvin. This pressure is nearly equal to the ambient pressure at cruise altitude. Hence the last turbine has now expanded to ambient and the kinetic energy originally utilized for providing thrust is now converted into shaft power. This power will now be used to drive the centrifugal vessel.

This defines the input condition to the rotating vessel. The total temperature drop is 92 Kelvin which is due to the pressure drop across a single stage turbine with no pressure drop in the stator. For the defined value of rotational speed of 50 revolutions per second, the mean blade speed, the temperature drop co-efficient and the flow co-efficient are calculated. This calculation is tabulated in Table 4-3.

Rotor	Performance Data	Symbol	Formula	Value	Units
Rotor	Efficiency	ηt		0.9	
Rotor	Pressure Ratio	Pturb	P_{07}/Pamb	1.85	
Rotor	Temperature Ratio	Tturb	Pturb $^{\gamma-1/\gamma}$	1.16	
Exhaust	Temperature	Tex	T_{07}/Tturb	595	
Rotor	Work Output	Wt	mCpΔTosηt	5.7	MWatts
Stage	Temperature Drop	ΔTos	T_{07}-Tex	92	°K
Exhaust	Pressure	Pex		25156	Pa
Rotational	Speed	N		50	rev/sec
Vessel	Speed	U	2πriN	316.5	m/s
Temperature	Drop Co-efficient	Ψ	$2C_p\Delta T_{os}/U^2$	2.06	
Flow	Co-efficient	φ	Ca/U	0.4781	

Table 4-3: Performance Data for the Centrifugal Expeller Turbine Rotor

Before proceeding further with the design, all data is checked for critical Mach number. For the given input value of temperature and pressure, the critical value of temperature, pressure, density, velocity and area are calculated and performance data is compared against it in order to prevent choking in the turbine stator and rotor and also to prevent the gas from entering the centrifugal shell at a sonic velocity. The data for critical value calculations is tabulated in Table 4-4. The input total temperature and total pressure for calculating the critical values at the stator inlet are the outlet total temperature and total pressure at the low power turbine station. Similarly for calculating the critical values at the rotor outlet, the input total temperature and total pressure are the total temperature and total pressure at the stator outlet. This is the temperature and pressure achieved after the rotor turbine undergoes complete expansion.

STATOR AND ROTOR CHOKING CALCULATIONS	Critical Temperature K Tc 2T07/γ+1	Critical Pressure Pa Pc P07/1.853	Critical Density Kg/m^3 ρc Pc/RTc	Critical Velocity m/s Cc sqrt(γRTc)	Critical Throat Area m^2 Ac m/(Cc*ρc)
STATOR	588.9	26194.8	0.1549	474.67	0.774
ROTOR	510.1	13575.8	0.0927	441.25	1.39

Table 4-4: Calculations for Critical Values for the Design of the Centrifugal Expeller

Moving further with the critical value calculations, the value of the critical stator and rotor gas outlet angles, α_2 and α_3 respectively is calculated. In order to maintain subsonic flow, the proposed gas angles must be less than the critical angles. Critical angles imply values for blade and gas angles that can lead to sonic flow. For the purpose of our design, the gas angles are specified, ensuring that the condition for sub-sonic gas flow is met with, and the blade angles are then designed accordingly. This is because the degree of deflection of the exhaust gas is important for the centrifugal mechanism to take effect. A larger amount of deflection of the gas will result in a higher whirl velocity and subsequently greater centrifugal force will be generated that will eventually create gas compression within the vessel.

The values for the critical gas angles are based on two criteria. One value is based on the critical resultant velocity and the other value is based on the critical whirl velocity. These values are also dependent on the axial velocity (Ca) which is assumed to be constant throughout the flow and is evaluated from the mass flow, the outlet area and the density at the low power turbine station outlet as stated in Table 4-1.

Critical velocity for the stator and rotor is calculated in Table 4-4. The values for both cases of dependence for the stator and rotor gas outlet angles are

tabulated in Table 4-5 and we have to satisfy the lower limit for the maximum value of the critical angle. The calculations are based on the preference of choosing the same gas outlet angle for the rotor and stator for ease of design as well as for achieving maximum deflection which is the prime requirement for the design of the centrifugal expeller.

Critical Angle Calculation	Critical Cos α	Critical Air Angle	Critical Tan α	Critical Whirl Angle
	Ca/Cc	acos(Ca/Cc)	Cc/2Ca	atan(Cc/2Ca)
STATOR α_2	0.3223	71.2 ˚	1.551	57.2 ˚
ROTOR α_3	0.3467	69.7 ˚	1.442	55.3 ˚

Table 4-5: Calculations for Critical Gas Angles for the Design of the Centrifugal Expeller

As can be seen in Table 4-5, different values for the critical gas angles of the stator and rotor from using the resultant velocity and the whirl velocity are calculated. As a design approach, we wish to draw similar deflection from both the stator and the rotor. Hence we need to consider the lower limit which is 55.3˚ in this case. Maintaining a margin of safety and error, the stator and rotor air outlet angles are chosen to be 50˚. This would also provide a whirl deflection of the same degree as the chosen air outlet angle. It is in our prime interest to maximize the degree of deflection in order for the centrifugal mechanism to work efficiently.

Blade Angle Calculations	Air Angle degrees			Blade Angle degrees	Degree of Reaction
symbol	α	**tanα**	**tanβ**	**β**	**Λ**
formula	**acos Ca/Cc**		**tanα-+1/φ**		**Ca/2U(tanβ$_3$-tanβ$_2$)**
STATOR β_2	50	1.192	-0.8995	-42.0	1
ROTOR β_3	50	1.192	3.2835	73.1	1

Table 4-6 : Calculating the Stator and Rotor Blade Outlet Angles from the Respective Air Outlet Angles

The blade angles are calculated by using the specified value of gas angles and working the design backwards. The blade angles depend on the gas angles and the flow co-efficient. This calculation is tabulated in Table 4-6. As can be seen, both α_2 and α_3 are specified for a 50˚deflection and the respective blade angles β_2 and β_3 are calculated. The degree of reaction is also calculated and a value of 1 confirms that this design is a stator impulse turbine and the entire pressure change occurs across the rotor for this single stage turbine. The stator is merely used to deflect the gas which is assumed to be exiting the low power station in the axial direction. However, in case where there exists a known pre-whirl from

the gas exiting the low power turbine station, the stator may not be used and the gas can be introduced directly into the centrifugal vessel through the rotor. The pre-whirl angle would then be the rotor inlet gas angle and the blade angles would then need to be calculated accordingly. The relationship between the gas angles and the blade angles is given by(Saravanamuttoo, 2008)

$$\tan\beta_2 = \tan\alpha_2 - 1/\varphi \text{ (stator)}$$

$$\tan\beta_3 = \tan\alpha_3 + 1/\varphi \text{ (rotor)}$$

The blade angles calculated in Table 4-6 will be used to determine the incidence angle, the camber angle, the stagger angle and the camber length which will be required for the purpose of designing the blade. Blade design shall follow later in this chapter.

4.4 CENTRIFUGAL VESSEL DESIGN CALCULATIONS

The exit whirl velocity component at the inlet to the centrifugal vessel shell is calculated based on the stator and rotor gas outlet angles according to Equation 4-2(Saravanamuttoo, 2008)

$$C_w = C_a(\tan\alpha_2 + tan\alpha_3)$$

Equation 4-2: The Whirl Velocity of the Gas Flow

Where C_w denotes the whirl velocity, C_a denotes the axial velocity and α_2 and α_3 denote the gas outlet angles from the stator and rotor respectively.

The total tangential velocity component of the gas entering the centrifugal vessel equals the sum of the whirl velocity of the gas and the angular velocity of the centrifugal vessel. The whirl velocity is less than the critical velocity of air exiting from the rotor as indicated in Table 4-4 and in Table 4-7.

The rotation of the centrifugal vessel provides a net advantage to the centrifugal expulsion mechanism primarily because it contributes significantly in increasing the tangential component of the rotating gas. For this phenomenon to take effect, the gas and the vessel must rotate in the same direction as is inherent by design. Once the gas enters the rotating centrifugal vessel a vortex is generated that gives rise to a static pressure. This pressure arises because of the centrifugal force that is produced due to the tangential velocity induced by the rotating gas. Hence a large value of tangential velocity is beneficial. If the blades are designed so as to increase the whirl velocity of the gas, there lies an upper limit of sonic value that would prevent the whirl velocity from increasing indefinitely. The velocity is increased otherwise by rotating the vessel and the

blades are designed so as to limit the whirl velocity. A tangential component is added to the velocity without approaching the critical Mach number. In addition to this prime function, the rotating vessel prevents the formation of a boundary layer and eliminates the loss of energy due to the viscous effect.

The dynamic head is calculated at the given velocity which enables us to calculate the static temperature and pressure from the inlet conditions. The pressure generated in the vessel at the given static temperature is then calculated using the vortex energy equation. Integrating the vortex energy Equation 4-1 and applying boundary values results in the following equation which is then used to calculate the static pressure generated inside the vessel due to the tangential velocity.

$$P = e^{C_{t/RT}^2}(r_{max} - r_{min})$$

Where $$r_{max} - r_{min} = r_e$$

Equation 4-3: Solution to the Vortex Energy Equation

Where C_t denotes the total tangential velocity which is the sum of the whirl velocity of the gas and the rotational velocity of the vessel, R is the universal gas constant and T denotes the temperature at which the rotating gas exists. The hub and tip radius of the vessel are denoted by r_{max} and r_{min} respectively. The difference of r_{max} and r_{min} equals r_e which is the effective inlet radius which has a value of 1.0075 m as given in Table 4-2. For a simplified model, the effective inlet radius is maintained at a constant value which provides an averaged out pressure value, even though the pressure could be higher at the widest diameter of the vessel.

Exit	Total	Exit	Exit	Exit	Exit	Condensation
Whirl	Tangential	Dynamic	Static	Static	Static	Pressure
Velocity	Velocity	Head	Temperature	Pressure Ratio	Pressure	Required
Cw	Ct	Td	Ts	PR	Ps	at Ts
$Ca(\tan\alpha_2+\tan\alpha_3)$	Cw+U	$Ct^2/2Cp$	Tex-Td	$\exp(Ct^2/RTex)$	Pex*PR	Preq
m/s	m/s	K	K		Atm	Atm
364	684	203	392	15	3.89	2.5

Table 4-7: Calculating the Pressure Generated by the Rotating Gas

According to Table 4-7 the whirl velocity of the gas entering the centrifugal vessel from the rotor is calculated from the axial velocity and the stator and the rotor air outlet angles as indicated in Equation 4-2. This whirl velocity is relative to the rotating vessel. The rotational blade speed of the vessel as calculated in Table 4-3 is added to this velocity to obtain the total tangential component of the

rotating gas. This tangential velocity is then used in Equation 4-3 to calculate the pressure ratio generated by the rotating gas. This pressure ratio acts on the initial exhaust static pressure to give the final static pressure of the gas. The dynamic head is also calculated using the tangential velocity of the gas and the static temperature of the gas is thus determined in Table 4-7. At the exit static temperature calculated, the saturated vapour pressure is the static pressure required for condensation as indicated in Table 4-7.

The static pressure generated by the centrifugal force creates a pressure ratio of 15 and increases the static pressure of the existing gas from 0.25156 Atm to 3.89 Atm through the centrifugal force generated during rotation. The static pressure required for condensation at this temperature is 2.5 Atm, as has been determined through the Clausius-Clapeyron equation and tabulated in Table 8-4 in section 8.1.3. This value provides adequate margin for losses since the pressure generated is greater than the pressure required for condensation.

The pressure increases at every successive rotation of the gas and the gas rotates and moves in the forward direction in the form of a vortex and continues to build up pressure. Eventually, the condensation pressure is achieved at the widest diameter of the vessel that is supported with the minimum volume. Once this pressure is attained in the vessel, the water vapour present in the exhaust gas will undergo a phase change at that temperature and condense and coalesce to form water droplets. The remaining exhaust gases, nitrogen and carbon-di-oxide will maintain their gaseous state since the temperature of the exhaust gas is above the critical temperature of these two gases. The latent heat released by water during condensation will be absorbed by the other two gases. Condensation nuclei such as soot and dust particles present in the exhaust gases will aid the phenomenon of condensation. The water condensed will be thrown outwards at the wall of the vessel and drained through a collection mechanism. The remaining gases shall exit through the expanding cone and escape into the atmosphere.

Maximum static pressure is generated at the widest diameter at the centre of the vessel. This region has the minimum volume because the inner core also has its widest diameter at the centre as is evident from Figure 3-4 and Figure 3-5. Hence maximum compression of the gas occurs at this position and initiates condensation. Once the phase change takes place and the water condensed is drained out at the periphery, the remaining two gases continue to rotate and move forward through the vessel and experience a reduction in pressure and density as the volume of the vessel expands. This increase in volume restores the gases to their initial state. Assuming that the gases have returned to their inlet state with a 2.25 % reduction in mass flow due to the condensation of water; they then pass through the exit stator which has the

same dimensions as the inlet stator. The exit stator deflects the whirl of the gases into axial flow and the gases can then exit into the atmosphere through the standard core exhaust nozzle.

The water formed through this process shall exist as a liquid at a temperature of 392 K and a pressure of 2.5 Atm. This water shall need to be removed from the centrifugal vessel at the same temperature and static pressure in order to maintain the condensed phase. Once transported out of the engine under pressure, it can be cooled to a temperature below 373 K by pumping it through the exposed surfaces of the aircraft, e.g. the leading edges of the wings or it can be used for cabin heating. The temperature of the water should be lowered to between 274 K and 372 K so that it remains as liquid water when pressurized to 1 atmosphere pressure. In this case, it shall remain as liquid water at sea level. However, if this water is meant to be released at an altitude as a liquid then it would need to be cooled further according to the pressure that it is meant to be released at in order for it to exist as a liquid at a reduced pressure. It is far more convenient to cool the water once it has been separated from the other gases because the bulk of the gas is removed and only 2.25%of the mass flow remains.

4.5 POWER CALCULATIONS FOR THE CENTRIFUGAL WATER EXPELLER

The power requirements of the condensation device need to be calculated in order to determine the compromise of the core exhaust thrust due to the installation of the centrifugal water expeller on the engine.

The water expeller includes a rotor which is driven by the exhaust gases exiting the LP turbine. This rotor generates sufficient power to rotate the device and the exhaust gases subsequently rotate within it. Owing to this rotation, pressure is generated inside the expeller vessel. This pressure enables the water vapor content of the core gases to achieve condensation. The power required to achieve the condensation pressure through the rotation of the vessel is calculated in order to determine whether this requirement is met by the power generated by the rotor. In addition to that, the power loss associated with the condensation of water is also determined as this result in a 2.25% reduction in the core mass flow. This loss is compensated by the remaining non-condensable exhaust gases N_2 and CO_2. The latent heat released during the condensation of water is absorbed by these two gases for a gain in kinetic energy. The net power loss after this compensation is thus evaluated.

The sonic velocity limit is applied to determine the maximum amount of latent heat absorbed by the gases in order to achieve sonic exit velocity of a choked

nozzle. This also enables us to determine the gas conditions at the vessel exit which is essential for size and dimensioning of the device.

In a similar manner, the thrust loss of the core gases due to the condensation of water and the resulting reduction in mass flow and velocity is also calculated. Hence all possible losses are identified and evaluated for the viability and validation of the design of the centrifugal water expeller.

4.5.1 INPUT DATA

The basic parameters essential for the calculations discussed above are given in Table 4-8. They are based on cruise flight at Mach 0.82 and an altitude of 10670 meters.

Input Parameters	**Value**
Mass Flow Rate of the Core Exhaust Gases	57kg/s
Mass Flow Rate of Condensed Water	1.34 kg/s
Specific Heat Capacity of the Core Exhaust Gases	1148J/Kg/K
Specific Heat Capacity of N_2 and CO_2 only	1050J/Kg/K
Ambient Pressure	23835 Pa
Ambient Temperature	218 K
Total Temperature Input to the Vessel	687 K
Total Pressure Input to the Vessel	48539 Pa
Angular Velocity of the Rotating Vessel	50 rev/s
Effective Radius of the Rotating Vessel	1.0075 m
Inlet Radius of the Rotating Vessel	1.25 m
Emission Index of Water	1.25

Table 4-8: Input Data for Power Calculations

4.5.2 DESIGN PARAMETERS

The design parameters computed previously that are required for the power calculations are given in Table 4-9 . They are based on cruise flight at Mach 0.82 and an altitude of 10670 meters.

OUTPUT PARAMETERS	VALUE
Rotor Work Output	5.7 MWatts
Total Temperature at Rotor Exit	595 K
Whirl Velocity at Rotor Exit	364.760 m/s
Tip Velocity at Rotor Exit at 50 rps	320 m/s
Total Tangential Velocity at Rotor Exit	684.760
Static Temperature at Rotor Exit	392 K
Design Condensation Pressure at 392 K	0.25 MPa
Pressure Ratio of the Vessel	15
Pressure of the Gas through Rotation	0.39 MPa
Fuel Flow Rate for Cruise Flight	1.0715 Kg/s
Mass Fraction of Water in the Exhaust Gas	0.225

Table 4-9: Design Specifications for Power Calculations

4.5.3 POWER CALCULATIONS

The power required to generate condensation pressure for a given mass flow is given by Equation 4-4 (Saravanamuttoo, 2008)

$$\boldsymbol{P_{cond} = mUC_a(tan\,\alpha_2 - tan\alpha_1)}$$

Equation 4-4: The Condensation Pressure

The power required to rotate the vessel at the same speed is given by Equation 4-5. The vessel has been approximated as two rotating solid cylinder with variable radius starting with the minimum radius of the vessel and ending at the maximum radius of the vessel. Each cone of the vessel shell is approximated as a single cylinder.

$$\boldsymbol{P_{vessel} = \frac{1}{2} m_v N^2 (r_v^2 - r_{max}^2)}$$

Equation 4-5: The Power Required for Rotating the Vessel

Considering the topology of the vessel shell, it can be divided into an expanding cone and a contracting cone as has been explained in chapter 3. The polar moment of inertia of two solid cylinders has been taken into account to calculate the torque and power required to rotate the vessel. It is possible to carry out a

more detailed calculation of the same by calculating the polar moment of inertia of the free shaft, the inner core and the outer shell of the vessel separately. However the approximation used above is sufficient to determine the overall power requirement of the system in order to ensure that that power required to drive the vessel is met by the power generated by the rotor. The total power required will be a sum of the power required to rotate the vessel and the gas contained within.

symbol	parameter	Value
C_a	Axial Velocity Of The Rotating Gas	153 m/s
m	Mass Flow Of The Rotating Gas	57 kg/s
n_w	Mass Fraction of Water in the Exhaust Gas	0.0225
U	Speed Of The Rotating Vessel	314 m/s
α_1	Air Inlet Angle at the Stator	0 degrees
α_2	Air Inlet Angle at the Rotor	50 degrees
N	Angular Velocity of the Rotating Vessel	50 rps
m_v	Mass of the Rotating Vessel	2000 kg
r_v	Radius at Vessel's Maximum Diameter	1.6 m
r_{max}	Radius at Vessel's Minimum Diameter	1.25 m

Table 4-10: The Condensation Pressure Parameters

According to the power equation, the power required to rotate the gas at 50 rps is determined to be 3.2 MW and the power required to rotate the vessel is 2.4 MW. This calculation assumes that power applied to rotate the vessel imparts energy to the rotating gas which in turn generates the condensation pressure. The total power required for generating the pressure (3.2MW+2.4 MW) is almost equal to the power generated by the rotor turbine of the water expeller (5.7 MW).Assuming that the bypass stream surrounding the centrifugal vessel will cause some hindrance to the rotation; the extra amount of power of 0.1 MW will be used to overcome this interference. It is also possible that any residual

power would be transferred to the gas due to the rotation of the vessel in the form of a pressure force so that the gases exit with an additional energy and hence thrust losses are minimized. This phenomenon is inherent by design.

4.5.4 LATENT HEAT COMPENSATION

The Latent Heat capacity of water Q_l is given by Equation 4-6.

$$\boldsymbol{Q_l = mn_w L_v}$$

Equation 4-6: Latent Heat Capacity of Water

$\boldsymbol{Lv}$ denotes the latent heat of condensation which holds a value of 2.23 MJ/Kg at the design static temperature of 392 K. The latent heat released by water according to the equation above is calculated to be 2.99 MW. This latent energy is absorbed by N_2 and CO_2. Nineteen percent of this latent heat is absorbed in the translational mode by the gases and provides a gain in kinetic energy. Hence, the additional power $\boldsymbol{P_l}$ gained by N_2 and CO_2 after absorbing the latent heat of water also equates to 567 KW. The rise in the total temperature of CO_2 and N_2 can thus be calculated by Equation 4-7.

$$\boldsymbol{P_l = (1 - n_w) m C_p \Delta T}$$

Equation 4-7: Latent Power Equation

Where, ΔT denotes the rise in total temperature of N_2 and CO_2. For a latent power value of 567 KW, the rise in temperature is calculated to be 9K. This enables us to calculate the final total temperature (T_f) and the final velocity (V_f) of CO_2 and N_2 at the vessel exit. Computed values are given in Table 4-12.

4.5.5 THE EXHAUST GASES AFTER CONDENSATION

The conditions of the exhaust gas after condensation are given in Table 4-11.

Parameter	**Units**	**Value**
Total Temperature	Kelvin	604
Total Pressure	Pascal	250000
Density	Kg/m^3	2.0
Axial Velocity	m/s	153

Table 4-11 : Conditions of the Non-condensable Exhaust Gases after Condensation

4.5.6 GAS CONDITIONS AT THE CORE NOZZLE

For the given mass flow, the specification of the nozzle exit temperature and the exit velocity need to be defined. In order to obtain maximum thrust within a given constraint of mass flow, the flow is made to exit at a velocity close to Mach 1 for a choked nozzle. The calculations above determine the condition and state of the gases exiting the vessel through an exhaust nozzle as given in Table 4-12.

Symbol	Parameter	Formula	Value
T_t	Total Temperature at Rotor Exit		595 K
T_s	Static Temperature Vessel Exit	$T_f - \frac{C_a^2}{2C_p}$	585
T_f	Final Stagnation Temperature at the Vessel Exit	$T_t + \Delta T$	604 K
T_c	Exhaust Gas Total Temperature at the Vessel Exit for Choked Nozzle	$T_c = \frac{2}{(\gamma + 1)} T_s$	509 K
V_c	Sonic Velocity at the Vessel Exit	$\sqrt{\gamma R T_c}$	441m/s
M_g	Exhaust Gas Mach number at the Vessel Exit (Choked Nozzle)		1

Table 4-12: Conditions at the Vessel Exit

4.5.7 THRUST LOSS COMPENSATION

The Thrust ($\boldsymbol{F_l}$) of the core exhaust is given by Equation 4-8.

$$\boldsymbol{F_l = m(C_j - C_a)}$$

Equation 4-8: Core Nozzle Thrust

m	Mass Flow of the Core Gases	57Kg/s
C_j	Initial Core Nozzle Exit Velocity at Mach 1	477 m/s
C_a	Aircraft Velocity at Mach 0.82	242 m/s

Table 4-13: Thrust Loss Compensation

The total thrust $\boldsymbol{F_l}$ of the core nozzle is calculated as 13 KN. The thrust compensation $\boldsymbol{Fc}$ due to the absorption of the latent power of water is given by Equation 4-9

$$\boldsymbol{F_c = (1 - n_w)m(V_c - C_a)}$$

Equation 4-9: Thrust Loss Compensation

The thrust compensation equals 11 KN. Hence the net thrust loss equals

Thrust Loss= Total Thrust – Thrust Compensation

This is calculated to be 2 KN. For a Cruise Thrust of 65 KN, the thrust loss is only 3 % of the overall thrust.

The rotor turbine generates 5.7 MW. The power required to drive the rotating vessel and the gas is determined to be 5.6 MW which make the water expeller a self-sustaining system. Pressure is generated inside the vessel due the rotation of the gas and the vessel.

The power compensation through latent heat for a gain in kinetic energy is calculated to be 567 KW.We need to apply the sonic velocity limit, assuming that the remaining gases shall exit at Mach 1.The maximum velocity at Mach 1equals 441 m/s at a static temperature of 509 K . The exit temperature of the gas at this velocity is 595 K. The latent power absorbed by N_2 and CO_2 contributes to a gain in exhaust gas temperature of 9K and this is the energy that is harnessed out of the exhaust water vapour content. As calculated above, the thrust loss is only 3 % of the overall thrust. Essentially, this is a self-regulating system whereby the residual energy of the gas is converted into a pressure force to condense and extract water and a fraction of the wasted thermal energy of the water vapor is recovered through inter-gaseous energy transfer.

The net energy balance indicates a thrust loss of 2KN in the process of energy conversion and a 2.25 percent reduction in the core mass flow. This equates to a 3 % loss in the overall thrust during cruise. This happens to be the upper limit of loss as it assumes that the remaining gases do not exit with residual pressure.

4.6 BLADE DESIGN

The blades for the stator and rotor are based on a standard NACA T6 base profile. X and Y dimensions of the blade profile are given according to the standard percentage of the camber line. The base profile is symmetric about the centreline with a thickness to chord ratio of 0.1. The leading edge radius is 12 percent of the thickness whereas the trailing edge radius is 6 percent of

thickness. A standard base profile with an assumed span is shown in Figure 4-4. This profile is scaled for a camber line length of 100 percent. Once the base profile is selected, the camber length for the rotor and stator need to be determined according to the chord length and blade angles.

The Abscissa and ordinate dimensions of the T6 base profile are sketched in Figure 4-5 as a percentage of the symmetric centre line which is also the camber line. This geometry is scaled for a relative camber line length of 100. A symmetric profile is used where the camber length and the chord length are the same and hence the profile is initially constructed at zero camber. Once the camber length is determined, the chord of the base profile is then scaled up to that camber length to provide the exact size of the aerofoil section. Since all co-ordinates of the profile section are drawn as a percentage of the camber length, the entire profile is scaled once the camber length is changed and the aspect ratio of the blade section is maintained. This section is then given the third dimension of blade span or height. The profile is then bent around the camber line according to the camber angle calculated.

Figure 4-4: The Standard NACA T6 Base Profile In a Perspective View

With reference to the critical value calculations for area in Table 4-4, blade dimensions are determined in Table 4-14. Initially, the blade height is determined as a ratio of the area to the circumference. The chord length is then taken as a third of the blade height according to the conventional design rule. The optimum pitch chord ratio is determined from an empirical relationship based on the inlet and outlet air and blade angles that have been determined in Table 4-6.This provides us with the pitch length and the number of blades required for the stator and the rotor.

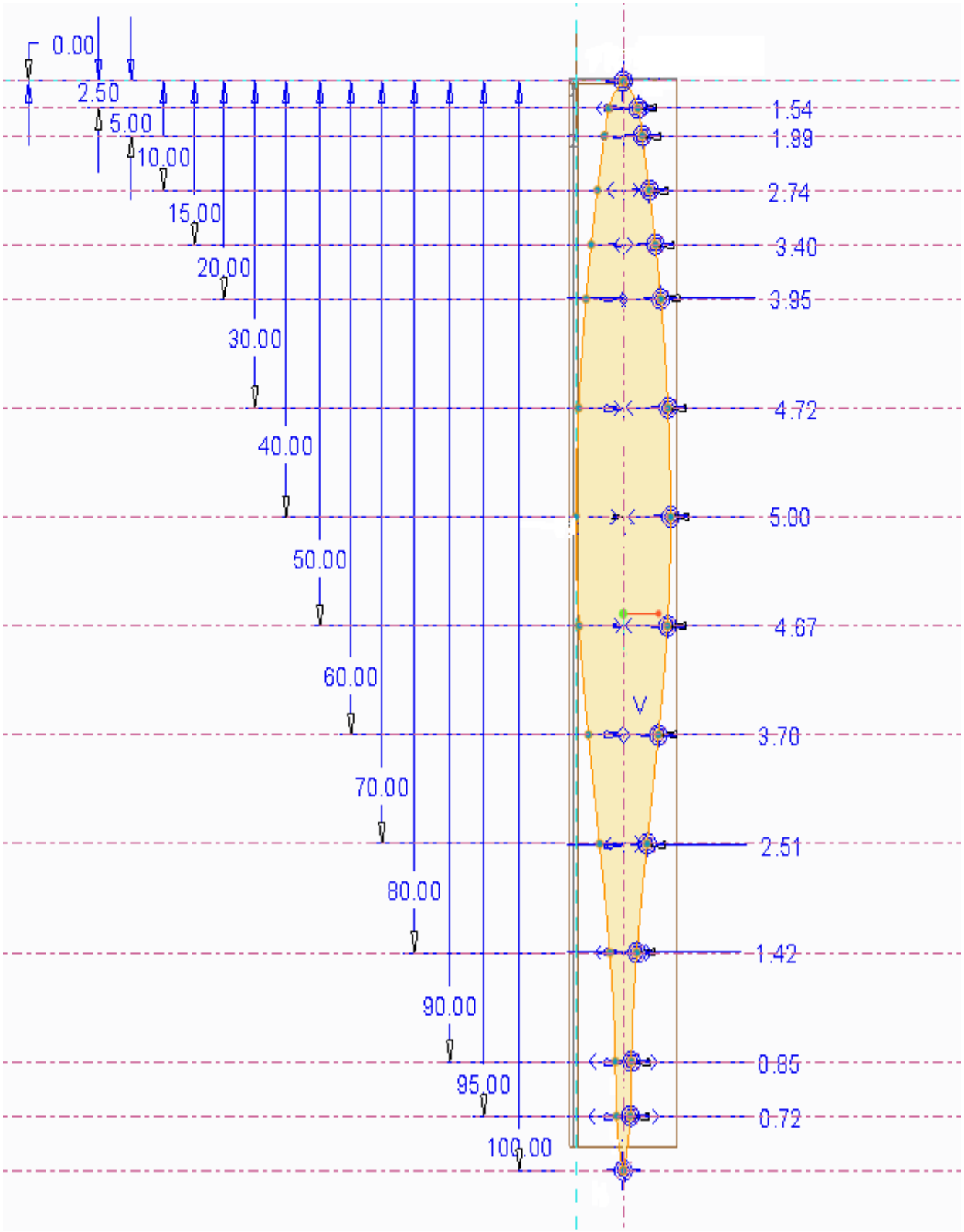

Figure 4-5: Abscissa and Ordinate Dimensions of the Blade Profile as a Ratio of Camber Length

	Sectional Throat Area	Sectional Radius	Blade Height	Chord Length	Pitch/Chord Ratio	Pitch Length	Number of Blades
	m^2	m	m	m		m	
BLADE	Ac	rc	hc	c	s/c	s	n
DESIGN	m/(Cc*ρc)	sqrt(Ac/π)	Ac/2πrc)	hc/3	s/c	s/c*c	2πrc/s
STATOR	1.658	0.7265	0.3633	0.1211	0.95	0.1150	39.7
ROTOR	2.981	0.9741	0.4871	0.1624	0.8	0.1299	47.1

Table 4-14: Calculating the Blade Dimensions for the Stator and Rotor

The pre-determined chord line is drawn at a stagger angle (δ_1 for stator and δ_2 for rotor) from the axial direction (vertical line) such that it cuts two horizontal lines. A straight line is then drawn at the blade inlet angle (β_1 for stator and β_2 for rotor) at the starting point of the chord line such that it cuts the horizontal line at the top of the chord. Another straight line is drawn at the ending point of the chord line at the blade outlet angle (β_2 for stator and β_3 for rotor) from the axial (vertical) direction. A circular arc is then constructed tangential to these two lines while maintaining the chord. The length of the circular arc is the camber length along which the aerofoil section is scaled. The camber length is geometrically measured and given in Table 4-15.The geometry construction for the rotor and stator camber length is given in Figure 4-6 and Figure 4-7.

Stator Blade outlet Angle degrees	Rotor Blade outlet Angle degrees	Stator Camber Angle degrees	Rotor Camber Angle degrees	Stator Stagger Angle degrees	Rotor Stagger Angle degrees	Stator Chord Length meters	Rotor Chord Length meters	Stator Camber Length meters	Rotor Camber Length meters
β2	β3	θ1	θ2	δ1	δ2	Cs	Cr	Ls	Lr
atan(tanα-1/ϕ)	atan(tanα+1/ϕ)	θ1=β1-β2	θ2=β2-β3	β1-θ1/2	β2-θ2/2				
-41.97	73.05	41.97	-115.02	20.985	-99.48	121	160	157	216

Table 4-15: Determining the Camber Length from Blade Geometry

The blade height is determined in Table 4-14 and needs to be adequately compensated for hub radius. A similar blade height is chosen for the stator and the rotor in this case since the stator is deflecting the gas only while other properties of the gas do not change. The blades are then bent according to the respective camber angle to finalize the blade design. As can be seen in Table 4-15 the stator and rotor camber are opposite in direction to each other. The three dimensional blade profiles for the stator and the rotor are illustrated in Figure 4-8 and Figure 4-9 . An odd number of blades will be chosen for the stator and the rotor in order to avoid vibrating resonant frequencies.

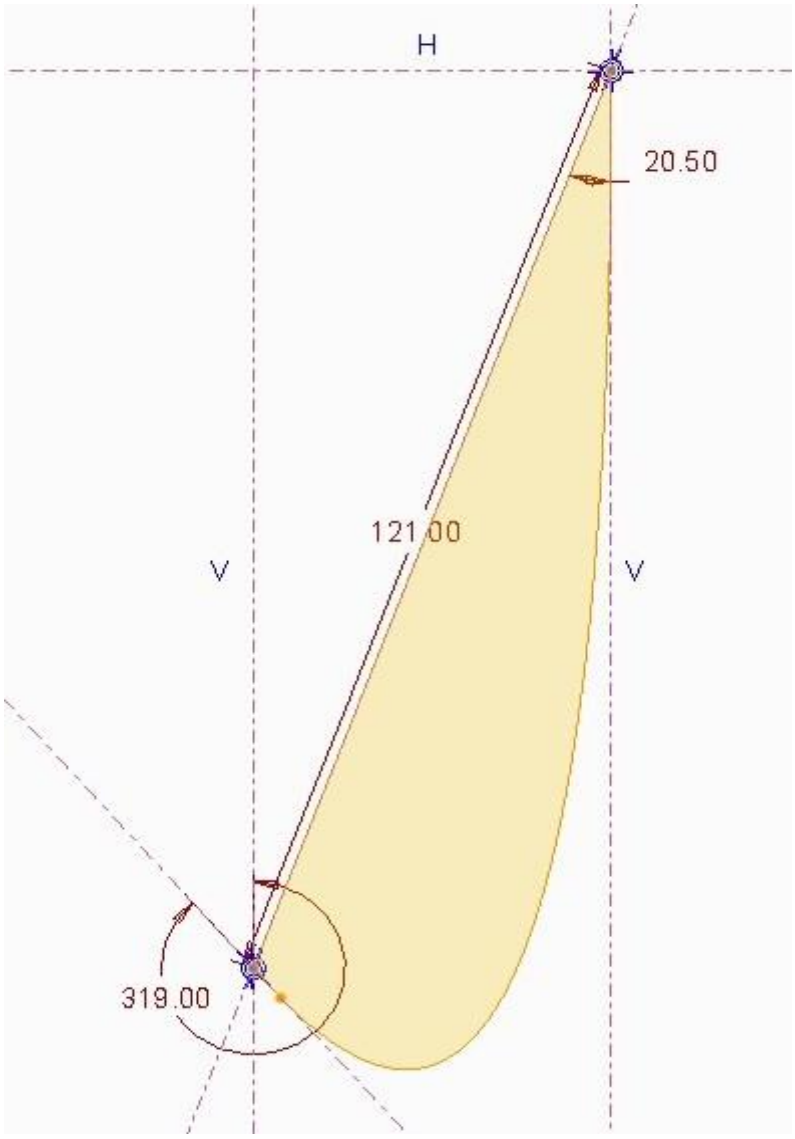

Figure 4-6: Calculating the Camber Length of the Stator Blade

According to Figure 4-6 and Table 4-15, the chord line of 121 mm is drawn at a stagger angle of 20.5˚ from the axial direction. Another vertical line is drawn at the blade inlet angle β_1 of 0˚ from the axial direction. The third line is constructed at the lower end at a blade outlet angle β_2 of -41˚ or 319˚ (360-41) from the axial direction. The camber line is then constructed as an arc which is tangent to these two lines and is cut by a chord of length 121mm. The length of the camber line is then measured geometrically to be 157 mm. Since the blade inlet angle is zero for this blade and the gas is approaching the blade at zero incidence, therefore it is slightly cambered and there is a minor difference between the chord length and the camber length. All angles are measured from the axial direction. This stator blade will deflect the gas entering axially by 41˚ and this angle will then be the blade inlet angle for the rotor blade.

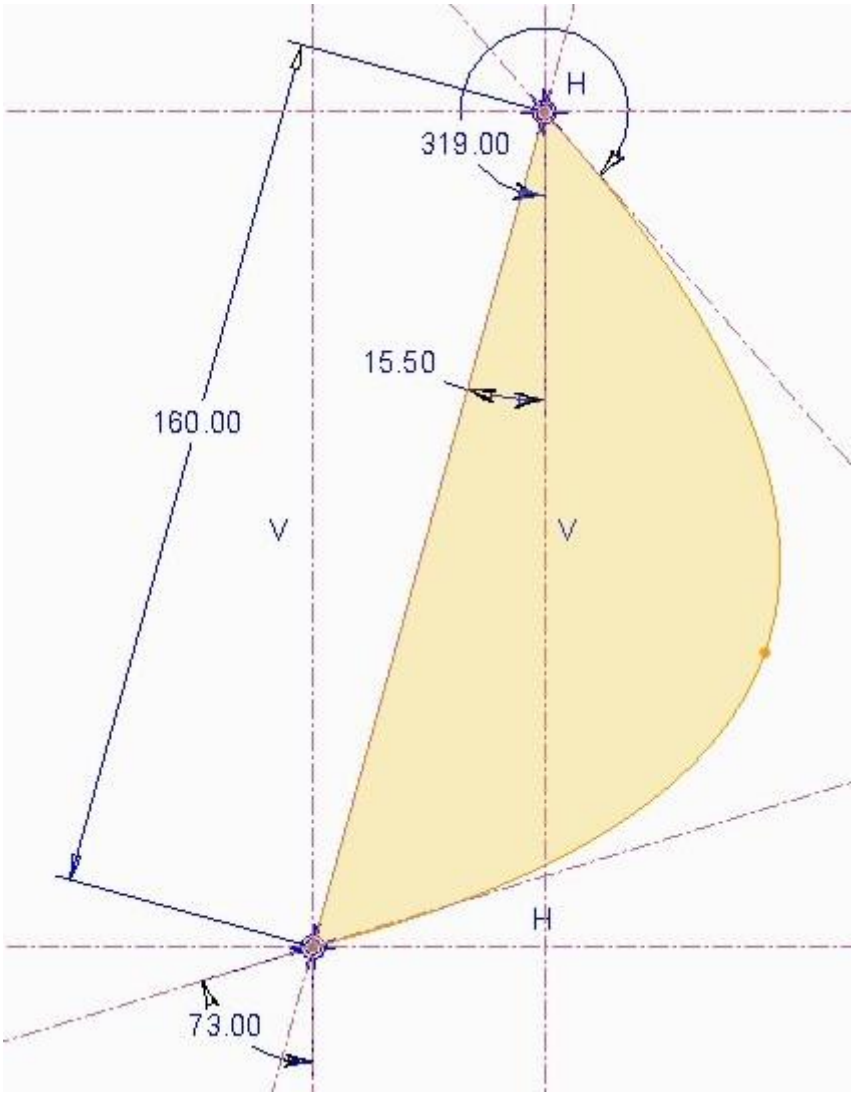

Figure 4-7: Calculating the Camber Length of the Rotor Blade

According to Figure 4-7 and Table 4-15, the chord line of 160 mm is drawn at a stagger angle of 15.5˚ from the axial direction. Another vertical line is drawn at the blade inlet angle β_2 of 319˚ from the axial direction. The third line is constructed at the lower end at a blade outlet angle β_3 of 73˚ from the axial direction. The camber line is then constructed as an arc which is tangent to these two lines and is cut by a chord of length 160 mm. The length of the camber line is measured geometrically to be 216 mm. Since the rotor blade inlet angle is equal to the stator blade outlet angle therefore this blade is considerably cambered and there is a major difference between the chord length and the camber length. All angles are measured from the axial direction. This rotor blade will deflect the gas entering the rotor by 31˚ which is the sum of the rotor blade inlet and outlet angle (β_{2+} β_3).

Figure 4-8 : The Stator Blade

Figure 4-9 : The Rotor Blade

4.7 STRUCTURAL ANALYSIS OF THE CENTRIFUGAL VESSEL

The structural analysis of the centrifugal vessel is performed to determine whether the vessel is able to withstand the centrifugal pressure force that is generated by the rotating gas. Since a high temperature and pressure is involved in this process it is essential to test the design of the vessel for structural strength.

A preliminary investigation is carried out in order to check the structural viability of this design by employing the finite element method. The component is modelled in the software PTC Creo™ and the static analysis utilizes its application specific to structural analysis. A linear elastic analysis is executed in PTC Creo Simulate™.

The Aluminium alloy Al6061 is specified as the design material for all its benefits of low density, elasticity and good thermal conductivity. Aluminium is also proven to aid condensation. The analysis is set up at the design temperature of 500 K in order to allow for a margin of safety. Stress and strain calculations are performed using the small strain analysis method.

The model is meshed into solid elements and the loads and constraints are then applied on the model surfaces. Tetrahedral mesh elements are used for the calculation. Stress distribution does not vary significantly through the vessel therefore the mesh is maintained at a relatively uniform size throughout the vessel. The volume mesh of the centrifugal vessel is illustrated in Figure 4-10.

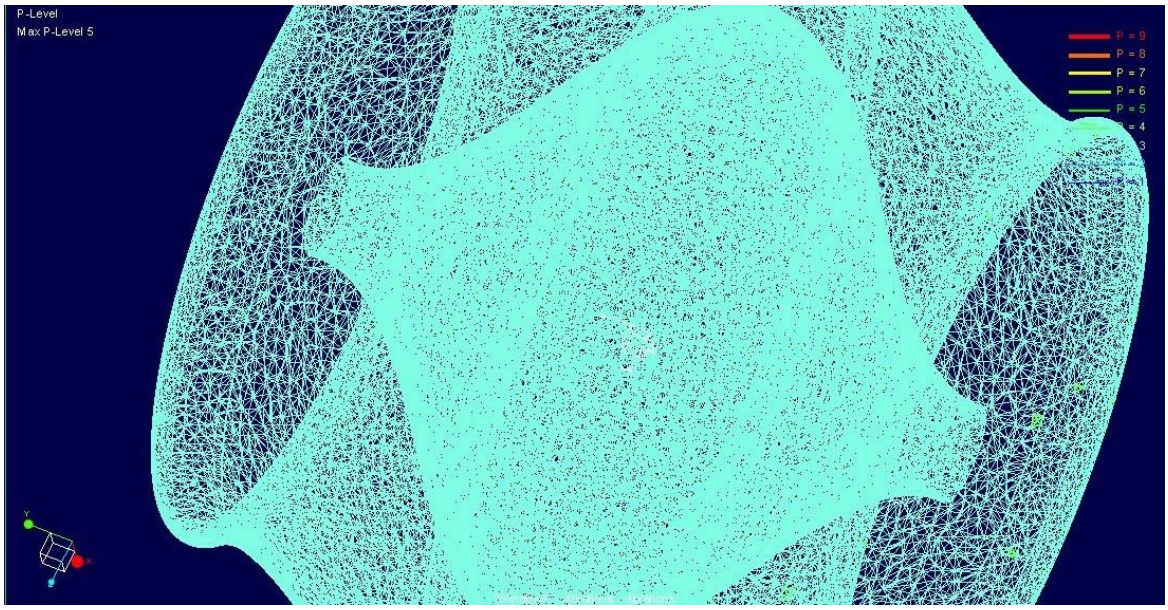

Figure 4-10: The Finite Element Mesh of the Centrifugal Vessel

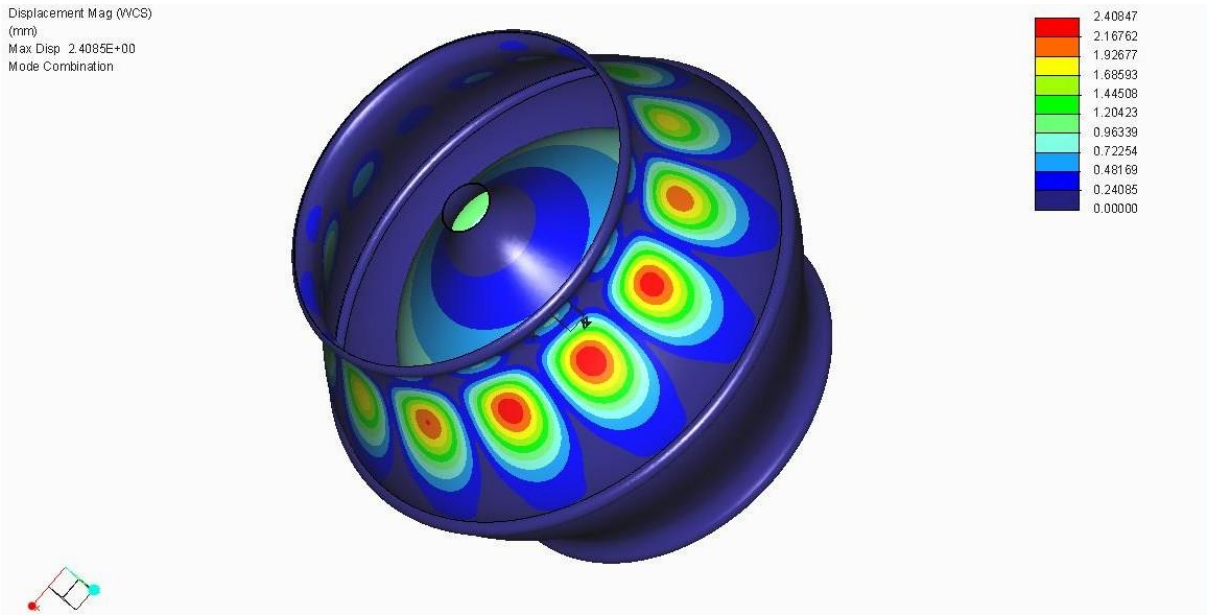

Figure 4-11: Modal Analysis of the Centrifugal Vessel Indicating Modal Displacement

Vibrational Mode	Fundamental Frequency Hz
Mode1	95.245
Mode2	106.564
Mode3	106.576
Mode4	109.709

Table 4-16: Fundamental Frequencies of the Modes of Vibration

The design study is initiated with a modal analysis in order to determine the fundamental modes of vibration. No loads are applied and the model is constrained on the outer rims on both sides. This is done in order to simulate the attachment of the rotor and the stator on either side. The fundamental frequencies of the first four modes of vibration are determined and tabulated in Table 4-16. These frequencies provide significant data to avoid resonance when the component is integrated with other components. Vibration of the vessel can also be critical otherwise; large vibrations can change the distribution of the flow and cause loss of condensation on the surface. The deflections arising due to the four modes are depicted in a combined mode in Figure 4-11.The maximum displacement that results due to vibration is also

calculated. A value of 2.408 mm confirms that the maximum displacement due to vibration lies within acceptable limits of elastic deflection. However, after the design is modified to avoid stress and strain distributions, the vibration modes will need to be recalculated accordingly.

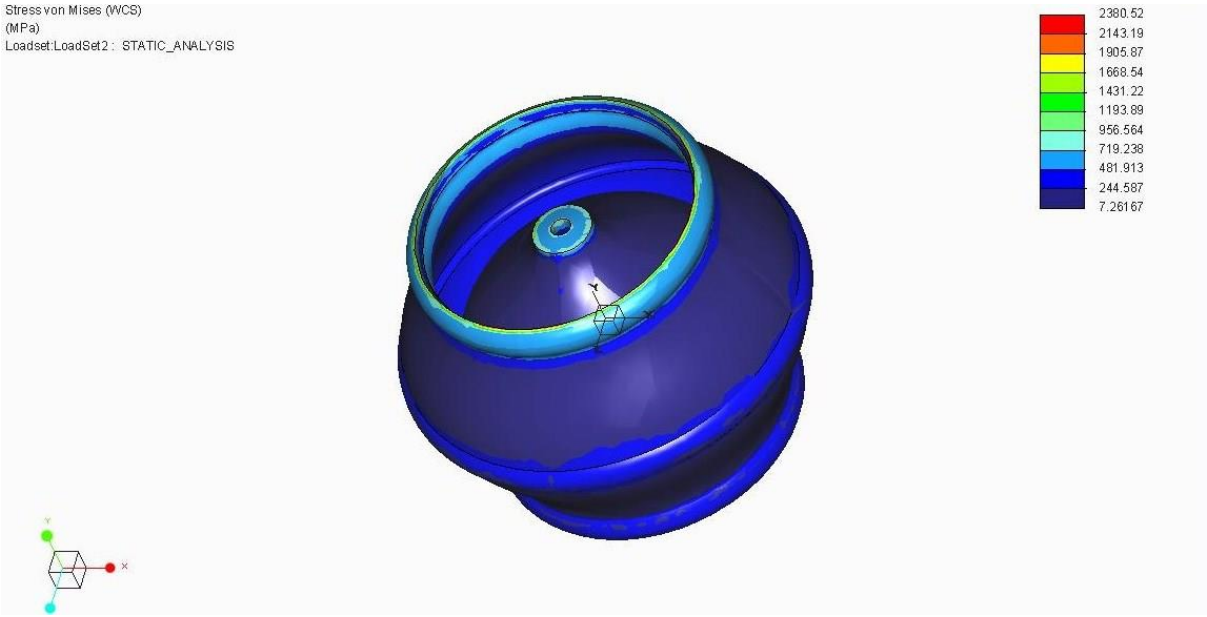

Figure 4-12: Von Mises Stress on the Centrifugal Vessel Due to the Applied Pressure using Al2014 at a Thickness of 100 mm

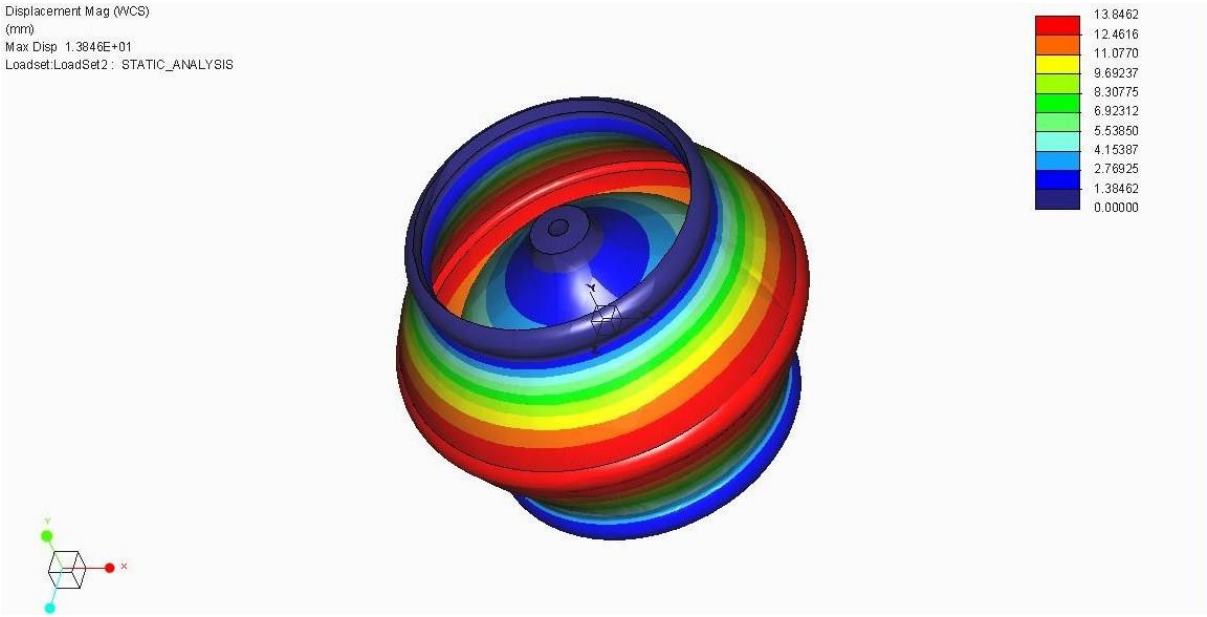

Figure 4-13: Displacement of the Centrifugal Vessel Due to the Applied Pressure using Al2014 at a Thickness of 100 mm

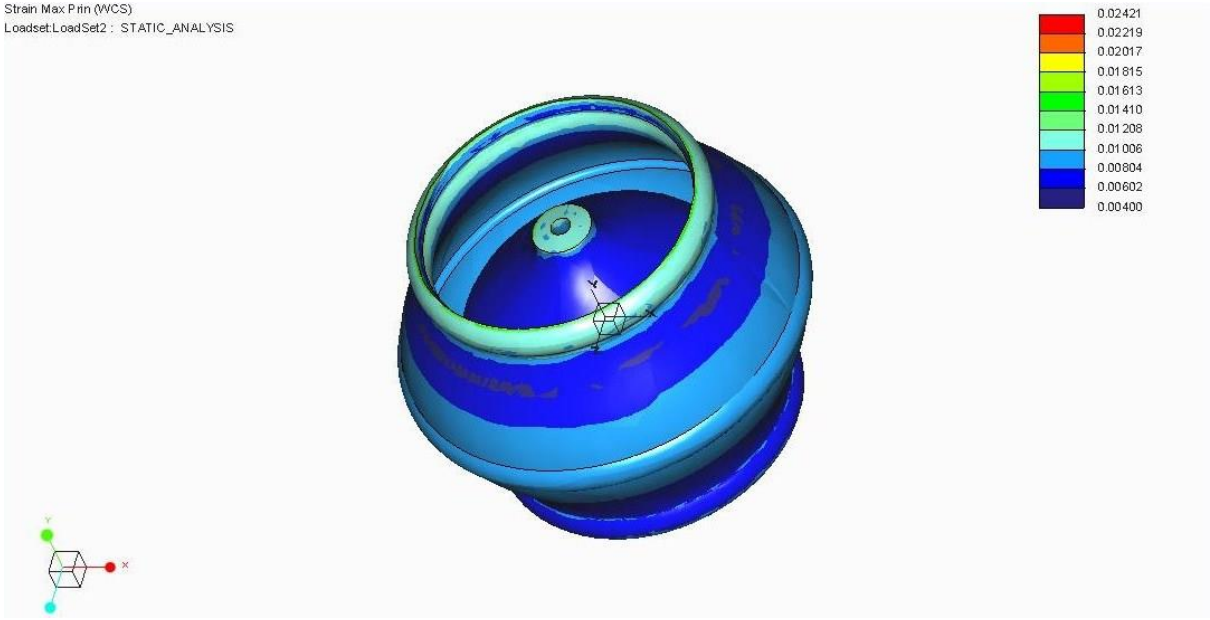

Figure 4-14: Strain of the Centrifugal Vessel due to the Applied Pressure using Al2014 at a Thickness of 100 mm

A pressure of 10 MPa is applied to the inner core as well as to the outer shell for the strength evaluation of the vessel shell. The vessel is analysed at a very high pressure as a design safety measure. Although the vessel is rotating, it is simulated as a static component in order to determine the stress induced by the contained pressure. The rotation of the shell does not affect the strength of the vessel to sustain pressure. The structural behaviour is only dependent on the geometrical design of the vessel under a given set of load conditions and the material used for manufacture.

The vessel is constrained at the inlet and outlet surface rims since it is supported by the two stators and the shaft at that location. The inner core is also constrained in a similar way since it is also supported by the same shaft. A uniform pressure is applied on the outer walls of the inner core and the inner walls of the outer shell. A temperature load of 500 K is also applied.

The stress due to the applied pressure load is uniformly distributed with no particular critical areas, as has been illustrated in Figure 4-12. The von misses stress is used as a criterion. Von misses stress provides an averaged out value that incorporates both axial and shear stress. The maximum value of induced stress is noted at the central periphery of the centrifugal vessel as expected. This happens to lie in the range of 250-500 MPa. The reason for this high value of stress is due to the temperature load of 500 K being applied to the vessel. High temperatures increase the stress concentration enormously.

The ultimate tensile strength of Aluminium alloys is in the range of 200 MPa. At a stress value beyond this limit, the behaviour of the material does not remain

elastic and plastic deformation occurs. Aluminium alloys do not possess high tensile strength at high temperatures. This model if tested at standard operating conditions of temperature and pressure will be able to sustain the applied load with the current design. However, in this particular case, either one can switch to another material with a higher value of tensile strength at high temperatures or the design can be modified to provide additional structural strength. The values for induced stresses will not change if the material properties in the analysis are changed. A material with the ultimate tensile strength in the range of 500-750 MPa would be able to sustain the existing design. The choice can be made from among the high strength alloys used for aerospace and aero-engine applications that can withstand high temperatures and are non-corrosive in the presence of water vapour. An intelligent decision might be required, additional structural strength by using aluminium will result in a weight penalty or an additional cost will be incurred in using a material with a higher tensile strength. This trade-off would need to be estimated.

If the design is intended to be modified structurally for the same material i.e. it is to be fabricated using an aluminium alloy, a rib would need to be designed across the central cross-section as reinforcement. With the addition of ribs, it is targeted that the maximum stress value will be brought down below 50 MPa in the worst case loading scenario. The high stress zone on the rim depicted in green in Figure 4-12 is due to the fact that constraints are applied in that region for the purpose of simulation and do not depict real values of induced stress.

Maximum displacement is observed at the centre of the vessel as illustrated in Figure 4-13. A very large displacement of nearly 15mm is observed at the centre. This equates to an increase in the diameter of the vessel by about 30 mm during operation. This value can be reduced by using a material with a greater stiffness than aluminium. The Young's modulus of aluminium is 69 GPa. A material with a higher value of young's modulus and ultimate tensile strength will be an ideal option. Again, another possibility of reducing the deflection is by adding reinforcements on the central diameter or by catering in the design around the vessel to accommodate this increase in size.

The strain plot in Figure 4-14 provides reasonable values. The maximum strain induced is one percent (neglecting regions where the shell is constrained) which happens to be a fairly acceptable value. The strain values are usually targeted below 8-10 % because ruptures occur at this percentage range for most materials.

The loads on the vessel will not vary rapidly during its operation and there is no impact load involved. The temperature or pressure of the vessel does not vary rapidly either; therefore a dynamic Finite Element analysis is not required at this stage of optimization. Once the geometry of the design is optimized through

many iterative cycles, a dynamic analysis can be performed on the model for the purpose of verification. For the current analysis, the pressure is applied uniformly all around the vessel. The pressure profile can be determined by performing a flow analysis. After the flow analysis is completed, the pressure profile for different operating conditions can be applied across the inner surface to simulate actual loading conditions. In addition, an assembled model can be used with static and rotating components to constrain the model more accurately. That analysis would then provide validation for initiating the mechanical design for this piece of equipment.

4.8 WEIGHT ESTIMATION OF THE CENTRIFUGAL WATER EXPELLER

The analysis was initially carried out at a thickness of 100mm for the shell with a length of 2000 mm and an inlet and outlet diameter of 1000mm. Al2014 which is an aerospace specific aluminum alloy was specified as the material with a stiffness of 73 GPa and a tensile strength of 490 MPa. With this current configuration, as discussed earlier, the stiffness value is low and a high value of displacement is experienced. The maximum displacement is experienced at the center. The supports and sealing are also attached to the center which shall also act as a constraint to restrain the displacement. We need a minimum thickness of the vessel to be 100mm in order to meet the ultimate tensile strength requirements. This results in a very heavy device. The simulation was revised by reducing the thickness of the device to 20 mm which is the minimum thickness for this scale of dimensions that can be practically manufactured. In order to achieve a reasonable weight and strength value the standard titanium alloy used for the manufacture of gas turbines Ti6Al4V was selected. Although it is denser than Al2014, the stiffness and ultimate tensile strength is higher and this alloy can also withstand higher temperatures. As can be seen in the table below, the displacement is reduced due to the use of a stiffer material. The weight has also been reduced considerably because a stronger material has been used and the thickness of the device can therefore be reduced. The specifications for both the materials and the results are tabulated in Table 4-17 and Table 4-18. Figure 4-28 provides a dimensional drawing of the vessel to provide a size and dimension perspective to the mechanical model.

Although the design is tested for very high pressures, in most of the cases, the weight of the device is not limited by the structural stress values but rather by the manufacturing constraints. As mentioned earlier, the minimum allowable thickness of the device is 20 mm for standard manufacturing techniques which then defines the weight of the device. The additional constraint is for the structural strength and stiffness at the high temperatures involved. These two

factors make Titanium Alloys the obvious choice in contrast to lightweight Aluminum alloys.

Material	Thickness (mm)	Volume (mm^3)	Maximum VonMises (Mpa)	Maximum Displacement (mm)	Maximum Strain	Vessel Weight (Kg)
Al2014	50	3.09E+09	448	14.2	0.0125	8400
Ti6Al4V	20	5.72E+08	879	11.9	0.00897	2000

Table 4-17 : Structural Analysis of the Vessel Using Two Different Materials

Material	Density (Kg/m^3)	Tensile Strength (Mpa)	Stiffness (GPa)	Temperature Limit
Al2014	2800	490	73	650
Ti6Al4V	4500	880	120	623

Table 4-18 : Material Properties for Al2014 and Ti6Al4V

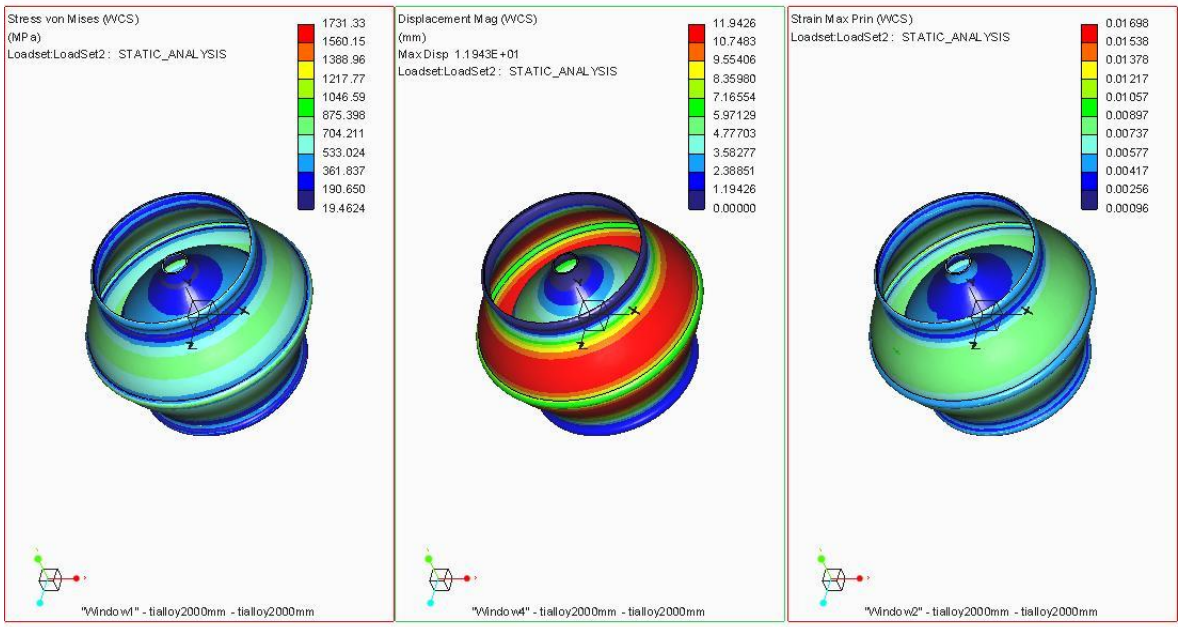

Figure 4-15: Stress, Displacement and Strain Analysis for the centrifugal Vessel using Ti6Al4V at a Thickness of 20 mm

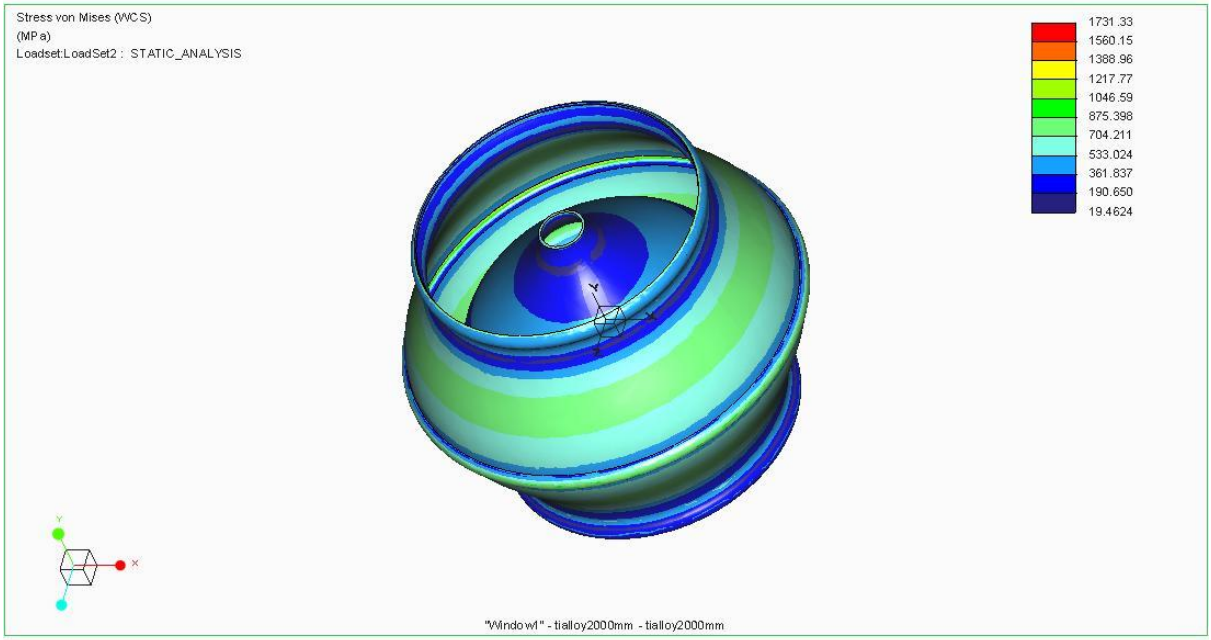

Figure 4-16: Stress Variation in the Centrifugal Vessel Due to the Applied Pressure and Constraints using Ti6Al4V at a Thickness of 20 mm

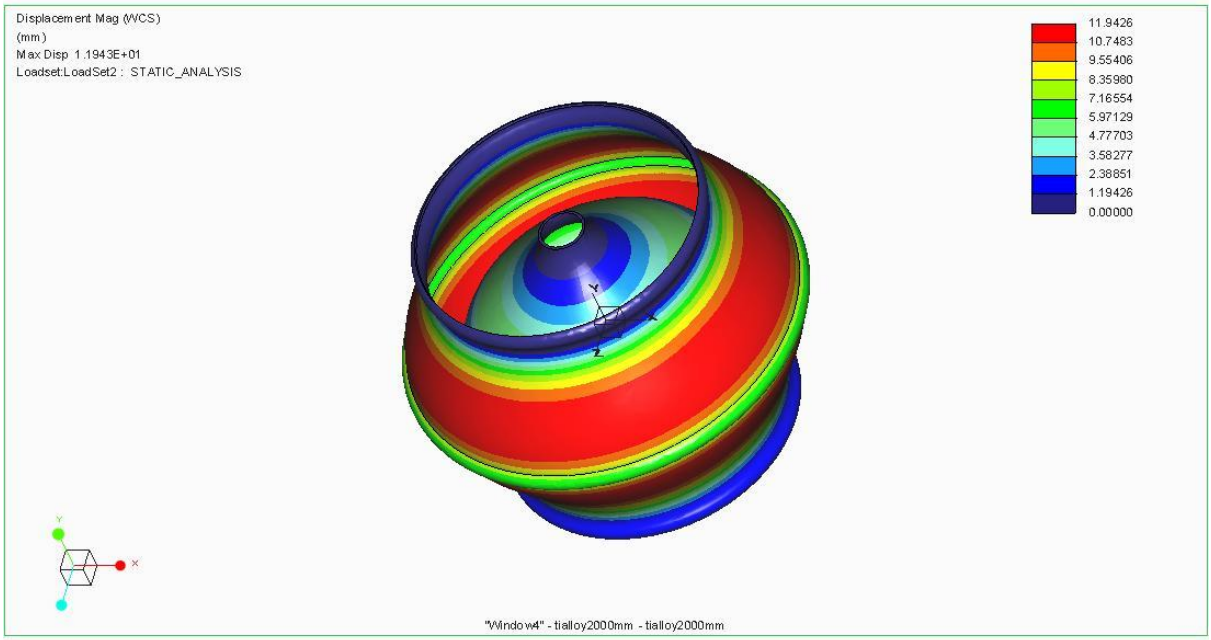

Figure 4-17 : Displacement Variation in the Centrifugal Vessel Due to the Applied Pressure and Constraints using Ti6Al4V at a Thickness of 20 mm

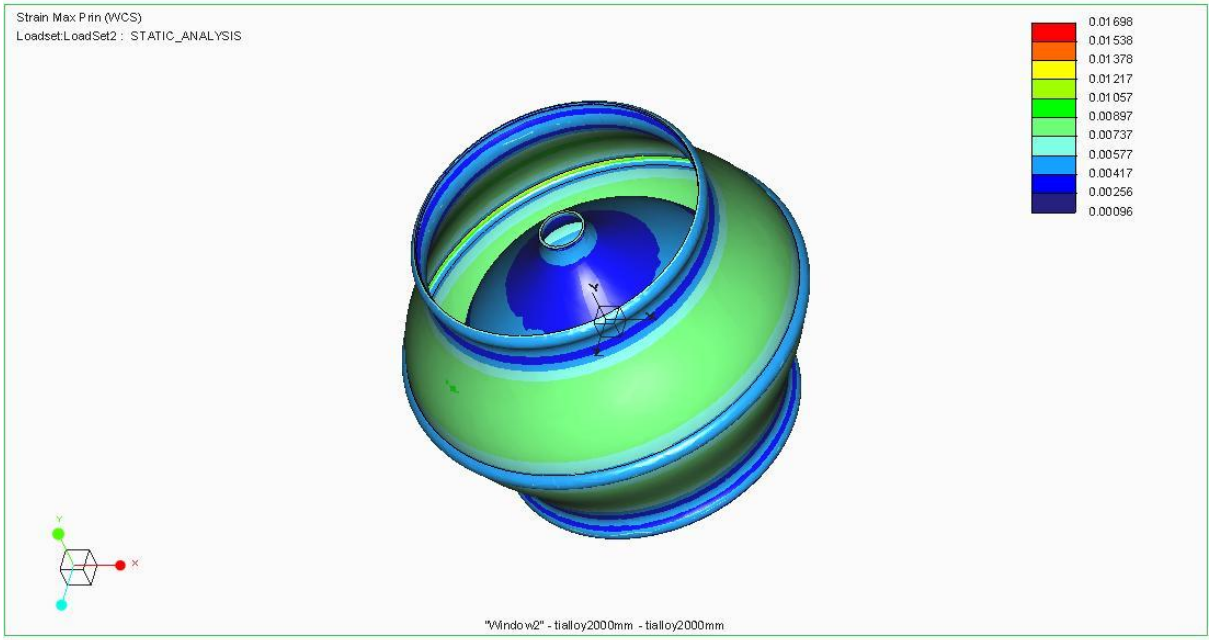

Figure 4-18 : Strain Variation in the Centrifugal Vessel Due to the Applied Pressure and Constraints using Ti6Al4V at a Thickness of 20 mm

4.9 PHILOSOPHY OF MECHANICAL DESIGN

The centrifugal water expeller vessel is designed as a tube, with the centre of the tube expanded, to look like two cones with their bases connected, and apexes at both ends opened, to allow through flow of exhaust gases.

As the exhaust gases pass through this vessel, the gas is made to rotate in a circular manner around the axis by deflector aerofoils. The aerofoils are shaped to deflect the gas flow almost tangentially, and thus force the gas flow to rotate. This set of deflector aerofoils are static, and hence called the stator.

As the rotating gases enter the vessel, a set of turbine blades are placed, with aerofoils shaped as scoops. The rotating gas apply force on the turbine blades, and as a reaction, the turbine rotates. The turbine is fixed to the vessel, and thus the turbine and vessel rotate together. The gases inside the turbine and the vessel itself rotate at the same angular velocity, thus the vessel and gases have a negligible relative velocity.

As the rotating gases enter the vessel, they are subject to their self-created centrifugal force discussed at length previously. At the downstream end, towards the exit of the vessel, is another stator. The purpose of this stator is to straighten out the rotating gas flow as it finally exits into the atmosphere.

The gas flow as shown in all the diagrams is from left to right, so we can describe it symbolically as:

Stator	→	Rotor + Vessel	→	Stator
(deflector)		(turbine + separator)		(straightener)

Since the stators are the static parts, they are made strong to also act as structural members capable of holding the rotating parts. The two stators are fitted with bearings and hold the shaft at either end. The turbine and the vessel are mounted on this shaft. The stators are held by girders connected to the pylons that hold the engine to the wing. The turbine and vessel are thus free to rotate, within the two stators, and the entire assembly is attached to the engine co-axially.

The water thus formed collects at the widest part of the vessel which is the largest circumference and has to be drained out. Design details are visible in Figure 4-20 and Figure 4-21. The two figures show the stator with stator blades (brown) on either side, the rotor with rotor blades (red), the vessel shell, the vessel collector connected to the drain, the shaft holding the equipment and the shaft bearings. The thin blue pipe in the figure indicates the flow of water within the drain.

The drain is also a stationary part, and is connected to the other stationary parts held by the pylon. The pylon holding the engine to the aircraft is being made use of to hold the vessel. The girders are covered with aerodynamic shrouds. The two conical sections shown in Figure 4-20 and Figure 4-21 are only meant for clarity; otherwise, the vessel is aerodynamically contoured to streamline the gas flow.

As the gas at the periphery is compressed to a certain extent, the cross-sectional area is proportionately reduced. This is where the water is formed, due to an increase in pressure, and rains on to the surface of the vessel. A canal is created to allow the water to flow into it. The canal is a part of the vessel, and is also rotating. It is visible as a circular protrusion at the maximum diameter of the vessel shell in Figure 4-20 and Figure 4-21. The water in the canal stays in, because of the gravity created due to the centrifugal force. The water would not fall out of the canal even in the presence of the Earth's gravitational force, since the gravitational force created within the vessel is many times greater than that of the Earth. This water is continuously being drained out from the collector so that a single phase flow can be maintained within the vessel shell. For clarity, the rotor and stator parts are shown in Figure

4-19 without the vessel shell. The rotor has been coloured red whereas the various stator parts including the shaft appear grey for differentiation.

Downstream from the periphery, the diameter is reduced and the lighter gases converge towards the centre. This is illustrated in Figure 4-22. It is evident from the figure that maximum compression of the gas occurs at the centre of the vessel. The residual gases have to be straightened out before they exit into the atmosphere. These residual gases can contribute to the propulsive thrust of the engine if they exit axially, otherwise if exiting with a whirl, they would only be creating an undesirable torque. The stator aerofoils are connected at the exhaust end for the purpose of converting the rotational gas flow into axial flow.

We return to the discussion of the formation of rainfall, and its flow into the canal. The rotating canals has perforations, along its bottom, or physically all along the periphery at its maximum diameter, called draining holes, from where water would be forced out radially, and into a collector. The collector is static, while the canal rotates within it, and thus, slides through it. The sides of the collector have rotating seals, to keep the water from leaking out into to the atmosphere. Figure 4-24 show the partial view of a section of the vessel showing the canal, drain holes and collector. The seals between the canal and the collector are shown in yellow, and the seal cover is shown in white.

Figure 4-25 illustrates the detail of the assembly showing the fittings. The two conical sections are inserted between the collectors, shown in brown, while the plug shown in blue is tightened by screws to the collector, along the numerous axes shown by the dashed lines. The plug (blue) also has drain holes for the water to flow into the collector. The physical properties of the rotating seals have to be able to contain a pressure of 2.5 atm at a temperature of 595°K, and be frictionless. Since this water is at a high temperature and pressure, the water thus drained out of the canal and into the collector has to continue its journey to a heat exchanger. No pump is required since the centrifugal force is itself pushing the water out. This water is then coiled around the vessel downstream of the collector and exposed to the cool bypass airflow as illustrated in Figure 4-23. The very high level of heat has to be dissipated to a comfortable level, for ease of handling. The vessel’s outer surface is exposed directly to the bypass airflow, to let the surface contribute somewhat to the condensation taking place inside. The contribution of the bypass airflow to the cooling of this system will also increase the temperature of the bypass air and hence shall indirectly contribute towards an increase in the net thrust.

4.9.1 SEALING

The vessel would be held by a ring channel at its largest diameter, the channel being part of the rigid static structure, with the vessel rotating within the

channel. This is where the maximum internal pressure is taking place due to the centrifugal force, and where sealing is most necessary, in order for the pressure to be maintained, and to prevent the high temperature water from escaping to the atmosphere. A diagram of the detail of the channel, seal and vessel is given in Figure 4-26 and Figure 4-27.

For clarity, the lubrication supply system, the coolant supply system and the hard points have been omitted. The seal is located between the fixed parts attached to the pylon, and the rotating parts of the vessel assembly. For clarity, the turbines are not shown. The seal should not be fixed on either wall of the rotor vessel nor the fixture stator. The freedom of the seal's movement would give allowance to the seal for thermal expansion. The lubricant delivery to the seals can be simplified, as the piping need only be done through the fixed parts of the above mechanism. Obvious points of delivery could be at the top of the vessel, through the holding pylon.

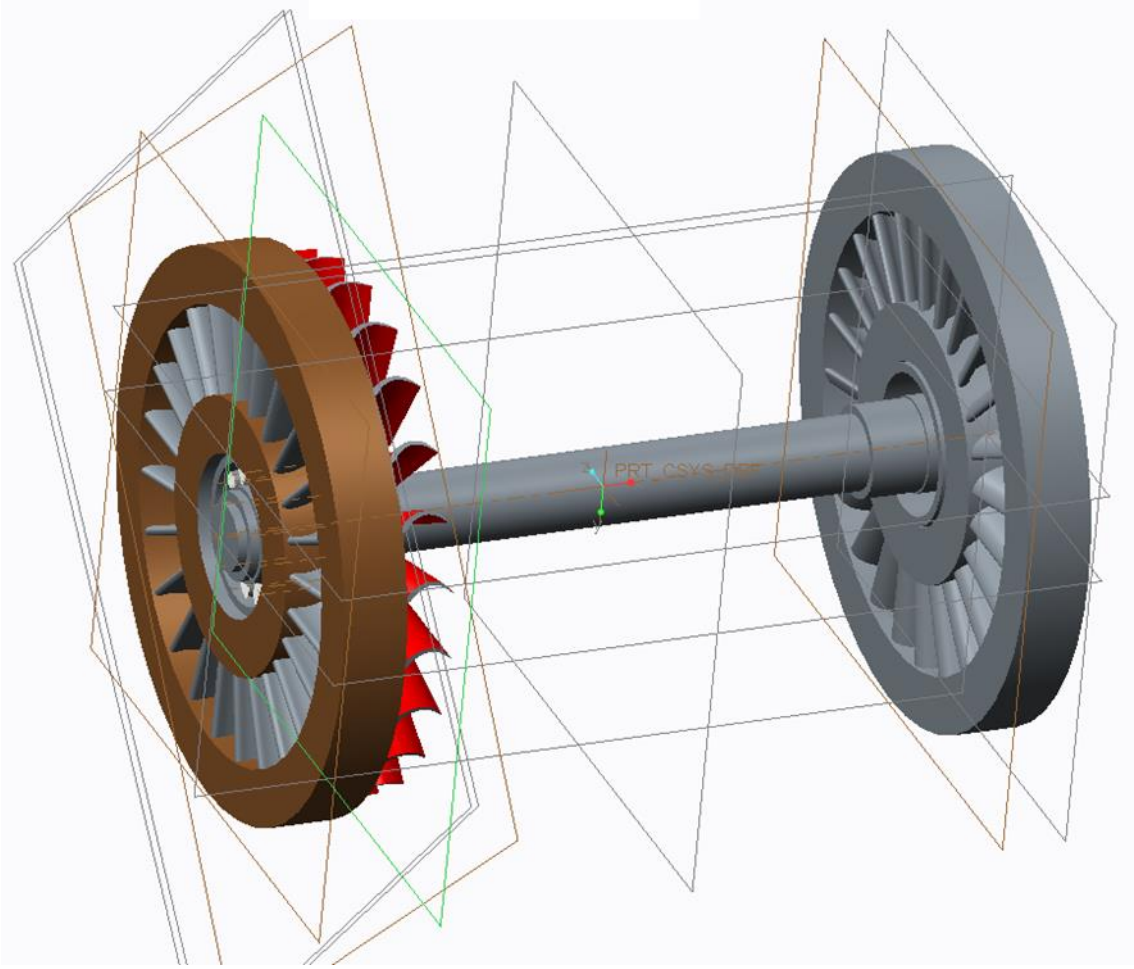

Figure 4-19: The Rotor Turbine (Red) on the Stator Shaft (grey)

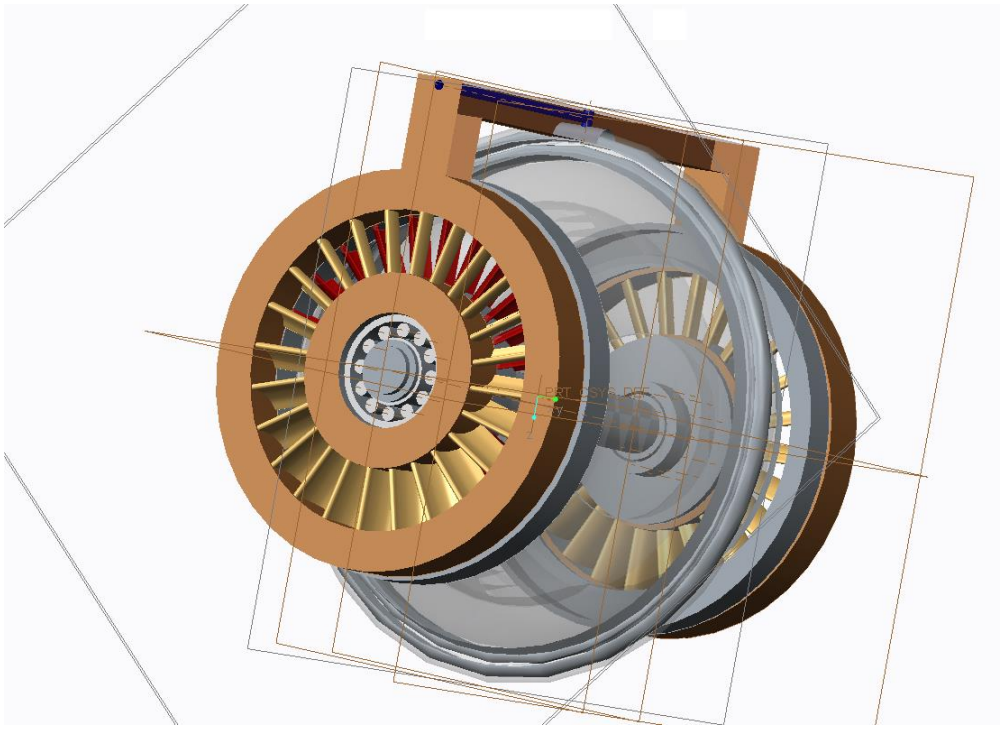

Figure 4-20: View from the Inlet End

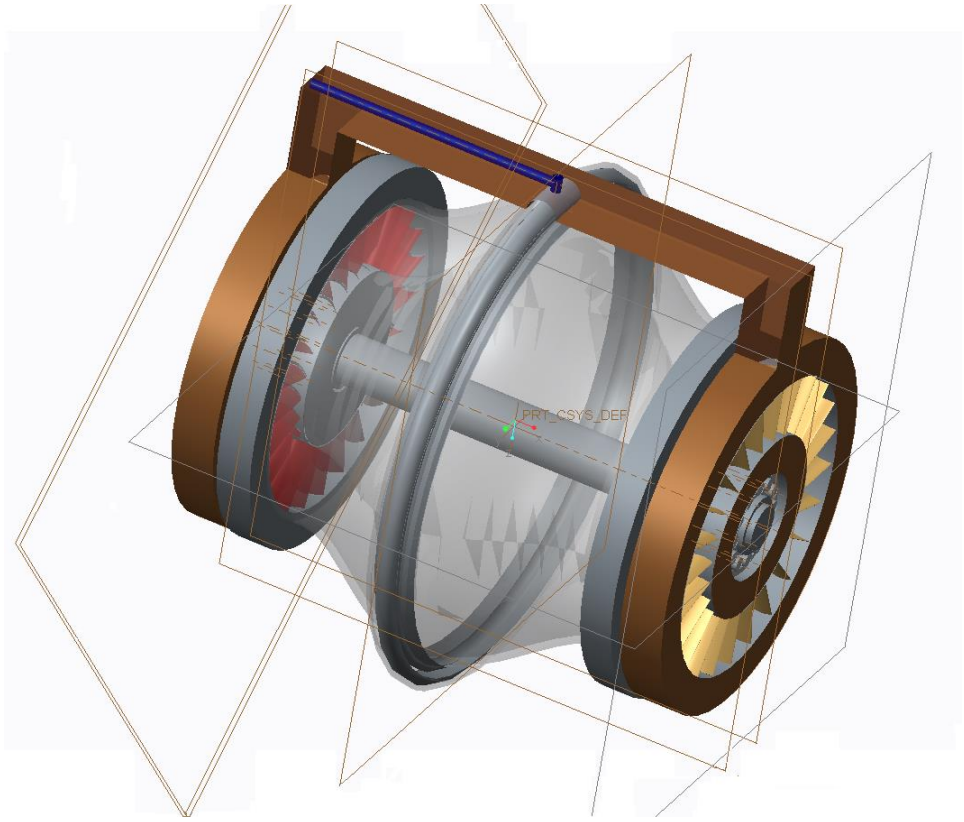

Figure 4-21: View from the Exhaust End

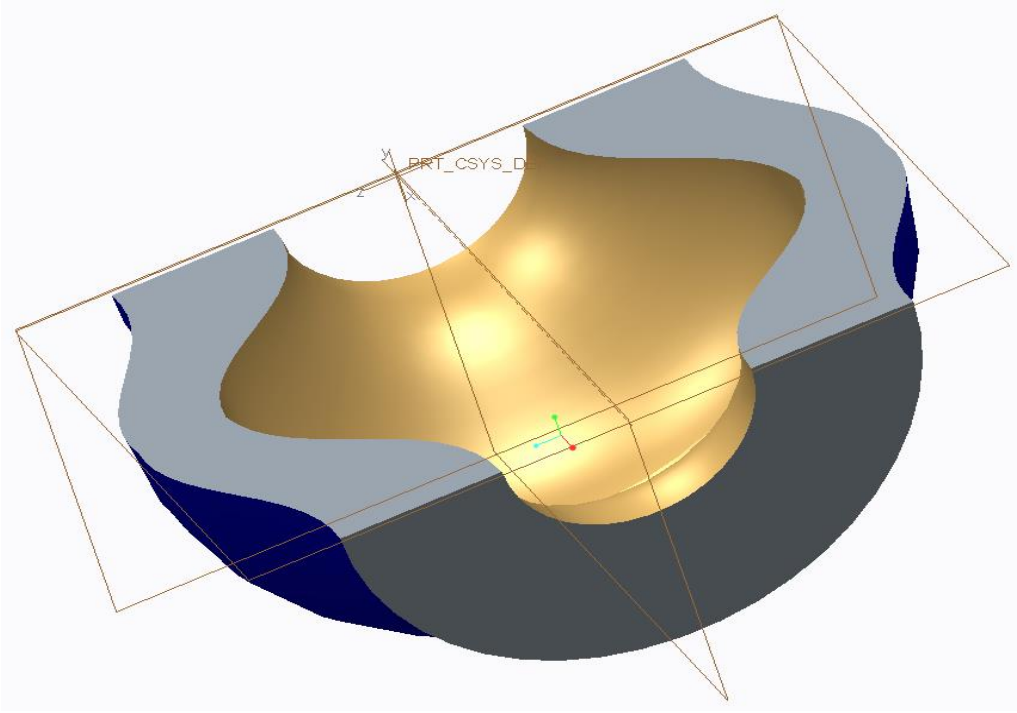

Figure 4-22: Sectional Diagram of the Exhaust Gas Flow through the Vessel

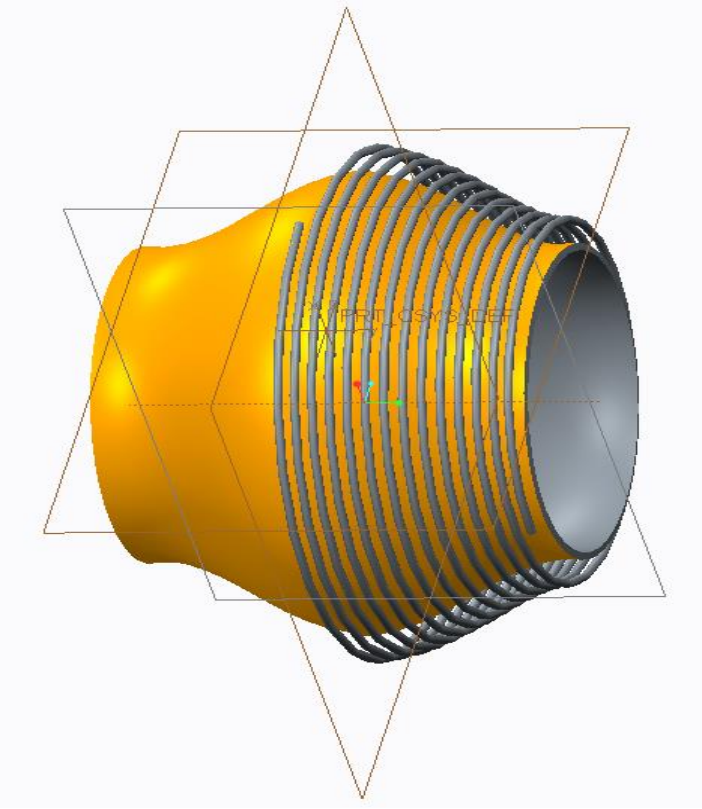

Figure 4-23: Hot Water Exposed to the Cool Bypass Airflow

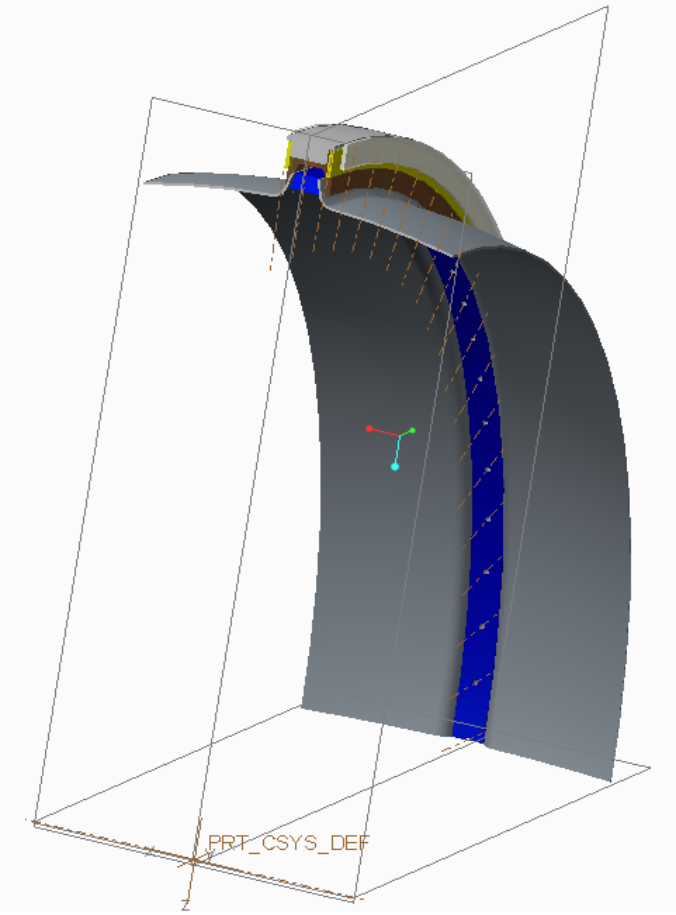

Figure 4-24: Partial View of a Section of the Vessel

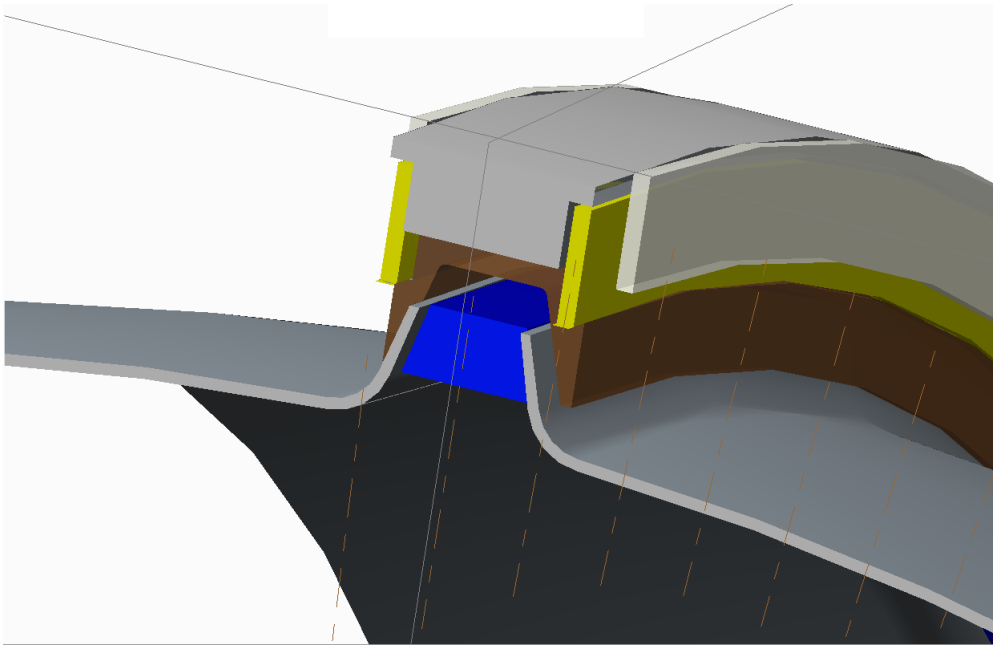

Figure 4-25: Fittings of the Collector Assembly

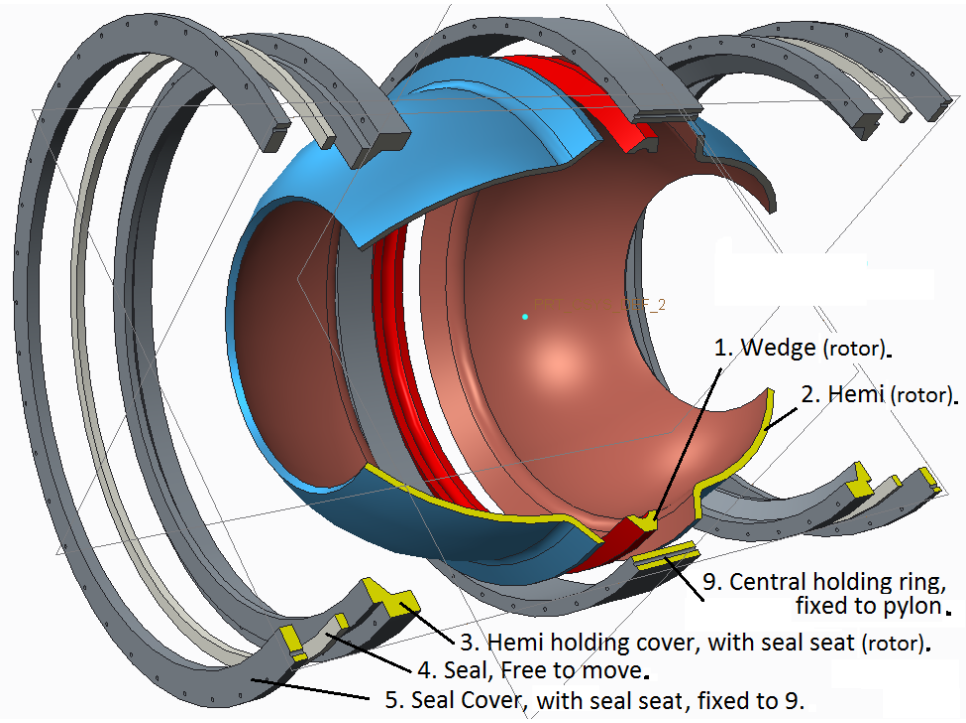

Figure 4-26 : Exploded View of the Rotating Vessel.

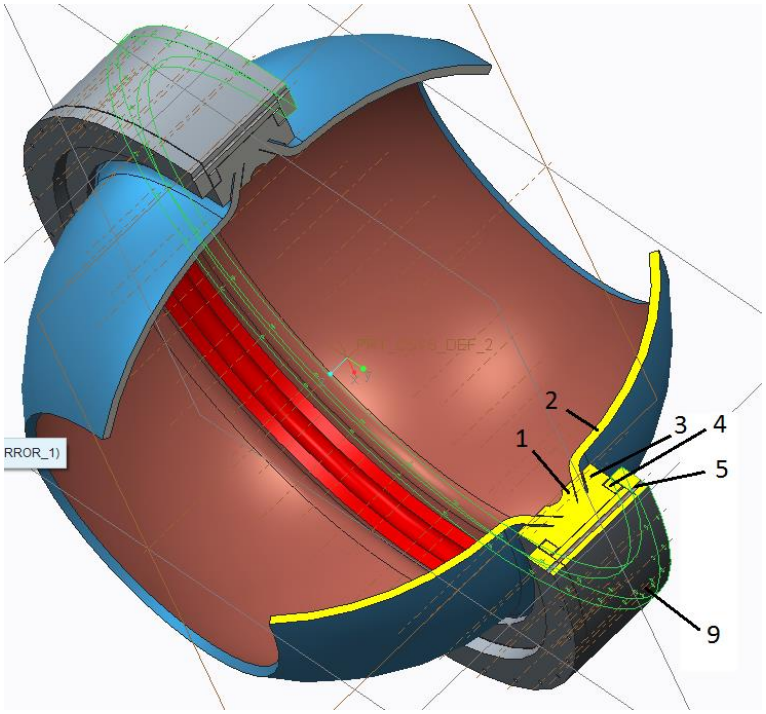

Figure 4-27: Assembled View of the Vessel, the Seals and the Holding Fixtures.

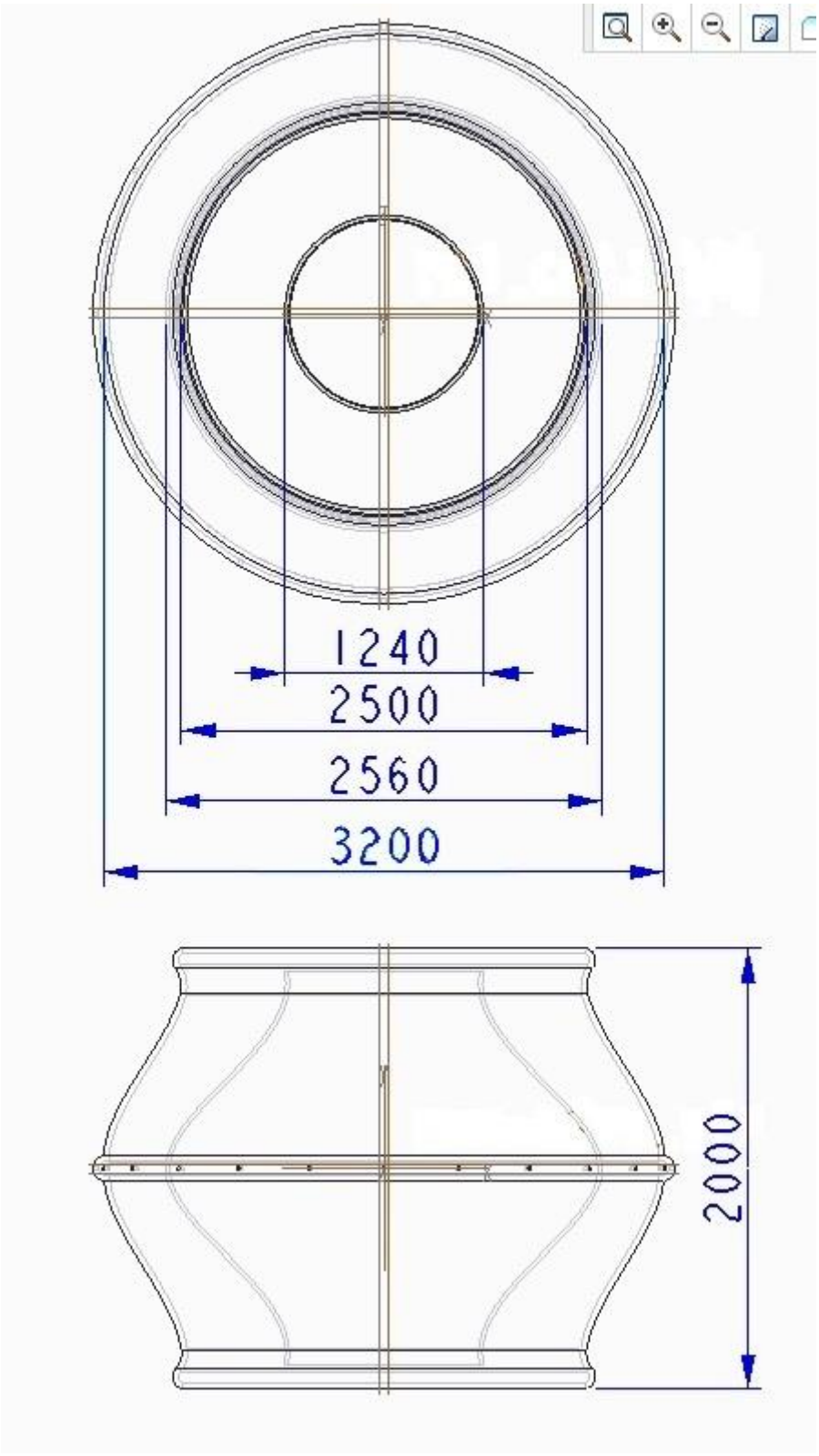

Figure 4-28: Dimensional Drawing of the Centrifugal Vessel

5 THERMOCHEMISTRY OF EMISSIONS

5.1 INTRODUCTION

A study of the thermochemistry of the combustion emissions is carried out to determine the behaviour of the core exhaust emissions at the final condensation temperature and pressure which is achieved by introducing the rotating gases into the centrifugal water expeller before they are being released into the atmosphere. The results of this analysis are presented to validate the design of the centrifugal water expeller. The results reveal the occurrence of intermolecular transfer of energy among the three prime combustion gases (CO_2, H_2O and N_2). The non-condensable exhaust gases, carbon-di-oxide and nitrogen; act as a heat sink and the latent heat of water released during condensation is absorbed by these two gases.

The analysis is initiated with a basic qualitative study of the molecular mechanics of the chemical species and progresses towards the quantitative exchange of energy quanta among the three gases during the process of condensation. This enables us to study the energy transitions as well as the change in the properties of the gases at the elevated temperature and pressure. The aim of this study is two folds; primarily to ascertain whether water will be able to lose its latent heat to the other two combustion gases for successful condensation and secondly to determine the state of the remaining gases at the nozzle exit for the core nozzle design. The gases are analyzed at the molecular level whereas the effect is correlated at the macro level.

Stoichiometric combustion is represented by the following generic formula:

$$C_xH_y + \left(x + \frac{y}{4}\right)O_2 + 3.7\left(x + \frac{y}{4}\right)N_2 \rightarrow xCO_2 + \frac{y}{2}H_2O + 3.7\left(x + \frac{y}{4}\right)N_2$$

Equation 5-1: Stoichiometric Combustion Equation for Generic Fuel

The left hand side of the equation indicates the reactants and the right hand side indicates the products of the combustion reaction. The energy of the product molecules consists of the translational, rotational, vibrational and electronic modes. Translational and rotational modes of energy are a direct function of temperature and can be determined through classical mechanics. Translational energy indicates the kinetic energy of the molecule whereas the rotational energy indicates the frictional heat possessed by the molecule. Vibrational and electronic modes of energy are quantized and can only be determined through quantum mechanics or experimentation. These two modes

of energy indicate the dissociation and photonic excitation of the molecules respectively. The translational and rotational energy is defined in quantum mechanics as the energy modes being quantized according to the spacing between the various quantum levels. Quantum levels for translational and rotational modes lie close together as compared to the quantum levels for the vibrational modes which are spaced far apart. Hence, in the translational and rotational modes, the molecules are able to easily move among various quantum levels and are thus excited translationally and rotationally with a lower input of energy. However, the quantum effects are minimized for high molecular weights and constrain volumes.

The vibrational and electronic quantum levels are spaced apart. The molecules require very high energy for excitation. This energy is not available at our design temperature. At the exhaust temperature close to 600 K the vibrational and electronic modes of energy lie in their ground states. Hence no dissociation or photonic excitation exists at that temperature. However, the translational and rotational modes of energy are excited at this temperature. This is evident from the speed and heat capacity of the exhaust gas.

The total degrees of freedom (DOF) possessed by a molecule for excitation are 3N, where N indicates the number of atoms in a molecule. A non-linear molecule possesses 3N-6 degrees of vibrational freedom whereas a linear molecule possesses 3N-5 degrees of vibrational freedom. Among the three prime exhaust gases, water is a non-linear molecule with a dipole moment whereas carbon-di-oxide and nitrogen are both linear molecules. The degrees of freedom possessed by each of the exhaust gas are given by Table 5-1.

Exhaust Gas	Translational DOF	Rotational DOF	Vibrational DOF
Water	3	3	3
Carbon-Di-Oxide	3	2	4
Nitrogen	3	2	1

Table 5-1: Degrees Of Freedom Possessed By the Exhaust Gases

The three vibrational degrees of freedom in water are called symmetric stretch, anti-symmetric stretch and angle bending. They represent tension, compression and bending of the inter-atomic bonds of the molecule. The four vibrational degrees of freedom in carbon-di-oxide are called symmetric stretch, anti-symmetric stretch planar angle bending, and out of plane angle bending. The last two modes are degenerates and vibrate at the same fundamental frequency.

Quantum excitation of molecules occurs in the vibrational rotational and electronic modes. Vibrational excitation occurs in the infra-red region, rotational excitation occurs in the microwave region and electronic excitation occurs in the UV-Visible region. This means that the molecules are activated in any of the three modes by absorbing energy from the electro-magnetic spectrum. After the absorption of energy, the activated molecules are then excited at a frequency that lies in the same energy band. Subsequently, a release of energy from the molecules also occurs at the same frequencies.

Vibrational frequencies hold importance for the combustion gases contained in the exhaust of an aero-engine. This is because thermal energy released in the chemical reaction of combustion is available to the molecules for absorption. This absorption of energy can induce vibrational excitation in the molecules. Vibrational excitation takes place at extremely high temperatures that are attained after complete combustion.

This excitation also results in the dissociation of the nitrogen molecules in the combustor and results in NOx formation. Once released into the atmosphere, the combustion gases are exposed to the Ultraviolet, Visible and the Infrared spectrum and hence get electronically and vibrationally excited. This explains the photochemical dissociation of the gases as well as the greenhouse effect in the upper atmosphere.

5.2 MOLECULAR DYNAMICS EQUATIONS

The intermolecular forces are a function of the distance between the two molecules. The short range forces are repulsive due to the existence of an electron cloud overlap between the two molecules. The long range forces are attractive, and arise due the presence of an electrostatic dipole. These long range forces give rise to the phenomenon of condensation with a release of energy in the process.

Since water is a polar molecule, it exhibits strong attractive forces and hence can condense through collision-coalescence. The intermolecular potential function of attractive forces between two molecules is given by Equation 5-2 (Atkins, 2010)

$$\boldsymbol{V = \frac{2}{3kT}\left(\frac{\mu a^2 \mu b^2}{4\pi\varepsilon_o r^6}\right)}$$

Equation 5-2: The Intermolecular Potential Function

5.2.1 NOTATIONS

The parameters and constants used in the molecular dynamics equations are listed in Table 5-2

PARAMETER	SYMBOL	VALUE	UNITS
Universal Gas Constant	R	8.3143	Joules/mole/Kelvin
Molecular Mass	M		Kg
Molecular Diameter	d	2.7×10^{-10}	Meters
Avogadro Number	N	6.02×10^{23}	Molecules
Loschmidt Number	n		Molecules/Meter^3
Vibrational Temperature	T_{vib}		Kelvin
Planck's Constant	h	6.62×10^{-34}	Joules. Second
Frequency of vibration	ϑ		Second^{-1}
Boltzmann Constant	k	1.38×10^{-23}	Joules/Molecule/Kelvin
Velocity of Light	c	3.0×10^{8}	Meters/Second
Quantum Level	q	0,1,2,3.....	
Number of Moles	n_0		
Temperature of the gas	T		Kelvin
Dipole Moment of molecule a,b	μ_a, μ_b		Coulomb. meter
Intermolecular distance	r		meter
Electric Constant	ε_o	8.85×10^{-12}	Coulomb^2/Newton/meter^2
Potential Function	V		Joules/meter

Table 5-2: Notations Used In the Equations for Molecular Dynamics

According (Turrell, 1997):

The average molecular speed $\boldsymbol{u}$ per unit mole is given by Equation 5-3

$$u = \sqrt{\frac{8RT}{\pi M}}$$

Equation 5-3: Average Molecular Speed

The root mean square velocity $\boldsymbol{v}$ of the gas molecules is given by Equation 5-4

Root mean square velocity is calculated because a distribution of speeds exists.

$$v = \sqrt{\frac{3RT}{M}}$$

Equation 5-4: Root Mean Square Velocity

The viscosity **η** of the gas molecules is given by Equation 5-5. It indicates the transport of momentum in the gas.

$$\eta = \frac{\mathrm{M}}{\mathrm{N}\pi\mathrm{d}^2}\sqrt{\frac{\mathrm{RT}}{\pi\mathrm{M}}}$$

Equation 5-5: Viscosity of the Gas Molecules

The diffusivity **D** of the gas molecules is given by Equation 5-6. It indicates the transport of mass in the gas.

$$D = \frac{1}{n\pi d^2}\sqrt{\frac{RT}{\pi M}}$$

Equation 5-6: The Diffusivity Of The Gas Molecules

The conductivity $\boldsymbol{k}$ of the gas molecules is given by Equation 5-7. It indicates the transport of kinetic energy in the gas.

$$k = \frac{1.5\ R}{N\pi d^2}\sqrt{\frac{RT}{\pi M}}$$

Equation 5-7: The Conductivity of the Gas Molecules

The number of collisions **C** of a given molecule with all the other molecules is given by Equation 5-8

$$C = \pi n u d^2\sqrt{2}$$

Equation 5-8: The Number of Collisions of the Gas Molecules

The mean free path $\boldsymbol{f}$ of the molecules is given by Equation 5-9

$$f = \frac{1}{\pi n d^2 \sqrt{2}}$$

Equation 5-9: The Mean Free Path of the Molecules

The molar specific heat capacity at constant volume $\boldsymbol{C_v}$ is given by Equation 5-10

$$C_v = \frac{3}{2}R$$

Equation 5-10: Specific Heat Capacity of a Gas

The molar translational energy $\boldsymbol{Et}$ is given by Equation 5-11

$$E_t = \frac{3}{2}n_0 RT$$

Equation 5-11: The Translational Energy of Gas Molecules

The molar rotational energy for linear molecules $\boldsymbol{Er}$ is given by

Equation 5-12

$$E_r = n_0 RT$$

Equation 5-12: The Rotational Energy of Gas Molecules

The vibrational energy $\boldsymbol{E_v}$ is given by Equation 5-13

$$E_v = \left(q + \frac{1}{2}\right) h\vartheta$$

Equation 5-13: The Vibrational Energy of Gas Molecules

The vibrational energy jump $\Delta \boldsymbol{E}$ is given by Equation 5-14

$$\Delta E = h\vartheta$$

Equation 5-14: The Vibrational Energy Jump of Gas Molecules

5.3 THE MOLECULAR DYNAMICS OF COMBUSTION GASES

The molecular dynamics of the combustion gases at different design temperatures and pressures have been calculated using the classical mechanics theory. Detailed calculations have been carried out for water, since the prime interest lies in the condensation of the water vapour present in the exhaust.

Vibrational energy calculations have also been carried out for the other two gases, CO_2 and N_2, in-order to determine their behaviour and to execute a comparative study for the purpose of determining the exchange of energy among the three gases. The behaviour of water changes in the presence of the other gases. Detailed molecular analysis provides evidence that the presence of nitrogen provides a net advantage in the heat loss from the water vapour.(Finzi et al., 1977) The vibrational energies of the three combustion gases have been calculated according to the fundamental vibrational frequencies of the molecules. Experimental values of the vibrational frequencies have been used for calculations.

Nitrogen being a linear di-atomic molecule possesses only one fundamental frequency whereas H_2O being a tri-atomic polar molecule possesses three fundamental vibrational frequencies and CO_2 being a linear tri-atomic molecule possesses four fundamental vibrational frequencies as indicated in Table 5-1 and Table 5-3. Table 5-3 also indicates that two vibrational modes of carbon-di-oxide vibrate at the same fundamental frequency and are thus called the degenerate modes. These degenerate modes can be excited at a low frequency.

Table 5-3 indicates that N_2 possesses high vibrational energy and hence this mode is difficult to excite. However, as will be discussed later, the translational modes of N_2 have the capacity to absorb energy from the other surrounding molecules. The vibrational energy of H_2O and CO_2 are of the same order. In this case it seems probable that if the water vapour undergoes a phase change at a given temperature and pressure, the latent heat released by the water vapour will be absorbed by one of the vibrational modes of CO_2 and the translational modes of N_2.Two vibrational modes of CO_2 are degenerate and hence exist at the same energy level. CO_2 has the lowest energy in this mode and therefore has the capacity to absorb energy in this mode from the surrounding molecules for activation. It should be noted that the vibrational energies in this case are independent of the temperature of the gases. The range of Infrared radiation varies from 400 per cm to 4000 per cm. The vibrational frequencies of CO_2 and H_2O lie within this range and hence Infra-red is readily absorbed and emitted by CO_2 and H_2O in the atmosphere.

Table 5-4 provides a list of constants and design data used for the computing the data tabulated in Table 5-3 and Table 5-5. Some of the data listed in Table 5-4(other than the values of the various constants) has been obtained through the aero-engine performance calculations. Calculations tabulated in Table 5-3 and Table 5-5 have been carried out manually using the classical molecular mechanics approach. The classical approach only computes the translational mode of energy whereas data for the other modes of energy is either obtained experimentally or through quantum mechanics calculations.

The classical mechanics equations described above and the data for various constants listed in Table 5-4 have been used to determine the molecular behaviour of water over a temperature range of 273 K to 647 K where the water can exist in the liquid phase. This data is tabulated in Table 5-5. It determines the variation of different molecular properties of water with a change in temperature. The distribution of the exhaust gas energy between the translational and rotational mode indirectly refers to the distribution among kinetic energy and absorption within the Infra-red spectrum.

Table 5-5 provides the molecular calculations for water at a range of temperatures initiating from 273 K up to a temperature value of 647 K which is the critical point of water. The velocity, viscosity, thermal conductivity, diffusivity, collisions and translational energy of the molecules all increase with an increase in temperature. The mean free path of the molecules does not change. The thermal energy of the molecules also increases with an increase in temperature. This indicates that water exhibits a change in its properties at an elevated temperature in the exhaust of an aero-engine.

Exhaust	**Experimental Vibrational**	**Vibrational**	**Vibrational**
Gases	**Frequency**	**Energy**	**Energy**
	v	**$E_{vib/molecule}$**	**$E_{vib/mole}$**
	1/λ	**hcv**	**hcvN**
Molecule	**/cm**	**KJ/molecule**	**KJ/mole**
H_2O	1799.2	3.57E-20	21.5
H_2O	3812.2	7.57E-20	45.6
H_2O	3945.8	7.84E-20	47.2
CO_2	2565	5.09E-20	30.7
CO_2	1480 (IR inactive)	2.94E-20	17.7
CO_2	526 (angle bending)	1.05E-20	6.3
CO_2	526 (angle bending)	1.05E-20	6.3
N_2	2360	4.62E-20	27.8

Table 5-3: Calculation of the Vibrational Energy of the Three Combustion Gases

LIST OF CONSTANTS USED		VALUE	UNITS
Avogadros number	*N*	6.02E+23	molecules/mole
Total molecular Flow rate of water		4.44E+25	molecules/sec
Universal Molar Gas Constant		8.314	J/mole/Kelvin
Gas Constant for N_2	*RN2*	296.9286	J/kg.K
Gas constant of Water	*Rw*	461.5	J/kg.K
Boltzmann's constant	*k*	1.38E-23	J/molecule.K
Latent heat of water at 100 ℃		2250000	J/kg
Latent heat of water at 0 ℃		2500000	J/kg
Specific. heat of water at constant Pressure		1952	J/kg.K
Specific heat of air at constant Pressure		1005	J/kg.K
Sp. heat of combustion gas at constant Pressure		1148	J/kg.K
Gamma air	γ	1.4	
Gamma combustion gas		1.33	
Molecular weight of water		0.018016	kg
Mass Flow rate of Fuel		1.025	kg/sec
Mole Flow rate of Fuel		6.02	moles/sec
Mole Flow rate of Water		73.7	moles/sec
Mass Flow rate of Water		1.327	kg/sec
Reduced Mass of Water molecule		1.57E-24	gm
Diameter of Water molecule		2.70E-10	meters
Gas constant for CO_2	*RCO2*	188.9545	J/kg.K
Loschmidt number	*P/kT*	4.57E+24	molecules/m³
Particle radius	*f(P,T)=r*	0.001	meters
Planck's Constant	*h*	6.62E-34	Joules.sec
velocity of light	*c*	3.00E+10	cm/sec
Molar latent heat of water at 0° C		45000	J/mole
Molar latent heat of water at 100° C		40500	J/mole

Table 5-4: Constants Used For Calculating the Molecular Dynamics of Combustion Gases

Temperature Exhaust Water	velocity r.m.s. of vapor	Translational Energy of vapor	Thermal velocity of vapor(avg)	Number of molecular collisions/s	Mean Free Path of water molecule	Viscosity of water molecule	Thermal Diffusivity of water	Thermal Energy
T	*Vrms*	1.5RT	*Vth*		molecule			kT
deg K	m/s	Joules/mole	m/s		meters	kg/m.sec	m²/sec	J/molecule
273	614.8	3405	566.4	8.1E+09	7.01E-08	2.61E-05	1.98E-05	3.77E-21
300	644.5	3742	593.8	8.5E+09	7.01E-08	2.74E-05	2.08E-05	4.14E-21
350	696.1	4365	641.3	9.2E+09	7.01E-08	2.96E-05	2.25E-05	4.83E-21
373	718.6	4652	662.1	9.4E+09	7.01E-08	3.06E-05	2.32E-05	5.15E-21
400	744.2	4989	685.6	9.8E+09	7.01E-08	3.17E-05	2.40E-05	5.52E-21
450	789.3	5613	727.2	1.0E+10	7.01E-08	3.36E-05	2.55E-05	6.21E-21
500	832.0	6236	766.5	1.1E+10	7.01E-08	3.54E-05	2.69E-05	6.90E-21
550	872.6	6860	803.9	1.1E+10	7.01E-08	3.71E-05	2.82E-05	7.59E-21
600	911.4	7484	839.7	1.2E+10	7.01E-08	3.88E-05	2.94E-05	8.28E-21
640	941.3	7982	867.2	1.2E+10	7.01E-08	4.00E-05	3.04E-05	8.83E-21
647	946.4	8070	872.0	1.2E+10	7.01E-08	4.03E-05	3.05E-05	8.93E-21

Table 5-5: Classical Mechanics Calculations of Water Vapour at the Exhaust Temperature and Pressure

5.4 THERMOCHEMISTRY OF THE EXHAUST GASES

A more detailed theoretical analysis is now carried out for all the three combustion gases over a wide range of design temperatures and pressures. Quantum mechanics calculations are employed to thoroughly analyse the translational, rotational and vibrational modes of energy for all gases. The analyses that follow have been performed with the technical assistance of Dr. Rumana Qureshi, Professor, Department of Chemistry, Quaid-e-Azam University, Islamabad, Pakistan.The data tabulated henceforth employs the ab-initio quantum mechanics calculations and has been obtained through the execution of the Gaussian G03W software using the Hatree-Fock method 6.31G basis set. This software code has been executed by Dr. Azra Yaqoub, Department of Chemistry, Quaid-e-Azam University, Islamabad, Pakistan for this analysis.

The partition functions **(Q)** for the translation, rotation and vibration energies of all the combustion gases in the exhaust is calculated. The molecular partition function (**Q**) provides an indication of the average number of states that are thermally accessible to a molecule at the temperature of the system(Ochterski, 2000). If the value of the partition function equals 1, then this implies that all the molecules are lying in their ground state. A value of the partition function greater than 1 indicates that the molecules have been excited to higher energy levels.

The results have been tabulated as computed. The units of calculation are Kilocalories/Mole (Kcal/mol). Since a comparative analysis has been performed and absolute values have not been used therefore no unit conversion is required. Initially the calculations were made for temperatures initiating from 350 K up to a temperature value of 450 K. This is the temperature range at which water can exist in the liquid state at realistically achievable values of pressure. An engine exhaust temperature (563 K) and exhaust pressure (0.2467 atm) as well as the ambient temperature and ambient pressure at cruise altitude were also included in the study.

The energy variation over a range of design temperatures and pressures has been calculated for all the three combustion gases: H_2O, CO_2 and N_2. These are the temperature and pressure points whereby condensation of water vapour can occur. In the case of water, as indicated by Table 5-6, the translational and rotational energy increase as temperature increases. The vibrational energy does not change with temperature. However, there is an increase in the vibrational heat capacity. The overall entropy also increases with an increase in temperature. The partition function for translation and rotation also increases with temperature which implies that these two energy modes are activated. The partition function of vibration equals one and hence no molecular vibration exists over this temperature band.

The behaviour of Carbon-di-Oxide is displayed in Table 5-7. All the three modes of energy, translation, rotation and vibration are active over this temperature band. The rotational and translational specific heat capacity is constant since it only depends on the gas constant and not on the temperature. The specific heat capacity of the vibration mode increases with an increase in temperature implying that more heat is absorbed at higher temperatures for the same level of photonic excitation. The partition function for all the three modes is also increasing with an increase in temperature since all energy modes are active. The partition function for vibration is increasing less rapidly with temperature as compared to the other two energy modes. This is specific to the quantum behaviour of the vibration mode. The overall entropy also increases with an increase in temperature.

Water									
Temperature	Pressure	E				Cv			
K	Atm	Trans	Rot	Vib	Total	Trans	Rot	Vib	Total
				Kcal/mol				Cal/Mole.K	
298.15	1	0.889	0.889	13.888	15.665	2.981	2.981	0.025	5.986
350	0.4934	1.043	1.043	13.89	15.976	2.981	2.981	0.065	6.027
373	0.9869	1.112	1.112	13.891	16.115	2.981	2.981	0.091	6.052
400	2.9607	1.192	1.192	13.894	16.279	2.981	2.981	0.127	6.088
450	14.8038	1.341	1.341	13.903	16.585	2.981	2.981	0.208	6.17
563	0.2467	1.678	1.678	13.939	17.295	2.981	2.981	0.442	6.404
Temperature	Pressure	Q				S			
K	Atm	Trans	Rot	Vib (V=0)	Total (V=0)	Trans	Rot	Vib	Total
								Cal/Mole.K	
298.15	1	3004320	84.3038	1.00016	2.53E+08	34.608	11.793	0.003	46.404
350	0.4934	9091390	107.225	1.00059	9.75E+08	36.809	12.271	0.01	49.089
373	0.9869	5329150	117.966	1.00093	6.29E+08	35.747	12.461	0.015	48.223
400	2.9607	2115510	131.004	1.0015	2.78E+08	33.911	12.669	0.022	46.603
450	14.8038	567959	156.32	1.00309	89057900	31.298	13.02	0.042	44.36
563	0.2467	59670700	218.755	1.01001	1.32E+10	40.548	13.688	0.113	54.348

Table 5-6: Thermochemistry of Water

Table 5-8 displays the behaviour of Nitrogen which exists as a linear di-atomic gas. Unlike water, no dipole moment exists in the nitrogen molecule. Translational and rotational energy increase with an increase in temperature whereas the vibrational energy remains constant. The specific heat capacity for all the three modes of energy increases with an increase in temperature. The partition function for the translation and rotation mode is increasing with temperature whereas that of vibration equals 1. Hence, no photonic excitation exists over this temperature band. The overall entropy also increases with an increase in temperature. Comparative data has also been provided in for the same set of calculations carried out at normal temperature and pressure as well

as at the temperature and pressure at a cruise altitude of 10,670 meters. It has been observed that for both the above mentioned states, the translational and rotational energy of all the gases is less than the energy at the exhaust temperature and pressure since these energies vary directly with temperature. However, the rotational and translational specific heat capacities remain constant. The vibrational energy remains constant with a minor change in the specific heat capacity. Vibrational modes of the exhaust are excited at extremely high temperature in the range of 1000 K. The overall entropy varies randomly for all gases at all the above temperature and pressure points. This is because entropy is a function of both temperature and pressure and pressure is a variable parameter. The absolute values of the various energy modes at the two ambient temperature and pressure points are not relevant in this study since the gases in the atmosphere are not contained within a constrain volume and the gas molecules are spread wide apart for any intermolecular interaction to occur. Nevertheless the comparison calibrates the behaviour of the exhaust gases over standard temperatures and pressures. Data for ozone and oxygen has also been tabulated along with the three exhaust gases since they exist in the atmosphere.

Carbon-di-	Oxide								
Temperature	Pressure	E				Cv			
		Trans	Rot	Vib	Total	Trans	Rot	Vib	Total
	Atm			Kcal/mol				Cal/Mole.K	
298.15	1	0.889	0.592	7.87	9.351	2.981	1.99	1.422	6.39
350	0.4934	1.043	0.696	7.957	9.696	2.981	1.99	1.955	6.92
373	0.9869	1.112	0.741	8.005	9.858	2.981	1.99	2.181	7.15
400	2.9607	1.192	0.795	8.067	10.055	2.981	1.99	2.436	7.4
450	14.8038	1.341	0.894	8.2	10.436	2.981	1.99	2.876	7.85
563	0.2467	1.678	1.119	8.575	11.372	2.981	1.99	3.734	8.7
Temperature	Pressure	Q				S			
		Trans	Rot	Vib	Total	Trans	Rot	Vib	Total
	Atm			(V=0)	(V=0)			Cal/Mole.K	
298.15	1	1.15E+07	2.65E+02	1.04E+00	3.17E+09	37.27	13.1	0.422	50.8
350	0.4934	3.47E+07	3.11E+02	1.09E+00	1.169E+10	39.47	13.4	0.712	53.6
373	0.9869	2.03E+07	3.31E+02	1.11E+00	7.44E+09	38.41	13.5	0.843	52.8
400	2.9607	8.07E+06	3.55E+02	1.13E+00	3.25E+07	36.57	13.7	1.005	51.2
450	14.8038	2.17E+06	3.99E+02	1.19E+00	1.03E+09	33.96	13.9	1.317	49.2
563	0.2467	2.28E+08	5.00E+02	1.36E+00	1.55E+11	43.21	14.3	2.058	59.6

Table 5-7 : Thermochemistry of Carbon-Di-Oxide

Nitrogen									
Temperature	Pressure	E				Cv			
		Trans	Rot	Vib	Total	Trans	Rot	Vib	Total
	Atm			Kcal/mol				Cal/Mole.K	
298.15	1	0.889	0.592	3.662	5.143	2.981	1.99	0.001	4.97
350	0.4934	1.043	0.696	3.662	5.401	2.981	1.99	0.006	4.97
373	0.9869	1.112	0.741	3.662	5.516	2.981	1.99	0.01	4.98
400	2.9607	1.192	0.795	3.663	5.65	2.981	1.99	0.017	4.99
450	14.8038	1.341	0.894	3.664	5.9	2.981	1.99	0.037	5.01
563	0.2467	1.678	1.119	3.673	6.47	2.981	1.99	0.123	5.09
Temperature	Pressure	Q				S			
		Trans	Rot	Vib	Total	Trans	Rot	Vib	Total
	Atm			(V=0)	(V=0)			Cal/Mole.K	
298.15	1	5.83E+06	5.21E+01	1.00E+00	3.03E+08	35.92	9.84	0	45.8
350	0.4934	1.76E+07	6.11E+01	1.00E+00	1.08E+09	38.12	10.2	0.001	48.3
373	0.9869	1.03E+07	6.51E+01	1.00E+00	6.73E+08	37.06	10.3	0.001	47.4
400	2.9607	4.10E+06	6.99E+01	1.00E+00	2.87E+08	35.23	10.4	0.002	45.7
450	14.8038	1.10E+06	7.86E+01	1.00E+00	8.66E+07	32.61	10.7	0.005	43.3
563	0.2467	1.16E+08	9.83E+01	1.00E+00	1.14E+10	41.86	11.1	0.022	53

Table 5-8: Thermochemistry of Nitrogen

5.5 THE CONDENSATION TEMPERATURE AND PRESSURE

This part of the work was carried out after the performance parameters of the centrifugal expeller were determined and the condensation design point was defined. Hence a final set of calculations were repeated at the design point temperature and pressure which is desired to be achieved. Earlier calculations were rather qualitative and were focused towards observing the general behavior of the gases with a variation in temperature and pressure and more specifically so at the water vapor condensation temperature and pressure. The Gaussian software was used again to compute the rotational and vibration frequencies and the thermo-chemical data for the exhaust gases at two finite states of temperature and pressure. These states are:

1. The excitation state at a temperature of 500 K and a pressure of 5.0 atm. This state provides an average value of the design state of the gas at which condensation of the water vapor content of the gas occurs.
2. The standard state at a temperature of 298 K and a pressure of 1 atm. This state is used as a reference for a quantitative comparison of data.

It has been observed from Table 5-12, Table 5-13 and Table 5-14 that the total partition function (Q) has the highest order of magnitude for CO_2 in the standard state and it is obvious from the tables that for all the three states, the total partition function for CO_2 has the highest order of magnitude whereas that of H_2O and N_2 is nearly equal. This infers that the CO_2 molecules have a greater probability of existing in the excited state as compared to the other two gases.

Analysis of the vibrational, rotational and translational components shows that CO_2 again has the highest value for the rotational partition function followed by the rotational partition function of H_2O. This data implies that CO_2 and H_2O have a greater probability to attain a rotationally excited state. A comparison of the translational function also predicts that CO_2 again has the highest value for the translational partition function followed by the translational partition function of N_2.The order of magnitude in this case is quite high as compared to the other two modes of energy implying a greater distribution in the excited translational states. The vibrational partition function for H_2O and N_2 is unity at all states whereas that for CO_2 has a value of unity for the standard state and a value of 1.28 for the excitation state. This infers that CO_2 can exist in the vibrationally excited state at the exhaust temperature and pressure which is the desired temperature for the condensation mechanism to be initiated.

The thermo-chemical data tabulated in Table 5-12, Table 5-13 and Table 5-14 provides values for specific heat capacity, the thermal energy and the entropy of the gases at the defined states of pressure and temperature. It is evident from the tables that the specific heat capacity of CO_2 has the highest magnitude followed by the specific heat capacity of H_2O.This trend is observed for both the states. Due to a lower value of specific heat capacity, Nitrogen gas gains heat easily as compared to the other two exhaust gases. The entropy values also reveal that the entropy of CO_2 is greater than that of H_2O and N_2.

5.6 RESULTS AND DISCUSSION

The value of the translational partition function is high and it implies that all the molecules possess high kinetic energy. Water (H_2O) and Carbon-di-oxide (CO_2) possess a higher value for the rotational partition function as compared to nitrogen (N_2). This is because H_2O is a polar molecule whereas as CO_2 and N_2 are linear molecules. The value of the vibrational partition function of CO_2 at the exhaust temperature of 500 K is 1.36 whereas that of H_2O and N_2 is 1. This implies that CO_2 is slightly excited whereas H_2O and N_2 are lying in their ground state and no vibrational excitation exists.

There is experimental evidence that rotational and vibrational relaxation of H_2O may take place at around 500 K in the presence of N_2 (Finzi et al., 1977). The vibrational relaxation of CO_2 by N_2 is also possible at this temperature (Houston,

2012). Thus, there is a possibility that some of the energy of CO_2 and H_2O may be carried away by N_2 and this shall enhance condensation. Some experimental work on liquid water provides evidence that an increase in pressure decreases the rotational relaxation rate and enables water to lose its energy quickly. Table 5-15 indicates that at the exhaust temperature and pressure, H_2O undergoes translational and rotational excitation; CO_2 undergoes translational, rotational and vibrational excitation whereas N_2 undergoes translational excitation only. As a consequence, N_2 absorbs the rotational and vibrational energy of water and transfers it to the translational mode. Hence as water molecules loose heat, the nitrogen molecules will gain speed.

Another interesting observation reveals that the entropy predicted for the higher pressure final state has a smaller value than the entropy at the standard state for all the three gases which point towards the fact that the gases are moving towards the more organized liquid phase. The experimental and predicted vibrational frequencies indicate that two low energy vibrational modes are present in CO_2 and the high value of vibrational partition function of CO_2 arises due to these modes. This predicts that CO_2 molecules can be excited by the thermal energy at the exhaust temperature.

With reference to Table 5-12 the infra-red (IR) intensity indicates the amount of electromagnetic radiation absorbed in the IR spectrum which is also released in the IR region and contributes to the greenhouse effect. This phenomenon occurs due to the changing dipole moment of the molecules as they vibrate. The IR intensity of the nitrogen molecule is zero as can be seen in Table 5-13 since N_2 is a non-polar molecule.

The value of the vibrational temperatures (Vib temp) in Table 5-12 indicates the temperature at which the thermal energy of the molecule matches the vibrational quanta of the molecule and is directly absorbed by the molecule for vibrational excitation to reach a level where photonic dissociation occurs. Vibrational Energy is independent of temperature below the vibrational temperature. This behavior is governed by Equation 5-15.The high value of the vibrational temperatures of water, Nitrogen and Carbon-di-oxide listed in Table 5-12, Table 5-13 and Table 5-14 respectively indicates that dissociation of these molecules does not occur within the engine even at the highest operating temperatures.

$$\boldsymbol{T_{vib} = h\vartheta/k}$$

Equation 5-15: The Vibrational Temperature of Molecules

5.7 VIBRATIONAL RELAXATION OF COMBUSTION GASES

A qualitative hypothesis is so far established regarding the intra-molecular heat transfer among the combustion gases exiting the exhaust of the jet engine. This hypothesis validated the design of the centrifugal water expeller whereby the latent heat of the water vapour released upon condensation is absorbed by the exhaust gases carbon-di-oxide (CO_2) and Nitrogen (N_2).

In addition to the above, a quantitative study is carried out to determine the energy absorption regime as well as the condition and state of the exhaust gases after the condensation of water in the centrifugal vessel. A simple model is established based on the prediction that the latent heat released by water during condensation is absorbed initially by CO_2 and then transferred to N_2 prior to being released into the atmosphere. This happens to be favourable phenomenon since energy is transferred from a greenhouse gas to a gas that does not contribute to the greenhouse effect. The atmospheric impact of this energy transition has also been determined. It implies that the contribution of the aero-engine exhaust to global warming is considerably reduced.

5.7.1 CONTEXTUAL STUDY

The vibrational relaxation of CO_2 and N_2 along a stagnation stream line has been investigated in (Joly, Marmignon and William, 1997)The experimental methods used to study the vibrational relaxation of CO_2 are the acoustic method (Huetz-Aubert, Louis and Taine, 1978), the spectrophotometric method and laser excited vibrational fluorescence. (Marinov 2 et al., 2012)

Although CO_2 and H_2O contribute significantly to the greenhouse effect in the atmosphere, the relaxation mechanism of CO_2 is more complicated than that of water as CO_2 has many vibrational levels among which some are resonating and there are numerous vibrational-translational (V-T) and vibrational-vibrational (V-V) intra-molecular and intermolecular processes involved.

“A parallelism exists between the CO_2, N_2 Gas Dynamics Laser and the production of non-equilibrium radiation in the exhaust plume” (Joly, Marmignon and William, 1997). Hence the conclusion from the investigation of the former can be applied to the latter.

The vibrational relaxation paths in a CO_2 –N_2 mixture present in the exhaust plume of jet engines and that occurring in the Mars atmosphere have been investigated in(Joly, Marmignon and Jacquet, 1999)There exists evidence that the vibrational relaxation of the CO_2 and N_2 mixture occurs in the Mars atmosphere and in the exhaust plume of jet engines.

A numerical method has been employed that treats ideal mixture of perfect gases. It is adopted to consider CO_2-N_2 mixtures where the internal vibrational levels are defined as chemical species. Nineteen V-V and V-T intra-molecular processes are considered between seven CO_2 and two N_2 levels. The few lowest vibrational levels of CO_2-N_2 mixture and V-V and V-T energy transfer between these levels is considered.

The radiation transition at a wavelength (λ) of 10.6 μm results in an exchange of energy between specific rotational levels of the two vibrational levels of CO_2: (001) and (100). This is a spontaneous emission. It is released into the atmosphere in a similar manner as the energy of the angle bending mode. "The prediction of radiation is related to the level population and depends on the V-V and V-T reaction rate". (Joly, Marmignon and Jacquet, 1999).This radiation transition corresponds to $1.87x10^{-20}$ Joules per molecule which is also equivalent to 11.257 KJ per mole. This process is intra-molecular.

All the above studies establish that Nitrogen acts as an energy reservoir for the absorption and transportation of energy from the other gases. This phenomenon has also been well identified in the earth's atmosphere.

5.7.2 THE ENERGY LEVELS OF GASES

According to the energy equation, the molecular vibrational energy jump $\Delta \boldsymbol{E}$ is given by Equation 5-16

$$\Delta \boldsymbol{E} = \boldsymbol{h}\frac{\boldsymbol{c}}{\boldsymbol{\lambda}}$$

Equation 5-16: The Vibrational Energy

PARAMETER	SYMBOL	VALUE	UNITS
Planck's Constant	*h*	$6.62x10^{-34}$	Joules. Second
Velocity of Light	c	3×10^{8}	Meters/second
Wavelength of Emitted or Absorbed Radiation	λ	10.6×10^{-6}	Meters
Frequency of Emitted or Absorbed Radiation	v	1/λ	1/Meters
Avogadro's Number	*N*	$6.02x10^{23}$	Molecules

Table 5-9: The Vibrational Energy Parameters

The molar energy is calculated by multiplying the molecular energy value with the Avogadro's number. The excitation energy mode notation for CO_2 is as follows:

CO_2 (a, b, c) = CO_2 (symmetric stretch, angle bending, anti- symmetric stretch)

5.7.3 V-V RELAXATION

The anti-symmetry mode of CO_2 excites the vibrational mode of N_2. This V-V intermolecular process is well establishes and is detailed in Equation 5-17 (Houston, 2012)

$$\mathbf{CO_2\ (001) + N_2\ (V=0) \rightarrow CO_2\ (000) + N_2\ (V=1)}$$

Equation 5-17: V-V Relaxation Equation

In this case, $\Delta \boldsymbol{E}$= 18 per cm which is equivalent to 357.48 x 10^{-24} Joules per molecule or 215 Joules per mole. This is the excess energy released during the process.

This process is also known as a Fermi-resonance process. It is two orders faster than V-T relaxation. The rate constant k_{vv} for this process is $10^{-12.62}$ cm^3 per second.(Keeton and Bass, 1976) This rate constant is also valid for an intra-molecular transition whereby energy transfer occurs between the symmetric stretch and the second state of angle bending of carbon-di-oxide. Basically, one intermolecular and one intra-molecular process share the same rate constant implying that they are interchangeable and hold an equal probability of occurrence.

5.7.4 V-T RELAXATION

The vibrational relaxation of CO_2 angle bending mode by N_2 is an example of V-T energy transfer as indicated by Equation 5-18(Houston, 2012).

$$\mathbf{CO_2\ (010) + N_2\ (V=0) \rightarrow CO_2\ (000) + N_2\ (V=0)}$$

Equation 5-18: V-T Relaxation Equation

The angle bending mode possesses the lowest vibrational energy and is therefore the easiest to excite. There exists evidence that the V-T relaxation of the angle bending mode occurs in the presence of other gases. This process is also known as the rate determining step for the relaxation of CO_2 since it is at the lowest vibrational level with an energy jump $\Delta \boldsymbol{E}$ 7974 Joules per mole.

The vibrational frequency (v) of the angle bending mode is 667 per cm. The excited angle bending mode of CO_2 is quenched in this process whereby the translation mode of nitrogen gains energy thereby increasing the speed of the

gas. According to Equation 5-11, the translation energy gained by nitrogen in this process is 7420 Joules per mole. This is nearly 93 percent of the vibrational energy released by CO_2. There exists evidence that the V-T relaxation of the angle bending mode occurs in the presence of other gases.

The greenhouse effect occurs when the angle bending mode of CO_2 is excited and it emits energy in the atmosphere. The rate constant k_{vt} for this process is 10^{-14} cm^3 per second. Another intra-molecular process of CO_2 whereby the third vibrational level is reactivated shares the same rate constant. All vibration modes have the same relaxation time whereas the V-T relaxation is significantly slower than the others.

5.7.5 INTRA-MOLECULAR ENERGY TRANSFER

Two cases of Fermi-resonance are also observed in intra-molecular energy transfer among the CO_2 angle bending and symmetric stretch mode. In the first instance of excitation, the second and the third rotational level of the angle bending mode couple together in order to excite the second rotational level of the symmetric mode within the molecule. The vibrational frequency of this mode is 1388 per cm which gives an energy jump of 16593 Joules per mole. Similarly the third rotational level of the third excitation level of the angle bending mode couples with the first excitation level of third rotational degree to excite the third level of rotation of the symmetric mode. This also excites and transfers energy to the first level of excitation of the anti-symmetric stretch where the excitation frequency is 2349 per cm and has an energy jump of 28082 Joules per mole. This energy then excites the first vibrational level of nitrogen.

These phenomena occur randomly in the atmosphere as well as in the exhaust plume of the aero-engines and that explain how CO_2 causes the greenhouse effect by emitting radiations of specific wavelengths.

In our analysis however, the intra-molecular transitions of CO_2 are not considered as we have a very specific model where the final outcome of intermolecular energy transfer between CO_2 and Nitrogen is of interest which occurs through V-V relaxation and V-T relaxation of CO_2. This is because the centrifugal condensation mechanism is a very contained and well defined system whereby the entire latent heat of water is absorbed by CO_2 and eventually transferred to nitrogen in the vibrational and translational mode. This happens prior to the release of the exhaust gases into the atmosphere. Intermediate intra-molecular transitions of CO_2 are therefore not important. They have been referenced here due to their contribution towards the greenhouse effect occurring in the atmosphere as well as to inform the reader about the phenomenon underlying this energy transition.

5.7.6 VIBRATIONAL RELAXATION TIME

Vibrational relaxation time is the time that is required for the transfer of energy from one molecular specie to another. This holds importance with reference to the environment in which the molecular species are contained in. It determines whether the intermolecular transfer of energy occurs within the spatial and temporal constraints so as to sustain the phenomenon of absorbing the latent heat of condensation of water by carbon-di-oxide and nitrogen in a steady state configuration. It also determines whether this energy transfer time scale is synchronized with the combustion time scale so as to comply with the by-production of the combustion gases. Some of the key parameters involved in determining the vibrational relaxation times are tabulated Table 5-10.

PARAMETER	SYMBOL	VALUE	UNITS
Universal Gas Constant	R	8.3143	Joules/mole/Kelvin
Molecular Mass	M		Kilograms
Molecular Diameter	d	2.7×10^{-10}	Meters
Avogadro's Number	N	6.02×10^{23}	Molecules
Absolute Temperature	T	537	Kelvin
Planck's Constant	h	6.62×10^{-34}	Joules.Second
Frequency of excitation	υ		Meter $^{-1}$
Boltzmann Constant	k	1.38×10^{-23}	Joules/Molecule/K
Velocity of Light	c	3.0×10^{8}	Meters/Second
Transition Probability	p		
Relaxation Time	τ		Seconds
Design Pressure	P	10.5×10^{6}	Pascal
Molecular Collisions	C		Second^{-1}
Molecular Speed	u		Meters/Second

Table 5-10 : Parameters for Calculating the Vibrational Relaxation Time

The equation for the vibrational relaxation time for a single mode of energy transfer according to is as follows (Dickens and Ripamonti, 1961):

$$\tau = \left\{ Cp \left[1 - \exp\left(\frac{hcv}{kT} \right) \right] \right\}^{-1}$$

Equation 5-19 : The Vibrational Relaxation Time

Since two molecular species are involved in this energy transition, therefore the molar mass M will be calculated using the reduced mass formula to find the effective molecular mass of both species. The reduced mass is calculated using the equation below:

$$M_r = \frac{M_{CO_2} M_{N_2}}{M_{CO_2} + M_{N_2}}$$

Equation 5-20 : Reduced Mass of Gaseous Species

Where:

M_r = Reduced Molar Mass of CO_2 and N_2

M_{CO2}= Molar Mass of CO_2

M_{N2}= Molar Mass of N_2

For a molecular mass of 0.044 Kg for CO_2 and 0.028 Kg for N_2, the reduced mass of both the species is calculated to be 0.017 Kg. For this value of reduced mass, the average molecular speed is calculated from Equation 5-3 to be 774 m/s and the number of collisions suffered by a molecule equates to 3.74 x 10^{11}per second according to Equation 5-8. With the availability of this data, the relaxation time can now be calculated for both Vibrational-Vibrational and Vibrational-Translational energy transfer of CO_2 by N_2.

5.7.7 VIBRATIONAL-VIBRATIONAL (V-V) RELAXATION TIME

According to (Fridman and Kennedy, 2004)the vibrational probability of V-V transition is 0.001. As discussed earlier, the excitation frequency at which this phenomenon occurs is 2349 cm^{-1}. This energy transition occurs when the anti-symmetric stretch vibrational mode gets excited by absorbing the heat released during the condensation of water. This energy is then transferred to the vibrational mode of Nitrogen with a minimal amount of energy released during the transition. The vibrational quantum of energy exchanged at this frequency is given by Equation 5-16. At the given frequency this equates to 4.665x10^{-20}

Joules per molecule. The relaxation time is thus calculated to be 2.6787x10^{-9} seconds (2.6787 nanoseconds.)

5.7.8 VIBRATIONAL-TRANSLATIONAL RELAXATION TIME

The experimental probability of the translational relaxation of CO_2 by N_2 at an excitation temperature of 500 K is measured to be 0.00178 according to (Houston, 2012). Vibrational-Translational relaxation occurs at a frequency of 667 cm^{-1}. The vibrational quantum of energy exchanged at this frequency is $hc\upsilon$ as given by Equation 5-14. At the given frequency this equates to 1.324 x10^{-20} Joules per molecule. The relaxation time is thus calculated to be 4.82 x10^{-9} seconds (4.82 nanoseconds) .This energy transition occurs when the angle bending vibrational mode gets excited by absorbing the heat released during the condensation of water. This energy is then transferred to the translational mode of Nitrogen.

The relaxation time of both vibrational-vibrational and vibrational translational energy transfer is of the same order. It can be inferred that both the processes are being executed simultaneously. The time required for the entire heat to be transferred to Nitrogen shall be double the calculated relaxation time. This is due to the fact that carbon-di-oxide initially absorbs heat from water due to the excitation of two of its vibrational modes and then transfers it to Nitrogen through the de-excitation of these modes. Thus these two processes occur in series. The excitation and de-excitation of carbon-di-oxide occurs at the same rate.

5.8 VIRIAL CO-EFFICIENTS

The value of the density is calculated by using the ideal gas equation. However, the behaviour of the gas deviates from that of an ideal gas at high pressures and low temperature and virial co-efficient need to be employed to calculate the exact value of the density.Hence, virial co-efficient are employed in order to determine the density of the remaining exhaust gases once the water has condensed under pressure. The virial gas equation is as follows:

$$\boldsymbol{P = \rho RT(1 + B\rho)}$$

Equation 5-21: The Virial Coefficient Equation

P= Static Pressure of the Gas	T= Absolute Temperature of the Gas
R= Universal Gas Constant	B= First Virial Co-efficient

This forms a quadratic equation which determines at least one valid value of density. The values of these co-efficient are determined experimentally and they are a function of the gaseous specie and temperature. Data for the combustion gases virial co-efficient at a temperature of 500 K has been obtained from (Dymond et al., 2002)

The Absolute temperature **T** remains constant and is approximated at 500K. The value of the gas constant R is 8.314 Joules/mole/ Kelvin is used for calculation. The pressure exerted by the two gases varies according to their molar ratio as indicated in the stoichiometric combustion equation. The value for the first virial co-efficient of CO_2 and N_2 as well as their molar ratio in the stoichiometric combustion equation along with the pressure values are given in Table 5-11:

COMBUSTION GAS	DENSITY (Kg/m^3)	VIRIALCO-EFF (m^3/mol)	MOLAR RATIO	PRESSURE (Pa)
Carbon-di-Oxide	ρ_1	-30×10^{-6}	0.121	250000
Nitrogen	ρ_2	$+16 \times 10^{-6}$	0.747	250000

Table 5-11 : Parameters for Density Calculation

According to the virial co-efficient equation and the table above, the quadratic equation for CO_2 becomes

$$97.7235\ \rho_1^2 - 143500\rho + 250000$$

Equation 5-22: Virial Equation for CO_2

Similarly, the quadratic equation for N_2 becomes

$$82\ \rho_2^2 + 143500\rho - 250000$$

Equation 5-23: Virial Equation for N_2

This equation gives a density value of 2.148 Kg m^{-3} for N_2 and a density value of 3.416 Kg m^{-3} for CO_2 for the specifications above. The overall density of the gas is calculated according to the molar ratio of the two species. This has a value of 2.01 Kg m^{-3}.

5.9 CONCLUSION

The analysis presented in this chapter substantiates the hypothesis of moisture extraction from the exhaust gases which is achieved by operating a pre-designed mechanism for condensation. Numerical data validates the premise of

an inter-gaseous exchange of heat energy. This phenomenon will enhance the liquefying capacity of the exhaust water vapour within the engine. A promising effect of this study is that it provides evidence towards the transfer of heat from the water vapour to nitrogen and carbon-di-oxide. This would facilitate the water vapour to lose its latent heat and condense within the engine, by using the other two gases as an additional heat sink. The condensation of the water vapour within the exhaust eventually prevents contrail formation in the atmosphere which is the ultimate objective of this research. The transfer of heat from water to nitrogen also happens to be a favourable outcome since, amongst the three exhaust gases; nitrogen is the only gas that does not contribute to the greenhouse effect. The excitation energy of this system is provided by the latent heat of water. The energy released by water during condensation is absorbed by Nitrogen and Carbon-di-Oxide through the phenomenon described above.

A sum of all the energy levels expanded during excitation of the gaseous species CO_2 and N_2 equates to the latent heat of water which has a value of 35280 Joules per mole.

Detailed sum of the energy balance is as follows.

A. The energy absorbed by CO_2 in the anti-symmetric excitation mode is 28084 Joules per mole at an excitation frequency of 2349 per cm.

B. The energy transferred to N_2 in the vibrational mode equals 27868 Joules per mole at an excitation frequency of 2331 per cm.

C. The excess energy released during the above V-V relaxation equals 215 Joules per mole. This is the excess energy that is wasted but it is an insignificant amount compared to the magnitude of the latent heat of water.

Hence it is evident that A is a sum of B and C.

The molar latent heat of water at a design static temperature of 392 K is calculated to be 40209 J/mol. The energy that is transferred to the vibrational mode of N_2 with an energy value of 27868 Joules per mole accounts for nearly 70 percent of the latent heat of water.

The angle bending mode of CO_2 is also excited and absorbs an energy value of 7974 Joules per mole at an excitation frequency of 667 per cm. This amounts to nearly twenty percent of the latent heat of water. A fraction of this energy is then transferred to the translational mode of N_2 as well as to the translational mode of CO_2. This energy contributes to a gain in the speed of the Nitrogen gas.

Owing to the de-excitation of the angle bending mode of CO_2, 7420 Joules per mole are absorbed by N_2 and CO_2 in the translational mode at the stagnation temperature of the system. This value is calculated from Equation 5-11. This is

nineteen percent of the latent energy of water. Translation energy is only a function of temperature and results in a gain in kinetic energy of the gas. The translational energy can be absorbed by both N_2 and CO_2 in their respective translational modes. The absorption of this energy determines the exit conditions of the two gases.

This calculation accounts for eighty-nine percent of the latent heat of water. The remaining eleven percent of the latent of heat of water is absorbed by carbon-di-oxide in its rotational mode. This value amounts to 4435 Joules per mole as tabulated in Table 5-14. This absorption of energy results in a gain in the internal energy of the gas that is dissipated into the atmosphere.

Hence we conclude that the major bulk of the latent heat of water goes into a non-condensable, non-polar gas Nitrogen which when released into the atmosphere in the excited state does not contribute to the greenhouse effect. The remaining latent heat of water is used for a gain in speed of the exhaust gases exiting the nozzle in order to compensate for the thrust loss associated with use of this mechanism on the engine.

Since the two gases can exit at the sonic velocity, there happens to be an upper limit to the energy that is being absorbed in the translational mode. According to the equation of translation energy, N_2 and CO_2 will absorb an equal amount of translational energy per mole, and hence nineteen percent of the latent heat is absorbed equally between the two gases. However since the molar concentration of N_2 is nearly five times greater than CO_2, the translation energy will be distributed over a greater number of molecules (nearly 5 times) as compared to CO_2. However this shall be compensated by the fact that the CO_2 molecule is 1.5 times heavier than the N_2 molecule. It is assumed that both gases will exit together at the same velocity.

Hence we conclude with the hypothesis that the latent heat released by water at the condensation temperature can be absorbed by the vibrational modes of CO_2 and the translational mode of N_2 for excitation. The vibrational relaxation of CO_2 will then emit this energy that will either be absorbed by N_2 for translational excitation or increase the infra-red excitation of CO_2. Infra-red excitation in the translational mode will contribute to the phenomenon of greenhouse effect once the gas is released into the atmosphere.This study concludes by confirming the theory of gaseous heat transfer among the combustion gases and provides a firm groundwork for proceeding towards the design and development of an exhaust gas moisture extraction system.

WATER					
Frequencies per cm	1808.8498	3881.475	4023.5268		
IR Intensity (km/mol)	112.4133	16.9186	70.967		
Vib temperature (K)	2602.53	5584.57	5788.95		
Temperature 298.150 Kelvin. Pressure 1.00000 Atm				**Reference State**	
WATER	**E (Thermal)**	**CV**	**S**		**Q**
	KCal/Mol	**Cal/Mol-K**	**Cal/Mol-K**		
Total	15.665	5.986	46.404	Total V=0	0.253317D+09
Electronic	0	0	0	Vib (V=0)	0.100016D+01
Translational	0.889	2.981	34.608	Electronic	0.100000D+01
Rotational	0.889	2.981	11.793	Translational	0.300432D+07
Vibrational	13.887	0.025	0.003	Rotational	0.843039D+02
Temperature 500.000 Kelvin. Pressure 5.00 Atm.				**Excited State**	
WATER	**E(Thermal)**	**CV**			**Q**
	KCal/Mol	**Cal/Mol-K**	**Cal/Mol-K**		
Total	17.13	6.345	47.895	Total V=0	0.516550D+09
Electronic	0	0	0	Vib (V=0)	0.100797D+01
Translational	1.601	2.981	34.255	Electronic	0.100000D+01
Rotational	1.601	2.981	13.547	Translational	0.251483D+07
Vibrational	13.928	0.384	0.093	Rotational	0.203778D+03

Table 5-12: Thermo-chemistry of Water at the Condensation Temperature and Pressure

NITROGEN					
Frequencies per cm	2511.5347				
IR Intensity (km/mol)	0				
Vib temperature (K)	3613.53				
Temperature 298.150 Kelvin. Pressure 1.00000 Atm				**Reference State**	
NITROGEN	**E(Thermal)**	**CV**	**S**		**Q**
	KCal/Mol	**Cal/Mol-K**	**Cal/Mol-K**		
Total	5.072	4.97	45.787	Total V=0	0.306493D+09
Electronic	0	0	0	Vib (V=0)	0.100001D+01
Translational	0.889	2.981	35.924	Electronic	0.100000D+01
Rotational	0.592	1.987	9.862	Translatio	0.582553D+07
Vibrational	3.59	0.002	0	Rotationa	0.526118D+02
Temperature 500.000 Kelvin. Pressure 5.00 Atm.				**Excited State**	
NITROGEN	**E(Thermal)**	**CV**	**S**		**Q**
	KCal/Mol	**Cal/Mol-K**	**Cal/Mol-K**		
Total	6.267	5.076	46.621	Total V=0	0.462636D+09
Electronic	0	0	0	Vib (V=0)	0.100120D+01
Translational	1.601	2.981	35.571	Electronic	0.100000D+01
Rotational	1.067	1.987	11.032	Translatio	0.487637D+07
Vibrational	3.599	0.108	0.018	Rotationa	0.947595D+02

.

Table 5-13: Thermo-chemistry of Nitrogen at the Condensation Temperature and Pressure

CARBON-DI-OXIDE						
Frequencies per cm	852.6121	852.6121	1287.7277	2117.642		
IR Intensity (km/mol)	65.0174	65.0174	0	900.5457		
Vib temperature (K)	1226.72	1226.72	1852.75	3046.81		
Temperature 298.150 Kelvin. Pressure 1.00000 Atm					**Reference State**	
CARBON-DI-OXIDE	**E(Thermal) KCal/Mol**	**CV Cal/Mol-K**	**S Cal/Mol-K**			**Q**
Total	8.876	6.266	50.808		Total V=0	0.330338D+10
Electronic	0	0	0		Vib (V=0)	0.103560D+01
Translational	0.889	2.981	37.27		Electronic	0.100000D+01
Rotational	0.592	1.987	13.172		Translational	0.114679D+08
Vibrational	7.395	1.298	0.367		Rotational	0.278153D+03
Temperature 500.000 Kelvin. Pressure 5.00 Atm.					**Excited State**	
CARBON-DI-OXIDE	**E (Thermal) KCal/Mol**	**CV Cal/Mol-K**	**S Cal/Mol-K**			**Q**
Total	10.668		53.048		Total V=0	0.617816D+10
Electronic	0	0	0		Vib (V=0)	0.128467D+01
Translational	1.601	2.981	36.917		Vib (V=0)1	0.111338D+01
Rotational	1.067	1.987	14.341		Vib (V=0)2	0.111338D+01
Vibrational	8	3.64	1.791		Electronic	0.100000D+01
Vibration1	1.495	1.309	0.728		Translational	0.959943D+07
Vibration2	1.495	1.309	0.728		Rotational	0.500983D+03

Table 5-14: Thermo-chemistry of Carbon-di-Oxide at the Condensation Temperature and Pressure

298.15 K	1 ATM																						
GAS	E				Cv				S					Q									
		Trans	Rot	Vib	Total	Trans	Rot	Vib	Total	Trans	Rot	Vib	Total		Trans	Rot	Vib	Total					
				Kcal/mol				Cal/Mole.K				Cal/Mole.K					(V=0)	(V=0)					
H2O		0.889	0.889	13.888	15.665	2.981	2.981	0.025	5.986	34.608	11.793	0.003	46.404		3.00E+06	8.43E+01	1.00E+00	2.53E+08					
CO2		0.889	0.592	7.87	9.351	2.981	1.987	1.422	6.39	37.27	13.072	0.422	50.784		1.15E+07	2.65E+02	1.04E+00	3.17E+09					
N2		0.889	0.592	3.662	5.143	2.981	1.987	0.001	4.969	35.924	9.842	0	45.766		5.83E+06	5.21E+01	1.00E+00	3.03E+08					
O3		0.889	0.889	5.538	7.316	2.981	2.981	0.726	6.688	37.529	20.113	0.195	57.837		1.31E+07	5.55E+03	1.02E+00	7.38E+10					
O2		0.889	0.592	2.857	4.338	2.981	1.987	0.012	4.98	36.321	10.336	0.001	46.658		7.11E+06	6.68E+01	1.00E+00	4.75E+08					
563K	0.2467 ATM																						
GAS	E				Cv				S					Q									
		Trans	Rot	Vib	Total	Trans	Rot	Vib	Total	Trans	Rot	Vib	Total		Trans	Rot	Vib	Total					
				Kcal/mol				Cal/Mole.K				Cal/Mole.K					(V=0)	(V=0)					
H2O		1.678	1.678	13.939	17.295	2.981	2.981	0.442	6.404	40.548	13.688	0.113	54.348		5.97E+07	2.19E+02	1.01E+00	1.32E+10					
CO2		1.678	1.119	8.575	11.372	2.981	1.987	3.734	8.702	43.21	14.335	2.058	59.603		2.28E+08	5.00E+02	1.36E+00	1.55E+11					
N2		1.678	1.119	3.673	6.47	2.981	1.987	0.123	5.091	41.864	11.105	0.022	52.99		1.16E+08	9.83E+01	1.00E+00	1.14E+10					
O3		1.678	1.678	5.996	9.352	2.981	2.981	2.69	8.652	43.565	22.007	1.226	66.798		2.72E+08	1.44E+04	1.13E+00	4.63E+12					
O2		1.678	1.119	2.891	5.688	2.981	1.987	0.318	5.286	42.357	11.599	0.074	54.03		1.48E+08	1.26E+02	1.01E+00	1.88E+10					
218 K	0.235 ATM																						
GAS	E				Cv				S					Q									
		Trans	Rot	Vib	Total	Trans	Rot	Vib	Total	Trans	Rot	Vib	Total		Trans	Rot	Vib	Total					
				Kcal/mol				Cal/Mole.K				Cal/Mole.K					(V=0)	(V=0)					
H2O		0.889	0.889	14.416	16.194	2.981	2.981	0.023	5.985	34.608	11.754	0.003	46.365		3.00E+06	8.27E+01	1.00E+00	2.48E+08					
CO2		0.65	0.433	8.03	9.113	2.981	1.987	0.721	5.689	38.592	12.392	0.174	51.158		2.23E+07	1.88E+02	1.01E+00	4.25E+09					
N2		0.65	0.433	3.943	5.026	2.981	1.987	0	4.968	37.247	9.141	0	46.387		1.13E+07	3.66E+01	1.00E+00	4.62E+04					
O3		0.65	0.65	5.5	6.8	2.981	2.981	0.252	6.213	38.852	19.179	0.051	58.082		2.54E+07	3.47E+03	1.03E+00	8.85E+10					
O2		0.65	0.433	2.857	3.94	2.981	1.987	0.001	4.969	37.643	1.987	0.001	4.969		1.38E+07	4.88E+02	1.00E+00	6.75E+08					

Table 5-15: Thermal Energies and Partition Function of All Gases at the Original State of the Exhaust Plume and the Atmosphere

6 ENGINE PERFORMANCE

The Performance analysis for the contrail-free engine has been carried out using the performance software TurboMatch that been developed at the Propulsion Centre, SATM, Cranfield University. The baseline input file for the software has been extracted from the online data in the engine library for TurboMatch that is accessible through the Cranfield domain. It was originally developed by Dr. Junfei Yin and later adapted to simulate the performance of the contrail-free aero- engine. The simulation model for the contrail-free aero engine has been developed by the author with the assistance of Fernando Lartategui Atela, MSc student Thermal Power, Cranfield University,UK.

All input files have been coded and executed using TurboMatch version 1.0. The simulation is a standard three spool configuration with two separate exhaust nozzles based on the specifications of the Rolls-Royce Trent 900 engine. The baseline engine is not an exact match of the Trent 900 but is based on its standard specifications and configuration of the Trent 900. All data and results are based on a single engine analyses.

6.1 THE CONTRAIL FREE AEROENGINE WITH THE TURBOFAN CONFIGURATION

The analysis was initiated by carrying out the design point analysis of the three spool high bypass standard turbofan engine to establish the take-off rating. This analysis was then extrapolated by running off-design cases for all flight conditions. The off-design run data at cruise was used to setup a design point analysis at cruise. The design point case was matched to the off-design case in order to maintain the uniformity of the engine under test. Ideally, the off-design run at cruise should have been used to simulate the contrail-free engine. However due to the limitations of the TurboMatch code in calculating the saturated vapour pressure of water at a given temperature for condensation purpose, this data needs to be input manually by executing a design point case for every condition and then providing an input value of the saturated vapour pressure for the exhaust gas temperature calculated by the TurboMatch code. Henceforth, all design point cases at different flight conditions have been matched to their corresponding off-design runs.

The contrail-free engine has been simulated as a set of design points at different flight conditions. The region of interest lies in eliminating contrails during cruise flight; hence the design point run of cruise is used to simulate the contrail free engine performance. The baseline for this cruise DP run is obtained

from the turbofan OD A.1 simulation by running the turbofan engine off-design at Cruise. Data for other flight conditions was obtained with the same input file by changing the altitude, Mach number, mass flow and TET. Certain modifications have been made to the mass flow and TET for optimizing the cruise run in a design point configuration that can be used to simulate the contrail-free engine.

The input file for the cruise DP has been provided in A.2. The essential parameters for all flight conditions were obtained by OD runs of the turbofan baseline Trent 900 file as provided in A.1. However, there are limitations to simulating the engine with the device attached at off-design condition. Since the design of this engine is unconventional, TurboMatch is unable to calculate the operating pressure of the condensation device. This data need to be calculated independently and then has to be input manually for every design point run at all flight conditions. The design point input file for the contrail-free engine A.2 has been developed with the assistance of Dr. Theoklis Nikolaidis, Lecturer, Propulsion Centre, SATM, Cranfield University, UK.

The pressure gain in the device has been simulated by adding a duct (Ducter brick in the TurboMatch code) with a negative pressure factor which indicates a gain in pressure. The loss in mass flow due to the condensation of water has been simulated with a splitter (Premas brick in the TurboMatch code) that bleeds out the mass flow. The duct simulates the pressure that is generated by the device whereas the splitter reduces the mass flow according to the fraction of the exhaust gas that has condensed into water. Twenty percent of the compressed air from the HPC is bled out for blade cooling and has been coded in the program accordingly. An auxiliary work of 3.5 MW is introduced into the LPT. This is the power required to rotate the expeller vessel for generating the condensation pressure.

Table 6-1 tabulates the data obtained from the engine performance simulation of the conventional turbofan and the contrail-free aero-engine for the entire flight profile. The values of the contrail-free engine are calculated at design points for each flight condition as this happens to be a requirement due to the limitation of the code to simulate the contrail-free engine using off-design cases. Design-point data has been calculated and matched to the data generated by running the basic code at off-design for all flight conditions as has been appended in A.1.

Table 6-1 provides the results for simulating the turbofan engine with and without the device in order to obtain a comparative analysis. For the contrail-free engine, the device is attached after the LPT. The core nozzle is connected to the exit of the device. Hence the device is attached between the LPT and the core nozzle.

The simulation has been executed for the complete flight mission starting with take-off and ending at Glide. It has been observed that the thrust of the engine at various flight conditions does not change due to the attachment of the device. All engine parameters remain fairly constant. A different pressure gain factor needs to be applied in order to condense water at different flight condition. The gain factor indicates the pressure ratio that is required to be generated by the device in order to achieve condensation. The static pressure is the initial pressure value of the gas prior to the process of condensation whereas the static temperature is the temperature of the gas at which condensation is achieved by generating a pressure equal to the saturated vapour pressure of water at that temperature.

The main region of interest lies in the cruise condition. With reference to Table 6-1 it can be inferred that water is condensed in the cruise and glide conditions. In order to obtain water at take-off and climb, the thrust would need to be compromised due to the high TET, therefore a very minimal gain factor has been set and no water is obtained during these two conditions. This is because the engine is operating at its maximum TET in these cases.

A very high pressure gain is required to condense water at this temperature because the saturated vapour pressure of water increases exponentially with an increase in the temperature of the exhaust gas. A high value of pressure gain results in a decrease in the thrust of the engine and hence can compromise the take-off rating of the engine. In order to avoid this scenario, condensation of water has not been attempted in the take-off and the climb conditions.

The static temperature and pressure in the calculation indicate the values at the exit of the nozzle in the TurboMatch simulation. However, the total temperature at the LPT and nozzle exit is the same. Owing to a fairly low velocity of 150 m/s at the LPT exit there is only a difference of 10 K between the static and total temperature at this station. In addition to that, the rotor of the device also reduces the temperature of the gas such that it is nearly equal to the exit static temperature of the nozzle. This is because the temperature is determined by the residual energy of the exhaust gas which is the same in both cases. It is converted to thrust if the gas is made to pass through the nozzle. With the device attached, the gas flows through the rotor of the device that converts the residual energy into power. Hence the static temperature after the transfer of this energy is constant. The exit condition in both the cases does not change i.e. the gas can only expand to ambient conditions.

As for the static pressure, the static pressure at the LPT exit is greater than the static pressure at the nozzle exit without the device being attached. Hence we are at a safe limit if we consider the static pressure at the exit of the nozzle. In the case of the device being attached, the rotor shall expand the exhaust gas to

near ambient pressure which is the same as the condition at the exit of the choked nozzle. This justifies our assumption of using the static temperature and pressure values at the nozzle exit. This is merely a limitation of the simulation of the device within TurboMatch. For detailed thermodynamic calculations in Chapter 4, the actual static temperature and pressure values have been used.

A different gain factor needs to be applied at a different flight condition in order to condense water. It is dependent on the static pressure of the gas. A non-significant value of gain factor has been used for the take-off and climb conditions because condensation of water is not aimed at since the TET at these two conditions is at the maximum operating value. An extremely large value of gain factor would be required to achieve condensation in these two cases.

However, this is only possible if the static temperature of the gas entering the device is below the critical temperature of water. In the case of take-off and climb condition of the turbofan the static temperature of the gas is above the critical temperature of water. The critical temperature of water is 647 K. Hence no amount of pressure applied can change the state of the exhaust gas vapour into liquid water. The flight condition where condensation occurs is illustrated in Table 6-1.

Introduction of the device at a minimal gain factor results in a reduction in the thrust. However the thrust rating of the engine at take-off is nevertheless maintained which is crucial in order to ascertain that the addition of the device will not affect the performance of the engine even at flight conditions where condensation of water is not of interest. This is because the device operates as a fixed attachment and cannot be by-passed during any phase of flight. This reduction in thrust at take-off and climb condition is evident in Table 6-1.

As for the cruise condition, the engine can operate at a lower TET for the same value of thrust with the device attached whereas in the glide condition the amount of thrust increases with the introduction of the device when the engine is operating at the same TET. In a similar manner to the cruise condition, the same amount of thrust can be achieved in the glide condition with a reduction in TET. However owing to the limitations of the TurboMatch code converging at low power settings at design point, the TET was not changed in the glide condition and a higher value of thrust was obtained.

The SFC in the take-off and climb condition does not change primarily because a very insignificant value of gain factor has been used. However in the case of the cruise and the glide condition, a reduction in SFC is observed. This is because of the reduction in the operating TET at cruise which is directly proportional to the SFC for a given value of thrust. In the case of the glide

condition we achieve a higher thrust value at the same TET which again results in the reduction in SFC. The mass flow has been maintained at a constant value since it is a function of the altitude and the engine size and not of the flight condition.

TAKE-OFF	ALT 0 MACH 0.0						
ENGINE	TET (K)	THRUST (KN)	SFC(mg/Ns)	W	GAIN	t (K)	p (atm)
TURBOFAN	1800	346	8.585	1225		746	1
CONTRAIL-FREE TURBOFAN	1800	340.31	8.729	1225	-0.25	711	1
CLIMB	ALT 5000 MACH 0.65						
ENGINE	TET (K)	THRUST (KN)	SFC(mg/Ns)	W	GAIN	t (K)	p (atm)
TURBOFAN	1800	148.741	16.012	950		716	0.626
CONTRAIL-FREE TURBOFAN	1800	142.046	16.767	950	-0.25	662	0.555
CRUISE	ALT 10670 MACH 0.82						
ENGINE	TET (K)	THRUST (KN)	SFC(mg/Ns)	W	GAIN	t (K)	p (atm)
TURBOFAN	1575	65.615	16.31	525		586	0.269
CONTRAIL-FREE TURBOFAN	1500	66.255	14.407	525	-60	418	4.266
GLIDE	ALT 10000 MACH 0.5						
ENGINE	TET (K)	THRUST (KN)	SFC(mg/Ns)	W	GAIN	t (K)	p (atm)
TURBOFAN	1380	62.119	13.968	550		533	0.261
CONTRAIL-FREE TURBOFAN	1380	83.413	10.402	550	-10	352	0.475

Table 6-1: Engine Performance Simulation of the Conventional Turbofan and the Contrail-Free Turbofan at Various Flight Conditions

LEGEND
NO CONTRAILS
PRESSURE GAIN NOT APPLICABLE
ENGINE TYPE
FLIGHT CONDITION
ENGINE PARAMETERS
CALCULATED VALUES

SYMBOL	ENGINE PARAMETER
TET	Turbine Entry Temperature
SFC	Specific Fuel Consumption
W	Mass Flow
GAIN	Pressure Gain Factor
t	Static Temperature at nozzle exit
p	Static Pressure at nozzle exit

Table 6-2: Legend for Tabulated Results and Engine Parameter Symbols

6.1.1 PRESSURE AND TEMPERATURE DISTRIBUTION AT CORE ENGINE STATIONS FOR THE TURBOFAN CONFIGURATION

Data has been obtained for the simulation of the baseline Trent 900 specification turbofan engine through performance runs in TurboMatch. Engine performance has been simulated for the entire flight mission. An average value of altitude and Mach number has been used to simulate the climb and glide condition that has been tabulated in Table 6-1. The stagnation temperature and stagnation pressure profiles are illustrated in Figure 6-1, Figure 6-2, Figure **6-3** and Figure 6-4. These profiles explain the effect of the introduction of the device into the engine and the change in performance in the new engine schematics. It is important to note that only the core engine stations have been plotted since the device is attached to the core exhaust and the bypass stream remains unaffected. The legend for the station numbers is provided in Table 6-3. Station 13 and station 14 are introduced with the addition of the device. They do not exist in the simple turbofan configuration. Nozzle station number has been maintained at 15 in both cases.

With reference to the take-off condition illustrated in Figure 6-1 a reduction in temperature and pressure is observed at the LPT exit with the introduction of the expeller device. This is due to the auxiliary work that the turbine undertakes in order to rotate the centrifugal expeller vessel.

However, with reference to the power calculations the auxiliary work at 3.5 MW is a mere fraction of the take-off rating .The temperature drop is 47.69 K and the pressure loss is 0.3299 atm. However the thrust rating is not compromised. No water is extracted since we are operating at the maximum TET on ground. Hence a minimum gain factor is set for simulation which is generated due to the rotation of the device. This results in a pressure gain of 0.2621 atm downstream

of the LPT turbine which in real terms is the auxiliary work done by the LPT converted into a pressure gain as per the gain factor set.

TurboFan Component	Station Number	TurboFan Component	Station Number
Ambient	0	Combustor exit	8
Intake	1	HPT inlet/ Bleed air mixing	9
Fan inlet	2	IPT inlet	10
Fan exit/ Bypass inlet	3	LPT inlet	11
IPC inlet	4	LPT exit/ Rotor Duct inlet	12
HPC inlet	5	Rotor Duct exit/Splitter inlet	13
HPC exit/ Bleed for cooling	6	Splitter exit/Nozzle inlet	14
Combustor inlet	7	Nozzle exit	15

Table 6-3: Station Number Notation for the Conventional Turbofan and the Contrail-Free Turbofan Engine

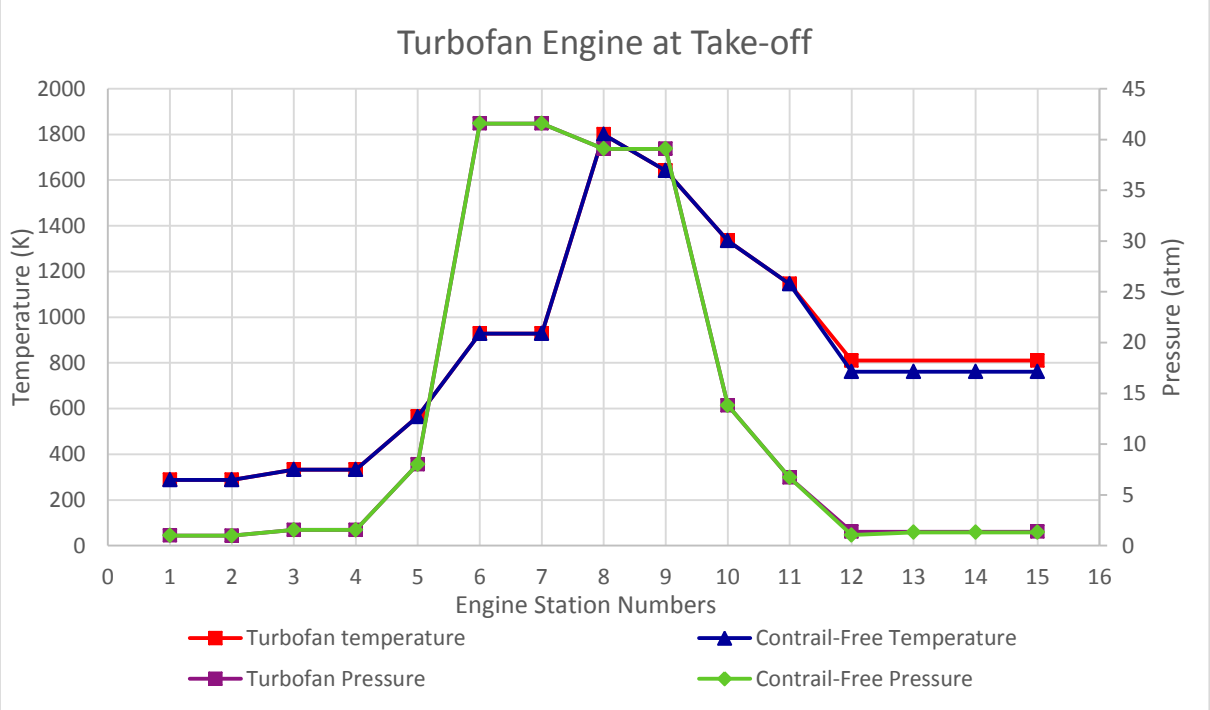

Figure 6-1: Temperature and Pressure Distribution at Engine Stations for the Conventional Turbofan and the Contrail-Free Turbofan at Take-Off

A similar behaviour is observed in the climb condition as illustrated in Figure 6-2 since the key parameters remain the same and again we are operating at the maximum TET, no mass flow condensation takes place and a minimal pressure gain is set for the device.

The shape of the two profiles in Figure 6-1 and Figure 6-2 is the same except that the maximum pressure achieved at the HPC exit is lower at the climb

condition due to the change in the ambient conditions when the aircraft is flying through a rarer atmosphere.

The cruise condition experiences a reduction in the operating TET when the device is attached to the engine as can be seen in Figure **6-3**. This results in lower temperature values at stations downstream of the combustor.

The effect of the auxiliary work on the temperature and pressure is more pronounced in the cruise flight condition primarily because it happens to be a greater fraction of the thrust in this case and is also enhanced by the reduction in the intake mass flow at the cruise altitude ambient condition.

The thrust at cruise is nearly reduced by a factor of 5 when compared to the take-off ground thrust. A reduction in the operating TET is accompanied by a reduction in the fuel flow. Hence the mass flow entering the turbine is reduced. However, the same amount of compressor work needs to be undertaken by the turbines and hence the pressure drop across all the three turbines is increased.

The additional pressure drop across the LPT (Station 11-12) is due to the effect of the auxiliary work performed by the LPT to rotate the expeller vessel. The steep rise in pressure beyond the LPT exit is due to the pressure generating functionality of the device and then a final pressure drop is experienced when the mass flow is reduced due to the condensation of water.

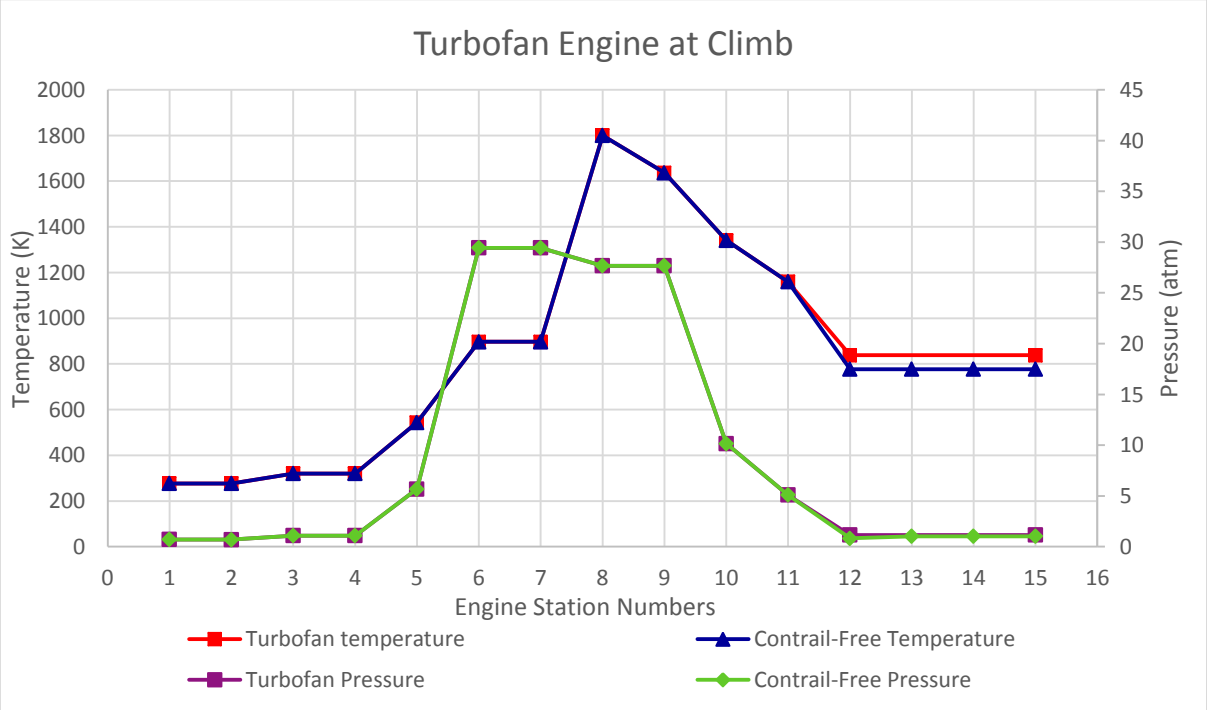

Figure 6-2: Temperature and Pressure Distribution at Engine Stations for the Conventional Turbofan and the Contrail-Free Turbofan at Climb

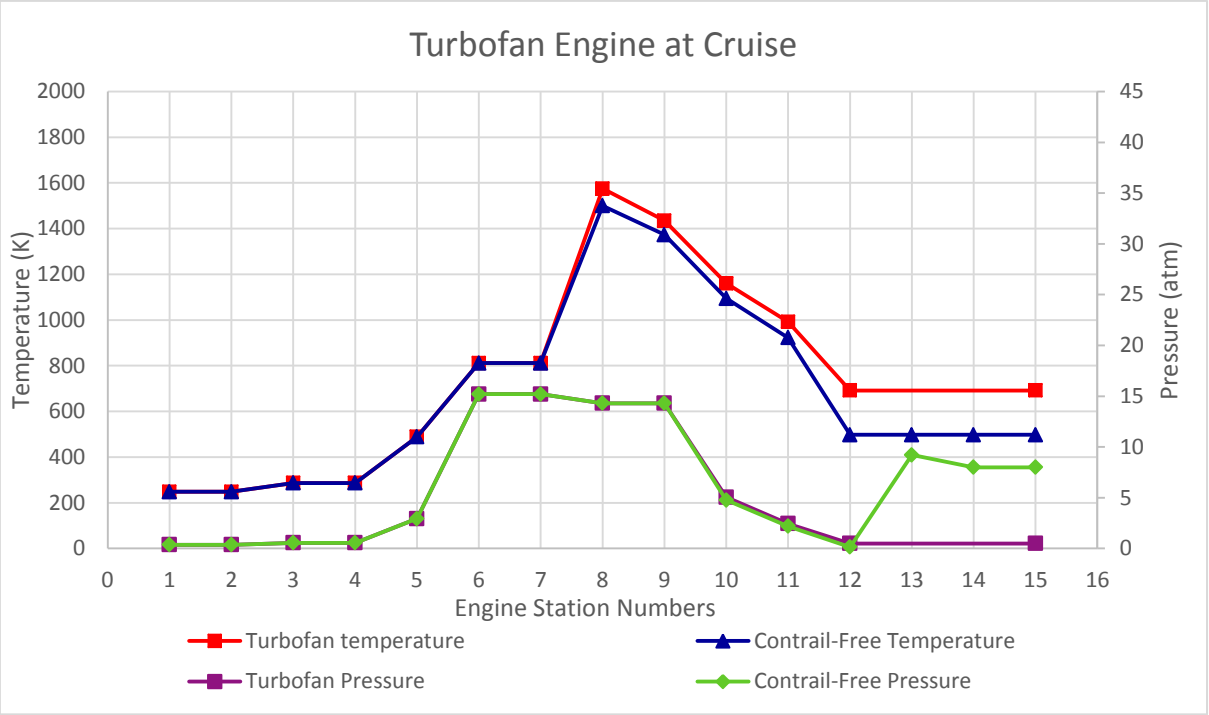

Figure 6-3: Temperature and Pressure Distribution at Engine Stations for the Conventional Turbofan and the Contrail-Free Turbofan at Cruise

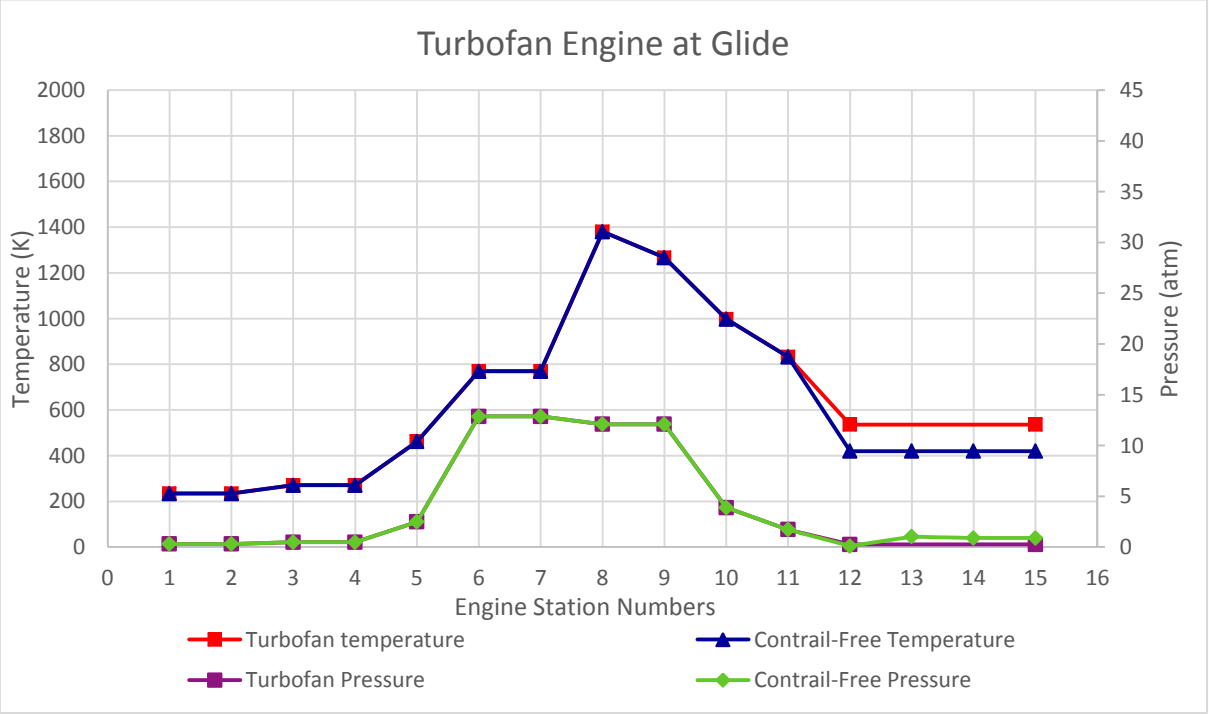

Figure 6-4: Temperature and Pressure Distribution at Engine Stations for the Conventional Turbofan and the Contrail-Free Turbofan at Glide

However, a residual stagnation pressure of 7.9 atm and a static pressure of 4.20 atm is observed at the nozzle exit. This might necessitate the requirement of a convergent-divergent nozzle. Another possibility could be to over expand the turbine to below ambient and then compress the flow such that it can exit through the standard convergent nozzle. This shall also allow further cooling of the gas flow.

The engine performance pattern at the glide phase is similar to the cruise phase as is indicated in the glide temperature and pressure profiles in Figure 6-4. Although the performance pattern is similar, the flight conditions are different in the two cases. Glide phase employs idle power settings during descent. No reduction in pressure is observed in the HPT and IPT. This is because we are operating at the same TET with and without the device. However the pressure drop across the LPT due to the auxiliary work is evident at the LPT exit (station 12) and then one can observe the effect of introducing the device on the pressure gain as well as the drop in the pressure once the water is extracted. The drop in temperature is only experienced at the LPT exit due to the auxiliary work involved and then the temperature remains unchanged downstream of the LPT.

6.2 THE CONTRAIL-FREE AEROENGINE WITH THE INTERCOOLED-RECUPERATED TURBOFAN CONFIGURATION

The analysis was initiated by carrying out the design point analysis of the three spool standard intercooled-recuperated turbofan engine to establish the take-off rating. This analysis was then extrapolated by running off-design cases for all flight conditions. The off-design run data at cruise was used to setup a design point analysis at cruise. The design point case was matched to the off-design case in order to maintain the uniformity of the engine under test. Ideally, the off-design run at cruise should have been used to simulate the contrail-free intrec engine. However due to the limitations of the TurboMatch code in calculating the saturated vapour pressure of water at a given temperature for condensation purpose, this data needs to be input manually by executing a design point case for every condition and then providing an input value of the saturated vapour pressure for the exhaust gas temperature calculated by the TurboMatch code. Henceforth, all design point cases at different flight conditions have been matched to their corresponding off-design runs.

The input file for the intercooled-recuperated turbofan engine A.3 has been created by including an intercooler and a recuperator to the existing turbofan Trent 900 file in order to maintain the same baseline specification and investigate the performance of an intercooled recuperated turbofan engine with

the attachment of the condensation device. A comparison can be drawn between the utilization of the simple turbofan engine and the intercooled recuperated configuration for the purpose of obtaining water during cruise flight conditions.

With reference to the TurboMatch simulation, a duct inserted between the LPT and the HPT compressor simulates the intercooler whereas the recuperator has been modelled as a heat exchanger with the cold side inserted between the HPC and the combustor and the hot side attached to the LPT exit. The cold stream for the intercooler is the bypass air flow and the hot stream is the compressed air from the LPC. In the case of the recuperator, the hot stream is the exhaust gas exiting the LPT and the cold stream is the pre-combusted air entering the combustor.

The input file for the contrail-free intercooled recuperated aero-engine A.4 has been created in exactly the same fashion as the contrail free file for the turbofan engine with the same baseline specifications in order to draw a clear and concise comparison between the two engines. The same brick elements have been added to both the original file.

The pressure gain in the device has been simulated by adding a duct (Ducter brick in the TurboMatch) with a negative pressure factor which indicates a gain in pressure and the loss in mass flow due to the condensation of water has been simulated with a splitter that bleeds out the mass flow (Premas brick in the TurboMatch code). The duct simulates the pressure that is generated by the device whereas the splitter reduces the mass flow according to the fraction of the exhaust gas that has condensed into water. The duct has been attached after the hot side of the recuperator which in reality indicates that the hot exhaust gas entering the device has undergone heat loss during recuperation and has transferred its heat to the pre-combusted air at the inlet to the combustor. Water loss has been simulated in a similar manner in both engines. An auxiliary work of 3.5 MW is introduced into the LPT. This is the power required to rotate the expeller vessel for generating the condensation pressure.

Table 6-4 tabulates the data obtained from the engine performance simulation of the intercooled-recuperated turbofan and the contrail-free intercooled-recuperated aero-engine for the entire flight profile. The values are calculated at design points for each flight condition as this happens to be a requirement due to the limitation of the code to simulate the contrail-free intrec engine using off-design cases. Design-point data has been calculated and matched to the data generated by running the basic code at off-design for all flight conditions as has been appended in A.3.Table 6-4 provides the results for simulating the intercooled recuperated engine with the device attached after the hot side of the recuperator such that the exhaust gas flow returning from the hot stream of the

recuperator enters the device. The core nozzle is connected to the exit of the device.

The simulation has been executed for the complete flight mission starting with take-off and ending at glide. It has been observed that the thrust of the engine at various flight conditions does not change due to the attachment of the device if the same TET is maintained in both the configurations i.e. with and without the device. All engine parameters remain fairly constant. A different pressure gain factor needs to be applied in order to condense water at different flight conditions. The gain factor indicates the pressure ratio that is required to be generated by the device in order to achieve condensation. The static pressure is the initial pressure value of the gas prior to the process of condensation once it has circulated through the hot side of the recuperating heat exchanger whereas the static temperature is the temperature of the gas at which condensation is achieved by generating a pressure equal to the saturated vapour pressure of water at the given temperature.

The main region of interest lies in the cruise condition. With reference to Table 6-4 it can be inferred that water is condensed in the cruise and glide conditions. In order to obtain water at take-off and climb, the thrust would need to be compromised due to the high TET, therefore a very minimal gain factor has been set and no water is obtained during these two conditions. This is because the engine is operating at its maximum TET in these cases. A very high pressure gain is required to condense water at this temperature because the saturated vapour pressure of water increases exponentially with an increase in the temperature of the exhaust gas. A high value of pressure gain results in a decrease in the thrust of the engine and hence can compromise the take-off rating of the engine. In order to avoid this scenario, condensation of water has not been attempted in the take-off and the climb conditions.

Although, unlike the turbofan engine, the nozzle exit temperature that is used as a reference for the LPT exhaust gas exit temperature is below the critical temperature of water to allow for the condensation to occur. This is because a temperature drop takes place when the core exhaust gas exiting the LPT is made to heat the pre-combusted compressed air that is entering the combustor. However, a high gain factor would need to be employed in order to generate pressure conducive to condensation. The phenomenon occurs in this configuration due to the involvement of the heat exchangers. The high gain factor will result in a reduction in thrust and a compromise on the take-off rating which is essentially not an option for take-off and climb.

The static temperature and pressure in the calculation indicate the values at the exit of the nozzle in the TurboMatch simulation. However, the total temperature at the LPT and nozzle exit is the same. Owing to a fairly low axial velocity of

150 m/s at the LPT exit there is only a difference of 10 K between the static and total temperature at this station. In addition to that, the rotor of the device also reduces the temperature of the gas such that it is nearly equal to the exit static temperature of the nozzle. This is because the temperature is determined by the residual energy of the exhaust gas which remains the same in both cases. It is converted to thrust if the gas is made to pass through the nozzle. With the device attached, the gas flows through the rotor of the device that converts the residual energy into power. Hence the static temperature after the transfer of this energy does not change. The exit condition in both the cases is the same i.e. the gas can only expand to ambient conditions.

As for the static pressure, the static pressure at the LPT exit is greater than the static pressure at the nozzle exit without the device being attached. Hence we are at a safe limit if we consider the static pressure at the exit of the nozzle. In the case of the device being attached, the rotor shall expand the exhaust gas to near ambient pressure which is the same as the condition at the exit of the choked nozzle. This justifies our assumption of using the static temperature and pressure values at the nozzle exit. This is merely a limitation of the simulation of the device within TurboMatch. For detailed thermodynamic calculations in Chapter 4, the actual static temperature and pressure values at the LPT exit have been used.

A different gain factor needs to be applied at a different flight condition in order to condense water. It is dependent on the static pressure of the gas. A non-significant value of gain factor has been used for the take-off and climb conditions because condensation of water is not aimed at since the TET at these two conditions is at the maximum operating value. Introduction of the device at a minimal gain factor results in a reduction in the thrust. However the thrust rating of the engine at take-off is nevertheless maintained which is crucial in order to ascertain that the addition of the device will not affect the performance of the engine even at flight condition where condensation of water is not of interest. This is because the device operates as a fixed attachment and cannot be by-passed during any phase of flight. The high gain factor will result in a reduction in thrust and a compromise on the take-off rating which is essentially not a viable option for take-off and climb.

In the case of the intercooled-recuperated engine, the thrust value is maintained during take-off and climb with the introduction of the device due to a minimal gain setting. The TET remains constant with and without the device. As for the cruise condition, the engine can also operate at the same TET with the device attached but experiences a slight decrease in thrust whereas in the glide condition the amount of thrust remains nearly constant with the introduction of the device. The SFC in the take-off and climb condition increases by a fraction

although a very insignificant value of gain factor has been used. However in the case of cruise and glide conditions, an increase in SFC is observed due to a reduction in thrust at a constant mass flow and a constant operating TET. The mass-flow has been maintained at a constant value since it is a function of the altitude and the engine size and not of the flight condition.

TAKE-OFF	ALT 0 MACH 0.0						
ENGINE	TET (K)	THRUST (KN)	SFC(mg/Ns)	W	GAIN	t (K)	p (atm)
INTERCOOLED-RECUPERATED	1700	353.123	8.693	1225		464	1.563
CONTRAIL-FREE INTREC	1700	351.354	9.059	1225	-0.25	448	1.528
CLIMB	ALT 5000 MACH 0.65						
ENGINE	TET (K)	THRUST (KN)	SFC(mg/Ns)	W	GAIN	t (K)	p (atm)
INTERCOOLED-RECUPERATED	1700	141.296	16.597	950		470	1.217
CONTRAIL-FREE INTREC	1700	141.044	17.431	950	-0.5	450	1.335
CRUISE	ALT 10670 MACH 0.82						
ENGINE	TET (K)	THRUST (KN)	SFC(mg/Ns)	W	GAIN	t (K)	p (atm)
INTERCOOLED-RECUPERATED	1550	65.413	17.644	525		436	0.609
CONTRAIL-FREE INTREC	1550	61.989	20.449	525	-8.5	399	2.6
GLIDE	ALT 10000 MACH 0.5						
ENGINE	TET (K)	THRUST (KN)	SFC(mg/Ns)	W	GAIN	t (K)	p (atm)
INTERCOOLED-RECUPERATED	1200	71.015	13.816	550		350	0.261
CONTRAIL-FREE INTREC	1200	69.789	15.688	550	-3	301	0.261

Table 6-4: Engine Performance Simulation of the Conventional Intrec and the Contrail-Free Intrec at Various Flight Conditions

LEGEND
NO CONTRAILS
PRESSURE GAIN NOT APPLICABLE
ENGINE TYPE
FLIGHT CONDITION
ENGINE PARAMETERS
CALCULATED VALUES

SYMBOL	ENGINE PARAMETER
TET	Turbine Entry Temperature
SFC	Specific Fuel Consumption
W	Mass Flow
GAIN	Pressure Gain Factor
t	Static Temperature at nozzle exit
p	Static Pressure at nozzle exit

Table 6-5: Legend for Tabulated Results and Engine Parameter Symbols

6.3 PRESSURE AND TEMPERATURE DISTRIBUTION AT CORE ENGINE STATIONS FOR THE INTERCOOLED RECUPERATEDTURBOFAN CONFIGURATION

The intercooled-recuperated turbofan engine has been developed on the baseline Trent 900 specifications turbofan engine by introducing an intercooler between the IPC and HPC to decrease the temperature of the compressed air entering the HPC, and a recuperator after the LPT exit that uses the hot core exhaust gas to heat the pre-combusted air entering the combustor from the HPC. Performance runs for the intercooled-recuperated configuration of a baseline turbofan have been executed in TurboMatch. In a similar manner to the turbofan, engine performance has been simulated for the entire flight mission. An average value of altitude and Mach number has been used to simulate the climb and glide condition, since the altitude and Mach number are changing continuously at these two conditions and this has been tabulated in Table 6-4. The stagnation temperature and stagnation pressure profiles are illustrated in Figure 6-5, Figure 6-6, Figure 6-7 and Figure 6-8.

These profiles explain the effect of the introduction of the device into the intercooled- recuperated engine and the change in performance in the new engine schematics. It is important to note that only the core engine stations have been plotted since the device is attached to the core exhaust and the bypass stream remains unaffected. The legend for the station numbers is provided in Table 6-6. Station 16 and station 17 are introduced with the addition of the device. They do not exist in the simple intercooled-recuperated configuration. Nozzle station number has been maintained at 18 in both cases. The performance of the intercooled-recuperated configuration has been analysed with the expeller device attached in order to determine the best configuration among the two engine schematics options that can be adopted if the device is meant to be attached to the engine. The device in this case is

attached at the exit of the recuperator. This implies that the core exhaust gas exiting the LPT has transferred some of its energy to the pre-combusted air and hence the gas enters the device at a lower temperature than if introduced directly from the LPT exit.

Intercooled -Recuperated Component	Station Number	Intercooled -Recuperated Component	Station Number
Intake	1	Combustor exit	10
Fan inlet	2	HPT inlet/ Bleed air mixing	11
Fan exit / Bypass inlet	3	IPT inlet	12
IPC inlet	4	LPT inlet	13
Intercooler inlet	5	LPT exit/Recuperator inlet (hot side)	14
Intercooler exit/HPC inlet	6	Recuperator exit (hot side)/Rotor duct inlet	15
HPC exit/ Bleed for Cooling	7	Rotor Duct exit/Splitter inlet	16
Recuperator inlet (cold side)	8	Splitter exit/Nozzle inlet	17
Recuperator exit/Combustor inlet	9	Nozzle exit	18

Table 6-6: Station Number Notation for the Conventional Intrec and the Contrail-Free Intrec Engine

With the device attached to the intercooled-recuperated engine, the maximum operating TET does not change at take-off as has been illustrated in Figure 6-5. This has been done to maintain the thrust rating in both cases although the take-off rating is 4 % higher than that of the simple turbofan configuration. This difference is acceptable since the weight of the intercooler and the recuperator heat exchangers needs to be compensated for. This issue has been discussed in Chapter 6 with reference to aircraft performance. With the device attached a reduction in temperature of 45 K is observed at the LPT exit due to the auxiliary work of 3.5 MW involved for rotating the expeller vessel of the device. This also reduces the temperature at the combustor inlet (station 9).Beyond the hot side recuperator exit (station 15), the temperature drop remains constant at 18 K. The reduction in temperature in both cases between station 5 and station 6 is due to the presence of the intercooler. The pressure across the intercooler does not change. The effect of the recuperator in the two cases is indicated between station 8 and station 9. A minimal pressure loss is also indicated. The overall pressure change is not significant in this case when the device is attached since water is not condensed at take-off and hence no mass flow reduction occurs. A drop in pressure of 0.65 atm is observed only at the exit of the LPT (station 14) because of the auxiliary work involved. An increase in pressure occurs across the device's expeller vessel (station 15 to station 16) due to the rotation of the vessel that is simulated as a pressure gain across the duct. The pressure increases back to the original value that is the same as the nozzle exit pressure without the device attached. As the temperature is lower at the inlet of the combustor due to the introduction of the device, the fuel flow through the

combustor is higher. This increases the SFC when the device is introduced while the thrust remains the same.

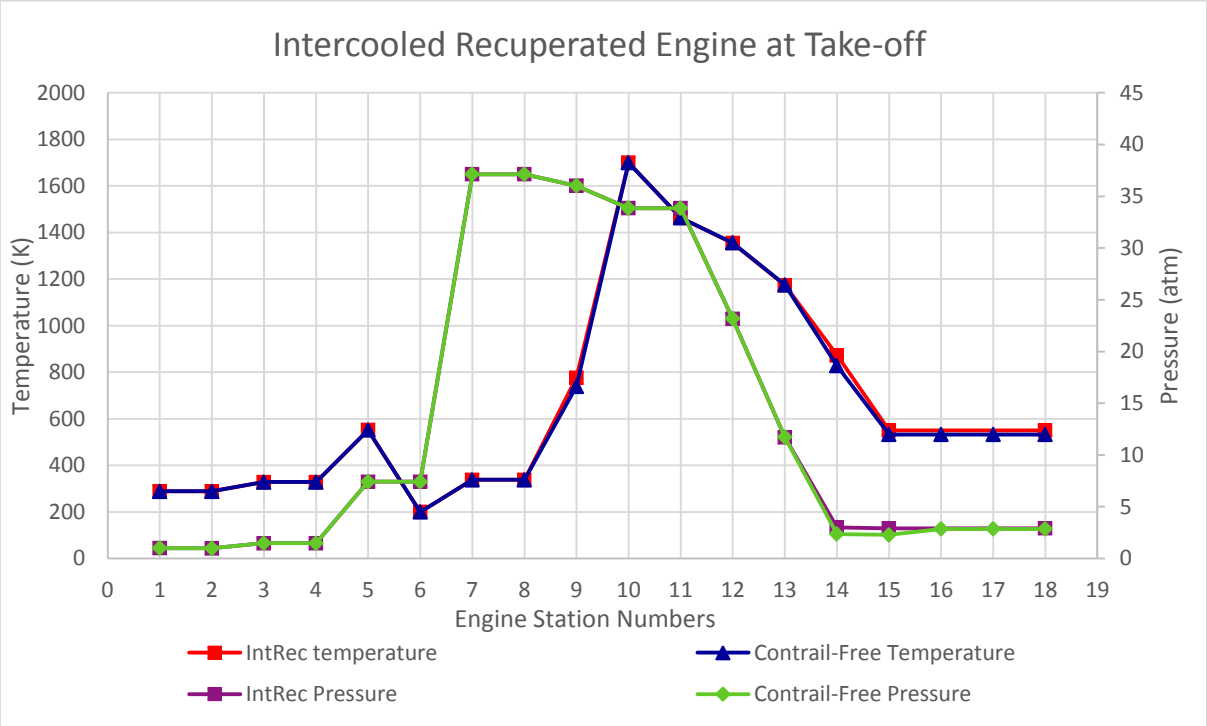

Figure 6-5: Temperature and Pressure Distribution at Engine Stations for the Conventional Intrec and the Contrail-Free Intrec at Take-Off

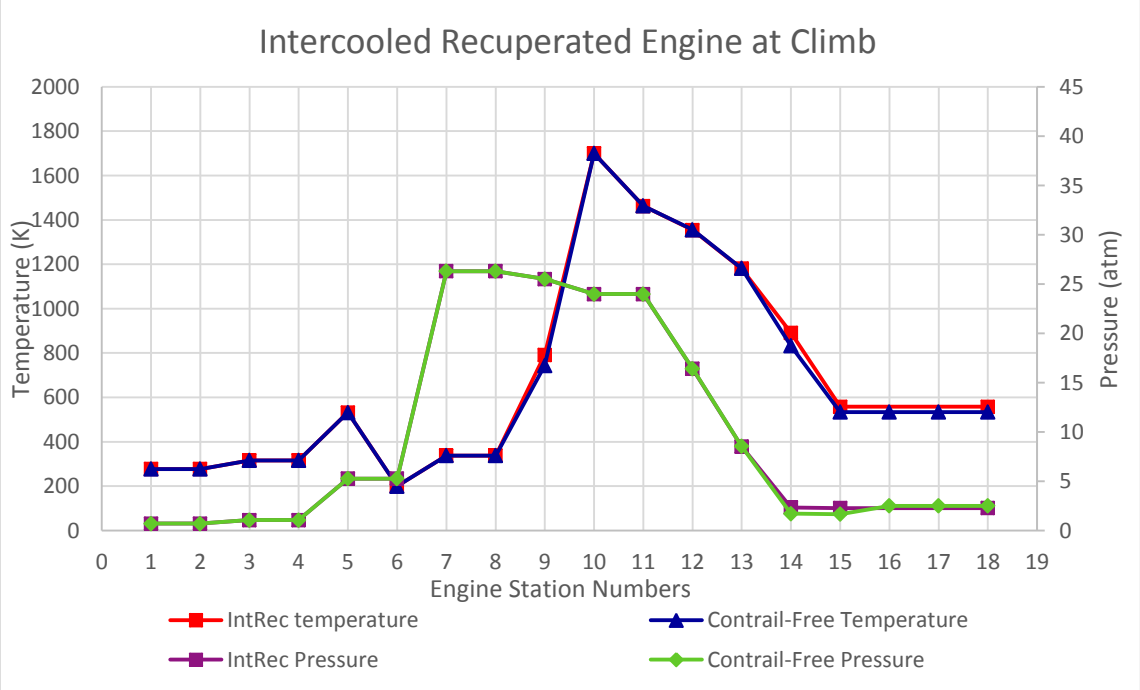

Figure 6-6: Temperature and Pressure Distribution at Engine Stations for the Conventional Intrec and the Contrail-Free Intrec at Climb

A similar behaviour is observed in the climb condition as illustrated in Figure 6-6 since the key parameters remain the same and again we are operating at the maximum TET, no mass flow condensation takes place and a minimal pressure gain is set for the device. The shape of the two profiles in Figure 6-5 and Figure 6-6 is the same except that the maximum pressure achieved at the HPC exit is lower at the climb condition due to the change in the ambient conditions when the aircraft is flying through a rarer atmosphere. The pattern remains the same as in take-off and only the pressure profile gets compressed with an overall reduction in the values of temperature and pressure during climb condition due to a change in altitude. The operating TET in the cruise condition does not change when the device is attached to the engine as can be seen in Figure 6-7.The effect of the auxiliary work on the temperature and pressure is more pronounced in the cruise flight condition primarily because it happens to be a greater fraction of the thrust in this case and is also enhanced by the reduction in the intake mass flow at the cruise altitude ambient condition.

The thrust at cruise is nearly reduced by a factor of 5 when compared to the take-off ground thrust. The temperature and pressure drop across the LPT (Station14 to Station15) is due to the effect of the auxiliary work performed by the LPT to rotate the expeller vessel of the device. The pressure drop across the LPT exit and the recuperator exit is 0.018 atm when the device is attached and 0.0354 without the device being attached. The temperature difference at the recuperator exit is 43 K between the two cases. This temperature difference remains constant till the exhaust gases exit the nozzle. The rise in pressure beyond the LPT exit is due to the functionality of the device and then a final pressure drop is experienced when the mass flow is reduced due to the condensation of water. There lies a temperature difference of 89 K at the inlet to the combustor. The temperature in this case is higher without the device. This fact implies that the fuel flow introduced into the combustion chamber would be increased when the device is attached and for the same cruise thrust, the SFC would be higher.

The engine performance pattern at the glide phase is similar to the cruise phase as is indicated in the glide temperature and pressure profiles in Figure 6-8. Although the performance pattern is similar, the flight conditions are different in the two cases. Glide phase employs idle power settings during descent. No reduction in pressure is observed in the HPT and IPT. This is because we are operating at the same TET with and without the device. However the pressure drop across the LPT due to the auxiliary work is evident at the LPT exit (station 14). It is difficult to observe the effect of introducing the device on the pressure gain as well as the drop in the pressure once the water is extracted.

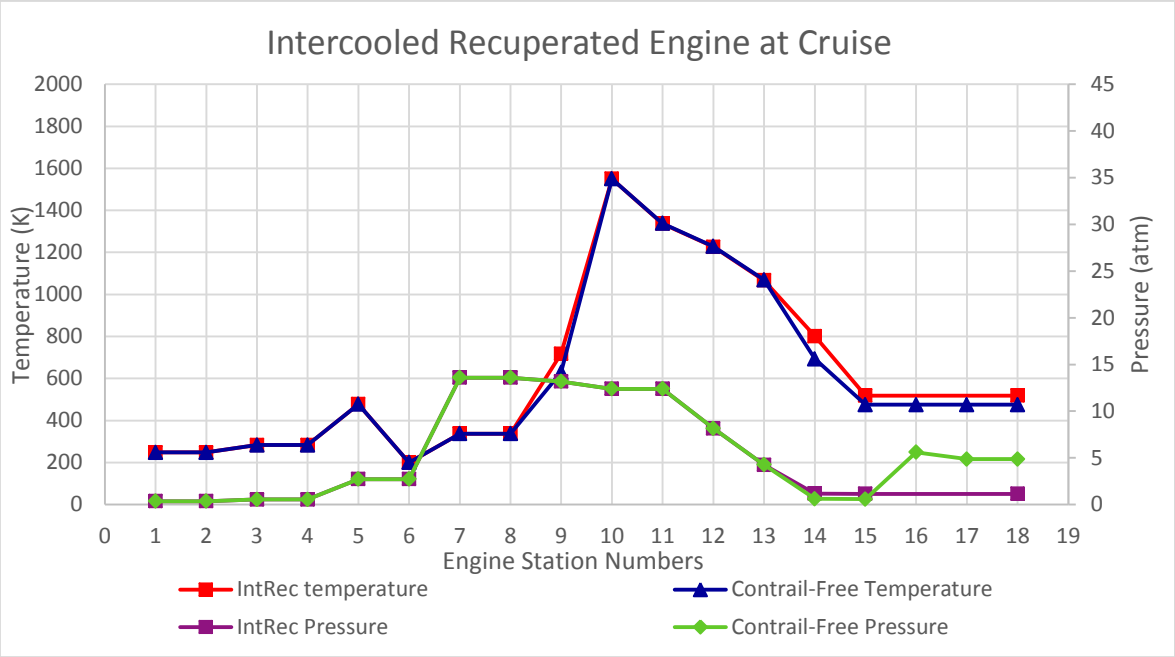

Figure 6-7: Temperature and Pressure Distribution at Engine Stations for the Conventional Intrec and the Contrail-Free Intrec at Cruise

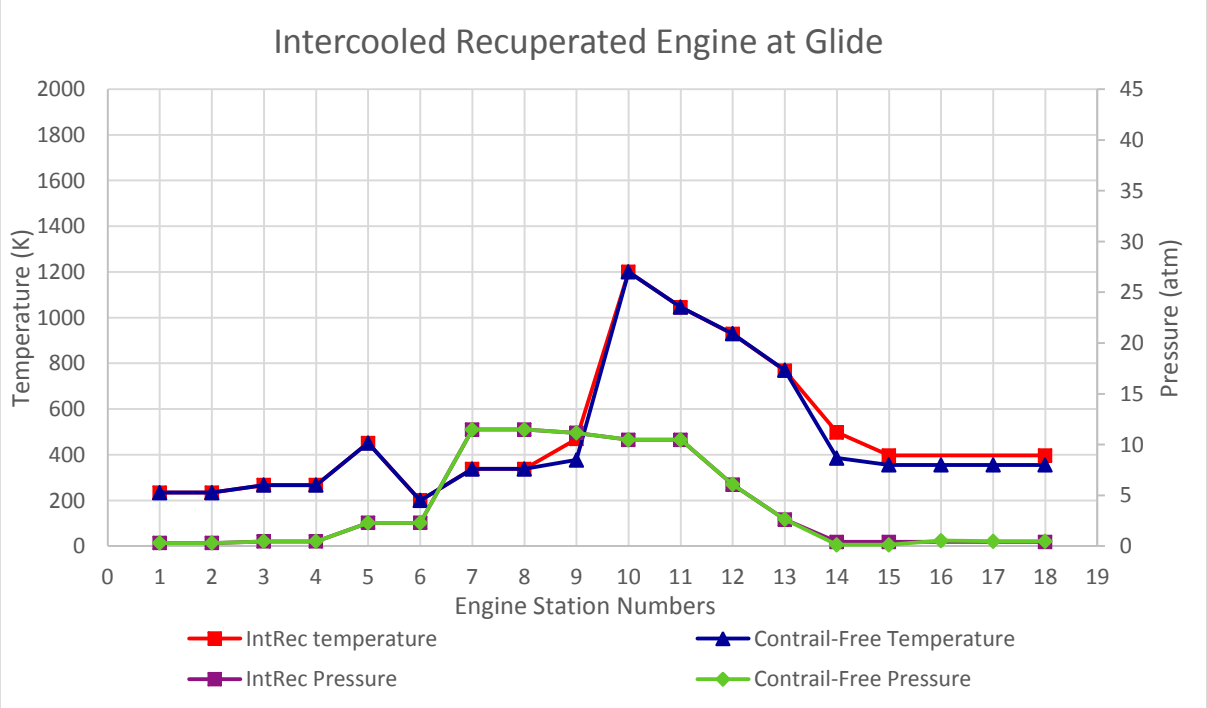

Figure 6-8: Temperature and Pressure Distribution at Engine Stations for the Conventional Intrec and the Contrail-Free Intrec at Glide

This is because a low value of pressure gain is used and the engine is already operating at a low value of TET of 1200K. The effect of the auxiliary work is very prominent in this case. The drop in temperature is only experienced at the LPT exit and at the exit of the recuperator due to the auxiliary work involved and then the temperature remains unchanged downstream.

However, a residual stagnation pressure of 4.87 atm and a static pressure of 2.6 atm is observed at the nozzle exit. This might necessitate the requirement of a convergent-divergent nozzle. Another possibility could be to over expand the turbine to below ambient and then compress the flow such that it can exit through the standard convergent nozzle. This shall also allow further cooling of the gas flow.

6.4 COMPARISON FOR THE CONTRAIL-FREE AERO ENGINE WITH THE TURBOFAN AND THE INTERCOOLED RECUPERATED CONFIGURATION

The attachment of the device for the purpose of water condensation is practical for both the configurations as has been analysed and tabulated. However, the intercooled recuperated configuration is more complex in terms of core flow paths and has a weight penalty of nearly 1500 Kg (Camilleri, Ogaji and Pilidis, 2011). This has been accommodated for in the Aircraft performance analysis in Chapter 7.

Both the engines match the thrust rating specification with the device attached. However a lower value of TET is required by the intercooled-recuperated at all flight conditions as compared to the turbofan engine. This is primarily because of the presence of the recuperator that enables the exhaust gas to achieve a comparatively lower temperature at the engine exit. As a result of this reduction in temperature, a lower pressure gain is required to achieve condensation of water with the intercooled-recuperated configuration. Hence the power input to drive the centrifugal water expeller is reduced if it is integrated with an intercooled-recuperated engine as compared to the standard turbofan engine.

Take-off and Climb conditions employ the maximum TET and therefore are not evaluated for water condensation. The SFC in both the cases remains the same for the take-off and the climb condition where only a minimal gain factor is employed and water is not condensed. Hence there is no loss of mass-flow in these two cases. The nozzle exit pressure is higher by a factor of 1.5 for the intercooled recuperated engine as compared to the turbofan engine. This is valid with and without the condensation device attached. This is because of the employment of the intercooler in between the IPC and the HPC. The intercooler reduces the overall compressor work that has to be undertaken by the turbines.

As a result, more residual energy is available in the gas exiting the turbine and entering the core nozzle.

Water condensation is achieved in the cruise and glide condition for both configurations. Again the intercooled-recuperated engine operates at a lower TET compared to the Turbofan. A reduction in TET is also experienced during the cruise phase in the case of the turbofan when simulated with the device attached. This is because of the pressure gain simulated with the introduction of the device which reduces the operating TET and SFC for a constant value of thrust. However a 6% reduction in thrust is experienced for the intercooled recuperated engine during the cruise phase when operating at a fixed TET. The TET has not been changed because it is difficult to achieve convergence with this complex configuration.

The difference in the pressure gain required at cruise condition varies by a factor of 7 among the two engines. The intercooled recuperated engine requires a very low value of pressure gain which is the probable cause of a thrust loss during the cruise phase. The SFC is higher in the intercooled-recuperated engine compared to the turbofan and increases with the addition of the device. The static temperature at the nozzle exit is lower with the Intercooled-recuperated engine at all flight conditions due to the lower operating TET and the presence of the recuperator. This temperature further reduces when the device is attached. The static temperature decreases with an increase in the gain factor. Static Pressure at the nozzle exit is higher with intercooled-recuperated engine in comparison to the turbofan. This pressure further increases according to the gain factor used in both cases which is dependent on the static temperature that determines the saturated vapour pressure of water at which a phase change would occur.

A similar behaviour is observed at Glide condition. However the same TET is maintained with and without the device in order to avoid convergence issues at low power settings. This results in an increase in thrust when the device is attached in the case of the turbofan engine. The thrust does not change for the intercooled-recuperated engine during the glide phase. Reduction in SFC happens when the device is attached to the turbofan and whereas the SFC of the intercooled-recuperated engine is the same with and without the device. The gain factor for the turbofan is higher by a factor of 4. The static temperature at nozzle exit for the turbofan is higher than that of the intercooled-recuperated engine, whereas the static pressure is the same in this condition and increases in both cases with the addition of the device.

An overall reduction in thrust is experienced by the intercooled-recuperated engine during the cruise and glide phase with the attachment of the device due to a loss in mass flow once the condensation of water occurs. As a result a

slight increase in SFC is also experienced. The take-off and climb thrust remain unaffected by the attachment of the device since water is not extracted in these two phases of flight. As for the Turbofan configuration, an increase in thrust and a reduction in SFC is experienced for the cruise and glide condition where water is condensed and vice versa for the take-off and glide condition where water is not extracted from the flow.

7 AIRCRAFT PERFORMANCE

An extensive aircraft performance analysis was carried out with a three spool high bypass turbofan engine based on Trent 900 engine specifications. This engine was integrated to a large wide-body aircraft similar to the A380 basic configuration in order to analyse the performance of the aircraft with the contrail-free engine. The baseline engine is not an exact match of the Trent 900 but is based on the standard specifications and configuration of the Trent 900. Similarly, the baseline aircraft is not an exact match of the A380-800 but is based on the standard specifications and configuration of the A380-800 aircraft. All data and results are based on a single engine analyses.

This analysis has been carried out using the in-house aircraft performance analysis software Hermes that has been developed at the Propulsion Centre, Department of Aerospace Engineering, and Cranfield University. This part of the research has been conducted as a joint project with the MSc student Fernando Lartategui Atela and the preparation of this chapter has been a collaborative effort between the author and the student. Further details of aircraft performance integrated with the contrail-free engine can be found in (Atela.F, 2016)

Parameter	Symbol	Definition	Notations
Lift coefficient	C_L	$C_L = \frac{2\,m\,g}{\rho\,{V_{TAS}}^2\,S\cos(\phi)}$	Φ= *Bank Angle* *mg=aircraft weight*
Lift	L	$L = \frac{C_L\,\rho\,{V_{TAS}}^2\,S}{2}$	ρ= *Air Density* *S= Wing Area*
Drag coefficient	C_D	$C_D = C_{D0} + C_{Dl}\,(C_L)^2$	C_{DO}=*Profile Drag*
Drag	D	$D = \frac{C_D\,\rho\,{V_{TAS}}^2\,S}{2}$	C_{Dl}= *Lift Induced Drag*

Table 7-1: Definition of Flight Parameters

Parameter	Definition
Indicated Airspeed (IAS)	$IAS = AirSpeedReading - mechanical\ calibration\ error$
Calibrated Airspeed (CAS)	$CAS = IAS - Pitot\ static\ pressure\ calibration\ errors$
Equivalent Airspeed (EAS)	$EAS = CAS - Compressibility\ effect$
True Airspeed (TAS)	$TAS = EAS - Air\ density\ change\ with\ altitude$

Table 7-2: Definition of Flight Speeds

Table 7-1 and Table 7-2 have been introduced to define the various flight parameters that shall be used in the discussion that follows in this chapter(Jenkinson, 1999).

7.1 TURBOFAN ENGINE INTEGRATED WITH THE AIRCRAFT

A standard three-spool turbofan engine based on the Trent 900 specifications has been incorporated into the conventional airframe geometry based on A380-800 specifications. The aircraft performance has been analysed and then compared against the performance of the contrail-free three-spool turbofan engine integrated to the same aircraft. All baseline parameters have been maintained in both configurations. The contrail-free engine refers to the baseline turbofan engine with the water expelling device attached to it which results in a subsequent change in the engine geometry. This entails an increase in the engine length and engine weight while maintaining all other parameters constant.

7.1.1 PERFORMANCE INPUT FOR THE AIRCRAFT AND THE TURBOFAN ENGINE

The aircraft performance analysis software HERMES requires two sets of input for program execution. This includes the geometric data and mission data for the aircraft as well as engine performance data for the entire mission profile.

The geometric file was tabulated for the aircraft based on A380 published data(Jane, 2010). This file was adapted from the Boeing 737 baseline specification geometric input file that exists in the HERMES software library. The input to the aircraft file B.1 includes aircraft geometry, specifications and details of the mission profile, ambient conditions for each flight phase, engine geometric data and engine thermodynamic data.

The engine input file B.2 requires data for engine performance that is obtained by the execution of the turbofan engine performance code A.1 with additional off-design conditions introduced for the entire mission profile. This data has been extracted through the TurboMatch execution and includes thrust, SFC, altitude, Mach number and TET. The data obtained was tabulated manually for the engine input file B.2.

7.1.2 PERFORMANCE OUTPUT FOR THE AIRCRAFT AND THE TURBOFAN ENGINE

Two sets of outputs have been obtained. One set of results provides data on the aircraft performance throughout the flight mission and the variation of aircraft performance parameters. This is called the aircraft flight path

performance output file B.2.1. The other set of results provide data on the engine performance throughout the flight mission and indicates changes in engine performance with a change in flight condition. This is called the engine flight path performance file B.2.2.

The results of the aircraft performance at each flight segment have been plotted. This includes the aircraft aerodynamic parameters and the engine parameters. A baseline run was executed for the conventional aircraft using the basic three spool turbofan engine configuration and benchmark values were obtained. The contrail free engine was then simulated by increasing the weight and length of the engine in the geometric input file B.1 for the HERMES software.

The initial estimate for the increase in length was 2 meters whereas that for the increase in weight was 2000 kg. This modification accounts for a 31% increase in engine weight and a 44% increase in engine length. The change in the aircraft take-off weight is only 1.4 % with four engines on board. The code was executed for both cases and a comparative analysis was drawn by plotting the conventional engine as well as the contrail-free engine with the device attached. This has been done for each flight phase separately with flight segments indicating the altitude of flight. The change in engine and aircraft parameters for all flight conditions has been discussed independently.

In the case of the basic turbofan, certain convergence issues arose during the calculation of the lift coefficient and the drag coefficient with the addition of 2000 kg of weight and 2 m of length to the original three spool turbofan engine geometry. Hence, for these two cases the weight was reduced to 1500 kg and the length was reduced to 1.4 m and the analysis was carried out to determine the coefficients. The results in this case met expectation and had logical values.

Although the difference between the basic turbofan and the contrail-free engine would be greater with the actual length and weight change, nevertheless the results are comparable and provide a basic overview of the behaviour of the engine with a change in geometry on the lift coefficient and the drag coefficient. Henceforth, all plots illustrating lift and drag coefficients for the turbofan configuration have been defined using the reduced engine length (1.4 m) and weight (1500 kg). The remaining plots use the initial estimates for length (2 m) and weight (2000 kg) addition.

This is a very minimal change in comparison to the overall engine weight and wetted area. These changes have only been applied to the basic turbofan configuration, whereas the intercooled-recuperated configuration has been analysed on initial estimates of length and weight addition.

7.1.2.1 CLIMB

Table 7-3 indicates the climb altitude and Mach number for each climb segment. This enables us to interpret the output plots with reference to the operating altitude. Data has been plotted versus Mach number instead of altitude for clarity of illustration.

A step change occurs for the lift coefficient, drag coefficient and the overall nacelle drag at segment 8 at an altitude of 3048 meters. This is because the aircraft climbs at a constant EAS of 128.6 m/s (250 knots) up to this altitude.

This speed is maintained at a constant value for noise restrictions close to ground. Then the aircraft accelerates to 164.6m/s (320 knots) and continues to climb to cruise Mach number of 0.8 which is achieved at an altitude of 8077.2 m at segment 15. A constant Mach number is then maintained in order to avoid approaching the critical Mach number. The maximum operating Mach for the A380 is 0.89.The critical Mach 1 at the throat of the intake due to ram pressure can result in choking of the flow.

Climb Segment	Altitude (m)	Mach number	Climb Segment	Altitude (m)	Mach number
0	0	-	9	3657.6	0.6063
1	557.2	0.3905	10	4267.2	0.6308
2	900	0.3987	11	4876.8	0.6567
3	1500	0.4135	12	5486.4	0.6842
4	1981.2	0.426	13	6096	0.7132
5	2438.4	0.4383	14	7620	0.7936
6	2743.2	0.4468	15	8077.2	0.8
7	3048	0.4555	16	9144	0.8
8	3048	0.583	17	10058	0.8

Table 7-3: Climb Altitude at Each Climb Segment Number for the Turbofan Engine

Figure 7-1 illustrates the change in Mach number with an increase in altitude during the climb phase. The Mach number increases continuously during climb starting from 0.3905 until it attains the initial cruise Mach number of 0.8. A step change is observed at an altitude of 3048 m where the aircraft accelerates from an EAS of 250 knots to 320 knots. The altitude remains constant during this acceleration.

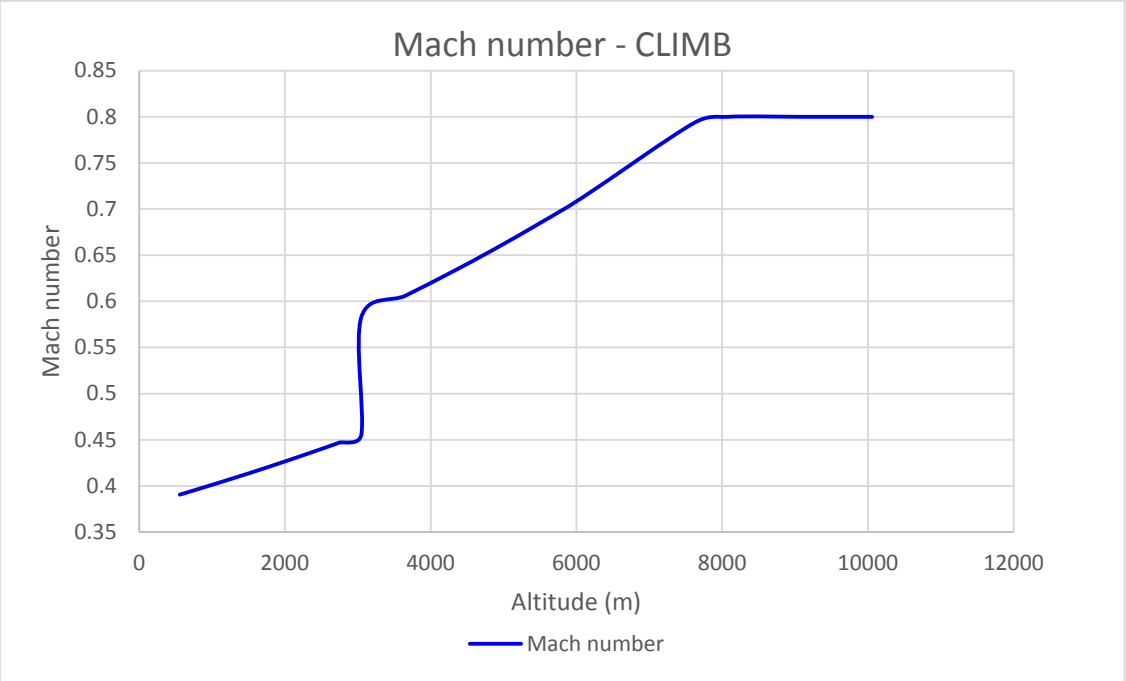

Figure 7-1: Mach Number Variation with Altitude during Climb for the Turbofan Engine

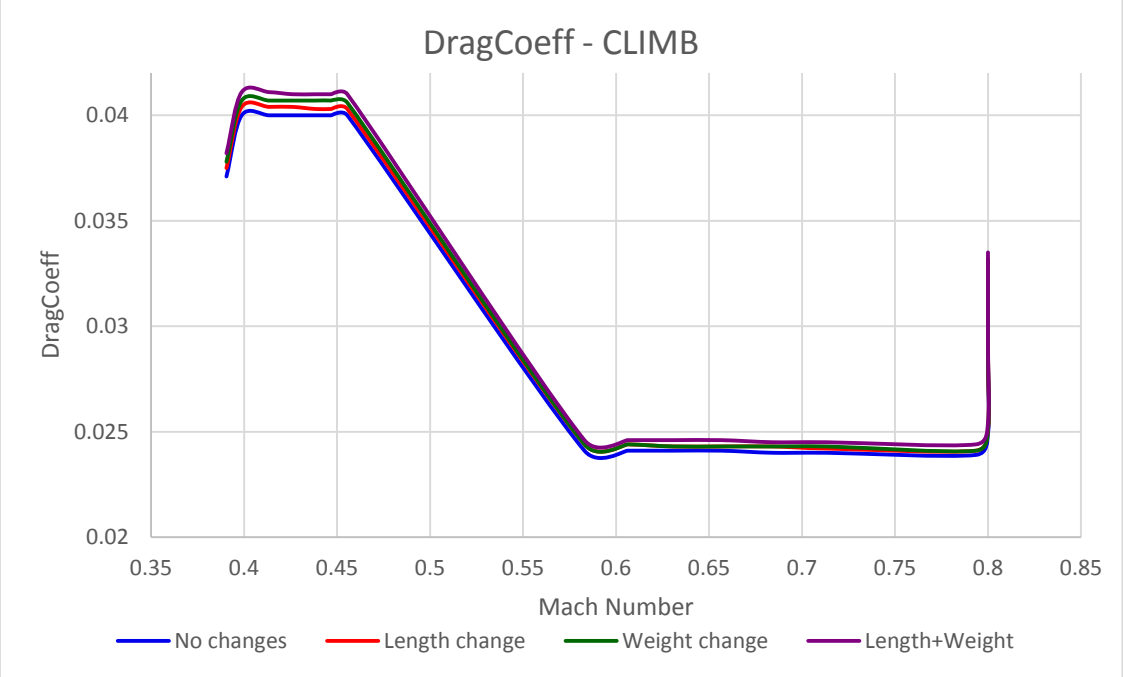

Figure 7-2: Drag Coefficient Variation with Mach Number During Climb for the Turbofan Engine

Figure 7-2 indicates the change in drag coefficient during the climb phase as the aircraft gains altitude and reaches the top of climb. The drag coefficient increases until an altitude of 900 m and then remains constant for as long as the EAS remains constant. This pattern is due to a change in the profile drag

because of a change in the configuration of the high lift devices after initial climb. The drag coefficient decreases steeply with an increase in EAS and then remains constant until an altitude of 8077.2 m at segment 15. After that it increases, until the first cruise altitude of 10058 is achieved at segment 17. This increase is due the constant Mach number and a decrease in EAS and TAS.

Initially climb is maintained at a constant EAS because climbing at constant Mach can lead to the aircraft reaching its stall speed. However at an altitude close to the cruise, the aircraft switches to a constant Mach number because a constant EAS at higher altitudes can lead to the critical Mach number.

The drag coefficient increase with an increase in length all through the profile by 1.1%. This is due to a change in the engine profile wetted area. An increase in weight results in a 1.9 % increase in the drag co-efficient. The overall effect of the device is a 3% increase in drag coefficient during the climb phase. The Mach number increases continuously during climb starting from 0.3905 until it attains the initial cruise Mach number of 0.8.

Figure 7-3 indicates the change in lift coefficient during the climb phase as the aircraft gains altitude and reaches the top of climb. The lift coefficient remains constant until segment 7 where an altitude of 3048 m is achieved. This is because the EAS remains constant until this altitude. It decreases steeply with an increase in EAS and then remains constant until an altitude of 8077.2 m at segment 15.This is because the EAS again has a constant value. After that it increases until the first cruise altitude of 10058 is achieved at segment 17. This increase in the lift coefficient after segment 15 is due to the constant Mach number maintained and a decrease in EAS and TAS.

Initially climb is maintained at a constant EAS because climbing at constant Mach can lead to the aircraft reaching its stall speed. However at an altitude close to the cruise, the aircraft switches to a constant Mach number because a constant EAS at higher altitudes can lead to the critical Mach number.

The lift co-efficient does not change with an increase in length all through the profile. Any change of less than 1% has been ignored. An increase in weight results in a 1.4% increase in the lift co-efficient. The overall effect of the device is a 1.7% increase in the lift coefficient during the climb phase. This is compensated by the increase in the lift induced drag during the climb phase.

Ideally an increase in weight should not affect the lift co-efficient. However during climb, the angle of attack needs to increase in order to compensate for the increase in the weight of the aircraft. This results in an increase in the lift co-efficient. The Mach number increases continuously during climb starting from 0.3905 until it attains the initial cruise Mach number of 0.8.

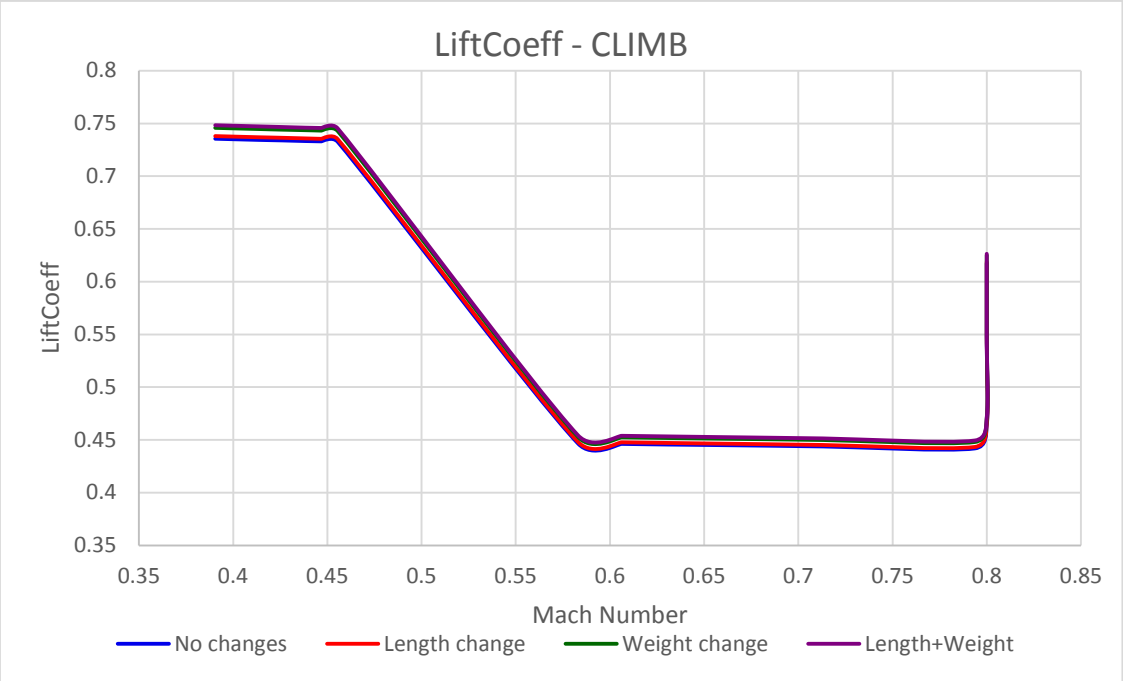

Figure 7-3: Lift Coefficient Variation during Climb for the Turbofan Engine

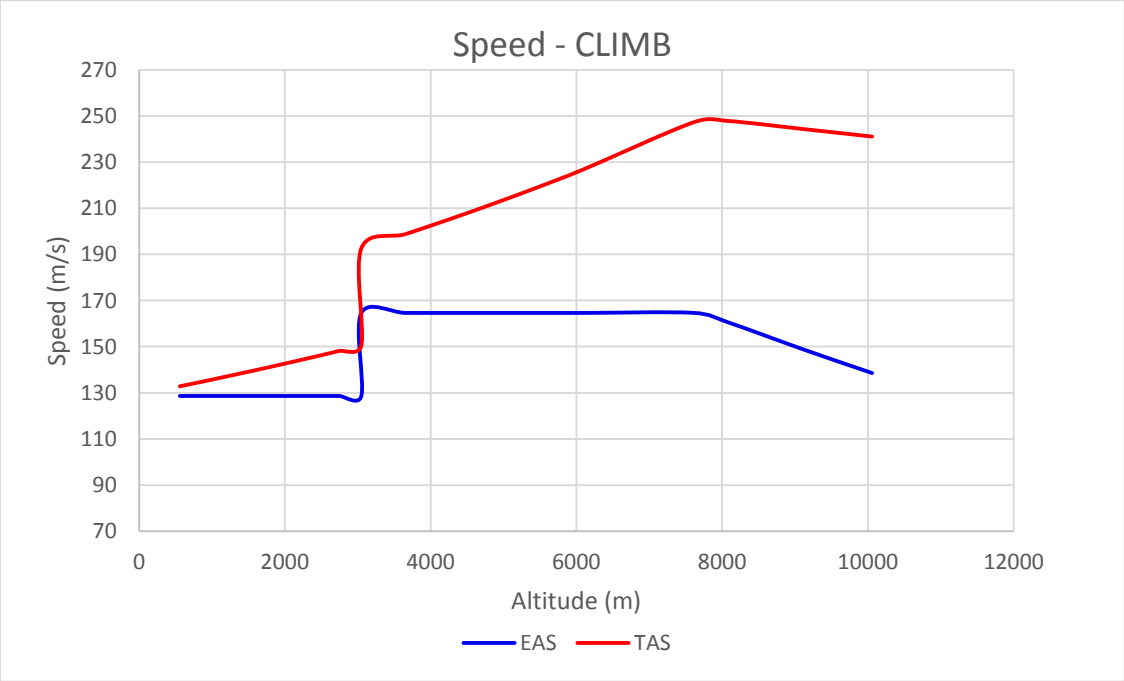

Figure 7-4: EAS and TAS Variation during Climb For the Turbofan Engine

Figure 7-4 illustrates the variation in the EAS and TAS during climb. The aircraft climbs at a constant EAS of 128.6 m/s (250 knots) up to an altitude of 3048 m at segment 7. This speed is maintained constant for noise restrictions close to

ground. Then it accelerates to 164.6m/s (320 knots) and continues to climb to cruise Mach number which is achieved at an altitude of 8077.2 m at segment 15. The TAS increases continuously during climb. This is because TAS is a function of EAS and is inversely proportional to the square root of the relative atmospheric density. Although EAS is maintained at a constant value, the density decreases as the aircraft gains altitude and hence TAS increases. TAS starts decreasing closer to the top of climb as a constant Mach number is maintained. The Mach number also increases with an increase in altitude in a similar manner to the TAS until it levels of to a constant value of 0.8 at segment 15 at an altitude of 8077 m.

Figure 7-5 illustrates the vertical rate of climb which decreases as altitude is gained. This decrease is due to a reduction in thrust because of a decrease in the inlet mass flow with an increase in altitude. Figure 7-5 indicates that the vertical rate of climb falls to zero at segment 7 at an altitude of 3048 m. This is because the segment following segment 7 also has the same altitude and the aircraft is only accelerating horizontally from an EAS of 250 knots to an EAS of 320 knots. The rate of climb decreases further on as the altitude is increased.

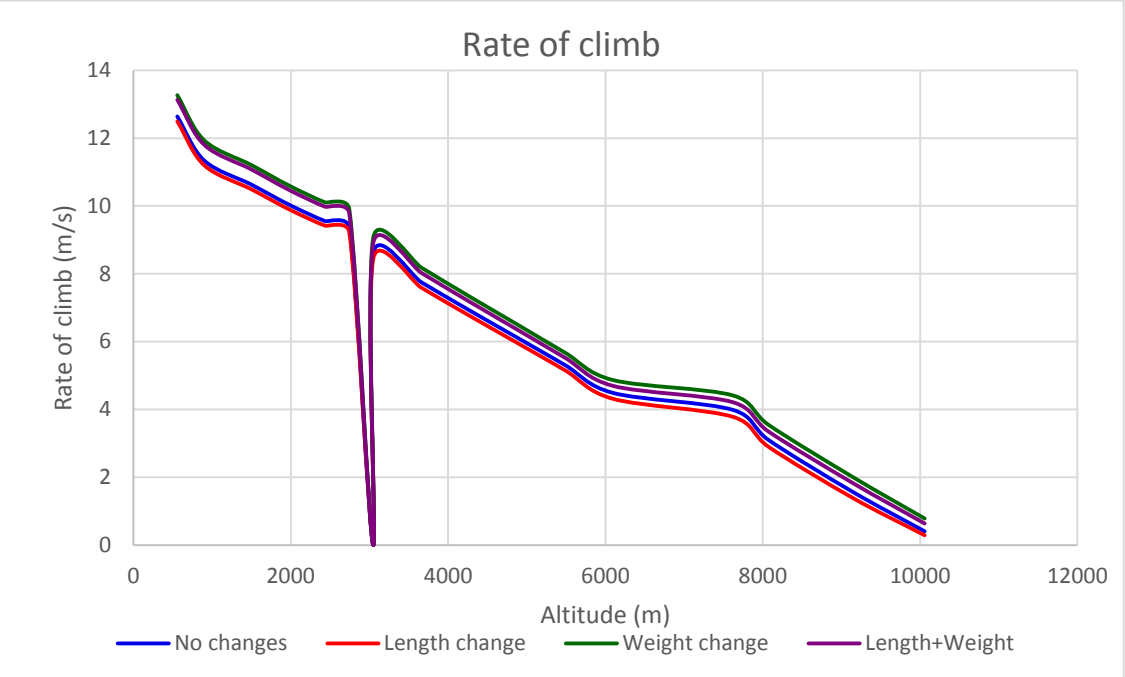

Figure 7-5: Rate of Climb for the Turbofan Engine

Figure 7-6 indicates the change in the nacelle drag during the climb phase as the aircraft gains altitude and reaches the top of climb. The nacelle drag remains constant until segment 7 where an altitude of 3048 m is achieved. This is because the EAS remains constant until this altitude. It increases steeply with an increase in EAS and then remains constant until an altitude of 8077.2 m at

segment 15.This is because the EAS has a constant value at this stage. After that it decreases until the first cruise altitude of 10058 is achieved at segment 17. This decrease in the drag after segment 15 is due the constant Mach number maintained and a decrease in EAS and TAS. Drag is proportional to the square of the EAS.

Initially climb is maintained at a constant EAS because climbing at constant Mach can lead to aircraft reaching its stall speed. However at an altitude close to the cruise, the aircraft switches to a constant Mach number because a constant EAS at higher altitudes can lead to the critical Mach number. The nacelle drag does not change with an increase in weight all through the profile. It is only a function of the change in length. An increase in length results in a 36 % increase in the overall nacelle drag. However, this is a very minimal increase when compared to the overall drag of the aircraft.

Figure 7-7 indicates the change in the thrust requirement during the climb phase as the aircraft gains altitude and reaches the top of climb. The thrust decreases linearly as the aircraft climbs and gains altitude. This is because the mass flow entering the engine reduces as the aircraft gains altitude due to a reduction in the air density with an increase in altitude.

The thrust does not change with an increase in weight or length of the engine all through the profile. It is only a function of the inlet mass-flow, ambient temperature and ambient pressure. These factors vary linearly with altitude. The thrust profile is linear except for an irregularity between segment 7 and segment 8 at an altitude of 3048 m. This is due to a transition in the EAS from 250 knots to 320 knots. The second irregularity in the curve is experienced between segment 14 and segment 15 at an altitude of 7620 m as indicated by the vertical line at Mach 0.8. This is because the aircraft switches to constant Mach number from constant EAS to avoid flying at the critical Mach number.

Figure 7-8 indicates the change in the SFC during the climb phase as the aircraft gains altitude and reaches the top of climb. The SFC increases linearly as the aircraft climbs and gains altitude. The aircraft needs to maintain EAS whereas the thrust decreases as altitude increases. Hence the SFC increases in order to maintain the EAS during climb. The SFC does not change with an increase in weight or length of the engine all through the profile. The SFC curve indicates a slope change between segment 7 and segment 8 at an altitude of 3048 m. This is due to a transition in the EAS from 250 knots to 320 knots. A small slope change in the curve is experienced between segment 14 and segment 15 at an initial altitude of 7620 m. This is because the aircraft switches to constant Mach number from constant EAS to avoid flying at the critical Mach number as indicated by the vertical line at Mach 0.8.

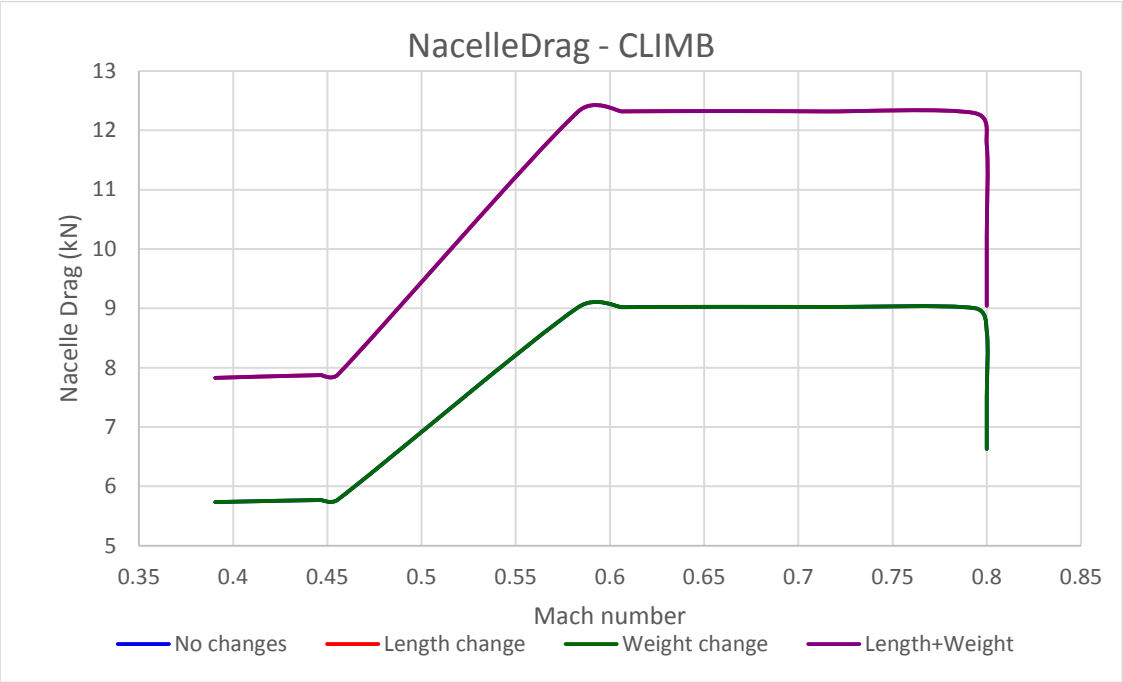

Figure 7-6: Nacelle Drag Variation during Climb for the Turbofan Engine

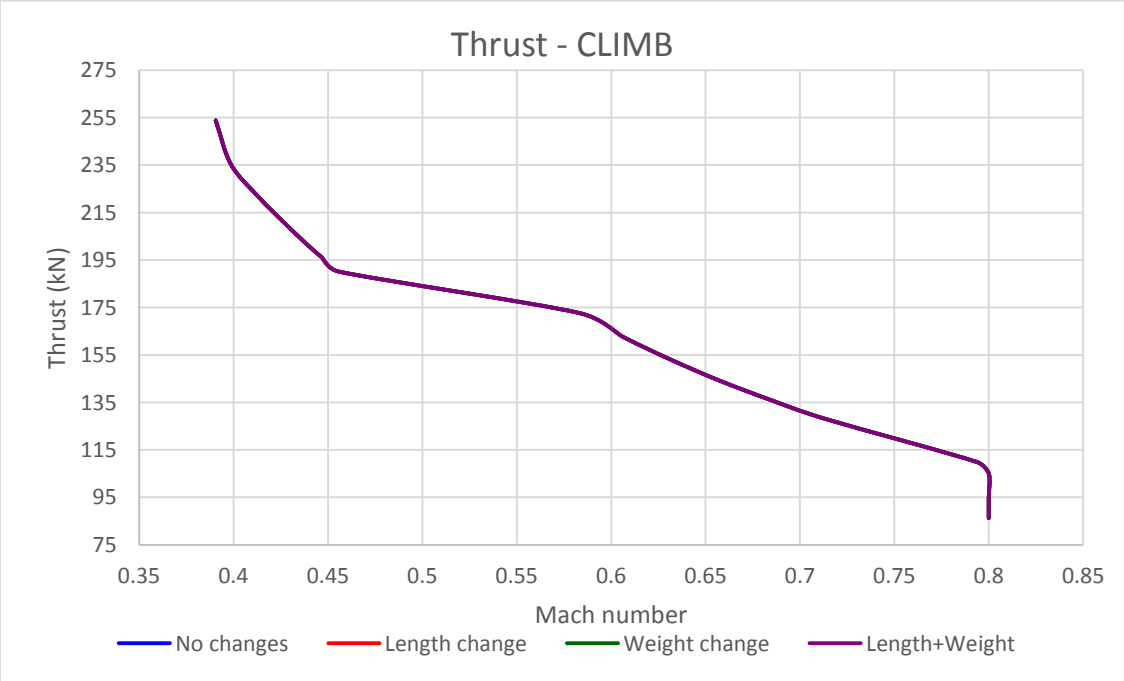

Figure 7-7: Thrust Variation during Climb for the Turbofan Engine

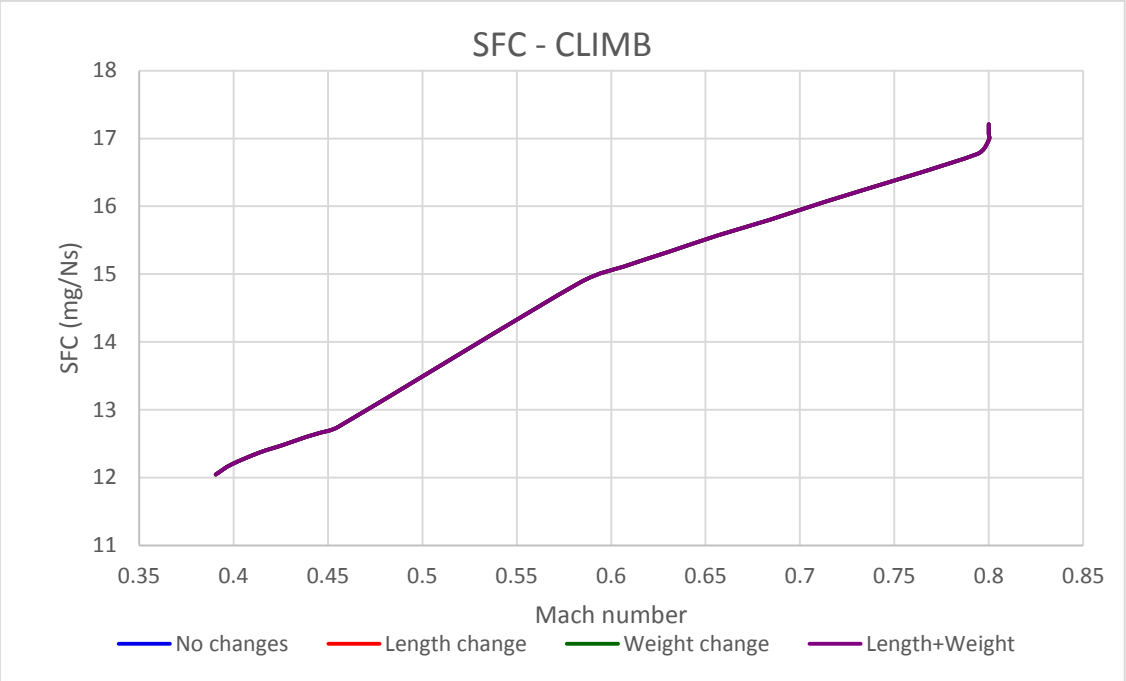

Figure 7-8: SFC Variation during Climb for the Turbofan Engine

7.1.2.2 CRUISE

Figure 7-9 illustrates the variation of the drag coefficient during the cruise phase of the flight mission. The drag reduces as the aircraft flies through the cruise phase. This is because as the aircraft moves along a straight and level flight path, it consumes fuel and its weight decreases continuously which results in a reduction in the lift induced drag. At the initial cruise altitude of 10058m, the drag co-efficient decreases steeply due to a reduction in the fuel weight of the aircraft at a constant altitude and constant Mach number. There is a slight increase in the drag co-efficient as the aircraft accelerates and climbs to the final cruise altitude of 10670m due to a decrease in EAS. Then again the drag co-efficient starts to decrease steeply with a reduction in fuel weight at a constant altitude and a constant cruise economy Mach number of 0.82. The drag coefficient of the aircraft increases by 0.6% with a change in length and increases by 0.6 % with a change in weight of the engine. The overall effect of the contrail-free engine on the cruise drag coefficient is only an increase in the drag by 1.1 %.

Figure 7-10 illustrates the variation of the lift coefficient during the cruise phase of the flight mission. The lift reduces as the aircraft flies through the cruise phase. This is because as the aircraft moves along a straight and level flight path, it consumes fuel and its weight decreases continuously which results in a reduction in the lift coefficient as it varies linearly with the weight of the aircraft. At the initial cruise altitude of 10058m, the lift co-efficient decreases steeply due

to a reduction in the fuel weight of the aircraft at a constant altitude and constant Mach number. There is a slight increase in the lift co-efficient as the aircraft accelerates and climbs to the final cruise altitude of 10670m due to a decrease in EAS .Then again the lift co-efficient starts to decrease steeply with a reduction in fuel weight at a constant altitude and a constant cruise economy Mach number of 0.82.The lift coefficient of the aircraft increases by 0.1% with a change in length and increases by 0.6% with a change in weight of the engine. The overall effect of the contrail-free engine on the cruise lift coefficient is only an increase in the lift coefficient by 0.6 % .

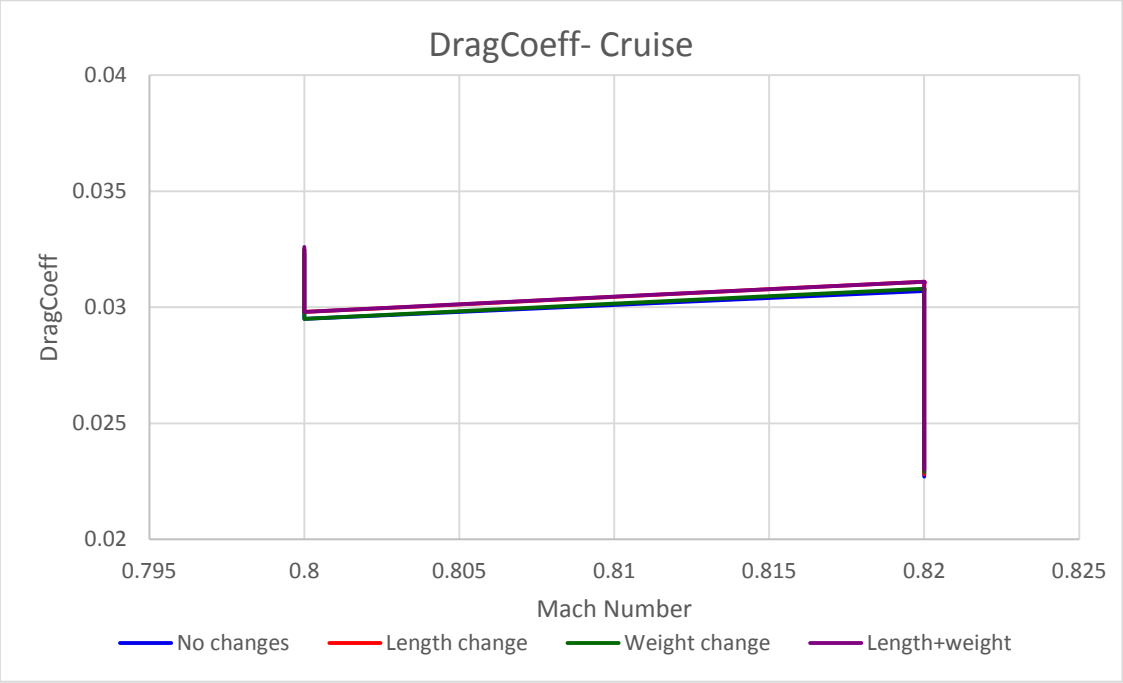

Figure 7-9: Drag Coefficient Variation during Cruise for the Turbofan Engine

Figure 7-11 illustrates the variation of the nacelle drag during the cruise phase of the flight mission. The nacelle drag remains constant as the aircraft flies at a constant altitude and constant Mach number. This is because the nacelle drag only consists of the profile drag and does not include the lift induced drag as in the case of the aircraft. The slight variation in the nacelle drag along the profile is due to a decrease in EAS with a gain in altitude. The nacelle drag is unaffected by the change in the engine weight. The nacelle drag is affected by an increase in the length of the engine. An increase in the length by 2 meters results in an overall increase in the nacelle drag by 36%. However, this is a small fraction when considering the total drag of the aircraft. The drag of the aircraft determines the thrust requirements at various flight conditions.

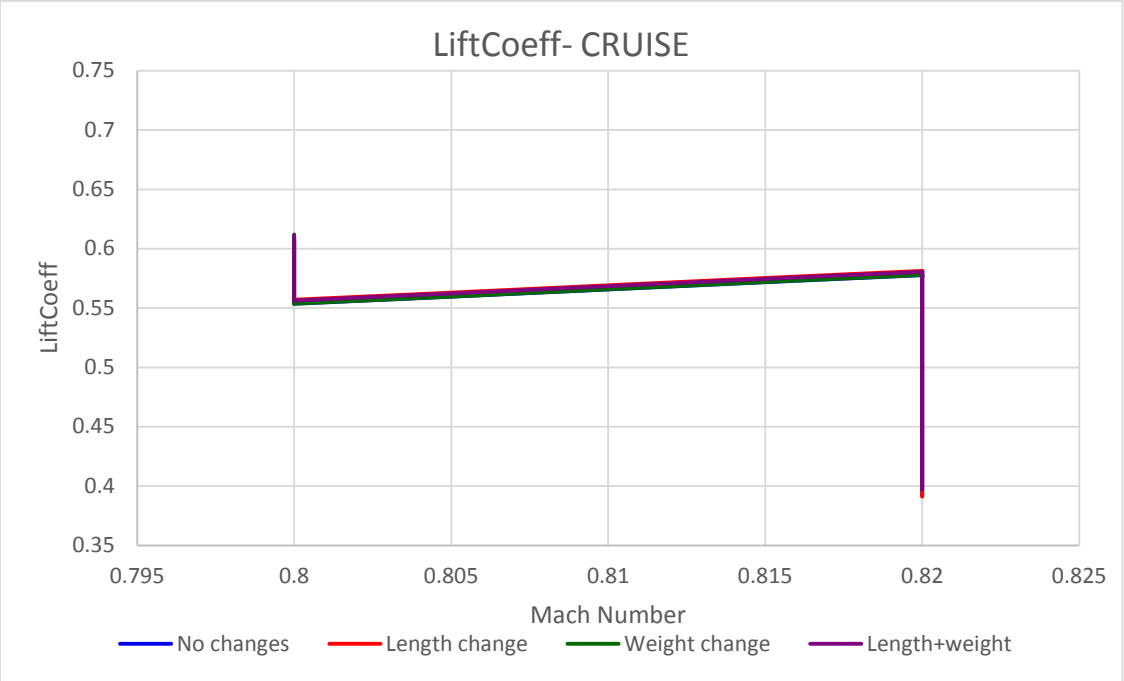

Figure 7-10: Lift Coefficient Variation during Cruise for the Turbofan Engine

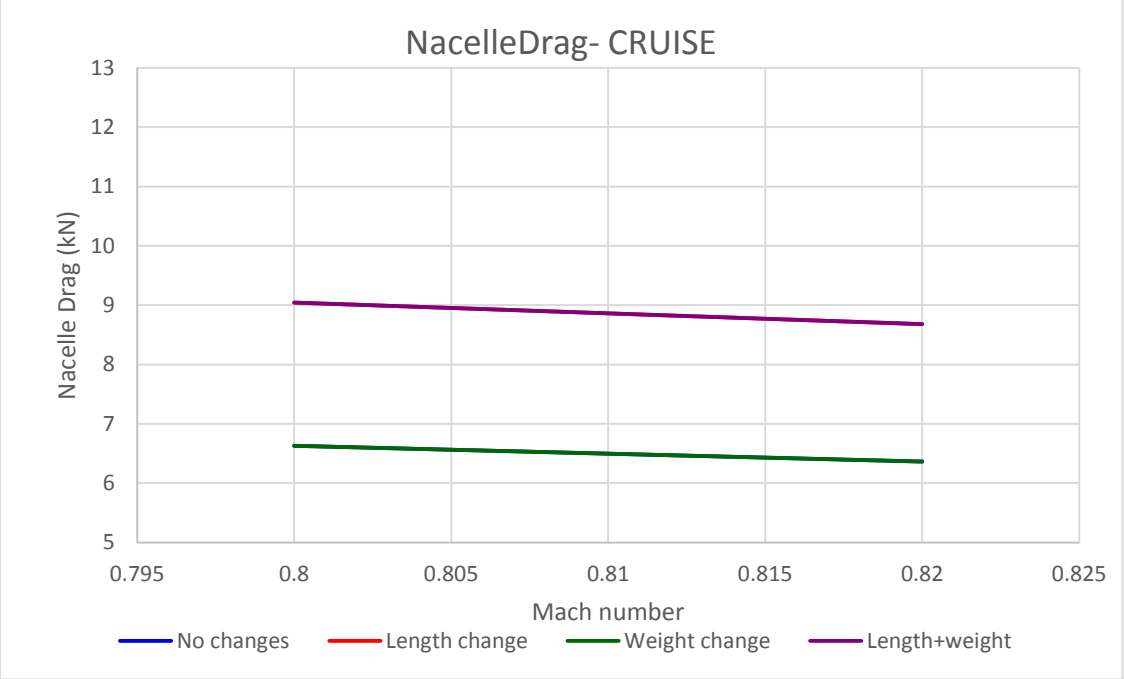

Figure 7-11: Nacelle Drag Variation during Cruise for the Turbofan Engine

Figure 7-12 indicates the change in the thrust requirement during the cruise phase as the aircraft covers distance. The thrust decreases as the aircraft flies along the flight path at a constant altitude. A continuous reduction in thrust occurs along the cruise trajectory as the aircraft burns fuel and experiences a reduction in weight. This results in a decrease in the drag and lift of the aircraft.

In order to maintain straight and level flight, the thrust needs to equate to the drag and hence reduces accordingly. The lift needs to be equal to the weight of the aircraft. At the initial cruise altitude of 10058m, the thrust decreases steeply due to a reduction in the fuel weight of the aircraft at a constant altitude and constant Mach number. It remains constant when the aircraft accelerates from Mach 0.8 to Mach 0.82 as the aircraft climbs from the initial cruise altitude to the final cruise altitude. Then again the thrust starts to decrease steeply with a reduction in fuel weight at a constant altitude and a constant cruise economy Mach number of 0.82. The thrust change with an increase in length of the engine is 0.6% all through the profile, whereas with a change in the weight of the engine, the thrust decreases by 2.2%. The overall decrease in thrust is 1.2%. Although, the thrust It is only a function of the inlet mass-flow, ambient temperature and ambient pressure, it is affected by a change in length and weight because the thrust needs to equate to the drag and the weight needs to be equal to the lift in order to maintain straight and level flight. Since lift and drag coefficients change with a change in the length and weight of the engine, the thrust also changes correspondingly.

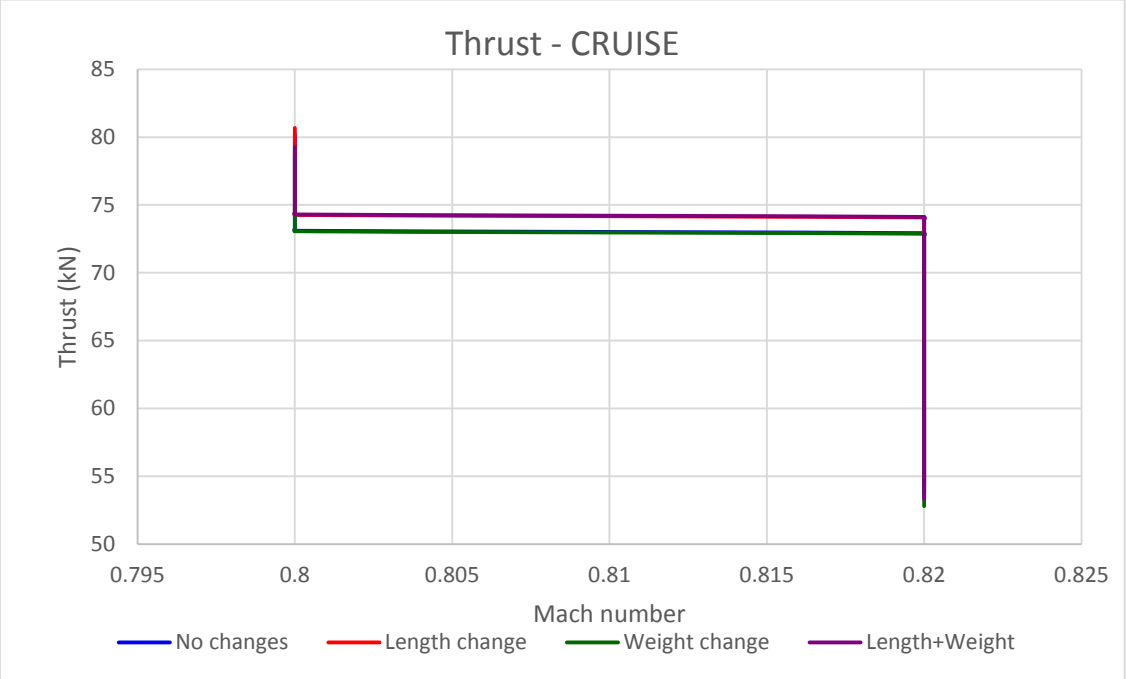

Figure 7-12: Thrust Variation during Cruise for the Turbofan Engine

Figure 7-13 illustrates the variation of SFC during cruise flight. The SFC decreases as the aircraft flies along the flight path at a constant altitude. A continuous reduction in SFC occurs along the cruise trajectory as the thrust requirement of the aircraft reduces due to a reduction in the cruise drag. A linear increase in SFC is experienced due to a change in cruise altitude from 10058 m to 10670 m. This is because of an increase the Mach number from 0.8

to the cruise economy Mach number of 0.82 at a higher altitude. The SFC increases with an increase in length of the engine by 0.05 % all through the profile, whereas with a change in the weight of the engine, the SFC decreases by 0.2%. The overall decrease in SFC is 0.12%. The reduction in SFC is due to a reduction in thrust at cruise for contrail-free engine. Once the Mach number becomes constant at 0.82, the SFC falls steeply as the aircraft loses weight during its flight path by burning fuel until the SFC reaches a value of 16.1 at the end of cruise.

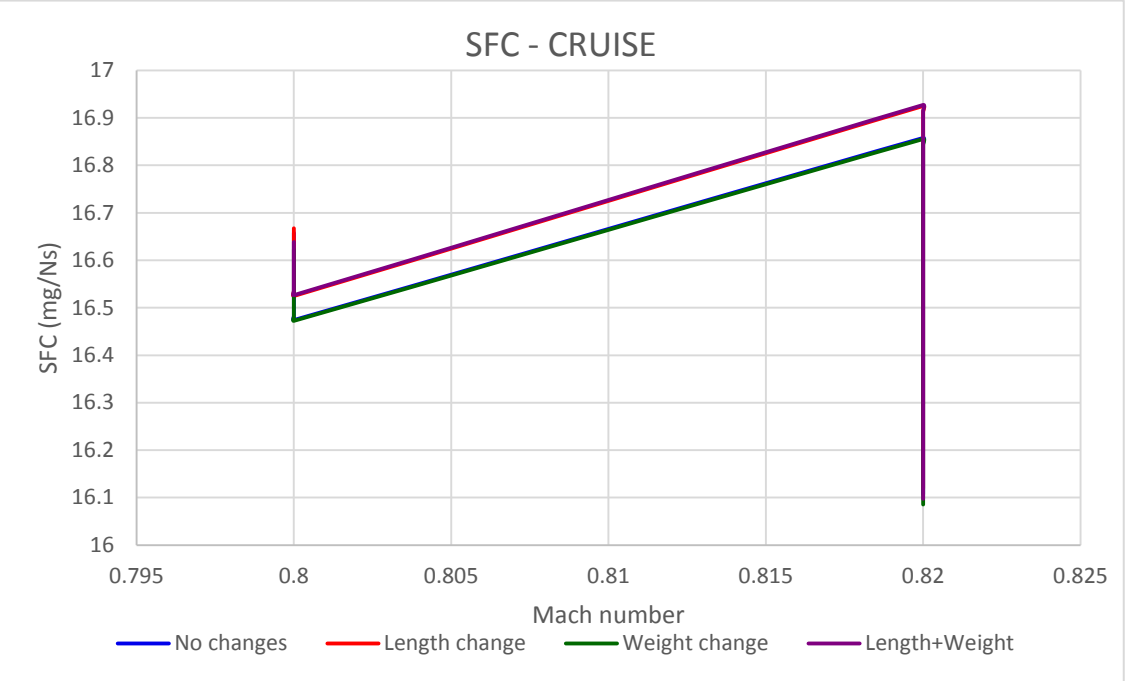

Figure 7-13: SFC Variation during Cruise for the Turbofan Engine

7.1.2.3 GLIDE

Table 7-4 indicates the glide altitude and Mach number for each glide segment. This enables us to interpret the output plots with reference to the operating altitude. Data has been plotted versus Mach number instead of altitude for clarity of illustration.

Figure 7-14 illustrates the change in Mach number with a decrease in altitude during the glide phase. The Mach number decreases continuously during glide starting from 0.7804 at the final cruise altitude until it attains the approach Mach number of 0.3945.

Figure 7-15 indicates the change in drag coefficient during the glide phase as the aircraft loses altitude and reaches the landing phase. The drag coefficient decreases at a very small rate until an altitude of 5335 m at segment 5 and then

increases until the landing phase is reached. This is because for initial descent, the rate of descent needs to be low in order to maintain cabin pressure. Beyond an altitude of 5335 m, the second phase of descent takes place where flaps and other drag increasing systems are deployed to enhance the profile drag which then increases linearly with a decrease in altitude. The drag coefficient increases with an increase in length by 0.4% and by 0.8% with an increase in the weight all through the profile. Hence the overall increase in the drag coefficient of the contrail free engine during the glide phase is 1.6%.All curves overlap due to the minimal change in the drag co-efficient with a change in the engine length and the engine weight.

Glide Segment	Altitude (m)	Mach number	Glide Segment	Altitude (m)	Mach number
1	10670	0.7804	6	4001.2563	0.5043
2	9336.2512	0.7275	7	2667.5075	0.4547
3	8002.5025	0.6542	8	1333.7588	0.4153
4	6668.7537	0.6177	9	0.01	0.3945
5	5335.005	0.5701	10	0.01	-

Table 7-4: Glide Altitude at Each Glide Segment Number for the Turbofan Engine

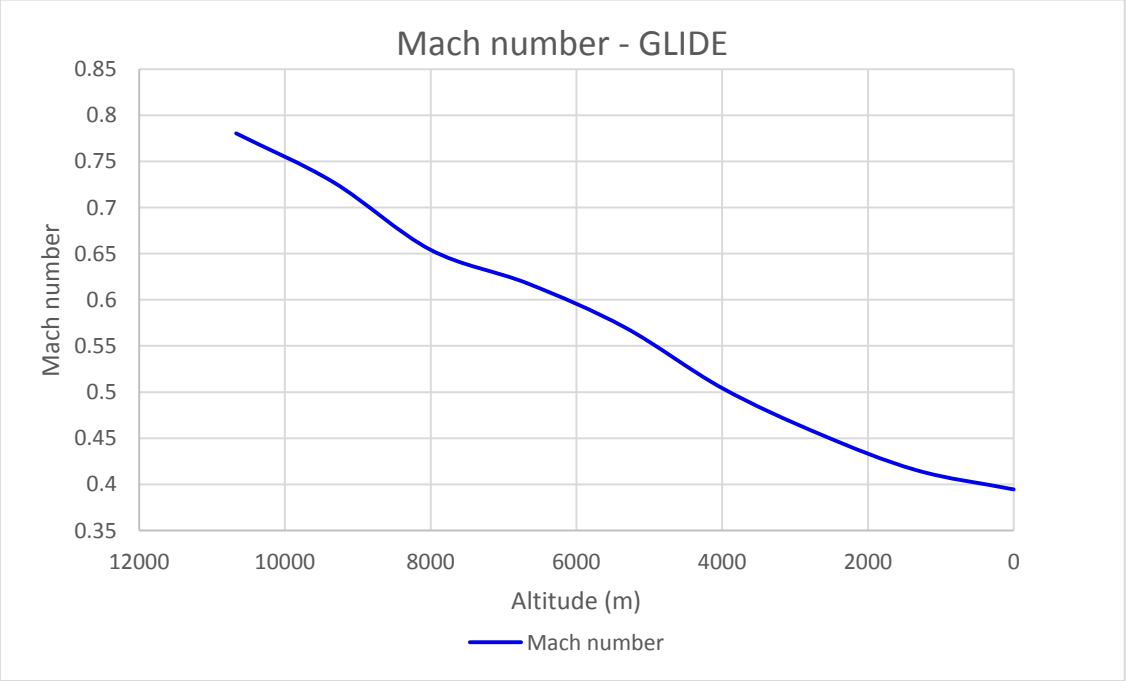

Figure 7-14: Mach Number Variation with Altitude during Glide for the Turbofan Engine

Figure 7-16 indicates the change in lift coefficient during the glide phase as the aircraft loses altitude and reaches the landing phase. The lift coefficient decreases until an altitude of 5335 m at segment 5 and then increases until the approach phase at segment 8. The lift coefficient is inversely proportional to the density, which increases as altitude reduces. Hence the coefficient of lift decreases. Beyond an altitude of 5335 m, the second phase of descent takes place where flaps and other high lift devices are deployed to enhance the profile drag. The engagement of the high lift systems increases the lift coefficient as well. The lift coefficient decreases after approach when the plane is flared out to achieve stall speed for landing. The lift co-efficient does not change with an increase in length all through the profile. However it increases by 1.4 % with an increase in the weight of the engine.

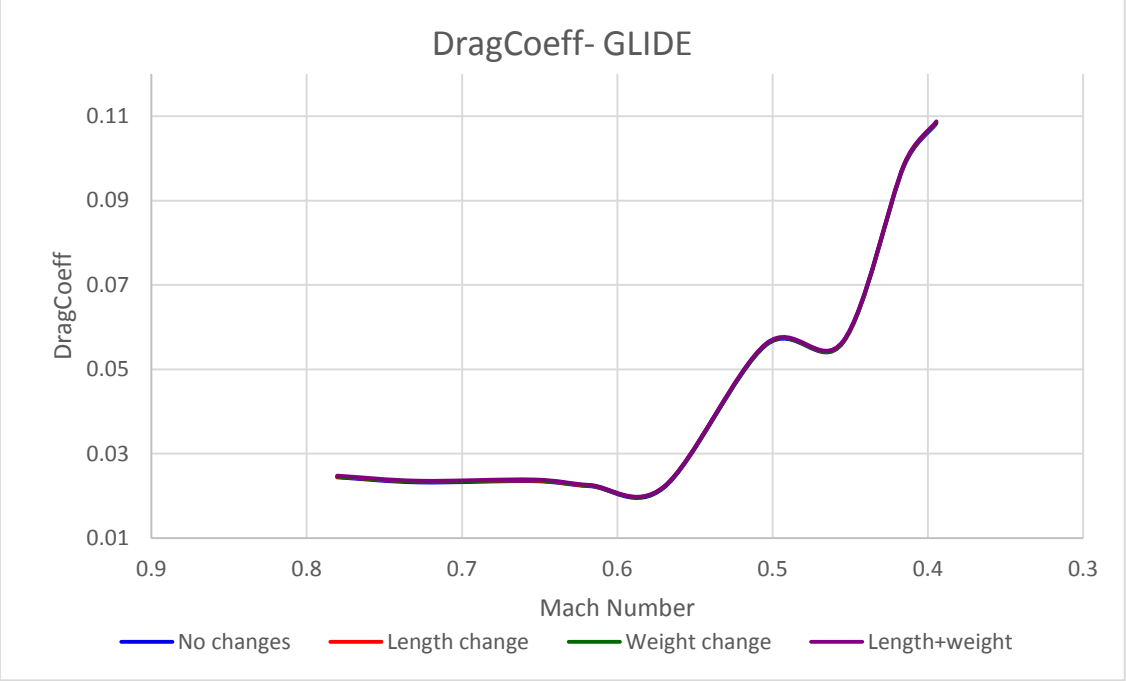

Figure 7-15: Drag Coefficient Variation during Glide for the Turbofan Engine

Figure 7-17 illustrates the variation in the EAS and the TAS during glide. The aircraft glides at a near constant EAS of 130m/s to 140 m/s all through the glide phase. This speed is maintained constant for noise restrictions close to the ground. The TAS decreases continuously during glide. This is because TAS is a function of EAS and is inversely proportional to the square root of the relative atmospheric density. Although EAS is maintained at a constant value, the density decreases as the aircraft loses altitude and hence TAS decreases. The Mach number also decreases with a decrease in altitude in a similar manner to the TAS until the landing phase is reached. The values for TAS, EAS and Mach have been input into the code and therefore do not change with a change in the

length or the weight of the engine. Hence they remain constant for both the conventional turbofan engine and the contrail free engine.

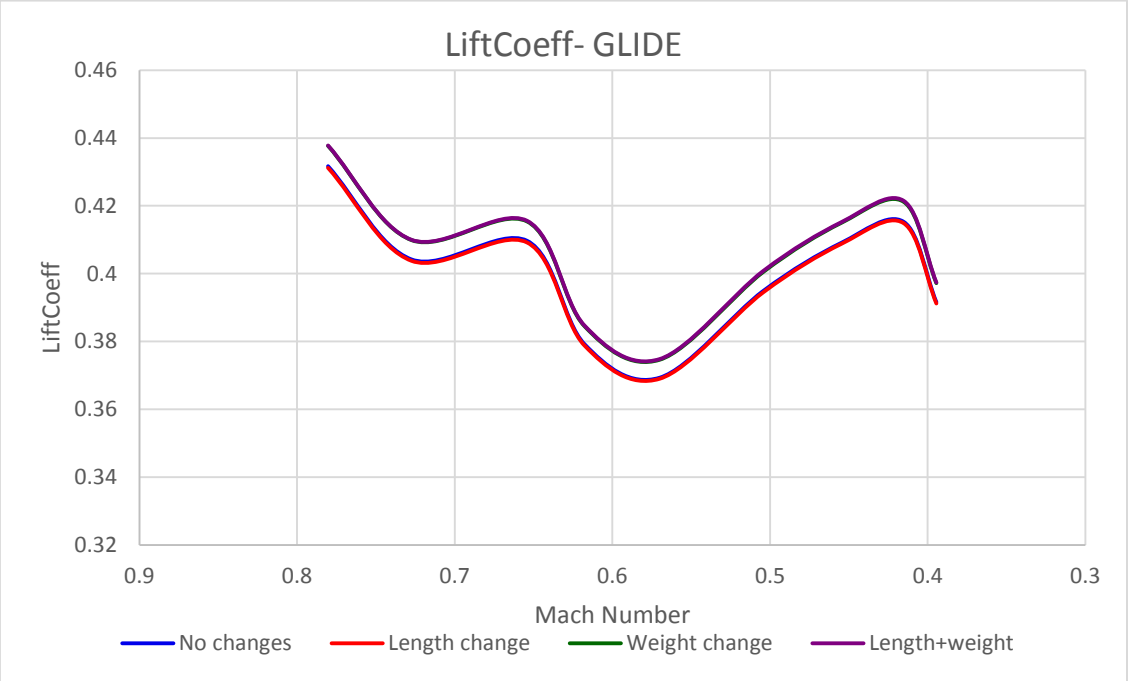

Figure 7-16: Lift Coefficient Variation during Glide for the Turbofan Engine

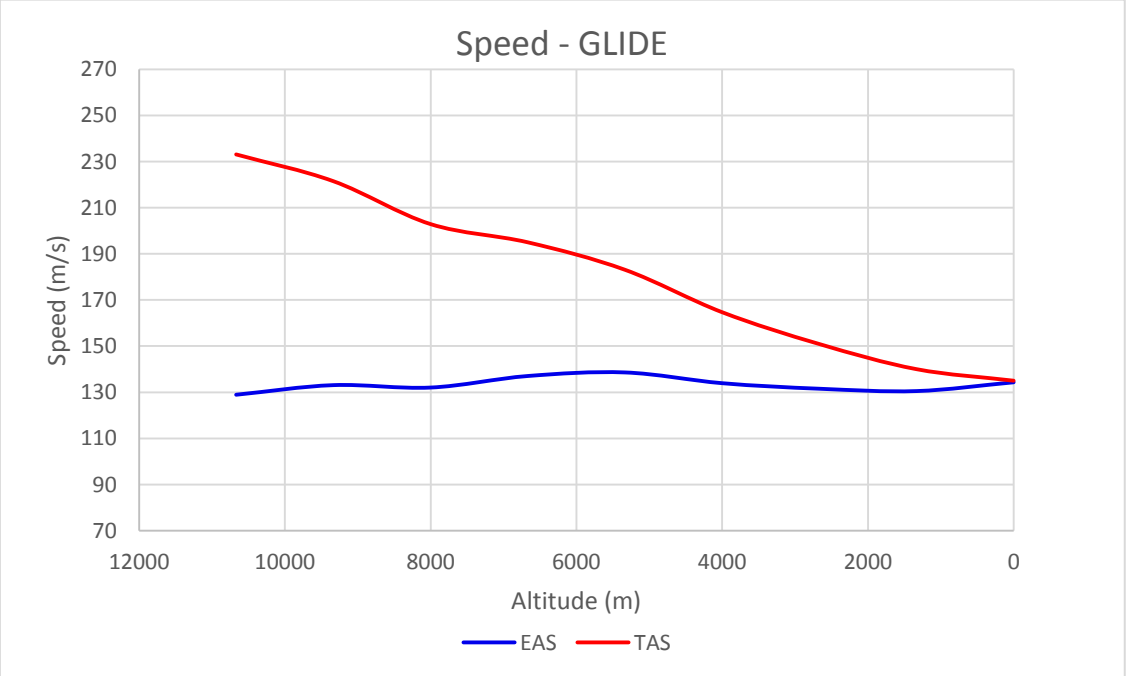

Figure 7-17: EAS and TAS Variation during Glide For the Turbofan Engine

Figure 7-18 illustrates the vertical rate of descent during the glide phase. The initial rate of descent decreases from 4m/s to 2 m/s at segment 4 at an altitude

of 6668m. This is because for initial descent, the rate of descent needs to be low in order to maintain cabin pressure. Beyond that it increases to 18 m/s until an altitude of 2667m at segment 7 is reached. This is because once cabin pressure is established; the aircraft loses altitude quickly until it enters the approach phase. Beyond that the rate of descent again reduces in order for the aircraft to land. The vertical rate of descent changes minimally with a change in the engine length or weight.

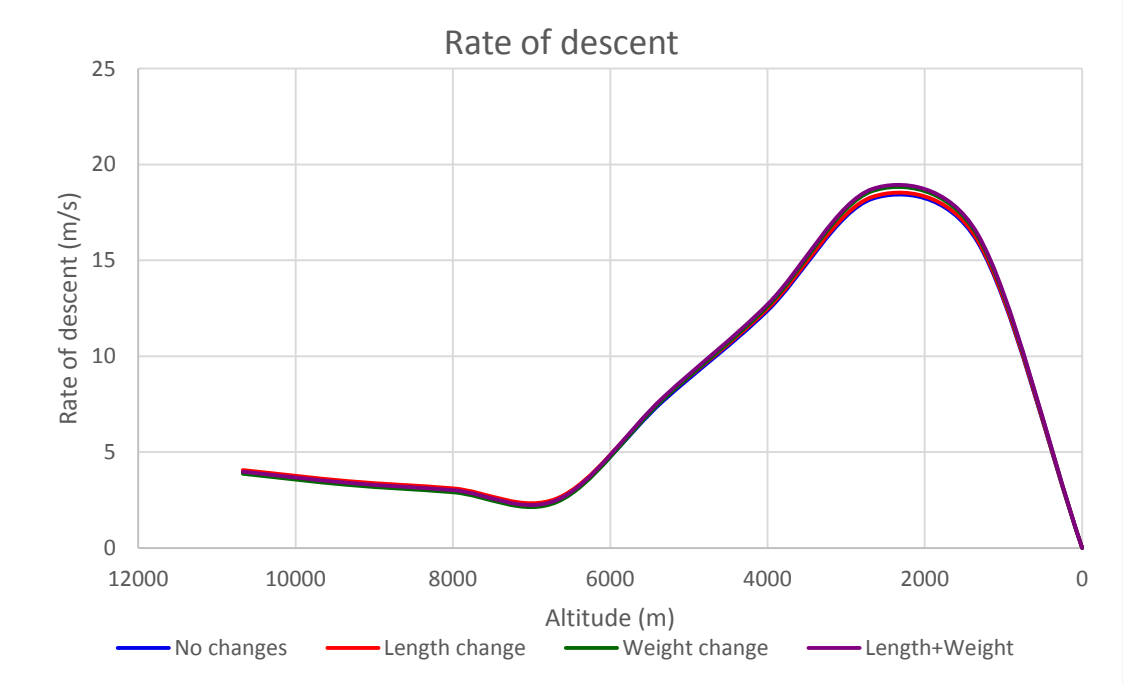

Figure 7-18: Absolute Vertical Rate of Descent for the Turbofan Engine

Figure 7-19 indicates the change in the nacelle drag during the glide phase as the aircraft loses altitude and approaches to land. The nacelle drag only varies by a maximum of 1 KN throughout the glide phase profile. This variation is proportional to the variation in the EAS during this phase. The nacelle drag does not change with an increase in weight all through the profile. It is only a function of the change in length. An increase in length results in a 36 % increase in the overall nacelle drag. However, this is a very minimal increase when compared to the overall drag of the aircraft.

Figure 7-20 indicates the thrust variation requirement during glide. The thrust increases gradually until segment 7 at an altitude of 2667 m close to the approach phase. This is due to an increase in the density as the aircraft descends which increases the mass-flow entering the engine at idle settings and hence results in a rise in thrust for a constant TET. As the aircraft enters the approach phase the thrust rises steeply as the engine is throttled to prevent undershoot. An increase in TET is also experienced with the increase in thrust.

The thrust value achieved during approach at segment 8 remains constant until the aircraft lands at segment 9. This behaviour does not change with a change in the length or the weight of the engine. Hence the contrail-free engine can land as per the standard of a conventional turbofan engine.

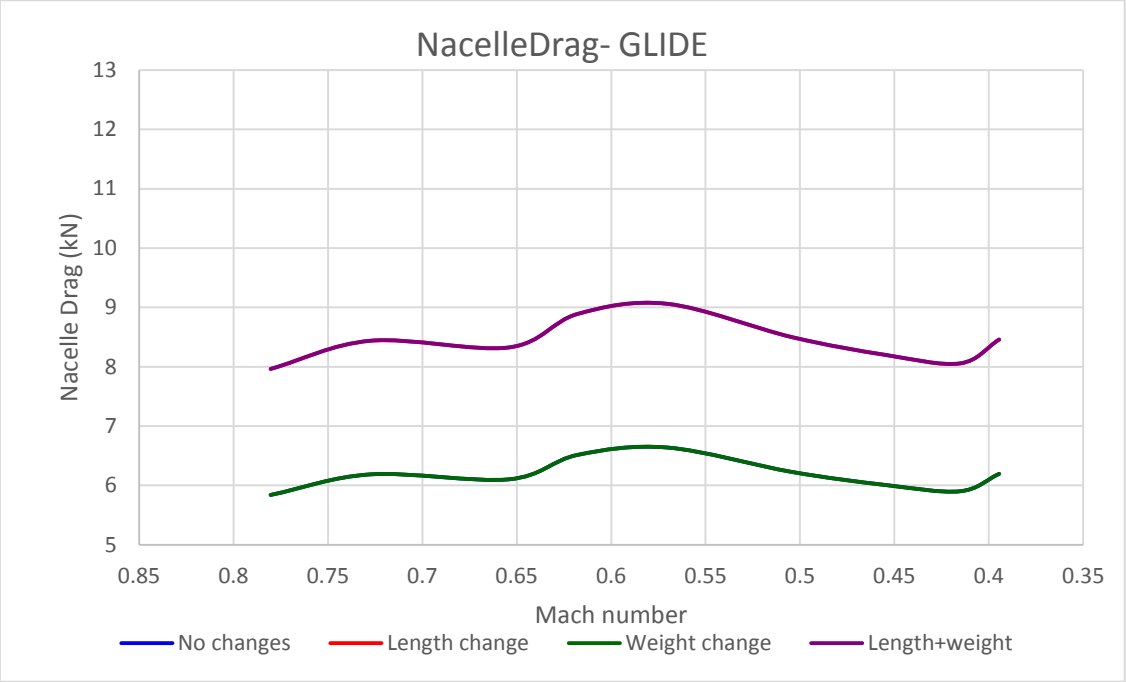

Figure 7-19: Nacelle Drag Variation during Glide for the Turbofan Engine

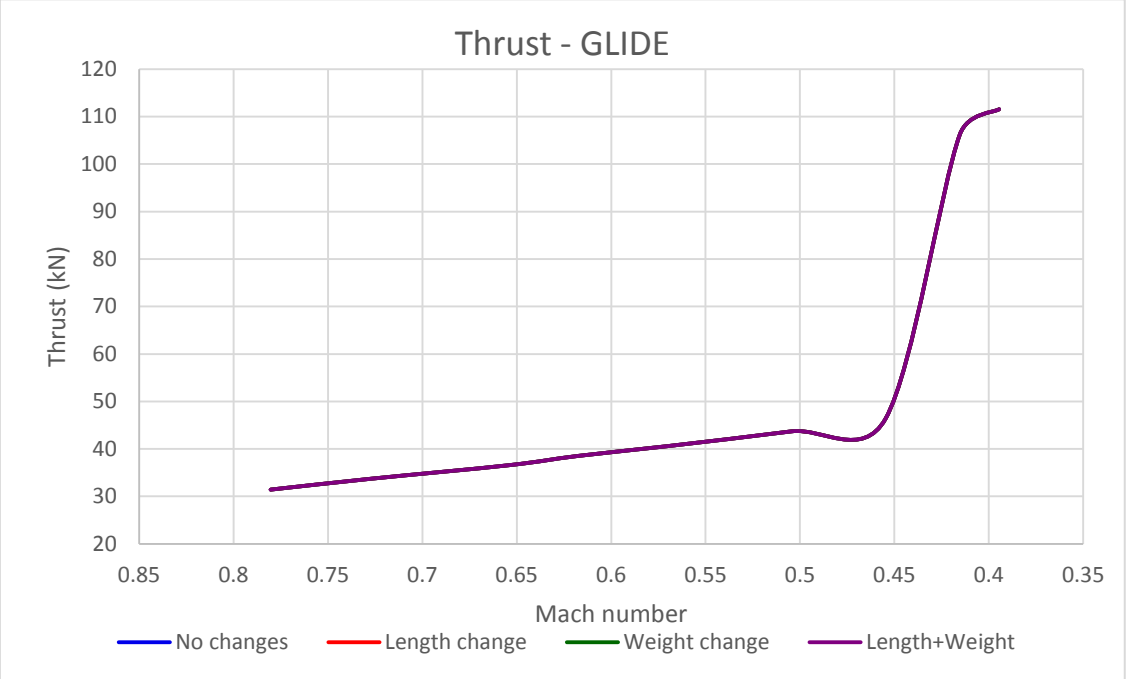

Figure 7-20: Thrust Variation during Glide for the Turbofan Engine

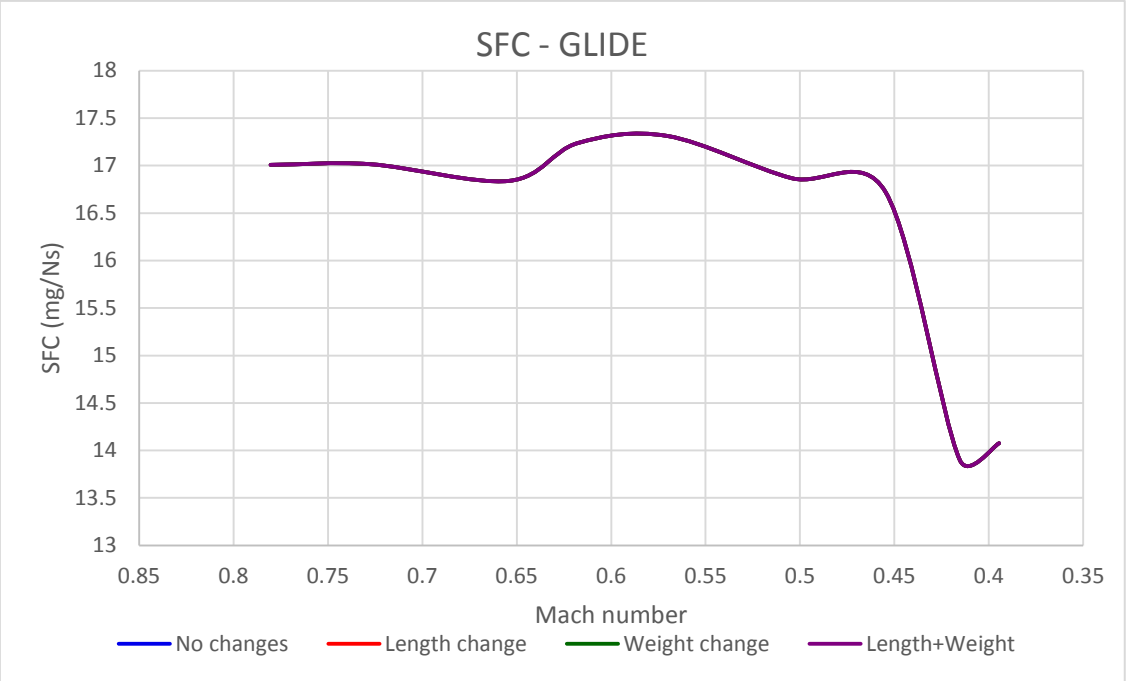

Figure 7-21: SFC Variation during Glide for the Turbofan Engine

Figure 7-21 illustrates the SFC variation during the glide phase. The SFC varies according to the change in the thrust in this phase. The SFC has a high value of 17 mg/Ns until the aircraft descends to an altitude of 2667 at segment 7. This is because thrust is very low during this part of the glide phase. Beyond that the SFC falls steeply to 14 mg/Ns as the aircraft enters the approach phase where again there is an increased requirement for thrust by the aircraft to land comfortably. This behaviour does not change with a change in the length or the weight of the engine.

7.2 THE INTERCOOLED-RECUPERATED TURBOFAN ENGINE INTEGRATED WITH THE AIRCRAFT

A standard three-spool intercooled-recuperated turbofan engine based on the Trent 900 specifications is integrated with the conventional airframe geometry based on A380-800 specifications. The aircraft performance is analysed and then compared against the performance of the contrail-free three-spool intercooled-recuperated turbofan engine integrated to the same aircraft. The baseline parameters are maintained in both configurations. The contrail-free engine in this case refers to the baseline intercooled-recuperated engine with the water expelling device attached to it which results in a subsequent change in the engine geometry. This entails an increase in the engine length and engine weight while maintaining all other parameters constant.

7.2.1 PERFORMANCE INPUT FOR THE AIRCRAFT AND THE INTERCOOLED-RECUPERATED ENGINE

In the case of the intercooled recuperated Trent 900 engine, the geometric input file for the A380 aircraft configuration is the same with the exception of the weight of the engine, as the intercooler and recuperator weights are included. These are constant values that need to be modified in the engine geometry section of the aircraft input file B.1, 1500 kg of extra weight has been added per engine in order to account for the additional weight of the intercooler and the recuperator(Camilleri, Ogaji and Pilidis, 2011). All other data remains unchanged in this file.

The engine input file B.3 for this configuration is different since the schematics of the intercooled-recuperated engine is not the same as the turbofan engine due to the inclusion of the heat exchangers. B.3 requires data for engine performance that is obtained by the execution of the intercooled-recuperated engine performance code A.3. This code was adapted to TurboMatch version 2.0 due to the convergence issues with version 1.0 since the inclusion of heat exchangers makes it difficult for the code to converge at low power settings. Additional off-design conditions are introduced for the entire mission profile in the new version 2.0. The data extracted was used to populate the engine input file B.3. The baseline engine is not an exact match of the Trent 900 but is based on the standard specifications and configuration of the Trent 900. Similarly, the baseline aircraft is not an exact match of the A380-800 but is based on the standard specifications and configuration of the A380-800 aircraft. All data and results are based on a single engine analyses.

7.2.2 PERFORMANCE OUTPUT FOR THE AIRCRAFT AND THE INTERCOOLED-RECUPERATED ENGINE

Two sets of outputs have been obtained. One set of results provides data on the aircraft performance throughout the flight mission with the variation of various aircraft performance parameters. This is called the aircraft flight path performance output file A.1.1. The other set of results provide data on the engine performance throughout the flight mission and indicates changes in engine performance with a change in flight condition. This is called the engine flight path performance file 0.

The results of the aircraft performance at each flight segment have been plotted below. This includes the aircraft aerodynamic parameters and the engine parameters. A baseline run was executed for the conventional aircraft and the intercooled-recuperated turbofan engine configuration and benchmark values were obtained. The contrail free engine was then simulated by increasing the

weight and length of this engine in the geometric input file B.1 for the Hermes software. The weight of the intercooler and the recuperator were also compensated in the input file B.1 by adding 1500 kg to the weight of the basic three spool turbofan configuration.

The initial estimate for the increase in length for the contrail-free intercooled recuperated engine was 2 meters whereas that for the increase in weight was 2000 kg exclusive of the weight if the intercooler and the recuperator. The code was executed for both cases and a comparative analysis has been drawn by plotting the conventional engine as well as the contrail-free engine with the device attached. This has been done for each flight phase separately with flight segments indicating the altitude of flight. The change in engine and aircraft parameters for all flight conditions has been discussed independently.

7.2.2.1 CLIMB

Table 7-5 indicates the climb altitude and Mach number for each climb segment. This enables us to interpret the output plots with reference to the operating altitude. Data has been plotted versus Mach number instead of altitude for clarity of illustration. A step change occurs for the lift coefficient, drag coefficient and the overall nacelle drag at segment 8 at an altitude of 3048 meters. This is because the aircraft climbs at a constant EAS of 128.6 m/s (250 knots) up to this altitude. This speed is maintained constant for noise restrictions close to ground. Then it accelerates to 164.6 m/s (320 knots) and continues to climb to cruise Mach number of 0.8 which is achieved at an altitude of 8077.2 m at segment 15. A constant Mach number is then maintained in order to avoid the critical Mach number. The maximum operating Mach for the A380 is 0.89.This value results in Mach 1 at the throat of the intake due to ram pressure.

Figure 7-22 illustrates the change in Mach number with an increase in altitude during the climb phase. The Mach number increases continuously during climb starting from 0.3905 until it attains the initial cruise Mach number of 0.8. A step change is observed at an altitude of 3048 m where the aircraft accelerates from an EAS of 250 knots to 320 knots. The altitude remains constant during this acceleration.

Figure 7-23 indicates the change in the overall drag coefficient during the climb phase as the aircraft gains altitude and reaches top of climb. The drag coefficient increases until an altitude of 900 m and then remains constant until the EAS remains constant. This is due to a change in profile drag because of a change in the configuration of the high lift devices after initial climb. It decreases steeply with an increase in EAS and then remains constant until an altitude of

8077.2 m at segment 15. After that it increases until the first cruise altitude of 10058 is achieved at segment 17. This increase is due the constant Mach number and a decrease in EAS and TAS. Initially climb is maintained at a constant EAS because climbing at constant Mach can lead to the aircraft reaching its stall speed. However at an altitude close to the cruise, the aircraft switches to a constant Mach number because a constant EAS at higher altitudes can lead to the critical Mach number .The drag coefficient changes with an increase in length all through the profile by 1.2%.This is due to a change in the engine profile wetted area. An increase in weight results in a 2.2% increase in the drag co-efficient. The overall effect of the device is a 3.4% increase in the drag coefficient during the climb phase.

Figure 7-24 indicates the change in the lift coefficient during the climb phase as the aircraft gains altitude and reaches the top of climb. The lift coefficient remains constant until segment 7 where an altitude of 3048 m is achieved. This is because the EAS remains constant until this altitude. It decreases steeply with an increase in EAS and then remains constant until an altitude of 8077.2 m at segment 15.This is because the EAS has a constant value. After that it increases until the first cruise altitude of 10058 is achieved at segment 17. This increase in the lift coefficient after segment 15 is due the constant Mach number maintained and a decrease in EAS and TAS. Initially climb is maintained at a constant EAS because climbing at constant Mach can lead to the aircraft reaching its stall speed. However at an altitude close to the cruise, the aircraft switches to a constant Mach number because a constant EAS at higher altitudes can lead to the critical Mach number.

Climb Segment	Altitude (m)	Mach number	Climb Segment	Altitude (m)	Mach number
0	0	-	9	3657.6	0.6063
1	557.2	0.3905	10	4267.2	0.6308
2	900	0.3987	11	4876.8	0.6567
3	1500	0.4135	12	5486.4	0.6842
4	1981.2	0.426	13	6096	0.7132
5	2438.4	0.4383	14	7620	0.7936
6	2743.2	0.4468	15	8077.2	0.8
7	3048	0.4555	16	9144	0.8
8	3048	0.583	17	10058	0.8

Table 7-5: Climb Altitude at Each Climb Segment Number for the Intrec Engine

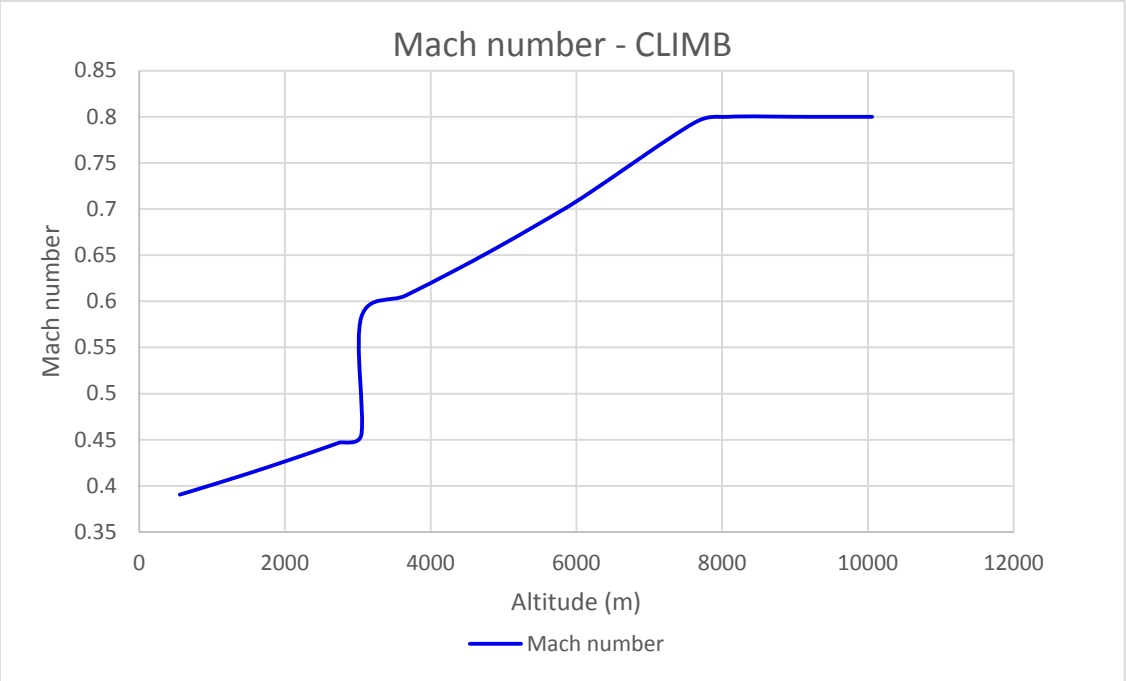

Figure 7-22: Mach Number Variation with Altitude during Climb for the Intrec Engine

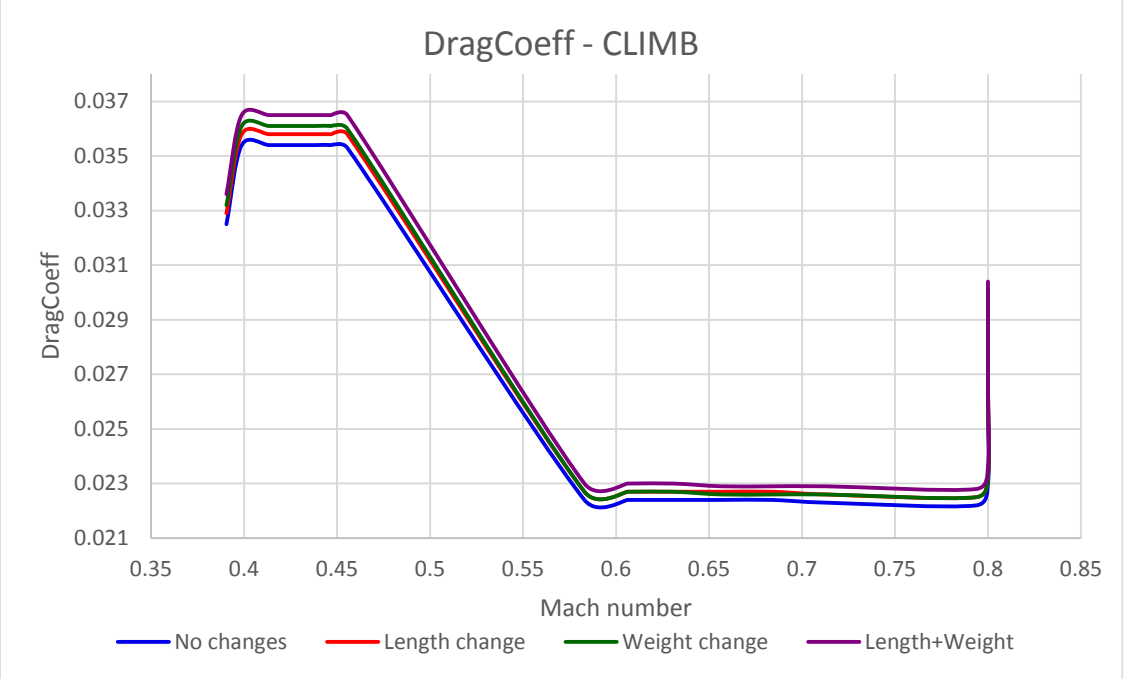

Figure 7-23: Drag Coefficient Variation during Climb for the Intrec Engine

The lift co-efficient does not change with an increase in length all through the profile. An increase in weight results in a 2% increase in the lift co-efficient. The overall effect of the device is a 2% increase in the lift coefficient during the climb phase. Ideally an increase in weight should not affect the lift co-efficient. However during climb, the angle of attack needs to increase in order to

compensate for the increase in the weight of the aircraft. This results in an increase in the lift co-efficient.

The Mach number increases continuously during climb starting from 0.3905 until it attains the initial cruise Mach number of 0.8. Figure 7-25 illustrates the variation in the EAS and the TAS during climb. The aircraft climbs at a constant EAS of 128.6 m/s (250 knots) up to an altitude of 3048 m at segment 7. This speed is maintained constant for noise restrictions close to ground. Then it accelerates to 164.6m/s (320 knots) and continues to climb to cruise Mach number which is achieved at an altitude of 8077.2 m at segment 15. The TAS increases continuously during climb. This is because TAS is a function of EAS and is inversely proportional to the square root of the relative atmospheric density.

Although EAS is maintained at a constant value, the density decreases as the aircraft gains altitude and hence TAS increases. TAS starts decreasing closer to the top of climb as a constant Mach number is maintained. The Mach number also increases with an increase in altitude in a similar manner to the TAS until it levels off to a constant value of 0.8 at segment 15 at an altitude of 8077 m.

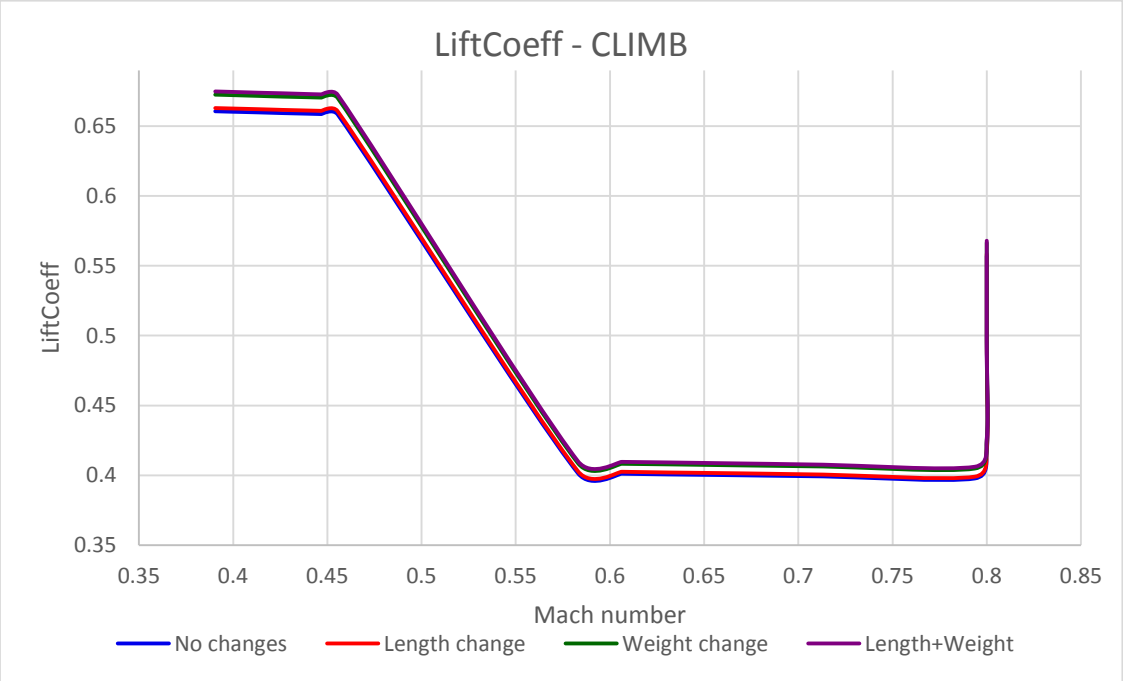

Figure 7-24: Lift Coefficient Variation during Climb for the Intrec Engine

Figure 7-26 illustrates the vertical rate of climb which decreases as altitude is gained. This decrease is due to a reduction in thrust because of a decrease in inlet mass flow with an increase in altitude. Figure 7-26 indicates that the vertical rate of climb falls to zero at segment 7 at an altitude of 3048 m. This is

because segment 7 and segment 8 have the same altitude and the aircraft is only accelerating horizontally from an EAS of 250 knots to an EAS of 320 knots. The rate of climb decreases further on as the altitude is increased. However, it does not change significantly with a change in the length and weight of the engine.

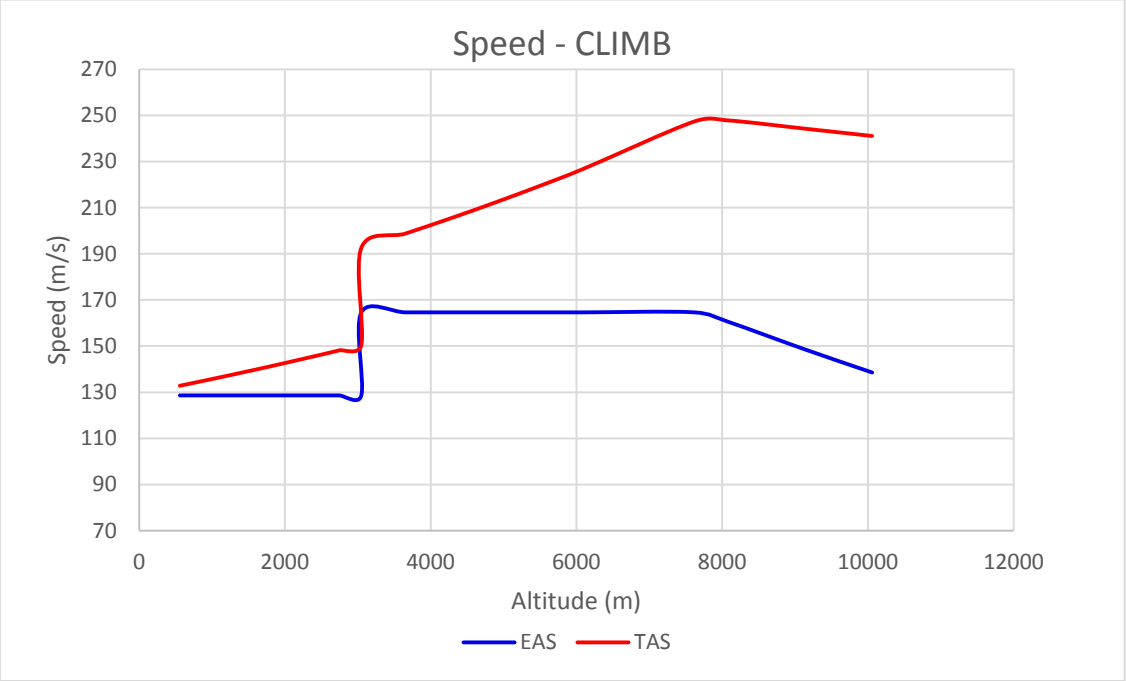

Figure 7-25: EAS and TAS Variation during Climb For the Intrec Engine

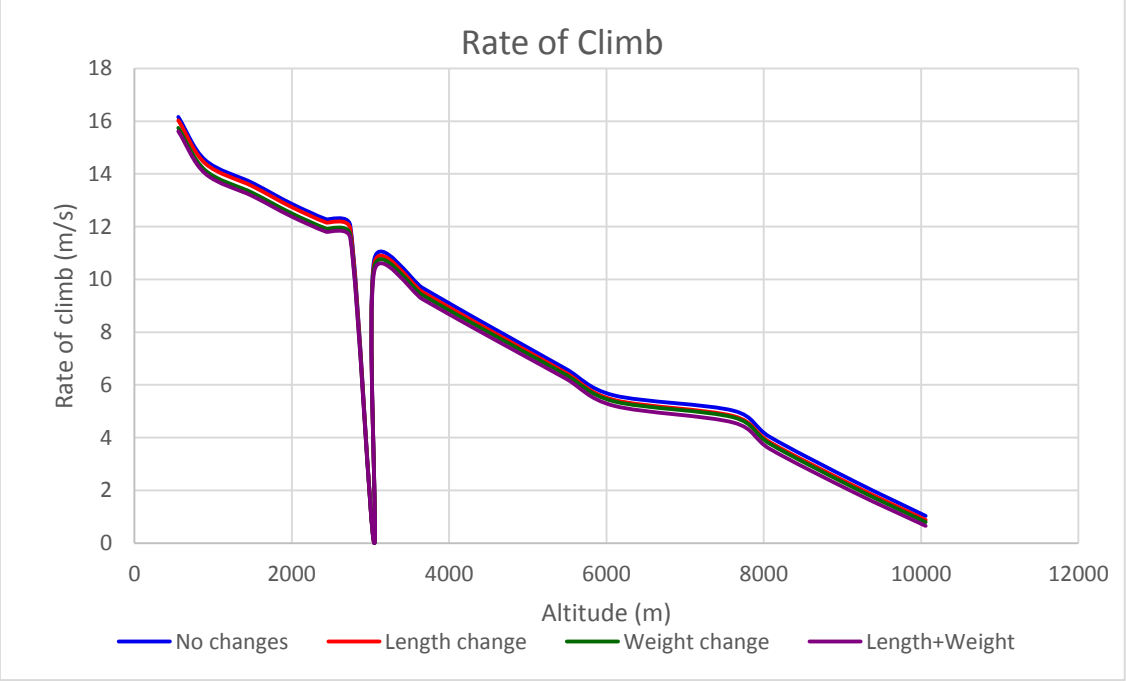

Figure 7-26: Vertical Rate of Climb for the Intrec Engine

Figure 7-27 indicates the change in the nacelle drag during the climb phase as the aircraft gains altitude and reaches the top of climb. The nacelle drag remains constant until segment 7 where an altitude of 3048 m is achieved. This is because the EAS remains constant until this altitude. It increases linearly with an increase in EAS and then remains constant until an altitude of 8077.2 m at segment 15.This is because the EAS has a constant value. After that it decreases until the first cruise altitude of 10058 is achieved at segment 17. This decrease in the drag after segment 15 is due the constant Mach number maintained and a decrease in EAS and TAS. The nacelle drag remains proportional to the EAS. The nacelle drag does not change with an increase in weight all through the profile. It is only a function of the change in length. An increase in length results in a 36% increase in the overall nacelle drag. However, this is a very minimal increase when compared to the overall drag of the aircraft.

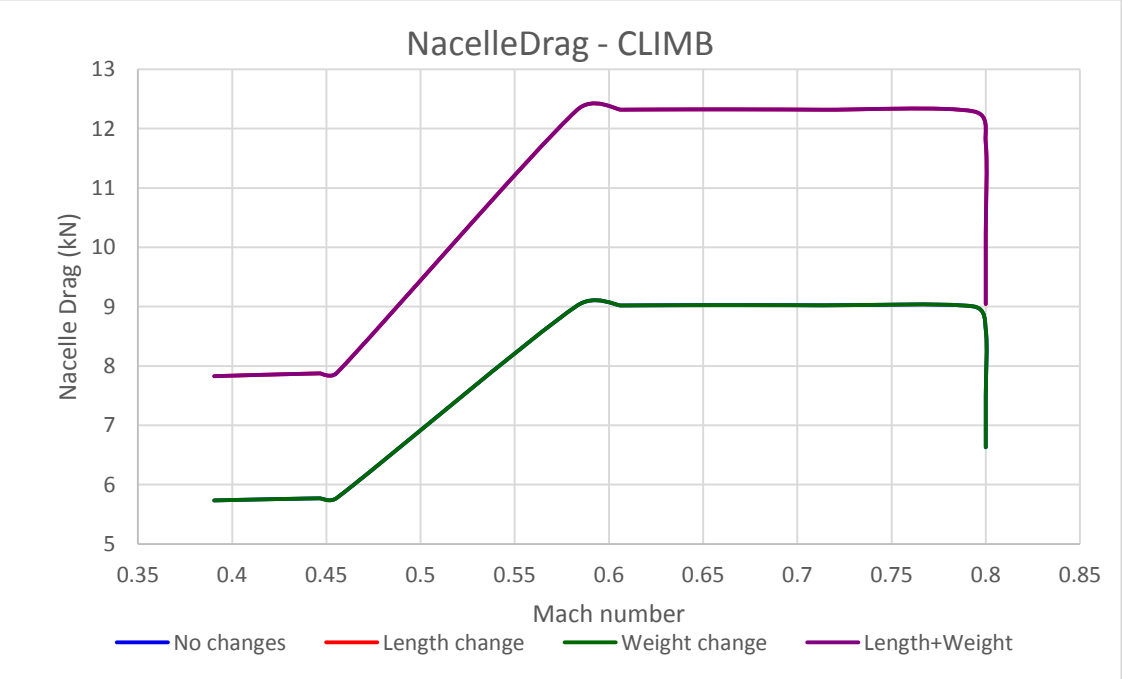

Figure 7-27: Nacelle Drag Variation during Climb for the Intrec Engine

Figure 7-28 indicates the change in the thrust requirement during the climb phase as the aircraft gains altitude and reaches the top of climb. The thrust decreases linearly as the aircraft climbs and gains altitude. This is because the mass flow entering the engine reduces as the aircraft gains altitude due to a reduction in air density with an increase in the altitude. The thrust does not change with an increase in weight or length of the engine all through the profile. It is only a function of the inlet mass-flow, ambient temperature and ambient pressure. These factors vary linearly with altitude. Hence all plots coincide. The thrust profile is linear except for an irregularity between segment 7 and segment

8 at an altitude of 3048 m. This is due to a transition in the EAS from 250 knots to 320 knots. The second irregularity in the curve is experienced between segment 14 and segment 15 at an altitude of 7620 m. This is because the aircraft switches to constant Mach number from constant EAS to avoid flying at the critical Mach number.

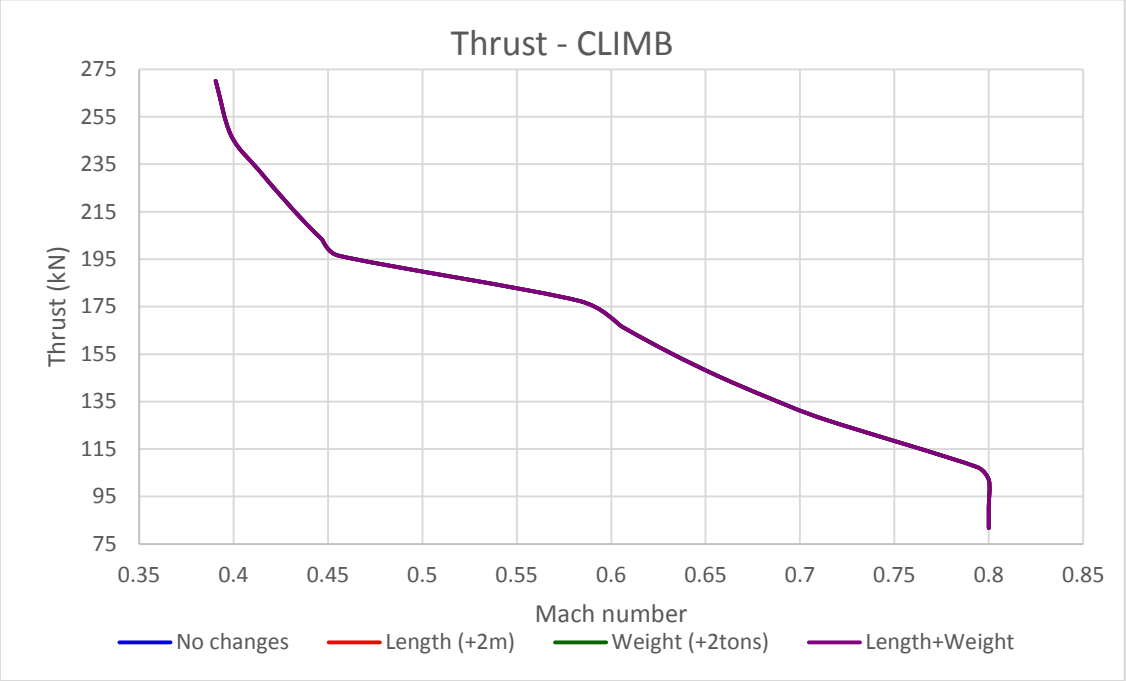

Figure 7-28: Thrust Variation during Climb for the Intrec Engine

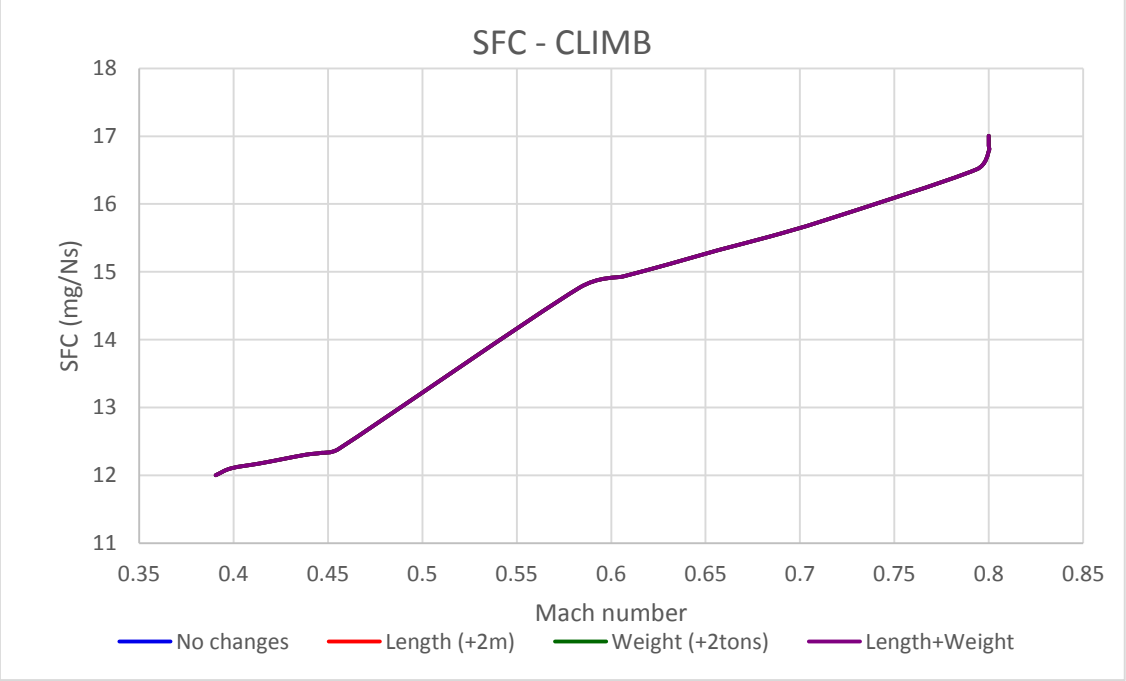

Figure 7-29: SFC Variation during Climb for the Intrec Engine

Figure 7-29 indicates the change in the SFC during the climb phase as the aircraft gains altitude and reaches the top of climb. The SFC increases linearly as the aircraft climbs and gains altitude. The aircraft needs to maintain EAS whereas the thrust is decreasing as altitude increases. Hence the SFC increases in order to maintain the EAS during climb. The SFC does not change with an increase in weight or length of the engine all through the profile. The SFC curve indicates a step change between segment 7 and segment 8 at an altitude of 3048 m. This is due to a transition in the EAS from 250 knots to 320 knots. A slope change in the curve is experienced between segment 14 and segment 15 at an altitude of 7620 m. This is because the aircraft switches to constant Mach number from constant EAS to avoid flying at the critical Mach number.

7.2.2.2 CRUISE

Figure 7-30 illustrates the variation of the drag coefficient during the cruise phase of the flight mission. The drag reduces as the aircraft flies through the cruise segments. This is because as the aircraft moves along a straight and level flight path, it consumes fuel and its weight decreases continuously which results in a reduction in the lift induced drag. The thrust requirement needs to equate to the drag for a straight and level flight.

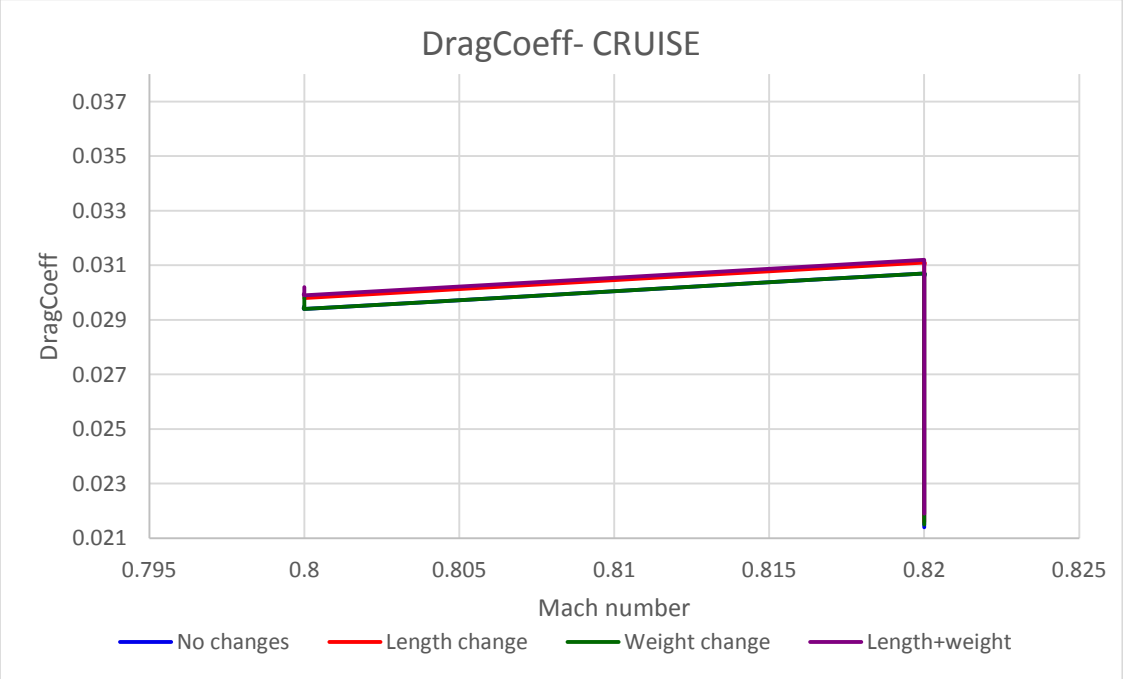

Figure 7-30: Drag Coefficient Variation during Cruise for the Intrec Engine

At the initial cruise altitude of 10058m, the drag co-efficient decreases steeply due to a reduction in the fuel weight of the aircraft at a constant altitude and

constant Mach number. There is a slight increase in the drag co-efficient as the aircraft accelerates and climbs to the final cruise altitude of 10670m due to a decrease in EAS. Then again the drag co-efficient starts to decrease steeply with a reduction in fuel weight at a constant altitude and a constant cruise economy Mach number of 0.82. The drag coefficient of the aircraft increases by 1% with a change in length and increase by 1.4% with a change in the weight of the engine. The overall effect of the contrail-free engine on the cruise drag coefficient is only an increase in the drag coefficient by 2.4%.

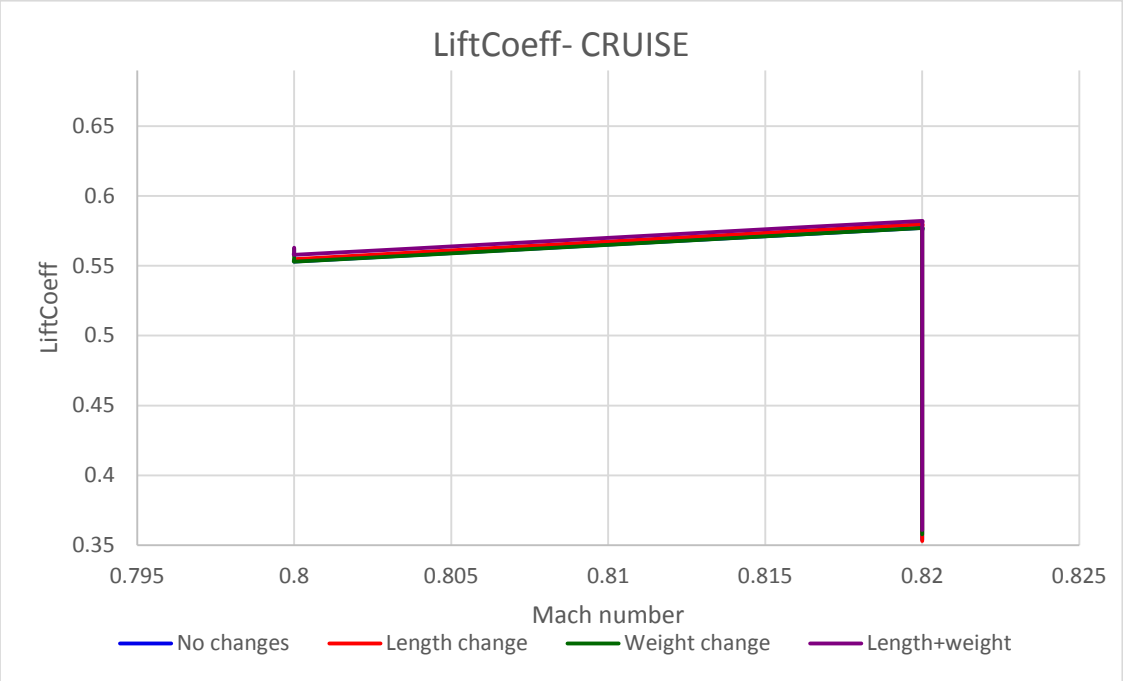

Figure 7-31: Lift Coefficient Variation during Cruise for the Intrec Engine

Figure 7-31 illustrates the variation of the lift coefficient during the cruise phase of the flight mission. The lift reduces as the aircraft flies through the cruise segments. This is because as the aircraft moves along a straight and level flight path, it consumes fuel and its weight decreases continuously which results in a reduction in the lift coefficient as lift varies linearly with the weight of the aircraft. At the initial cruise altitude of 10058m, the lift co-efficient decreases steeply due to a reduction in the fuel weight of the aircraft at a constant altitude and constant Mach number. There is a slight increase in the lift co-efficient as the aircraft accelerates and climbs to the final cruise altitude of 10670m due to a decrease in EAS .Then again the lift co-efficient starts to decrease steeply with a reduction in fuel weight at a constant altitude and a constant cruise economy Mach number of 0.82.The lift coefficient of the aircraft increases by 0.2% with a change in length and increases by 1.6% with a change in weight of the engine. The overall effect of the contrail-free engine on the cruise lift coefficient is only an increase in the lift by 1.7 %.

Figure 7-32 illustrates the variation of the nacelle drag during the cruise phase of the flight mission. The nacelle drag remains constant as the aircraft flies at a constant altitude and constant Mach number. This is because the nacelle drag only comprises of the profile drag and does not include the lift induced drag as in the case of the aircraft. The slight variation in the nacelle drag along the profile is due to a decrease in EAS with a gain in altitude. The nacelle drag is unaffected by the change in the engine weight. The nacelle drag is affected by an increase in the length of the engine. An increase in the length by 2 meters results in an overall increase in the nacelle drag by 36%. However, this is a small fraction when considering the total drag of the aircraft. The drag of the aircraft determines the thrust requirements at various flight conditions.

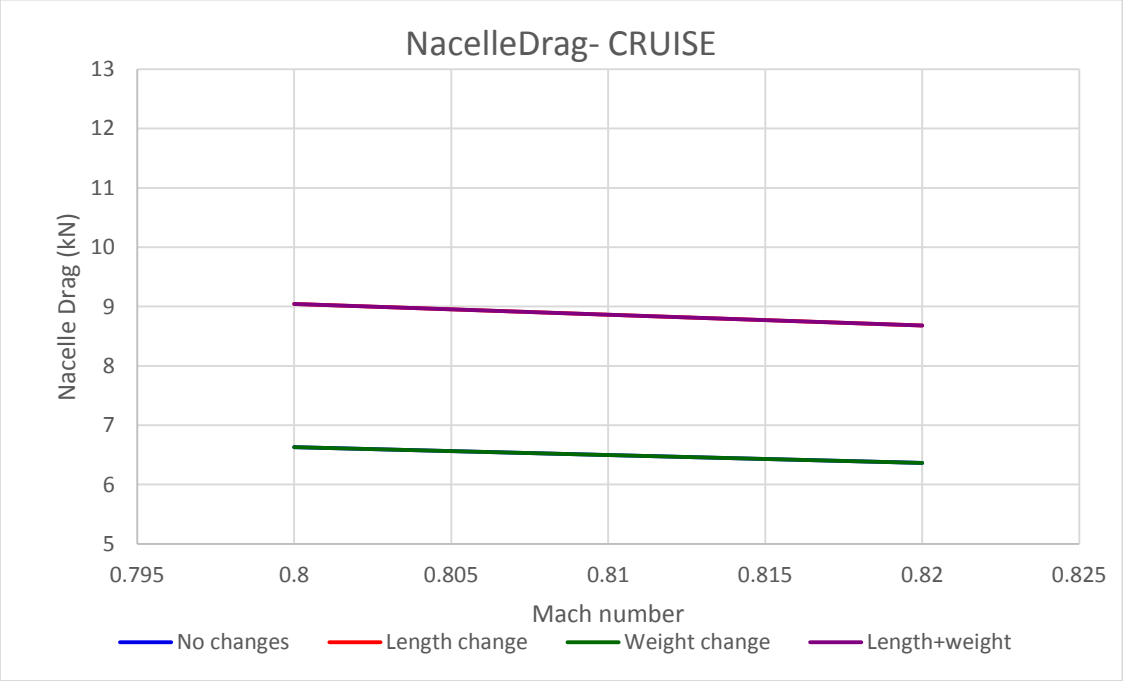

Figure 7-32: Nacelle Drag during Cruise for the Intrec Engine

Figure 7-33 indicates the change in the thrust during the cruise phase as the aircraft covers distance. The thrust decreases as the aircraft flies along the flight path at a constant altitude. A continuous reduction in thrust occurs along the cruise trajectory as the aircraft burns fuel and experiences a reduction in weight. This results in a decrease in the drag and lift of the aircraft. In order to maintain straight and level flight, the thrust needs to equate to the drag and hence reduces accordingly. The lift needs to be equal to the weight of the aircraft. . At the initial cruise altitude of 10058m, the thrust decreases steeply due to a reduction in the fuel weight of the aircraft at a constant altitude and constant Mach number. It remains constant when the aircraft accelerates from Mach 0.8 to Mach 0.82 as the aircraft climbs from the initial cruise altitude to the final cruise altitude. Then again the thrust starts to decrease steeply with a reduction

in fuel weight at a constant altitude and a constant cruise economy Mach number of 0.82.

The change in thrust requirement with an increase in length of the engine is 1% all through the profile, whereas with a change in the weight of the engine, the thrust increases by 1.5%. The overall increase in thrust requirement is 2.5%. Although, the thrust It is only a function of the inlet mass-flow, ambient temperature and ambient pressure, it is affected by a change in length and weight because the thrust needs to equate to the drag and the weight needs to be equal the lift in order to maintain straight and level flight. Since lift and drag coefficients change with a change in the length and weight of the engine, the thrust requirement also changes correspondingly.

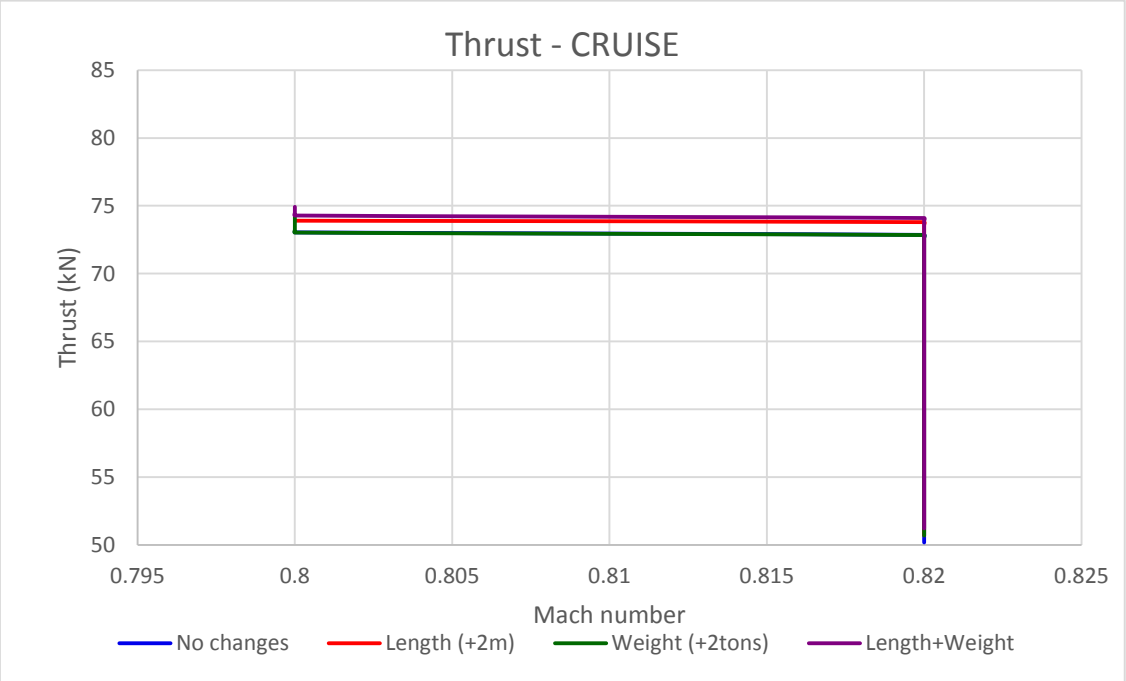

Figure 7-33: Thrust variation during Cruise for the Intrec Engine

Figure 7-34 illustrates the variation of SFC during cruise flight. The SFC decreases as the aircraft flies along the flight path at a constant altitude. A continuous reduction in SFC occurs along the cruise trajectory as the thrust requirement of the aircraft reduces due to a reduction in cruise drag. A linear increase in SFC is experienced due to a change in the cruise altitude from 10058 m to 10670 m. This is because of an increase the Mach number from 0.8 to the cruise economy Mach number of 0.82 at a higher altitude.

The SFC change with an increase in length of the engine is 0.2 % all through the profile, whereas with a change in the weight of the engine, the SFC increases by 0.2%. The overall increase in SFC is 0.4%. The increase in SFC is

due to an increase in thrust requirement at cruise for the intercooled-recuperated contrail-free engine.

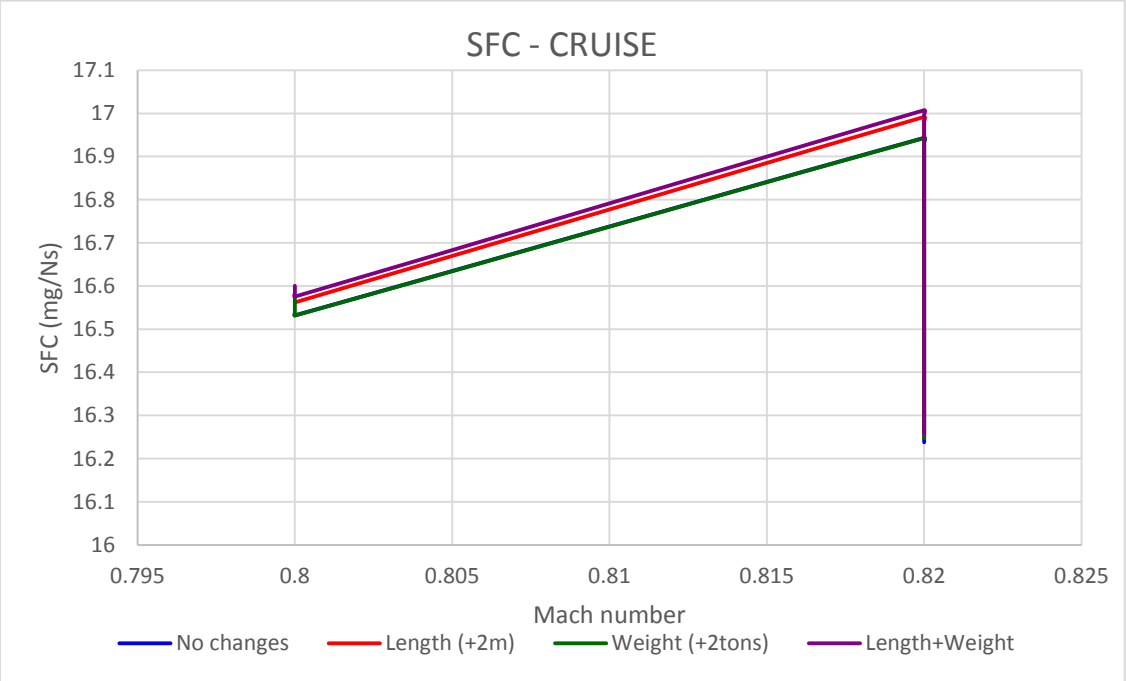

Figure 7-34: SFC variation During Cruise for the Intrec Engine

7.2.2.3 GLIDE

Table 7-6 indicates the glide altitude and Mach number for each glide segment. This enables us to interpret the output plots with reference to the operating altitude. Data has been plotted versus Mach instead of altitude for clarity of illustration.

Glide Segment	Altitude (m)	Mach number	Glide Segment	Altitude (m)	Mach number
1	10670	0.7804	6	4001.2563	0.5043
2	9336.2512	0.7275	7	2667.5075	0.4547
3	8002.5025	0.6542	8	1333.7588	0.4153
4	6668.7537	0.6177	9	0.01	0.3945
5	5335.005	0.5701	10	0.01	-

Table 7-6: Glide Altitude at Each Glide Segment Number for the Intrec Engine

Figure 7-35 illustrates the change in Mach number with a decrease in altitude during the glide phase. The Mach number decreases continuously during glide

starting from 0.7804 at the final cruise altitude until it attains the approach Mach number of 0.3945.

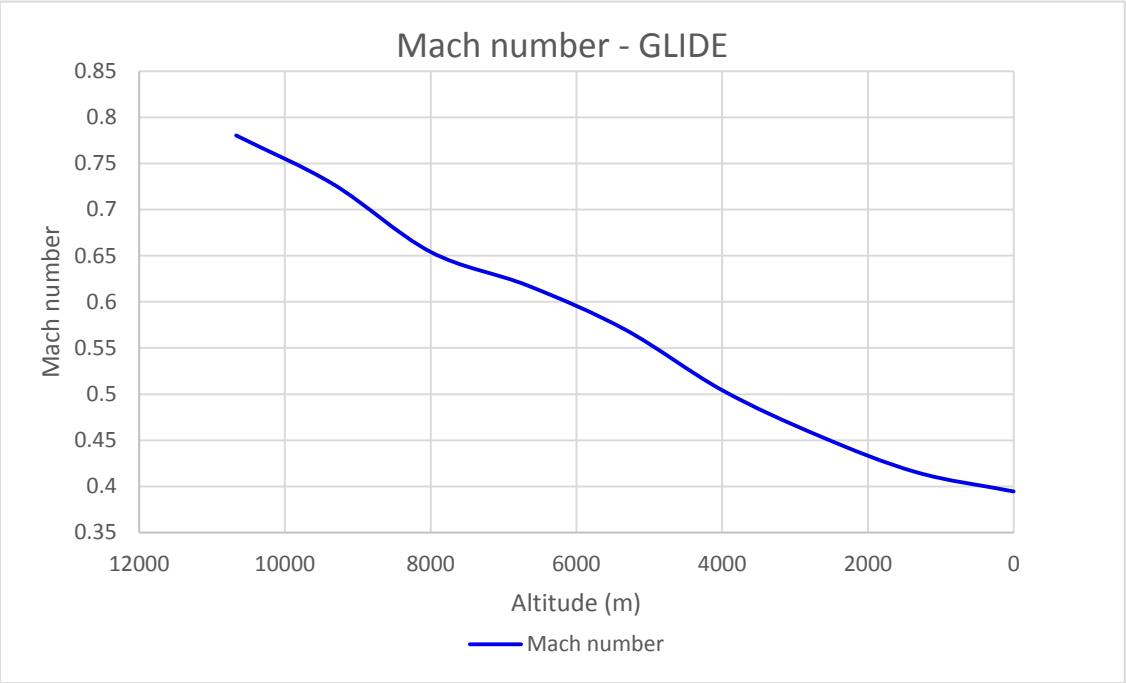

Figure 7-35: Mach Number Variation with Altitude during Glide for the Intrec Engine

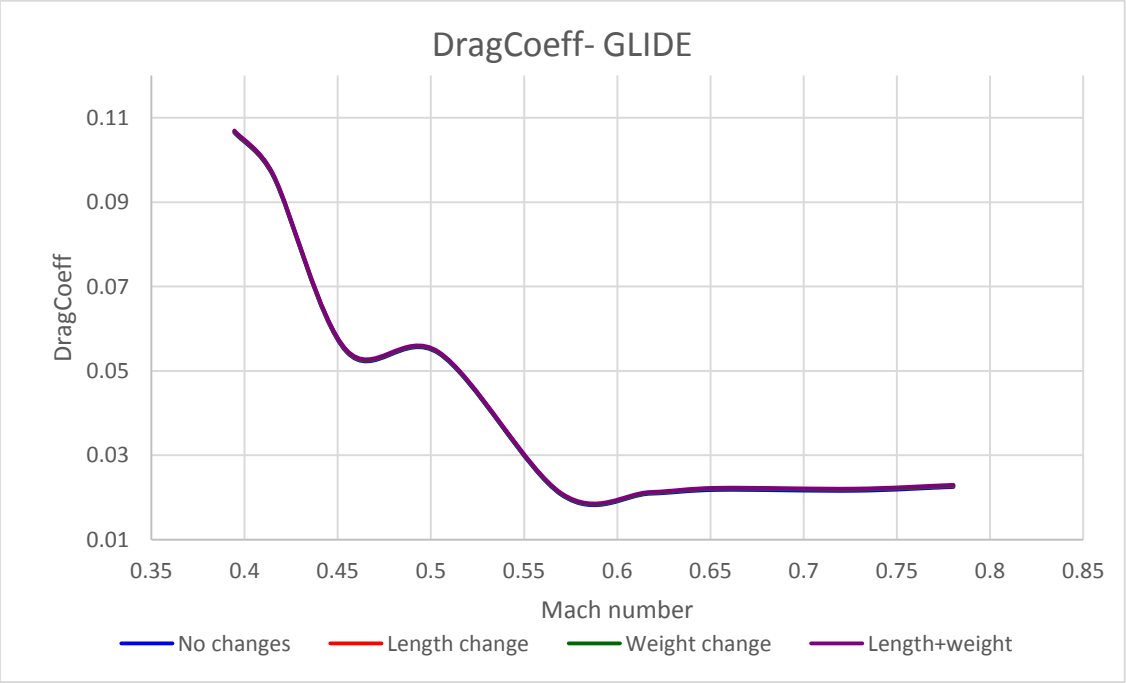

Figure 7-36: Drag Coefficient Variation during Glide for the Intrec Engine

Figure 7-36 indicates the change in drag coefficient during the glide phase as the aircraft loses altitude and reaches the landing phase. The drag coefficient

decreases at a very small rate until an altitude of 5335 m at segment 5 and then increases until the landing phase is reached. This is because for initial descent, the rate of descent needs to be low in order to maintain cabin pressure. Beyond an altitude of 5335 m, the second phase of descent takes place where flaps and other drag increasing systems are deployed to enhance the profile drag. The drag then increases linearly with a decrease in altitude. The drag coefficient increases by 0.9% with an increase in length and by 1.3% with an increase in weight all through the profile. Hence the drag coefficient profile of the contrail free engine has an overall increase of 2.2% during the glide phase when compared to that of the intercooled recuperated engine.

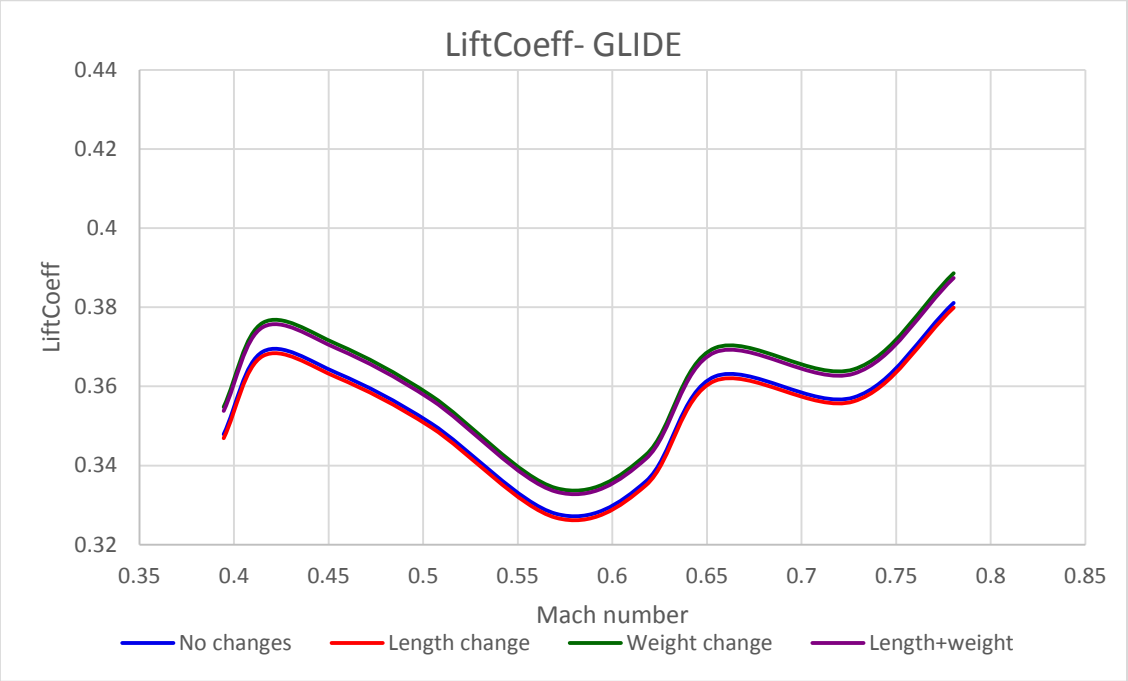

Figure 7-37: Lift Coefficient Variation during Glide for the Intrec Engine

Figure 7-37 indicates the change in lift coefficient during the glide phase as the aircraft loses altitude and reaches the landing phase. The lift coefficient decreases until an altitude of 5335 m at segment 5 and then increases until the approach phase at segment 8 is reached. The lift coefficient is inversely proportional to the density, which increases as altitude reduces. Hence the coefficient of lift decreases. Beyond an altitude of 5335 m, the second phase of descent takes place where flaps and other high lift devices are deployed to enhance the profile drag. The engagement of the high lift systems increases the lift coefficient as well. The lift coefficient decreases after approach when the plane is flared out to achieve stall speed for landing. The lift coefficient does not change with an increase in length all through the profile. However it increases by 1.7 % with an increase in the weight of the engine.

Figure 7-38 illustrates the variation in the EAS and the TAS during glide. The aircraft glides at a near constant EAS of 130m/s to 140 m/s all through the glide phase. This speed is maintained constant for noise restrictions close to ground. The TAS decreases continuously during glide. This is because TAS is a function of EAS and is inversely proportional to the square root of the relative atmospheric density.

Although EAS is maintained at a constant value, the density decreases as the aircraft loses altitude and hence TAS decreases. The Mach number also decreases with a decrease in altitude in a similar manner to the TAS until the landing phase is reached. The values for TAS, EAS and Mach have been input into the code and therefore do not change with a change in the length or the weight of the engine. Hence they remain constant for both the intercooled-recuperated engine and the contrail free engine.

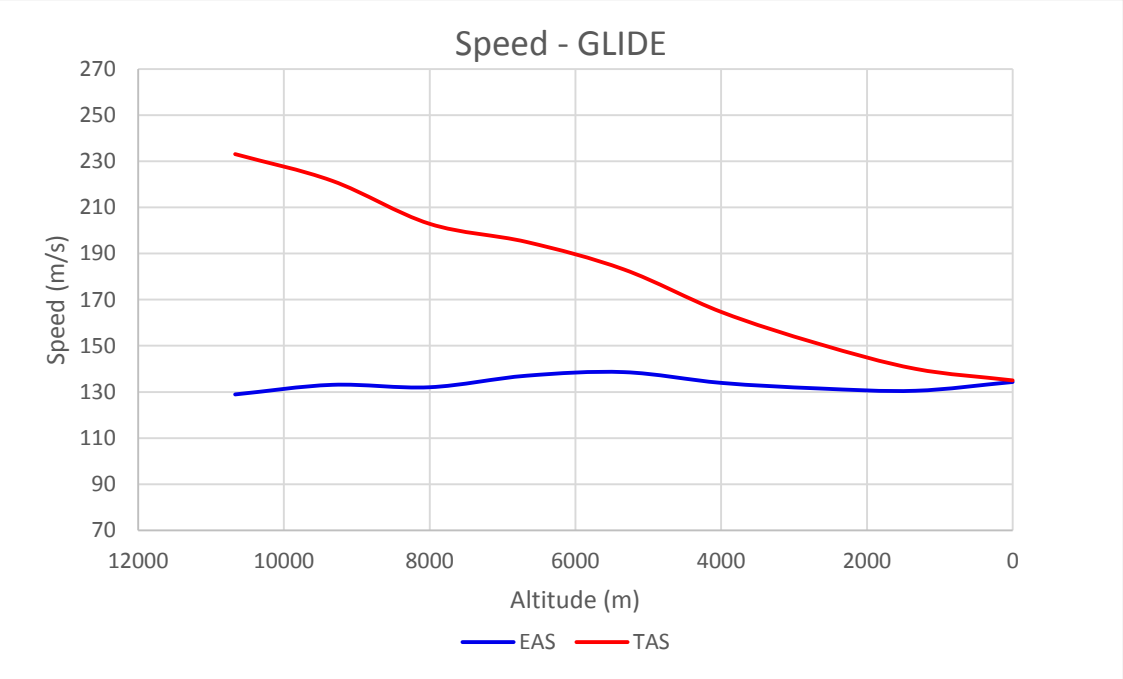

Figure 7-38: EAS and TAS Variation During Glide For the Intrec Engine

Figure 7-39 illustrates the vertical rate of descent during the glide phase. The initial rate of descent decreases from 6 m/s to 4 m/s at segment 4 at an altitude of 6668m. This is because for initial descent, the rate of descent needs to be low in order to maintain cabin pressure. Beyond that it increases to 22 m/s up to an altitude of 1333 m at segment 8. This is because once cabin pressure is established; the aircraft loses altitude quickly until it enters the approach phase. Beyond that the rate of descent again reduces in order for the aircraft to land and touchdown softly. The vertical rate of descent changes minimally with a change in the engine length or weight.

Figure 7-40 indicates the change in the nacelle drag during the glide phase as the aircraft loses altitude and approaches to land. The nacelle drag only varies by a maximum of 1 KN throughout the glide phase profile. This variation is proportional to the variation in the EAS during this phase. The nacelle drag does not change with an increase in weight all through the profile. It is only a function of the change in length. An increase in length results in a 36 % increase in the overall nacelle drag. However, this is a very minimal increase when compared to the overall drag of the aircraft.

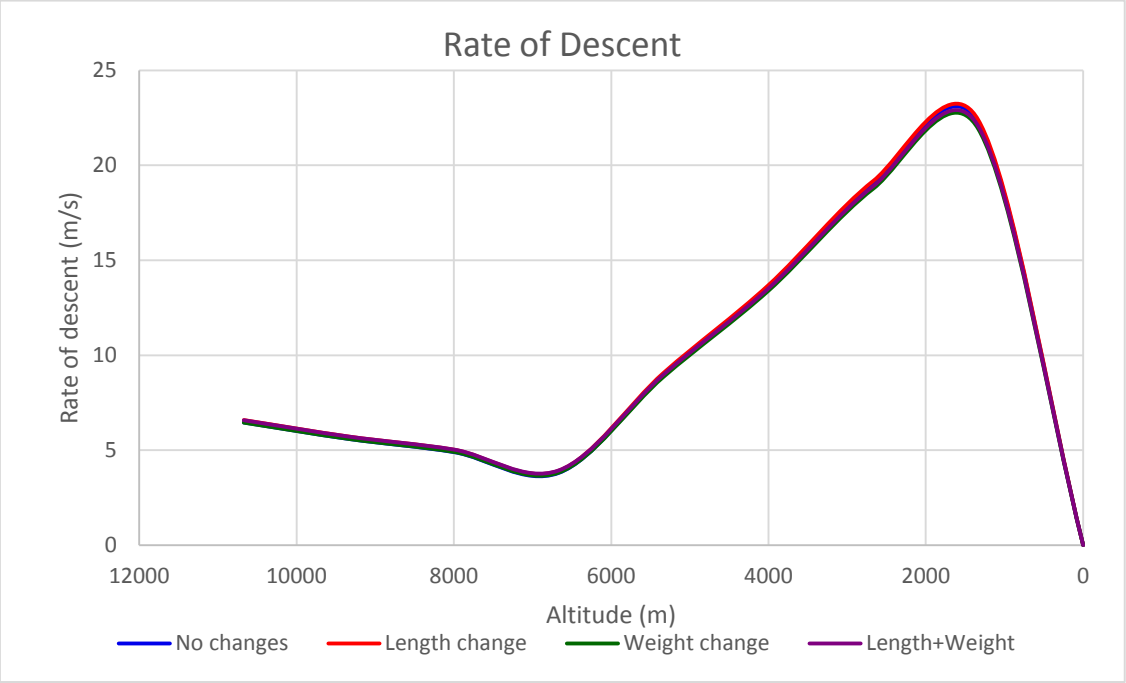

Figure 7-39: Absolute Rate of Descent for the Intrec Engine

Figure 7-41 indicates the thrust variation during glide. The thrust increases gradually until segment 7 at an altitude of 2667 m close to the approach phase. This is due to an increase in the air density as the aircraft descends which increases the mass-flow entering the engine at idle settings and hence results in a rise in thrust for a constant TET.

As the aircraft enters the approach phase the thrust rises steeply as the engine is throttled to prevent undershoot. An increase in TET is also experienced with the increase in thrust. The thrust value increases until the aircraft lands at segment 9. This behaviour does not change with a change in the length or the weight of the engine. Hence the contrail-free engine can land as per the standard of an intercooled-recuperated engine.

Figure 7-42 illustrates the SFC variation during the glide phase. The SFC varies according to the change in the thrust in this phase. The SFC has a high value

of 19 mg/Ns at the start of the glide phase. It decreases linearly until it descends to the approach altitude of 1333 m at segment 8. The SFC at this point is 13.4 mg/Ns. A high SFC at the start of the glide phase is due to a low value of thrust. It varies inversely with the thrust.

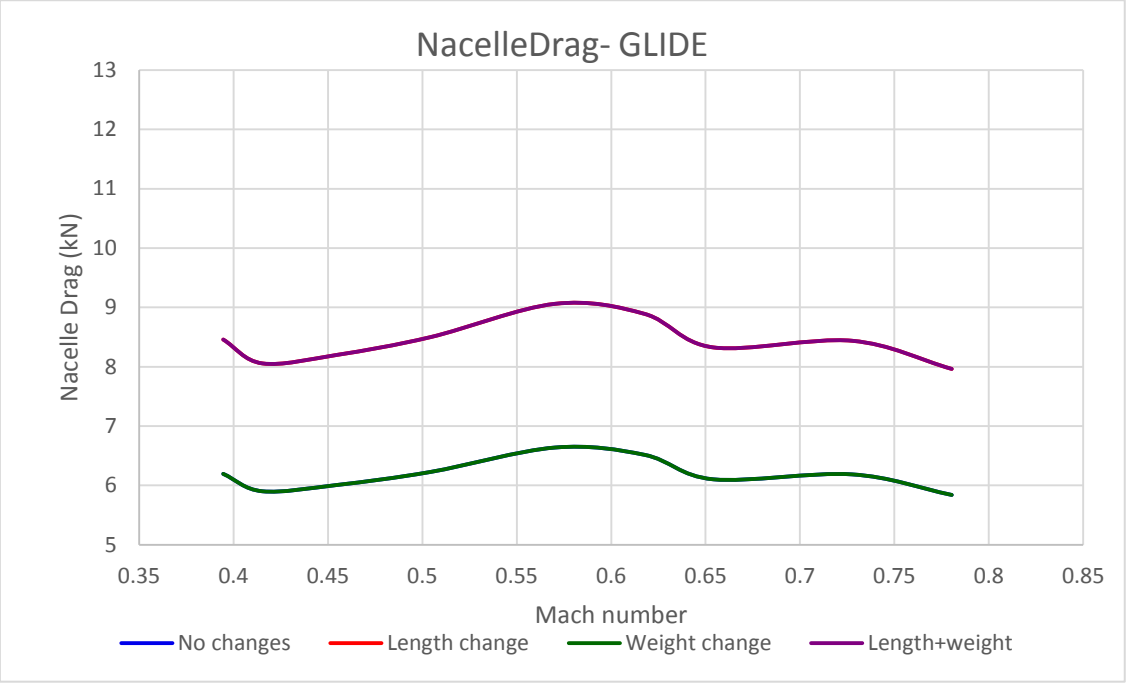

Figure 7-40: Nacelle Drag during Glide for the Intrec Engine

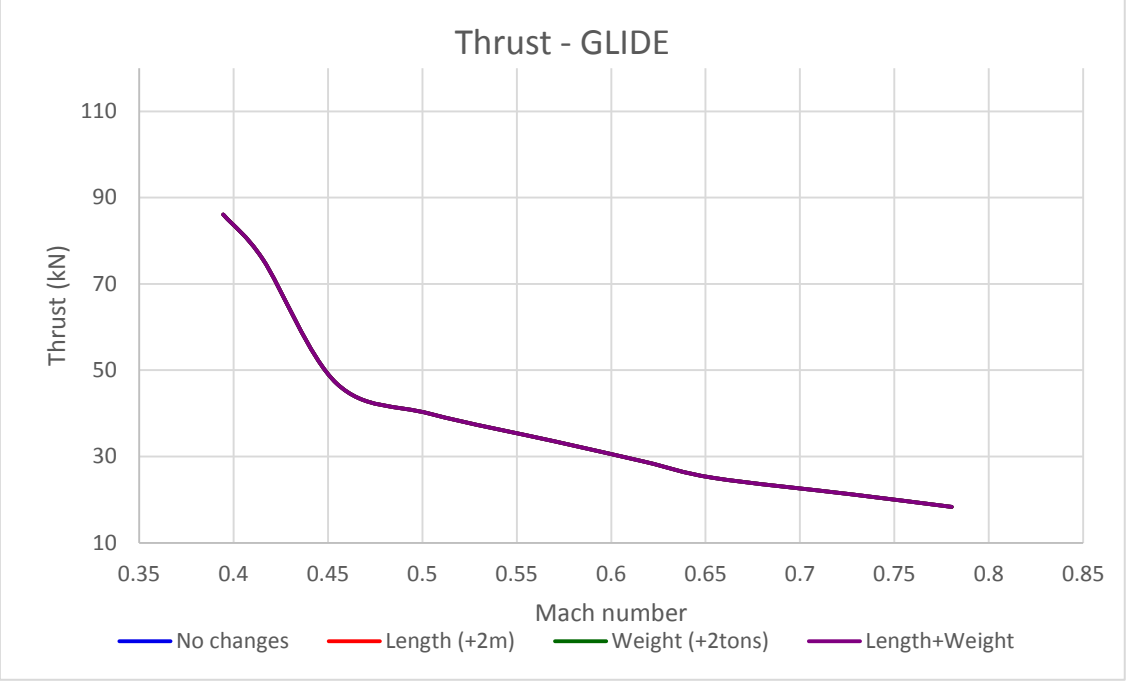

Figure 7-41: Thrust Variation during Glide for the Intrec Engine

The SFC remains constant after the approach phase until the aircraft lands and comes to a complete stop. The SFC does not change with a change in the length or the weight of the engine.

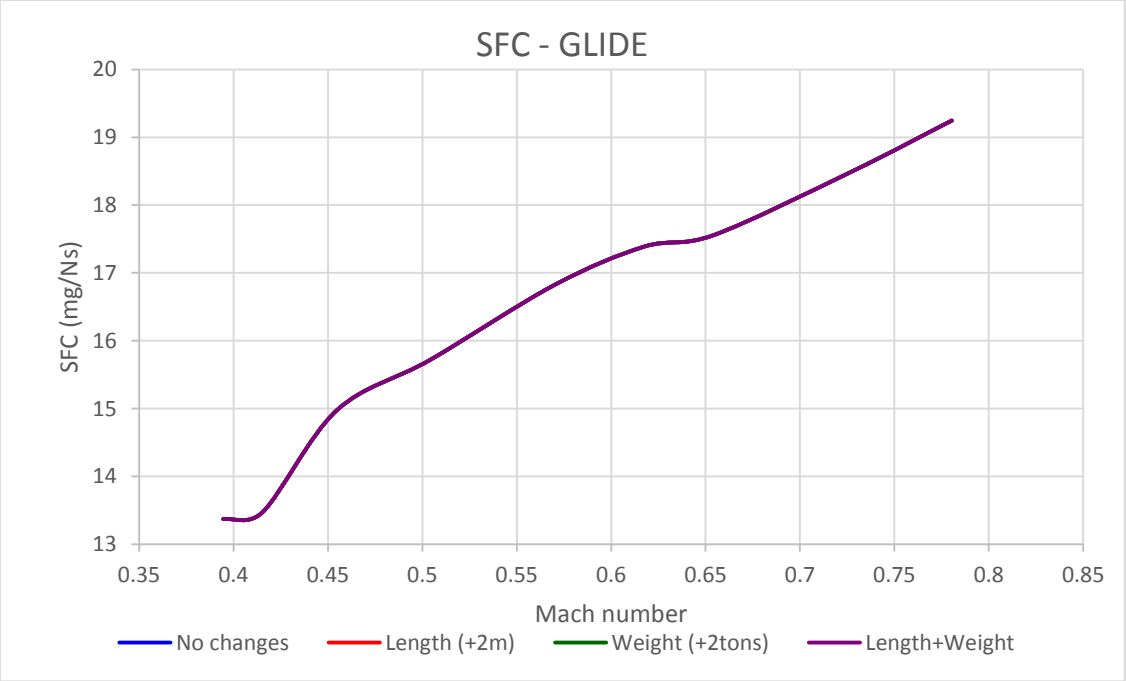

Figure 7-42: SFC Variation during Glide for the Intrec Engine

7.3 ENGINE DRAG CALCULATIONS

A preliminary investigation was carried out to determine the increase in the nacelle drag due to the attachment of the device into the engine. The device is attached in between the LPT and the nozzle and hence lies at the boundary of the mid-body and the after-body of the nacelle. The contribution of the mid-body drag is in the range of 7.5 to 10 % of the overall nacelle drag while the drag of the aft-body is nearly 60 % (Williams,2010).

In the case of the contrail free engine, a maximum increase in length of 2 meters has been estimated for the initial design specifications. This results in an overall increase in nacelle drag of 36% during the cruise phase as tabulated in Table 7-7. All aerodynamic properties and engine parameters have been determined at a cruise altitude of 10670 meters as given in Table 7-8. The methodology to calculate the nacelle drag is detailed in Table 7-9. This methodology has been adopted from (Williams,2010).

These results have been verified by the simulation in the engine performance software which has been executed for the contrail-free aero-engine with an increase in the length and weight of the engine.

ENGINE LENGTH (m)	Nacelle Wetted Area (m^2)	Reynolds Number	Skin Friction Coefficient (Cfn)	Form Factor (Fn)	Nacelle Drag Coefficient (Dn)	Nacelle Drag (N)
Original Length	42.08	2.91E+07	2.40E-03	1.25	3.36E-03	1584.73
Extended Length	60.59	4.18E+07	2.27E-03	1.25	3.18E-03	2161.48

Table 7-7: Calculation for Nacelle Drag for the Contrail-free Engine at Cruise

PARAMETERS	VALUE	PARAMETERS	VALUE
Original Length (m)	4.547	Kinematic Viscosity m^2/s	3.806E-05
Diameter (m)	2.946	Mach Number (Mn)	0.82
True Air Speed(TAS in m/s)	243.15	Altitude at Cruise(m)	10670
Density (Kg/m^3)	0.38	Extended Length (m)	6.547

Table 7-8: Parameters for Nacelle Drag Calculations

Formulae for Nacelle Drag Calculations
Wetted Area Engine Nacelle Wetted Area = 2 x pi x (Diameter / 2) x Length;
Reynolds Number Reynolds Number = TASx Length / Kinematic Viscosity ;
Skin Friction Coefficient Cfn = 0.455 / ((log10 (Reynolds)) $^{2.58}$ x (1. + 0.144 * Mn^2) $^{0.65}$);
Form Factor (including interference factor) Fn = 1.25;
Overall Nacelle Drag Dn = 1.12xCfn x Fn Drag = 0.5 x Density x TAS^2 x Wetted_Area x Dn

Table 7-9: Methodology to Calculate Nacelle Drag

7.4 AIRCRAFT PERFORMANCE COMPARISON FOR THE TURBOFAN AND THE INTERCOOLED-RECUPERATED ENGINE

Figure 7-43 illustrates the comparison of the thrust variation between the turbofan engine and the intercooled-recuperated engine during the flight mission. This comparison is valid for the original configuration as well as for the contrail free configuration. Both engines start taxiing at 100 KN and accelerate to the take-off rating of 346 for the basic turbofan and 360 KN for the intercooled-recuperated turbofan. The higher thrust value for the intercooled-recuperated engine is due to the utility of the intercooler and the recuperator heat exchanger.

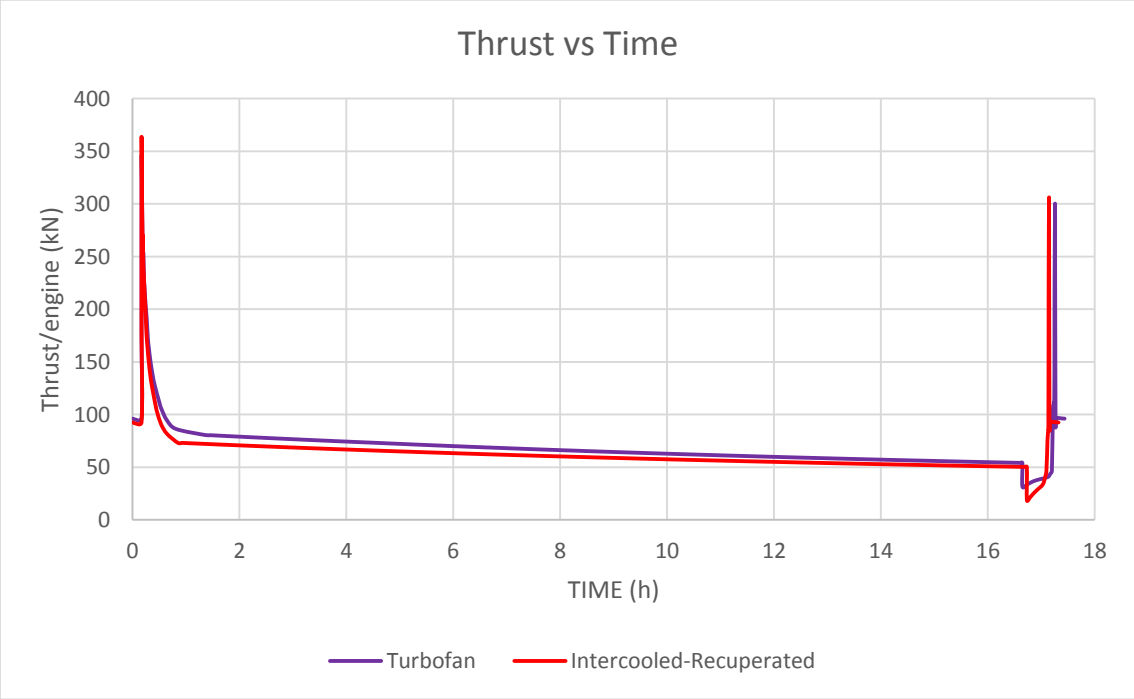

Figure 7-43: Thrust Variation with Time during the Flight Mission for the Turbofan and the Intrec Engine

The thrust requirement decreases steeply during climb for 38 minutes and then decreases gradually during cruise for 16 hours in both cases. This simulation has been performed for the maximum possible range and endurance of the A380-800 aircraft. The climb thrust is the same in the two configurations whereas the cruise thrust is at maximum 10 % higher in the case of the turbofan configuration. This discrepancy is because of the different power settings for code convergence in the two engines as they both have a different configuration. The thrust reduces to 31 KN during the glide phase for the turbofan and 20 KN for the intercooled-recuperated engine. The thrust

increases to 100KN for the turbofan and 76 KN for the intercooled-recuperated engine once the aircraft enter the approach phase. During the glide and the approach phase, the operating TET for the intercooled recuperated engine is lower than that of the turbofan engine. This is because different convergence parameters are applied in both cases at low power settings. After landing the thrust increases again in both cases up to 300 KN for the engagement of the thrust-reversers. Beyond that it further reduces to 92 KN for taxiing in both cases until the aircraft come to a complete stop.

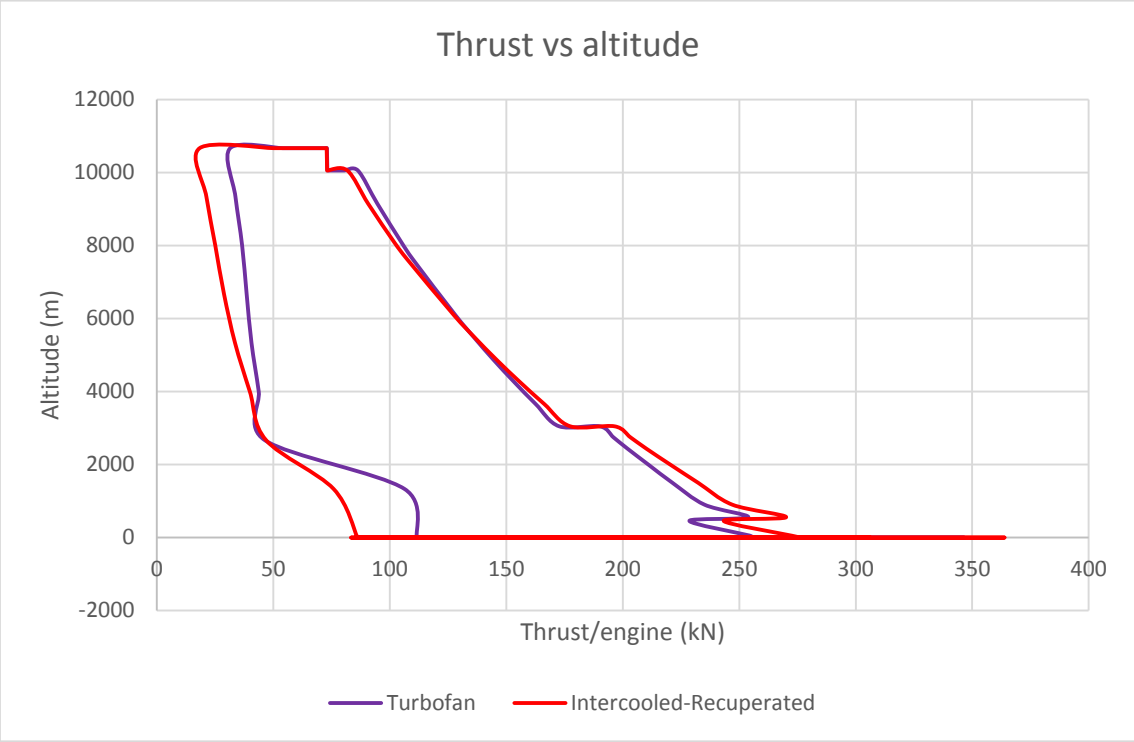

Figure 7-44: Thrust Variation with Altitude during the Flight Mission for the Turbofan and the Intrec Engine

Figure 7-44 also illustrates the variation of thrust with altitude for both engine configurations. Both engines take-off from ground altitude at their respective take-off thrust. They climb with the same gradient but the climb thrust of the turbofan engine is 4 % less than that of the intercooled-recuperated engine for the initial climb up to an altitude of 3048 m at a velocity of 250 knots. Beyond this altitude the aircraft accelerates to 320 knots and both engines climb at the same thrust.

The cruise thrust is lower for the intercooled-recuperated engine. This difference becomes prominent at the end of the cruise phase. During the glide phase, the rate of change of thrust is lower for the turbofan in comparison to the intercooled recuperated engine. As for the final approach the thrust requirement of the turbofan engine is higher than that of the intercooled-recuperated engine.

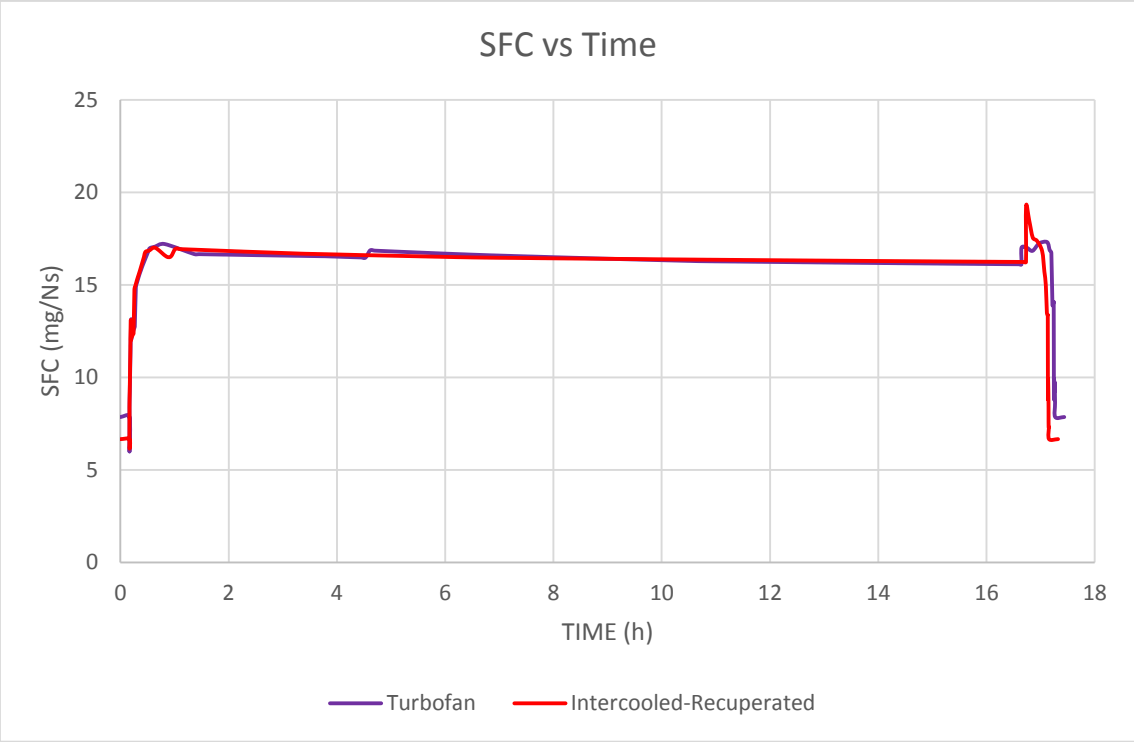

Figure 7-45: SFC Variation during the Flight Mission for the Turbofan and the Intrec Engine

Figure 7-45 illustrates the variation of SFC during the flight mission for both engine configurations. The SFC requirement at take-off for the turbofan is 7.85 mg/Ns whereas that of the intercooled recuperated engine is 6.66 mg/Ns. The SFC increases to its maximum value of 16.9 mg/Ns during climb until the first cruise altitude is attained. It decreases gradually during cruise flight. The SFC for both cases is the same for cruise flight. A slight increase in SFC is experienced for a brief interval at the start of the glide phase as the engines need to adjust to the low power setting. Beyond that, the SFC decrease steeply as the aircraft descends at idle power and lands eventually. The final point on the curve indicates the SFC during taxi which is at the same values as the initial taxi for both cases.

Figure 7-46 illustrates the TET variation during the flight mission. At take-off the TET for the intercooled-recuperated engine is 100 K lower than that of the turbofan engine. The same TET difference applies to the climb phase since the aircraft climbs at the maximum operating take-off TET. The difference in TET reduces to 50 K during the initial cruise phase among the two engines but then eventually at the end of the cruise, both engines achieve the same TET of 1500 K. This discrepancy is because of the different power settings for code convergence in the two engines as they both have a different configuration. The TET difference between the two engines for the glide and the approach phase is 60 K and that during landing for thrust reversal is 175 K. This is because

different convergence parameters are applied in both cases at low power settings The higher TET in the turbofan result in higher thrust values in that configuration.

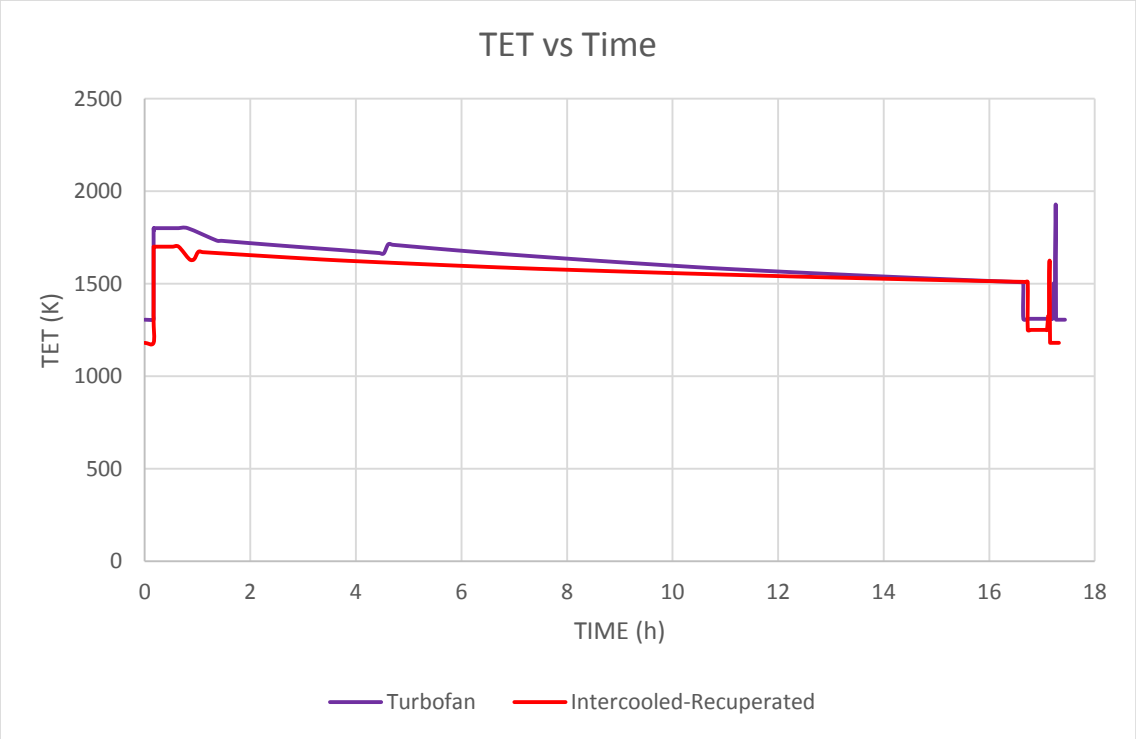

Figure 7-46: TET Variation during the Flight Mission for the Turbofan and the Intrec Engine.

7.5 CONCLUSION

This detailed study investigates the performance of the contrail-free engine in the basic three spool turbofan as well as the three spool intercooled-recuperated turbofan configuration and concludes that the inclusion of the water- expelling device into the engine does not alter the performance of the aircraft drastically. In the perspective of the performance of the aircraft integrated with the engine, this is essentially a change in the geometry of the engine. Only fractional changes have been observed in the aerodynamic parameters of the aircraft and the engine due to this inclusion. A modification in the length and weight of the engine therefore does not contribute to a significant change in the overall performance of the aircraft. Hence the integration of the contrail-free engine into any conventional aircraft is validated to be a practically implementable and technically viable perspective.

8 BACKGROUND STUDIES

8.1 WATER IN THE ATMOSPHERE

Water vapour accounts for 0.25% of the mass of the atmosphere on average. It has a residence time that ranges from a few seconds to days and this makes water a highly variable constituent. Water is released from aircraft exhaust emissions into the upper troposphere. This water is released as vapour at a high temperature whereby it condenses in the cooler atmosphere to form contrails and eventually cirrus clouds.

In one example reported by Knollenberg (1972), “the amount of moisture released by the burning of jet fuel from a research aircraft was 1.7 grams of water for every meter of flight path. However, the total water measured in a persistent contrail produced by the aircraft was conservatively measured to be between 20700 to 41200 grams of water for every meter of the contrail path!” Almost the entire contrail is created from the moisture in the atmosphere through the process of collision-coalescence. According to Schumann et al. (2015) contrail water maybe 10^3 to 10^6 times the amount of water emitted.

The tropospheric region constitutes 80% of the mass of the atmosphere. Commercial aircraft cruise along the upper troposphere just below the tropopause. The lower troposphere hosts all kinds of weather patterns. Hence the flight altitude is an intermediary layer between the troposphere and the stratosphere and has been chosen as such as the optimum flight altitude in order to fly above the weather. This study aims to devise a method to reduce the greenhouse effect of water vapour that is released from the exhaust emissions of the aircraft into the upper troposphere. The main focus revolves around condensing the water within the engine before releasing a predetermined size of water droplets into the atmosphere so as to prevent the formation of contrails at the cruise altitude.

8.1.1 WATER PHYSICS

A basic study is undertaken unfolding the behaviour of water in the atmosphere. The parameters governing this behaviour are tabulated in Table 8-1. The most crucial parameters for this study are the saturated vapour pressure of water at a given temperature as well as the size of the condensate particle formed at any given conditions of temperature and pressure. The size of the condensate particle of water defines its state and is a function of the saturated vapour pressure, ambient temperature and ambient pressure. A particle in the order of 0.1 microns acts as a cloud condensation nucleus promoting cloud formation through collision-coalescence and hence the phenomenon of cloud seeding

occurs naturally in the atmosphere. High altitude ambient conditions are favourable for water vapour's existence at this scale.(Heymsfield et al., 2010)

A particle in the order of 1 micron would exist within a cloud or a contrail. Water vapour is manifested in this state when it is released from the core engine exhaust and condenses in the atmosphere at cruise altitude. Direct measurement of contrails through airborne instruments has specified the dimensions of contrails in this order.(Jeberger et al., 2013) and (Gleitsmann and Zellne, 1998)

A particle in the order of 100 microns is a raindrop (Noppel, 2007). This state of water occurs close to the ground where the ambient temperature and pressure is relatively high and rainfall is experienced on the earth's surface. Condensation at a high pressure is the dominant effect in this case.

The aim of this study is to determine conditions conducive to the condensation of water as large size water droplets or rain. The exhaust water vapour content is manipulated within the engine to achieve this state. The size of the condensate particle is fixed at 1000 microns (Bright, 2011) and the Kelvin equation is worked backwards to determine the required temperature and pressure for this scale of condensation to occur.

Water vapour follows the Dalton's Law of partial pressure for gases. The partial pressure exerted by water in a mixture of chemically non-reacting gases is a ratio of the total pressure exerted by the gases according to the molar ratio of water within the mixture. The mole fraction of water vapour in the air is 0.622 according to the molecular weight of water and air respectively. The condensation and extraction of the water vapour from the mixture of the exhaust gases results in a reduction in the overall pressure of the remaining gases according to the molar ratio of water in the combustion gas.

PARAMETER	**SYMBOL**	**UNIT**	**VALUE**
Actual Vapour Pressure	P	Pa	
Saturated Vapour Pressure	P_0/SVP	Pa	
Surface Tension of Water	σ	J/m^2	0.076
Loschmidt Number	n	$Molecules/m^{-3}$	$3.3*10^{28}$
Radius of Droplet	r	m	
Gas Constant	R	J/kg/K	287
Temperature	T	K	

Relative Humidity	RH	%	
Condensation Temperature	T_d	K	
Latent Heat Of Vaporization	L_v	J/kg	
Molar Weight Of Water	M_w	Kg	0.018
Required Pressure	P_1	Pa	
Required Temperature	T_1	K	
Boltzmann Constant	k	J/K/molecule	$1.38*10^{-23}$
Molar Ratio of Water	W_s	-	0.622
Specific Heat Capacity of Water	c_{pw}	J/Kg/K	1952
Ambient Temperature (ISA)	T_{amb}	K	
Ambient Pressure (ISA)	P_{amb}	Pa	
Altitude	h	m	

Table 8-1: Parameters Used for Determining the Condensation Behaviour of Water

The saturated vapour pressure of water at a given temperature is calculated by the Clausius-Clapeyron equation(Hobbs, 2000).

$$\boldsymbol{P_0 = 611e^{5420\left(\frac{1}{273}-\frac{1}{T}\right)}}$$

Equation 8-1: The Clausius-Clapeyron equation

The variation in the saturated vapour pressure of water with temperature is illustrated in Figure 8-1, the phase diagram of water where the different states of water are identified with respect to the variation in the temperature and the pressure. The Clausius-Clapeyron Equation can also be approximated by the following Taylor Series(Seinfeld, Pandis and Knovel, 2006):

$$\boldsymbol{P_0 = 101325e^{\left(13.3185a\ -\ 1.97a^2-0.6445a^3-0.1299a^4\right)}}$$

where

$$\boldsymbol{a = 1 - \left(\frac{373.15}{T}\right)}$$

Equation 8-2 : Taylor Series Approximation of the Clausius-Clapeyron Equation

The Relative Humidity at a given pressure is

$$\boldsymbol{RH = \frac{P}{P_0}}$$

Equation 8-3: The Relative Humidity

The change in temperature due to isentropic compression or expansion can be calculated by the Poisson's equation

$$\boldsymbol{\frac{T_1}{T} = \left(\frac{P_1}{P}\right)^{R/C_P}}$$

Equation 8-4: The Poisson's Equation

The latent heat of vaporization of water varies with temperature according to the following equation(Seinfeld, Pandis and Knovel, 2006)

$$\boldsymbol{L_v = 2.5 \times 10^6 \left(\frac{273.15}{T_d}\right)^{0.167+3.67\times10^{-4}T}}$$

Equation 8-5: The Latent Heat of Vaporization

The kelvin equation provides the minimum critical size of the particle that can exist in a stable equilibrium and hence allow the condensate to grow in size.(John and Keith, 2006)

$$\boldsymbol{r = \frac{2\sigma}{\left(nkT \times \ln\frac{P}{P_0}\right)}}$$

Equation 8-6: The Kelvin Equation

It is evident from Equation 8-6 that for a positive radius of the droplet, ($P>P_0$) the mixture has to be supersaturated with respect to its environment. In a sub-saturated environment, ($P<P_0$) the condensate particle formed is in unstable equilibrium that evaporates back into vapour. The particle size of the water produced determines its behaviour. If the particle size is of the order of 0.02 microns, it acts as a condensation nucleus, if it is of the order of 20 microns it behaves as water vapour and if the size is as large as 200 microns then water is in the form of rain drops.(Noppel, 2007)

In order to calculate the saturated vapour pressure of water, the ambient temperature and pressure need to be known. The operating altitude lies between 10000 and 11000 meters. Given the flight altitude both static

temperature and static pressure are calculated using the international standard atmosphere (Kurzke, 2007).

Below 11000m the ambient ISA temperature is:

$$T_{amb} = 288.15 - 6.5\ \frac{h}{1000}$$

Equation 8-7: Ambient Temperature below 11000 meters

Ambient pressure in this altitude range is

$$P_{amb} = 101325\ \left(1 - \frac{0.0225577\ h}{1000}\right)^{5.25588}$$

Equation 8-8: Ambient Pressure below 11000 meters

Between 11000m and 25000m the temperature is constant and equals 216.65K. Ambient pressure at this altitude range is:

$$P_{amb} = 22632\ e^{\frac{11000-h}{6341.62}}$$

Equation 8-9: Ambient Pressure between 11000 and 25000 meters

Above 25000m the temperature increases again, according to the formula:

$$T_{amb} = 216.65 + 3(h - 25000)/1000$$

Equation 8-10 Ambient Temperature above 25000 meters

And ambient pressure in this altitude range is:

$$P_{amb} = 2488.6\ \left(\frac{216.15}{T_{amb}}\right)^{11.8}$$

Equation 8-11 Ambient Pressure above 25000 meters

Once ISA static pressure and temperature are calculated for a given altitude, the air density (ρ), sound velocity (Vs) and Mach number can be calculated according to the equations:

$$V_S = \sqrt{\gamma RT}$$

Equation 8-12: Velocity of Sound

$$Mach = V/V_S$$

Equation 8-13: Mach number

$$\rho = P/RT$$

Equation 8-14: The Ideal Gas Equation

Employing the equations that govern the behaviour of water and the ones describing the variation of temperature and pressure with altitude, the saturated vapour pressure as well as the size of the condensate particle formed in the atmosphere is determined. The values are given in the Table 8-2. The saturation vapour pressure in the atmosphere is far less than the ambient pressure and therefore, the environment is conducive for the engine vapour condensation to occur. The vapour particles thus formed are of the order of 0.1 micron which indicates that the water vapour present in the atmosphere will act as a cloud condensation nucleus and hence induce contrails and cirrus cloud formation.

Atmospheric temperature and pressure are a function of altitude and can be expressed according to the equations described above. The saturated vapour pressure of water is a function of temperature and hence can be calculated for a given altitude as tabulated in Table 8-2. The Loschmidt number indicates the number of molecules in a unit volume of gas. This constant is a function of both the temperature and the pressure of a gas. For a given altitude, the size of the condensation nuclei formed is given by the Kelvin equation. Particle radii of the order of 0.1 microns are formed in Nature. These are stable water vapour particles that act as condensation nuclei for the formation of clouds. For vapour condensation to occur, the saturated vapour pressure at a given temperature should exceed the existing pressure at that temperature. This is evident for the entire altitude range in Table 8-2. Data for saturated vapour pressure, Loschmidt number and particle radius is calculated for an altitude range of 0 to 11000 meters as tabulated. Particle radii, as calculated are of the order of 0.1 micron, and indicate a super-saturated environment which would facilitate the formation of condensation nuclei. Calculations show that there is an increase in

size of the particles formed at higher altitudes. Nevertheless, the order of the size does not change and the condensate particle can only act as a cloud seed to induce cloud and contrail formation.

Atmospheric Physics					
Altitude	Temperature Ambient	Pressure Ambient	Saturated Vapor Pressure S.V.P.	Loschmidt number	Particle radius
	f (altitude)	f (altitude)	f (T)	P/kT	f (P,T)
meters	deg K	Pascal	Pascal	molecules/m3	microns
0	288.15	101325.00	1735.29	2.54811E+25	0.3688
1000	281.65	89874.56	1124.21	2.31232E+25	0.3860
2000	275.15	79495.20	713.53	2.09359E+25	0.4057
3000	268.65	70108.52	443.03	1.89106E+25	0.4281
4000	262.15	61640.21	268.65	1.70386E+25	0.4537
5000	255.65	54019.88	158.81	1.53119E+25	0.4827
6000	249.15	47180.99	91.34	1.37223E+25	0.5157
7000	242.65	41060.71	51.00	1.22622E+25	0.5533
8000	236.15	35599.78	27.58	1.0924E+25	0.5961
9000	229.65	30742.42	14.40	9.70047E+24	0.6450
10000	223.15	26436.23	7.24	8.58467E+24	0.7010
11000	216.65	22632.03	3.49	7.56982E+24	0.7653

Table 8-2: Variation of Water Vapour Particle Radius with Altitude

8.1.2 WATER IN THE EXHAUST

The stoichiometric equation for complete combustion provides the ratio of the combustion gas constituents of Kerosene fuel:

$$C_{12}H_{26} + 18.5(O_2+4N_2) = 12CO_2 + 13H_2O + 74N_2$$

Equation 8-15 : The Stoichiometric Combustion Equation for Kerosene

The Molar Ratio of chemical specie equals the number of moles of the specie divided by the total no of moles in the mixture, hence:

1. Molar ratio of Water from Equation 8-15 = 13/ (12+13+74) =0.131

2. Molar ratio of CO_2 from Equation 8-15 =12/ (12+13+74) =0.121

For a given value of exhaust temperature and pressure the pressure exerted by water vapour can be calculated by multiplying the molar ratio of water by the total pressure of the exhaust gases. This enables us to determine the loss in the pressure of the combustion gas once water condenses out of it.

As tabulated in Table 8-3 , water contained in the exhaust emissions exists at a certain temperature and pressure. Saturation vapour pressure at that temperature can be calculated using the Clausius-Clapeyron equation. The vapour can either be compressed to the saturation pressure at a given temperature or cooled to the extent that the saturation pressure at a given temperature equals the ambient pressure. When both the pressures are known values, the temperature drop required to achieve condensation can be determined. The size of the condensate particle is then calculated by the Kelvin equation. Once the water has condensed, the pressure exerted by the remaining gases can be calculated according to the Dalton's law of partial pressure.

Calculations for vapour pressure, particle radii, Loschmidt number and relative humidity are carried out for actual engine performance data at various engine stations, as tabulated in Table 8-3. Engine data has been obtained from the performance analysis of a standard high bypass three spool turbofan engine based on the parameters of the Trent 900 engine.

A negative value for particle radii for the three turbines and the hot nozzle indicate that the condensate particle is unstable and thus re-evaporates as soon as it is formed. The humidity value indicates that the environment is highly unsaturated at the given temperatures. A positive particle radius in the bypass stream of the order of 1 micron indicates the presence of naturally occurring moisture.

Engine Exhaust, Actual Values							
Station	Temperature	Pressure	Saturated Vapor	Loschmidt	Particle	Pressure	Humidity
	Exhaust	Exhaust	Pressure S.V.P.	number	radius		relative
	T	P	f(T)	P/kT	f(P,T)		P/SVP
	deg K	Pascal	Pascal	molecules/	microns	Bar	%
HPT	1600	2960165	8.65E+09	1.341E+26	-0.00643	29.60165	0.034213
IPT	1259	882382	3.46E+09	5.079E+25	-0.02082	8.82382	0.025527
LPT	1087	434536	1.75E+09	2.897E+25	-0.04214	4.34536	0.024843
Nozzle	663	45134	7.21E+07	4.933E+24	-0.45657	0.45134	0.062596
Bypass	311	64759	6.91E+03	1.509E+25	1.04901	0.64759	936.9914

Table 8-3: Variation of Water Vapour Particle Radius inside the Engine

With reference to Table 8-3, water vapour in the exhaust of the engine under consideration exists at a temperature of 663K and a pressure of 45134 Pa. The saturated vapour pressure at this temperature is 72103599 Pa. This value is far greater than the exhaust pressure; hence, condensation of the water vapour is not possible. However, when this vapour is released into the atmosphere at an

altitude of 10,000 meters, and is cooled to an ambient temperature of 223 K and expanded to an ambient pressure of 26436 Pa, it automatically becomes super-saturated in its environment, which has a saturated vapour pressure of 7.24 Pa, and hence the condensation of water vapour occurs. This is the phenomenon behind contrail formation!

8.1.3 CONDENSATION DESIGN POINT CALCULATIONS

The calculations in Table 8-4 provide the key specifications required for the design of a condensation heat exchanger that is able to extract moisture from the exhaust emissions and condense it into sizeable stable water droplets. Pressure and temperature values are determined through this calculation, while mass flow rates of air and exhaust gases are obtained through the engine performance analysis.

The prime objective of this calculation is to cool the exhaust to a temperature where it becomes super-saturated with moisture, and water vapour in the exhaust gases condenses into liquid water. This condensation is to be achieved within the engine. The size of the condensate particle is extremely critical. A large size water droplet of the order of 1000 microns is desired to prevent contrail formation. In the case of the engine exhaust, only a condensation nucleus of a few microns is achieved as an initial state of the water vapour, as indicated in Table 8-3.

Engine Exhaust, Design Points for Condensation						
Temperature	Pressure	Saturated Vapor	Loschmidt	Particle	Pressure	Humidity
Exhaust	Exhaust	Pressure S.V.P.	Number	Radius		relative
T	P	f(T)	P/kT	f(P,T)		P/SVP
deg K	Pascal	Pascal	olecules/m3	microns	Bar	%
300	3.65E+03	3.65E+03	8.811E+23	1000	0.0365	100.0
350	4.82E+04	4.82E+04	9.977E+24	1000	0.4819	100.0
400	3.34E+05	3.34E+05	6.049E+25	1000	3.339	100.0
450	1.50E+06	1.50E+06	2.423E+26	1000	15.05	100.0
500	5.02E+06	5.02E+06	7.273E+26	1000	50.18	100.0
550	1.34E+07	1.34E+07	1.771E+27	1000	134.4	100.0
600	3.06E+07	3.06E+07	3.691E+27	1000	305.6	100.0
650	6.12E+07	6.12E+07	6.826E+27	1000	612.3	100.0

Table 8-4 : Calculation for Condensation Design Point Temperature and Pressure

The size of the condensate particle is controlled by using the Kelvin equation, and working it backwards for the required pressure at the desired particle size. For a given temperature, the Loschmidt number is determined, and the Kelvin equation is used to calculate the pressure required for a particle size of 1000

microns at that temperature. The saturated-vapour pressure at that temperature is also calculated.

Table 8-4 shows the various available temperature and pressure values that, if achieved, would result in the condensation of water vapour into liquid water droplets. Practically achievable values need to be selected from the data. The maximum limit for temperature has been set at 650 K since the critical temperature of water is 647 K and no amount of pressure can convert water vapour into the liquid phase beyond this temperature. This is evident from the phase diagram of water in Figure 8-1.

For the engine under consideration, the exhaust gases exist at a temperature of 663 K and a pressure of 45234 *Pa*. In order to achieve the selected design point, the exhaust gases need to be cooled to a temperature of 350 K with no change of pressure. Hence, the temperature value of 350 K and a pressure of 48234 *Pa* are selected to be the design point parameters for the design of the conventional, temperature based condensation heat exchanger.

However, the design point changes for the design of the centrifugal water expeller which is a pressure based condensation device. The combustion gas is compressed at its existing temperature to achieve the required saturated vapour pressure in order to undergo a phase change.

The size of the condensate particle is critical. It can be inferred that the size of the particle produced is inversely proportional to the super-saturation level. This implies that if the moisture is cooled, it would condense as soon as the humidity level reaches 100% and the size of the droplets formed would be relatively large as calculated by the Kelvin equation.

Referring to Table 8-2, it is observed that when the moisture is introduced into the atmosphere where the saturation pressure is much lower than the ambient pressure and the humidity level is much larger than 100%, the size of the water vapour particle formed in this highly supersaturated environment is of the order of a few microns. This enables these particles to act as cloud condensation nuclei.

On the contrary, if the moisture in the exhaust is cooled to the condensation temperature, the relative humidity barely reaches 100% and large sized visible droplets are formed. This actually works to our advantage and is a desirable feature in the context of contrail prevention. A similar behaviour can be observed in nature whereby large sized water droplets cause rainfall at low altitudes and naturally occurring moisture forms clouds at high altitudes. This approach has been adopted to proceed with the idea of condensing the moisture within the engine exhaust to obtain large collectable water droplets.

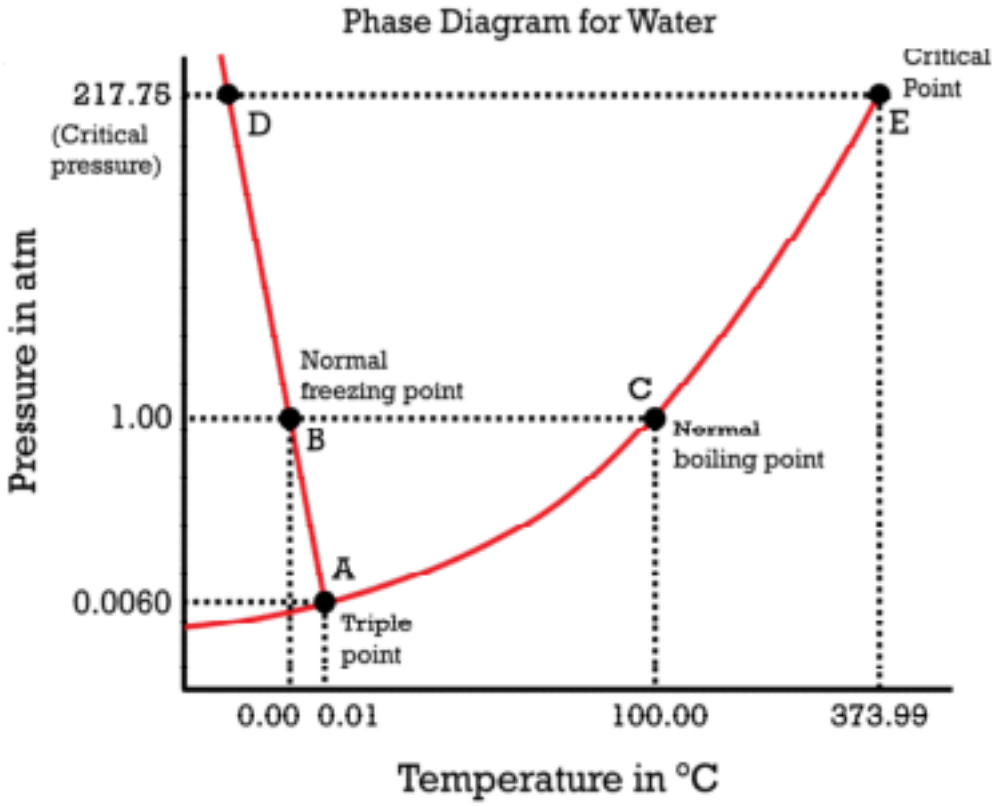

Figure 8-1: The Phase Diagram of Water (courtesy: www.chemguide.co.uk)

8.2 THE CENTRIFUGAL COMPRESSOR

Several schemes are considered to extract the moisture from the core exhaust gases, while giving due consideration to the high velocities and volumes involved. The utmost priority is to avoid the conventional heat exchangers owing to the weight, size and flow reversal constraints.

Moreover, such heat exchangers also necessitate modification for airborne applications since they are originally designed for ground based applications. A heat exchanger for aero-engines thus needs to be designed according to stringent specifications of light weight, low frontal cross-section, high specific heat ratio and other unique specifications, distracting the scope of this work. However, even if such a hypothetical heat exchanger were constructed, not much heat can be dissipated to the ambient by-pass flow through any hypothetical heat exchanger, since the total heat capacity of the bypass mass flow is limited. The only cooling possible is by complete mixing of the exhaust flow with the bypass flow. This puts us back to where we started! We don't have a heat exchanger, but end up having a mixer. And that is what nature is already doing to the exhaust plume in the atmosphere!

One of the basic approaches adopted is to compress the exhaust gases using a simple compression device so as to achieve the desired design point temperature and pressure whereby condensation would be initiated and then the water produced could be removed by the centrifugal action of the compressor. Starting with a simple centrifugal compressor, the impeller is modified to be cooled at the outside by the bypass air so as to ensure that temperature rise does not take place while the exhaust gases are undergoing compression.

Design data is calculated for both an intercooled recuperated aero engine and a simple turbofan engine of the same scale using the Trent-900 baseline specifications. The compressor is placed after the last turbine that is, the low power turbine. The core exhaust in a turbofan engine contributes to the thrust of the engine. Since thrust could no longer be directly obtained from the exhaust because the compression device diverts the energy of the exhaust, the low power turbine is modified so that it expands to ambient pressure. This results in a further drop in temperature and the excess power generated by the turbine is used to drive the additional compressor. This can be practically achieved for an intercooled recuperated engine since it is more thermally efficient than a simple turbofan configuration and a temperature gradient is available between the low pressure turbine and the high pressure compressor for successful recuperation.

The calculations for the intercooled recuperated engine are discussed. The centrifugal compressor that is meant to act as a condensation device is placed after the last turbine stage and it is surrounded by the bypass stream at its outer walls.

8.2.1 THE INTERCOOLED RECUPERATED ENGINE

The following data and specifications defined in Table 8-5,Table 8-7 and Table 8-6 is used for designing the centrifugal compressor for the intercooled recuperated engine. Excess power is derived from the low power turbine by expanding it to ambient pressure. This expansion also results in a drop in temperature of the exhaust gas. The isentropic expansion calculations for the excess power derived from the LPT are tabulated in Table 8-6. Assuming a standard turbine efficiency of 0.9, the excess power derived amounts to 6.5 MWatts. This value correlates to a tip speed of 300 m/s as calculated in Table 8-8.This is the maximum speed that the compressor can be driven at using the excess power.

Table 8-8 calculates the compression across the centrifugal impeller at various tip speeds. A tip speed of 300 m/s is the maximum speed that can be generated with the excess power available from the LPT. This tip speed lies within the design limit of 460 m/s which induces the maximum allowable centrifugal stress

for conventional aluminium alloys. This tip speed results in a static pressure ratio of 4.14 across the impeller and a temperature rise of 73 Kelvin. The undesirable rise of temperature is controlled by surrounding the impeller with the bypass air that would prevent the temperature rise. Detailed calculations for design specifications are worked out.

The compressor is designed to run on the low power shaft which has a rotational speed of 50 revolutions per second. This value of the rotational speed has been obtained from the engine performance data. The power input factor and slip factor for the compressor are assumed to be 1.04 and 0.9 respectively(Saravanamuttoo, 2008). All other inputs tabulated are obtained from the intercooled recuperated aero-engine design point performance calculation output data. A conventional engine station number notation has been used throughout for both input and output data in the tables that follow.

Intermediary calculation constant	$\psi\varepsilon/Cp$		C1	0.0008153
Intermediary calculation constant	$\gamma/\gamma-1$		C2	4.03
Intermediary calculation constant	η/T_{07}		C3	0.0011354

Table 8-5: Intermediary Calculation Constants

	TURBINE	**POWER**	**CALCULATION**		
Ambient	Pressure	Pamb		23835	Pascal
Ambient	Temperature	Tamb		218	K
Cruise	Altitude	Alt		10670	m
Turbine	Efficiency	ηt		0.9	
Turbine	Pressure Ratio	Pturb	$P_{07}/Pamb$	1.9525488	
Turbine	Temperature Ratio	Tturb	$Pturb^{\gamma-1/\gamma}$	1.1820898	
Exhaust	Temperature	Tex	T_{07}/Tturb	581.17412	K
Turbine	Power	PowerTurb	mCp(T_{07}-Tex)ηt	6560358	Watts

Table 8-6: Low Power Turbine Excess Power Output for the Intercooled Recuperated Engine

The compressor is placed on the LPT shaft after the last turbine and obtains its intake flow from the combustion gases that exit from the last turbine stage. The requirement is to generate the maximum possible pressure in the combustion gas so that a phase change is initiated that result in the condensation of water**.**

Constants Used		Symbol	Value	Units
Specific Heat Capacity		*Cp*	1148	J/kg K
Power Input Factor		*ψ*	1.04	
Slip Factor		*ε*	0.9	
Rotational Speed (3000 rpm)		*N*	50	rev/sec
Mass Flow		*m*	60	kg/sec
Efficiency		*η*	0.78	
Bypass Nozzle dia.		*Dby*	3.05	meters
Shaft dia. (Eye Root)		*Er*	0.3	meters
Inlet dia. (Eye Tip)		*Et*	2	meters
Inlet Velocity (LPT station)		V_{07}	153	m/sec
Inlet Temperature (LPT station)		T_{07}	687	°K
Inlet Pressure (LPT station)		P_{07}	46539	Pa
Radial velocity = Inlet velocity			153	m/sec
Constant Used	Formulae	Symbol	Value	Units
Gamma Gas		*γ*	1.33	
Eye Root Speed	*NπEr*	*Vr*	47.124	m/sec
Eye Tip Speed	*NπEt*	*Vt*	314.16	m/sec
Air Angle at Root	atan(V_{07}/*Vr*)	α root	1.27	deg
Air Angle at Tip	atan(V_{07}/*Vt*)	α tip	0.45	deg
Gas Constant		*R*	287	J/kgK

Table 8-7 : Centrifugal Compressor Design Inputs for a Pre-Nozzle Attachment Scheme

The condensation is meant to occur when the vapour is compressed in the impeller and then diffuses into the diffuser which induces a rise in static pressure. Due to the rotation of the impeller, a centrifugal force is generated such that the water vapour is thrown outwards towards the walls of the compressor. The walls are cooled by the bypass flow. Condensed liquid water is meant to be collected on the internal walls and is drained out.

The exhaust nozzle is assumed to be placed after the centrifugal compressor so that it generates thrust from the uncondensed core gases and releases them

into the atmosphere. The bypass nozzle remains unchanged and generates thrust in the conventional manner. The design calculations for the centrifugal compressor at various tip speeds for a pre-nozzle attachment are tabulated in Table 8-8. A set of values have been obtained by varying the tip speed to the structural limits of design. Design speed is then chosen according to the availability of power to drive the compressor, since this device would act as an external load on the engine.

The drawback of using a conventional centrifugal compressor for this purpose is that it results in a considerable rise in temperature for a minimal rise in pressure. The calculations in Table 8-8 show that it is not possible to attain the design point temperature and pressure with this configuration. Referring to Table 8-7, the temperature and pressure at station 7 is 687 K and 46539 Pa respectively. When the low power turbine is further expanded to ambient, the temperature and pressure at the LPT station before the nozzle drops to 581 K and 23835 Pa respectively as indicated by Table 8-6.

Although the temperature has been reduced to a value below the critical point of water which makes condensation possible, the maximum pressure ratio across the impeller is limited to 4.14 as discussed through Table 8-8. This happens when the inlet temperature to the compressor is considered to be equal to 581 K. This would result in a pressure rise to 1.93 atm. According to Table 8-4 this would require the exhaust gas to be further cooled to 384 K for the water vapour to condense at the said pressure.

As the temperature rise across the impeller is 73K, the total drop in temperature required is 270K. The total amount of heat loss required for the given mass flow would then amount to 17.6 MWatts. A further 3.4 MWatts would need to be lost as latent heat by the water vapour in order to condense from the vapour phase into the liquid phase. The total amount of heat loss amounts to 21 MWatts.

The convective cooling capacity of the bypass stream is nearly insignificant compared to the magnitude of heat loss required due to a large mass flow and the existence of latent heat. The inability of the bypass stream to absorb this amount of heat has been discussed thoroughly with numerical values in the chapter of heat exchange analysis.

The results of these calculations do not prove favourable and it is numerically deduced that a conventional centrifugal compressor cannot be used as a condensation device due to the excessive amount of heat generated during compression. Such a device is design wise optimized for extremely low temperature intakes at high altitudes and is therefore unsuitable for combustion gas intakes at exhaust temperatures.

Tip Speed	Impeller Diameter	Temperature Rise	Compressor Pressure Ratio	Power Required	Whirl Velocity
U	Dimp	Trise	Pcomp		
	U/πN	$C1U^2$	$(1+C3Trise)^{C2}$	mCpDimp/η	εU
m/sec	meters	°K		MWatts	m/sec
250	1.592	51	1.25	4.275	225
300	1.91	73.4	1.38	6.156	270
350	2.228	99.9	1.54	8.379	315
400	2.546	130.5	1.74	10.944	360
450	2.865	165.1	2	13.851	405
500	3.183	203.8	2.31	17.1	450
550	3.501	246.6	2.7	20.691	495

Tip Speed	Dynamic Head	Pressure Ratio across Impeller	Temp. at Impeller Output	Static Temp at Impeller output	Static Pressure Ratio at Impeller Output
U	THD	Pratio	Timp	Tstat	Pstat
	$V_{07}^2/2Cp$		T_{07}+Trise	T_{07}+Trise-THD	$(Pratio\ Tstat/Timp)^{C2}$
m/sec	°K		°K	°K	
250	10.2	1.29	738	727.8	2.67
300	10.2	1.44	760.4	750.2	4.14
350	10.2	1.63	786.9	776.7	6.85
400	10.2	1.88	817.5	807.3	12.01
450	10.2	2.18	852.1	841.9	22.19
500	10.2	2.57	890.8	880.6	42.92
550	10.2	3.06	933.6	923.4	86.38

Tip Speed	Pressure at Impeller Output	Pressure at Impeller Output	Density at Impeller Output	Area at Impeller Output	Depth of Impeller at Tip
U	Pimp	Pimp	ρimp	Aimp	dimp
	Pstat P_{07}	Pstat x P_{07}	Pimp/RTimp	$m/\rho imp V_{07}$	Aimp/πDimp
m/sec	Pa	Atm	J/kgK	$meter^2$	meters
250	124272.1	1.24	0.5868	0.6349	0.127
300	192625.9	1.93	0.8827	0.4221	0.070
350	318588.0	3.19	1.4107	0.2641	0.038
400	558753.8	5.59	2.3816	0.1564	0.020
450	1032529.6	10.33	4.2221	0.0882	0.010
500	1997491.8	19.97	7.8128	0.0477	0.005
550	4020144.7	40.2	15.0031	0.0248	0.002

Table 8-8 : Design Calculation for the Centrifugal Compressor at Various Tip Speeds

8.3 HEAT EXCHANGER ANALYSIS

A novel idea presented recently in literature describes using an unmixed heat exchanger to dissipate the thermal energy of the core exhaust into the cold bypass flow(Taylor, Noppel and Singh, 2007). This concept is studied comprehensively in the present work. The concept of using the bypass flow to cool the core exhaust sounds very attractive, and the thermodynamic feasibility is studied. The performance data of a three spool high bypass turbofan engine was used to work out an example. An unmixed heat exchanger is considered and the mass flow requirements are calculated.

The heat exchanger analysis is based on unmixed, parallel flow, convective heat transfer, where the core exhaust is cooled by the bypass flow in a concentric cylindrical configuration. Design parameters for this analysis are obtained from the engine performance analysis carried out where gas properties are determined at all engine stations and their values have been used for this assessment.

8.3.1 CONVECTIVE HEAT TRANSFER

The Reynolds number for convective flow is given by

$$\boldsymbol{Re} = \frac{\boldsymbol{\rho DV}}{\boldsymbol{\mu}}$$

Equation 8-16: The Reynolds Co-Efficient For Convective Flow

A value of the Reynolds number greater than $5x10^5$ implies turbulent flow. The Prandtl number $\boldsymbol{Pr}$ for convective flow is given by

$$\boldsymbol{Pr} = \frac{\boldsymbol{\mu Cp}}{\boldsymbol{k}}$$

Equation 8-17: The Prandtl Co-Efficient For Convective Flow

The Nusselt number $\boldsymbol{Nu}$ for convective flow is given by

$$\boldsymbol{Nu} = \frac{\boldsymbol{hD}}{\boldsymbol{k}}$$

Equation 8-18: The Nusselt Co-Efficient For Convective Flow

Parameter	Symbol
Density of the fluid	ρ
Velocity of the fluid	V
Conductivity of the fluid	k
Specific Heat Capacity at constant Pressure	Cp
Viscosity of the fluid	μ
Hydraulic Diameter of the cylinder	D
Convectivity of the fluid	h

Table 8-9: Parameters for Calculating the Nusselt Number of the Bypass Stream

The hydraulic diameter of the vessel for concentric cylinders equals mean diameter of the inner cylinder subtracted from the mean diameter of the outer cylinder. The wall thickness of the cylinders is assumed to be negligible compared to the diameters, and hence the conductivity term in the equation can be ignored. The overall heat transfer co-efficient $\boldsymbol{U}$ for flow through concentric cylinders is given by:

$$\boldsymbol{U = \frac{1}{\frac{1}{hi} + \frac{Ai ln\left({ro}/{ri}\right)}{2\pi kcL} + \frac{Ai}{Aoho}}}$$

Equation 8-19: The Overall Heat Transfer Co-Efficient

Parameter	Symbol
Convectivity of the Hot Core Fluid	$\boldsymbol{hi}$
Convectivity of the Cold Bypass Fluid	$\boldsymbol{ho}$
Inner Surface Area of the Cylinder,	$\boldsymbol{Ai}$
Outer Surface Area of the Cylinder	$\boldsymbol{Ao}$
Inner Radius of the Cylinder	$\boldsymbol{ri}$
Outer Radius of the Cylinder	$\boldsymbol{ro}$
Conductivity of the Cylinder Material	$\boldsymbol{kc}$
Length of the Cylinder	$\boldsymbol{L}$

Table 8-10 : Parameters for Calculating the Overall Heat Transfer Coefficient

Assuming negligible thickness for the cylinder and hence complete heat conduction, the second term in the denominator will be neglected and the overall heat transfer co-efficient remains a function of only the convectivity of the core and bypass streams. Heat tends to convect away from the core flow to the bypass flow. The convective heat transfer of both the core and the bypass stream need to be calculated in order to calculate the overall heat transfer co-efficient.

8.3.2 ENGINE CORE STREAM FLOW

The core exhaust stream is the hot fluid of the heat exchanger that is used to convect away the heat to the cold bypass flow. The properties of the core exhaust fluid are given in Table 8-11. Part of core flow and bypass flow data has been extracted from the engine performance analysis of a standard high bypass three spool engine. This analysis has been appended in A1.

Core Exhaust		
Parameter	**Unit**	**Value**
Temperature	K	697
Pressure	Pa	47300
Mass Flow	kg/s	57
Velocity	m/s	153
Viscosity	Ns/m^2	$3.26x10^{-5}$
Density	Kg/m^3	0.236
Specific Heat	J/(KgK)	1148
Diameter	m	1.496
Conductivity	W/(mK)	0.05015
Reynolds Number	ρDV/μ	$5.1x10^6$
Prandtl Number	μCp/k	0.74625

Table 8-11: Properties of the Core Fluid

8.3.3 ENGINE BYPASS STREAM FLOW

The bypass stream is the cold fluid of the heat exchanger that is used to absorb the heat from the hot core exhaust. The properties of the bypass fluid are given in the Table 8-12:

BYPASS FLOW		
Parameter	Unit	Value
Temperature	K	289
Pressure	Pa	57000
Mass Flow	kg/s	452
Velocity	m/s	170
Viscosity	Ns/m^2	$1.59x10^{-5}$
Density	Kg/m^3	0.6872
Specific Heat	J/(KgK)	1005.821
Diameter	m	3.1
Conductivity	W/(mK)	0.02624
Reynolds Number	ρDV/μ	$2.3x10^7$
Prandtl Number	μCp/k	0.6089

Table 8-12: Properties of the Bypass Fluid

For the fluid properties of the bypass stream given in Table 8-12, Reynolds number is calculated to be 2.27 x 10^7. Similarly, the Reynolds number for the core is calculated to be 1.67 x 10^6 using data given in Table 8-11. These values indicate that both the bypass flow and the core flow are turbulent. The Prandtl number as calculated in the Table 8-12 is 0.7708.For turbulent flow in concentric cylinders(Cengel, 2006)

$$\boldsymbol{Nu = 0.023\, Re^{0.8} Pr^{0.3}}$$

Equation 8-20: Convective Heat Transfer Relationship for Dimensionless Coefficients

The above equation gives a value of convective heat transfer coefficient of 67 Watts/m^2 for the core flow and 128 Watts/m^2 for the bypass flow. The overall convection co-efficient is therefore calculated to be 44 Watts/m^2.Heat transfer through convection is given by

$$\boldsymbol{\dot{Q} = hA\Delta T}$$

Equation 8-21: Convective Heat Transfer

Parameter	**Symbol**
Convective Heat Transfer Coefficient	$\boldsymbol{h}$
Area of the Convective Surface	$\boldsymbol{A}$
Temperature Difference between the Hot and the Cold Fluid	$\boldsymbol{\Delta T}$
Mass Flow Rate of Hot Stream	$\boldsymbol{m_h}$

Mass Flow Rate of Cold Stream	$\boldsymbol{m_c}$
Specific Heat Capacity of Hot Stream	$\boldsymbol{C_{ph}}$
Specific Heat Capacity of Cold Stream	$\boldsymbol{C_{pc}}$
Temperature of the Hot Stream	$\boldsymbol{T_h}$
Temperature of the Cold Stream	$\boldsymbol{T_c}$
Equilibrium Temperature Required for Condensation	$\boldsymbol{T_w}$

Table 8-13: Parameters for Heat Transfer

For condensation to take place at the given pressure of 57 KPa, the exhaust gas fluid needs to cool down to a temperature of 350 K as indicated in Table 8-4. Assuming that both hot and cold streams acquire the same temperature, heat transfer $\dot{Q}$ is the minimum of the two values as given by Equation 8-22 and Equation 8-23 (Holman, 1997):

$$\dot{\boldsymbol{Q}} = \boldsymbol{m_h Cp_h (T_h - T_w)}$$

Equation 8-22: Steady-State Heat Transfer between the Hot and Cold Stream

Or by

$$\dot{\boldsymbol{Q}} = \boldsymbol{m_c Cp_c (T_c - T_w)}$$

Equation 8-23: Steady-State Heat Transfer between the Hot and Cold Stream

In this case, the core exhaust signifies the hot stream, and the bypass flow implies the cold stream. T_w equals 350 K which is the desired temperature required for condensation to occur in the exhaust flow. The heat transfer capacity of the bypass fluid for various lengths of the cylinder with a transfer surface diameter of 1.5645 meters, which is the actual diameter of the exhaust nozzle, is given in Table 8-14. The heat transfer rate required for both the streams to attain this temperature is calculated to be 22 MW.

Heat Exchanger Length	**Heat Transfer Area for D_{avg}= 1.56 m**	**Bypass Flow Convective Heat Transfer**
$\boldsymbol{L}$	$\boldsymbol{\pi DL}$	**Capacity**
m	**m^2**	**Watts**
0.25	1.2285	51

0.5	2.457	108
0.75	3.6855	162
1	4.914	216
1.25	6.1425	270
1.5	7.371	324
1.75	8.5995	378
2	9.828	432

Table 8-14: Convective Heat Transfer Capacity of the Bypass Flow

Once the core exhaust has cooled down to the condensation temperature, additional heat transfer is required for a phase change from vapour to liquid. This latent heat is given by the following equation:

$$\dot{Q}_L = \dot{m} L_v$$

Equation 8-24: Latent Heat Transfer Required for Condensation of Vapour

Where $\dot{Q}_L$the latent heat transfer is required for a phase change, $\dot{m}$ is the mass flow rate of water and L_v is the latent heat of vaporization. The mass fraction of water in the exhaust gases is 0.025, and therefore the mass flow rate of water equals mass fraction of water multiplied by the mass flow rate of the exhaust gas. This equals 1.3394 kg/sec. Using data of water vapour properties from Table 8-15, the latent heat of vaporization at the equilibrium temperature is 2.31 MJ/Kg. Hence the latent heat transfer of water is determined to be 3.1 MWatts.

The total heat transfer required to convert the entire vapour in the exhaust gas into liquid amounts to 25.1 MWatts. This is a huge amount for the bypass flow to absorb and an infinitely long cylinder would be required to achieve this. The convective heat transfer through the bypass is only a small fraction of the total heat transfer required in this configuration of unmixed parallel flows.

The convective heat transfer coefficient required for various lengths of the cylinder is calculated. Considering that the length of an engine is about 4 to 5 meters, a reasonable length for the heat exchanger could be another 2 meters, which would require a convective coefficient of 2.5 MWatts/m^2 which is nearly 5000 times greater than the convective coefficient of the bypass air. Hence, it is not possible for the bypass flow to cool down the core exhaust flow to a practical level. This analysis is valid in the case of a simple parallel flow concentric cylinder flow consideration. The surface area available for convection is the outer surface of the inner cylinder. Thermal resistance of the cylinder wall is considered negligible, and 100% conduction through the wall is assumed.

HEAT EXCHANGER DESIGN SPECIFICATIONS		
PRESSURE	Pa	47300
CONDENSATION TEMPERATURE	K	350
LATENT HEAT	J/Kg	2309000
DENSITY LIQUID	Kg/m^3	971.8
DENSITY VAPOUR	Kg/m^3	0.2935
SPECIFIC HEAT liquid **(Cpl)**	J/(KgK)	4197
SPECIFIC HEAT (vapour (**Cpv**)	J/(KgK)	1962
VISCOSITY LIQUID	Ns/m^2	0.000355
VISCOSITY VAPOUR	Ns/m^2	0.00001159
THERMAL CONDUCTIVITY of liquid	W/(mK)	0.67
THERMAL CONDUCTIVITY of vapour	W/(mK)	0.023
PRANDTL NUMBER of liquid		2.22
PRANDTL NUMBER of vapour		1

Table 8-15: Properties of Water at the Condensation Temperature and Pressure

8.3.4 INCREASING THE TRANSFER SURFACE AREA

The heat transfer calculations carried out above is based on a simple co-axial pipe configuration as shown in Figure 8-2 as shown by the image on the right. The inner cylinder contains the core exhaust gases and the outer cylinder contains the bypass air.

However, the interfacing surface area, available for heat exchange can be increased by using a daisy shaped inner cylinder for this concentric cylinder arrangement. The modified shape is shown by the image on the left. This is the maximum enhancement that can be done with this configuration.

Although the rate of heat transfer will enhance, the improvement will nevertheless be unable to meet the requirement for the desired quantity of heat transfer required for the condensation of water vapour present in the combustion gases.

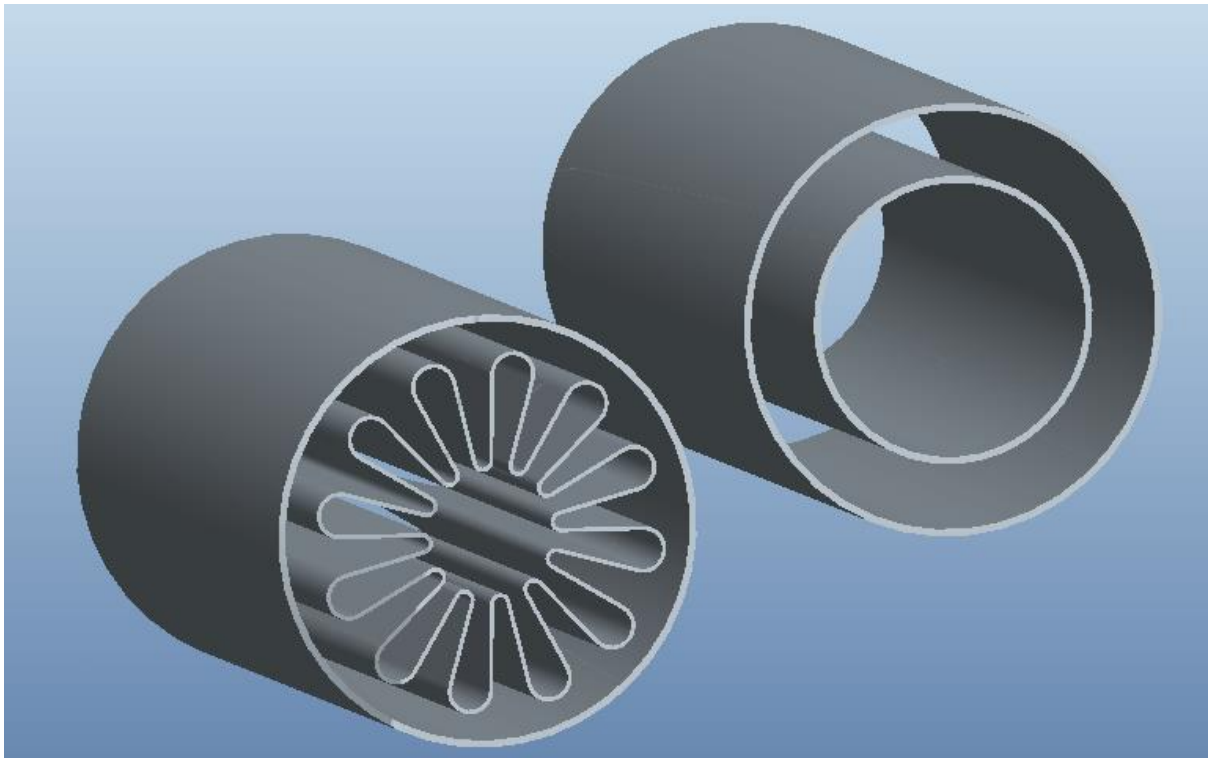

Figure 8-2: Increasing the Transfer Surface Area, Using a Daisy Shaped Inner Cylinder

8.3.5 RADIATIVE HEAT TRANSFER OF THE EXHAUST GASES

Radiative heat transfer also contributes to the overall heat transfer from the combustion gases into the environment. Some basic values have been calculated to determine its contribution. The emissive power of a gas is given by(Holman, 1997):

$$\boldsymbol{E_g = \varepsilon_g \sigma T_g^4}$$

Equation 8-25: The Emissive Power of a Gas

Where **σ** denotes the Stefan-Boltzmann constant and has a value of 5.67×10^{-8} W m^{-2} K^{-4} and $\boldsymbol{A_s}$ indicates the temperature of the radiating surface. The total heat $\dot{Q}r$ emitted by the gas is given by:

$$\boldsymbol{\dot{Q}r = A_s \varepsilon_g \sigma T_g^4}$$

Equation 8-26: The Total Heat Emission

The absorptivity of a gas is given by:

$$\boldsymbol{\propto_g = \varepsilon_g C_g \left(\frac{T_g}{T_s}\right)^n}$$

Equation 8-27: The Absorptivity of the Gas

Where: n is a gas specific property $\propto_g$= Absorptivity, ε_g= emissivity, C_g = pressure correction factor and T_g = temperature of the gas, while T_s = temperature of the radiating surface. At an exhaust gas temperature and pressure of 697 K and 47300 *Pa* respectively, and bypass temperature and pressure of 289 K and 57000 *Pa* respectively, For CO_2 we have:

$$\propto_c = \varepsilon_c C_c \left(\frac{T_c}{T_s}\right)^{0.65}$$

Equation 8-28: Absorptivity of CO_2 in the Engine Combustion Gas Mixture

Where the absorptivity of CO_2, $\propto_c = 0.11$, as computed from the given values of ε_c = 0.085, C_c = 0.65 and T_c = 697 K and T_s = 289 K. For water:

$$\propto_w = \varepsilon_w C_w \left(\frac{T_w}{T_s}\right)^{0.45}$$

Equation 8-29: Absorptivity of Water in the Engine Gas Mixture

Where the absorptivity of water, $\propto_w = 0.20$, as computed from the given values of ε_w = 0.15, C_w = 0.9 and T_w = 697K and T_s = 289 K.

$$\varepsilon_g = \varepsilon_w + \varepsilon_c - \Delta\varepsilon$$

Equation 8-30: Emissivity of the Combustion Gases

Where $\Delta\varepsilon$ =0.005 and accounts for the overlap of the two gases.

From Equation 8-30 above, ε_g = 0.305, hence the emissive heat transfer from the combustion gasses of the aircraft exhaust equals 2.788 KW/m^2. These calculations have been carried out by assuming a radiative cylinder with a mean beam length L = 0.95D, where D = diameter of the engine exhaust nozzle.

This radiative heat transfer of the gases shall supplement to the heat transfer capacity of the bypass flow as indicated in Table 8-14. For a maximum length assumption of the heat exchanger to be 2 meters, the heat transfer surface is computed to be 9.828 m^2. Hence the total emissive heat transfer for this area shall amount to 40 KWatts. This shall enhance the heat transfer capacity of the bypass flow as the core gas radiates to the bypass air.

However, the magnitude of the heat transfer required for condensation to occur remains excessive in comparison. This calculation nevertheless indicates that the absorptivity and emissivity of water vapour are greater than those of carbon-di-oxide. This validates the hypothesis regarding the radiative forcing of aviation induced contrails to be greater than that of carbon-di-oxide emissions.

8.4 ENVIRONMENTAL IMPACT OF AVIATION

8.4.1 INTRODUCTION

The earth's surface is transparent to incoming radiation and opaque to outgoing radiation, which keeps the earth warm. However, this atmospheric balance can be disturbed if the opacity is increased due to global warming. Global warming occurs as a result of the increase in the concentration of the greenhouse gases namely carbon dioxide ozone and water. Water is one of the most important greenhouse gases as it is very effective in trapping outgoing radiations. Incoming radiations for wavelengths less than 4 microns (μm) are absorbed by the atmosphere as well as the earth's surface whereas the outgoing radiation emitted by the earth's surface of greater than 4 microns (μm) are trapped by the greenhouse gases.(Wallace and Hobbs, 2006)

The atmosphere on the other hand is transparent to the visible spectrum, opaque to the ultraviolet (UV) band and has variable opacity across the infra-red (IR) region. Among the other major atmospheric gases N_2 does not figure in the absorption at all whereas O_3 only absorbs little in the UV and IR region. Water (H_2O) and carbon-di-oxide (CO_2) are tri-atomic molecules which possess rotational and vibrational degrees of freedom that can be easily excited by Infra-red radiations.

Mono atomic noble gases in the atmosphere are transparent to radiation. Gases with certain asymmetric molecular structures are highly effective in absorbing radiation, and are thus known as greenhouse gases, of which, the most important are H_2O, CO_2 and O_3. These greenhouse gasses are generally transparent to white light (all wavelengths) and the sunlight penetrates to heat up the Earth during the day. At night, the Earth loses heat to outer space by emitting infra-red radiation, however, the greenhouse gasses reflect some of the IR heat back to Earth. This is the phenomenon behind global warming. Natural clouds filter out both ways, and their contribution is in equilibrium.

8.4.2 THE GREENHOUSE EFFECT

The total solar radiation reaching the Earth is 1373 Watts/meter^2 when the Earth is at a mean distance from the Sun. This value is known as the Solar Constant. The solar radiation is reduced in the atmosphere due to absorption. According to the Wien's Law, the peak of the terrestrial spectrum occurs at 14μm, which is the average wavelength of IR radiation to space. The average mean surface temperature of the earth is 288 K and the mean solar wavelength is 0.6 μm. "The absorption of radiation by the atmosphere surrounding the earth increases the earth's surface temperature by a factor of 1.19. The atmosphere absorbs 25 percent of the incoming flux and re-radiates IR back down to the

earth's surface which results in an increase in the surface temperature of the earth. The outgoing radiation from the earth's surface is also absorbed within the atmosphere and partly refracted into outer space (Marshall and Plumb, 1965)

The solar band ranges from 0.3μm to 0.5 μm. From amongst the visible spectrum, O_2 absorbs radiation of wavelength of the order of 0.6 μm. Ozone absorbs UV below 0.3μm completely, and between 0.3μm and 0.4μm considerably. The absorption of IR radiation is dominated by H_2O and CO_2. They absorb this energy, and then release this energy in the range of 5μm to 8μm and above 13μm as they are large molecules and therefore they emit and scatter considerably. When at high temperatures inside a combustion chamber they emit in a narrow band of wavelength. O_2 and N_2 scatter radiation at a short wavelength compared to their molecule size. (Ambaum, 2010)

8.4.3 AVIATION AND THE ATMOSPHERE

The fuel burn of aviation contributes to 3 percent of the overall carbon-di-oxides global emissions. At present there are 15000 aircrafts around 10000 airports that consume 140 Tg of fuel per year. This figure is expected to rise to 300 Tg by the year 2015(Chapman, 2007)

The contribution of aviation to the atmospheric balance is critical due to the atmospheric placement of the combustion products. 85% of the aircraft exhaust is released above the planetary boundary layer. i.e. above 2 km out of which 70% is released in the upper troposphere (UT) and the lower stratosphere (LS) between 9 and 13 km. There exists minimal vertical mixing and diurnal variation in wind direction and therefore aircraft exhaust is released in narrow flight routes and corridors which impact on regional and global scales. Traffic patterns are inhomogeneous. The bulk of traffic lies inside "well defined traffic corridors" in the northern atmosphere(Spiro, Purvis-Roberts and Stigliani, 2012).

The fuel to air ratio of modern combustors is greater than 1:50 which implies that a large amount of ambient air is ingested and processed. Among the combustion by-products released, CO_2 and H_2O are the primary greenhouse gases. SOx, NOx and hydrocarbons are also released as a fractional by-product. They are also reactive gases which affect ozone and methane levels by forming aerosols. Unburnt Hydrocarbons at a visible size of greater than 1 micron (µm) form smoke. (Alan, 2016)

Most commercial aircraft combustors have a combustion efficiency of greater than 99 percent. The amount of fuel burn for the same efficiency can be increased by increasing the gas temperature and pressure but that increases NOx emissions. The chemical lifetime of aircraft exhaust such as NOx, soot and

sulphates injected into the upper troposphere and the lower stratosphere are comparable to the atmospheric mixing time. (Alan, 2016)

Aircraft chemical perturbations are expected to be localized in regions around the flight corridors are responsible for increasing the atmospheric CO_2 levels by 1ppmv or 2 percent over 50 years. CO_2 is long-lived and well mixed. It is impossible to distinguish between that emitted by aircraft and other sources. Aircraft H_2O perturbations are less than 1 percent. H_2O has a short tropospheric residence time ranging from days to weeks (Alan, 2016).

The total NOx emission from current global aviation is 0.5 Tg per year of which 60 percent is released in the upper troposphere and 40 percent in the lower stratosphere. NOx participates in the solar initiated free radical reactions of ozone formation and depletion. This formation and depletion balance is a sensitive function of the altitude. (Alan, 2016)

The overall effect of aircraft emissions in the upper troposphere and the lower stratosphere region is to increase the ozone levels by six percent in the heavy traffic areas and 0.4 percent in the total ozone column. (Alan, 2016).

8.4.4 CONTRAILS

Contrail induced cirrus clouds trap outgoing longwave radiation more effectively than they reflect incoming solar shortwave radiation. This tends to warm the climate. Contrail formation is a sensitive function of cloud particle size, altitude and the ambient temperature and pressure. The size of cloud condensation nuclei (CCN) varies from 0.05 µm to 0.02 µm. Plume is formed by 10^6 particles per kilogram of fuel. The concentration of cloud condensation nuclei (CCN) also affects the growth of cloud cover by 1 to 2 percent per decade. There has been an overall 5 percent increase in traffic route cloud cover during the last 30 years of air travel. (Chen and Gettelman, 2013)

The overall radiative forcing is substantially larger by a factor of 2 to 5 than the forcing by aircraft alone. There exists a trade-off to increase flight altitude to reduce contrail formation at the expense of increasing the ozone sensitivity to NOx. The higher altitude (16-20 km) release of supersonic NOx and H_2O emissions is predicted to generally enhance ozone depleting cycles relative to ozone forming ones which could lead to a net decrease in ozone concentration.(Zerefos et al., 2003)

Contrail formation is observed at temperatures as high as 215 degrees Kelvin. It is difficult to differentiate between long lived contrails and cirrus clouds. Most persistent contrails have a visible optical depth between 0.1 and 0.4.The numbers of crystals in a contrail remain constant after formation in the supersaturated conditions. The local turbulence also affects the formation

because water vapour and temperature are not homogeneously distributed. Contrails can form within cirrus clouds where they are manifested by reduced particle size or local thickening. Contrails transmit more radiation at a certain wavelength and the effective diameter varies from 5µm to 50µm.(Yang et al., 2010)

Schmidt in Germany (1941) and Applemann in the United States (1953) developed the currently accepted theory of contrail formation. Their theory showed that the threshold temperature depended on the ambient pressure, temperature and humidity outside of the aircraft, and on the ratio of water vapour and heat released into the atmosphere by the aircraft exhaust. From this theory, Applemann developed a graphical method to determine when an aircraft would or would not form a contrail. (Review and Sciences, 2003)

“Whilst the IPCC (Lee, D.S. Clare, P.E. Haywood, J. Kärcher, B. Lunnon, R.W. Pilling, I. and Slingo, 2000) concluded that the present day effects of aviation from all forcing are relatively small compared to other sources (3.5% of 1992 levels), it is the rapid growth of aviation that gives rise to concern. The scenarios used by the IPCC for 2050 utilized average projected traffic growth rates (1990-2050) ranging between 2.2% and 4.7% per year. Under the scenario Fa1, the total fossil fuel consumption by aviation is projected to be 3% (compared to 2.4% in 1992) but the contribution to total RF is 5%.Air traffic has undergone very rapid expansion since the late 1950’s. Growth rates in terms of Revenue Passenger Kilometres –RPK, were of the order 15% per year in the 1970’s, 9% in 1980’s and slowing to around 5% in 1990’s and are expected to remain at such growth rates until 2015”

“For the assessment of 2050 aviation-induced cirrus coverage, IPCC (1999, Chapter 3) adopted a different approach. A correlation between cirrus coverage and aviation fuel consumption was used to extrapolate increased global cirrus coverage of 0-0.8%.Assuming the same radiative sensitivity, a range of 0-0.16 W /m^2 was speculated. The response time by 2050 is rather short. A global mean temperature response based upon the global RF value was calculated by IPCC (1999, Chapter 6) to be an increase of 0.9 K in 2050 over 1990 values based upon the I990 scenario. Of this 0.9 K, approximately 5% was attributable (~0.5 K) to aviation (Scenario Fa1)”.

9 CONCLUSION

This project falls under the category of environmental studies for civil aircraft with an investigation into the global warming and global cooling potential of the aero-gas turbine power plants that are extensively used in aviation because of their exceptional power to weight characteristics. The investigation will encompass a comparative assessment of traditional and novel prime mover cycles including the performance of the engine and the environmental analysis of the system. The originality of work lies in the technical and environmental innovation of gas turbines that is based on current and novel engine cycles for an advanced airframe application in a wide range of operations.

The research has been undertaken across a range of disciplines; diverse technologies have been put in together for the first time and implemented to address a serious environmental concern of the aviation industry. Although these technologies have had their applications elsewhere, but have never been applied together to solve the environmental issues associated with the aviation industry.

It is anticipated that this research shall give the aviation industry a new vision whereby it foresees not only reducing the negative impact of aviation emission by eliminating contrails but adopt an approach to treat the water containing emissions as a resource. The implementation of this invention shall shift the negative impact of aviation on the global environment towards a positive contribution from the aviation industry towards the environment. Hence the aviation industry shall move from a problem towards a solution. This research is a first attempt in this direction and leaves scope for various prospective studies.

The research was initiated with the performance analysis of a high bypass three spool turbofan engine that is based on the Trent 900 and A380 published data in order to obtain all design parameters and engine conditions at the cruise altitude. Atmospheric science and water physics were also studied to determine the behaviour of the water vapour in the exhaust when released into the atmosphere and various design points were calculated whereby condensation could occur.

A heat transfer analysis was then carried out to determine the possibility of the exhaust gases losing their heat through a simple heat exchange mechanism between the core gas flow and the bypass flow. However, the magnitude of heat loss required proved to be excessive and could not be achieved through a simple heat exchanger within the size and weight constraints. Hence new concepts for an original water condensation system were evolved. A conventional centrifugal compressor was also assessed in order to determine its functionality as a condensation device for the exhaust water

vapour.Calculation concluded that the centrifugal compressor could not provide the functionality required for a water condensation device at the given state of the exhaust gases. Proceeding further, three new ideas were conceptualized and the preliminary mechanical design was developed for further analysis. This completed the initial phase of the research.

In the next phase of the research, thermo-chemistry of the combustion gases at the molecular level was analyzed to determine the effect of the presence of the other exhaust gases on the condensation behavior of the water vapor. The results of the study were optimistic and indicated that the presence of the non-condensable gases in the exhaust plume favored the condensation of water. This provided confirmation for advancing towards the task of designing a water vapor condensation and extraction system for the vapor content of the exhaust gases.

This design was further complemented with a quantitative analysis of the inter-gaseous exchange of energy at the molecular level during the condensation process that gave evidence of the fact that the latent heat released by water during condensation is absorbed by the remaining exhaust gases thereby minimizing the energy losses associated with this phenomenon. Nearly 20 percent of this energy contributes to a gain in the kinetic energy of the exhaust gases.

This study also established the fact that the bulk of the heat is transferred into Nitrogen which happens to be a favorable outcome of employing this device since Nitrogen is a non-greenhouse gas in contrast to water and Carbon-di-oxide and does not contribute to the phenomenon of global warming when released into the atmosphere. Secondly the greenhouse impact of carbon-di-oxide also reduces significantly since carbon-di-oxide is de-excited during this energy transition.

Research was then progressed towards the design of the centrifugal water expeller. A mathematical model was developed and the mechanical details were realized which were modelled in a 3D CAD model with extensive detail of component design and assembly. Initial design estimates resulted in a 2 m increase in the length of the engine and a 200 Kg addition in the weight while maintaining the average engine diameter for Trent 900 baseline specifications. This is essentially a 30 % increase in the dimensions of the engine.

This was followed by the performance analysis for an engine with the centrifugal water expeller integrated into it. It employed the use of the TurboMatch software in-order to execute a design point analysis for this novel engine configuration. The contrail-free engine complied with the take-off rating of a standard 3 spool turbofan engine. A 3 % reduction in overall thrust was experienced during cruise

flight. However, this trade-off is accepted for the environmental benefits achieved through the engagement of this device with the engine.

During the last phase of the research, the engine performance analysis was then used to perform an aircraft performance analysis for an aircraft integrated with the contrail-free engine using the in-house software Hermes. In the perspective of the performance of the aircraft integrated with the contrail-free engine, this is essentially a change in the geometry of the engine. Only fractional changes were observed in the aerodynamic parameters of the aircraft and the engine due to this inclusion. A modification in the length and weight of the engine therefore does not contribute to a significant change in the overall performance of the aircraft. Hence the integration of the contrail-free engine into any conventional aircraft is validated to be a practically implementable and technically viable perspective.

The centrifugal expeller device developed during the course of this research is a novel addition to the family of gas-turbine components that shall revolutionize the aero-engine industry and mark the beginning of the first contrail-free aircraft flight!

10 FUTURE WORK

The thesis has emerged as a multidisciplinary project whereby the major aspects of the design of the centrifugal water expeller have been addressed in the perspective of the evolution of the contrail-free engine. Nevertheless excessive detail has been avoided as the focus remains to establish the proof of concept of design whereas detailed studies in different domains can be undertaken in the future while considering this thesis to be the foundation of the research. Some recommendations in each of the research aspects follow for future studies and evaluation.

The theoretical proof of concept is established through this project. An experimental stream can now be initiated for validation. The methods and knowledge brought together show great promise and should be explored further to make the concept viable on practical aircraft engines. Some of the predictable issues would arise, and their possible solutions are discussed. The current research can be used as a platform to launch these propositions.

Water Injection

The engine exhaust gases could be provided with water injection, in order to act like condensation centers, to aid the condensation process of the flow of the exhaust gases in the centrifugal vessel. This water injection would also cool the exhaust gases, helping the operating point down. The injected water would also be recovered in the expulsion process of water, along with the water from the exhaust gases. That is this injected water would also not escape into the atmosphere.

As shown earlier, the water produced is 1.25 times the mass of the fuel burnt, and if all the water produced by combustion is extracted, saved and carried aboard the aircraft all the way to the destination, then practical issues arise. It should be noted that the aircraft would not be 1.25 times heavier, but just 1.25 times heavier than the fuel burnt in flight. For Kerosene, the amount of water produces burnt displaces an equal amount of fuel burnt since water is denser than Kerosene.

a) The water thus produced has to be stored somewhere. If the water is stored in the emptied chambers of the fuel tanks using membranes to separate water from the fuel, the tanks would have to be thoroughly cleaned before re-fueling, creating an additional duty for the ground crew, and taking up additional time before the next takeoff.
b) Additional water tanks in the wings are impractical, since they have to be larger than the fuel tanks and necessitate a modification of the plan-form of the aircraft.

c) As the aircraft flies, the water stored aboard makes the aircraft get heavier, instead of getting lighter as in conventional exhaust of all combustion products.
d)
e) The heavier aircraft causes an increase in fuel consumption, instead of reduced fuel consumption as in conventional aircraft.

f) During landings, the landing gear has to cope with a heavier aircraft, which in some aircraft; the landing gear might not be capable of. The landing gear should not have to be strengthened. Other implications of landing with water would also need to be investigated.

One possible solution would be to throw out bulk of water or discharge small accumulated quantities of water in lumps or ropes and streams in flight. The bulk would take time to drop enough distance to disperse as rain drops of water, and would need to be released at an altitude that is lower than the altitude where cloud formation could possibly occur.

Water Storage Tanks

A study would have to be undertaken to determine the minimum size of the bulk of water that could be thrown out of the aircraft where vapor does not form through its path downwards. This would determine the minimum size of the small high pressure, high temperature water tank needed. This water tank could be accommodated within, or within an extension of the pylon, holding the engine and the expeller attachment.

Maximum Take-off Thrust

The expeller attachment creates an obstruction for the exhaust thrust. This has not been quantified yet; however, the requirement is that maximum thrust should be available at takeoff. During takeoff, the contrails are not created. Thus, the expeller can be disabled at takeoff. One option is to have a mechanism of variable pitch aero-foils in the stators and the rotor. Thus, allowing clear and linear passage of the exhaust gases. It is highly probable that considerable research has already been done for variable pitch aero-foils, so their modification and ingenious adaptation to the expeller can be done.

Internal Cooling of the Stator and Turbine Blades

The technology of the internal cooling of the blades already exists in the aero-engine industry. However, considerable modification and adaptation would be needed to apply the technology to deliver the coolant to blades in the expeller

device. Considering that the vessel is itself part of a rotating mechanism, a unique solution might be needed.

Aero-foil Optimization

Aero-foil designs would need to be undertaken to determine the optimum contours relevant to the requirements of the expeller, such that the expeller performance and minimum thrust loss are together taken care of.

External aero-foils

It is also possible to rotate the vessel using energy from the external by-pass air-flow. Aero-foils attached to the rotating vessel externally could be designed to be placed in the by-pass airflow, causing minimum obstruction and disturbance to the by-pass air-flow.

This concept might reduce the complexity of the stator and rotor on the inside of the vessel, however, taking energy from the high temperature thrust does reduce the temperature of the exhaust, which is conducive to condensation of water. Thus the internal blades were preferred to external blades. However, a study might turn out to be fruitful.

Vessel's External Profile

The expeller's external profile should be aero-dynamically un-obtrusive, and shaped to prevent boundary layer separation. Since it is a rotating part, radial symmetry does come into play. However, if the axis of rotation could be at an angle, a certain lift could be gained, such that the expeller carries a part, or all, of its own weight.

External Surface of the Vessel

The vessel's exterior should preferably be able to radiate its internal heat to the by-pass airflow. Since the by-pass airflow can possibly absorb a very small portion of the condensed water's heat, a black external surface would make a small improvement.

Internal Surface of the Vessel

The internal surface of the expeller should be a material where condensation can form large droplets, for example, copper and silver. Silver being expensive, a thin layer would be debated upon; however, the ablative and corrosive properties of the exhaust would soon deplete this layer.

Copper would happily react with the nitrates in the exhaust, and corrode away. Thus, a material would need to be selected that would not corrode, nor erode, in the harsh environment of high temperature, high speed thrust of the exhaust.

Structural Strength of the Vessel

The structural properties of the vessel as a whole need not be under stated, and should conform to the industry standards. The proposal here is to produce the vessel in at least three layers. The outermost layer with properties of black body radiation as defined above, the innermost layer with condensation inducing properties as defined above, and the middle layer, or layers, with properties of strength, rigidity, etc. A detailed dynamic structural analysis of the device would need to be carried out with moving parts involved in order to determine the exact safety margins of the design.

Multi-Layer Construction

If the flow characteristics of the materials are similar, the three or more layers could be stacked as flat blanks, and formed on a spinning machine. If the middle layer is too inflexible, and requires a strong spin deformation, then the different materials could be spun independently to approximately their required sizes. They could be put one inside the other, and finally given a spin together. All the collars and troughs could be made in a single go. Thus there would be no air gaps between the layers. The ablative surfaces could have thick sections, so that the expeller could have a long life. It would be helpful if all the layers are good thermal conductors.

Most importantly, the coefficients of thermal expansion of all the materials should be close together. The manufacturing techniques applicable to high pressure vessels need to be explored in detail. A careful selection of the materials is also required in order to comply with the weight constraints of the device.

Sealing Material

There are three, or possibly four, different materials used here, with different coefficients of thermal expansion. They could be aluminum, ceramic and steel. The sealing material could possibly be ceramic, or another material yet to be defined, such that it fulfils the specifications of surface speed, pressure retention, porosity, flexibility, corrosive resistance, thermal expansion, etc.

The seal has been simplified to a simple ring, with a section of reasonable dimensions of thickness and diameters, so as to seal water at high pressure and high temperature, allowing miniscule leakage, so that the high internal pressure can be maintained. The design of the seal involves precision since the shell is rotating. The vessel design described earlier has a design allowance that will be taking up the thermal expansion difference of the materials of the seal, and the vessel. Further work is needed to determine a suitable seal material within the requirements of the system.

Lubrication

Suitable lubricants have to be selected, according to their applications. The means of their delivery to their respective points have to be determined, and modification of parts to allow the delivery has to be designed.

Weather Modification

Weather behaviour would tend to change due to a reduced amount of water vapour being released into the atmosphere through aircraft emission. Artificial rain can be induced by releasing the separated exhaust water in the lower atmosphere at any altitude which possesses weather patterns. Release of water with additional nucleation centres like silver Iodide for seeding can induce artificial rainfall at an accelerated rate. Introducing large water droplets into warm clouds stimulates the growth of raindrops by collision coalescence. The impact of artificial rain and the release of water in the atmosphere can be studied to determine its effect on the weather and the water cycle in order to validate the likelihood of a favourable outcome towards global cooling.

The behaviour of the exhaust gases at the transformed levels of energy at the exit of the engine and when released into the atmosphere needs to be investigated further. Nitrogen is likely to transport the latent heat of water absorbed during condensation into the atmosphere. The behaviour of the Nitrogen energy reservoir in the atmosphere would need to be analysed for this purpose.

A climate model such as “AirClim”, or “TomCat” could be employed to quantify the effect of the de-excited CO_2 and N_2 carrying the energy into the atmosphere. This model could also be used to assess the effect of releasing water at various altitudes.

A quantitative study can also be carried out on the behaviour of the combustion gases by using an alternate fuel other than kerosene. The use of hydrogen fuel can be explored for the same purpose.

Water containment and Utility Model

A detailed study of flight systems would be required to determine if the water produced could be used on board by the engine and the aircraft systems to replace the water carried aboard for in flight use. It might also be possible to substitute the use of compressor bleed air with water for some purposes. Drainage storage and handling model of water could be created inclusive of the proposition of further cooling the separated water through a heat exchange mechanism in order for it to exist as a liquid at a wide range of ambient conditions that are essentially a function of the altitude.

Fluid Dynamics

A detailed Computational Fluid Dynamics (CFD) analysis can be performed to determine the behaviour of the fluid under action and the variation of the fluid properties in the radial and axial direction. The characteristics of the exhaust gas in this configuration are governed by the compressible Navier-Stokes equation. It determines the pressure, temperature, density and velocity changes involved when the gas undergoes centrifugal compression. The solution to the said equation can be obtained using the finite element method. The CFD analyses can be complemented with scaled down experimentation of gas flow. This shall enable a more accurate modelling of the centrifugal water expeller and hence result in an optimized design of the device and improved performance.

Engine Simulation

An engine performance simulation tool such as “TurboMatch” would need to be adapted to include a built in contrail model for calculating the pressure to condense water at a given temperature or vice versa; hence, calculating the condensation conditions within the engine. The condensation mechanism model should be an inherent part of the code. The effect of extracting the water out of the emissions would need to be quantified to account for the change in the mass flow of the core exhaust as well the altered condition of the gases exiting the nozzle. This shall enable the use of the software to execute off-design analyses for engines with the water expeller attached. Since the expeller is now defined as a component in the turbomachinery family, a specific module could be added to the code for modelling its characteristics. Further investigations can be undertaken for the thrust and fuel burn penalty of carrying water aboard on standard engines. This can then be extrapolated towards aircraft redesign as a vision of the future for flying heavier and perhaps landing with water.

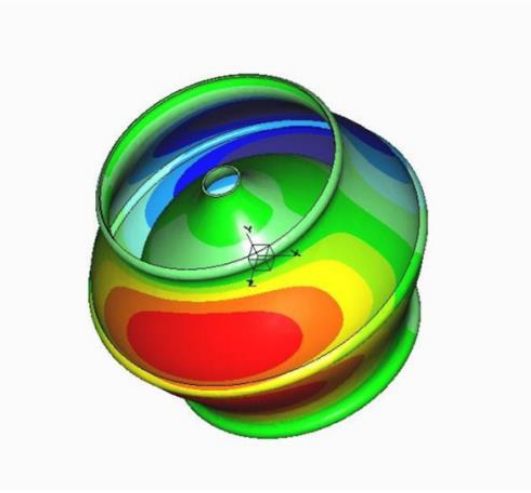

REFERENCES

Alan, S. (2016) ‘Air travel’s impact on Earth’s climate’, *Encyclopaedia of Global Warming*, pp. 3–6.

Ambaum, M.H.P. (2010) Thermal Physics of the Atmosphere. Wiley Online Library.

Anderson, C.E., Birstein, S.J. and Silverman, B.A., Us Air Force, 1970.*Method and Apparatus for Suppressing Contrails*. U.S. Patent 3,517,505.

Atela, F.L. (2016) *Aircraft Performance with On-board Water Condensed from Engine Core Exhaust for Contrail Prevention*. Cranfield University.

Atkins, P. (2010) *Physical Chemistry.* Oxford University Press.

Bright, C.G. (2011) *Aircraft Contrail Dispersion*. GB patent 2475280 A.

Burkhardt, U. and Kärcher, B. (2011) ‘Global radiative forcing from contrail cirrus’, *Nature Climate Change*, 1(1), pp. 54–58.

Camilleri, R. et al. (2011) ‘Applying heat pipes to a novel concept aero engine part 2 - Design of a heat-pipe heat exchanger for an intercooled-recuperated aero engine’, *Aeronautical Journal*, 115(1169), pp. 403–410.

Cengel, Y.A. (2006) *Heat and Mass Transfer*: *A Practical Approach* McGraw Hill Higher Education.

Chapman, L. (2007) ‘Transport and climate change: a review’, *Journal of Transport Geography,* 15(5), pp. 354–367.

Chen, C.C. and Gettelman, A. (2013) ‘Simulated radiative forcing from contrails and contrail cirrus’, *Atmospheric Chemistry and Physics, 13(24), pp. 12525–12536.*

Dickens, P.G. and Ripamonti, A. (1961) ‘Calculation of vibrational relaxation times in gases’, *Transactions of the Faraday Society, 57 Royal Society of Chemistry, pp. 735–745*.

Dymond, J.H. et al. (2002) *Virial Coefficients of Pure Gases and Mixtures*. Springer Germany.

Filippone, A. (2010) ‘Cruise altitude flexibility of jet transport aircraft’*, Aerospace Science and Technology, 14(4), pp. 283–294.*

Finzi, J. et al. (1977) ‘Vibrational relaxation of water vapor’, *The Journal of Chemical Physics, 67, p. 4053.*

Fridman, A. and Kennedy, L.A. (2004*) Plasma Physics and Engineering*. CRC press.

Gleitsmann, G. and Zellne, R. (1998) 'The effects of ambient temperature and relative humidity on particle formation in the jet regime of commercial aircrafts: A modelling study', *Atmospheric Environment, 32(18), pp. 3079–3087*.

Haglind, F. (2008) 'Potential of lowering the contrail formation of aircraft exhausts by engine re-design', *Aerospace Science and Technology, 12(6), pp. 490–497.*

Heymsfield, A. et al. (2010) 'Contrail microphysics', *Bulletin of the American Meteorological Society, 91(4), pp. 465–472.*

Hobbs, P. V (2000*) Basic Physical Chemistry for the Atmospheric Sciences.* Cambridge University Press.

Holman, J.P. (1997*) Heat Transfer*, 8 th. McGraw-Hill Book Company (UK) Ltd.,

Houston, P.L. (2012) *Chemical Kinetics and Reaction Dynamics*. Courier Corporation.

Huetz-Aubert, M. et al. (1978) 'An optic-acoustic study of collisional vibrational relaxation in mixtures of CO_2 with a diatomic gas. Application to CO_2-CO and CO_2-N_2', *Physica B+C, 93(2), pp. 237–252.*

Jackson, P., 1998*. Jane's all the World's Aircraft 1998-1999*.Mc.Graw Hill

Jeberger, P. et al. (2013) 'Aircraft type influence on contrail properties', *Atmospheric Chemistry and Physics, 13(23), pp. 11965–11984.*

Jenkinson, L. (1999) *Civil Jet Aircraft Design*. 1st edn. Butterworth-Heinemann.

John, J. and Keith, T. (2006) *Gas Dynamics.* Pearson Education.

Joly, V. et al. (1999) 'Vibrational relaxation of CO_2 in a CO_2-N_2 mixture. Part 2: Application to a one-dimensional problem', *Aerospace Science and Technology, 3(5), pp. 313–322.*

Joly, V. et al. (1997) Vibrational relaxation of CO_2 in a CO_2-N_2 mixture along a stagnation streamline. : AIAA, 1997, Paper / *American Institute of Aeronautics and Astronautics; AIAA-97/2554.*

Keeton, R.G. and Bass, H.E. (1976) 'Vibrational and rotational relaxation of water vapour by water vapour, nitrogen, and argon at 500 K', *The Journal of the Acoustical Society of America, 60, p. 78.*

Kurzke, J. (2007) *GasTurb 11, User Manual*. Germany: Joachim Kurzke.

Lee, D.S., Clare, P.E., Haywood, J., Kärcher, B., Lunnon, R.W., Pilling, I., Slingo, A. and Tilston, J.R., 2000. *Identifying the uncertainties in radiative forcing of climate from aviation contrails and aviation-induced cirrus*. Report DERA/AS/PT/CR000102, DERA, UK.

Marinov 2, D. et al. (2012) 'Surface vibrational relaxation of N 2 studied by CO2 titration with time-resolved quantum cascade laser absorption spectroscopy', *Journal of Physics D: Applied Physics, 45(17)* (1)LPP, Ecole Polytechnique, CNRS; (2)Institute of Physics, St Petersburg State University; (3)INP Greifswald

Marshall, J. and Plumb, R.A. (1965) *Atmosphere, Ocean and Climate Dynamics: an Introductory Text.* Academic Press.

Noppel, F.G. (2007) *Contrail and Cirrus Cloud Avoidance Technology.* Cranfield University.

Noppel, F.G., Singh, R. and Taylor, M.D., Rolls-Royce Plc, 2013. *Method and Apparatus for Suppressing Aero-Engine Contrails*. U.S. Patent 8,402,736.

Noppel, F.G., Singh, R. and Taylor, M.D., Rolls-Royce Plc, 2008. *Method and Apparatus for Suppressing Aero-Engine Contrails*. U.S. Patent Application 12/450,691.

Ochterski, J.W. (2000) *Thermochemistry in Gaussian*. Gaussian Inc.

Qureshi, M.L. (2016a) *A Mechanical Device to Suppress Contrail Formation.* US patent 62328087 A

Qureshi, M.L. (2016a) *A Mechanical Device to Suppress Contrail Formation.* GB patent 2531632

Qureshi, M.L. (2016b) *A Device to Suppress Contrail Formation*.GB patent 2531629

Saravanamuttoo, H.I.H. (2008) *Gas Turbine Theory*. Pearson Prentice Hall.

Schumann, U. (2000) 'Influence of propulsion efficiency on contrail formation', *Aerospace Science and Technology, 4(6), pp. 391–401.*

Schumann, U. et al. (2015) 'Dehydration effects from contrails in a coupled contrail-climate model', *Atmospheric Chemistry and Physics, 15(19), pp. 11179–11199.*

Seinfeld, J.H. et al. (2006) *Atmospheric Chemistry and Physics*. J. Wiley.

Singh, S., Scipar, Inc., 1988. *Method of Suppressing Formation of Contrails and Solution Therefor*. U.S. Patent 4,766,725.

Spiro, T.G. et al. (2012) *Chemistry of the Environment*. University Science Books.

Taylor, M.D., Noppel, F.G. and Singh, R., Rolls-Royce plc, 2011. *Gas Turbine Engine Having a Heat Exchanger Arrangement for Exhaust Gas Flows*. U.S. Patent 7,971,438.

Turrell, G. (1997) *Gas Dynamics Theory and Application.* John Wiley.

Wallace, J.M. and Hobbs, P. V (2006) *Atmospheric Science: An Introductory Survey*. Academic press.

Weihs, P. et al. (2015) 'Potential impact of contrails on solar energy gain', *Atmospheric Measurement Techniques, 8(3), pp. 1089–1096.*

Williams, V. et al. (2002) 'Reducing the climate change impacts of aviation by restricting cruise altitudes', *Transportation Research Part D: Transport and Environment, 7(6), pp. 451–464.*

Yang, P. et al. (2010) 'Contrails and induced cirrus', *Bulletin of the American Meteorological Society, 91(4), pp. 473–478.*

Zerefos, C.S. et al. (2003) 'Evidence of impact of aviation on cirrus cloud formation', *Atmospheric Chemistry and Physics, 3(1996), pp. 1633–1644.*

APPENDICES

Appendix A TURBOMATCH

A.1 PERFORMANCE CODE FOR THE 3 SPOOL TURBOFAN ENGINE TRENT 900 BASELINE SPECIFICATIONS

A.1.1 INPUT FILE AT TAKE-OFF DESIGN AND OFF-DESIGN POINT

```
 THE FIRST RUN IS THE DESIGN POINT AT TAKE-OFF TO ESTABLISH THE TAKE-OFF
RATING OF 340 KN
// extracted from the TurboMatch Tutorial
//X:\SoE\TURBOMATCH\TurboMatch\civ\RR_Trent900.dat
// Created by: Dr. Junfei Yin ; Adapted by: Fernando Lartategui Atela


  OD SI KE CT FP
  -1
  -1
 INTAKE  S1-2         D1-4            R100
 COMPRE  S2-3         D5-10           R101   V5    V6
 PREMAS  S3,4,14      D11-14                 V11
 DUCTER  S14-15       D15-18          R102
 NOZCON  S15-16,1     D19             R103
 COMPRE  S4-5         D20-25          R104   V20   V21
 COMPRE  S5-6         D26-31          R105   V26   V27
 PREMAS  S6,7,17      D32-35
 DUCTER  S17-18       D36-39          R106
 BURNER  S7-8         D40-42          R107
 MIXEES  S8,18,9
 TURBIN  S9-10        D43-50,105,51           V44
 TURBIN  S10-11       D52-59,104,60           V53
 TURBIN  S11-12       D61-68,101,69           V62
 NOZCON  S12-13,1     D70             R108
 PERFOR  S1,0,0       D71-74,103,100,102,108,0,107,0,0,0
 CODEND
  ! INTAKE - Aeroplane inlet
  1   0.0         ! ALTITUDE
  2   0.0         ! ISA DEVIATION
```

```
 3   0.0          ! MACH NO.
 4   0.99         ! PRESSURE RECOVERY
 ! COMPRE - Fan uses Trent 800
 5   -1.0         ! SURGE MARGINE
 6    1.0         ! ROTATIONAL SPEED,N1
 7   1.56         ! FAN PRESSURE RATIO
 8   0.874        ! EFFICIENCY
 9   0.0          ! ERROR SELECTOR
 10  1.0          ! MAP NUMBER
 ! PREMAS -  Bypass - Main
 11  0.111111     ! LAMDA (BYPASS RATIO 8.5)
 12  0.0          ! MASS FLOW LOSS
 13  1.0          ! PRESSURE FACTOR
 14  0.0          ! PRESSURE LOSS
! Bypass duct
 15  0.0          ! REHEAT SELECTOR
 16  0.01         ! PRESSURE LOSS 1%
 17  0.0          ! REHEAT COMB.EFFICIENCY
 18  0.0          ! MAX REHEAT FUEL FLOW
 !Bypass Convergent Zozzle
 19  -1.0         ! Fan Exhaust Nozzle: fixed Area
 !  IP COMPRESSOR
 20  0.85         ! SURGE MARGIN
 21  1.0          ! ROTATIONAL SPEED
 22  5.188        ! PRESSURE RATIO
 23  0.846        ! EFFICIENCY
 24  1.0          ! ERROR SELECTOR
 25  4.0          ! MAP NUMBER
 !  HP COMPRESSOR
 26  0.85         ! SURGE MARGIN
 27  1.0          ! ROTATIONAL SPEED
 28  5.188        ! PRESSURE RATIO
 29  0.851        ! EFFICIENCY
 30  1.0          ! ERROR SELECTOR
 31  5.0          ! MAP NUMBER
 !  HPT Turbine COOLING BYPASS
 32  0.80         ! BYPASS RATIO
```

```
33  0.0          ! MASS FLOW LOSS
34  1.0          ! PRESSURE FACTOR
35  0.0          ! PRESSURE LOSS
!  Ducter Cooling
36  0.0          ! REHEAT SELECTOR
37  0.01         ! PRESSURE LOSS 1%
38  0.0          ! REHEAT COMB.EFFICIENCY
39  0.0          ! MAX REHEAT FUEL FLOW
!  BURNER
40  0.06         ! PRESSURE LOSS
41  0.998        ! COMBUSTION EFFICIENCY
42  -1.0         ! FUEL FLOW
!  TURBINE-HP
43  0.0          ! AUX.WORK
44  0.8          ! REL NON-D MASS FLOW
45  0.6          ! REL NON-D SPEED
46  0.885        ! EFFICIENCY
47 -1.0          ! REL ROT.SPEED(COMP TURB=-1)
48  3.0          ! COMP NO. FROM LOW END
49  5.0          ! TURBINE MAP
50 -1.0          ! POWER LAW
51  0.0          ! NGV
!  TURBINE-IP
52  0.0          ! AUX.WORK
53  0.8          ! REL NON-D MASS FLOW
54  0.6          ! REL NON-D SPEED
55  0.909        ! EFFICIENCY
56 -1.0          ! REL ROT.SPEED
57  2.0          ! COMP NO. FROM LOW END
58  5.0          ! TURBINE MAP
59 -1.0          ! POWER LAW
60  0.0          ! NGV
!  TURBINE-LP
61  0.0          ! AUX.WORK
62  0.8          ! REL NON-D MASS FLOW
63  0.6          ! REL NON-D SPEED
64  0.915        ! EFFICIENCY
```

```
 65 -1.0          ! REL ROT.SPEED
 66  1.0          ! COMP NO. FROM LOW END
 67  5.0          ! TURBINE MAP
 68 -1.0          ! POWER LAW
 69  0.0          ! NGV
 !  Core CONVERGENT NOZZLE
 70 -1.0          ! SWITHCH, AREA FIXED
 !  PERFORMANCE
 71 -1.0          ! POWER (-1=TURBOJET/FAN)
 72 -1.0          ! PROPELLER EFFICIENCY(")
 73  0.0          ! SCALING INDEX
 74  0.0          ! REQ'D D.P. THRUST
 -1
 1 2  1225.0      ! INLET MASS FLOW(Kg/s)
 8 6  1800.0      ! TET(K)
 -1
*************************************************
```

A.1.2 DESIGN POINT OUTPUT AT TAKE-OFF

```
          The Units for this Run are as follows:-
 Temperature = K   Pressure = Atmospheres   Length = metres
 Area = sq metres  Mass Flow = kg/sec       Velocity = metres/sec
 Force = Newtons   s.f.c.(Thrust) =  mg/N sec   s.f.c.(Power = mg/J
 Sp. Thrust =    N/kg/sec     Power =   Watts
    ***** DESIGN POINT ENGINE CALCULATIONS *****
 ***** AMBIENT AND INLET PARAMETERS *****
 Alt. =      0.0      I.S.A. Dev. =    0.000       Mach No. =  0.00
 Etar = 0.9900        Momentum Drag =      0.00
 ***** COMPRESSOR  1 PARAMETERS *****
 PRSF =  0.13725E+01     ETASF =  0.10038E+01     WASF =
0.20785E+01
 Z = 0.85000             PR =   1.560             ETA = 0.87400
 PCN =   1.0000          CN = 1.00000             COMWK =
0.54966E+08
 ***** CONVERGENT NOZZLE  1 PARAMETERS *****
 NCOSF =  0.10000E+01
 Area =  3.2875          Exit Velocity =  276.54
Gross Thrust=294577.84         Nozzle Coeff. =  0.97828E+00
```

***** COMPRESSOR 2 PARAMETERS *****

PRSF = 0.41059E+01 ETASF = 0.10193E+01 WASF = 0.53198E+00

Z = 0.85000 PR = 5.188 ETA = 0.84600

PCN = 1.0000 CN = 1.00000 COMWK = 0.32239E+08

***** COMPRESSOR 3 PARAMETERS *****

PRSF = 0.63781E+00 ETASF = 0.10631E+01 WASF = 0.46443E+00

Z = 0.85000 PR = 5.188 ETA = 0.85100

PCN = 1.0000 CN = 1.00000 COMWK = 0.53712E+08

***** COMBUSTION CHAMBER PARAMETERS *****

ETASF = 0.99800E+00

ETA = 0.99800 DLP = 2.4941 WFB = 2.9705

***** TURBINE 1 PARAMETERS *****

CNSF = 0.89138E+02 ETASF = 0.10550E+01 TFSF = 0.15229E+01

DHSF = 0.41330E+05

TF = 219.627 ETA = 0.88500 CN = 2.200

AUXWK = 0.00000E+00

***** TURBINE 2 PARAMETERS *****

CNSF = 0.80382E+02 ETASF = 0.10836E+01 TFSF = 0.59683E+00

DHSF = 0.30506E+05

TF = 219.627 ETA = 0.90900 CN = 2.200

AUXWK = 0.00000E+00

***** TURBINE 3 PARAMETERS *****

CNSF = 0.74471E+02 ETASF = 0.10907E+01 TFSF = 0.31253E+00

DHSF = 0.60595E+05

TF = 219.627 ETA = 0.91500 CN = 2.200

AUXWK = 0.00000E+00

***** CONVERGENT NOZZLE 2 PARAMETERS *****

NCOSF = 0.10000E+01

Area = 0.7766 Exit Velocity = 378.57

Gross Thrust = 51423.04 Nozzle Coeff. = 0.97667E+00

Scale Factor on above Mass Flows, Areas, Thrusts & Powers = 1.0

Station	F.A.R.	Mass Flow	Pstatic	Ptotal	Tstatic	Ttotal	Vel	Area
1	0.00000	1225.000	1.00000	1.00000	288.15	288.15	0.0	******
2	0.00000	1225.000	******	0.99000	******	288.15	******	******
3	0.00000	1225.000	******	1.54440	******	332.82	******	******
4	0.00000	136.111	******	1.54440	******	332.82	******	******
5	0.00000	136.111	******	8.01235	******	564.70	******	******
6	0.00000	136.111	******	41.56808	******	928.24	******	******
7	0.00000	108.889	******	41.56808	******	928.24	******	******
8	0.02728	111.859	******	39.07400	******	1800.00	******	******
9	0.02182	139.081	******	39.07400	******	1641.64	******	******
10	0.02182	139.081	******	13.80923	******	1334.96	******	******
11	0.02182	139.081	******	6.69935	******	1145.85	******	******
12	0.02182	139.081	******	1.37839	******	809.76	******	******
13	0.02182	139.081	1.00000	1.37839	746.28	809.76	378.6	0.7766
14	0.00000	1088.889	******	1.54440	******	332.82	******	******
15	0.00000	1088.889	******	1.52896	******	332.82	******	******
16	0.00000	1088.889	1.00000	1.52896	294.76	332.82	276.5	3.2875
17	0.00000	27.222	******	41.56808	******	928.24	******	******
18	0.00000	27.222	******	41.15240	******	928.24	******	******

Gross Thrust = 346000.84

Momentum Drag = 0.00

Net Thrust = 346000.84

Fuel Flow = 2.9705

s.f.c. = 8.58519

Sp. Thrust = 282.450

A.1.3 OUTPUT FOR OFF-DESIGN RUNS

```
  1 2000
  3 0.65          !climb
  -1
 8 6 1800
  -1
 ***** OFF DESIGN ENGINE CALCULATIONS. Converged after   3 Loops
 ***** AMBIENT AND INLET PARAMETERS *****
 Alt. =   2000.0      I.S.A. Dev. =    0.000       Mach No. =  0.65
 Etar = 0.9900        Momentum Drag = 274639.28
 ***** COMPRESSOR  1 PARAMETERS *****
 PRSF =  0.13725E+01     ETASF =  0.10038E+01     WASF =
0.20785E+01
 Z = 0.80439             PR =   1.529             ETA = 0.87669
 PCN =   1.0168          CN = 0.99914             COMWK =
0.56048E+08
 ***** CONVERGENT NOZZLE  1 PARAMETERS *****
 NCOSF =  0.10000E+01
 Area =  3.2875          Exit Velocity =  338.67  Gross Thrust =
391430.47
 Nozzle Coeff. =  0.98098E+00
 ***** COMPRESSOR  2 PARAMETERS *****
 PRSF =  0.41059E+01     ETASF =  0.10193E+01     WASF =
0.53198E+00
 Z = 0.85447             PR =   5.052             ETA = 0.85059
 PCN =   0.9914          CN = 0.97750             COMWK =
0.31600E+08
 ***** COMPRESSOR  3 PARAMETERS *****
 PRSF =  0.63781E+00     ETASF =  0.10631E+01     WASF =
0.46443E+00
 Z = 0.84168             PR =   5.104             ETA = 0.85496
 PCN =   1.0016          CN = 0.99316             COMWK =
0.52497E+08
 ***** COMBUSTION CHAMBER PARAMETERS *****
 ETASF =  0.99800E+00
 ETA = 0.99800           DLP = 2.4596             WFB =   2.8771
 ***** TURBINE  1 PARAMETERS *****
 CNSF =  0.89138E+02     ETASF =  0.10550E+01     TFSF= 0.15229E+01
 DHSF =0.41330E+05  TF =219.603 ETA =0.88471 CN =2.203 AUXWK =0.0
```

***** TURBINE 2 PARAMETERS *****

CNSF = 0.80382E+02 ETASF = 0.10836E+01 TFSF = 0.59683E+00

DHSF = 0.30506E+05

TF = 219.402 ETA = 0.90908 CN = 2.180

AUXWK = 0.00000E+00

***** TURBINE 3 PARAMETERS *****

CNSF = 0.74471E+02 ETASF = 0.10907E+01 TFSF = 0.31253E+00

DHSF = 0.60595E+05

TF = 219.575 ETA = 0.91244 CN = 2.236

AUXWK = 0.00000E+00

***** CONVERGENT NOZZLE 2 PARAMETERS *****

NCOSF = 0.10000E+01 Area = 0.7766 Exit Velocity = 446.84 Gross Thrust = 59464.82 Nozzle Coeff. = 0.97869E+00

Scale Factor on above Mass Flows, Areas, Thrusts & Powers=1.0

Station	F.A.R.	Mass Flow	Pstatic	Ptotal	Tstatic	Ttotal	Vel	Area
1	0.00000	1270.287	0.78452	1.04228	275.15	298.45	216.2	******
2	0.00000	1270.287	******	1.03185	******	298.45	******	******
3	0.00000	1270.287	******	1.57790	******	342.34	******	******
4	0.00000	133.119	******	1.57790	******	342.34	******	******
5	0.00000	133.100	******	7.97176	******	574.38	******	******
6	0.00000	133.100	******	40.68716	******	937.02	******	******
7	0.00000	106.480	******	40.68716	******	937.02	******	******
8	0.02702	109.357	******	38.22752	******	1800.00	******	******
9	0.02162	135.977	******	38.22752	******	1643.06	******	******
10	0.02162	135.977	******	13.52300	******	1336.41	******	******
11	0.02162	135.977	******	6.55328	******	1146.77	******	******

```
    12   0.02162   135.977    ******   1.23438  ******  795.67
******  ******

    13   0.02162   135.977   0.78452   1.23438  706.84  795.67
446.8  0.7766

    14   0.00000  1137.226    ******   1.57790  ******  342.34
******  ******

    15   0.00000  1137.226    ******   1.56212  ******  342.34
******  ******

    16   0.00000  1137.226   0.82539   1.56212  285.29  342.34
338.7  3.2875

    17   0.00000    26.620    ******  40.68716  ******  937.02
******  ******

    18   0.00000    26.620    ******  40.28029  ******  937.02
******  ******

  Gross Thrust = 450895.25

 Momentum Drag = 274639.28

    Net Thrust = 176255.97

     Fuel Flow =    2.8771

        s.f.c. =  16.32314

    Sp. Thrust =   138.753

 ***********************************************

 1 5000           !climb2

 -1

 -1

 ***** OFF DESIGN ENGINE CALCULATIONS. Converged after   3 Loops

 ***** AMBIENT AND INLET PARAMETERS *****

 Alt. =   5000.0      I.S.A. Dev. =    0.000       Mach No. =  0.65

 Etar = 0.9900        Momentum Drag = 194254.02

 ***** COMPRESSOR  1 PARAMETERS *****

 PRSF =  0.13725E+01     ETASF =  0.10038E+01     WASF =
0.20785E+01

 Z = 0.84764             PR =   1.597             ETA = 0.85299

 PCN =   1.0125          CN = 1.03205             COMWK=0.43578E+08

 ***** CONVERGENT NOZZLE  1 PARAMETERS *****

 NCOSF =  0.10000E+01

 Area =  3.2875          Exit Velocity =  329.38

Gross Thrust = 285444.84  Nozzle Coeff. =  0.98090E+00

 ***** COMPRESSOR  2 PARAMETERS *****

 PRSF =  0.41059E+01     ETASF =  0.10193E+01     WASF= 0.53198E+00

 Z = 0.85040             PR =   5.328             ETA = 0.83560
```

```
 PCN =   1.0015          CN = 1.01522          COMWK = 0.24418E+08

 ***** COMPRESSOR  3 PARAMETERS *****

 PRSF =  0.63781E+00     ETASF =  0.10631E+01     WASF =
0.46443E+00

 Z = 0.85603             PR =   5.243             ETA = 0.84706

 PCN =   0.9969          CN = 1.00346          COMWK =  0.40443E+08

 ***** COMBUSTION CHAMBER PARAMETERS *****

 ETASF =  0.99800E+00

 ETA = 0.99800           DLP = 1.8657             WFB =   2.2537

 ***** TURBINE  1 PARAMETERS *****

 CNSF =  0.89138E+02     ETASF =  0.10550E+01   TFSF =  0.15229E+01

 DHSF =  0.41330E+05    TF =  219.671            ETA = 0.88544
CN =  2.194    AUXWK =  0.00000E+00

 ***** TURBINE  2 PARAMETERS *****

 CNSF =  0.80382E+02     ETASF =  0.10836E+01   TFSF =  0.59683E+00

 DHSF = 0.30506E+05  TF = 219.593  ETA = 0.90856 CN =  2.204

 AUXWK =  0.00000E+00

 ***** TURBINE  3 PARAMETERS *****

 CNSF =  0.74471E+02     ETASF =  0.10907E+01   TFSF =  0.31253E+00

 DHSF =  0.60595E+05  TF =  220.644  ETA = 0.91650  CN =  2.229

 AUXWK =  0.00000E+00

 ***** CONVERGENT NOZZLE  2 PARAMETERS *****

 NCOSF =  0.10000E+01  Area =  0.7766  Exit Velocity =  489.05
Gross Thrust =  50206.70   Nozzle Coeff. =  0.97998E+00

 Scale Factor on above Mass Flows, Areas, Thrusts & Powers= 1.0

 Station  F.A.R. Mass Flow   Pstatic    Ptotal Tstatic  Ttotal
Vel    Area

     1   0.00000   932.013   0.53307   0.70825  255.65  277.32
208.4  ******

     2   0.00000   932.013    ******   0.70117  ******  277.32
******  ******

     3   0.00000   932.013    ******   1.11993  ******  323.89
******  ******

     4   0.00000   102.514    ******   1.11993  ******  323.89
******  ******

     5   0.00000   102.506    ******   5.96714  ******  557.35
******  ******

     6   0.00000   102.506    ******  31.28353  ******  921.38
******  ******

     7   0.00000    82.005    ******  31.28353  ******  921.38
******  ******
```

```
     8   0.02748    84.258    ******  29.41781  ****** 1800.00
******  ******

     9   0.02199   104.759    ******  29.41781  ****** 1640.53
******  ******

    10   0.02199   104.759    ******  10.39882  ****** 1334.02
******  ******

    11   0.02199   104.759    ******   5.01815  ****** 1143.87
******  ******

    12   0.02199   104.759    ******   0.93113  ******  789.42
******  ******

    13   0.02199   104.759   0.53307   0.93113  682.30  789.42
489.0  0.7766

    14   0.00000   829.515    ******   1.11993  ******  323.89
******  ******

    15   0.00000   829.515    ******   1.10873  ******  323.89
******  ******

    16   0.00000   829.515   0.58542   1.10873  269.80  323.89
329.4  3.2875

    17   0.00000    20.501    ******  31.28353  ******  921.38
******  ******

    18   0.00000    20.501    ******  30.97070  ******  921.38
******  ******

  Gross Thrust = 335651.53
 Momentum Drag = 194254.02
    Net Thrust = 141397.53
     Fuel Flow =    2.2537
        s.f.c. =  15.93881
    Sp. Thrust =   151.712
 ***********************************************
  3 0.55           !glide
 -1
 8 6 1300
  -1
      ***** OFF DESIGN ENGINE CALCULATIONS. Converged after 8 Loops
 ***** AMBIENT AND INLET PARAMETERS *****
 Alt. =   5000.0      I.S.A. Dev. =    0.000       Mach No. =  0.55
 Etar = 0.9900        Momentum Drag = 112636.73
 ***** COMPRESSOR  1 PARAMETERS *****
 PRSF =  0.13725E+01     ETASF =  0.10038E+01   WASF =  0.20785E+01
 Z = 0.53038    PR =   1.221      ETA = 0.84624
 PCN =   0.7344          CN = 0.75703          COMWK =  0.12091E+08
```

```
***** CONVERGENT NOZZLE  1 PARAMETERS *****
NCOSF =  0.10000E+01
Area =  3.2875    Exit Velocity =  246.80 Gross Thrust = 141870.41
Nozzle Coeff. =  0.97770E+00
***** COMPRESSOR  2 PARAMETERS *****
PRSF =  0.41059E+01     ETASF =  0.10193E+01     WASF =
0.53198E+00
Z = 0.90462             PR =   3.796             ETA = 0.86125
PCN =   0.7023          CN = 0.75233        COMWK =  0.79591E+07
***** COMPRESSOR  3 PARAMETERS *****
PRSF =  0.63781E+00     ETASF =  0.10631E+01   WASF =  0.46443E+00
Z = 0.80619             PR =   4.428             ETA = 0.86115
PCN =   0.8209          CN = 0.92432          COMWK =  0.13876E+08
***** COMBUSTION CHAMBER PARAMETERS *****
ETASF =  0.99800E+00
ETA = 0.99800           DLP = 0.8240             WFB =   0.6875
***** TURBINE  1 PARAMETERS *****
CNSF =  0.89138E+02     ETASF =  0.10550E+01   TFSF =  0.15229E+01
DHSF =  0.41330E+05 TF =  216.327 ETA = 0.87641  CN =  2.121
AUXWK =  0.00000E+00
***** TURBINE  2 PARAMETERS *****
CNSF =  0.80382E+02     ETASF =  0.10836E+01  TFSF =  0.59683E+00
DHSF =  0.30506E+05 TF =  210.770 ETA = 0.89642 CN =  1.821
AUXWK =  0.00000E+00
***** TURBINE  3 PARAMETERS *****
CNSF =  0.74471E+02     ETASF =  0.10907E+01   TFSF =  0.31253E+00
DHSF =  0.60595E+05  TF =  202.082  ETA = 0.88169  CN =  1.903
AUXWK =  0.00000E+00
***** CONVERGENT NOZZLE  2 PARAMETERS *****
NCOSF =  0.10000E+01 Area =  0.7766 Exit Velocity =  208.26
Gross Thrust =  10421.81 Nozzle Coeff. =  0.97325E+00

Scale Factor on above Mass Flows, Areas, Thrusts & Powers =1.0
Station  F.A.R. Mass Flow   Pstatic    Ptotal Tstatic  Ttotal
Vel    Area
     1   0.00000   638.679   0.53307   0.65486  255.65  271.17
176.4  ******
     2   0.00000   638.679    ******   0.64831  ******  271.17
******  ******
```

```
     3   0.00000   638.679    ******   0.79186  ******  290.04
******  ******

     4   0.00000    50.730    ******   0.79186  ******  290.04
******  ******

     5   0.00000    50.730    ******   3.00589  ******  445.38
******  ******

     6   0.00000    50.730    ******  13.30951  ******  706.88
******  ******

     7   0.00000    40.584    ******  13.30951  ******  706.88
******  ******

     8   0.01694    41.271    ******  12.48550  ****** 1300.00
******  ******

     9   0.01355    51.417    ******  12.48550  ****** 1189.83
******  ******

    10   0.01355    51.417    ******   4.51418  ******  961.27
******  ******

    11   0.01355    51.417    ******   2.28526  ******  825.90
******  ******

    12   0.01355    51.417    ******   0.60396  ******  612.19
******  ******

    13   0.01355    51.417   0.53307   0.60396  591.99  612.19
208.3  0.7766

    14   0.00000   587.949    ******   0.79186  ******  290.04
******  ******

    15   0.00000   587.949    ******   0.78394  ******  290.04
******  ******

    16   0.00000   587.949   0.53307   0.78394  259.71  290.04
246.8  3.2875

    17   0.00000    10.146    ******  13.30951  ******  706.88
******  ******

    18   0.00000    10.146    ******  13.17642  ******  706.88
******  ******

  Gross Thrust = 152292.22
 Momentum Drag = 112636.73
    Net Thrust =  39655.49
     Fuel Flow =    0.6875
        s.f.c. =  17.33587
    Sp. Thrust =    62.090
 ***********************************************
 -1
 8 6 1400         !glide2
 -1
***** OFF DESIGN ENGINE CALCULATIONS. Converged after   4 Loops
```

***** AMBIENT AND INLET PARAMETERS *****

Alt. = 5000.0 I.S.A. Dev. = 0.000 Mach No. = 0.55

Etar = 0.9900 Momentum Drag = 123676.41

***** COMPRESSOR 1 PARAMETERS *****

PRSF = 0.13725E+01 ETASF = 0.10038E+01 WASF = 0.20785E+01

Z = 0.62604 PR = 1.304 ETA = 0.86246

PCN = 0.8070 CN = 0.83188 COMWK = 0.17447E+08

***** CONVERGENT NOZZLE 1 PARAMETERS *****

NCOSF = 0.10000E+01 Area = 3.2875 Exit Velocity = 268.58 Gross Thrust = 167932.61 Nozzle Coeff. = 0.97866E+00

***** COMPRESSOR 2 PARAMETERS *****

PRSF = 0.41059E+01 ETASF = 0.10193E+01 WASF = 0.53198E+00

Z = 0.88822 PR = 4.269 ETA = 0.87060

PCN = 0.7913 CN = 0.83912 COMWK = 0.10944E+08

***** COMPRESSOR 3 PARAMETERS *****

PRSF = 0.63781E+00 ETASF = 0.10631E+01 WASF = 0.46443E+00

Z = 0.81426 PR = 4.679 ETA = 0.86115

PCN = 0.8633 CN = 0.94701 COMWK = 0.18776E+08

***** COMBUSTION CHAMBER PARAMETERS *****

ETASF = 0.99800E+00M ETA = 0.99800 DLP = 1.0490 WFB = 0.9381

***** TURBINE 1 PARAMETERS *****

CNSF = 0.89138E+02 ETASF = 0.10550E+01 TFSF = 0.15229E+01

DHSF = 0.41330E+05 TF = 217.939 ETA = 0.88105 CN = 2.150

AUXWK = 0.00000E+00

***** TURBINE 2 PARAMETERS *****

CNSF = 0.80382E+02 ETASF = 0.10836E+01 TFSF = 0.59683E+00

DHSF = 0.30506E+05 TF = 215.503 ETA = 0.89760CN = 1.979

AUXWK = 0.00000E+00

***** TURBINE 3 PARAMETERS *****

CNSF = 0.74471E+02 ETASF = 0.10907E+01 TFSF = 0.31253E+00

DHSF = 0.60595E+05 TF = 211.581 ETA = 0.89120 CN = 2.021

AUXWK = 0.00000E+00

***** CONVERGENT NOZZLE 2 PARAMETERS *****

NCOSF = 0.10000E+01

Area = 0.7766 Exit Velocity = 262.18 Gross Thrust = 16178.65

Nozzle Coeff. = 0.97442E+00

Scale Factor on above Mass Flows, Areas, Thrusts & Powers= 1.0

Station	F.A.R.	Mass Flow	Pstatic	Ptotal	Tstatic	Ttotal	Vel	Area
1	0.00000	701.277	0.53307	0.65486	255.65	271.17	176.4	******
2	0.00000	701.277	******	0.64831	******	271.17	******	******
3	0.00000	701.277	******	0.84534	******	295.97	******	******
4	0.00000	62.391	******	0.84534	******	295.97	******	******
5	0.00000	62.390	******	3.60912	******	469.33	******	******
6	0.00000	62.390	******	16.88534	******	754.81	******	******
7	0.00000	49.912	******	16.88534	******	754.81	******	******
8	0.01880	50.850	******	15.83630	******	1400.00	******	******
9	0.01504	63.329	******	15.83630	******	1280.63	******	******
10	0.01504	63.329	******	5.63647	******	1033.16	******	******
11	0.01504	63.329	******	2.77796	******	884.25	******	******
12	0.01504	63.329	******	0.64490	******	636.77	******	******
13	0.01504	63.329	0.53307	0.64490	605.08	636.77	262.2	0.7766
14	0.00000	638.884	******	0.84534	******	295.97	******	******
15	0.00000	638.884	******	0.83688	******	295.97	******	******
16	0.00000	638.884	0.53307	0.83688	260.11	295.97	268.6	3.2875
17	0.00000	12.478	******	16.88534	******	754.81	******	******
18	0.00000	12.478	******	16.71648	******	754.81	******	******

Gross Thrust = 184111.28

Momentum Drag = 123676.41

Net Thrust = 60434.86

Fuel Flow = 0.9381

s.f.c. = 15.52302

```
    Sp. Thrust =    86.178
 ***********************************************
 1 10670          !cruise
 3 0.82
 -1
 8 6 1625
 -1
***** OFF DESIGN ENGINE CALCULATIONS. Converged after   8 Loops
 ***** AMBIENT AND INLET PARAMETERS *****
 Alt. =  10670.0      I.S.A. Dev. =    0.000       Mach No. =  0.82
 Etar = 0.9900        Momentum Drag = 123683.38
 ***** COMPRESSOR  1 PARAMETERS *****
 PRSF =  0.13725E+01     ETASF =  0.10038E+01     WASF =
0.20785E+01
 Z = 0.84531             PR =   1.594             ETA = 0.85453
 PCN =   0.9572          CN = 1.03113         COMWK =  0.21167E+08
 ***** CONVERGENT NOZZLE  1 PARAMETERS *****
 NCOSF =  0.10000E+01
 Area =  3.2875   Exit Velocity =  311.63  Gross Thrust = 160375.52
 Nozzle Coeff. =  0.97890E+00
 ***** COMPRESSOR  2 PARAMETERS *****
 PRSF =  0.41059E+01     ETASF =  0.10193E+01     WASF =
0.53198E+00
 Z = 0.85153             PR =   5.331             ETA = 0.83577
 PCN =   0.9471          CN = 1.01491   COMWK =  0.11918E+08
 ***** COMPRESSOR  3 PARAMETERS *****
 PRSF =  0.63781E+00     ETASF =  0.10631E+01     WASF =
0.46443E+00
 Z = 0.85650             PR =   5.247             ETA = 0.84676
 PCN =   0.9449          CN = 1.00374    COMWK =  0.19868E+08
 ***** COMBUSTION CHAMBER PARAMETERS *****
 ETASF =  0.99800E+00
 ETA = 0.99800           DLP = 0.9703         WFB =   1.0715
 ***** TURBINE  1 PARAMETERS *****
 CNSF =  0.89138E+02     ETASF =  0.10550E+01  TFSF =  0.15229E+01
 DHSF =  0.41330E+05 TF =  219.616            ETA = 0.88547
CN =  2.189    AUXWK =  0.00000E+00
 ***** TURBINE  2 PARAMETERS *****
 CNSF =  0.80382E+02     ETASF =  0.10836E+01   TFSF =  0.59683E+00
```

DHSF = 0.30506E+05 TF = 220.069 ETA = 0.91061 CN = 2.200

AUXWK = 0.00000E+00

***** TURBINE 3 PARAMETERS *****

CNSF = 0.74471E+02 ETASF = 0.10907E+01 TFSF = 0.31253E+00

DHSF = 0.60595E+05 TF = 220.750 ETA = 0.91690 CN = 2.229

AUXWK = 0.00000E+00

***** CONVERGENT NOZZLE 2 PARAMETERS *****

NCOSF = 0.10000E+01 Area = 0.7766 Exit Velocity = 481.28
Gross Thrust = 28444.49 Nozzle Coeff. = 0.98100E+00

Scale Factor on above Mass Flows, Areas, Thrusts & Powers= 1.0

Station	F.A.R.	Mass Flow	Pstatic	Ptotal	Tstatic	Ttotal	Vel	Area
1	0.00000	508.443	0.23517	0.36587	218.79	248.33	243.3	******
2	0.00000	508.443	******	0.36221	******	248.33	******	******
3	0.00000	508.443	******	0.57753	******	289.85	******	******
4	0.00000	55.840	******	0.57753	******	289.85	******	******
5	0.00000	55.840	******	3.07888	******	500.40	******	******
6	0.00000	55.840	******	16.15466	******	833.87	******	******
7	0.00000	44.672	******	16.15466	******	833.87	******	******
8	0.02399	45.743	******	15.18435	******	1625.00	******	******
9	0.01919	56.911	******	15.18435	******	1480.46	******	******
10	0.01919	56.911	******	5.34141	******	1197.67	******	******
11	0.01919	56.911	******	2.57692	******	1022.91	******	******
12	0.01919	56.911	******	0.47389	******	697.92	******	******
13	0.01919	56.911	0.25518	0.47389	591.67	697.92	481.3	0.7766
14	0.00000	452.603	******	0.57753	******	289.85	******	******
15	0.00000	452.603	******	0.57176	******	289.85	******	******

```
    16   0.00000   452.603   0.30213   0.57176  241.45  289.85
311.6  3.2875
    17   0.00000    11.168    ******  16.15466  ******  833.87
******  ******
    18   0.00000    11.168    ******  15.99311  ******  833.87
******  ******
  Gross Thrust = 188820.02
 Momentum Drag = 123683.38
    Net Thrust =  65136.63
     Fuel Flow =    1.0715
        s.f.c. =  16.45063
    Sp. Thrust =   128.110
 ***********************************************
 1 10000
 3 0.8
 -1
 -1
 ***** OFF DESIGN ENGINE CALCULATIONS. Converged after   1 Loops
 ***** AMBIENT AND INLET PARAMETERS *****
 Alt. =  10000.0      I.S.A. Dev. =    0.000       Mach No. =  0.80
 Etar = 0.9900        Momentum Drag = 130768.23
 ***** COMPRESSOR  1 PARAMETERS *****
 PRSF =  0.13725E+01     ETASF =  0.10038E+01     WASF =
0.20785E+01  Z = 0.83944    PR =   1.584      ETA = 0.86065
 PCN =   0.9591          CN = 1.02595   COMWK =  0.22529E+08
 ***** CONVERGENT NOZZLE  1 PARAMETERS *****
 NCOSF =  0.10000E+01  Area =  3.2875  Exit Velocity =  313.32
Gross Thrust = 170978.88 Nozzle Coeff. =  0.97932E+00
 ***** COMPRESSOR  2 PARAMETERS *****
 PRSF =  0.41059E+01     ETASF =  0.10193E+01   WASF =  0.53198E+00
 Z = 0.85186             PR =   5.281             ETA = 0.83968
 PCN =   0.9469          CN = 1.00921         COMWK =  0.12673E+08
 ***** COMPRESSOR  3 PARAMETERS *****
 PRSF =  0.63781E+00     ETASF =  0.10631E+01  WASF =  0.46443E+00
 Z = 0.85386             PR =   5.222             ETA = 0.84854
 PCN =   0.9460          CN = 1.00206         COMWK =  0.21145E+08
 ***** COMBUSTION CHAMBER PARAMETERS *****
 ETASF =  0.99800E+00 ETA = 0.99800  DLP = 1.0358 WFB =   1.1371
 ***** TURBINE  1 PARAMETERS *****
```

```
 CNSF =  0.89138E+02     ETASF =0.10550E+01     TFSF =  0.15229E+01
 DHSF =  0.41330E+05  TF =  219.609 ETA = 0.8853  CN =  2.191
 AUXWK =  0.00000E+00
 ***** TURBINE  2 PARAMETERS *****
 CNSF =  0.80382E+02     ETASF =  0.10836E+01  TFSF =  0.59683E+00
 DHSF =  0.30506E+05 TF =  219.962 ETA = 0.91026  CN =  2.199
 AUXWK =  0.00000E+00
 ***** TURBINE  3 PARAMETERS *****
 CNSF =  0.74471E+02   ETASF =  0.10907E+01 TFSF =  0.31253E+00
 DHSF =  0.60595E+05  TF =  220.485 ETA = 0.91575  CN =  2.233
 AUXWK =  0.00000E+00
 ***** CONVERGENT NOZZLE  2 PARAMETERS *****
 NCOSF =  0.10000E+01  Area =  0.7766 Exit Velocity =  481.50
Gross Thrust =  29468.44  Nozzle Coeff. =  0.98083E+00
 Scale Factor on above Mass Flows, Areas, Thrusts & Powers=1.0
 Station  F.A.R. Mass Flow   Pstatic    Ptotal Tstatic  Ttotal
Vel    Area
     1   0.00000   545.601   0.26084   0.39775  223.15  251.82
239.7  ******
     2   0.00000   545.601    ******   0.39377  ******  251.82
******  ******
     3   0.00000   545.601    ******   0.62379  ******  293.00
******  ******
     4   0.00000    59.439    ******   0.62379  ******  293.00
******  ******
     5   0.00000    59.441    ******   3.29418  ******  503.25
******  ******
     6   0.00000    59.441    ******  17.20166  ******  836.46
******  ******
     7   0.00000    47.553    ******  17.20166  ******  836.46
******  ******
     8   0.02391    48.690    ******  16.16587  ****** 1625.00
******  ******
     9   0.01913    60.578    ******  16.16587  ****** 1480.88
******  ******
    10   0.01913    60.578    ******   5.68847  ****** 1198.11
******  ******
    11   0.01913    60.578    ******   2.74657  ****** 1023.53
******  ******
    12   0.01913    60.578    ******   0.50449  ******  698.59
******  ******
```

```
    13   0.01913    60.578   0.27176   0.50449  592.24  698.59
481.5  0.7766
    14   0.00000   486.166    ******   0.62379  ******  293.00
******  ******
    15   0.00000   486.166    ******   0.61755  ******  293.00
******  ******
    16   0.00000   486.166   0.32630   0.61755  244.07  293.00
313.3  3.2875
    17   0.00000    11.888    ******  17.20166  ******  836.46
******  ******
    18   0.00000    11.888    ******  17.02964  ******  836.46
******  ******

  Gross Thrust = 200447.31
 Momentum Drag = 130768.23
    Net Thrust =  69679.08
     Fuel Flow =    1.1371
        s.f.c. =  16.31932
    Sp. Thrust =   127.711
 ***********************************************
 1 1000           !approach
 3 0.4
 -1
 8 6 1400
 -1
      ***** OFF DESIGN ENGINE CALCULATIONS. Converged after 9 Loops
 ***** AMBIENT AND INLET PARAMETERS *****
 Alt. =   1000.0      I.S.A. Dev. =    0.000       Mach No. =  0.40
 Etar = 0.9900        Momentum Drag = 119288.57
 ***** COMPRESSOR  1 PARAMETERS *****
 PRSF =  0.13725E+01     ETASF =  0.10038E+01   WASF =  0.20785E+01
 Z = 0.58720             PR =   1.231             ETA = 0.86067
 PCN =   0.7338          CN = 0.73056   COMWK =  0.18418E+08
 ***** CONVERGENT NOZZLE  1 PARAMETERS *****
 NCOSF =  0.10000E+01  Area =  3.2875 Exit Velocity =  225.81
Gross Thrust = 179237.92  Nozzle Coeff. =  0.97629E+00
 ***** COMPRESSOR  2 PARAMETERS *****
 PRSF =  0.41059E+01   ETASF =  0.10193E+01  WASF =  0.53198E+00
 Z = 0.90600             PR =   3.734             ETA = 0.85981
 PCN =   0.7171          CN = 0.74133       COMWK =  0.12158E+08
 ***** COMPRESSOR  3 PARAMETERS *****
```

```
 PRSF =  0.63781E+00     ETASF =  0.10631E+01   WASF =  0.46443E+00

 Z = 0.81345 PR =   4.434   ETA = 0.86115 PCN =   0.8457
CN = 0.92176             COMWK =  0.21357E+08

 ***** COMBUSTION CHAMBER PARAMETERS *****

 ETASF =  0.99800E+0 ETA = 0.99800 DLP = 1.2146  WFB =   1.1045

 ***** TURBINE  1 PARAMETERS *****

 CNSF =  0.89138E+02     ETASF =  0.10550E+01   TFSF =  0.15229E+01

 DHSF =  0.41330E+05 TF =  215.564  ETA = 0.87418  CN =  2.107

 AUXWK =  0.00000E+00

***** TURBINE  2 PARAMETERS *****

 CNSF =  0.80382E+02     ETASF =  0.10836E+01  TFSF =  0.59683E+00

 DHSF =  0.30506E+05  TF =  208.478  ETA = 0.89361  CN =  1.787

 AUXWK =  0.00000E+00

 ***** TURBINE  3 PARAMETERS *****

 CNSF =  0.74471E+02     ETASF =  0.10907E+01  TFSF =  0.31253E+00

 DHSF =  0.60595E+05 TF =  197.398 ETA = 0.88222  CN =  1.822

 AUXWK =  0.00000E+00

 ***** CONVERGENT NOZZLE  2 PARAMETERS *****

 NCOSF =  0.10000E+01 Area =  0.7766 Exit Velocity =  201.51

 Gross Thrust =  14561.7   Nozzle Coeff. =  0.97290E+00

 Scale Factor on above Mass Flows, Areas, Thrusts & Powers=1.0

 Station  F.A.R. Mass Flow   Pstatic    Ptotal Tstatic  Ttotal
Vel    Area

     1   0.00000   886.223   0.88697   0.99041  281.65  290.68
134.6  ******

     2   0.00000   886.223    ******   0.98051  ******  290.68
******  ******

     3   0.00000   886.223    ******   1.20731  ******  311.38
******  ******

     4   0.00000    73.173    ******   1.20731  ******  311.38
******  ******

     5   0.00000    73.173    ******   4.50805  ******  475.40
******  ******

     6   0.00000    73.173    ******  19.98979  ******  752.19
******  ******

     7   0.00000    58.538    ******  19.98979  ******  752.19
******  ******

     8   0.01887    59.643    ******  18.77515  ****** 1400.00
******  ******

     9   0.01509    74.277    ******  18.77515  ****** 1280.19
******  ******
```

```
    10   0.01509    74.277    ******   6.85859  ****** 1040.33
******  ******

    11   0.01509    74.277    ******   3.52717  ******  899.60
******  ******

    12   0.01509    74.277    ******   0.98549  ******  678.32
******  ******

    13   0.01509    74.277   0.88697   0.98549  659.74  678.32
201.5  0.7766

    14   0.00000   813.050    ******   1.20731  ******  311.38
******  ******

    15   0.00000   813.050    ******   1.19524  ******  311.38
******  ******

    16   0.00000   813.050   0.88697   1.19524  285.91  311.38
225.8  3.2875

    17   0.00000    14.635    ******  19.98979  ******  752.19
******  ******

    18   0.00000    14.635    ******  19.78990  ******  752.19
******  ******

  Gross Thrust = 193799.66

 Momentum Drag = 119288.57

    Net Thrust =  74511.09

     Fuel Flow =    1.1045

        s.f.c. =  14.82304

    Sp. Thrust =    84.077

 ***********************************************

 1 0.0            !taxi

 3 0.1

 -1

 8 6 1300

  -1

 ***** OFF DESIGN ENGINE CALCULATIONS. Converged after   5 Loops

 ***** AMBIENT AND INLET PARAMETERS *****

 Alt. =      0.0      I.S.A. Dev. =    0.000       Mach No. =  0.10

 Etar = 0.9900        Momentum Drag =  22523.12

 ***** COMPRESSOR  1 PARAMETERS *****

 PRSF =  0.13725E+01     ETASF =  0.10038E+01     WASF =
0.20785E+01

 Z = 0.64319             PR =   1.162             ETA = 0.85212

 PCN =   0.5750          CN = 0.57438         COMWK =  0.98527E+07

***** CONVERGENT NOZZLE  1 PARAMETERS *****

 NCOSF =  0.10000E+01
```

```
 Area =  3.2875   Exit Velocity =  153.17  Gross Thrust =  90810.41
 Nozzle Coeff. =  0.97347E+00
 ***** COMPRESSOR  2 PARAMETERS *****
 PRSF =  0.41059E+01     ETASF =  0.10193E+01   WASF =  0.53198E+00
 Z = 0.94392             PR =   2.976             ETA = 0.82652
 PCN =   0.5847          CN = 0.61219         COMWK =  0.70968E+07
 ***** COMPRESSOR  3 PARAMETERS *****
 PRSF =  0.63781E+00     ETASF =  0.10631E+01   WASF =  0.46443E+00
 Z = 0.82391             PR =   4.095             ETA = 0.85833
 PCN =   0.7662          CN = 0.87094        COMWK =  0.13290E+08
 ***** COMBUSTION CHAMBER PARAMETERS *****
 ETASF =  0.99800E+00 ETA = 0.99800  DLP = 0.8044  WFB =0.7449
 ***** TURBINE  1 PARAMETERS *****
 CNSF =  0.89138E+02   ETASF =  0.10550E+01  TFSF =  0.15229E+01
 DHSF =  0.41330E+05   TF =  210.205   ETA = 0.86016 CN =  1.984
 AUXWK =  0.00000E+00
 ***** TURBINE  2 PARAMETERS *****
 CNSF =  0.80382E+02     ETASF =  0.10836E+01   TFSF =  0.59683E+00
 DHSF =  0.30506E+05  TF =  193.719 ETA = 0.85660 CN =  1.505
 AUXWK =  0.00000E+00
 ***** TURBINE  3 PARAMETERS *****
 CNSF =  0.74471E+02     ETASF =  0.10907E+01  TFSF =  0.31253E+00
 DHSF =  0.60595E+05 TF =  172.957  ETA = 0.85235 CN =  1.461
 AUXWK =  0.00000E+00
 ***** CONVERGENT NOZZLE  2 PARAMETERS *****
 NCOSF =  0.10000E+01 Area =  0.7766 Exit Velocity =  133.52
 Gross Thrust =   6929.06 Nozzle Coeff. =  0.97181E+00
 Scale Factor on above Mass Flows, Areas, Thrusts & Powers=1.0
 Station  F.A.R. Mass Flow   Pstatic    Ptotal Tstatic  Ttotal
Vel    Area
     1   0.00000   661.764   1.00000   1.00702  288.15  288.73
34.0  ******
     2   0.00000   661.764    ******   0.99695  ******  288.73
******  ******
     3   0.00000   661.764    ******   1.15811  ******  303.56
******  ******
     4   0.00000    52.626    ******   1.15811  ******  303.56
******  ******
```

```
     5   0.00000    52.657    ******   3.44691  ******  437.07
******  ******

     6   0.00000    52.657    ******  14.11675  ******  679.29
******  ******

     7   0.00000    42.125    ******  14.11675  ******  679.29
******  ******

     8   0.01768    42.870    ******  13.31238  ****** 1300.00
******  ******

     9   0.01415    53.402    ******  13.31238  ****** 1185.15
******  ******

    10   0.01415    53.402    ******   5.13659  ******  974.74
******  ******

    11   0.01415    53.402    ******   2.82801  ******  859.17
******  ******

    12   0.01415    53.402    ******   1.04605  ******  693.85
******  ******

    13   0.01415    53.402   1.00000   1.04605  685.51  693.85
133.5  0.7766

    14   0.00000   609.020    ******   1.15811  ******  303.56
******  ******

    15   0.00000   609.020    ******   1.14652  ******  303.56
******  ******

    16   0.00000   609.020   1.00000   1.14652  291.91  303.56
153.2  3.2875

    17   0.00000    10.531    ******  14.11675  ******  679.29
******  ******

    18   0.00000    10.531    ******  13.97558  ******  679.29
******  ******

  Gross Thrust =  97739.48
 Momentum Drag =  22523.12
    Net Thrust =  75216.35
     Fuel Flow =    0.7449
        s.f.c. =   9.90296
    Sp. Thrust =   113.660
```

A.2 THE CONTRAIL- FREE AERO ENGINE WITH TURBOFAN TRENT 900 BASELINE SPECIFICATION

DESIGN POINT RUN AT CRUISE CONDITION

\\ Created by Sarah Qureshi ; Adapted from RR_Trent900.dat

```
  OD SI KE CT FP
  -1
  -1
```

```
INTAKE  S1-2         D1-4            R100
COMPRE  S2-3         D5-10           R101   V5    V6
PREMAS  S3,4,18      D11-14                 V11
DUCTER  S18-19       D15-18          R102
NOZCON  S19-20,1     D19             R103
COMPRE  S4-5         D20-25          R104   V20   V21
COMPRE  S5-6         D26-31          R105   V26   V27
PREMAS  S6,7,17      D32-35
DUCTER  S17-18       D36-39          R106
BURNER  S7-8         D40-42          R107
MIXEES  S8,18,9
TURBIN  S9-10        D43-50,105,51          V44
TURBIN  S10-11       D52-59,104,60          V53
TURBIN  S11-12       D61-68,101,69          V62
DUCTER  S12-13       D75-78          R109
PREMAS  S13,14,0     D79-82
NOZCON  S14-15,1     D70             R108
PERFOR  S1,0,0       D71-74,103,100,102,108,0,107,0,0,0
CODEND

 ! INTAKE - Aeroplane inlet
 1   10670          ! ALTITUDE
 2   0.0          ! ISA DEVIATION
 3   0.82          ! MACH NO.
 4   0.99         ! PRESSURE RECOVERY
 ! COMPRE - Fan uses Trent 800
 5   -1.0         ! SURGE MARGINE
 6    1.0         ! ROTATIONAL SPEED,N1
 7   1.56         ! FAN PRESSURE RATIO
 8   0.874        ! EFFICIENCY
 9   0.0          ! ERROR SELECTOR
 10  1.0          ! MAP NUMBER
 ! PREMAS -  Bypass - Main
 11  0.111111     ! LAMDA (BYPASS RATIO 8.5)
 12  0.0          ! MASS FLOW LOSS
 13  1.0          ! PRESSURE FACTOR
 14  0.0          ! PRESSURE LOSS
```

```
! Bypass duct
15  0.0         ! REHEAT SELECTOR
16  0.01        ! PRESSURE LOSS 1%
17  0.0         ! REHEAT COMB.EFFICIENCY
18  0.0         ! MAX REHEAT FUEL FLOW
!Bypass Convergent Zozzle
19  -1.0        ! Fan Exhaust Nozzle: fixed Area
!  IP COMPRESSOR
20  0.85        ! SURGE MARGIN
21  1.0         ! ROTATIONAL SPEED
22  5.188       ! PRESSURE RATIO
23  0.846       ! EFFICIENCY
24  1.0         ! ERROR SELECTOR
25  4.0         ! MAP NUMBER
!  HP COMPRESSOR
26  0.85        ! SURGE MARGIN
27  1.0         ! ROTATIONAL SPEED
28  5.188       ! PRESSURE RATIO
29  0.851       ! EFFICIENCY
30  1.0         ! ERROR SELECTOR
31  5.0         ! MAP NUMBER
!  HPT Turbine COOLING BYPASS
32  0.80        ! BYPASS RATIO
33  0.0         ! MASS FLOW LOSS
34  1.0         ! PRESSURE FACTOR
35  0.0         ! PRESSURE LOSS
!  Ducter Cooling
36  0.0         ! REHEAT SELECTOR
37  0.01        ! PRESSURE LOSS 1%
38  0.0         ! REHEAT COMB.EFFICIENCY
39  0.0         ! MAX REHEAT FUEL FLOW
!  BURNER
40  0.06        ! PRESSURE LOSS
41  0.998       ! COMBUSTION EFFICIENCY
42  -1.0        ! FUEL FLOW
!  TURBINE-HP
43  0.0         ! AUX.WORK
```

```
44  0.8          ! REL NON-D MASS FLOW
45  0.6          ! REL NON-D SPEED
46  0.885        ! EFFICIENCY
47 -1.0          ! REL ROT.SPEED(COMP TURB=-1)
48  3.0          ! COMP NO. FROM LOW END
49  1.0          ! TURBINE MAP
50 -1.0          ! POWER LAW
51  0.0          ! NGV
!  TURBINE-IP
52  0.0          ! AUX.WORK
53  0.8          ! REL NON-D MASS FLOW
54  0.6          ! REL NON-D SPEED
55  0.909        ! EFFICIENCY
56 -1.0          ! REL ROT.SPEED
57  2.0          ! COMP NO. FROM LOW END
58  1.0          ! TURBINE MAP
59 -1.0          ! POWER LAW
60  0.0          ! NGV
!  TURBINE-LP
61  3500000         ! AUX.WORK
62  0.8          ! REL NON-D MASS FLOW
63  0.6          ! REL NON-D SPEED
64  0.915        ! EFFICIENCY
65 -1.0          ! REL ROT.SPEED
66  1.0          ! COMP NO. FROM LOW END
67  1.0          ! TURBINE MAP
68 -1.0          ! POWER LAW
69  0.0          ! NGV
!  DUCTER CONTRAILS
75  0.0          ! REHEAT SELECTOR
76  -60          ! PRESSURE GAIN
77  0.0          ! REHEAT COMB.EFFICIENCY
78  0.0          ! MAX REHEAT FUEL FLOW
! PREMAS -  CONTRAILS
 79  0.9765       ! LAMDA (WATER LOSS FROM MASS FLOW 0.0235)
 80  0.0          ! MASS FLOW LOSS
 81  0.9765       ! PRESSURE FACTOR LOSS DUE TO LOSS OF WATER
```

```
  82  0.0          ! PRESSURE LOSS
 !  Core CONVERGENT NOZZLE
 70 -1.0          ! SWITHCH, AREA FIXED
 !  PERFORMANCE
 71 -1.0          ! POWER (-1=TURBOJET/FAN)
 72 -1.0          ! PROPELLER EFFICIENCY(")
 73  0.0          ! SCALING INDEX
 74  0.0          ! REQ'D D.P. THRUST
 -1
 1 2  525.0       ! INLET MASS FLOW(Kg/s)
 8 6  1500.0      ! TET(K)
 -1
*********************************************
```

The Units for this Run are as follows:-

Temperature = K Pressure = Atmospheres Length = metres

Area = sq metres Mass Flow = kg/sec Velocity = metres/sec

Force = Newtons s.f.c.(Thrust) = mg/N sec s.f.c.(Power) = mug/J

Sp. Thrust = N/kg/sec Power = Watts 1

```
      ***** DESIGN POINT ENGINE CALCULATIONS *****
 ***** AMBIENT AND INLET PARAMETERS *****
 Alt. =  10670.0      I.S.A. Dev. =    0.000       Mach No. =  0.82
 Etar = 0.9900        Momentum Drag = 127711.08
 ***** COMPRESSOR  1 PARAMETERS *****
 PRSF =  0.13725E+01     ETASF =  0.10038E+01     WASF =
0.22602E+01
 Z = 0.85000             PR =   1.560             ETA = 0.87400
 PCN =   1.0000          CN = 1.00000       COMWK =  0.20303E+08
 ***** CONVERGENT NOZZLE  1 PARAMETERS *****
 NCOSF =  0.10000E+01
 Area =  3.4469          Exit Velocity =  310.05
Gross Thrust = 162791.59 Nozzle Coeff. =  0.97925E+00
 ***** COMPRESSOR  2 PARAMETERS *****
 PRSF =  0.41059E+01     ETASF =  0.10193E+01  WASF =  0.57858E+00
 Z = 0.85000             PR =   5.188             ETA = 0.84600
```

```
 PCN =   1.0000          CN = 1.00000        COMWK =  0.11928E+08
 ***** COMPRESSOR  3 PARAMETERS *****
 PRSF =  0.63781E+00     ETASF =  0.10631E+01  WASF =  0.50616E+00
 Z = 0.85000             PR =   5.188            ETA = 0.85100
 PCN =   1.0000          CN = 1.00000        COMWK =  0.20017E+08
 ***** COMBUSTION CHAMBER PARAMETERS *****
 ETASF =  0.99800E+00  ETA = 0.99800 DLP = 0.9125 WFB =   0.9546
 ***** TURBINE  1 PARAMETERS *****
 CNSF =  0.10375E+03   ETASF =  0.10307E+01     TFSF =  0.26137E+01
 DHSF =  0.69293E+04  TF =  401.640 ETA = 0.88500 CN =  2.800
 AUXWK =  0.00000E+00
 ***** TURBINE  2 PARAMETERS *****
 CNSF =  0.92640E+02     ETASF =  0.10587E+01  TFSF =  0.97541E+00
 DHSF =  0.51787E+04 TF =  401.640 ETA = 0.90900   CN =  2.800
 AUXWK =  0.00000E+00
 ***** TURBINE  3 PARAMETERS *****
 CNSF =  0.85076E+02     ETASF =  0.10656E+01 TFSF =  0.49037E+00
 DHSF =  0.14313E+05 TF =  401.640 ETA = 0.91500 CN =  2.800
 AUXWK =  0.75000E+07
 ***** CONVERGENT NOZZLE  2 PARAMETERS *****
 NCOSF =  0.10000E+01 Area =  0.0351 Exit Velocity =  407.53
Gross Thrust =  31174.42  Nozzle Coeff. =  0.80269E+00
Scale Factor on above Mass Flows, Areas, Thrusts & Powers=1.0000
 Station  F.A.R. Mass Flow   Pstatic    Ptotal Tstatic  Ttotal
Vel    Area
     1   0.00000   525.000   0.23517   0.36587  218.79  248.33
243.3  ******
     2   0.00000   525.000    ******   0.36221  ******  248.33
******  ******
     3   0.00000   525.000    ******   0.56504  ******  286.91
******  ******
     4   0.00000    58.333    ******   0.56504  ******  286.91
******  ******
     5   0.00000    58.333    ******   2.93145  ******  488.81
******  ******
     6   0.00000    58.333    ******  15.20836  ******  811.62
******  ******
     7   0.00000    46.667    ******  15.20836  ******  811.62
******  ******
```

```
     8   0.02045    47.621    ******  14.29586  ****** 1500.00
******  ******

     9   0.01636    59.288    ******  14.29586  ****** 1372.99
******  ******

    10   0.01636    59.288    ******   4.76384  ****** 1094.67
******  ******

    11   0.01636    59.288    ******   2.19938  ******  923.21
******  ******

    12   0.01636    59.288    ******   0.15098  ******  497.81
******  ******

    13   0.01636    59.288    ******   9.20987  ******  497.81
******  ******

    14   0.01636    51.497    ******   7.99969  ******  497.81
******  ******

    15   0.01636    51.497   4.26617   7.99969  418.14  497.81
407.5  0.0351

    16   0.00000     0.000    ******   0.00000  ******    0.00
******  ******

    17   0.00000    11.667    ******  15.20836  ******  811.62
******  ******

    18   0.00000    11.667    ******  15.05628  ******  811.62
******  ******

    19   0.00000   466.667    ******   0.55939  ******  286.91
******  ******

    20   0.00000   466.667   0.29560   0.55939  238.99  286.91
310.0  3.4469


  Gross Thrust = 193966.02
 Momentum Drag = 127711.08
    Net Thrust =  66254.94
     Fuel Flow =    0.9546
        s.f.c. =  14.40726
    Sp. Thrust =   126.200
```

A.3 PERFORMANCE CODE FOR THE 3 SPOOL INTER-COOLED RECUPERATED TURBOFAN ENGINE TRENT 900 BASELINE SPECIFICATION

A.3.1 INPUT FILE AT TAKE-OFF DESIGN AND OFF-DESIGN POINT

```
//Created by: Sarah Qureshi and Fernando Lartategui Atela
// Adapted from: RR_Trent900.dat
  OD SI KE CT FP
```

```
 -1
 -1
INTAKE  S1-2         D1-4            R100
COMPRE  S2-3         D5-10           R101   V5    V6
PREMAS  S3,4,19      D11-14                 V11
DUCTER  S19-20       D15-18          R102
NOZCON  S20-21,1     D19             R103
COMPRE  S4-5         D20-25          R104   V20   V21
DUCTER  S5-6         D75-78          R209
COMPRE  S6-7         D26-31          R105   V26   V27
PREMAS  S7,8,17      D32-35
DUCTER  S17-18       D36-39          R106
HETCOL  S8,9         D79-82
BURNER  S9-10        D40-42          R107
MIXEES  S10,18,11
TURBIN  S11-12       D43-50,105,51          V44
TURBIN  S12-13       D52-59,104,60          V53
TURBIN  S13-14       D61-68,101,69          V62
HETHOT S8,14,15      D83-86
NOZCON  S15,16,1     D70                    R108
PERFOR  S1,0,0       D71-74,103,100,102,108,0,107,0,0,0
CODEND

 ! INTAKE - Aeroplane inlet
 1   0.0         ! ALTITUDE
 2   0.0         ! ISA DEVIATION
 3   0.0         ! MACH NO.
 4   0.99        ! PRESSURE RECOVERY
 ! COMPRE - Fan uses Trent 800
 5   -1.0        ! SURGE MARGINE
 6    1.0        ! ROTATIONAL SPEED,N1
 7   1.5        ! FAN PRESSURE RATIO
 8   0.875       ! EFFICIENCY
 9   0.0         ! ERROR SELECTOR
 10  1.0         ! MAP NUMBER
 ! PREMAS -  Bypass - Main
 11  0.111111    ! LAMDA (BYPASS RATIO 8.5)
```

```
12  0.0         ! MASS FLOW LOSS
13  1.0         ! PRESSURE FACTOR
14  0.0         ! PRESSURE LOSS
! Bypass duct
15  0.0         ! REHEAT SELECTOR
16  0.01        ! PRESSURE LOSS 1%
17  0.0         ! REHEAT COMB.EFFICIENCY
18  0.0         ! MAX REHEAT FUEL FLOW
!Bypass Convergent Zozzle
19  -1.0        ! Fan Exhaust Nozzle: fixed Area
!  IP COMPRESSOR
20  0.85        ! SURGE MARGIN
21  1.0         ! ROTATIONAL SPEED
22  5.0         ! PRESSURE RATIO
23  0.845       ! EFFICIENCY
24  1.0         ! ERROR SELECTOR
25  4.0         ! MAP NUMBER
!  HP COMPRESSOR
26  0.85        ! SURGE MARGIN
27  1.0         ! ROTATIONAL SPEED
28  5.0         ! PRESSURE RATIO
29  0.85        ! EFFICIENCY
30  1.0         ! ERROR SELECTOR
31  5.0         ! MAP NUMBER
!  HPT Turbine COOLING BYPASS
32  0.80        ! BYPASS RATIO
33  0.0         ! MASS FLOW LOSS
34  1.0         ! PRESSURE FACTOR
35  0.0         ! PRESSURE LOSS
!  Ducter Cooling
36  0.0         ! REHEAT SELECTOR
37  0.01        ! PRESSURE LOSS 1%
38  0.0         ! REHEAT COMB.EFFICIENCY
39  0.0         ! MAX REHEAT FUEL FLOW
!  BURNER
40  0.06        ! PRESSURE LOSS
41  0.998       ! COMBUSTION EFFICIENCY
```

```
42  -1.0        ! FUEL FLOW
!  TURBINE-HP
43  0           ! AUX.WORK
44  0.8         ! REL NON-D MASS FLOW
45  0.6         ! REL NON-D SPEED
46  0.885       ! EFFICIENCY
47 -1.0         ! REL ROT.SPEED(COMP TURB=-1)
48  3.0         ! COMP NO. FROM LOW END
49  5.0         ! TURBINE MAP
50 -1.0         ! POWER LAW
51  0.0         ! NGV
!  TURBINE-IP
52  0           ! AUX.WORK
53  0.8         ! REL NON-D MASS FLOW
54  0.6         ! REL NON-D SPEED
55  0.909       ! EFFICIENCY
56 -1.0         ! REL ROT.SPEED
57  2.0         ! COMP NO. FROM LOW END
58  5.0         ! TURBINE MAP
59 -1.0         ! POWER LAW
60  0.0         ! NGV
!  TURBINE-LP
61  0           ! AUX.WORK
62  0.8         ! REL NON-D MASS FLOW
63  0.6         ! REL NON-D SPEED
64  0.915       ! EFFICIENCY
65 -1.0         ! REL ROT.SPEED
66  1.0         ! COMP NO. FROM LOW END
67  5.0         ! TURBINE MAP
68 -1.0         ! POWER LAW
69  0.0         ! NGV
!  Core CONVERGENT NOZZLE
70 -1.0         ! SWITHCH, AREA FIXED
!  PERFORMANCE
71 -1.0         ! POWER (-1=TURBOJET/FAN)
72 -1.0         ! PROPELLER EFFICIENCY(")
73  0.0         ! SCALING INDEX
```

```
 74  0.0          ! REQ'D D.P. THRUST
! INTERCOOLER
 75 2.0           ! INTERCOOLER SELECTOR
 76 0.0           ! PRESSURE LOSS
 77 1.0           ! INTERCOOLER EFFICIENCY
 78 -1.0          ! MAX. REHEAT FUEL FLOW
 ! HETCOL
79 0.01           ! COLD SIDE PRESSURE LOSS INLET TO XCHANGER
80 0.82           ! EFFECTIVENESS
81 1.0            ! TYPE 1, RECUPERATOR 3, REGENERATOR
82 0.0            ! MASS FLOW LEAKAGE
!HETHOT
83 0.01           ! HOT SIDE PRESSURE LOSS, INLET TO RECUPERATOR
84 0.82           ! HEAT EXCHANGER EFFECTIVENESS
85 1.0            ! TYPE 1(RECUPERATOR)
86 0.0            ! MASS FLOW LEAKAGE
 -1
 1  2  1225.0     ! INLET MASS FLOW(Kg/s)
 10 6  1700.0     ! TET(K)
 6 6 200.0
 -1
************************************************
```

A.3.2 OUT FOR DESIGN POINT AT TAKE-OFF

```
      ***** DESIGN POINT ENGINE CALCULATIONS *****
***** AMBIENT AND INLET PARAMETERS *****
Alt. =      0.0      I.S.A. Dev. =    0.000       Mach No. =  0.00
Etar = 0.9900        Momentum Drag =      0.00
***** COMPRESSOR  1 PARAMETERS *****
PRSF =  0.12255E+01     ETASF =  0.10050E+01     WASF =
0.20785E+01
Z = 0.85000             PR =   1.500             ETA = 0.87500
PCN =   1.0000          CN = 1.00000        COMWK =  0.49775E+08
***** CONVERGENT NOZZLE  1 PARAMETERS *****
NCOSF =  0.10000E+01  Area =  3.4583  Exit Velocity =  262.48
Gross Thrust = 279438.59  Nozzle Coeff. =  0.97769E+00


***** COMPRESSOR  2 PARAMETERS *****
```

```
PRSF =  0.39216E+01     ETASF =  0.10181E+01  WASF =  0.54975E+00
Z = 0.85000             PR =   5.000             ETA = 0.84500
PCN =   1.0000          CN = 1.00000     COMWK =  0.30985E+08
***** DUCT/AFTER BURNING 1 PARAMETERS *****
ETA =  1.0000           DLP = 0.0000             WFB =   0.0000
DUCTER IS USED AS AN INTERCOOLER!
****INTERCOOLER****HEAT REMOVED:48797.75      KWATTS
  ***** COMPRESSOR  3 PARAMETERS *****
PRSF =  0.60918E+00     ETASF =  0.10619E+01  WASF =  0.29826E+00
Z = 0.85000             PR =   5.000             ETA = 0.85000
PCN =   1.0000          CN = 1.00000    COMWK =  0.18794E+08
HETYP =  1.0 HEUA =      160.893
HETYP =  1.0 HEUA =      178.606
HETYP =  1.0 HEUA =      177.617
HETYP =  1.0 HEUA =      177.659
***** HEAT EXCHANGER COLD SIDE PARAMETERS *****
ETAD =  0.82000E+00    ETA = 0.82000           DLP = 0.3713
***** COMBUSTION CHAMBER PARAMETERS *****
ETASF =  0.99800E+00   ETA = 0.99800 DLP = 2.2052  WFB =   3.0696
***** TURBINE  1 PARAMETERS *****
CNSF =  0.84143E+02     ETASF =  0.10550E+01  TFSF =  0.14112E+01
DHSF =  0.16026E+05  TF =  219.627 ETA = 0.88500CN =  2.200
AUXWK =  0.00000E+00
***** TURBINE  2 PARAMETERS *****
CNSF =  0.80981E+02     ETASF =  0.10836E+01 TFSF =  0.10071E+01
DHSF =  0.28466E+05  TF =  219.627 ETA = 0.90900  CN =  2.200
AUXWK =  0.00000E+00
***** TURBINE  3 PARAMETERS *****
CNSF =  0.75383E+02     ETASF =  0.10907E+01 TFSF =  0.55245E+00
DHSF =  0.52539E+05  TF =  219.627 ETA = 0.91500 CN =  2.200
AUXWK =  0.00000E+00
HETYP =  1.0 HEUA =      177.659
***** HEAT EXCHANGER HOT SIDE PARAMETERS *****
ETAD =  0.82000E+00 HEUA =      177.659 ETASF =  0.00000E+00
ETA =  0.8200           DLP = 0.0307     TOTHOT =   550.5212

***** CONVERGENT NOZZLE  2 PARAMETERS *****
```

NCOSF = 0.10000E+01 Area = 0.2626 Exit Velocity = 428.11

Gross Thrust = 74720.74 Nozzle Coeff. = 0.97379E+00

Scale Factor on above Mass Flows, Areas, Thrusts & Powers=1.0

Station	F.A.R.	Mass Flow	Pstatic	Ptotal	Tstatic	Ttotal	Vel	Area
1	0.00000	1225.000	1.00000	1.00000	288.15	288.15	0.0	******
2	0.00000	1225.000	******	0.99000	******	288.15	******	******
3	0.00000	1225.000	******	1.48500	******	328.61	******	******
4	0.00000	136.111	******	1.48500	******	328.61	******	******
5	0.00000	136.111	******	7.42500	******	551.78	******	******
6	0.00000	136.111	******	7.42500	******	200.00	******	******
7	0.00000	136.111	******	37.12502	******	337.65	******	******
8	0.00000	108.889	******	37.12502	******	337.65	******	******
9	0.00000	108.889	******	36.75377	******	776.53	******	******
10	0.02819	111.958	******	34.54854	******	1700.00	******	******
11	0.02255	139.181	******	34.54854	******	1462.82	******	******
12	0.02255	139.181	******	23.63845	******	1354.94	******	******
13	0.02255	139.181	******	11.96398	******	1174.09	******	******
14	0.02255	139.181	******	3.07159	******	872.83	******	******
15	0.02255	139.181	******	3.04088	******	550.52	******	******
16	0.02255	139.181	1.62767	3.04088	464.08	550.52	428.1	0.2626
17	0.00000	27.222	******	37.12502	******	337.65	******	******
18	0.00000	27.222	******	36.75377	******	337.65	******	******
19	0.00000	1088.889	******	1.48500	******	328.61	******	******

```
    20   0.00000  1088.889    ******   1.47015  ******  328.61
******  ******
    21   0.00000  1088.889   1.00000   1.47015  294.31  328.61
262.5  3.4583


  Gross Thrust = 354159.34
 Momentum Drag =      0.00
    Net Thrust = 354159.34
     Fuel Flow =    3.0696
        s.f.c. =   8.66738
    Sp. Thrust =   289.110
```

A.3.3 OUTPUT FOR OFF-DESIGN RUNS

```
  1 2000
  3 0.65           !Climb
  -1
  10 6 1700
  -1
***** OFF DESIGN ENGINE CALCULATIONS. Converged after   5 Loops
 ***** AMBIENT AND INLET PARAMETERS *****
 Alt. =   2000.0      I.S.A. Dev. =    0.000       Mach No. =  0.65
 Etar = 0.9900        Momentum Drag = 274433.62
 ***** COMPRESSOR  1 PARAMETERS *****
 PRSF =  0.12255E+01     ETASF =  0.10050E+01 WASF =  0.20785E+01
 Z = 0.75947             PR =   1.440             ETA = 0.86873
 PCN =   1.0085          CN = 0.99092        COMWK =  0.48099E+08
 ***** CONVERGENT NOZZLE  1 PARAMETERS *****
 NCOSF =  0.10000E+01  Area =  3.4583   Exit Velocity =  333.71
Gross Thrust = 372506.47  Nozzle Coeff. =  0.98063E+00
 ***** COMPRESSOR  2 PARAMETERS *****
 PRSF =  0.39216E+01     ETASF =  0.10181E+01  WASF =  0.54975E+00
 Z = 0.84501             PR =   4.825             ETA = 0.84966
 PCN =   0.9883          CN = 0.97712        COMWK =  0.29508E+08
 ***** DUCT/AFTER BURNING 1 PARAMETERS *****
 ETA =  1.0000           DLP = 0.0000             WFB =   0.0000
 DUCTER IS USED AS AN INTERCOOLER!
 ****INTERCOOLER****HEAT REMOVED:47653.79      KWATTS
  ***** COMPRESSOR  3 PARAMETERS *****
 PRSF =  0.60918E+00     ETASF =  0.10619E+01   WASF =  0.29826E+00
```

```
 Z = 0.84157             PR =   4.945             ETA = 0.85338
 PCN =   0.9974          CN = 0.99743          COMWK =  0.17866E+08
 ***** HEAT EXCHANGER COLD SIDE PARAMETERS *****
 ETA = 0.82805           DLP = 0.3585
 ***** COMBUSTION CHAMBER PARAMETERS *****
 ETASF =  0.99800E+00 ETA = 0.99800  DLP = 2.1558 WFB =   2.9385
 ***** TURBINE  1 PARAMETERS *****
 CNSF =  0.84143E+02     ETASF =  0.10550E+01  TFSF =  0.14112E+01
 DHSF =  0.16026E+05  TF =  219.523 ETA = 0.88489  CN =  2.195
 AUXWK =  0.00000E+00
 ***** TURBINE  2 PARAMETERS *****
 CNSF =  0.80981E+02     ETASF =  0.10836E+01   TFSF =  0.10071E+01
 DHSF =  0.28466E+05 TF =  219.424  ETA = 0.90938  CN =  2.173
 AUXWK =  0.00000E+00
 ***** TURBINE  3 PARAMETERS *****
 CNSF =  0.75383E+02     ETASF =  0.10907E+01 TFSF =  0.55245E+00
 DHSF =  0.52539E+05  TF =  219.657 ETA = 0.91393 CN =  2.216
 AUXWK =  0.00000E+00
 ***** HEAT EXCHANGER HOT SIDE PARAMETERS *****
 ETA =  0.8281           DLP = 0.0296     TOTHOT =   550.1146
 ***** CONVERGENT NOZZLE  2 PARAMETERS *****
 NCOSF =  0.10000E+01  Area =  0.2626 Exit Velocity =  427.96
Gross Thrust =  76178.91  Nozzle Coeff. =  0.96606E+00
 Scale Factor on above Mass Flows, Areas, Thrusts & Powers =
1.0000
 Station  F.A.R. Mass Flow   Pstatic    Ptotal Tstatic  Ttotal
Vel    Area
     1   0.00000  1269.336   0.78452   1.04228  275.15  298.45
216.2  ******
     2   0.00000  1269.336    ******   1.03185  ******  298.45
******  ******
     3   0.00000  1269.336    ******   1.48585  ******  336.15
******  ******
     4   0.00000   131.032    ******   1.48585  ******  336.15
******  ******
     5   0.00000   131.032    ******   7.16901  ******  556.72
******  ******
     6   0.00000   131.032    ******   7.16901  ******  200.00
******  ******
     7   0.00000   131.032    ******  35.44961  ******  335.94
******  ******
```

```
     8   0.00000   104.825    ******  35.44961  ******  335.94
******  ******

     9   0.00000   104.825    ******  35.09112  ******  782.08
******  ******

    10   0.02803   107.764    ******  32.93528  ****** 1700.00
******  ******

    11   0.02243   133.970    ******  32.93528  ****** 1462.47
******  ******

    12   0.02243   133.970    ******  22.64232  ****** 1355.90
******  ******

    13   0.02243   133.970    ******  11.55962  ****** 1176.98
******  ******

    14   0.02243   133.970    ******   2.95555  ******  874.62
******  ******

    15   0.02243   133.970    ******   2.92591  ******  550.11
******  ******

    16   0.02243   133.970   1.56605   2.92591  463.72  550.11
428.0  0.2626

    17   0.00000    26.206    ******  35.44961  ******  335.94
******  ******

    18   0.00000    26.206    ******  35.09511  ******  335.94
******  ******

    19   0.00000  1138.305    ******   1.48585  ******  336.15
******  ******

    20   0.00000  1138.305    ******   1.47099  ******  336.15
******  ******

    21   0.00000  1138.305   0.78452   1.47099  280.81  336.15
333.7  3.4583

  Gross Thrust = 448685.38

 Momentum Drag = 274433.62

    Net Thrust = 174251.73

     Fuel Flow =    2.9385

        s.f.c. =  16.86366

    Sp. Thrust =   137.278

***********************************************

  1 5000           !Climb2

  -1

  -1

***** OFF DESIGN ENGINE CALCULATIONS. Converged after   1 Loops

 ***** AMBIENT AND INLET PARAMETERS *****

 Alt. =   5000.0      I.S.A. Dev. =    0.000       Mach No. =  0.65

 Etar = 0.9900        Momentum Drag = 192585.14
```

```
 ***** COMPRESSOR  1 PARAMETERS *****
 PRSF =  0.12255E+01     ETASF =  0.10050E+01   WASF =  0.20785E+01
 Z = 0.80354             PR =   1.493             ETA = 0.86310
 PCN =   1.0007          CN = 1.02007         COMWK =  0.36200E+08
 ***** CONVERGENT NOZZLE  1 PARAMETERS *****
 NCOSF =  0.10000E+01   Area =  3.4583   Exit Velocity =  325.54
Gross Thrust = 268376.28  Nozzle Coeff. =  0.98086E+00
 ***** COMPRESSOR  2 PARAMETERS *****
 PRSF =  0.39216E+01     ETASF =  0.10181E+01   WASF =  0.54975E+00
 Z = 0.86422             PR =   5.153             ETA = 0.83804
 PCN =   0.9908          CN = 1.00979      COMWK =  0.22397E+08
 ***** DUCT/AFTER BURNING 1 PARAMETERS *****
 ETA =  1.0000           DLP = 0.0000             WFB =   0.0000
 DUCTER IS USED AS AN INTERCOOLER!
 ****INTERCOOLER****HEAT REMOVED:34124.50      KWATTS
   ***** COMPRESSOR  3 PARAMETERS *****
 PRSF =  0.60918E+00     ETASF =  0.10619E+01   WASF =  0.29826E+00
 Z = 0.84196             PR =   4.960             ETA = 0.85292
 PCN =   0.9997          CN = 0.99971          COMWK =  0.13528E+08
 ***** HEAT EXCHANGER COLD SIDE PARAMETERS *****
 ETA = 0.88143           DLP = 0.2709
 ***** COMBUSTION CHAMBER PARAMETERS *****
 ETASF =  0.99800E+00  ETA = 0.99800           DLP = 1.6840
WFB =   2.1569
 ***** TURBINE  1 PARAMETERS *****
 CNSF =  0.84143E+02     ETASF =  0.10550E+01   TFSF =  0.14112E+01
 DHSF =  0.16026E+05
 TF =  219.844      ETA = 0.88577 CN =  2.200 AUXWK =  0.00000E+00
 ***** TURBINE  2 PARAMETERS *****
 CNSF =  0.80981E+02     ETASF =  0.10836E+01   TFSF =  0.10071E+01
 DHSF =  0.28466E+05 TF =  219.929            ETA = 0.91093
CN =  2.180 AUXWK =  0.00000E+00
 ***** TURBINE  3 PARAMETERS *****
 CNSF =  0.75383E+02     ETASF =  0.10907E+01   TFSF =  0.55245E+00
 DHSF =  0.52539E+05 TF =  220.81 ETA = 0.91925   CN =  2.201
 AUXWK =  0.00000E+00
 ***** HEAT EXCHANGER HOT SIDE PARAMETERS *****
```

```
 ETA =  0.8814           DLP = 0.0222     TOTHOT =   549.0889

 ***** CONVERGENT NOZZLE  2 PARAMETERS *****

 NCOSF =  0.10000E+01

 Area =  0.2626  Exit Velocity =  427.59  Gross Thrust =58758.04

 Nozzle Coeff. =  0.96127E+00

 Scale Factor on above Mass Flows, Areas, Thrusts & Powers= 1.0

 Station  F.A.R. Mass Flow   Pstatic    Ptotal Tstatic  Ttotal
Vel    Area

     1   0.00000   924.006   0.53307   0.70825  255.65  277.32
208.4  ******

     2   0.00000   924.006    ******   0.70117  ******  277.32
******  ******

     3   0.00000   924.006    ******   1.04700  ******  316.35
******  ******

     4   0.00000    98.992    ******   1.04700  ******  316.35
******  ******

     5   0.00000    98.992    ******   5.39542  ******  538.56
******  ******

     6   0.00000    98.919    ******   5.39542  ******  200.00
******  ******

     7   0.00000    98.919    ******  26.76331  ******  336.34
******  ******

     8   0.00000    79.135    ******  26.76331  ******  336.34
******  ******

     9   0.00000    79.135    ******  26.49237  ******  809.29
******  ******

    10   0.02726    81.292    ******  24.80835  ****** 1700.00
******  ******

    11   0.02180   101.075    ******  24.80835  ****** 1462.12
******  ******

    12   0.02180   101.075    ******  17.03590  ****** 1355.04
******  ******

    13   0.02180   101.075    ******   8.66556  ****** 1174.82
******  ******

    14   0.02180   101.075    ******   2.23784  ******  872.79
******  ******

    15   0.02180   101.075    ******   2.21560  ******  549.09
******  ******

    16   0.02180   101.075   1.18011   2.21560  462.76  549.09
427.6  0.2626

    17   0.00000    19.784    ******  26.76331  ******  336.34
******  ******

    18   0.00000    19.784    ******  26.49568  ******  336.34
******  ******
```

```
    19   0.00000   825.133    ******   1.04700  ******  316.35
******  ******
    20   0.00000   825.133    ******   1.03653  ******  316.35
******  ******
    21   0.00000   825.133   0.54707   1.03653  263.52  316.35
325.5  3.4583
  Gross Thrust = 327134.31
 Momentum Drag = 192585.14
    Net Thrust = 134549.17
     Fuel Flow =    2.1569
        s.f.c. =  16.03042
    Sp. Thrust =   145.615
***********************************************
  3 0.55           !Glide
  -1
  10 6 1425
  -1
***** OFF DESIGN ENGINE CALCULATIONS. Converged after   8 Loops
 ***** AMBIENT AND INLET PARAMETERS *****
 Alt. =   5000.0      I.S.A. Dev. =    0.000       Mach No. =  0.55
 Etar = 0.9900        Momentum Drag = 128064.03
 ***** COMPRESSOR  1 PARAMETERS *****
 PRSF =  0.12255E+01     ETASF =  0.10050E+01     WASF =
0.20785E+01
 Z = 0.65058             PR =   1.296             ETA = 0.86571
 PCN =   0.8326          CN = 0.85825             COMWK =
0.17585E+08
 ***** CONVERGENT NOZZLE  1 PARAMETERS *****
 NCOSF =  0.10000E+01
 Area =  3.4583          Exit Velocity =  266.61  Gross Thrust =
174144.84
 Nozzle Coeff. =  0.97858E+00
 ***** COMPRESSOR  2 PARAMETERS *****
 PRSF =  0.39216E+01     ETASF =  0.10181E+01     WASF =
0.54975E+00
 Z = 0.98130             PR =   4.350             ETA = 0.82158
 PCN =   0.7810          CN = 0.82387             COMWK =
0.11057E+08
 ***** DUCT/AFTER BURNING 1 PARAMETERS *****
 ETA =  1.0000           DLP = 0.0000             WFB =   0.0000
```

```
 DUCTER IS USED AS AN INTERCOOLER!
 ****INTERCOOLER****HEAT REMOVED:16751.74      KWATTS
  ***** COMPRESSOR  3 PARAMETERS *****
 PRSF =  0.60918E+00     ETASF =  0.10619E+01   WASF =  0.29826E+00
 Z = 0.74596             PR =   3.989             ETA = 0.86014
 PCN =   0.9193          CN = 0.91931          COMWK =  0.66510E+07
 ***** HEAT EXCHANGER COLD SIDE PARAMETERS *****
 ETA = 0.90200           DLP = 0.1630
 ***** COMBUSTION CHAMBER PARAMETERS *****
 ETASF =  0.99800E+00 ETA = 0.99800  DLP = 0.9170   WFB =   1.0154
 ***** TURBINE  1 PARAMETERS *****
 CNSF =  0.84143E+02     ETASF =  0.10550E+01   TFSF =  0.14112E+01
 DHSF =  0.16026E+05 TF =  218.727   ETA = 0.88131 CN =  2.207
 AUXWK =  0.00000E+00
 ***** TURBINE  2 PARAMETERS *****
 CNSF =  0.80981E+02   ETASF =  0.10836E+01  TFSF =  0.10071E+01
 DHSF =  0.28466E+05 TF =  218.336   ETA = 0.908 CN =  1.877
 AUXWK =  0.00000E+00
 ***** TURBINE  3 PARAMETERS *****
 CNSF =  0.75383E+02     ETASF =  0.10907E+01 TFSF =  0.55245E+00
 DHSF =  0.52539E+05 TF =  218.759 ETA = 0.91030CN =  2.005
 AUXWK =  0.00000E+00
 ***** HEAT EXCHANGER HOT SIDE PARAMETERS *****
 ETA =  0.9020           DLP = 0.0118     TOTHOT =   469.2071
 ***** CONVERGENT NOZZLE  2 PARAMETERS *****
 NCOSF =  0.10000E+01 Area =  0.2626 Exit Velocity =  395.70
 Gross Thrust =  26036.56 Nozzle Coeff. =  0.97999E+00
 Scale Factor on above Mass Flows, Areas, Thrusts & Powers=1.0
 Station  F.A.R. Mass Flow   Pstatic    Ptotal Tstatic  Ttotal
Vel    Area
     1   0.00000   726.156   0.53307   0.65486  255.65  271.17
176.4  ******
     2   0.00000   726.156    ******   0.64831  ******  271.17
******  ******
     3   0.00000   726.156    ******   0.84039  ******  295.31
******  ******
     4   0.00000    58.693    ******   0.84039  ******  295.31
******  ******
```

```
     5   0.00000    58.693    ******   3.65584  ******  481.35
******  ******

     6   0.00000    58.707    ******   3.65584  ******  200.00
******  ******

     7   0.00000    58.707    ******  14.58154  ******  313.01
******  ******

     8   0.00000    46.965    ******  14.58154  ******  313.01
******  ******

     9   0.00000    46.965    ******  14.41854  ******  680.95
******  ******

    10   0.02162    47.981    ******  13.50152  ****** 1425.00
******  ******

    11   0.01730    59.722    ******  13.50152  ****** 1227.90
******  ******

    12   0.01730    59.722    ******   9.28188  ****** 1135.65
******  ******

    13   0.01730    59.722    ******   4.71246  ******  979.38
******  ******

    14   0.01730    59.722    ******   1.21254  ******  720.90
******  ******

    15   0.01730    59.722    ******   1.20071  ******  469.21
******  ******

    16   0.01730    59.722   0.64123   1.20071  393.82  469.21
395.7  0.2626

    17   0.00000    11.741    ******  14.58154  ******  313.01
******  ******

    18   0.00000    11.741    ******  14.43572  ******  313.01
******  ******

    19   0.00000   667.484    ******   0.84039  ******  295.31
******  ******

    20   0.00000   667.484    ******   0.83198  ******  295.31
******  ******

    21   0.00000   667.484   0.53307   0.83198  259.96  295.31
266.6  3.4583


  Gross Thrust = 200181.39
 Momentum Drag = 128064.03
    Net Thrust =  72117.36
     Fuel Flow =    1.0154
        s.f.c. =  14.07972
    Sp. Thrust =    99.314
 ***********************************************
 -1
```

```
  10 6 1390        !Glide2
  -1
***** OFF DESIGN ENGINE CALCULATIONS. Converged after   2 Loops
 ***** AMBIENT AND INLET PARAMETERS *****
 Alt. =   5000.0      I.S.A. Dev. =    0.000       Mach No. =  0.55
 Etar = 0.9900        Momentum Drag = 125089.05
 ***** COMPRESSOR  1 PARAMETERS *****
 PRSF =  0.12255E+01     ETASF =  0.10050E+01     WASF =
0.20785E+01
 Z = 0.62503             PR =   1.275             ETA = 0.86185
 PCN =   0.8145          CN = 0.83962         COMWK =  0.16111E+08
 ***** CONVERGENT NOZZLE  1 PARAMETERS *****
 NCOSF =  0.10000E+01  Area =  3.4583  Exit Velocity =  261.16
Gross Thrust = 167117.55  Nozzle Coeff. =  0.97834E+00
 ***** COMPRESSOR  2 PARAMETERS *****
 PRSF =  0.39216E+01     ETASF =  0.10181E+01  WASF =  0.54975E+00
 Z = 0.98912             PR =   4.210             ETA = 0.81916
 PCN =   0.7550          CN = 0.79847       COMWK =  0.10097E+08
 ***** DUCT/AFTER BURNING 1 PARAMETERS *****
 ETA =  1.0000           DLP = 0.0000             WFB =   0.0000
 DUCTER IS USED AS AN INTERCOOLER!
 ***INTERCOOLER****HEAT REMOVED:15369.70      KWATTS
   ***** COMPRESSOR  3 PARAMETERS *****
 PRSF =  0.60918E+00     ETASF =  0.10619E+01  WASF =  0.29826E+00
 Z = 0.73448             PR =   3.899             ETA = 0.86014
 PCN =   0.9128          CN = 0.91278        COMWK =  0.61316E+07
 ***** HEAT EXCHANGER COLD SIDE PARAMETERS *****
 ETA = 0.90200           DLP = 0.1539
 ***** COMBUSTION CHAMBER PARAMETERS *****
 ETASF =  0.99800E+00 ETA = 0.99800  DLP = 0.8494 WFB =0.9263
 ***** TURBINE  1 PARAMETERS *****
 CNSF =  0.84143E+02     ETASF =  0.10550E+01 TFSF =  0.14112E+01
 DHSF =  0.16026E+05 TF =  218.305 ETA = 0.87917 CN =  2.219
 AUXWK =  0.00000E+00
 ***** TURBINE  2 PARAMETERS *****
 CNSF =  0.80981E+02     ETASF =  0.10836E+01 TFSF =  0.10071E+01
 DHSF =  0.28466E+05 TF =  218.496  ETA = 0.90831  CN =  1.837
 AUXWK =  0.00000E+00
```

***** TURBINE 3 PARAMETERS *****

CNSF = 0.75383E+02 ETASF = 0.10907E+01 TFSF = 0.55245E+00

DHSF = 0.52539E+05 TF = 218.727 ETA = 0.91113 CN = 1.987

AUXWK = 0.00000E+00

***** HEAT EXCHANGER HOT SIDE PARAMETERS *****

ETA = 0.9020 DLP = 0.0109 TOTHOT = 459.7221

***** CONVERGENT NOZZLE 2 PARAMETERS *****

NCOSF = 0.10000E+01 Area = 0.2626 Exit Velocity = 391.73

Gross Thrust = 23255.87 Nozzle Coeff. = 0.98085E+00

Scale Factor on above Mass Flows, Areas, Thrusts & Powers = 1.0000

Station	F.A.R.	Mass Flow	Pstatic	Ptotal	Tstatic	Ttotal	Vel	Area
1	0.00000	709.287	0.53307	0.65486	255.65	271.17	176.4	******
2	0.00000	709.287	******	0.64831	******	271.17	******	******
3	0.00000	709.287	******	0.82655	******	293.81	******	******
4	0.00000	55.212	******	0.82655	******	293.81	******	******
5	0.00000	55.212	******	3.47971	******	474.52	******	******
6	0.00000	55.218	******	3.47971	******	200.00	******	******
7	0.00000	55.218	******	13.56681	******	310.77	******	******
8	0.00000	44.174	******	13.56681	******	310.77	******	******
9	0.00000	44.174	******	13.41293	******	663.22	******	******
10	0.02097	45.101	******	12.56355	******	1390.00	******	******
11	0.01678	56.144	******	12.56355	******	1198.28	******	******
12	0.01678	56.144	******	8.61155	******	1107.37	******	******
13	0.01678	56.144	******	4.38262	******	954.78	******	******
14	0.01678	56.144	******	1.12832	******	701.49	******	******
15	0.01678	56.144	******	1.11738	******	459.72	******	******

```
    16   0.01678    56.144   0.59636   1.11738  385.70  459.72
391.7  0.2626
    17   0.00000    11.044    ******  13.56681  ******  310.77
******  ******
    18   0.00000    11.044    ******  13.43115  ******  310.77
******  ******
    19   0.00000   654.061    ******   0.82655  ******  293.81
******  ******
    20   0.00000   654.061    ******   0.81829  ******  293.81
******  ******
    21   0.00000   654.061   0.53307   0.81829  259.88  293.81
261.2  3.4583


  Gross Thrust = 190373.42
 Momentum Drag = 125089.05
    Net Thrust =  65284.37
     Fuel Flow =    0.9263
        s.f.c. =  14.18884
    Sp. Thrust =    92.042
**********************************************
1 10670          !Cruise
  3 0.82
  -1
  10 6 1660
  -1
***** OFF DESIGN ENGINE CALCULATIONS. Converged after   7 Loops
 ***** AMBIENT AND INLET PARAMETERS *****
 Alt. =  10670.0      I.S.A. Dev. =    0.000       Mach No. = 0.82
 Etar = 0.9900        Momentum Drag = 125537.25
 ***** COMPRESSOR  1 PARAMETERS *****
 PRSF =  0.12255E+01     ETASF =  0.10050E+01   WASF =  0.20785E+01
 Z = 0.83828             PR =   1.535             ETA = 0.85199
 PCN =   0.9650          CN = 1.03945         COMWK =  0.19691E+08
 ***** CONVERGENT NOZZLE  1 PARAMETERS *****
 NCOSF =  0.10000E+01  Area =  3.4583   Exit Velocity =  309.77
Gross Thrust = 159393.86 Nozzle Coeff. =  0.97949E+00
 ***** COMPRESSOR  2 PARAMETERS *****
 PRSF =  0.39216E+01     ETASF =  0.10181E+01   WASF =  0.54975E+00
 Z = 0.91795             PR =   5.491             ETA = 0.81550
 PCN =   0.9507          CN = 1.01832         COMWK =  0.12154E+08
```

```
***** DUCT/AFTER BURNING 1 PARAMETERS *****
 ETA =  1.0000           DLP = 0.0000            WFB =   0.0000
 DUCTER IS USED AS AN INTERCOOLER!
 ****INTERCOOLER****HEAT REMOVED:17005.65      KWATTS
 ***** COMPRESSOR  3 PARAMETERS *****
 PRSF =  0.60918E+00     ETASF =  0.10619E+01   WASF =  0.29826E+00
 Z = 0.83032             PR =   4.827             ETA = 0.85787
 PCN =   0.9865          CN = 0.98651         COMWK =  0.73228E+07
 ***** HEAT EXCHANGER COLD SIDE PARAMETERS *****
 ETA = 0.90200           DLP = 0.1505
 ***** COMBUSTION CHAMBER PARAMETERS *****
 ETASF =  0.99800E+00 ETA = 0.99800   DLP = 0.9330 WFB =   1.1530
 ***** TURBINE  1 PARAMETERS *****
 CNSF =  0.84143E+02     ETASF =  0.10550E+01 TFSF =  0.14112E+01
 DHSF =  0.16026E+05 TF =  219.322  ETA = 0.8840 CN =  2.197
 AUXWK =  0.00000E+00
 ***** TURBINE  2 PARAMETERS *****
 CNSF =  0.80981E+02     ETASF =  0.10836E+01  TFSF =  0.10071E+01
 DHSF =  0.28466E+05 TF =  219.377 ETA = 0.90988 CN =  2.117
 AUXWK =  0.00000E+00
 ***** TURBINE  3 PARAMETERS *****
 CNSF =  0.75383E+02  ETASF =  0.10907E+01 TFSF =  0.55245E+00
 DHSF =  0.52539E+05 TF =  220.483  ETA = 0.91948 CN =  2.149
 AUXWK =  0.00000E+00
 ***** HEAT EXCHANGER HOT SIDE PARAMETERS *****
 ETA =  0.9020           DLP = 0.0122     TOTHOT =   536.1929
 ***** CONVERGENT NOZZLE  2 PARAMETERS *****
 NCOSF =  0.10000E+01  Area =  0.2626  Exit Velocity =  422.63
Gross Thrust =  33491.09 Nozzle Coeff. =  0.94876E+00
 Scale Factor on above Mass Flows, Areas, Thrusts & Powers= 1.0
 Station  F.A.R. Mass Flow   Pstatic    Ptotal Tstatic  Ttotal
Vel    Area
     1   0.00000   516.064   0.23517   0.36587  218.79  248.33
243.3  ******
     2   0.00000   516.064    ******   0.36221  ******  248.33
******  ******
     3   0.00000   516.064    ******   0.55608  ******  286.39
******  ******
```

```
     4   0.00000    55.005    ******   0.55608  ******  286.39
******  ******

     5   0.00000    55.005    ******   3.05355  ******  504.34
******  ******

     6   0.00000    55.018    ******   3.05355  ******  200.00
******  ******

     7   0.00000    55.018    ******  14.74040  ******  332.71
******  ******

     8   0.00000    44.014    ******  14.74040  ******  332.71
******  ******

     9   0.00000    44.014    ******  14.58987  ******  798.19
******  ******

    10   0.02620    45.167    ******  13.65689  ****** 1660.00
******  ******

    11   0.02096    56.171    ******  13.65689  ****** 1427.84
******  ******

    12   0.02096    56.171    ******   9.37997  ****** 1323.03
******  ******

    13   0.02096    56.171    ******   4.76547  ****** 1146.11
******  ******

    14   0.02096    56.171    ******   1.22282  ******  848.72
******  ******

    15   0.02096    56.171    ******   1.21060  ******  536.19
******  ******

    16   0.02096    56.171   0.64746   1.21060  451.56  536.19
422.6  0.2626

    17   0.00000    11.004    ******  14.74040  ******  332.71
******  ******

    18   0.00000    11.004    ******  14.59300  ******  332.71
******  ******

    19   0.00000   461.060    ******   0.55608  ******  286.39
******  ******

    20   0.00000   461.060    ******   0.55052  ******  286.39
******  ******

    21   0.00000   461.060   0.29082   0.55052  238.56  286.39
309.8  3.4583


Gross Thrust = 192884.95

Momentum Drag = 125537.25

Net Thrust =  67347.70

Fuel Flow =    1.1530

s.f.c. =  17.11987

Sp. Thrust =   130.503
```

```
          ********************************************
1 10000          !Cruise2
  3 0.8
  -1
  -1
***** OFF DESIGN ENGINE CALCULATIONS. Converged after   1 Loops
 ***** AMBIENT AND INLET PARAMETERS *****
 Alt. =  10000.0      I.S.A. Dev. =    0.000       Mach No. =  0.80
 Etar = 0.9900        Momentum Drag = 133088.48
 ***** COMPRESSOR  1 PARAMETERS *****
 PRSF =  0.12255E+01     ETASF =  0.10050E+01   WASF =  0.20785E+01
 Z = 0.83321             PR =   1.529             ETA = 0.85616
 PCN =   0.9687          CN = 1.03623          COMWK =  0.21151E+08
 ***** CONVERGENT NOZZLE  1 PARAMETERS *****
 NCOSF =  0.10000E+01 Area =  3.4583      Exit Velocity =  311.61
Gross Thrust = 170416.86 Nozzle Coeff. =  0.97981E+00
 ***** COMPRESSOR  2 PARAMETERS *****
 PRSF =  0.39216E+01     ETASF =  0.10181E+01   WASF =  0.54975E+00
 Z = 0.91316             PR =   5.447             ETA = 0.82002
 PCN =   0.9543          CN = 1.01614         COMWK =  0.13063E+08
 ***** DUCT/AFTER BURNING 1 PARAMETERS *****
 ETA =  1.0000           DLP = 0.0000             WFB =   0.0000
 DUCTER IS USED AS AN INTERCOOLER!
 ****INTERCOOLER****HEAT REMOVED:18480.27      KWATTS
   ***** COMPRESSOR  3 PARAMETERS *****
 PRSF =  0.60918E+00     ETASF =  0.10619E+01   WASF =  0.29826E+00
 Z = 0.82932             PR =   4.824             ETA = 0.85812
 PCN =   0.9868          CN = 0.98676          COMWK =  0.78601E+07
 ***** HEAT EXCHANGER COLD SIDE PARAMETERS *****
 ETA = 0.90200           DLP = 0.1618
 ***** COMBUSTION CHAMBER PARAMETERS *****
 ETASF =  0.99800E+00
 ETA = 0.99800           DLP = 1.0033             WFB =   1.2386
 ***** TURBINE  1 PARAMETERS *****
 CNSF =  0.84143E+02     ETASF =  0.10550E+01   TFSF =  0.14112E+01
 DHSF =  0.16026E+05  TF =  219.596    ETA = 0.88502    CN =  2.197
 AUXWK =  0.00000E+00
 ***** TURBINE  2 PARAMETERS *****
```

```
 CNSF =  0.80981E+02     ETASF =  0.10836E+01   TFSF =  0.10071E+01
 DHSF =  0.28466E+05 TF =  219.487 ETA = 0.91027 CN =  2.125
 AUXWK =  0.00000E+00
 ***** TURBINE  3 PARAMETERS *****
 CNSF =  0.75383E+02     ETASF =  0.10907E+01  TFSF =  0.55245E+00
 DHSF =  0.52539E+05  TF =  220.569  ETA = 0.91968 CN =  2.157
 AUXWK =  0.00000E+00
 ***** HEAT EXCHANGER HOT SIDE PARAMETERS *****
 ETA =  0.9020           DLP = 0.0131     TOTHOT =   536.1324
 ***** CONVERGENT NOZZLE  2 PARAMETERS *****
 NCOSF =  0.10000E+01 Area =  0.2626 Exit Velocity =  422.60
Gross Thrust =  35808.51 Nozzle Coeff. =  0.95079E+00
 Scale Factor on above Mass Flows, Areas, Thrusts & Powers=   1.0
 Station  F.A.R. Mass Flow   Pstatic    Ptotal Tstatic  Ttotal
Vel    Area
     1   0.00000   555.282   0.26084   0.39775  223.15  251.82
239.7  ******
     2   0.00000   555.282    ******   0.39377  ******  251.82
******  ******
     3   0.00000   555.282    ******   0.60192  ******  289.81
******  ******
     4   0.00000    59.101    ******   0.60192  ******  289.81
******  ******
     5   0.00000    59.101    ******   3.27893  ******  507.74
******  ******
     6   0.00000    59.103    ******   3.27893  ******  200.00
******  ******
     7   0.00000    59.103    ******  15.81798  ******  332.60
******  ******
     8   0.00000    47.282    ******  15.81798  ******  332.60
******  ******
     9   0.00000    47.282    ******  15.65614  ******  798.19
******  ******
    10   0.02620    48.521    ******  14.65281  ****** 1660.00
******  ******
    11   0.02096    60.341    ******  14.65281  ****** 1427.83
******  ******
    12   0.02096    60.341    ******  10.07131  ****** 1323.10
******  ******
    13   0.02096    60.341    ******   5.11646  ****** 1146.08
******  ******
```

```
    14   0.02096    60.341    ******   1.31355  ******  848.73
******  ******

    15   0.02096    60.341    ******   1.30042  ******  536.13
******  ******

    16   0.02096    60.341   0.69549   1.30042  451.51  536.13
422.6  0.2626

    17   0.00000    11.821    ******  15.81798  ******  332.60
******  ******

    18   0.00000    11.821    ******  15.65980  ******  332.60
******  ******

    19   0.00000   496.181    ******   0.60192  ******  289.81
******  ******

    20   0.00000   496.181    ******   0.59590  ******  289.81
******  ******

    21   0.00000   496.181   0.31484   0.59590  241.41  289.81
311.6  3.4583


  Gross Thrust = 206225.38
 Momentum Drag = 133088.48
    Net Thrust =  73136.90
     Fuel Flow =    1.2386
        s.f.c. =  16.93524
    Sp. Thrust =   131.711
***********************************************
  1 1000           !Approach
  3 0.4
  -1
  10 6 1350
  -1
***** OFF DESIGN ENGINE CALCULATIONS. Converged after   7 Loops
 ***** AMBIENT AND INLET PARAMETERS *****
 Alt. =   1000.0      I.S.A. Dev. =    0.000       Mach No. =  0.40
 Etar = 0.9900        Momentum Drag = 126479.62
 ***** COMPRESSOR  1 PARAMETERS *****
 PRSF =  0.12255E+01     ETASF =  0.10050E+01   WASF =  0.20785E+01
 Z = 0.62798             PR =   1.242             ETA = 0.86995
 PCN =   0.7771          CN = 0.77375         COMWK =  0.20179E+08
 ***** CONVERGENT NOZZLE  1 PARAMETERS *****
 NCOSF =  0.10000E+01  Area =  3.4583      Exit Velocity =  229.07
Gross Thrust = 194117.36  Nozzle Coeff. =  0.97644E+00
```

```
***** COMPRESSOR  2 PARAMETERS *****
PRSF =  0.39216E+01     ETASF =  0.10181E+01   WASF =  0.54975E+00
Z = 0.97960             PR =   3.800             ETA = 0.82372
PCN =   0.7187          CN = 0.73749          COMWK =  0.12687E+08
***** DUCT/AFTER BURNING 1 PARAMETERS *****
ETA =  1.0000           DLP = 0.0000             WFB =   0.0000
DUCTER IS USED AS AN INTERCOOLER!
****INTERCOOLER****HEAT REMOVED:20870.15      KWATTS
 ***** COMPRESSOR  3 PARAMETERS *****
PRSF =  0.60918E+00     ETASF =  0.10619E+01     WASF =
0.29826E+00
Z = 0.72044             PR =   3.766             ETA = 0.85987
PCN =   0.9009          CN = 0.90092             COMWK =
0.77330E+07
***** HEAT EXCHANGER COLD SIDE PARAMETERS *****
ETA = 0.90200           DLP = 0.2005
***** COMBUSTION CHAMBER PARAMETERS *****
ETASF =  0.99800E+00  ETA = 0.99800   DLP = 1.0881  WFB =   1.1595
***** TURBINE  1 PARAMETERS *****
CNSF =  0.84143E+02     ETASF =  0.10550E+01  TFSF =  0.14112E+01
DHSF =  0.16026E+05  TF =  217.763 ETA = 0.87718   CN =  2.222
AUXWK =  0.00000E+00
***** TURBINE  2 PARAMETERS *****
CNSF =  0.80981E+02     ETASF =  0.10836E+01   TFSF =  0.10071E+01
DHSF =  0.28466E+05  TF =  217.747 ETA = 0.90500  CN =  1.775
AUXWK =  0.00000E+00
***** TURBINE  3 PARAMETERS *****
CNSF =  0.75383E+02     ETASF =  0.10907E+01  TFSF =  0.55245E+00
DHSF =  0.52539E+05 TF =  217.672 ETA = 0.91217 CN =  1.924
AUXWK =  0.00000E+00
***** HEAT EXCHANGER HOT SIDE PARAMETERS *****
ETA =  0.9020           DLP = 0.0138     TOTHOT =   449.3759
***** CONVERGENT NOZZLE  2 PARAMETERS *****
NCOSF =  0.10000E+01  Area =  0.2626 Exit Velocity =  347.16
Gross Thrust =  24811.29 Nozzle Coeff. =  0.97924E+00
Scale Factor on above Mass Flows, Areas, Thrusts & Powers= 1.0000
```

Station	F.A.R.	Mass Flow	Pstatic	Ptotal	Tstatic	Ttotal	Vel	Area
1	0.00000	939.647	0.88697	0.99041	281.65	290.68	134.6	******
2	0.00000	939.647	******	0.98051	******	290.68	******	******
3	0.00000	939.647	******	1.21819	******	312.07	******	******
4	0.00000	71.853	******	1.21819	******	312.07	******	******
5	0.00000	71.853	******	4.62854	******	486.24	******	******
6	0.00000	71.824	******	4.62854	******	200.00	******	******
7	0.00000	71.824	******	17.42897	******	307.40	******	******
8	0.00000	57.459	******	17.42897	******	307.40	******	******
9	0.00000	57.459	******	17.22850	******	644.99	******	******
10	0.02018	58.619	******	16.14042	******	1350.00	******	******
11	0.01614	72.984	******	16.14042	******	1164.29	******	******
12	0.01614	72.984	******	11.05875	******	1075.57	******	******
13	0.01614	72.984	******	5.63116	******	927.19	******	******
14	0.01614	72.984	******	1.46857	******	681.66	******	******
15	0.01614	72.984	******	1.45477	******	449.38	******	******
16	0.01614	72.984	0.88697	1.45477	391.08	449.38	347.2	0.2626
17	0.00000	14.365	******	17.42897	******	307.40	******	******
18	0.00000	14.365	******	17.25468	******	307.40	******	******
19	0.00000	867.845	******	1.21819	******	312.07	******	******
20	0.00000	867.845	******	1.20601	******	312.07	******	******
21	0.00000	867.845	0.88697	1.20601	285.85	312.07	229.1	3.4583

```
  Gross Thrust = 218928.66
 Momentum Drag = 126479.62
    Net Thrust =  92449.04
     Fuel Flow =    1.1595
        s.f.c. =  12.54168
    Sp. Thrust =    98.387
*********************************************
  1 0              !Taxi
  3 0.1
  -1
  10 6 1360
  -1
***** OFF DESIGN ENGINE CALCULATIONS. Converged after   3 Loops
 ***** AMBIENT AND INLET PARAMETERS *****
 Alt. =      0.0      I.S.A. Dev. =    0.000       Mach No. =  0.10
 Etar = 0.9900        Momentum Drag =  30834.37
 ***** COMPRESSOR  1 PARAMETERS *****
 PRSF =  0.12255E+01     ETASF =  0.10050E+01     WASF =
0.20785E+01
 Z = 0.73735             PR =   1.274             ETA = 0.89504
 PCN =   0.7557          CN = 0.75495             COMWK =
0.21006E+08
 ***** CONVERGENT NOZZLE  1 PARAMETERS *****
 NCOSF =  0.10000E+01
 Area =  3.4583     Exit Velocity =  198.87
Gross Thrust = 161201.73 Nozzle Coeff. =  0.97510E+00
 ***** COMPRESSOR  2 PARAMETERS *****
 PRSF =  0.39216E+01     ETASF =  0.10181E+01  WASF =  0.54975E+00
 Z = 0.98371             PR =   3.810             ETA = 0.82178
 PCN =   0.7182          CN = 0.73731       COMWK =  0.13239E+08
 ***** DUCT/AFTER BURNING 1 PARAMETERS *****
 ETA =  1.0000           DLP = 0.0000             WFB =   0.0000
 DUCTER IS USED AS AN INTERCOOLER!
 ****INTERCOOLER****HEAT REMOVED:21725.40      KWATTS
 ***** COMPRESSOR  3 PARAMETERS *****
 PRSF =  0.60918E+00     ETASF =  0.10619E+01   WASF =  0.29826E+00
 Z = 0.72139             PR =   3.752             ETA = 0.86003
```

```
 PCN =   0.8983          CN = 0.89831    COMWK =  0.80127E+07
 ***** HEAT EXCHANGER COLD SIDE PARAMETERS *****
 ETA = 0.90200           DLP = 0.2078
 ***** COMBUSTION CHAMBER PARAMETERS *****
 ETASF =  0.99800E+00 ETA = 0.99800 DLP = 1.1430  WFB =   1.2122
 ***** TURBINE  1 PARAMETERS *****
 CNSF =  0.84143E+02     ETASF =  0.10550E+01 TFSF =  0.14112E+01
 DHSF =  0.16026E+05  TF =  218.285   ETA = 0.87978  CN =  2.207
 AUXWK =  0.00000E+00
 ***** TURBINE  2 PARAMETERS *****
 CNSF =  0.80981E+02     ETASF =  0.10836E+01   TFSF =  0.10071E+01
 DHSF =  0.28466E+05  TF =  217.471  ETA = 0.90430 CN =  1.766
 AUXWK =  0.00000E+00
 ***** TURBINE  3 PARAMETERS *****
 CNSF =  0.75383E+02     ETASF =  0.10907E+01  TFSF =  0.55245E+00
 DHSF =  0.52539E+05 TF =  217.004   ETA = 0.91204  CN =  1.862
 AUXWK =  0.00000E+00
 ***** HEAT EXCHANGER HOT SIDE PARAMETERS *****
 ETA =  0.9020           DLP = 0.0142     TOTHOT =   452.6439
 ***** CONVERGENT NOZZLE  2 PARAMETERS *****
 NCOSF =  0.10000E+01 Area =  0.262 Exit Velocity =  328.15
Gross Thrust =  24366.80 Nozzle Coeff. =  0.97845E+00
 Scale Factor on above Mass Flows, Areas, Thrusts & Powers= 1.0
 Station  F.A.R. Mass Flow   Pstatic    Ptotal Tstatic  Ttotal
Vel    Area
     1   0.00000   905.961   1.00000   1.00702  288.15  288.73
34.0  ******
     2   0.00000   905.961    ******   0.99695  ******  288.73
******  ******
     3   0.00000   905.961    ******   1.26974  ******  311.82
******  ******
     4   0.00000    74.676    ******   1.26974  ******  311.82
******  ******
     5   0.00000    74.676    ******   4.83787  ******  486.70
******  ******
     6   0.00000    74.679    ******   4.83787  ******  200.00
******  ******
     7   0.00000    74.679    ******  18.15175  ******  307.03
******  ******
```

```
     8   0.00000    59.743    ******  18.15175  ******  307.03
******  ******

     9   0.00000    59.743    ******  17.94390  ******  652.75
******  ******

    10   0.02029    60.955    ******  16.80091  ****** 1360.00
******  ******

    11   0.01623    75.891    ******  16.80091  ****** 1172.55
******  ******

    12   0.01623    75.891    ******  11.57309  ****** 1084.27
******  ******

    13   0.01623    75.891    ******   5.90977  ******  935.60
******  ******

    14   0.01623    75.891    ******   1.56130  ******  690.30
******  ******

    15   0.01623    75.891    ******   1.54709  ******  452.64
******  ******

    16   0.01623    75.891   1.00000   1.54709  400.80  452.64
328.1  0.2626

    17   0.00000    14.936    ******  18.15175  ******  307.03
******  ******

    18   0.00000    14.936    ******  17.97023  ******  307.03
******  ******

    19   0.00000   831.268    ******   1.26974  ******  311.82
******  ******

    20   0.00000   831.268    ******   1.25704  ******  311.82
******  ******

    21   0.00000   831.268   1.00000   1.25704  292.10  311.82
198.9  3.4583

  Gross Thrust = 185568.52
 Momentum Drag =  30834.37
    Net Thrust = 154734.16
     Fuel Flow =    1.2122
        s.f.c. =   7.83396
    Sp. Thrust =   170.796
```

A.4 THE CONTRAIL FREE AERO ENGINE WITH 3 SPOOL INTERCOOLED-RECUPERATED TURBOFAN ENGINE TRENT 900 BASELINE SPECIFICATION

\\ Created by Sarah Qureshi ; Adapted from RR_Trent900.dat

```
  OD SI KE CT FP
  -1
  -1
```

```
INTAKE  S1-2         D1-4            R100
COMPRE  S2-3         D5-10           R101   V5    V6
PREMAS  S3,4,19      D11-14                 V11
DUCTER  S19-20       D15-18          R102
NOZCON  S20-21,1     D19             R103
COMPRE  S4-5         D20-25          R104   V20   V21
DUCTER  S5-6         D75-78          R209
COMPRE  S6-7         D26-31          R105   V26   V27
PREMAS  S7,8,21      D32-35
DUCTER  S21-22       D36-39          R106
HETCOL  S8,9         D79-82
BURNER  S9-10        D40-42          R107
MIXEES  S10,22,11
TURBIN  S11-12       D43-50,105,51          V44
TURBIN  S12-13       D52-59,104,60          V53
TURBIN  S13-14       D61-68,101,69          V62
HETHOT S8,14,15      D83-86
DUCTER  S15-16       D87-90          R110
PREMAS  S16,17,0     D91-94
NOZCON  S17,18,1     D70                    R108
PERFOR  S1,0,0       D71-74,103,100,102,108,0,107,0,0,0
CODEND

 ! INTAKE - Aeroplane inlet
 1   10670         ! ALTITUDE
 2   0.0         ! ISA DEVIATION
 3   0.82         ! MACH NO.
 4   0.99        ! PRESSURE RECOVERY
 ! COMPRE - Fan uses Trent 800
 5   -1.0        ! SURGE MARGINE
 6    1.0        ! ROTATIONAL SPEED,N1
 7   1.5        ! FAN PRESSURE RATIO
 8   0.875       ! EFFICIENCY
 9   0.0         ! ERROR SELECTOR
 10  1.0         ! MAP NUMBER
 ! PREMAS -  Bypass - Main
 11  0.111111    ! LAMDA (BYPASS RATIO 8.5)
```

```
12  0.0         ! MASS FLOW LOSS
13  1.0         ! PRESSURE FACTOR
14  0.0         ! PRESSURE LOSS
! Bypass duct
15  0.0         ! REHEAT SELECTOR
16  0.01        ! PRESSURE LOSS 1%
17  0.0         ! REHEAT COMB.EFFICIENCY
18  0.0         ! MAX REHEAT FUEL FLOW
!Bypass Convergent Zozzle
19  -1.0        ! Fan Exhaust Nozzle: fixed Area
!  IP COMPRESSOR
20  0.85        ! SURGE MARGIN
21  1.0         ! ROTATIONAL SPEED
22  5.0         ! PRESSURE RATIO
23  0.845       ! EFFICIENCY
24  1.0         ! ERROR SELECTOR
25  4.0         ! MAP NUMBER
!  HP COMPRESSOR
26  0.85        ! SURGE MARGIN
27  1.0         ! ROTATIONAL SPEED
28  5.0         ! PRESSURE RATIO
29  0.85        ! EFFICIENCY
30  1.0         ! ERROR SELECTOR
31  5.0         ! MAP NUMBER
!  HPT Turbine COOLING BYPASS
32  0.80        ! BYPASS RATIO
33  0.0         ! MASS FLOW LOSS
34  1.0         ! PRESSURE FACTOR
35  0.0         ! PRESSURE LOSS
!  Ducter Cooling
36  0.0         ! REHEAT SELECTOR
37  0.01        ! PRESSURE LOSS 1%
38  0.0         ! REHEAT COMB.EFFICIENCY
39  0.0         ! MAX REHEAT FUEL FLOW
!  BURNER
40  0.06        ! PRESSURE LOSS
41  0.998       ! COMBUSTION EFFICIENCY
```

```
42  -1.0        ! FUEL FLOW
!  TURBINE-HP
43  0.0         ! AUX.WORK
44  0.8         ! REL NON-D MASS FLOW
45  0.6         ! REL NON-D SPEED
46  0.885       ! EFFICIENCY
47 -1.0         ! REL ROT.SPEED(COMP TURB=-1)
48  3.0         ! COMP NO. FROM LOW END
49  1.0         ! TURBINE MAP
50 -1.0         ! POWER LAW
51  0.0         ! NGV
!  TURBINE-IP
52  0.0        ! AUX.WORK
53  0.8         ! REL NON-D MASS FLOW
54  0.6         ! REL NON-D SPEED
55  0.909       ! EFFICIENCY
56 -1.0         ! REL ROT.SPEED
57  2.0         ! COMP NO. FROM LOW END
58  1.0         ! TURBINE MAP
59 -1.0         ! POWER LAW
60  0.0         ! NGV
!  TURBINE-LP
61  3500000     ! AUX.WORK
62  0.8         ! REL NON-D MASS FLOW
63  0.6         ! REL NON-D SPEED
64  0.915       ! EFFICIENCY
65 -1.0         ! REL ROT.SPEED
66  1.0         ! COMP NO. FROM LOW END
67  1.0         ! TURBINE MAP
68 -1.0         ! POWER LAW
69  0.0         ! NGV
!  Core CONVERGENT NOZZLE
70 -1.0         ! SWITHCH, AREA FIXED
!  PERFORMANCE
71 -1.0         ! POWER (-1=TURBOJET/FAN)
72 -1.0         ! PROPELLER EFFICIENCY(")
73  0.0         ! SCALING INDEX
```

```
 74  0.0          ! REQ'D D.P. THRUST
! INTERCOOLER
75 2.0            !INTERCOOLER SELECTOR
76 0.0            ! PRESSURE LOSS
77 1.0            ! INTERCOOLER EFFICIENCY
78 -1.0           ! MAX. REHEAT FUEL FLOW
! HETCOL
79 0.03             ! COLD SIDE PRESSURE LOSS INLET TO XCHANGER
80 0.82             ! EFFECTIVENESS
81 1.0              ! TYPE 1, RECUPERATOR 3, REGENERATOR
82 0.0              ! MASS FLOW LEAKAGE
!HETHOT
83 0.03             ! HOT SIDE PRESSURE LOSS, INLET TO RECUPERATOR
84 0.82             ! HEAT EXCHANGER EFFECTIVENESS
85 1.0              ! TYPE 1(RECUPERATOR)
86 0.0              ! MASS FLOW LEAKAGE
! DUCTER CONTRAILS
 87  0.0          ! REHEAT SELECTOR
 88  -8.5          ! PRESSURE GAIN
 89  0.0          ! REHEAT COMB.EFFICIENCY
 90  0.0          ! MAX REHEAT FUEL FLOW
! PREMAS  CONTRAILS
 91  0.9765       ! LAMDA (WATER LOSS FROM MASS FLOW 0.0235)
 92  0.0          ! MASS FLOW LOSS
 93  0.9765       ! PRESSURE FACTOR GAIN
 94  0.0          ! PRESSURE LOSS
 -1
 1  2  525.0      ! INLET MASS FLOW(Kg/s)
 10 6  1550.0      ! TET(K)
6 6 200.0
-1
***********************************************
    ***** DESIGN POINT ENGINE CALCULATIONS *****
***** AMBIENT AND INLET PARAMETERS *****
Alt. =  10670.0      I.S.A. Dev. =    0.000       Mach No. =  0.82
Etar = 0.9900        Momentum Drag = 127711.08
```

```
***** COMPRESSOR  1 PARAMETERS *****
PRSF =  0.12255E+01     ETASF =  0.10050E+01   WASF =  0.22602E+01
Z = 0.85000             PR =   1.500             ETA = 0.87500
PCN =   1.0000          CN = 1.00000         COMWK =  0.18386E+08
***** CONVERGENT NOZZLE  1 PARAMETERS *****
NCOSF =  0.10000E+01 Area =  3.5618   Exit Velocity =  308.07
Gross Thrust = 158571.62 Nozzle Coeff. =  0.97980E+00
***** COMPRESSOR  2 PARAMETERS *****
PRSF =  0.39216E+01     ETASF =  0.10181E+01 WASF =  0.59789E+00
Z = 0.85000             PR =   5.000             ETA = 0.84500
PCN =   1.0000          CN = 1.00000   COMWK =  0.11462E+08
***** DUCT/AFTER BURNING 1 PARAMETERS *****
ETA =  1.0000           DLP = 0.0000             WFB =   0.0000
DUCTER IS USED AS AN INTERCOOLER!
****INTERCOOLER****HEAT REMOVED:16416.23      KWATTS
  ***** COMPRESSOR  3 PARAMETERS *****
PRSF =  0.60918E+00     ETASF =  0.10619E+01     WASF =
0.34938E+00
Z = 0.85000             PR =   5.000             ETA = 0.85000
PCN =   1.0000          CN = 1.00000    COMWK =  0.80544E+07
HETYP =  1.0 HEUA =       71.792
HETYP =  1.0 HEUA =       76.531
HETYP =  1.0 HEUA =       76.293
HETYP =  1.0 HEUA =       76.303
***** HEAT EXCHANGER COLD SIDE PARAMETERS *****
ETAD =  0.82000E+00 ETA = 0.82000  DLP = 0.4075
***** COMBUSTION CHAMBER PARAMETERS *****
ETASF =  0.99800E+00 ETA = 0.99800   DLP = 0.790 WFB =   1.2676
***** TURBINE  1 PARAMETERS *****
CNSF =  0.10242E+03     ETASF =  0.10307E+01 TFSF =  0.22681E+01
DHSF =  0.28262E+04 TF =  401.640  ETA = 0.88500  CN =  2.800
AUXWK =  0.00000E+00
***** TURBINE  2 PARAMETERS *****
CNSF =  0.98131E+02     ETASF =  0.10587E+01   TFSF =  0.15636E+01
DHSF =  0.43749E+04  TF =  401.640   ETA = 0.90900 CN =  2.800
AUXWK =  0.00000E+00
***** TURBINE  3 PARAMETERS *****
CNSF =  0.91563E+02     ETASF =  0.10656E+01   TFSF =  0.88170E+00
```

DHSF = 0.11319E+05 TF = 401.640 ETA = 0.91500 CN = 2.800

AUXWK = 0.75000E+07

HETYP = 1.0 HEUA = 76.303

***** HEAT EXCHANGER HOT SIDE PARAMETERS *****

ETAD = 0.82000E+00 HEUA = 76.303 ETASF = 0.00000E+00

ETA = 0.8200 DLP = 0.0183 TOTHOT = 475.2595

***** CONVERGENT NOZZLE 2 PARAMETERS *****

NCOSF = 0.10000E+01 Area = 0.0566 Exit Velocity = 398.08

Gross Thrust = 31128.24 Nozzle Coeff. = 0.85251E+00

Scale Factor on above Mass Flows, Areas, Thrusts & Powers=1.0

Station	F.A.R.	Mass Flow	Pstatic	Ptotal	Tstatic	Ttotal	Vel	Area
1	0.00000	525.000	0.23517	0.36587	218.79	248.33	243.3	******
2	0.00000	525.000	******	0.36221	******	248.33	******	******
3	0.00000	525.000	******	0.54331	******	283.26	******	******
4	0.00000	58.333	******	0.54331	******	283.26	******	******
5	0.00000	58.333	******	2.71656	******	477.48	******	******
6	0.00000	58.333	******	2.71656	******	200.00	******	******
7	0.00000	58.333	******	13.58280	******	337.65	******	******
8	0.00000	46.667	******	13.58280	******	337.65	******	******
9	0.00000	46.667	******	13.17531	******	628.90	******	******
10	0.02716	47.934	******	12.38479	******	1550.00	******	******
11	0.02173	59.601	******	12.38479	******	1337.94	******	******
12	0.02173	59.601	******	8.15969	******	1228.27	******	******
13	0.02173	59.601	******	4.27154	******	1069.36	******	******
14	0.02173	59.601	******	0.60887	******	692.80	******	******
15	0.02173	59.601	******	0.59060	******	475.26	******	******

```
    16   0.02173    59.601    ******   5.61069  ******  475.26
******  ******

    17   0.02173    51.769    ******   4.87345  ******  475.26
******  ******

    18   0.02173    51.769   2.59962   4.87345  399.43  475.26
398.1  0.0566

    19   0.00000   466.667    ******   0.54331  ******  283.26
******  ******

    20   0.00000   466.667    ******   0.53788  ******  283.26
******  ******

    21   0.00000    11.667   0.28423  13.58280  235.96  337.65
308.1  3.5618

    22   0.00000    11.667    ******  13.44697  ******  337.65
******  ******


  Gross Thrust = 189699.88
 Momentum Drag = 127711.08
    Net Thrust =  61988.80
     Fuel Flow =    1.2676
        s.f.c. =  20.44918
    Sp. Thrust =   118.074
```

Appendix B HERMES

B.1 GEOMETRIC INPUT FILE FOR THE AIRCRAFT A380

```
!Input file for the geometric, mission and engine specifications of
the aircraft a380-800; Engine: TRENT900 ; Created by: Sarah Qureshi
Adapted from Boeing 737-800; Engine: CFM 56-7B27 input file
ENGINE_SPEC:RR_trent900
!GEOMETRIC DETAILS
! Wing Geometry
845             ! AcWingAInit - Wing area
7.5             ! AcWingAspr - Aspect ratio
0.203           ! AcWingCThir - Thickness chord ratio
33.5            ! AcWingSwpa - Sweep angle (in degrees)
0.26            ! AcWingTpr - Taper ratio
0.132           ! AcWingRtThir - Root thinkness ratio
0.087           ! AcWingOtThir - Outer thikness ratio
! Tailplane Geometry
222.57          ! AcTailAInit - Tailplane area
4.4             ! AcTailAspr - Aspect ratio
0.203           ! AcTailCThir - Thickness chord ratio
30.             ! AcTailSwpa - Sweep angle (in degrees)
0.383           ! AcTailTpr - Taper ratio
0.132           ! AcTailRtThir - Root thinkness ratio
0.087           ! AcTailOtThir - Outer thikness ratio
! Fin Geometry
134.2           ! AcFinA - Fin area
28.99           ! AcFinSpan - Span
0.115           ! AcFinCThir - Thickness chord ratio
28.99           ! AcFinSwpa - Sweep angle (in degrees)
0.424           ! AcFinTpr - Taper ratio
0.132           ! AcFinRtThir - Root thinkness ratio
0.087           ! AcFinOtThir - Outer thikness ratio
! Fuselage Geometry
7.14            ! AcFusDia - Diameter
70.4            ! AcFusLen - Length
! Landing Gear Characteristics
2               ! AcLGTyp1 - Landing gear type ***0=default, 1=Bogie,
2=Small twin wheel***
```

```
1                   ! AcLgTyp2= 0,1,2
1                   ! AcLgTyp3= 0,1,2
1                   ! AcLgTyp4= 0,1,2,-1 *** -1=if the aircraft only
has 3 LG -1 has to be declared
1                   ! AcLgTyp5= 0,1,2,-1 *** for the last 2 values
2                   ! AcLGDepl - Number of segments with LG down for
descent
! High lift systems
1                   ! AcFlapSegTo -Number of Segments with flaps
deployed during TO
3                   ! AcFlapSegApp - Number of Segments with flaps
deployed for approach
2                   ! ACFlapSegLand - Number of Segments with flaps
deployed during Landing
1.10        ! AcExtSrTo - Wing area extension ratio TO
1.15        ! AcExtSrApp - Wing area extension ratio approach
1.20        ! AcExtSrLand - Wing area extension ratio Landing
5.0                 ! AcFlapAngleTo - Flap Angle TO IN DEGREES
20.0        ! AcFlapAngleApp - Flap Angle Approach
30.0        ! AcFlapAngleLand - Flap Angle Land
1                   ! AcFlapSlots - Number of Flap Slots (1-3)
! Engine Geometry
2.946          ! EngNacDiaInit - Diameter (JANE's)
4.547          ! EngNacLenInit - Length (JANE's)
!XXXXXXXXXXXXXXXXXXXXXXXXXXXXXXXXXXXXXXXXXXXXXX
!MISSION/WEIGHT SPECIFICATION DATA
270010        ! AcAfrWtInit - Airframe weight (IHS)
4             ! AcEngNb - Number of Engines
6436          ! EngWtInit - Engine weight,  (kg/engine) (JANE's)
90975.        ! AcPldWt - Payload weight, (kg) (IHS)
100000        ! AcFuelWtInit - Fuel weight,  (kg) (NOT NECESSARY)
90975         ! AcPldWtmax  - Maximum payload weight, kg (IHS)
259465        ! AcFuelWtmax - Maximum fuel weight,  kg (IHS)
385995.       ! AcLandWtmax - Maximum landing weight, kg (IHS)
560000        ! AcToWtmax - Maximum take-off weight, kg (Source:
Jane’s)
0.0           ! DVFuelRatio - Diversion fuel weight to total fuel
weight (%)
0.1           ! AcFuelContpc - Relative contigency fuel to remain
after landing (%)
```

```
14816          ! AcRng - Range to be flown (km)       ! Mission (2)
0.0            ! AcRngdv - Diversion Range to be flown (km)
2              ! AcMisType - Mission to be flown (1-fixed fuel get
range) or (2-fixed range for given Pload get fuel)
1              ! DvMission - specify if diversion mission is to be
run (1- NO diversion mission) or (2- YES to diversion mission)
!XXXXXXXXXXXXXXXXXXXXXXXXXXXXXXXXXXXXXXXXXXXXXXXX
!CRUISE MAIN/DIVERSION AND HOLDING DATA
2              ! number of cruise altitudes and Mach numbers
1                   ! number of cruise Temperature Deviations from
ISA day (the trip is splitted equally into this number of parts.
Every part has the respective DTisa)
1              ! number of diversion cruise altitudes
5.             ! Cruise small segment time Interval in (min). This
value affects the accuracy of the calculations, so keep it small.
10058.,10670.            ! Cruise altitudes in [m] (WARNING: THE
ALTITUDES CANNOT BE THE SAME!!!!!!!!!!)
0.800,0.820        ! Cruise Mach numbers, the same number with
cruise altitudes
3.                 ! Cruise ambient temperature deviation from ISA,
in [K]
0.         ! Diversion cruise altitudes (m)
0.0          ! Diversion cruise Mach numbers,
0.0            ! Diversion cruise ambient temperature deviation
from ISA, in [K]
457.0          ! Holding altitude (m)
30.            ! Hold Time in (min)
!XXXXXXXXXXXXXXXXXXXXXXXXXXXXXXXXXXXXXXXXXXXXXXXX
!CLIMB DATA
22          ! Climb segments Number
! Altitudes(m)    | DTisa(K) | EAS(knots) | Power(0.-1.)
557.20 3. 250. 1.
900.00 3. 250. 1.
1500.00 3. 250. 1.
1981.20 3. 250. 1.
2438.40 3. 250. 1.
2743.20 3. 250. 1.
3048.00 3. 250. 1.
3048.10 3. 320. 1.
3657.60 3. 320. 1.
```

```
4267.20 3. 320. 1.
4876.80 3. 320. 1.
5486.40 3. 320. 1.
6096.00 3. 320. 1.
7620.00 3. 320. 1.
8077.20 3. 320. 1.
9144.00 3. 320. 1.
10058.00 3. 320. 1.
10668.00 3. 320. 1.
11227.00 3. 320. 1.
11887.00 3. 320. 1.
12000.00 3. 320. 1.
12496.8 3. 320.  1.
!XXXXXXXXXXXXXXXXXXXXXXXXXXXXXXXXXXXXXXXXXXXXXXXXXX
!DESCENT DATA
10          ! Descent segments Number
! The altitudes are dependent on the final cruise altitude. So they
are calculated inside the code.
! DTisa(K)  | TAS(knots) | Power(0.-1.) ****Note: the last 3 power
settings use the Approach rating
3. 233.1 1.                  ! Flight Idle Rating
3. 221.5 1.                  ! Flight Idle Rating
3. 202.9 1.                  ! Flight Idle Rating
3. 195.0 1.                  ! Flight Idle Rating
3. 183.1 1.                  ! Flight Idle Rating
3. 164.7 1.                  ! Flight Idle Rating
3. 150.9 1.                  ! Flight Idle Rating
3. 140.0 1.                 ! Approach Rating
3. 135.0 1.                  ! Approach Rating
3. 135.0 1.                  ! Approach Rating
!XXXXXXXXXXXXXXXXXXXXXXXXXXXXXXXXXXXXXXXXXXXXXXXXXX
!LANDING DATA
0.01       ! Note: Do not put final landing altitude = 0.0, use a
very small value instead.
135.00     ! Approach speed (TAS), in [m/s]
3.00       ! Deviation from standard atmosphere for Landing in [K]
6.00       ! Duration of Landing phase in [min]
!XXXXXXXXXXXXXXXXXXXXXXXXXXXXXXXXXXXXXXXXXXXXXXXXXX
```

```
!TAXI and TAKE-OFF DATA
0.02      ! AcTaxiCf1 - Runway Friction Coefficient
0.3       ! AcTaxiCf2 - Runway Friction Coefficient,BREAKES-OFF
10.0      ! AcTaxiTime - Taxi time in [min] (12mins for LR, 9mins
for SR)
1.0       ! AcToTime - Take-off time in [min]
0.00      ! AcToALT - Take-off altitude in [m]
3.00    ! Take-off temperature deviation from ISA in [K]
0.0           ! TakeOff Derate (Real Values from 0 to 1, 0.0->100%
of Maximum Thrust, 1.0->0% of Maximum Thrust)
!XXXXXXXXXXXXXXXXXXXXXXXXXXXXXXXXXXXXXXXXXXXXXXX
!NUMERICAL TOLERANCES AND INITIAL GUESSES
1.D-11                        ! Climb and Descent internal loops
relative accuracy
1.D-09                        ! Main mission range relative accuracy
1.D-09                        ! Diversion mission range relative
accuracy
1.D-07                        ! Fuel weight outer iteration loop
relative accuracy
480.D00                       ! Main mission duration guess 1 (for
secant method, modify it only if there is a convergence problem)
260.D00                       ! Main mission duration guess 2 (for
secant method, modify it only if there is a convergence problem)
!XXXXXXXXXXXXXXXXXXXXXXXXXXXXXXXXXXXXXXXXXXXXXXX
!TMATCHCALLS SPECIFICATIONS (*****HERMES DOES NOT READ THIS
PART*****)
!-------------------------------------------------------------------
--------
!Number of points in the Engine Design Point input file to be
skipped
!before the mission profile starts (including the design point)
1
!-------------------------------------------------------------------
!Burner exit station number
8
!-------------------------------------------------------------------
!ENGINE TET RANGE FOR EACH PHASE
24                     ! TET number for Take Off
2                      ! TET number for Climb
24                     ! TET number for Main and Diversion Cruise
```

```
2                       ! TET number for Flight Idle(Descent) and
Ground Idle
2                       ! TET number for Approach
20.                     ! TET step change in [K] for Take Off
20.                     ! TET step change in [K] for Climb
5.                      ! TET step change in [K] for Main and
Diversion Cruise
10.                     ! TET step change in [K] for Flight
Idle(Descent) and Ground Idle
5.                      ! TET step change in [K] for Approach
1800.            ! Max TET in [K] for Take Off
1800.            ! Max TET in [K] for Climb
1685.            ! Max TET in [K] for Main Mission Cruise
1310.            ! Max TET in [K] for Flight Idle(Descent) and
Ground Idle
1500.            ! Max TET in [K] for Approach
!-------------------------------------------------------------------
!ADDITIONAL ENGINE PERFORMANCE STATION VECTOR DATA (STATION, ITEM)
1                       ! Number of additional engine performance
station vector data
!Station | Item
8 6
!-------------------------------------------------------------------
!ADDITIONAL ENGINE PERFORMANCE BRICK DATA (DESCRIPTION, BRICK NO,
ITEM)
0                       ! Number of additional engine performance
brick data
!Description | BrickNo | Item     (WARNING: The BrickNo is defined
according to the tabular output file of turbomatch )
!-------------------------------------------------------------------
!ADDITIONAL OFF DESIGN ENGINE CONFIGURATIONS (LIKE BLEEDS etc.)
!Specify additional off design specification for each flight phase
(e.g. for brick data 26 "26 0.95")
0                       ! Number of additional off design
specifications for each flight phase
!You have to specify the same number of additional specs for all
the phases, i.e. if you specify something you have to do it for
every flight phase
!-------------------------------------------------------------------
!INPUT AND OUTPUT FILE PATHS
!Engine Design Point Specification file (input to
Hermes)RR_trent900.dat
```

B.2 INPUT FILE FOR THE TURBOFAN TRENT 900 ENGINE

```
HERMES Engine Performance Input Data File - All Data Refer to a
Single Engine !File created by: Fernando Lartategui Atela
```

Adapted from Boeing 737-800; Engine: CFM 56-7B27 engine file

```
!Engine performance data calculated from Turbomatch version 1.0 and
tabulated manually.
Altitude,Mach,DTisa:Increasing order, Thrust:Decreasing order

! TakeOff Rating Engine Performance Data Table Structure
  2 ! Take-Off Altitudes
  1 ! Take-Off DTisa Numbers
  9 ! Take-Off Mach Numbers
  2 ! Take-Off Data Rows
  2 ! Take-Off Additional Performance Data Columns
! Climb Rating Engine Performance Data Table Structure
 22 ! Climb Altitudes
  1 ! Climb DTisa Numbers
  1 ! Climb Mach Numbers
  2 ! Climb Data Rows
  2 ! Climb Additional Performance Data Columns
! Cruise Rating Engine Performance Data Table Structure
  2 ! Cruise Altitudes
  1 ! Cruise DTisa Numbers
  1 ! Cruise Mach Numbers
 24 ! Cruise Data Rows
  2 ! Cruise Additional Performance Data Columns
! Descent Rating Engine Performance Data Table Structure
 10 ! Descent Altitudes
  1 ! Descent DTisa Numbers
  1 ! Descent Mach Numbers
  2 ! Descent Data Rows
  2 ! Descent Additional Performance Data Columns
! Approach Rating Engine Performance Data Table Structure
  3 ! Approach Altitudes
  1 ! Approach DTisa Numbers
  1 ! Approach Mach Numbers
  2 ! Approach Data Rows
  2 ! Approach Additional Performance Data Columns
```

! Ground Idle Rating Engine Performance Data Table Structure

1 ! GroundIdle Altitudes

1 ! GroundIdle DTisa Numbers

9 ! GroundIdle Mach Numbers

2 ! GroundIdle Data Rows

2 ! GroundIdle Additional Performance Data Columns

! Engine Performance at Take-Off Rating

Net Thrust (kN)	**SFC (mg/Ns)**	**Altitude (m)**	**Dtisa**	**Mach**	**TET**
346.001	8.585	0	3	0	1800
338.698	8.476	0	3	0	1780
326.978	9.093	0	3	0.05	1800
340.366	8.995	0	3	0.05	1780
309.325	9.635	0	3	0.1	1800
302.646	9.523	0	3	0.1	1780
293.621	10.192	0	3	0.15	1800
286.678	10.095	0	3	0.15	1780
279.645	10.762	0	3	0.2	1800
272.777	10.669	0	3	0.2	1780
267.275	11.341	0	3	0.25	1800
259.994	11.263	0	3	0.25	1780
254.938	11.973	0	3	0.3	1800
247.107	11.933	0	3	0.3	1780
243.269	12.657	0	3	0.35	1800
235.79	12.604	0	3	0.35	1780
233.135	13.333	0	3	0.4	1800
225.705	13.291	0	3	0.4	1780
333.191	8.598	457.2	3	0	1800
327.201	8.49	457.2	3	0	1780
314.898	9.105	457.2	3	0.05	1800
308.544	9.011	457.2	3	0.05	1780
298.12	9.643	457.2	3	0.1	1800
291.947	9.547	457.2	3	0.1	1780
283.203	10.197	457.2	3	0.15	1800
277.185	10.097	457.2	3	0.15	1780
269.969	10.764	457.2	3	0.2	1800
263.82	10.667	457.2	3	0.2	1780
258.281	11.34	457.2	3	0.25	1800
252.371	11.23	457.2	3	0.25	1780
246.628	11.983	457.2	3	0.3	1800

239.958	11.899	457.2	3	0.3	1780
236.596	12.598	457.2	3	0.35	1800
229.482	12.542	457.2	3	0.35	1780
226.588	13.283	457.2	3	0.4	1800
219.426	13.239	457.2	3	0.4	1780

! Engine Performance at Climb Rating

Net Thrust (kN)	**SFC (mg/Ns)**	**Altitude (m)**	**Dtisa**	**Mach**	**TET**
244.471	12.118	450	3	0.31	1800
237.949	12.023	450	3	0.31	1780
235.124	12.191	900	3	0.319	1800
228.859	12.119	900	3	0.319	1780
221.328	12.367	1500	3	0.331	1800
216.578	12.262	1500	3	0.331	1780
211.324	12.479	1981.2	3	0.341	1800
206.677	12.379	1981.2	3	0.341	1780
201.965	12.598	2438.4	3	0.351	1800
197.533	12.497	2438.4	3	0.351	1780
196.045	12.668	2743.2	3	0.357	1800
191.723	12.568	2743.2	3	0.357	1780
190.158	12.749	3048	3	0.364	1800
185.942	12.65	3048	3	0.364	1780
172.689	14.869	3048.1	3	0.547	1800
167.846	14.812	3048.1	3	0.547	1780
162.6	15.108	3657.6	3	0.568	1800
158.7	15.018	3657.6	3	0.568	1780
153.291	15.332	4267.2	3	0.591	1800
149.665	15.238	4267.2	3	0.591	1780
144.406	15.573	4876.8	3	0.616	1800
140.932	15.485	4876.8	3	0.616	1780
136.101	15.803	5486.4	3	0.641	1800
132.801	15.717	5486.4	3	0.641	1780
128.12	16.066	6096	3	0.669	1800
125.024	15.98	6096	3	0.669	1780
109.917	16.768	7620	3	0.744	1800
107.473	16.652	7620	3	0.744	1780
105.079	16.978	8077.2	3	0.769	1800
102.637	16.879	8077.2	3	0.769	1780
94.66	17.067	9144	3	0.785	1800
92.495	16.964	9144	3	0.785	1780
86.266	17.21	10058	3	0.805	1800

84.311	17.104	10058	3	0.805	1780
80.96	17.321	10668	3	0.82	1800
79.137	17.215	10668	3	0.82	1780
75.449	17.3	11227	3	0.82	1800
73.767	17.191	11227	3	0.82	1780
67.986	17.301	11887	3	0.82	1800
66.475	17.191	11887	3	0.82	1780
66.785	17.3	12000	3	0.82	1800
65.299	17.191	12000	3	0.82	1780
61.749	17.301	12497	3	0.82	1800
60.376	17.192	12497	3	0.82	1780

! Engine Performance at Cruise Rating

Net Thrust (kN)	**SFC (mg/Ns)**	**Altitude (m)**	**Dtisa**	**Mach**	**TET**
75.298	16.558	10058	3	0.8	1685
74.757	16.547	10058	3	0.8	1680
74.268	16.525	10058	3	0.8	1675
73.776	16.503	10058	3	0.8	1670
73.285	16.482	10058	3	0.8	1665
72.796	16.461	10058	3	0.8	1660
72.309	16.44	10058	3	0.8	1655
71.825	16.418	10058	3	0.8	1650
71.34	16.397	10058	3	0.8	1645
70.859	16.376	10058	3	0.8	1640
70.379	16.355	10058	3	0.8	1635
69.901	16.334	10058	3	0.8	1630
69.425	16.313	10058	3	0.8	1625
68.95	16.292	10058	3	0.8	1620
68.478	16.271	10058	3	0.8	1615
68.007	16.25	10058	3	0.8	1610
67.538	16.228	10058	3	0.8	1605
67.055	16.209	10058	3	0.8	1600
66.5	16.202	10058	3	0.8	1595
65.96	16.191	10058	3	0.8	1590
65.428	16.18	10058	3	0.8	1585
64.894	16.169	10058	3	0.8	1580
64.307	16.162	10058	3	0.8	1575
63.675	16.165	10058	3	0.8	1570
70.614	16.724	10670	3	0.82	1685
70.183	16.699	10670	3	0.82	1680
69.74	16.674	10670	3	0.82	1675

69.297	16.65	10670	3	0.82	1670
68.856	16.626	10670	3	0.82	1665
68.414	16.602	10670	3	0.82	1660
67.955	16.581	10670	3	0.82	1655
67.499	16.559	10670	3	0.82	1650
67.044	16.538	10670	3	0.82	1645
66.591	16.517	10670	3	0.82	1640
66.14	16.495	10670	3	0.82	1635
65.691	16.474	10670	3	0.82	1630
65.243	16.453	10670	3	0.82	1625
64.797	16.431	10670	3	0.82	1620
64.353	16.41	10670	3	0.82	1615
63.91	16.389	10670	3	0.82	1610
63.469	16.368	10670	3	0.82	1605
63.029	16.347	10670	3	0.82	1600
62.591	16.325	10670	3	0.82	1595
62.155	16.304	10670	3	0.82	1590
61.721	16.283	10670	3	0.82	1585
61.232	16.271	10670	3	0.82	1580
60.723	16.262	10670	3	0.82	1575
60.229	16.251	10670	3	0.82	1570

! Engine Performance at Descent Rating

Net Thrust (kN)	**SFC (mg/Ns)**	**Altitude (m)**	**Dtisa**	**Mach**	**TET**
43.338	18.583	0	3	0.394	1310
40.803	19.018	0	3	0.394	1300
43.572	18.532	10	3	0.395	1310
40.758	19.038	10	3	0.395	1300
45.747	17.2	1333.5	3	0.415	1310
43.001	17.622	1333.5	3	0.415	1300
46.339	16.723	2667	3	0.455	1310
44.138	16.955	2667	3	0.455	1300
43.71	16.867	4000.5	3	0.504	1310
41.499	17.186	4000.5	3	0.504	1300
40.59	17.312	5334	3	0.57	1310
38.794	17.523	5334	3	0.57	1300
38.521	17.238	6667.5	3	0.618	1310
37.171	17.331	6667.5	3	0.618	1300
36.572	16.839	8001	3	0.654	1310
35.138	17.016	8001	3	0.654	1300
33.708	17.015	9334.5	3	0.727	1310

32.448	17.175	9334.5	3	0.727	1300
31.427	17.008	10668	3	0.8	1310
30.108	17.221	10668	3	0.8	1300

! Engine Performance at Approach Rating

Net Thrust (kN)	SFC (mg/Ns)	Altitude (m)	Dtisa	Mach	TET
111.548	14.076	0	3	0.394	1500
109.637	14.118	0	3	0.394	1495
112.291	13.988	10	3	0.395	1500
109.451	14.136	10	3	0.395	1495
106.246	13.898	1333.5	3	0.415	1500
104.67	13.9	1333.5	3	0.415	1495

! Engine Performance at Ground Idle Rating

Net Thrust (kN)	SFC (mg/Ns)	Altitude (m)	Dtisa	Mach	TET
96.074	7.854	0	3	0	1305
94.287	7.882	0	3	0	1300
90.683	8.33	0	3	0.025	1305
88.954	8.355	0	3	0.025	1300
85.673	8.82	0	3	0.05	1305
83.987	8.852	0	3	0.05	1300
81.028	9.331	0	3	0.075	1305
79.352	9.374	0	3	0.075	1300
76.655	9.87	0	3	0.1	1305
75.039	9.92	0	3	0.1	1300
72.566	10.436	0	3	0.125	1305
71.02	10.492	0	3	0.125	1300
68.776	11.026	0	3	0.15	1305
67.273	11.091	0	3	0.15	1300
65.209	11.645	0	3	0.175	1305
63.73	11.723	0	3	0.175	1300
61.881	12.292	0	3	0.2	1305
60.419	12.382	0	3	0.2	1300

B.2.1 AIRCRAFT FLIGHT PATH PERFORMANCE OUTPUT WITH A380-800 AIRCRAFT AND TURBOFAN TRENT900 ENGINE

ENGINE_SPEC:RR_trent900

```
 Aircraft weight L1 at beginning of climb:   645728.322077508
 Fuel burnt till top of climb (kg):   27867.9695123020
 Check :   27867.9695123020
 Aircraft weight(kg) at top of climb:   617860.352565206
 Distance flown during climb (km):   932.541823378191
 Climb duration (min):    67.4038563011300
 A/C weight at beginning of cruise:    617860.352565206
Cruise data
Dt of each cruise segement:   5.00 min
First and last cruise segment duration:   2.50 min
 Nacelle. Drag Coeff (Mid-Cr):  6.708458838222480E-004
 Nacelle. Drag (Mid-Cr):   6.36419327795167      (kN)
 Cruise duration:   919.399552620642      (min)
 Aircraft weight at END of cruise (kg):   380772.400906589
 Distance flown during cruise (km):   13466.3494852038
 A/C weight at beginning of cruise, Check:   617860.352565206
 Aircraft weight L1 at beginning of descent:   380772.400906589
 Fuel burnt in descent segment (kg):   5828.61340509956
 Aircraft weight (kg) at END of descent (kg):    374943.787501490
 Distance flown during descent (km):   417.108691448709
 Descent duration (min):    35.6752983842790
 Fuel burnt during landing (kg):    2261.01641785721
 (NOTE: Landing distance not included in range)
 Distance flown during landing (km):   48.6000000000000
 ----------------------------------------
 STALL SPEED (m/s)           =        84.146208
 FAILURE SPEED (V1)          =        87.737213
 LIFT-OFF SPEED (m/s)        =        92.560829
 V2         (m/s)       =       100.975449
 ----------------------------------------
 ********************************************************
 **         ALL ENGINES OPERATE (AEO)          **
 ********************************************************
 ------------------------------------------------------------
 GROUND DISTANCE (GROUND ROLL)          (km)       =
3.258915
 DISTANCE TO THE SCREEN HEIGHT          (km)       =
0.317668
```

```
 FAR TAKE-OFF DISTANCE            (km)       =         4.113071
 ================================================================
 HEIGHT AT END OF TRANSITION      (m)        =        55.900482
 ================================================================
 TAKE-OFF FLIGHT PATH             (km)       =         4.260511
 ----------------------------------------------------------------
 TOTAL TAKE-OFF FLIGHT PATH TO ALT. = 1500FT (km)   =
7.962373
 ================================================================
 ********************************************************
 **         ONE ENGINE INOPERATIVE (OEI)       **
 ********************************************************
 ----------------------------------------------------------------
 BALANCED FIELD LENGTH            (km)       =         4.457000
 ----------------------------------------------------------------
 FROM THE SCREEN TO THE END OF TRANSITION (km)           =
0.125279
 ----------------------------------------------------------------
 CLIMB TO 400FT                   (km)       =         0.700915
 ACCELERATION TO VC(250KT)        (km)       =         1.953544
 CLIMB TO 1500FT            (km)       =         5.166972
 ================================================================
 TAKE-OFF FLIGHT PATH             (km)       =        7.821430
 ----------------------------------------------------------------
 TOTAL TAKE-OFF FLIGHT PATH TO ALT. = 1500FT (TOFP)(km) =
12.278430
 ================================================================
 The fuel weight in Kg for TAXI is:
2390.72809149038
 The fuel weight in Kg for TAKE-OFF is:
712.900460400000
 ================================================================
 Main Mission Range:        14816.0000000307      km
 Range Error:   2.070709250336332E-010 %
 Main Block Range:          14872.5623728311      km
 Main Mission TIME:         1022.47870730605      min
 Main Block TIME:           17.3246451217675      hr
 Mean Mission speed:       241.504621631140      m/s
 Mean Block speed:         238.461873057110      m/s
```

```
 Main Mission Fuel:          270784.534576018       kg
 Main Block Fuel:            273045.550993875       kg
=================================================================

  Overall Flight duration:   1022.47870730605       min
17.0413117884342       hr
```

AIRCRAFT PERFORMANCE DURING CLIMB CONDITION

Seg_No	ALT (m)	ALT (ft)	TIME(min)	TIME(hrs)	Thrust (KN) /Engine	SFC (mg/Ns)	Segment Fuel(kg)	EAS (m/s)	TAS (m/s)
1	557.2	1828.084	0	0	253.818	12.045	0	128.6111	132.8122
2	900	2952.7559	0.4572	0.0076	235.124	12.191	325.0446	128.6111	135.057
3	1500	4921.2598	1.3496	0.0225	221.328	12.367	600.2214	128.6111	139.1224
4	1981.2	6500	2.1135	0.0352	211.324	12.479	492.7203	128.6111	142.5142
5	2438.4	8000	2.8827	0.048	201.965	12.598	478.2949	128.6111	145.8507
6	2743.2	9000	3.4215	0.057	196.045	12.668	325.1309	128.6111	148.1392
7	3048	10000	3.9714	0.0662	190.158	12.749	323.8704	128.6111	150.4809
8	3048	10000	5.1495	0.0858	172.689	14.869	708.3406	164.6222	192.6156
9	3657.6	12000	6.3445	0.1057	162.6	15.108	720.628	164.6222	198.8231
10	4267.2	14000	7.6717	0.1279	153.291	15.332	765.7356	164.6222	205.3292
11	4876.8	16000	9.1585	0.1526	144.406	15.573	820.7172	164.6222	212.1532
12	5486.4	18000	10.8429	0.1807	136.101	15.803	889.4989	164.6222	219.316
13	6096	20000	12.7873	0.2131	128.12	16.066	982.3581	164.6222	226.84
14	7620	25000	18.5589	0.3093	109.917	16.768	2706.5814	164.6222	247.3963
15	8077.2	26500	20.518	0.342	105.079	16.978	852.8077	160.5787	247.8568
16	9144	30000	26.462	0.441	94.66	17.067	2425.1969	148.4628	244.2294
17	10058	32998.6877	36.8318	0.6139	86.266	17.21	3858.5588	138.5464	241.0781

Seg_No	Mach	Climb Rate (m/s)	Dist_(m)	Dist_(m) Cum	Climb Gradient (deg)	DragCoeff aircraft	LiftCoeff aircraft	DragCoeff Nacelle	Drag Nacelle (KN)
1	0.3905	12.4973	0	0	5.3308	0.0375	0.7406	0.0007	5.7336
2	0.3987	11.2054	3657.9259	3657.9259	4.6728	0.0404	0.7402	0.0007	5.7395
3	0.4135	10.4983	7316.142	10974.0679	4.2636	0.0404	0.7395	0.0007	5.7496
4	0.426	9.9069	6436.6618	17410.7297	3.9307	0.0403	0.739	0.0007	5.7574
5	0.4383	9.4273	6638.2847	24049.0144	3.6696	0.0403	0.7384	0.0007	5.7647
6	0.4468	9.2381	4742.8444	28791.8588	3.5405	0.0403	0.738	0.0007	5.7694
7	0.4555	0	4916.8929	33708.7517	0	0.0403	0.7377	0.0007	5.7741
8	0.583	8.5024	12125.8629	45834.6146	2.4875	0.0243	0.4497	0.0006	9.0143
9	0.6063	7.655	14019.3514	59853.966	2.1694	0.0242	0.4492	0.0006	9.0194
10	0.6308	6.8337	16080.538	75934.504	1.8751	0.0242	0.4487	0.0006	9.0229
11	0.6567	6.0317	18610.8399	94545.3439	1.6015	0.0242	0.4481	0.0006	9.0245
12	0.6842	5.2253	21794.8709	116340.2149	1.3418	0.0242	0.4475	0.0006	9.0241
13	0.7132	4.4008	26017.8697	142358.0846	1.0633	0.0241	0.4468	0.0006	9.0213
14	0.7936	3.8896	82099.9413	224458.0259	0.8999	0.024	0.4449	0.0006	9.002
15	0.8	2.9912	29103.2873	253561.3132	0.6965	0.025	0.467	0.0006	8.6114
16	0.8	1.469	87742.4866	341303.7998	0.3469	0.0288	0.5442	0.0007	7.4933
17	0.8	0.3325	150973.3944	492277.1942	0.0794	0.033	0.6211	0.0007	6.6297

AIRCRAFT PERFORMANCE DURING CRUISE CONDITION (I)

Seg No	TIME (hrs)	ALT (m)	ALT (ft)	Thrust (KN /Engine	SFC (mg/Ns)	Segment Fuel(kg)	Dist(km)	Fuel Cum (Kg)	Dist(km) Cum	L/D	DragCoeff aircraft	LiftCoeff aircraft	DragCoeff Nacelle	Drag (KN) Nacelle
1	0.0416	10058	32.9987	80.4754	16.6633	804.0653	36.1381	804.0653	36.1381	18.8294	0.0324	0.6106	0.0007	6.6297
2	0.1249	10058	32.9987	80.3677	16.6611	1605.767	72.2762	2409.833	108.4144	18.8301	0.0324	0.6098	0.0007	6.6297
3	0.2082	10058	32.9987	80.1531	16.6567	1601.059	72.2762	4010.892	180.6906	18.8314	0.0323	0.6083	0.0007	6.6297
4	0.2915	10058	32.9987	79.9396	16.6524	1596.379	72.2762	5607.271	252.9668	18.8325	0.0322	0.6067	0.0007	6.6297
5	0.3748	10058	32.9987	79.7273	16.6481	1591.727	72.2762	7198.997	325.2431	18.8336	0.0321	0.6051	0.0007	6.6297
6	0.458	10058	32.9987	79.5162	16.6438	1587.102	72.2762	8786.1	397.5193	18.8345	0.032	0.6035	0.0007	6.6297
7	0.5413	10058	32.9987	79.3062	16.6395	1582.506	72.2762	10368.61	469.7955	18.8353	0.032	0.6019	0.0007	6.6297
8	0.6246	10058	32.9987	79.0974	16.6353	1577.936	72.2762	11946.54	542.0718	18.8359	0.0319	0.6004	0.0007	6.6297
9	0.7079	10058	32.9987	78.8898	16.631	1573.394	72.2762	13519.94	614.348	18.8365	0.0318	0.5988	0.0007	6.6297
10	0.7911	10058	32.9987	78.6832	16.6268	1568.879	72.2762	15088.81	686.6243	18.8369	0.0317	0.5973	0.0007	6.6297
11	0.8744	10058	32.9987	78.4778	16.6227	1564.39	72.2762	16653.2	758.9005	18.8371	0.0316	0.5957	0.0007	6.6297
12	0.9577	10058	32.9987	78.2735	16.6185	1559.928	72.2762	18213.13	831.1767	18.8373	0.0315	0.5942	0.0007	6.6297
13	1.041	10058	32.9987	78.0704	16.6144	1555.492	72.2762	19768.62	903.453	18.8373	0.0315	0.5926	0.0007	6.6297
14	1.1243	10058	32.9987	77.8683	16.6103	1551.082	72.2762	21319.71	975.7292	18.8372	0.0314	0.5911	0.0007	6.6297
15	1.2075	10058	32.9987	77.6673	16.6062	1546.698	72.2762	22866.4	1048.005	18.837	0.0313	0.5896	0.0007	6.6297
16	1.2908	10058	32.9987	77.4674	16.6021	1542.34	72.2762	24408.74	1120.282	18.8366	0.0312	0.588	0.0007	6.6297
17	1.3741	10058	32.9987	77.2686	16.5981	1538.007	72.2762	25946.75	1192.558	18.8361	0.0311	0.5865	0.0007	6.6297
18	1.4574	10058	32.9987	77.0709	16.594	1533.7	72.2762	27480.45	1264.834	18.8355	0.0311	0.585	0.0007	6.6297
19	1.5407	10058	32.9987	76.8742	16.59	1529.418	72.2762	29009.87	1337.11	18.8347	0.031	0.5835	0.0007	6.6297
20	1.6239	10058	32.9987	76.6786	16.5861	1525.16	72.2762	30535.03	1409.387	18.8339	0.0309	0.582	0.0007	6.6297
21	1.7072	10058	32.9987	76.484	16.5821	1520.927	72.2762	32055.96	1481.663	18.8329	0.0308	0.5805	0.0007	6.6297
22	1.7905	10058	32.9987	76.2905	16.5782	1516.719	72.2762	33572.68	1553.939	18.8318	0.0307	0.579	0.0007	6.6297
23	1.8738	10058	32.9987	76.098	16.5743	1512.535	72.2762	35085.21	1626.215	18.8305	0.0307	0.5775	0.0007	6.6297
24	1.9571	10058	32.9987	75.9066	16.5704	1508.376	72.2762	36593.59	1698.492	18.8291	0.0306	0.576	0.0007	6.6297
25	2.0403	10058	32.9987	75.7161	16.5665	1504.24	72.2762	38097.83	1770.768	18.8276	0.0305	0.5745	0.0007	6.6297
26	2.1236	10058	32.9987	75.5267	16.5627	1500.128	72.2762	39597.95	1843.044	18.826	0.0304	0.573	0.0007	6.6297
27	2.2069	10058	32.9987	75.3383	16.5588	1496.039	72.2762	41093.99	1915.32	18.8243	0.0304	0.5715	0.0007	6.6297
28	2.2902	10058	32.9987	75.1509	16.555	1491.974	72.2762	42585.97	1987.597	18.8224	0.0303	0.57	0.0007	6.6297
29	2.3734	10058	32.9987	74.9645	16.5512	1487.932	72.2762	44073.9	2059.873	18.8204	0.0302	0.5685	0.0007	6.6297
30	2.4567	10058	32.9987	74.779	16.5474	1483.913	72.2762	45557.81	2132.149	18.8183	0.0301	0.5671	0.0007	6.6297
31	2.54	10058	32.9987	74.5946	16.5397	1479.559	72.2762	47037.37	2204.425	18.816	0.0301	0.5656	0.0007	6.6297
32	2.6233	10058	32.9987	74.4111	16.5314	1475.184	72.2762	48512.56	2276.702	18.8136	0.03	0.5641	0.0007	6.6297
33	2.7066	10058	32.9987	74.2287	16.5232	1470.838	72.2762	49983.39	2348.978	18.8111	0.0299	0.5627	0.0007	6.6297
34	2.7898	10058	32.9987	74.0473	16.5151	1466.523	72.2762	51449.92	2421.254	18.8085	0.0298	0.5612	0.0007	6.6297
35	2.8731	10058	32.9987	73.8669	16.5071	1462.235	72.2762	52912.15	2493.53	18.8057	0.0298	0.5598	0.0007	6.6297
36	2.9564	10058	32.9987	73.6874	16.4992	1457.989	72.2762	54370.14	2565.806	18.8029	0.0297	0.5583	0.0007	6.6297
37	3.0397	10058	32.9987	73.509	16.4916	1453.786	72.2762	55823.93	2638.083	18.7999	0.0296	0.5569	0.0007	6.6297
38	3.123	10058	32.9987	73.3315	16.484	1449.609	72.2762	57273.54	2710.359	18.7968	0.0296	0.5555	0.0007	6.6297
39	3.2062	10058	32.9987	73.155	16.4764	1445.455	72.2762	58718.99	2782.635	18.7935	0.0295	0.554	0.0007	6.6297
40	3.2895	10670	35.0066	72.9774	16.8611	1475.611	73.4276	60194.6	2856.063	18.7907	0.0308	0.5782	0.0007	6.3642
41	3.3728	10670	35.0066	72.7904	16.8502	1470.882	73.4276	61665.48	2929.49	18.7892	0.0307	0.5767	0.0007	6.3642
42	3.4561	10670	35.0066	72.6044	16.8395	1466.185	73.4276	63131.67	3002.918	18.7877	0.0306	0.5751	0.0007	6.3642
43	3.5394	10670	35.0066	72.4195	16.8287	1461.52	73.4276	64593.19	3076.346	18.786	0.0305	0.5736	0.0007	6.3642
44	3.6226	10670	35.0066	72.2357	16.8181	1456.887	73.4276	66050.07	3149.773	18.7842	0.0305	0.5721	0.0007	6.3642
45	3.7059	10670	35.0066	72.053	16.8075	1452.285	73.4276	67502.36	3223.201	18.7822	0.0304	0.5706	0.0007	6.3642
46	3.7892	10670	35.0066	71.8713	16.7969	1447.715	73.4276	68950.07	3296.628	18.7801	0.0303	0.5691	0.0007	6.3642
47	3.8725	10670	35.0066	71.6906	16.7865	1443.175	73.4276	70393.25	3370.056	18.7779	0.0302	0.5676	0.0007	6.3642
48	3.9557	10670	35.0066	71.511	16.776	1438.666	73.4276	71831.92	3443.483	18.7756	0.0302	0.5661	0.0007	6.3642
49	4.039	10670	35.0066	71.3325	16.7657	1434.188	73.4276	73266.1	3516.911	18.7731	0.0301	0.5646	0.0007	6.3642
50	4.1223	10670	35.0066	71.1549	16.7554	1429.74	73.4276	74695.84	3590.339	18.7706	0.03	0.5631	0.0007	6.3642
51	4.2056	10670	35.0066	70.9784	16.7451	1425.321	73.4276	76121.16	3663.766	18.7678	0.0299	0.5617	0.0007	6.3642
52	4.2889	10670	35.0066	70.8029	16.735	1420.932	73.4276	77542.1	3737.194	18.765	0.0299	0.5602	0.0007	6.3642
53	4.3721	10670	35.0066	70.6284	16.7248	1416.572	73.4276	78958.67	3810.621	18.762	0.0298	0.5587	0.0007	6.3642
54	4.4554	10670	35.0066	70.4548	16.7148	1412.241	73.4276	80370.91	3884.049	18.7589	0.0297	0.5573	0.0007	6.3642
55	4.5387	10670	35.0066	70.2823	16.7048	1407.939	73.4276	81778.85	3957.477	18.7557	0.0296	0.5558	0.0007	6.3642
56	4.622	10670	35.0066	70.1107	16.6949	1403.675	73.4276	83182.52	4030.904	18.7523	0.0296	0.5543	0.0007	6.3642
57	4.7053	10670	35.0066	69.9401	16.6853	1399.452	73.4276	84581.97	4104.332	18.7489	0.0295	0.5529	0.0007	6.3642
58	4.7885	10670	35.0066	69.7705	16.6757	1395.256	73.4276	85977.23	4177.759	18.7453	0.0294	0.5514	0.0007	6.3642
59	4.8718	10670	35.0066	69.6018	16.6665	1391.114	73.4276	87368.35	4251.187	18.7415	0.0293	0.55	0.0007	6.3642
60	4.9551	10670	35.0066	69.434	16.6574	1387.005	73.4276	88755.35	4324.615	18.7377	0.0293	0.5486	0.0007	6.3642
61	5.0384	10670	35.0066	69.2672	16.6484	1382.921	73.4276	90138.27	4398.042	18.7337	0.0292	0.5471	0.0007	6.3642
62	5.1217	10670	35.0066	69.1013	16.6394	1378.861	73.4276	91517.13	4471.47	18.7296	0.0291	0.5457	0.0007	6.3642

AIRCRAFT PERFORMANCE DURING CRUISE CONDITION (II)

Seg No	TIME (hrs)	ALT (m)	ALT (ft)	Thrust (KN /Engine	SFC (mg/Ns)	Segment Fuel(kg)	Dist(km)	Fuel Cum (Kg)	Dist(km) Cum	L/D	DragCoeff aircraft	LiftCoeff aircraft	DragCoeff Nacelle	Drag (KN) Nacelle
63	5.2049	10670	35.0066	68.9364	16.6304	1374.827	73.4276	92891.96	4544.897	18.7253	0.0291	0.5443	0.0007	6.3642
64	5.2882	10670	35.0066	68.7723	16.6215	1370.82	73.4276	94262.78	4618.325	18.721	0.029	0.5429	0.0007	6.3642
65	5.3715	10670	35.0066	68.6091	16.6126	1366.839	73.4276	95629.62	4691.753	18.7165	0.0289	0.5414	0.0007	6.3642
66	5.4548	10670	35.0066	68.4469	16.6038	1362.883	73.4276	96992.5	4765.18	18.7119	0.0289	0.54	0.0007	6.3642
67	5.538	10670	35.0066	68.2855	16.5961	1359.042	73.4276	98351.54	4838.608	18.7072	0.0288	0.5386	0.0007	6.3642
68	5.6213	10670	35.0066	68.125	16.5888	1355.248	73.4276	99706.79	4912.035	18.7023	0.0287	0.5372	0.0007	6.3642
69	5.7046	10670	35.0066	67.9654	16.5815	1351.478	73.4276	101058.3	4985.463	18.6973	0.0287	0.5358	0.0007	6.3642
70	5.7879	10670	35.0066	67.8066	16.5738	1347.7	73.4276	102406	5058.89	18.6922	0.0286	0.5344	0.0007	6.3642
71	5.8712	10670	35.0066	67.6487	16.5662	1343.943	73.4276	103749.9	5132.318	18.687	0.0285	0.533	0.0007	6.3642
72	5.9544	10670	35.0066	67.4917	16.5587	1340.211	73.4276	105090.1	5205.746	18.6816	0.0285	0.5316	0.0007	6.3642
73	6.0377	10670	35.0066	67.3355	16.5515	1336.527	73.4276	106426.7	5279.173	18.6762	0.0284	0.5302	0.0007	6.3642
74	6.121	10670	35.0066	67.1801	16.5443	1332.865	73.4276	107759.5	5352.601	18.6706	0.0283	0.5289	0.0007	6.3642
75	6.2043	10670	35.0066	67.0255	16.5371	1329.225	73.4276	109088.7	5426.028	18.6649	0.0283	0.5275	0.0007	6.3642
76	6.2876	10670	35.0066	66.8718	16.53	1325.605	73.4276	110414.3	5499.456	18.659	0.0282	0.5261	0.0007	6.3642
77	6.3708	10670	35.0066	66.7189	16.5229	1322.007	73.4276	111736.4	5572.884	18.6531	0.0281	0.5247	0.0007	6.3642
78	6.4541	10670	35.0066	66.5668	16.5158	1318.426	73.4276	113054.8	5646.311	18.647	0.0281	0.5234	0.0007	6.3642
79	6.5374	10670	35.0066	66.4155	16.5084	1314.842	73.4276	114369.6	5719.739	18.6408	0.028	0.522	0.0007	6.3642
80	6.6207	10670	35.0066	66.2651	16.5011	1311.279	73.4276	115680.9	5793.166	18.6344	0.0279	0.5206	0.0007	6.3642
81	6.704	10670	35.0066	66.1154	16.4938	1307.742	73.4276	116988.6	5866.594	18.628	0.0279	0.5193	0.0007	6.3642
82	6.7872	10670	35.0066	65.9665	16.4869	1304.246	73.4276	118292.9	5940.022	18.6214	0.0278	0.5179	0.0007	6.3642
83	6.8705	10670	35.0066	65.8184	16.48	1300.771	73.4276	119593.7	6013.449	18.6147	0.0278	0.5166	0.0007	6.3642
84	6.9538	10670	35.0066	65.6711	16.4731	1297.317	73.4276	120891	6086.877	18.6079	0.0277	0.5152	0.0007	6.3642
85	7.0371	10670	35.0066	65.5245	16.4662	1293.882	73.4276	122184.9	6160.304	18.6009	0.0276	0.5139	0.0007	6.3642
86	7.1203	10670	35.0066	65.3787	16.4594	1290.468	73.4276	123475.3	6233.732	18.5939	0.0276	0.5126	0.0007	6.3642
87	7.2036	10670	35.0066	65.2337	16.4525	1287.071	73.4276	124762.4	6307.16	18.5867	0.0275	0.5112	0.0007	6.3642
88	7.2869	10670	35.0066	65.0894	16.4454	1283.67	73.4276	126046.1	6380.587	18.5794	0.0274	0.5099	0.0007	6.3642
89	7.3702	10670	35.0066	64.9459	16.4383	1280.288	73.4276	127326.4	6454.015	18.572	0.0274	0.5086	0.0007	6.3642
90	7.4535	10670	35.0066	64.8032	16.4313	1276.927	73.4276	128603.3	6527.442	18.5644	0.0273	0.5072	0.0007	6.3642
91	7.5367	10670	35.0066	64.6612	16.4246	1273.607	73.4276	129876.9	6600.87	18.5568	0.0273	0.5059	0.0007	6.3642
92	7.62	10670	35.0066	64.5199	16.4179	1270.307	73.4276	131147.2	6674.297	18.549	0.0272	0.5046	0.0007	6.3642
93	7.7033	10670	35.0066	64.3793	16.4112	1267.027	73.4276	132414.2	6747.725	18.5411	0.0271	0.5033	0.0007	6.3642
94	7.7866	10670	35.0066	64.2395	16.4046	1263.765	73.4276	133678	6821.153	18.5331	0.0271	0.502	0.0007	6.3642
95	7.8699	10670	35.0066	64.1004	16.398	1260.522	73.4276	134938.5	6894.58	18.5249	0.027	0.5007	0.0007	6.3642
96	7.9531	10670	35.0066	63.9621	16.3915	1257.298	73.4276	136195.8	6968.008	18.5167	0.027	0.4994	0.0007	6.3642
97	8.0364	10670	35.0066	63.8244	16.3849	1254.091	73.4276	137449.9	7041.435	18.5083	0.0269	0.4981	0.0007	6.3642
98	8.1197	10670	35.0066	63.6875	16.3784	1250.902	73.4276	138700.8	7114.863	18.4998	0.0269	0.4968	0.0007	6.3642
99	8.203	10670	35.0066	63.5512	16.3719	1247.731	73.4276	139948.5	7188.291	18.4912	0.0268	0.4955	0.0007	6.3642
100	8.2863	10670	35.0066	63.4157	16.3655	1244.579	73.4276	141193.1	7261.718	18.4825	0.0267	0.4942	0.0007	6.3642
101	8.3695	10670	35.0066	63.2808	16.359	1241.444	73.4276	142434.6	7335.146	18.4736	0.0267	0.4929	0.0007	6.3642
102	8.4528	10670	35.0066	63.1467	16.3526	1238.327	73.4276	143672.9	7408.573	18.4647	0.0266	0.4916	0.0007	6.3642
103	8.5361	10670	35.0066	63.0132	16.3462	1235.225	73.4276	144908.1	7482.001	18.4556	0.0266	0.4903	0.0007	6.3642
104	8.6194	10670	35.0066	62.8804	16.3395	1232.119	73.4276	146140.2	7555.429	18.4464	0.0265	0.4891	0.0007	6.3642
105	8.7026	10670	35.0066	62.7483	16.3329	1229.031	73.4276	147369.3	7628.856	18.4371	0.0265	0.4878	0.0007	6.3642
106	8.7859	10670	35.0066	62.6168	16.3263	1225.96	73.4276	148595.2	7702.284	18.4276	0.0264	0.4865	0.0007	6.3642
107	8.8692	10670	35.0066	62.4861	16.3199	1222.924	73.4276	149818.1	7775.711	18.4181	0.0263	0.4853	0.0007	6.3642
108	8.9525	10670	35.0066	62.3559	16.3137	1219.909	73.4276	151038	7849.139	18.4084	0.0263	0.484	0.0007	6.3642
109	9.0358	10670	35.0066	62.2265	16.3074	1216.911	73.4276	152255	7922.566	18.3986	0.0262	0.4827	0.0007	6.3642
110	9.119	10670	35.0066	62.0977	16.3012	1213.93	73.4276	153468.9	7995.994	18.3887	0.0262	0.4815	0.0007	6.3642
111	9.2023	10670	35.0066	61.9696	16.295	1210.964	73.4276	154679.9	8069.422	18.3787	0.0261	0.4802	0.0007	6.3642
112	9.2856	10670	35.0066	61.8421	16.2889	1208.015	73.4276	155887.9	8142.849	18.3686	0.0261	0.479	0.0007	6.3642
113	9.3689	10670	35.0066	61.7152	16.2829	1205.093	73.4276	157093	8216.277	18.3583	0.026	0.4777	0.0007	6.3642
114	9.4522	10670	35.0066	61.589	16.2798	1202.4	73.4276	158295.4	8289.704	18.348	0.026	0.4765	0.0007	6.3642
115	9.5354	10670	35.0066	61.4634	16.2767	1199.72	73.4276	159495.1	8363.132	18.3375	0.0259	0.4752	0.0007	6.3642
116	9.6187	10670	35.0066	61.3384	16.2736	1197.055	73.4276	160692.1	8436.56	18.3269	0.0259	0.474	0.0007	6.3642
117	9.702	10670	35.0066	61.214	16.2707	1194.412	73.4276	161886.5	8509.987	18.3162	0.0258	0.4727	0.0007	6.3642
118	9.7853	10670	35.0066	61.0902	16.2685	1191.836	73.4276	163078.4	8583.415	18.3053	0.0258	0.4715	0.0007	6.3642
119	9.8686	10670	35.0066	60.967	16.2663	1189.273	73.4276	164267.7	8656.842	18.2944	0.0257	0.4703	0.0007	6.3642
120	9.9518	10670	35.0066	60.8444	16.2641	1186.723	73.4276	165454.4	8730.27	18.2833	0.0257	0.469	0.0007	6.3642
121	10.0351	10670	35.0066	60.7223	16.262	1184.185	73.4276	166638.6	8803.698	18.2721	0.0256	0.4678	0.0007	6.3642
122	10.1184	10670	35.0066	60.6009	16.2593	1181.62	73.4276	167820.2	8877.125	18.2608	0.0256	0.4666	0.0007	6.3642
123	10.2017	10670	35.0066	60.48	16.2566	1179.068	73.4276	168999.3	8950.553	18.2494	0.0255	0.4654	0.0007	6.3642
124	10.2849	10670	35.0066	60.3597	16.2539	1176.528	73.4276	170175.8	9023.98	18.2379	0.0254	0.4642	0.0007	6.3642

AIRCRAFT PERFORMANCE DURING CRUISE CONDITION (III)

Seg No	TIME (hrs)	ALT (m)	ALT (ft)	Thrust (KN /Engine	SFC (mg/Ns)	Segment Fuel(kg)	Dist(km)	Fuel Cum (Kg)	Dist(km) Cum	L/D	DragCoeff aircraft	LiftCoeff aircraft	DragCoeff Nacelle	Drag (KN) Nacelle
125	10.3682	10670	35.0066	60.2399	16.2512	1174.002	73.4276	171349.8	9097.408	18.2262	0.0254	0.4629	0.0007	6.3642
126	10.4515	10670	35.0066	60.1208	16.2486	1171.489	73.4276	172521.3	9170.836	18.2145	0.0253	0.4617	0.0007	6.3642
127	10.5348	10670	35.0066	60.0022	16.2459	1168.988	73.4276	173690.3	9244.263	18.2026	0.0253	0.4605	0.0007	6.3642
128	10.6181	10670	35.0066	59.8842	16.2433	1166.5	73.4276	174856.8	9317.691	18.1906	0.0252	0.4593	0.0007	6.3642
129	10.7013	10670	35.0066	59.7667	16.2407	1164.024	73.4276	176020.8	9391.118	18.1785	0.0252	0.4581	0.0007	6.3642
130	10.7846	10670	35.0066	59.6498	16.2381	1161.561	73.4276	177182.3	9464.546	18.1662	0.0252	0.4569	0.0007	6.3642
131	10.8679	10670	35.0066	59.5334	16.2355	1159.11	73.4276	178341.5	9537.973	18.1539	0.0251	0.4557	0.0007	6.3642
132	10.9512	10670	35.0066	59.4176	16.2329	1156.672	73.4276	179498.1	9611.401	18.1414	0.0251	0.4545	0.0007	6.3642
133	11.0345	10670	35.0066	59.3024	16.2304	1154.245	73.4276	180652.4	9684.829	18.1288	0.025	0.4533	0.0007	6.3642
134	11.1177	10670	35.0066	59.1877	16.2278	1151.831	73.4276	181804.2	9758.256	18.1162	0.025	0.4521	0.0007	6.3642
135	11.201	10670	35.0066	59.0735	16.2253	1149.429	73.4276	182953.6	9831.684	18.1033	0.0249	0.4509	0.0007	6.3642
136	11.2843	10670	35.0066	58.9599	16.2227	1147.039	73.4276	184100.7	9905.111	18.0904	0.0249	0.4497	0.0007	6.3642
137	11.3676	10670	35.0066	58.8468	16.2202	1144.661	73.4276	185245.3	9978.539	18.0774	0.0248	0.4485	0.0007	6.3642
138	11.4509	10670	35.0066	58.7342	16.2177	1142.295	73.4276	186387.6	10051.97	18.0642	0.0248	0.4474	0.0007	6.3642
139	11.5341	10670	35.0066	58.6222	16.2152	1139.941	73.4276	187527.6	10125.39	18.051	0.0247	0.4462	0.0007	6.3642
140	11.6174	10670	35.0066	58.5106	16.2127	1137.598	73.4276	188665.2	10198.82	18.0376	0.0247	0.445	0.0007	6.3642
141	11.7007	10670	35.0066	58.3997	16.2103	1135.267	73.4276	189800.4	10272.25	18.0241	0.0246	0.4438	0.0007	6.3642
142	11.784	10670	35.0066	58.2892	16.2078	1132.948	73.4276	190933.4	10345.68	18.0105	0.0246	0.4426	0.0007	6.3642
143	11.8672	10670	35.0066	58.1792	16.2054	1130.64	73.4276	192064	10419.1	17.9968	0.0245	0.4415	0.0007	6.3642
144	11.9505	10670	35.0066	58.0698	16.2029	1128.344	73.4276	193192.4	10492.53	17.9829	0.0245	0.4403	0.0007	6.3642
145	12.0338	10670	35.0066	57.9609	16.2005	1126.059	73.4276	194318.4	10565.96	17.969	0.0244	0.4391	0.0007	6.3642
146	12.1171	10670	35.0066	57.8525	16.1981	1123.785	73.4276	195442.2	10639.39	17.9549	0.0244	0.438	0.0007	6.3642
147	12.2004	10670	35.0066	57.7446	16.1957	1121.522	73.4276	196563.7	10712.81	17.9407	0.0243	0.4368	0.0007	6.3642
148	12.2836	10670	35.0066	57.6372	16.1933	1119.271	73.4276	197683	10786.24	17.9265	0.0243	0.4356	0.0007	6.3642
149	12.3669	10670	35.0066	57.5303	16.1909	1117.031	73.4276	198800	10859.67	17.9121	0.0243	0.4345	0.0007	6.3642
150	12.4502	10670	35.0066	57.4238	16.1885	1114.802	73.4276	199914.8	10933.1	17.8975	0.0242	0.4333	0.0007	6.3642
151	12.5335	10670	35.0066	57.3179	16.1862	1112.583	73.4276	201027.4	11006.53	17.8829	0.0242	0.4322	0.0007	6.3642
152	12.6168	10670	35.0066	57.2125	16.1838	1110.376	73.4276	202137.8	11079.95	17.8682	0.0241	0.431	0.0007	6.3642
153	12.7	10670	35.0066	57.1076	16.1815	1108.18	73.4276	203246	11153.38	17.8533	0.0241	0.4299	0.0007	6.3642
154	12.7833	10670	35.0066	57.0031	16.1792	1105.994	73.4276	204352	11226.81	17.8383	0.024	0.4287	0.0007	6.3642
155	12.8666	10670	35.0066	56.8992	16.1769	1103.819	73.4276	205455.8	11300.24	17.8233	0.024	0.4276	0.0007	6.3642
156	12.9499	10670	35.0066	56.7957	16.1745	1101.654	73.4276	206557.4	11373.66	17.8081	0.0239	0.4265	0.0007	6.3642
157	13.0332	10670	35.0066	56.6927	16.1723	1099.501	73.4276	207656.9	11447.09	17.7928	0.0239	0.4253	0.0007	6.3642
158	13.1164	10670	35.0066	56.5902	16.17	1097.357	73.4276	208754.3	11520.52	17.7774	0.0239	0.4242	0.0007	6.3642
159	13.1997	10670	35.0066	56.4881	16.1677	1095.224	73.4276	209849.5	11593.95	17.7618	0.0238	0.423	0.0007	6.3642
160	13.283	10670	35.0066	56.3865	16.1654	1093.102	73.4276	210942.6	11667.37	17.7462	0.0238	0.4219	0.0007	6.3642
161	13.3663	10670	35.0066	56.2854	16.1632	1090.99	73.4276	212033.6	11740.8	17.7304	0.0237	0.4208	0.0007	6.3642
162	13.4495	10670	35.0066	56.1848	16.1609	1088.888	73.4276	213122.5	11814.23	17.7146	0.0237	0.4197	0.0007	6.3642
163	13.5328	10670	35.0066	56.0846	16.1587	1086.796	73.4276	214209.3	11887.66	17.6986	0.0236	0.4185	0.0007	6.3642
164	13.6161	10670	35.0066	55.9849	16.1565	1084.715	73.4276	215294	11961.08	17.6825	0.0236	0.4174	0.0007	6.3642
165	13.6994	10670	35.0066	55.8856	16.1543	1082.644	73.4276	216376.7	12034.51	17.6663	0.0236	0.4163	0.0007	6.3642
166	13.7827	10670	35.0066	55.7868	16.1521	1080.582	73.4276	217457.2	12107.94	17.65	0.0235	0.4152	0.0007	6.3642
167	13.8659	10670	35.0066	55.6884	16.1499	1078.531	73.4276	218535.8	12181.37	17.6336	0.0235	0.414	0.0007	6.3642
168	13.9492	10670	35.0066	55.5905	16.1477	1076.489	73.4276	219612.3	12254.79	17.6171	0.0234	0.4129	0.0007	6.3642
169	14.0325	10670	35.0066	55.4931	16.1455	1074.458	73.4276	220686.7	12328.22	17.6005	0.0234	0.4118	0.0007	6.3642
170	14.1158	10670	35.0066	55.3961	16.1434	1072.436	73.4276	221759.2	12401.65	17.5837	0.0234	0.4107	0.0007	6.3642
171	14.1991	10670	35.0066	55.2995	16.1412	1070.424	73.4276	222829.6	12475.08	17.5668	0.0233	0.4096	0.0007	6.3642
172	14.2823	10670	35.0066	55.2034	16.1391	1068.422	73.4276	223898	12548.5	17.5499	0.0233	0.4085	0.0007	6.3642
173	14.3656	10670	35.0066	55.1077	16.137	1066.429	73.4276	224964.4	12621.93	17.5328	0.0232	0.4074	0.0007	6.3642
174	14.4489	10670	35.0066	55.0125	16.1348	1064.446	73.4276	226028.9	12695.36	17.5156	0.0232	0.4063	0.0007	6.3642
175	14.5322	10670	35.0066	54.9177	16.1327	1062.472	73.4276	227091.3	12768.79	17.4983	0.0232	0.4052	0.0007	6.3642
176	14.6155	10670	35.0066	54.8233	16.1306	1060.508	73.4276	228151.9	12842.22	17.4809	0.0231	0.4041	0.0007	6.3642
177	14.6987	10670	35.0066	54.7293	16.1285	1058.553	73.4276	229210.4	12915.64	17.4634	0.0231	0.403	0.0007	6.3642
178	14.782	10670	35.0066	54.6358	16.1265	1056.608	73.4276	230267	12989.07	17.4458	0.023	0.4019	0.0007	6.3642
179	14.8653	10670	35.0066	54.5427	16.1244	1054.672	73.4276	231321.7	13062.5	17.428	0.023	0.4008	0.0007	6.3642
180	14.9486	10670	35.0066	54.45	16.1223	1052.745	73.4276	232374.4	13135.93	17.4102	0.023	0.3997	0.0007	6.3642
181	15.0318	10670	35.0066	54.3578	16.1203	1050.828	73.4276	233425.3	13209.35	17.3923	0.0229	0.3986	0.0007	6.3642
182	15.1151	10670	35.0066	54.2659	16.1182	1048.92	73.4276	234474.2	13282.78	17.3742	0.0229	0.3975	0.0007	6.3642
183	15.1984	10670	35.0066	54.1745	16.1162	1047.02	73.4276	235521.2	13356.21	17.356	0.0228	0.3964	0.0007	6.3642
184	15.2817	10670	35.0066	54.0835	16.1142	1045.13	73.4276	236566.3	13429.64	17.3378	0.0228	0.3954	0.0007	6.3642
185	15.3233	10670	35.0066	53.9929	16.1121	521.6244	36.7138	237088	13466.35	17.3194	0.0228	0.3943	0.0007	6.3642

AIRCRAFT PERFORMANCE DURING GLIDE CONDITION

Seg_No	ALT (m)	ALT (ft)	TIME(min)	TIME(hrs)	Thrust (KN) /Engine	SFC (mg/Ns)	Segment Fuel(kg)	EAS (m/s)	TAS (m/s)
1	10670	35006.5617	0	0	31.4236	17.008	0	128.91	233.1
2	9336.2512	30630.7456	5.5954	0.0933	33.705	17.015	743.918	133.0816	221.5
3	8002.5025	26254.9295	12.1341	0.2022	36.5688	16.8392	933.3662	132.0309	202.9
4	6668.7537	21879.1134	19.4851	0.3248	38.5192	17.2376	1128.5545	137.0328	195
5	5335.005	17503.2972	28.3287	0.4721	40.5884	17.3119	1450.2464	138.5827	183.1
6	4001.2563	13127.4811	31.2475	0.5208	43.7082	16.8673	504.5833	133.9239	164.7
7	2667.5075	8751.665	33.0518	0.5509	46.338	16.7231	327.4511	131.5169	150.9
8	1333.7588	4375.8489	34.2786	0.5713	106.2448	13.898	229.9313	130.4957	140
9	0.01	0.0328	35.6753	0.5946	111.5487	14.0759	510.5626	134.3026	135
Seg_No	**Mach**	**Descent Rate (m/s)**	**Dist_(m)**	**Dist_(m) Cum**	**Descent Gradient (deg)**	**DragCoeff aircraft**	**LiftCoeff aircraft**	**DragCoeff Nacelle**	**Drag Nacelle (KN)**
1	0.7804	-3.9728	0	0	-1.0013	0.0245	0.4347	0.0007	5.8395
2	0.7275	-3.3996	76298.1842	76298.1842	-0.9178	0.0233	0.4071	0.0007	6.1862
3	0.6542	-3.024	83240.7526	159538.9368	-0.8708	0.0236	0.4126	0.0007	6.1026
4	0.6177	-2.5136	87737.8555	247276.7923	-0.7618	0.0224	0.3818	0.0007	6.5153
5	0.5701	-7.6158	100304.2222	347581.0145	-2.5076	0.022	0.3719	0.0007	6.638
6	0.5043	-12.3199	30425.9462	378006.9607	-4.4642	0.0558	0.3977	0.0007	6.2271
7	0.4547	-18.12	17031.5591	395038.5198	-7.1013	0.0564	0.412	0.0007	6.007
8	0.4153	-15.9156	10623.9086	405662.4284	-6.6026	0.0984	0.4183	0.0007	5.9011
9	0.3945	0	11446.263	417108.6914	0	0.1085	0.3943	0.0007	6.1947

B.2.2 ENGINE FLIGHT PATH PERFORMANCE OUTPUT WITH A380-800 AIRCRAFT AND TURBOFAN TRENT900 ENGINE

Phase	Seg No	ALT (m)	DTisa (K)	Mach	TIME (hrs)	TIME (min)	TIME (sec)	Thrust (kN /Engine	SFC (g/kNs)	TET [K]
1	1	0	3	0	0	0	0	96.074	7.854	1305
1	2	0	3	0	0.16667	10	600	96.074	7.854	1305
1	3	0	3	0	0.16681	10.00833	600.5	173.0005	6.0029	1326.2207
1	4	0	3	0	0.16708	10.025	601.5	242.2007	7.03574	1515.7324
1	5	0	3	0	0.16736	10.04167	602.5	311.4009	8.06858	1705.2441
1	6	0	3	0	0.16764	10.05833	603.5	346.001	8.585	1800
1	7	0	3	0.068	0.17253	10.35174	621.10418	329.42697	9.22054	1787.0481
1	8	0	3	0.135	0.17742	10.64514	638.70836	298.25664	10.02758	1800
1	9	0	3	0.203	0.18231	10.93854	656.31254	278.93722	10.79513	1800
1	10	0	3	0.27	0.1872	11.23195	673.91673	262.22148	11.59988	1800
1	11	10.668	3	0.295	0.18811	11.28666	677.1995	255.95021	11.91134	1800
1	12	55.9	3	0.298	0.18845	11.30723	678.43378	254.33439	11.95291	1800
1	13	457.2	3	0.39	0.19853	11.91198	714.71893	228.56965	13.14737	1800
2	14	557.2	3	0.391	0.19881	11.92865	715.71893	253.818	12.045	1800
2	15	900	3	0.399	0.20643	12.38581	743.14885	235.124	12.191	1800
2	16	1500	3	0.414	0.2213	13.27824	796.6944	221.328	12.367	1800
2	17	1981.2	3	0.426	0.23404	14.04217	842.53025	211.324	12.479	1800

Phase	Seg No	ALT (m)	DTisa (K)	Mach	TIME (hrs)	TIME (min)	TIME (sec)	Thrust (kN /Engine	SFC (g/kNs)	TET [K]
2	18	2438.4	3	0.438	0.24686	14.81133	888.67967	201.965	12.598	1800
2	19	2743.2	3	0.447	0.25584	15.35019	921.01132	196.045	12.668	1800
2	20	3048	3	0.456	0.265	15.90008	954.00504	190.158	12.749	1800
2	21	3048	3	0.583	0.28464	17.07816	1024.6899	172.689	14.869	1800
2	22	3657.6	3	0.606	0.30455	18.27312	1096.3873	162.6	15.108	1800
2	23	4267.2	3	0.631	0.32667	19.60035	1176.021	153.291	15.332	1800
2	24	4876.8	3	0.657	0.35145	21.0871	1265.2263	144.406	15.573	1800
2	25	5486.4	3	0.684	0.37953	22.77153	1366.2921	136.101	15.803	1800
2	26	6096	3	0.713	0.41193	24.71592	1482.9553	128.12	16.066	1800
2	27	7620	3	0.794	0.50813	30.48759	1829.2556	109.917	16.768	1800
2	28	8077.2	3	0.8	0.54078	32.44665	1946.799	105.079	16.978	1800
2	29	9144	3	0.8	0.63984	38.39066	2303.4397	94.66	17.067	1800
2	30	10058	3	0.8	0.81267	48.76045	2925.6272	86.266	17.21	1800
3	31	10058	3	0.8	1.36385	81.83087	4909.8524	80.47543	16.66327	1732.8506
3	32	10058	3	0.8	1.44713	86.82761	5209.6566	80.36774	16.66108	1731.8552
3	33	10058	3	0.8	1.53041	91.82435	5509.4608	80.15308	16.65672	1729.8714
3	34	10058	3	0.8	1.61368	96.82108	5809.265	79.93961	16.65238	1727.8984
3	35	10058	3	0.8	1.69696	101.8178	6109.0692	79.72732	16.64806	1725.9364
3	36	10058	3	0.8	1.78024	106.8146	6408.8734	79.5162	16.64377	1723.9852
3	37	10058	3	0.8	1.86352	111.8113	6708.6776	79.30623	16.6395	1722.0447
3	38	10058	3	0.8	1.9468	116.808	7008.4818	79.09742	16.63525	1720.1148
3	39	10058	3	0.8	2.03008	121.8048	7308.286	78.88976	16.63103	1718.1955
3	40	10058	3	0.8	2.11336	126.8015	7608.0902	78.68322	16.62683	1716.2867
3	41	10058	3	0.8	2.19664	131.7982	7907.8944	78.47782	16.62265	1714.3884
3	42	10058	3	0.8	2.27992	136.795	8207.6986	78.27354	16.6185	1712.5003
3	43	10058	3	0.8	2.3632	141.7917	8507.5028	78.07036	16.61437	1710.6226
3	44	10058	3	0.8	2.44647	146.7885	8807.307	77.86829	16.61026	1708.755
3	45	10058	3	0.8	2.52975	151.7852	9107.1112	77.66732	16.60617	1706.8976
3	46	10058	3	0.8	2.61303	156.7819	9406.9154	77.46743	16.60211	1705.0502
3	47	10058	3	0.8	2.69631	161.7787	9706.7196	77.26862	16.59807	1703.2128
3	48	10058	3	0.8	2.77959	166.7754	10006.524	77.07089	16.59405	1701.3853
3	49	10058	3	0.8	2.86287	171.7721	10306.328	76.87422	16.59005	1699.5677
3	50	10058	3	0.8	2.94615	176.7689	10606.132	76.67861	16.58607	1697.7598
3	51	10058	3	0.8	3.02943	181.7656	10905.936	76.48405	16.58212	1695.9616
3	52	10058	3	0.8	3.11271	186.7623	11205.741	76.29052	16.57818	1694.1731
3	53	10058	3	0.8	3.19598	191.7591	11505.545	76.09804	16.57427	1692.3941
3	54	10058	3	0.8	3.27926	196.7558	11805.349	75.90658	16.57037	1690.6246
3	55	10058	3	0.8	3.36254	201.7526	12105.153	75.71615	16.5665	1688.8646
3	56	10058	3	0.8	3.44582	206.7493	12404.957	75.52672	16.56265	1687.1139
3	57	10058	3	0.8	3.5291	211.746	12704.762	75.33831	16.55882	1685.3725
3	58	10058	3	0.8	3.61238	216.7428	13004.566	75.15089	16.55501	1683.6404
3	59	10058	3	0.8	3.69566	221.7395	13304.37	74.96447	16.55122	1681.9174
3	60	10058	3	0.8	3.77894	226.7362	13604.174	74.77903	16.54745	1680.2036
3	61	10058	3	0.8	3.86222	231.733	13903.978	74.59457	16.53969	1678.3392
3	62	10058	3	0.8	3.9455	236.7297	14203.783	74.41113	16.53144	1676.4635
3	63	10058	3	0.8	4.02877	241.7265	14503.587	74.2287	16.52324	1674.6006
3	64	10058	3	0.8	4.11205	246.7232	14803.391	74.04728	16.51513	1672.757
3	65	10058	3	0.8	4.19533	251.7199	15103.195	73.86686	16.50706	1670.9234
3	66	10058	3	0.8	4.27861	256.7167	15402.999	73.68744	16.49921	1669.0981
3	67	10058	3	0.8	4.36189	261.7134	15702.804	73.50899	16.49158	1667.281
3	68	10058	3	0.8	4.44517	266.7101	16002.608	73.33152	16.48399	1665.4737

Phase	Seg No	ALT (m)	DTisa (K)	Mach	TIME (hrs)	TIME (min)	TIME (sec)	Thrust (kN /Engine	SFC (g/kNs)	TET [K]
3	69	10058	3	0.8	4.52845	271.7069	16302.412	73.15502	16.47642	1663.6709
3	70	10670	3	0.82	4.61173	276.7036	16602.216	72.97742	16.86109	1712.4179
3	71	10670	3	0.82	4.69501	281.7003	16902.02	72.79036	16.85024	1710.2478
3	72	10670	3	0.82	4.77828	286.6971	17201.825	72.6044	16.83945	1708.0905
3	73	10670	3	0.82	4.86156	291.6938	17501.629	72.41952	16.82873	1705.9457
3	74	10670	3	0.82	4.94484	296.6906	17801.433	72.23571	16.81807	1703.8133
3	75	10670	3	0.82	5.02812	301.6873	18101.237	72.05297	16.80747	1701.6933
3	76	10670	3	0.82	5.1114	306.684	18401.041	71.87128	16.79693	1699.5856
3	77	10670	3	0.82	5.19468	311.6808	18700.846	71.69064	16.78645	1697.49
3	78	10670	3	0.82	5.27796	316.6775	19000.65	71.51104	16.77603	1695.4065
3	79	10670	3	0.82	5.36124	321.6742	19300.454	71.33248	16.76568	1693.335
3	80	10670	3	0.82	5.44452	326.671	19600.258	71.15493	16.75538	1691.2753
3	81	10670	3	0.82	5.5278	331.6677	19900.063	70.97841	16.74514	1689.2275
3	82	10670	3	0.82	5.61107	336.6645	20199.867	70.80289	16.73496	1687.1913
3	83	10670	3	0.82	5.69435	341.6612	20499.671	70.62837	16.72483	1685.1667
3	84	10670	3	0.82	5.77763	346.6579	20799.475	70.45484	16.71477	1683.1536
3	85	10670	3	0.82	5.86091	351.6547	21099.279	70.28229	16.70476	1681.1519
3	86	10670	3	0.82	5.94419	356.6514	21399.084	70.11073	16.69492	1679.1843
3	87	10670	3	0.82	6.02747	361.6481	21698.888	69.94012	16.68529	1677.2587
3	88	10670	3	0.82	6.11075	366.6449	21998.692	69.77048	16.67572	1675.344
3	89	10670	3	0.82	6.19403	371.6416	22298.496	69.60179	16.66651	1673.4401
3	90	10670	3	0.82	6.27731	376.6383	22598.3	69.43404	16.65742	1671.5467
3	91	10670	3	0.82	6.36058	381.6351	22898.105	69.26722	16.64838	1669.6624
3	92	10670	3	0.82	6.44386	386.6318	23197.909	69.10133	16.63935	1667.7815
3	93	10670	3	0.82	6.52714	391.6286	23497.713	68.93636	16.63037	1665.9111
3	94	10670	3	0.82	6.61042	396.6253	23797.517	68.7723	16.62146	1664.0532
3	95	10670	3	0.82	6.6937	401.622	24097.321	68.60915	16.6126	1662.2075
3	96	10670	3	0.82	6.77698	406.6188	24397.126	68.44689	16.60379	1660.3721
3	97	10670	3	0.82	6.86026	411.6155	24696.93	68.28553	16.59612	1658.6005
3	98	10670	3	0.82	6.94354	416.6122	24996.734	68.12504	16.58878	1656.8523
3	99	10670	3	0.82	7.02682	421.609	25296.538	67.96541	16.58148	1655.1134
3	100	10670	3	0.82	7.1101	426.6057	25596.342	67.80665	16.57384	1653.3733
3	101	10670	3	0.82	7.19337	431.6024	25896.147	67.64874	16.56622	1651.6419
3	102	10670	3	0.82	7.27665	436.5992	26195.951	67.49168	16.55866	1649.9196
3	103	10670	3	0.82	7.35993	441.5959	26495.755	67.33547	16.55145	1648.203
3	104	10670	3	0.82	7.44321	446.5927	26795.559	67.1801	16.54428	1646.4956
3	105	10670	3	0.82	7.52649	451.5894	27095.363	67.02555	16.53714	1644.7963
3	106	10670	3	0.82	7.60977	456.5861	27395.168	66.87182	16.53002	1643.0996
3	107	10670	3	0.82	7.69305	461.5829	27694.972	66.71892	16.52293	1641.4119
3	108	10670	3	0.82	7.77633	466.5796	27994.776	66.56683	16.51582	1639.732
3	109	10670	3	0.82	7.85961	471.5763	28294.58	66.41554	16.50844	1638.0548
3	110	10670	3	0.82	7.94288	476.5731	28594.384	66.26506	16.5011	1636.3864
3	111	10670	3	0.82	8.02616	481.5698	28894.189	66.11537	16.49385	1634.7258
3	112	10670	3	0.82	8.10944	486.5666	29193.993	65.96648	16.48688	1633.0677
3	113	10670	3	0.82	8.19272	491.5633	29493.797	65.81838	16.47996	1631.4185
3	114	10670	3	0.82	8.276	496.56	29793.601	65.67105	16.47306	1629.7773
3	115	10670	3	0.82	8.35928	501.5568	30093.405	65.5245	16.4662	1628.1417
3	116	10670	3	0.82	8.44256	506.5535	30393.21	65.37871	16.45936	1626.5147
3	117	10670	3	0.82	8.52584	511.5502	30693.014	65.23369	16.45254	1624.8956
3	118	10670	3	0.82	8.60912	516.547	30992.818	65.08943	16.44542	1623.2784
3	119	10670	3	0.82	8.6924	521.5437	31292.622	64.94592	16.43835	1621.6695

Phase	Seg No	ALT (m)	DTisa (K)	Mach	TIME (hrs)	TIME (min)	TIME (sec)	Thrust (kN /Engine	SFC (g/kNs)	TET [K]
3	120	10670	3	0.82	8.77567	526.5404	31592.426	64.80317	16.4313	1620.0691
3	121	10670	3	0.82	8.85895	531.5372	31892.231	64.66115	16.42457	1618.4702
3	122	10670	3	0.82	8.94223	536.5339	32192.035	64.51988	16.41789	1616.8793
3	123	10670	3	0.82	9.02551	541.5307	32491.839	64.37934	16.41125	1615.2966
3	124	10670	3	0.82	9.10879	546.5274	32791.643	64.23953	16.40462	1613.7193
3	125	10670	3	0.82	9.19207	551.5241	33091.447	64.10044	16.39803	1612.1494
3	126	10670	3	0.82	9.27535	556.5209	33391.252	63.96207	16.39147	1610.5877
3	127	10670	3	0.82	9.35863	561.5176	33691.056	63.82441	16.38492	1609.0296
3	128	10670	3	0.82	9.44191	566.5143	33990.86	63.68746	16.3784	1607.4769
3	129	10670	3	0.82	9.52518	571.5111	34290.664	63.55122	16.37192	1605.9321
3	130	10670	3	0.82	9.60846	576.5078	34590.468	63.41567	16.36545	1604.394
3	131	10670	3	0.82	9.69174	581.5045	34890.273	63.28082	16.35902	1602.8616
3	132	10670	3	0.82	9.77502	586.5013	35190.077	63.14666	16.35262	1601.337
3	133	10670	3	0.82	9.8583	591.498	35489.881	63.01318	16.34621	1599.8194
3	134	10670	3	0.82	9.94158	596.4948	35789.685	62.88038	16.33954	1598.3035
3	135	10670	3	0.82	10.0249	601.4915	36089.489	62.74827	16.3329	1596.7953
3	136	10670	3	0.82	10.1081	606.4882	36389.294	62.61683	16.3263	1595.2948
3	137	10670	3	0.82	10.1914	611.485	36689.098	62.48605	16.31995	1593.7965
3	138	10670	3	0.82	10.2747	616.4817	36988.902	62.35595	16.31368	1592.3044
3	139	10670	3	0.82	10.358	621.4784	37288.706	62.2265	16.30744	1590.8199
3	140	10670	3	0.82	10.4413	626.4752	37588.51	62.0977	16.30123	1589.3399
3	141	10670	3	0.82	10.5245	631.4719	37888.315	61.96956	16.29503	1587.8636
3	142	10670	3	0.82	10.6078	636.4687	38188.119	61.84206	16.28886	1586.3947
3	143	10670	3	0.82	10.6911	641.4654	38487.923	61.71521	16.28286	1584.9408
3	144	10670	3	0.82	10.7744	646.4621	38787.727	61.58899	16.27976	1583.6502
3	145	10670	3	0.82	10.8577	651.4589	39087.531	61.46338	16.27668	1582.3659
3	146	10670	3	0.82	10.9409	656.4556	39387.336	61.33838	16.27361	1581.0877
3	147	10670	3	0.82	11.0242	661.4523	39687.14	61.21398	16.27068	1579.823
3	148	10670	3	0.82	11.1075	666.4491	39986.944	61.09018	16.26849	1578.6069
3	149	10670	3	0.82	11.1908	671.4458	40286.748	60.96698	16.26631	1577.3966
3	150	10670	3	0.82	11.274	676.4425	40586.552	60.84435	16.26415	1576.1921
3	151	10670	3	0.82	11.3573	681.4393	40886.357	60.72231	16.26198	1574.9931
3	152	10670	3	0.82	11.4406	686.436	41186.161	60.60085	16.25928	1573.7637
3	153	10670	3	0.82	11.5239	691.4328	41485.965	60.47998	16.25659	1572.5402
3	154	10670	3	0.82	11.6072	696.4295	41785.769	60.35967	16.25391	1571.3226
3	155	10670	3	0.82	11.6904	701.4262	42085.573	60.23995	16.25124	1570.1108
3	156	10670	3	0.82	11.7737	706.423	42385.378	60.12079	16.24859	1568.9047
3	157	10670	3	0.82	11.857	711.4197	42685.182	60.0022	16.24595	1567.7044
3	158	10670	3	0.82	11.9403	716.4164	42984.986	59.88417	16.24332	1566.5098
3	159	10670	3	0.82	12.0236	721.4132	43284.79	59.7667	16.24071	1565.3209
3	160	10670	3	0.82	12.1068	726.4099	43584.594	59.64979	16.2381	1564.1376
3	161	10670	3	0.82	12.1901	731.4066	43884.399	59.53344	16.23551	1562.9599
3	162	10670	3	0.82	12.2734	736.4034	44184.203	59.41763	16.23293	1561.7878
3	163	10670	3	0.82	12.3567	741.4001	44484.007	59.30237	16.23037	1560.6212
3	164	10670	3	0.82	12.44	746.3969	44783.811	59.18766	16.22781	1559.4601
3	165	10670	3	0.82	12.5232	751.3936	45083.615	59.07349	16.22527	1558.3046
3	166	10670	3	0.82	12.6065	756.3903	45383.42	58.95986	16.22274	1557.1544
3	167	10670	3	0.82	12.6898	761.3871	45683.224	58.84676	16.22022	1556.0097
3	168	10670	3	0.82	12.7731	766.3838	45983.028	58.73419	16.21771	1554.8704
3	169	10670	3	0.82	12.8563	771.3805	46282.832	58.62216	16.21522	1553.7364
3	170	10670	3	0.82	12.9396	776.3773	46582.636	58.51065	16.21274	1552.6078

Phase	Seg No	ALT (m)	DTisa (K)	Mach	TIME (hrs)	TIME (min)	TIME (sec)	Thrust (kN /Engine	SFC (g/kNs)	TET [K]
3	171	10670	3	0.82	13.0229	781.374	46882.441	58.39966	16.21027	1551.4844
3	172	10670	3	0.82	13.1062	786.3708	47182.245	58.28919	16.20781	1550.3663
3	173	10670	3	0.82	13.1895	791.3675	47482.049	58.17924	16.20536	1549.2535
3	174	10670	3	0.82	13.2727	796.3642	47781.853	58.06981	16.20292	1548.1459
3	175	10670	3	0.82	13.356	801.361	48081.657	57.96089	16.2005	1547.0434
3	176	10670	3	0.82	13.4393	806.3577	48381.462	57.85247	16.19808	1545.9461
3	177	10670	3	0.82	13.5226	811.3544	48681.266	57.74456	16.19568	1544.8539
3	178	10670	3	0.82	13.6059	816.3512	48981.07	57.63716	16.19329	1543.7668
3	179	10670	3	0.82	13.6891	821.3479	49280.874	57.53025	16.19091	1542.6848
3	180	10670	3	0.82	13.7724	826.3446	49580.679	57.42385	16.18854	1541.6078
3	181	10670	3	0.82	13.8557	831.3414	49880.483	57.31793	16.18618	1540.5358
3	182	10670	3	0.82	13.939	836.3381	50180.287	57.21251	16.18383	1539.4688
3	183	10670	3	0.82	14.0223	841.3349	50480.091	57.10758	16.18149	1538.4067
3	184	10670	3	0.82	14.1055	846.3316	50779.895	57.00314	16.17917	1537.3496
3	185	10670	3	0.82	14.1888	851.3283	51079.7	56.89918	16.17685	1536.2973
3	186	10670	3	0.82	14.2721	856.3251	51379.504	56.7957	16.17455	1535.25
3	187	10670	3	0.82	14.3554	861.3218	51679.308	56.6927	16.17226	1534.2074
3	188	10670	3	0.82	14.4386	866.3185	51979.112	56.59017	16.16997	1533.1697
3	189	10670	3	0.82	14.5219	871.3153	52278.916	56.48812	16.1677	1532.1368
3	190	10670	3	0.82	14.6052	876.312	52578.721	56.38654	16.16544	1531.1087
3	191	10670	3	0.82	14.6885	881.3088	52878.525	56.28543	16.16319	1530.0853
3	192	10670	3	0.82	14.7718	886.3055	53178.329	56.18478	16.16095	1529.0666
3	193	10670	3	0.82	14.855	891.3022	53478.133	56.0846	16.15872	1528.0526
3	194	10670	3	0.82	14.9383	896.299	53777.937	55.98488	16.1565	1527.0433
3	195	10670	3	0.82	15.0216	901.2957	54077.742	55.88561	16.15428	1526.0386
3	196	10670	3	0.82	15.1049	906.2924	54377.546	55.7868	16.15208	1525.0385
3	197	10670	3	0.82	15.1882	911.2892	54677.35	55.68845	16.14989	1524.043
3	198	10670	3	0.82	15.2714	916.2859	54977.154	55.59055	16.14771	1523.0521
3	199	10670	3	0.82	15.3547	921.2826	55276.958	55.49309	16.14554	1522.0657
3	200	10670	3	0.82	15.438	926.2794	55576.763	55.39608	16.14338	1521.0838
3	201	10670	3	0.82	15.5213	931.2761	55876.567	55.29952	16.14123	1520.1065
3	202	10670	3	0.82	15.6046	936.2729	56176.371	55.2034	16.13909	1519.1336
3	203	10670	3	0.82	15.6878	941.2696	56476.175	55.10771	16.13696	1518.1651
3	204	10670	3	0.82	15.7711	946.2663	56775.979	55.01247	16.13484	1517.2011
3	205	10670	3	0.82	15.8544	951.2631	57075.784	54.91765	16.13273	1516.2414
3	206	10670	3	0.82	15.9377	956.2598	57375.588	54.82327	16.13063	1515.2862
3	207	10670	3	0.82	16.0209	961.2565	57675.392	54.72932	16.12854	1514.3353
3	208	10670	3	0.82	16.1042	966.2533	57975.196	54.6358	16.12646	1513.3887
3	209	10670	3	0.82	16.1875	971.25	58275	54.5427	16.12438	1512.4464
3	210	10670	3	0.82	16.2708	976.2467	58574.805	54.45003	16.12232	1511.5084
3	211	10670	3	0.82	16.3541	981.2435	58874.609	54.35778	16.12026	1510.5747
3	212	10670	3	0.82	16.4373	986.2402	59174.413	54.26595	16.11822	1509.6452
3	213	10670	3	0.82	16.5206	991.237	59474.217	54.17453	16.11618	1508.7199
3	214	10670	3	0.82	16.6039	996.2337	59774.021	54.08353	16.11416	1507.7989
3	215	10670	3	0.82	16.6455	998.7321	59923.923	53.99294	16.11214	1506.882
4	216	10670	3	0.78	16.6467	998.7987	59927.923	31.42358	17.00799	1310
4	217	9336.3	3	0.728	16.7399	1004.394	60263.646	33.705	17.01499	1310
4	218	8002.5	3	0.654	16.8489	1010.933	60655.972	36.56877	16.8392	1310
4	219	6668.8	3	0.618	16.9714	1018.284	61097.027	38.51917	17.23762	1310
4	220	5335	3	0.57	17.1188	1027.127	61627.644	40.58844	17.31194	1310
4	221	4001.3	3	0.504	17.1674	1030.046	61802.774	43.70823	16.86725	1310

Phase	Seg No	ALT (m)	DTisa (K)	Mach	TIME (hrs)	TIME (min)	TIME (sec)	Thrust (kN /Engine	SFC (g/kNs)	TET [K]
4	222	2667.5	3	0.455	17.1975	1031.851	61911.034	46.338	16.72305	1310
4	223	1333.8	3	0.415	17.218	1033.077	61984.64	106.24482	13.89798	1500
4	224	0.01	3	0.395	17.2412	1034.474	62068.441	111.54874	14.07591	1500
5	226	0.01	3	0.203	17.2407	1034.441	62066.441	111.54874	14.07591	1500
5	227	0.01	3	0.199	17.2413	1034.475	62068.527	111.54874	14.07591	1500
5	228	0.01	3	0.195	17.2452	1034.714	62082.822	140.47851	8.80032	1391.3513
5	229	0.01	3	0.194	17.2466	1034.797	62087.822	182.84972	9.35572	1513.6699
5	230	0.01	3	0.193	17.248	1034.88	62092.822	225.326	9.91349	1636.2251
5	231	0.01	3	0.061	17.2568	1035.406	62124.386	300.24764	9.21631	1803.9666
5	232	0.01	3	0.058	17.2582	1035.49	62129.386	251.58231	9.41492	1853.4021
5	233	0.01	3	0.055	17.2596	1035.573	62134.386	202.36659	9.74967	1928.2758
5	234	0.01	3	0.041	17.2663	1035.979	62158.724	87.55889	8.63555	1305
5	235	0.01	3	0	17.269	1036.14	62168.375	96.074	7.854	1305
5	236	0.01	3	0	17.4357	1046.14	62768.375	96.074	7.854	1305

B.3 INPUT FILE FOR THE INTERCOOLED-RECUPERATED TURBOFAN TRENT 900 ENGINE

```
HERMES Engine Performance Input Data File - All Data Refer to a
Single Engine !File created by: Fernando Lartategui Atela

!Engine performance data calculated from Turbomatch version 2.0 and
tabulated manually.

Altitude,Mach,DTisa:Increasing order, Thrust:Decreasing order

! TakeOff Rating Engine Performance Data Table Structure

  2 ! Take-Off Altitudes

  1 ! Take-Off DTisa Numbers

  9 ! Take-Off Mach Numbers

  2 ! Take-Off Data Rows

  2 ! Take-Off Additional Performance Data Columns

! Climb Rating Engine Performance Data Table Structure

 22 ! Climb Altitudes

  1 ! Climb DTisa Numbers

  1 ! Climb Mach Numbers

  2 ! Climb Data Rows

  2 ! Climb Additional Performance Data Columns

! Cruise Rating Engine Performance Data Table Structure

  2 ! Cruise Altitudes

  1 ! Cruise DTisa Numbers

  1 ! Cruise Mach Numbers

 24 ! Cruise Data Rows

  2 ! Cruise Additional Performance Data Columns

! Descent Rating Engine Performance Data Table Structure
```

```
 10 ! Descent Altitudes
  1 ! Descent DTisa Numbers
  1 ! Descent Mach Numbers
  2 ! Descent Data Rows
  2 ! Descent Additional Performance Data Columns
! Approach Rating Engine Performance Data Table Structure
  3 ! Approach Altitudes
  1 ! Approach DTisa Numbers
  1 ! Approach Mach Numbers
  2 ! Approach Data Rows
  2 ! Approach Additional Performance Data Columns
! Ground Idle Rating Engine Performance Data Table Structure
  1 ! GroundIdle Altitudes
  1 ! GroundIdle DTisa Numbers
  9 ! GroundIdle Mach Numbers
  2 ! GroundIdle Data Rows
2 ! GroundIdle Additional Performance Data Columns
3
! Engine Performance at Take-Off Rating
```

Net Thrust (kN)	**SFC (mg/Ns)**	**Altitude (m)**	**Dtisa**	**Mach**	**TET**
363.71	8.605	0	3	0	1700
354.55	8.481	0	3	0	1680
344.03	9.109	0	3	0.05	1700
334.97	8.986	0	3	0.05	1680
326.36	9.634	0	3	0.1	1700
317.28	9.515	0	3	0.1	1680
310.36	10.187	0	3	0.15	1700
301.41	10.066	0	3	0.15	1680
295.8	10.759	0	3	0.2	1700
286.89	10.645	0	3	0.2	1680
282.67	11.36	0	3	0.25	1700
273.9	11.248	0	3	0.25	1680
270.86	11.986	0	3	0.3	1700
262.32	11.874	0	3	0.3	1680
260.29	12.636	0	3	0.35	1700
251.98	12.528	0	3	0.35	1680
250.87	13.312	0	3	0.4	1700
242.57	13.209	0	3	0.4	1680
348.86	8.583	457.2	3	0	1700
340	8.461	457.2	3	0	1680

329.78	9.092	457.2	3	0.05	1700
321.42	8.959	457.2	3	0.05	1680
313.13	9.605	457.2	3	0.1	1700
304.73	9.48	457.2	3	0.1	1680
297.95	10.151	457.2	3	0.15	1700
289.5	10.028	457.2	3	0.15	1680
284.33	10.712	457.2	3	0.2	1700
275.84	10.597	457.2	3	0.2	1680
271.78	11.307	457.2	3	0.25	1700
263.51	11.192	457.2	3	0.25	1680
260.53	11.925	457.2	3	0.3	1700
252.4	11.812	457.2	3	0.3	1680
250.47	12.567	457.2	3	0.35	1700
242.39	12.461	457.2	3	0.35	1680
241.51	13.233	457.2	3	0.4	1700
233.59	13.13	457.2	3	0.4	1680

! Engine Performance at Climb Rating

Net Thrust (kN)	**SFC (mg/Ns)**	**Altitude (m)**	**Dtisa**	**Mach**	**TET**
258.59	12.052	450	3	0.31	1700
250.5	11.94	450	3	0.31	1680
247.07	12.103	900	3	0.319	1700
239.27	11.997	900	3	0.319	1680
232.37	12.173	1500	3	0.331	1700
225.03	12.065	1500	3	0.331	1680
220.8	12.239	1981.2	3	0.341	1700
214.13	12.124	1981.2	3	0.341	1680
210.05	12.304	2438.4	3	0.351	1700
204.15	12.185	2438.4	3	0.351	1680
203.35	12.332	2743.2	3	0.357	1700
197.67	12.222	2743.2	3	0.357	1680
196.51	12.386	3048	3	0.364	1700
191.29	12.269	3048	3	0.364	1680
177.44	14.763	3048.1	3	0.547	1700
171.5	14.661	3048.1	3	0.547	1680
166.3	14.932	3657.6	3	0.568	1700
161.01	14.821	3657.6	3	0.568	1680
155.73	15.115	4267.2	3	0.591	1700
150.96	15.009	4267.2	3	0.591	1680
145.72	15.32	4876.8	3	0.616	1700
141.41	15.22	4876.8	3	0.616	1680
136.35	15.522	5486.4	3	0.641	1700
132.31	15.419	5486.4	3	0.641	1680

127.47	15.761	6096	3	0.669	1700
123.68	15.658	6096	3	0.669	1680
107.48	16.512	7620	3	0.744	1700
104.4	16.414	7620	3	0.744	1680
102.03	16.779	8077.2	3	0.769	1700
99.163	16.678	8077.2	3	0.769	1680
90.714	16.86	9144	3	0.785	1700
88.254	16.746	9144	3	0.785	1680
81.738	17.006	10058	3	0.805	1700
79.33	16.884	10058	3	0.805	1680
76.056	17.112	10668	3	0.82	1700
73.808	16.991	10668	3	0.82	1680
70.537	17.066	11227	3	0.82	1700
68.441	16.946	11227	3	0.82	1680
63.549	17.069	11887	3	0.82	1700
61.66	16.946	11887	3	0.82	1680
62.445	17.068	12000	3	0.82	1700
60.592	16.944	12000	3	0.82	1680
57.709	17.071	12497	3	0.82	1700
56.013	16.947	12497	3	0.82	1680

! Engine Performance at Cruise Rating

Net Thrust (kN)	**SFC (mg/Ns)**	**Altitude (m)**	**Dtisa**	**Mach**	**TET**
78.748	16.789	10058	3	0.8	1675
78.148	16.758	10058	3	0.8	1670
77.497	16.727	10058	3	0.8	1665
76.84	16.694	10058	3	0.8	1660
76.205	16.663	10058	3	0.8	1655
75.57	16.601	10058	3	0.8	1650
74.935	16.601	10058	3	0.8	1645
74.273	16.575	10058	3	0.8	1640
73.591	16.551	10058	3	0.8	1635
72.926	16.528	10058	3	0.8	1630
72.188	16.501	10058	3	0.8	1625
71.429	16.475	10058	3	0.8	1620
70.679	16.45	10058	3	0.8	1615
69.94	16.424	10058	3	0.8	1610
69.2	16.4	10058	3	0.8	1605
68.455	16.377	10058	3	0.8	1600
67.704	16.355	10058	3	0.8	1595
66.929	16.34	10058	3	0.8	1590
66.157	16.323	10058	3	0.8	1585
65.377	16.312	10058	3	0.8	1580

64.629	16.298	10058	3	0.8	1575
63.839	16.285	10058	3	0.8	1570
63.012	16.268	10058	3	0.8	1565
62.208	16.257	10058	3	0.8	1560
73.217	16.962	10670	3	0.82	1675
72.633	16.932	10670	3	0.82	1670
72.02	16.901	10670	3	0.82	1665
71.415	16.869	10670	3	0.82	1660
70.82	16.837	10670	3	0.82	1655
70.227	16.805	10670	3	0.82	1650
69.638	16.774	10670	3	0.82	1645
69.05	16.744	10670	3	0.82	1640
68.464	16.714	10670	3	0.82	1635
67.891	16.683	10670	3	0.82	1630
67.242	16.661	10670	3	0.82	1625
66.542	16.635	10670	3	0.82	1620
65.845	16.607	10670	3	0.82	1615
65.148	16.584	10670	3	0.82	1610
64.458	16.558	10670	3	0.82	1605
63.79	16.532	10670	3	0.82	1600
63.101	16.505	10670	3	0.82	1595
62.43	16.481	10670	3	0.82	1590
61.721	16.464	10670	3	0.82	1585
60.989	16.451	10670	3	0.82	1580
60.191	16.434	10670	3	0.82	1575
59.419	16.419	10670	3	0.82	1570
58.665	16.406	10670	3	0.82	1565
57.908	16.391	10670	3	0.82	1560

! Engine Performance at Descent Rating

Net Thrust (kN)	**SFC (mg/Ns)**	**Altitude (m)**	**Dtisa**	**Mach**	**TET**
61.93	14.314	0	3	0.394	1250
54.195	14.817	0	3	0.394	1225
61.818	14.333	10	3	0.395	1250
54.072	14.843	10	3	0.395	1225
54.605	14.413	1333.5	3	0.415	1250
47.849	14.918	1333.5	3	0.415	1225
46.882	14.975	2667	3	0.455	1250
41.097	15.506	2667	3	0.455	1225
39.886	15.72	4000.5	3	0.504	1250
34.94	16.308	4000.5	3	0.504	1225
33.517	16.824	5334	3	0.57	1250
29.3	17.506	5334	3	0.57	1225

28.805	17.389	6667.5	3	0.618	1250
25.247	18.074	6667.5	3	0.618	1225
25.059	17.555	8001	3	0.654	1250
21.986	18.237	8001	3	0.654	1225
21.239	18.494	9334.5	3	0.727	1250
18.695	19.248	9334.5	3	0.727	1225
18.335	19.245	10668	3	0.8	1250
16.065	20.047	10668	3	0.8	1225

! Engine Performance at Approach Rating

Net Thrust (kN)	**SFC (mg/Ns)**	**Altitude (m)**	**Dtisa**	**Mach**	**TET**
86.082	13.37	0	3	0.394	1325
77.498	13.631	0	3	0.394	1300
85.911	13.388	10	3	0.395	1325
77.335	13.651	10	3	0.395	1300
75.832	13.471	1333.5	3	0.415	1325
68.221	13.737	1333.5	3	0.415	1300

! Engine Performance at Ground Idle Rating

Net Thrust (kN)	**SFC (mg/Ns)**	**Altitude (m)**	**Dtisa**	**Mach**	**TET**
92.449	6.66	0	3	0	1180
80.54	6.719	0	3	0	1150
87.129	7.069	0	3	0.025	1180
75.71	7.15	0	3	0.025	1150
82.488	7.474	0	3	0.05	1180
71.267	7.603	0	3	0.05	1150
77.961	7.921	0	3	0.075	1180
67.167	8.08	0	3	0.075	1150
73.692	8.395	0	3	0.1	1180
63.381	8.583	0	3	0.1	1150
70.04	8.857	0	3	0.125	1180
59.866	9.113	0	3	0.125	1150
66.452	9.369	0	3	0.15	1180
56.628	9.669	0	3	0.15	1150
63.162	9.903	0	3	0.175	1180
53.609	10.56	0	3	0.175	1150
60.087	10.461	0	3	0.2	1180
50.816	10.879	0	3	0.2	1150

A.1.1 AIRCRAFT FLIGHT PATH PERFORMANCE OUTPUT WITH A380-800 AIRCRAFT AND INTERCOOLED-RECUPERATED TRENT900 ENGINE

```
ENGINE_SPEC:RR_trent900
Aircraft weight L1 at beginning of climb:   576092.330671755
 Fuel burnt till top of climb (kg):   15735.3499949827
 Check :   15735.3499949828
 Aircraft weight(kg) at top of climb:   560356.980676772
 Distance flown during climb (km):   500.172978150581
 Climb duration (min):    36.8204082830832
A/C weight at beginning of cruise:    560356.980676772
Cruise data
Dt of each cruise segement:   5.00 min
First and last cruise segment duration:   2.50 min
 Nacelle. Drag Coeff (Mid-Cr):  6.708458838222480E-004
 Nacelle. Drag (Mid-Cr):   6.36419327795167      (kN)
 Cruise duration:   955.414828922424      (min)
 Aircraft weight at END of cruise (kg):   333819.746804090
 Distance flown during cruise (km):   14038.1960650024
 A/C weight at beginning of cruise, Check:   560356.980676772
Aircraft weight L1 at beginning of descent:   333819.746804090
 Fuel burnt in descent segment (kg):   3054.78231721509
 Aircraft weight(kgs) at END of descent (kg):    330764.964486875
 Distance flown during descent (km):   277.630956816078
 Descent duration (min):    24.0972886053265
 Fuel burnt during landing (kg):    1657.31846861221
 (NOTE: Landing distance not included in range)
 Distance flown during landing (km):   48.6000000000000
----------------------------------------
STALL SPEED (m/s)           =        79.487532
FAILURE SPEED (V1)          =        81.133173
LIFT-OFF SPEED (m/s)        =        87.436286
V2         (m/s)       =        95.385039
----------------------------------------
*********************************************************
**         ALL ENGINE OPERATE (AEO)           **
*********************************************************
```

```
 ---------------------------------------------------------------
 GROUND DISTANCE (GROUND ROLL)          (km)       =
2.319467
 DISTANCE TO THE SCREEN HEIGHT          (km)       =
0.300101
 FAR TAKE-OFF DISTANCE            (km)       =         3.012503
 ===============================================================
 HEIGHT AT END OF TRANSITION      (m)        =        49.882072
 ===============================================================
 TAKE-OFF FLIGHT PATH             (km)       =         3.238690
 ---------------------------------------------------------------
 TOTAL TAKE-OFF FLIGHT PATH TO ALT. = 1500FT (km)   =
6.084111
 ===============================================================
 *********************************************************
 **         ONE ENGINE INOPERATIVE (OEI)      **
 *********************************************************
 ---------------------------------------------------------------
 BALANCED FIELD LENGTH            (km)       =         3.310000
 ---------------------------------------------------------------
 FROM THE SCREEN TO THE END OF TRANSITION (km)           =
0.225853
 ---------------------------------------------------------------
 CLIMB TO 400FT                   (km)       =         0.572792
 ACCELERATION TO VC(250KT)        (km)       =         1.818715
 CLIMB TO 1500FT            (km)       =         3.818932
 ===============================================================
 TAKE-OFF FLIGHT PATH             (km)       =        6.210438
 ---------------------------------------------------------------
 TOTAL TAKE-OFF FLIGHT PATH TO ALT. = 1500FT (TOFP)(km) =
9.520438
 ===============================================================
 The fuel weight in Kg for TAXI is:
1809.01617695458
 The fuel weight in Kg for TAKE-OFF is:
751.133892000000
 ===============================================================
 Main Mission Range:        14815.9999999690      km
 Range Error:   2.090195616300884E-010  %
 Main Block Range:          14870.6841105395      km
```

```
 Main Mission TIME:          1016.33252581083      min
 Main Block TIME:            17.2222087635139      hr
 Mean Mission speed:        242.965099572911      m/s
 Mean Block speed:          239.849931154718      m/s
 Main Mission Fuel:          245327.366184880      kg
 Main Block Fuel:            246984.684653492      kg
 ================================================================

  Overall Flight duration:   1016.33252581083      min
16.9388754301806      hr
```

AIRCRAFT PERFORMANCE DURING CLIMB CONDITION

Seg_No	ALT (m)	ALT (ft)	TIME(min)	TIME(hrs)	Thrust (KN) /Engine	SFC (mg/Ns)	Segment Fuel(kg)	EAS (m/s)	TAS (m/s)
1	557.2	1828.084	0	0	270.11	12.001	0	128.6111	132.8122
2	900	2952.7559	0.3536	0.0059	247.07	12.103	264.4466	128.6111	135.057
3	1500	4921.2598	1.0422	0.0174	232.37	12.173	480.8696	128.6111	139.1224
4	1981.2	6500	1.6294	0.0272	220.8	12.239	389.7698	128.6111	142.5142
5	2438.4	8000	2.2204	0.037	210.05	12.304	375.0064	128.6111	145.8507
6	2743.2	9000	2.6342	0.0439	203.35	12.332	252.8219	128.6111	148.1392
7	3048	10000	3.0561	0.0509	196.51	12.386	250.2306	128.6111	150.4809
8	3048	10000	3.9731	0.0662	177.44	14.763	558.5614	164.6222	192.6156
9	3657.6	12000	4.9182	0.082	166.3	14.932	578.818	164.6222	198.8231
10	4267.2	14000	5.9672	0.0995	155.73	15.115	609.0319	164.6222	205.3292
11	4876.8	16000	7.1433	0.1191	145.72	15.32	647.3816	164.6222	212.1532
12	5486.4	18000	8.4764	0.1413	136.35	15.522	695.8589	164.6222	219.316
13	6096	20000	10.0149	0.1669	127.47	15.761	761.8525	164.6222	226.84
14	7620	25000	14.5487	0.2425	107.48	16.512	2062.6826	164.6222	247.3963
15	8077.2	26500	16.0679	0.2678	102.03	16.779	635.7494	160.5787	247.8568
16	9144	30000	20.4842	0.3414	90.714	16.86	1718.061	148.4628	244.2294
17	10058	32998.6877	26.9572	0.4493	81.738	17.006	2268.2304	138.5464	241.0781

Seg_No	Mach	Climb Rate (m/s)	Dist_(m)	Dist_(m) Cum	Climb Gradient (deg)	DragCoeff aircraft	LiftCoeff aircraft	DragCoeff Nacelle	Drag Nacelle (KN)
1	0.3905	16.1597	0	0	6.8797	0.0325	0.6607	0.0007	5.7336
2	0.3987	14.5223	2820.7308	2820.7308	6.047	0.0354	0.6604	0.0007	5.7395
3	0.4135	13.6578	5632.4505	8453.1812	5.5397	0.0354	0.6599	0.0007	5.7496
4	0.426	12.892	4938.21	13391.3913	5.1095	0.0354	0.6594	0.0007	5.7574
5	0.4383	12.2784	5092.9346	18484.3258	4.7748	0.0354	0.659	0.0007	5.7647
6	0.4468	12.0391	3636.3576	22120.6835	4.6099	0.0354	0.6587	0.0007	5.7694
7	0.4555	0	3767.9145	25888.5979	0	0.0353	0.6584	0.0007	5.7741
8	0.583	10.7502	9438.2148	35326.8127	3.1439	0.0224	0.4015	0.0006	9.0143
9	0.6063	9.6851	11081.7462	46408.5589	2.744	0.0224	0.4011	0.0006	9.0194
10	0.6308	8.6392	12704.5536	59113.1125	2.37	0.0224	0.4006	0.0006	9.0229
11	0.6567	7.6212	14716.6292	73829.7417	2.0232	0.0224	0.4002	0.0006	9.0245
12	0.6842	6.6037	17245.3015	91075.0431	1.6956	0.0224	0.3997	0.0006	9.0241
13	0.7132	5.6023	20583.6021	111658.6452	1.3535	0.0223	0.3992	0.0006	9.0213
14	0.7936	5.0159	64485.3751	176144.0203	1.1604	0.0222	0.3977	0.0006	9.002
15	0.8	4.0259	22566.4103	198710.4306	0.9374	0.023	0.4175	0.0006	8.6114
16	0.8	2.3534	65188.0113	263898.4419	0.5557	0.0261	0.487	0.0007	7.4933
17	0.8	1.0308	94237.043	358135.4849	0.2461	0.0296	0.557	0.0007	6.6297

AIRCRAFT PERFORMANCE DURING CRUISE CONDITION (I)

Seg No	TIME (hrs)	ALT (m)	ALT (ft)	Thrust (KN) /Engine	SFC (mg/Ns)	Segment Fuel(kg)	Dist(km)	Fuel Cum (Kg)	Dist(km) Cum	L/D	DragCoeff aircraft	LiftCoeff aircraft	DragCoeff Nacelle	Drag (KN) Nacelle
1	0.0417	10058	32.9987	73.1271	16.535	725.8068	36.1774	725.8068	36.1774	18.793	0.0295	0.5538	0.0007	6.6297
2	0.1251	10058	32.9987	73.0389	16.5319	1449.5961	72.3549	2175.4029	108.5323	18.7913	0.0294	0.5531	0.0007	6.6297
3	0.2084	10670	35.0066	72.8557	16.9434	1481.9548	73.5075	3657.3577	182.0397	18.7897	0.0307	0.5772	0.0007	6.3642
4	0.2918	10670	35.0066	72.6682	16.9338	1477.2997	73.5075	5134.6574	255.5472	18.7882	0.0306	0.5757	0.0007	6.3642
5	0.3752	10670	35.0066	72.4817	16.9243	1472.6863	73.5075	6607.3438	329.0547	18.7866	0.0306	0.5741	0.0007	6.3642
6	0.4585	10670	35.0066	72.2963	16.915	1468.1062	73.5075	8075.4499	402.5621	18.7848	0.0305	0.5726	0.0007	6.3642
7	0.5419	10670	35.0066	72.112	16.9057	1463.5566	73.5075	9539.0065	476.0696	18.7829	0.0304	0.5711	0.0007	6.3642
8	0.6253	10670	35.0066	71.9288	16.8962	1459.0188	73.5075	10998.0253	549.577	18.7808	0.0303	0.5696	0.0007	6.3642
9	0.7086	10670	35.0066	71.7466	16.8865	1454.493	73.5075	12452.5183	623.0845	18.7786	0.0303	0.5681	0.0007	6.3642
10	0.792	10670	35.0066	71.5654	16.877	1449.9973	73.5075	13902.5157	696.592	18.7763	0.0302	0.5666	0.0007	6.3642
11	0.8754	10670	35.0066	71.3853	16.8674	1445.5293	73.5075	15348.045	770.0994	18.7739	0.0301	0.5651	0.0007	6.3642
12	0.9587	10670	35.0066	71.2062	16.8578	1441.0796	73.5075	16789.1246	843.6069	18.7713	0.03	0.5636	0.0007	6.3642
13	1.0421	10670	35.0066	71.0282	16.8482	1436.6594	73.5075	18225.7839	917.1143	18.7686	0.0299	0.5621	0.0007	6.3642
14	1.1255	10670	35.0066	70.8511	16.8387	1432.2684	73.5075	19658.0523	990.6218	18.7658	0.0299	0.5606	0.0007	6.3642
15	1.2089	10670	35.0066	70.6751	16.8292	1427.9042	73.5075	21085.9566	1064.1293	18.7628	0.0298	0.5591	0.0007	6.3642
16	1.2922	10670	35.0066	70.5	16.8197	1423.5684	73.5075	22509.5249	1137.6367	18.7597	0.0297	0.5576	0.0007	6.3642
17	1.3756	10670	35.0066	70.326	16.8103	1419.261	73.5075	23928.7859	1211.1442	18.7565	0.0297	0.5562	0.0007	6.3642
18	1.459	10670	35.0066	70.1529	16.8011	1414.9902	73.5075	25343.7761	1284.6517	18.7532	0.0296	0.5547	0.0007	6.3642
19	1.5423	10670	35.0066	69.9808	16.792	1410.7583	73.5075	26754.5344	1358.1591	18.7497	0.0295	0.5532	0.0007	6.3642
20	1.6257	10670	35.0066	69.8097	16.783	1406.5539	73.5075	28161.0882	1431.6666	18.7461	0.0294	0.5518	0.0007	6.3642
21	1.7091	10670	35.0066	69.6396	16.7741	1402.3767	73.5075	29563.465	1505.174	18.7424	0.0294	0.5503	0.0007	6.3642
22	1.7924	10670	35.0066	69.4704	16.7654	1398.2491	73.5075	30961.7141	1578.6815	18.7385	0.0293	0.5489	0.0007	6.3642
23	1.8758	10670	35.0066	69.3021	16.7569	1394.1482	73.5075	32355.8622	1652.189	18.7345	0.0292	0.5474	0.0007	6.3642
24	1.9592	10670	35.0066	69.1348	16.7483	1390.0735	73.5075	33745.9357	1725.6964	18.7304	0.0291	0.546	0.0007	6.3642
25	2.0426	10670	35.0066	68.9684	16.7398	1386.0236	73.5075	35131.9593	1799.2039	18.7262	0.0291	0.5446	0.0007	6.3642
26	2.1259	10670	35.0066	68.8029	16.7313	1381.9983	73.5075	36513.9576	1872.7113	18.7218	0.029	0.5431	0.0007	6.3642
27	2.2093	10670	35.0066	68.6383	16.7229	1377.9986	73.5075	37891.9562	1946.2188	18.7173	0.0289	0.5417	0.0007	6.3642
28	2.2927	10670	35.0066	68.4747	16.7145	1374.0243	73.5075	39265.9805	2019.7263	18.7127	0.0289	0.5403	0.0007	6.3642
29	2.376	10670	35.0066	68.3119	16.7058	1370.0389	73.5075	40636.0194	2093.2337	18.7079	0.0288	0.5388	0.0007	6.3642
30	2.4594	10670	35.0066	68.1501	16.697	1366.0763	73.5075	42002.0957	2166.7412	18.7031	0.0287	0.5374	0.0007	6.3642
31	2.5428	10670	35.0066	67.9891	16.6883	1362.139	73.5075	43364.2347	2240.2486	18.6981	0.0287	0.536	0.0007	6.3642
32	2.6261	10670	35.0066	67.829	16.6809	1358.3287	73.5075	44722.5634	2313.7561	18.693	0.0286	0.5346	0.0007	6.3642
33	2.7095	10670	35.0066	67.6698	16.6755	1354.7019	73.5075	46077.2653	2387.2636	18.6877	0.0285	0.5332	0.0007	6.3642
34	2.7929	10670	35.0066	67.5114	16.6701	1351.0964	73.5075	47428.3617	2460.771	18.6823	0.0285	0.5318	0.0007	6.3642
35	2.8762	10670	35.0066	67.3539	16.6648	1347.5119	73.5075	48775.8736	2534.2785	18.6768	0.0284	0.5304	0.0007	6.3642
36	2.9596	10670	35.0066	67.1972	16.6593	1343.9367	73.5075	50119.8103	2607.7859	18.6712	0.0283	0.529	0.0007	6.3642
37	3.043	10670	35.0066	67.0413	16.6535	1340.3532	73.5075	51460.1635	2681.2934	18.6654	0.0283	0.5276	0.0007	6.3642
38	3.1264	10670	35.0066	66.8863	16.6478	1336.7909	73.5075	52796.9544	2754.8009	18.6596	0.0282	0.5262	0.0007	6.3642
39	3.2097	10670	35.0066	66.7321	16.6421	1333.2494	73.5075	54130.2038	2828.3083	18.6536	0.0281	0.5249	0.0007	6.3642
40	3.2931	10670	35.0066	66.5786	16.6364	1329.7288	73.5075	55459.9326	2901.8158	18.6474	0.0281	0.5235	0.0007	6.3642
41	3.3765	10670	35.0066	66.426	16.6303	1326.2007	73.5075	56786.1333	2975.3232	18.6412	0.028	0.5221	0.0007	6.3642
42	3.4598	10670	35.0066	66.2742	16.6242	1322.6846	73.5075	58108.818	3048.8307	18.6348	0.0279	0.5207	0.0007	6.3642
43	3.5432	10670	35.0066	66.1232	16.6182	1319.1893	73.5075	59428.0073	3122.3382	18.6283	0.0279	0.5194	0.0007	6.3642
44	3.6266	10670	35.0066	65.973	16.6121	1315.7146	73.5075	60743.7219	3195.8456	18.6217	0.0278	0.518	0.0007	6.3642
45	3.7099	10670	35.0066	65.8236	16.6063	1312.2724	73.5075	62055.9942	3269.3531	18.6149	0.0278	0.5166	0.0007	6.3642
46	3.7933	10670	35.0066	65.6749	16.6014	1308.9223	73.5075	63364.9165	3342.8605	18.6081	0.0277	0.5153	0.0007	6.3642
47	3.8767	10670	35.0066	65.5271	16.5965	1305.5913	73.5075	64670.5078	3416.368	18.6011	0.0276	0.5139	0.0007	6.3642
48	3.9601	10670	35.0066	65.3799	16.5917	1302.2792	73.5075	65972.787	3489.8755	18.5939	0.0276	0.5126	0.0007	6.3642
49	4.0434	10670	35.0066	65.2336	16.5868	1298.9859	73.5075	67271.7729	3563.3829	18.5867	0.0275	0.5112	0.0007	6.3642
50	4.1268	10670	35.0066	65.088	16.5817	1295.6893	73.5075	68567.4622	3636.8904	18.5793	0.0274	0.5099	0.0007	6.3642
51	4.2102	10670	35.0066	64.9432	16.5763	1292.3804	73.5075	69859.8426	3710.3979	18.5718	0.0274	0.5085	0.0007	6.3642
52	4.2935	10670	35.0066	64.7991	16.5709	1289.0905	73.5075	71148.9331	3783.9053	18.5642	0.0273	0.5072	0.0007	6.3642
53	4.3769	10670	35.0066	64.6557	16.5654	1285.8194	73.5075	72434.7525	3857.4128	18.5565	0.0273	0.5059	0.0007	6.3642
54	4.4603	10670	35.0066	64.5131	16.5601	1282.5671	73.5075	73717.3195	3930.9202	18.5486	0.0272	0.5045	0.0007	6.3642
55	4.5436	10670	35.0066	64.3712	16.5546	1279.325	73.5075	74996.6445	4004.4277	18.5406	0.0271	0.5032	0.0007	6.3642
56	4.627	10670	35.0066	64.2301	16.5491	1276.0962	73.5075	76272.7407	4077.9352	18.5325	0.0271	0.5019	0.0007	6.3642
57	4.7104	10670	35.0066	64.0897	16.5437	1272.8859	73.5075	77545.6266	4151.4426	18.5243	0.027	0.5006	0.0007	6.3642
58	4.7937	10670	35.0066	63.95	16.5382	1269.6939	73.5075	78815.3205	4224.9501	18.516	0.027	0.4993	0.0007	6.3642
59	4.8771	10670	35.0066	63.811	16.5328	1266.5201	73.5075	80081.8405	4298.4575	18.5075	0.0269	0.4979	0.0007	6.3642
60	4.9605	10670	35.0066	63.6727	16.5274	1263.3619	73.5075	81345.2025	4371.965	18.4989	0.0268	0.4966	0.0007	6.3642
61	5.0439	10670	35.0066	63.5351	16.522	1260.2213	73.5075	82605.4238	4445.4725	18.4902	0.0268	0.4953	0.0007	6.3642
62	5.1272	10670	35.0066	63.3983	16.5166	1257.0985	73.5075	83862.5223	4518.9799	18.4813	0.0267	0.494	0.0007	6.3642
63	5.2106	10670	35.0066	63.2621	16.5113	1253.9934	73.5075	85116.5157	4592.4874	18.4724	0.0267	0.4927	0.0007	6.3642
64	5.294	10670	35.0066	63.1267	16.506	1250.9058	73.5075	86367.4216	4665.9948	18.4633	0.0266	0.4914	0.0007	6.3642

AIRCRAFT PERFORMANCE DURING CRUISE CONDITION (II)

Seg No	TIME (hrs)	ALT (m)	ALT (ft)	Thrust (KN) /Engine	SFC (mg/Ns)	Segment Fuel(kg)	Dist(km)	Fuel Cum (Kg)	Dist(km) Cum	L/D	DragCoeff aircraft	LiftCoeff aircraft	DragCoeff Nacelle	Drag (KN) Nacelle
65	5.3773	10670	35.0066	62.9919	16.5011	1247.8639	73.5075	87615.2855	4739.5023	18.4541	0.0266	0.4901	0.0007	6.3642
66	5.4607	10670	35.0066	62.8578	16.4963	1244.8455	73.5075	88860.131	4813.0098	18.4448	0.0265	0.4888	0.0007	6.3642
67	5.5441	10670	35.0066	62.7244	16.4915	1241.8439	73.5075	90101.975	4886.5172	18.4354	0.0264	0.4876	0.0007	6.3642
68	5.6274	10670	35.0066	62.5916	16.4868	1238.859	73.5075	91340.8339	4960.0247	18.4258	0.0264	0.4863	0.0007	6.3642
69	5.7108	10670	35.0066	62.4595	16.4821	1235.8905	73.5075	92576.7245	5033.5321	18.4161	0.0263	0.485	0.0007	6.3642
70	5.7942	10670	35.0066	62.3281	16.4786	1233.0284	73.5075	93809.7528	5107.0396	18.4063	0.0263	0.4837	0.0007	6.3642
71	5.8776	10670	35.0066	62.1974	16.4754	1230.2073	73.5075	95039.9601	5180.5471	18.3964	0.0262	0.4824	0.0007	6.3642
72	5.9609	10670	35.0066	62.0672	16.4723	1227.4011	73.5075	96267.3612	5254.0545	18.3864	0.0262	0.4812	0.0007	6.3642
73	6.0443	10670	35.0066	61.9377	16.4692	1224.6097	73.5075	97491.9709	5327.562	18.3762	0.0261	0.4799	0.0007	6.3642
74	6.1277	10670	35.0066	61.8089	16.4661	1221.8329	73.5075	98713.8038	5401.0694	18.3659	0.0261	0.4786	0.0007	6.3642
75	6.211	10670	35.0066	61.6807	16.4633	1219.0892	73.5075	99932.893	5474.5769	18.3555	0.026	0.4774	0.0007	6.3642
76	6.2944	10670	35.0066	61.5531	16.461	1216.4	73.5075	101149.293	5548.0844	18.345	0.026	0.4761	0.0007	6.3642
77	6.3778	10670	35.0066	61.4261	16.4588	1213.7245	73.5075	102363.0175	5621.5918	18.3343	0.0259	0.4749	0.0007	6.3642
78	6.4611	10670	35.0066	61.2998	16.4565	1211.0626	73.5075	103574.0801	5695.0993	18.3236	0.0258	0.4736	0.0007	6.3642
79	6.5445	10670	35.0066	61.174	16.4543	1208.4142	73.5075	104782.4943	5768.6067	18.3127	0.0258	0.4723	0.0007	6.3642
80	6.6279	10670	35.0066	61.0489	16.4521	1205.7793	73.5075	105988.2737	5842.1142	18.3017	0.0257	0.4711	0.0007	6.3642
81	6.7112	10670	35.0066	60.9243	16.4496	1203.141	73.5075	107191.4147	5915.6217	18.2905	0.0257	0.4698	0.0007	6.3642
82	6.7946	10670	35.0066	60.8004	16.447	1200.5008	73.5075	108391.9155	5989.1291	18.2793	0.0256	0.4686	0.0007	6.3642
83	6.878	10670	35.0066	60.6771	16.4444	1197.8741	73.5075	109589.7895	6062.6366	18.2679	0.0256	0.4674	0.0007	6.3642
84	6.9614	10670	35.0066	60.5543	16.4417	1195.2609	73.5075	110785.0504	6136.1441	18.2564	0.0255	0.4661	0.0007	6.3642
85	7.0447	10670	35.0066	60.4322	16.4391	1192.661	73.5075	111977.7114	6209.6515	18.2448	0.0255	0.4649	0.0007	6.3642
86	7.1281	10670	35.0066	60.3106	16.4365	1190.0744	73.5075	113167.7858	6283.159	18.2331	0.0254	0.4637	0.0007	6.3642
87	7.2115	10670	35.0066	60.1896	16.434	1187.5013	73.5075	114355.2871	6356.6664	18.2213	0.0254	0.4624	0.0007	6.3642
88	7.2948	10670	35.0066	60.0692	16.4316	1184.9573	73.5075	115540.2444	6430.1739	18.2093	0.0253	0.4612	0.0007	6.3642
89	7.3782	10670	35.0066	59.9494	16.4293	1182.4262	73.5075	116722.6706	6503.6814	18.1972	0.0253	0.46	0.0007	6.3642
90	7.4616	10670	35.0066	59.8302	16.427	1179.9079	73.5075	117902.5785	6577.1888	18.185	0.0252	0.4587	0.0007	6.3642
91	7.5449	10670	35.0066	59.7115	16.4247	1177.4023	73.5075	119079.9808	6650.6963	18.1727	0.0252	0.4575	0.0007	6.3642
92	7.6283	10670	35.0066	59.5934	16.4224	1174.9093	73.5075	120254.8901	6724.2037	18.1603	0.0251	0.4563	0.0007	6.3642
93	7.7117	10670	35.0066	59.4759	16.4201	1172.4288	73.5075	121427.3189	6797.7112	18.1477	0.0251	0.4551	0.0007	6.3642
94	7.7951	10670	35.0066	59.3589	16.418	1169.9703	73.5075	122597.2892	6871.2187	18.135	0.025	0.4539	0.0007	6.3642
95	7.8784	10670	35.0066	59.2425	16.416	1167.5328	73.5075	123764.8219	6944.7261	18.1222	0.025	0.4527	0.0007	6.3642
96	7.9618	10670	35.0066	59.1266	16.414	1165.1074	73.5075	124929.9293	7018.2336	18.1093	0.0249	0.4515	0.0007	6.3642
97	8.0452	10670	35.0066	59.0113	16.412	1162.6941	73.5075	126092.6233	7091.741	18.0963	0.0249	0.4503	0.0007	6.3642
98	8.1285	10670	35.0066	58.8965	16.41	1160.2927	73.5075	127252.916	7165.2485	18.0831	0.0248	0.4491	0.0007	6.3642
99	8.2119	10670	35.0066	58.7822	16.408	1157.9032	73.5075	128410.8193	7238.756	18.0699	0.0248	0.4479	0.0007	6.3642
100	8.2953	10670	35.0066	58.6686	16.4061	1155.5256	73.5075	129566.3449	7312.2634	18.0565	0.0247	0.4467	0.0007	6.3642
101	8.3786	10670	35.0066	58.5554	16.4038	1153.1399	73.5075	130719.4848	7385.7709	18.043	0.0247	0.4455	0.0007	6.3642
102	8.462	10670	35.0066	58.4428	16.4016	1150.7655	73.5075	131870.2503	7459.2783	18.0294	0.0246	0.4443	0.0007	6.3642
103	8.5454	10670	35.0066	58.3307	16.3994	1148.4029	73.5075	133018.6532	7532.7858	18.0156	0.0246	0.4431	0.0007	6.3642
104	8.6287	10670	35.0066	58.2191	16.3972	1146.0521	73.5075	134164.7053	7606.2933	18.0018	0.0245	0.4419	0.0007	6.3642
105	8.7121	10670	35.0066	58.1081	16.395	1143.7129	73.5075	135308.4182	7679.8007	17.9878	0.0245	0.4407	0.0007	6.3642
106	8.7955	10670	35.0066	57.9976	16.3928	1141.3854	73.5075	136449.8036	7753.3082	17.9737	0.0245	0.4395	0.0007	6.3642
107	8.8789	10670	35.0066	57.8876	16.3906	1139.0694	73.5075	137588.873	7826.8156	17.9595	0.0244	0.4383	0.0007	6.3642
108	8.9622	10670	35.0066	57.7781	16.3884	1136.7649	73.5075	138725.6379	7900.3231	17.9452	0.0244	0.4372	0.0007	6.3642
109	9.0456	10670	35.0066	57.6692	16.3863	1134.4718	73.5075	139860.1097	7973.8306	17.9307	0.0243	0.436	0.0007	6.3642
110	9.129	10670	35.0066	57.5607	16.3841	1132.1901	73.5075	140992.2998	8047.338	17.9162	0.0243	0.4348	0.0007	6.3642
111	9.2123	10670	35.0066	57.4528	16.382	1129.9196	73.5075	142122.2194	8120.8455	17.9015	0.0242	0.4337	0.0007	6.3642
112	9.2957	10670	35.0066	57.3454	16.3799	1127.6603	73.5075	143249.8797	8194.3529	17.8867	0.0242	0.4325	0.0007	6.3642
113	9.3791	10670	35.0066	57.2385	16.3777	1125.4122	73.5075	144375.2919	8267.8604	17.8718	0.0241	0.4313	0.0007	6.3642
114	9.4624	10670	35.0066	57.132	16.3756	1123.1751	73.5075	145498.467	8341.3679	17.8568	0.0241	0.4302	0.0007	6.3642
115	9.5458	10670	35.0066	57.0261	16.3735	1120.9491	73.5075	146619.4161	8414.8753	17.8417	0.024	0.429	0.0007	6.3642
116	9.6292	10670	35.0066	56.9207	16.3714	1118.734	73.5075	147738.1501	8488.3828	17.8264	0.024	0.4278	0.0007	6.3642
117	9.7126	10670	35.0066	56.8158	16.3694	1116.5298	73.5075	148854.6798	8561.8903	17.811	0.024	0.4267	0.0007	6.3642
118	9.7959	10670	35.0066	56.7113	16.3673	1114.3363	73.5075	149969.0162	8635.3977	17.7956	0.0239	0.4255	0.0007	6.3642
119	9.8793	10670	35.0066	56.6074	16.3652	1112.1537	73.5075	151081.1699	8708.9052	17.78	0.0239	0.4244	0.0007	6.3642
120	9.9627	10670	35.0066	56.5039	16.3632	1109.9817	73.5075	152191.1516	8782.4126	17.7642	0.0238	0.4232	0.0007	6.3642
121	10.046	10670	35.0066	56.4009	16.3611	1107.8204	73.5075	153298.9719	8855.9201	17.7484	0.0238	0.4221	0.0007	6.3642
122	10.1294	10670	35.0066	56.2984	16.3591	1105.6696	73.5075	154404.6415	8929.4276	17.7325	0.0237	0.4209	0.0007	6.3642
123	10.2128	10670	35.0066	56.1964	16.3571	1103.5293	73.5075	155508.1708	9002.935	17.7164	0.0237	0.4198	0.0007	6.3642
124	10.2961	10670	35.0066	56.0948	16.3551	1101.3994	73.5075	156609.5702	9076.4425	17.7002	0.0237	0.4186	0.0007	6.3642
125	10.3795	10670	35.0066	55.9937	16.3531	1099.28	73.5075	157708.8502	9149.9499	17.684	0.0236	0.4175	0.0007	6.3642
126	10.4629	10670	35.0066	55.8931	16.3511	1097.1708	73.5075	158806.021	9223.4574	17.6676	0.0236	0.4164	0.0007	6.3642
127	10.5462	10670	35.0066	55.7929	16.3491	1095.0719	73.5075	159901.0929	9296.9649	17.651	0.0235	0.4152	0.0007	6.3642
128	10.6296	10670	35.0066	55.6932	16.3471	1092.9832	73.5075	160994.0761	9370.4723	17.6344	0.0235	0.4141	0.0007	6.3642

AIRCRAFT PERFORMANCE DURING CRUISE CONDITION (III)

Seg No	TIME (hrs)	ALT (m)	ALT (ft)	Thrust (KN) /Engine	SFC (mg/Ns)	Segment Fuel(kg)	Dist(km)	Fuel Cum (Kg)	Dist(km) Cum	L/D	DragCoeff aircraft	LiftCoeff aircraft	DragCoeff Nacelle	Drag (KN) Nacelle
129	10.713	10670	35.0066	55.594	16.3451	1090.9047	73.5075	162084.9808	9443.9798	17.6177	0.0234	0.413	0.0007	6.3642
130	10.7964	10670	35.0066	55.4953	16.3432	1088.8362	73.5075	163173.817	9517.4872	17.6008	0.0234	0.4118	0.0007	6.3642
131	10.8797	10670	35.0066	55.3969	16.3412	1086.7778	73.5075	164260.5948	9590.9947	17.5839	0.0234	0.4107	0.0007	6.3642
132	10.9631	10670	35.0066	55.2991	16.3393	1084.7293	73.5075	165345.3241	9664.5022	17.5668	0.0233	0.4096	0.0007	6.3642
133	11.0465	10670	35.0066	55.2017	16.3374	1082.6907	73.5075	166428.0148	9738.0096	17.5496	0.0233	0.4085	0.0007	6.3642
134	11.1298	10670	35.0066	55.1047	16.3355	1080.662	73.5075	167508.6768	9811.5171	17.5323	0.0232	0.4073	0.0007	6.3642
135	11.2132	10670	35.0066	55.0082	16.3335	1078.6431	73.5075	168587.3199	9885.0245	17.5148	0.0232	0.4062	0.0007	6.3642
136	11.2966	10670	35.0066	54.9122	16.3316	1076.6339	73.5075	169663.9538	9958.532	17.4973	0.0232	0.4051	0.0007	6.3642
137	11.3799	10670	35.0066	54.8165	16.3297	1074.6344	73.5075	170738.5883	10032.0395	17.4797	0.0231	0.404	0.0007	6.3642
138	11.4633	10670	35.0066	54.7214	16.3279	1072.6446	73.5075	171811.2328	10105.5469	17.4619	0.0231	0.4029	0.0007	6.3642
139	11.5467	10670	35.0066	54.6266	16.326	1070.6643	73.5075	172881.8971	10179.0544	17.444	0.023	0.4018	0.0007	6.3642
140	11.63	10670	35.0066	54.5323	16.3241	1068.6936	73.5075	173950.5907	10252.5618	17.4261	0.023	0.4007	0.0007	6.3642
141	11.7134	10670	35.0066	54.4384	16.3223	1066.7323	73.5075	175017.323	10326.0693	17.408	0.023	0.3996	0.0007	6.3642
142	11.7968	10670	35.0066	54.345	16.3204	1064.7804	73.5075	176082.1034	10399.5768	17.3897	0.0229	0.3985	0.0007	6.3642
143	11.8802	10670	35.0066	54.252	16.3186	1062.8379	73.5075	177144.9413	10473.0842	17.3714	0.0229	0.3974	0.0007	6.3642
144	11.9635	10670	35.0066	54.1594	16.3167	1060.9047	73.5075	178205.8461	10546.5917	17.353	0.0228	0.3963	0.0007	6.3642
145	12.0469	10670	35.0066	54.0672	16.3149	1058.9808	73.5075	179264.8269	10620.0991	17.3345	0.0228	0.3952	0.0007	6.3642
146	12.1303	10670	35.0066	53.9755	16.3131	1057.0661	73.5075	180321.893	10693.6066	17.3158	0.0228	0.3941	0.0007	6.3642
147	12.2136	10670	35.0066	53.8841	16.3113	1055.1606	73.5075	181377.0536	10767.1141	17.297	0.0227	0.393	0.0007	6.3642
148	12.297	10670	35.0066	53.7932	16.3095	1053.2641	73.5075	182430.3177	10840.6215	17.2782	0.0227	0.3919	0.0007	6.3642
149	12.3804	10670	35.0066	53.7027	16.3077	1051.3767	73.5075	183481.6944	10914.129	17.2592	0.0226	0.3908	0.0007	6.3642
150	12.4637	10670	35.0066	53.6127	16.3059	1049.4983	73.5075	184531.1927	10987.6365	17.2401	0.0226	0.3897	0.0007	6.3642
151	12.5471	10670	35.0066	53.523	16.3041	1047.6289	73.5075	185578.8216	11061.1439	17.2209	0.0226	0.3886	0.0007	6.3642
152	12.6305	10670	35.0066	53.4337	16.3023	1045.7684	73.5075	186624.59	11134.6514	17.2016	0.0225	0.3875	0.0007	6.3642
153	12.7139	10670	35.0066	53.3449	16.3006	1043.9167	73.5075	187668.5068	11208.1588	17.1821	0.0225	0.3865	0.0007	6.3642
154	12.7972	10670	35.0066	53.2565	16.2988	1042.0739	73.5075	188710.5807	11281.6663	17.1626	0.0225	0.3854	0.0007	6.3642
155	12.8806	10670	35.0066	53.1684	16.2971	1040.2398	73.5075	189750.8205	11355.1738	17.1429	0.0224	0.3843	0.0007	6.3642
156	12.964	10670	35.0066	53.0808	16.2953	1038.4145	73.5075	190789.2349	11428.6812	17.1232	0.0224	0.3832	0.0007	6.3642
157	13.0473	10670	35.0066	52.9935	16.2936	1036.5978	73.5075	191825.8327	11502.1887	17.1033	0.0223	0.3822	0.0007	6.3642
158	13.1307	10670	35.0066	52.9067	16.2919	1034.7897	73.5075	192860.6224	11575.6961	17.0833	0.0223	0.3811	0.0007	6.3642
159	13.2141	10670	35.0066	52.8202	16.2902	1032.9902	73.5075	193893.6126	11649.2036	17.0632	0.0223	0.38	0.0007	6.3642
160	13.2974	10670	35.0066	52.7342	16.2885	1031.1992	73.5075	194924.8118	11722.7111	17.0431	0.0222	0.3789	0.0007	6.3642
161	13.3808	10670	35.0066	52.6485	16.2868	1029.4168	73.5075	195954.2286	11796.2185	17.0227	0.0222	0.3779	0.0007	6.3642
162	13.4642	10670	35.0066	52.5632	16.2851	1027.6427	73.5075	196981.8713	11869.726	17.0023	0.0222	0.3768	0.0007	6.3642
163	13.5475	10670	35.0066	52.4783	16.2834	1025.8771	73.5075	198007.7484	11943.2334	16.9818	0.0221	0.3758	0.0007	6.3642
164	13.6309	10670	35.0066	52.3938	16.2817	1024.1197	73.5075	199031.8681	12016.7409	16.9612	0.0221	0.3747	0.0007	6.3642
165	13.7143	10670	35.0066	52.3097	16.2801	1022.3707	73.5075	200054.2388	12090.2484	16.9404	0.0221	0.3736	0.0007	6.3642
166	13.7977	10670	35.0066	52.226	16.2784	1020.63	73.5075	201074.8689	12163.7558	16.9196	0.022	0.3726	0.0007	6.3642
167	13.881	10670	35.0066	52.1426	16.2768	1018.8975	73.5075	202093.7663	12237.2633	16.8986	0.022	0.3715	0.0007	6.3642
168	13.9644	10670	35.0066	52.0596	16.2751	1017.1731	73.5075	203110.9394	12310.7707	16.8776	0.022	0.3705	0.0007	6.3642
169	14.0478	10670	35.0066	51.977	16.2735	1015.4569	73.5075	204126.3963	12384.2782	16.8564	0.0219	0.3694	0.0007	6.3642
170	14.1311	10670	35.0066	51.8948	16.2718	1013.7487	73.5075	205140.1451	12457.7857	16.8351	0.0219	0.3684	0.0007	6.3642
171	14.2145	10670	35.0066	51.8129	16.2702	1012.0486	73.5075	206152.1937	12531.2931	16.8138	0.0218	0.3673	0.0007	6.3642
172	14.2979	10670	35.0066	51.7314	16.2686	1010.3565	73.5075	207162.5503	12604.8006	16.7923	0.0218	0.3663	0.0007	6.3642
173	14.3812	10670	35.0066	51.6503	16.267	1008.6724	73.5075	208171.2227	12678.308	16.7707	0.0218	0.3652	0.0007	6.3642
174	14.4646	10670	35.0066	51.5695	16.2654	1006.9962	73.5075	209178.2188	12751.8155	16.749	0.0217	0.3642	0.0007	6.3642
175	14.548	10670	35.0066	51.4891	16.2638	1005.3278	73.5075	210183.5467	12825.323	16.7271	0.0217	0.3631	0.0007	6.3642
176	14.6314	10670	35.0066	51.4091	16.2622	1003.6673	73.5075	211187.214	12898.8304	16.7052	0.0217	0.3621	0.0007	6.3642
177	14.7147	10670	35.0066	51.3294	16.2606	1002.0146	73.5075	212189.2286	12972.3379	16.6832	0.0216	0.3611	0.0007	6.3642
178	14.7981	10670	35.0066	51.2501	16.2591	1000.3696	73.5075	213189.5982	13045.8453	16.6611	0.0216	0.36	0.0007	6.3642
179	14.8815	10670	35.0066	51.1712	16.2575	998.7324	73.5075	214188.3306	13119.3528	16.6388	0.0216	0.359	0.0007	6.3642
180	14.9648	10670	35.0066	51.0926	16.256	997.1028	73.5075	215185.4334	13192.8603	16.6165	0.0215	0.358	0.0007	6.3642
181	15.0482	10670	35.0066	51.0143	16.2544	995.4809	73.5075	216180.9143	13266.3677	16.594	0.0215	0.3569	0.0007	6.3642
182	15.1316	10670	35.0066	50.9364	16.2529	993.8665	73.5075	217174.7808	13339.8752	16.5715	0.0215	0.3559	0.0007	6.3642
183	15.2149	10670	35.0066	50.8589	16.2513	992.2597	73.5075	218167.0405	13413.3826	16.5488	0.0214	0.3549	0.0007	6.3642
184	15.2983	10670	35.0066	50.7817	16.2498	990.6604	73.5075	219157.7009	13486.8901	16.5261	0.0214	0.3538	0.0007	6.3642
185	15.3817	10670	35.0066	50.7048	16.2483	989.0686	73.5075	220146.7696	13560.3976	16.5032	0.0214	0.3528	0.0007	6.3642
186	15.465	10670	35.0066	50.6283	16.2468	987.4843	73.5075	221134.2539	13633.905	16.4802	0.0213	0.3518	0.0007	6.3642
187	15.5484	10670	35.0066	50.5522	16.2452	985.9073	73.5075	222120.1612	13707.4125	16.4571	0.0213	0.3508	0.0007	6.3642
188	15.6318	10670	35.0066	50.4764	16.2437	984.3377	73.5075	223104.4989	13780.92	16.4339	0.0213	0.3498	0.0007	6.3642
189	15.7152	10670	35.0066	50.4009	16.2422	982.7755	73.5075	224087.2744	13854.4274	16.4107	0.0213	0.3487	0.0007	6.3642
190	15.7985	10670	35.0066	50.3258	16.2408	981.2205	73.5075	225068.4949	13927.9349	16.3873	0.0212	0.3477	0.0007	6.3642
191	15.8819	10670	35.0066	50.251	16.2393	979.6728	73.5075	226048.1677	14001.4423	16.3638	0.0212	0.3467	0.0007	6.3642
192	15.9236	10670	35.0066	50.1765	16.2378	489.0661	36.7537	226537.2339	14038.1961	16.3402	0.0212	0.3457	0.0007	6.3642

AIRCRAFT PERFORMANCE DURING GLIDE CONDITION

Seg_No	ALT (m)	ALT (ft)	TIME(min)	TIME(hrs)	Thrust (KN) /Engine	SFC (mg/Ns)	Segment Fuel(kg)	EAS (m/s)	TAS (m/s)
1	10670	35006.5617	0	0	18.3306	19.2461	0	128.91	233.1
2	9336.2512	30630.7456	3.4428	0.0574	21.2352	18.495	308.4555	133.0816	221.5
3	8002.5025	26254.9295	7.4195	0.1237	25.0547	17.5561	398.1852	132.0309	202.9
4	6668.7537	21879.1134	11.9569	0.1993	28.8015	17.3892	512.3682	137.0328	195
5	5335.005	17503.2972	17.8073	0.2968	33.5134	16.8244	748.3897	138.5827	183.1
6	4001.2563	13127.4811	20.2922	0.3382	39.8824	15.7206	356.1308	133.9239	164.7
7	2667.5075	8751.665	21.931	0.3655	46.8793	14.9753	261.8762	131.5169	150.9
8	1333.7588	4375.8489	23.0982	0.385	75.83	13.471	208.8535	130.4957	140
9	0.01	0.0328	24.0973	0.4016	86.0818	13.37	260.523	134.3026	135
Seg_No	**Mach**	**Descent Rate (m/s)**	**Dist_(m)**	**Dist_(m) Cum**	**Descent Gradient (deg)**	**DragCoeff aircraft**	**LiftCoeff aircraft**	**DragCoeff Nacelle**	**Drag Nacelle (KN)**
1	0.7804	-6.4568	0	0	-1.6271	0.0225	0.3811	0.0007	5.8395
2	0.7275	-5.5898	46933.3849	46933.3849	-1.5089	0.0216	0.3572	0.0007	6.1862
3	0.6542	-4.8991	50614.6181	97548.003	-1.4106	0.0218	0.3625	0.0007	6.1026
4	0.6177	-3.7996	54146.6141	151694.6171	-1.1514	0.0209	0.336	0.0007	6.5153
5	0.5701	-8.9458	66347.7459	218042.363	-2.9448	0.0206	0.3278	0.0007	6.638
6	0.5043	-13.564	25892.7882	243935.1513	-4.9129	0.0541	0.3506	0.0007	6.2271
7	0.4547	-19.0459	15459.516	259394.6673	-7.4601	0.0545	0.3633	0.0007	6.007
8	0.4153	-22.2488	10099.3946	269494.0619	-9.1913	0.0962	0.3688	0.0007	5.9011
9	0.3945	0	8136.8949	277630.9568	0	0.1065	0.3479	0.0007	6.1947

A.1.2 ENGINE FLIGHT PATH PERFORMANCE OUTPUT WITH A380-800 AIRCRAFT AND INTERCOOLED-RECUPERATED TRENT900 ENGINE

Phase	Seg No	ALT (m)	DTisa (K)	Mach	TIME (hrs)	TIME (min)	TIME (sec)	Thrust (kN) /Engine	SFC (g/kNs)	TET [K]
1	1	0	3	0	0	0	0	92.449	6.66	1180
1	2	0	3	0	0.16667	10	600	92.449	6.66	1180
1	3	0	3	0	0.16681	10.00833	600.5	181.855	6.14321	1302.9367
1	4	0	3	0	0.16708	10.025	601.5	254.597	7.12792	1461.762
1	5	0	3	0	0.16736	10.04167	602.5	327.339	8.11264	1620.5873
1	6	0	3	0	0.16764	10.05833	603.5	363.71	8.605	1700
1	7	0	3	0.06388	0.17132	10.2794	616.76375	339.12603	9.2547	1700
1	8	0	3	0.12775	0.17501	10.50046	630.02751	317.47901	9.94095	1700
1	9	0	3	0.19163	0.17869	10.72152	643.29126	298.23744	10.66324	1700
1	10	0	3	0.25551	0.18238	10.94258	656.55502	281.36943	11.42894	1700
1	11	10.668	3	0.27877	0.18329	10.9973	659.83801	275.62859	11.71882	1700
1	12	49.88207	3	0.2873	0.18394	11.03618	662.17066	272.71812	11.82051	1700
1	13	457.2	3	0.3901	0.19172	11.50337	690.20247	243.28414	13.10113	1700
2	14	557.2	3	0.39054	0.192	11.52004	691.20247	270.11	12.001	1700
2	15	900	3	0.39869	0.19789	11.8736	712.41572	247.07	12.103	1700
2	16	1500	3	0.41353	0.20937	12.56219	753.7315	232.37	12.173	1700
2	17	1981.2	3	0.42598	0.21916	13.1494	788.96401	220.8	12.239	1700

Phase	Seg No	ALT (m)	DTisa (K)	Mach	TIME (hrs)	TIME (min)	TIME (sec)	Thrust (kN) /Engine	SFC (g/kNs)	TET [K]
2	18	2438.4	3	0.4383	0.22901	13.74046	824.42778	210.05	12.304	1700
2	19	2743.2	3	0.44679	0.2359	14.1542	849.25191	203.35	12.332	1700
2	20	3048	3	0.45551	0.24294	14.57616	874.56932	196.51	12.386	1700
2	21	3048	3	0.58305	0.25822	15.49312	929.58716	177.44	14.763	1700
2	22	3657.6	3	0.60628	0.27397	16.43822	986.29311	166.3	14.932	1700
2	23	4267.2	3	0.63081	0.29145	17.48726	1049.23541	155.73	15.115	1700
2	24	4876.8	3	0.65674	0.31105	18.66329	1119.79755	145.72	15.32	1700
2	25	5486.4	3	0.68415	0.33327	19.99642	1199.78499	136.35	15.522	1700
2	26	6096	3	0.71318	0.35892	21.53494	1292.09627	127.47	15.761	1700
2	27	7620	3	0.79359	0.43448	26.06878	1564.12678	107.48	16.512	1700
2	28	8077.2	3	0.8	0.4598	27.58794	1655.2763	102.03	16.779	1700
2	29	9144	3	0.8	0.5334	32.00429	1920.25724	90.714	16.86	1700
2	30	10058	3	0.8	0.64129	38.47726	2308.6356	81.738	17.006	1700
3	31	10058	3	0.8	0.84736	50.84154	3050.49212	73.12707	16.53495	1631.5118
3	32	10058	3	0.8	0.93073	55.84371	3350.62244	73.03891	16.53191	1630.8489
3	33	10670	3	0.82	1.0141	60.84588	3650.75275	72.8557	16.94344	1671.9067
3	34	10670	3	0.82	1.09747	65.84805	3950.88306	72.66816	16.93381	1670.301
3	35	10670	3	0.82	1.18084	70.85022	4251.01338	72.48171	16.92435	1668.766
3	36	10670	3	0.82	1.26421	75.85239	4551.14369	72.29633	16.91497	1667.2539
3	37	10670	3	0.82	1.34758	80.85457	4851.274	72.11202	16.90565	1665.7506
3	38	10670	3	0.82	1.43095	85.85674	5151.40431	71.92877	16.89617	1664.2461
3	39	10670	3	0.82	1.51432	90.85891	5451.53463	71.74657	16.88654	1662.7403
3	40	10670	3	0.82	1.59768	95.86108	5751.66494	71.56542	16.87696	1661.2432
3	41	10670	3	0.82	1.68105	100.86325	6051.79525	71.38531	16.8674	1659.7505
3	42	10670	3	0.82	1.76442	105.86543	6351.92556	71.20622	16.85777	1658.2456
3	43	10670	3	0.82	1.84779	110.8676	6652.05588	71.02816	16.8482	1656.7492
3	44	10670	3	0.82	1.93116	115.86977	6952.18619	70.85111	16.83867	1655.2615
3	45	10670	3	0.82	2.01453	120.87194	7252.3165	70.67508	16.82918	1653.778
3	46	10670	3	0.82	2.0979	125.87411	7552.44682	70.50004	16.81973	1652.3022
3	47	10670	3	0.82	2.18127	130.87629	7852.57713	70.32599	16.81034	1650.8347
3	48	10670	3	0.82	2.26464	135.87846	8152.70744	70.15293	16.8011	1649.3712
3	49	10670	3	0.82	2.34801	140.88063	8452.83775	69.98084	16.79204	1647.9104
3	50	10670	3	0.82	2.43138	145.8828	8752.96807	69.80973	16.78304	1646.4578
3	51	10670	3	0.82	2.51475	150.88497	9053.09838	69.63957	16.77408	1645.0133
3	52	10670	3	0.82	2.59812	155.88714	9353.22869	69.47036	16.76545	1643.5745
3	53	10670	3	0.82	2.68149	160.88932	9653.35901	69.3021	16.75686	1642.1437
3	54	10670	3	0.82	2.76486	165.89149	9953.48932	69.13477	16.74832	1640.7208
3	55	10670	3	0.82	2.84823	170.89366	10253.61963	68.96837	16.73982	1639.3035
3	56	10670	3	0.82	2.9316	175.89583	10553.74994	68.80289	16.73135	1637.8916
3	57	10670	3	0.82	3.01497	180.898	10853.88026	68.63833	16.72292	1636.4874
3	58	10670	3	0.82	3.09834	185.90018	11154.01057	68.47467	16.71455	1635.0911
3	59	10670	3	0.82	3.18171	190.90235	11454.14088	68.31192	16.70577	1633.6729
3	60	10670	3	0.82	3.26508	195.90452	11754.27119	68.15006	16.69702	1632.2606
3	61	10670	3	0.82	3.34844	200.90669	12054.40151	67.9891	16.68831	1630.856
3	62	10670	3	0.82	3.43181	205.90886	12354.53182	67.82902	16.6809	1629.5225
3	63	10670	3	0.82	3.51518	210.91104	12654.66213	67.66981	16.6755	1628.2959
3	64	10670	3	0.82	3.59855	215.91321	12954.79245	67.51144	16.67013	1627.0758
3	65	10670	3	0.82	3.68192	220.91538	13254.92276	67.35391	16.66479	1625.8622

Phase	Seg No	ALT (m)	DTisa (K)	Mach	TIME (hrs)	TIME (min)	TIME (sec)	Thrust (kN) /Engine	SFC (g/kNs)	TET [K]
3	66	10670	3	0.82	3.76529	225.91755	13555.05307	67.19721	16.65934	1624.6801
3	67	10670	3	0.82	3.84866	230.91972	13855.18338	67.04134	16.65355	1623.5667
3	68	10670	3	0.82	3.93203	235.92189	14155.3137	66.88629	16.64779	1622.4592
3	69	10670	3	0.82	4.0154	240.92407	14455.44401	66.73205	16.64206	1621.3575
3	70	10670	3	0.82	4.09877	245.92624	14755.57432	66.57864	16.63636	1620.2617
3	71	10670	3	0.82	4.18214	250.92841	15055.70463	66.42602	16.63034	1619.168
3	72	10670	3	0.82	4.26551	255.93058	15355.83495	66.27422	16.62424	1618.079
3	73	10670	3	0.82	4.34888	260.93275	15655.96526	66.12321	16.61818	1616.9958
3	74	10670	3	0.82	4.43225	265.93493	15956.09557	65.97299	16.61214	1615.9182
3	75	10670	3	0.82	4.51562	270.9371	16256.22589	65.82357	16.60629	1614.8463
3	76	10670	3	0.82	4.59899	275.93927	16556.3562	65.67493	16.60139	1613.78
3	77	10670	3	0.82	4.68236	280.94144	16856.48651	65.52706	16.59651	1612.7192
3	78	10670	3	0.82	4.76573	285.94361	17156.61682	65.37995	16.59165	1611.6639
3	79	10670	3	0.82	4.8491	290.94579	17456.74714	65.2336	16.58682	1610.614
3	80	10670	3	0.82	4.93247	295.94796	17756.87745	65.088	16.58174	1609.5652
3	81	10670	3	0.82	5.01584	300.95013	18057.00776	64.94316	16.57628	1608.5156
3	82	10670	3	0.82	5.09921	305.9523	18357.13807	64.79906	16.57085	1607.4715
3	83	10670	3	0.82	5.18257	310.95447	18657.26839	64.65571	16.56545	1606.4327
3	84	10670	3	0.82	5.26594	315.95665	18957.3987	64.5131	16.56008	1605.3993
3	85	10670	3	0.82	5.34931	320.95882	19257.52901	64.37122	16.55462	1604.3505
3	86	10670	3	0.82	5.43268	325.96099	19557.65933	64.23008	16.54913	1603.294
3	87	10670	3	0.82	5.51605	330.96316	19857.78964	64.08966	16.54366	1602.2429
3	88	10670	3	0.82	5.59942	335.96533	20157.91995	63.94996	16.53823	1601.1973
3	89	10670	3	0.82	5.68279	340.9675	20458.05026	63.81098	16.53282	1600.157
3	90	10670	3	0.82	5.76616	345.96968	20758.18058	63.67271	16.5274	1599.1488
3	91	10670	3	0.82	5.84953	350.97185	21058.31089	63.53514	16.52201	1598.1505
3	92	10670	3	0.82	5.9329	355.97402	21358.4412	63.39828	16.51665	1597.1574
3	93	10670	3	0.82	6.01627	360.97619	21658.57152	63.26212	16.51131	1596.1693
3	94	10670	3	0.82	6.09964	365.97836	21958.70183	63.12666	16.50601	1595.1862
3	95	10670	3	0.82	6.18301	370.98054	22258.83214	62.99188	16.5011	1594.1869
3	96	10670	3	0.82	6.26638	375.98271	22558.96245	62.85778	16.4963	1593.1876
3	97	10670	3	0.82	6.34975	380.98488	22859.09277	62.72436	16.49153	1592.1935
3	98	10670	3	0.82	6.43312	385.98705	23159.22308	62.59162	16.48678	1591.2043
3	99	10670	3	0.82	6.51649	390.98922	23459.35339	62.45954	16.48206	1590.2201
3	100	10670	3	0.82	6.59986	395.9914	23759.4837	62.32812	16.47856	1589.2815
3	101	10670	3	0.82	6.68323	400.99357	24059.61402	62.19735	16.47542	1588.3593
3	102	10670	3	0.82	6.7666	405.99574	24359.74433	62.06723	16.4723	1587.4417
3	103	10670	3	0.82	6.84997	410.99791	24659.87464	61.93775	16.4692	1586.5285
3	104	10670	3	0.82	6.93333	416.00008	24960.00496	61.8089	16.46611	1585.6199
3	105	10670	3	0.82	7.0167	421.00225	25260.13527	61.68068	16.46328	1584.7246
3	106	10670	3	0.82	7.10007	426.00443	25560.26558	61.55309	16.46102	1583.8531
3	107	10670	3	0.82	7.18344	431.0066	25860.39589	61.42612	16.45876	1582.9858
3	108	10670	3	0.82	7.26681	436.00877	26160.52621	61.29976	16.45652	1582.1227
3	109	10670	3	0.82	7.35018	441.01094	26460.65652	61.17401	16.45429	1581.2637
3	110	10670	3	0.82	7.43355	446.01311	26760.78683	61.04887	16.45206	1580.4089
3	111	10670	3	0.82	7.51692	451.01529	27060.91714	60.92433	16.44962	1579.5948
3	112	10670	3	0.82	7.60029	456.01746	27361.04746	60.80039	16.44698	1578.8182
3	113	10670	3	0.82	7.68366	461.01963	27661.17777	60.67705	16.44435	1578.0454

Phase	Seg No	ALT (m)	DTisa (K)	Mach	TIME (hrs)	TIME (min)	TIME (sec)	Thrust (kN) /Engine	SFC (g/kNs)	TET [K]
3	114	10670	3	0.82	7.76703	466.0218	27961.30808	60.55431	16.44174	1577.2764
3	115	10670	3	0.82	7.8504	471.02397	28261.4384	60.43216	16.43914	1576.511
3	116	10670	3	0.82	7.93377	476.02615	28561.56871	60.3106	16.43655	1575.7494
3	117	10670	3	0.82	8.01714	481.02832	28861.69902	60.18963	16.43397	1574.9911
3	118	10670	3	0.82	8.10051	486.03049	29161.82933	60.06923	16.43163	1574.2114
3	119	10670	3	0.82	8.18388	491.03266	29461.95965	59.94942	16.42931	1573.4354
3	120	10670	3	0.82	8.26725	496.03483	29762.08996	59.83018	16.42699	1572.6631
3	121	10670	3	0.82	8.35062	501.037	30062.22027	59.7115	16.42468	1571.8945
3	122	10670	3	0.82	8.43399	506.03918	30362.35058	59.5934	16.42239	1571.1295
3	123	10670	3	0.82	8.51736	511.04135	30662.4809	59.47586	16.4201	1570.3683
3	124	10670	3	0.82	8.60073	516.04352	30962.61121	59.35888	16.41796	1569.6013
3	125	10670	3	0.82	8.68409	521.04569	31262.74152	59.24245	16.41596	1568.8293
3	126	10670	3	0.82	8.76746	526.04786	31562.87184	59.12658	16.41396	1568.0609
3	127	10670	3	0.82	8.85083	531.05004	31863.00215	59.01126	16.41197	1567.2962
3	128	10670	3	0.82	8.9342	536.05221	32163.13246	58.89648	16.40999	1566.535
3	129	10670	3	0.82	9.01757	541.05438	32463.26277	58.78225	16.40802	1565.7775
3	130	10670	3	0.82	9.10094	546.05655	32763.39309	58.66856	16.40606	1565.0236
3	131	10670	3	0.82	9.18431	551.05872	33063.5234	58.5554	16.40383	1564.2761
3	132	10670	3	0.82	9.26768	556.0609	33363.65371	58.44278	16.4016	1563.5322
3	133	10670	3	0.82	9.35105	561.06307	33663.78403	58.33069	16.39938	1562.7919
3	134	10670	3	0.82	9.43442	566.06524	33963.91434	58.21913	16.39717	1562.055
3	135	10670	3	0.82	9.51779	571.06741	34264.04465	58.1081	16.39497	1561.3217
3	136	10670	3	0.82	9.60116	576.06958	34564.17496	57.99759	16.39278	1560.5918
3	137	10670	3	0.82	9.68453	581.07175	34864.30528	57.88761	16.3906	1559.8653
3	138	10670	3	0.82	9.7679	586.07393	35164.43559	57.77814	16.38843	1559.1423
3	139	10670	3	0.82	9.85127	591.0761	35464.5659	57.66918	16.38627	1558.4226
3	140	10670	3	0.82	9.93464	596.07827	35764.69621	57.56074	16.38412	1557.7064
3	141	10670	3	0.82	10.01801	601.08044	36064.82653	57.45281	16.38198	1556.9935
3	142	10670	3	0.82	10.10138	606.08261	36364.95684	57.34539	16.37985	1556.2839
3	143	10670	3	0.82	10.18475	611.08479	36665.08715	57.23846	16.37773	1555.5777
3	144	10670	3	0.82	10.26812	616.08696	36965.21747	57.13204	16.37562	1554.8748
3	145	10670	3	0.82	10.35149	621.08913	37265.34778	57.02612	16.37353	1554.1752
3	146	10670	3	0.82	10.43486	626.0913	37565.47809	56.92069	16.37144	1553.4788
3	147	10670	3	0.82	10.51822	631.09347	37865.6084	56.81576	16.36936	1552.7857
3	148	10670	3	0.82	10.60159	636.09565	38165.73872	56.71132	16.36729	1552.0959
3	149	10670	3	0.82	10.68496	641.09782	38465.86903	56.60736	16.36523	1551.4092
3	150	10670	3	0.82	10.76833	646.09999	38765.99934	56.50389	16.36318	1550.7258
3	151	10670	3	0.82	10.8517	651.10216	39066.12965	56.4009	16.36114	1550.0456
3	152	10670	3	0.82	10.93507	656.10433	39366.25997	56.29839	16.35911	1549.3685
3	153	10670	3	0.82	11.01844	661.1065	39666.39028	56.19635	16.35708	1548.6945
3	154	10670	3	0.82	11.10181	666.10868	39966.52059	56.09479	16.35507	1548.0237
3	155	10670	3	0.82	11.18518	671.11085	40266.65091	55.99371	16.35307	1547.3561
3	156	10670	3	0.82	11.26855	676.11302	40566.78122	55.89309	16.35107	1546.6915
3	157	10670	3	0.82	11.35192	681.11519	40866.91153	55.79294	16.34909	1546.03
3	158	10670	3	0.82	11.43529	686.11736	41167.04184	55.69325	16.34711	1545.3715
3	159	10670	3	0.82	11.51866	691.11954	41467.17216	55.59402	16.34515	1544.7161
3	160	10670	3	0.82	11.60203	696.12171	41767.30247	55.49525	16.34319	1544.0638
3	161	10670	3	0.82	11.6854	701.12388	42067.43278	55.39694	16.34124	1543.4144

Phase	Seg No	ALT (m)	DTisa (K)	Mach	TIME (hrs)	TIME (min)	TIME (sec)	Thrust (kN) /Engine	SFC (g/kNs)	TET [K]
3	162	10670	3	0.82	11.76877	706.12605	42367.56309	55.29909	16.3393	1542.7681
3	163	10670	3	0.82	11.85214	711.12822	42667.69341	55.20168	16.33737	1542.1247
3	164	10670	3	0.82	11.93551	716.1304	42967.82372	55.10473	16.33545	1541.4843
3	165	10670	3	0.82	12.01888	721.13257	43267.95403	55.00822	16.33354	1540.8469
3	166	10670	3	0.82	12.10225	726.13474	43568.08435	54.91215	16.33164	1540.2124
3	167	10670	3	0.82	12.18562	731.13691	43868.21466	54.81653	16.32974	1539.5808
3	168	10670	3	0.82	12.26898	736.13908	44168.34497	54.72135	16.32786	1538.9521
3	169	10670	3	0.82	12.35235	741.14125	44468.47528	54.62661	16.32598	1538.3263
3	170	10670	3	0.82	12.43572	746.14343	44768.6056	54.5323	16.32411	1537.7034
3	171	10670	3	0.82	12.51909	751.1456	45068.73591	54.43843	16.32225	1537.0834
3	172	10670	3	0.82	12.60246	756.14777	45368.86622	54.34498	16.3204	1536.4662
3	173	10670	3	0.82	12.68583	761.14994	45668.99654	54.25197	16.31856	1535.8518
3	174	10670	3	0.82	12.7692	766.15211	45969.12685	54.15938	16.31672	1535.2403
3	175	10670	3	0.82	12.85257	771.15429	46269.25716	54.06721	16.31489	1534.6315
3	176	10670	3	0.82	12.93594	776.15646	46569.38747	53.97547	16.31308	1534.0256
3	177	10670	3	0.82	13.01931	781.15863	46869.51779	53.88414	16.31127	1533.4224
3	178	10670	3	0.82	13.10268	786.1608	47169.6481	53.79324	16.30947	1532.8219
3	179	10670	3	0.82	13.18605	791.16297	47469.77841	53.70275	16.30767	1532.2242
3	180	10670	3	0.82	13.26942	796.16515	47769.90872	53.61267	16.30589	1531.6293
3	181	10670	3	0.82	13.35279	801.16732	48070.03904	53.52301	16.30411	1531.037
3	182	10670	3	0.82	13.43616	806.16949	48370.16935	53.43375	16.30234	1530.4475
3	183	10670	3	0.82	13.51953	811.17166	48670.29966	53.3449	16.30058	1529.8606
3	184	10670	3	0.82	13.6029	816.17383	48970.42998	53.25645	16.29883	1529.2765
3	185	10670	3	0.82	13.68627	821.176	49270.56029	53.16841	16.29708	1528.6949
3	186	10670	3	0.82	13.76964	826.17818	49570.6906	53.08077	16.29535	1528.1161
3	187	10670	3	0.82	13.85301	831.18035	49870.82091	52.99353	16.29362	1527.5398
3	188	10670	3	0.82	13.93638	836.18252	50170.95123	52.90668	16.2919	1526.9662
3	189	10670	3	0.82	14.01974	841.18469	50471.08154	52.82023	16.29019	1526.3952
3	190	10670	3	0.82	14.10311	846.18686	50771.21185	52.73418	16.28848	1525.8268
3	191	10670	3	0.82	14.18648	851.18904	51071.34216	52.64851	16.28678	1525.261
3	192	10670	3	0.82	14.26985	856.19121	51371.47248	52.56323	16.28509	1524.6977
3	193	10670	3	0.82	14.35322	861.19338	51671.60279	52.47834	16.28341	1524.137
3	194	10670	3	0.82	14.43659	866.19555	51971.7331	52.39383	16.28174	1523.5788
3	195	10670	3	0.82	14.51996	871.19772	52271.86342	52.30971	16.28007	1523.0232
3	196	10670	3	0.82	14.60333	876.1999	52571.99373	52.22597	16.27841	1522.4701
3	197	10670	3	0.82	14.6867	881.20207	52872.12404	52.1426	16.27676	1521.9194
3	198	10670	3	0.82	14.77007	886.20424	53172.25435	52.05962	16.27511	1521.3713
3	199	10670	3	0.82	14.85344	891.20641	53472.38467	51.97701	16.27348	1520.8257
3	200	10670	3	0.82	14.93681	896.20858	53772.51498	51.89477	16.27185	1520.2825
3	201	10670	3	0.82	15.02018	901.21075	54072.64529	51.81291	16.27023	1519.7418
3	202	10670	3	0.82	15.10355	906.21293	54372.7756	51.73141	16.26861	1519.2035
3	203	10670	3	0.82	15.18692	911.2151	54672.90592	51.65029	16.267	1518.6677
3	204	10670	3	0.82	15.27029	916.21727	54973.03623	51.56953	16.2654	1518.1343
3	205	10670	3	0.82	15.35366	921.21944	55273.16654	51.48913	16.26381	1517.6032
3	206	10670	3	0.82	15.43703	926.22161	55573.29686	51.4091	16.26222	1517.0746
3	207	10670	3	0.82	15.5204	931.22379	55873.42717	51.32943	16.26065	1516.5484
3	208	10670	3	0.82	15.60377	936.22596	56173.55748	51.25012	16.25907	1516.0245
3	209	10670	3	0.82	15.68714	941.22813	56473.68779	51.17116	16.25751	1515.503

Phase	Seg No	ALT (m)	DTisa (K)	Mach	TIME (hrs)	TIME (min)	TIME (sec)	Thrust (kN) /Engine	SFC (g/kNs)	TET [K]
3	210	10670	3	0.82	15.77051	946.2303	56773.81811	51.09256	16.25595	1514.9839
3	211	10670	3	0.82	15.85387	951.23247	57073.94842	51.01432	16.2544	1514.4671
3	212	10670	3	0.82	15.93724	956.23465	57374.07873	50.93643	16.25286	1513.9526
3	213	10670	3	0.82	16.02061	961.23682	57674.20905	50.85888	16.25132	1513.4405
3	214	10670	3	0.82	16.10398	966.23899	57974.33936	50.78169	16.24979	1512.9306
3	215	10670	3	0.82	16.18735	971.24116	58274.46967	50.70485	16.24827	1512.423
3	216	10670	3	0.82	16.27072	976.24333	58574.59998	50.62835	16.24675	1511.9178
3	217	10670	3	0.82	16.35409	981.2455	58874.7303	50.55219	16.24524	1511.4147
3	218	10670	3	0.82	16.43746	986.24768	59174.86061	50.47638	16.24374	1510.914
3	219	10670	3	0.82	16.52083	991.24985	59474.99092	50.40091	16.24225	1510.4155
3	220	10670	3	0.82	16.6042	996.25202	59775.12123	50.32578	16.24076	1509.9193
3	221	10670	3	0.82	16.68757	1001.25419	60075.25155	50.25098	16.23928	1509.4252
3	222	10670	3	0.82	16.72925	1003.75528	60225.3167	50.17652	16.2378	1508.9334
4	223	10670	3	0.78043	16.73037	1003.82195	60229.3167	18.33064	19.24613	1250
4	224	9336.25125	3	0.72751	16.78775	1007.2647	60435.88211	21.23519	18.49499	1250
4	225	8002.5025	3	0.65423	16.85402	1011.24147	60674.48803	25.0547	17.55606	1250
4	226	6668.75375	3	0.61766	16.92965	1015.77887	60946.73245	28.80148	17.38916	1250
4	227	5335.005	3	0.57008	17.02715	1021.62928	61297.75676	33.51345	16.82443	1250
4	228	4001.25625	3	0.50434	17.06857	1024.11414	61446.84834	39.88239	15.72063	1250
4	229	2667.5075	3	0.45471	17.09588	1025.75298	61545.17865	46.87934	14.97528	1250
4	230	1333.75875	3	0.41534	17.11534	1026.92012	61615.20691	75.83003	13.47102	1325
4	231	0.01	3	0.3945	17.13199	1027.91923	61675.15402	86.08183	13.37002	1325
5	233	0.01	3	0.20295	17.13143	1027.8859	61673.15402	86.08183	13.37002	1325
5	234	0.01	3	0.19889	17.13184	1027.91064	61674.63837	86.08183	13.37002	1325
5	235	0.01	3	0.19582	17.13467	1028.08021	61684.8129	148.50888	8.80162	1366.7766
5	236	0.01	3	0.19431	17.13606	1028.16355	61689.8129	193.34715	9.35287	1466.4313
5	237	0.01	3	0.1928	17.13745	1028.24688	61694.8129	238.31725	9.90785	1566.3537
5	238	0.01	3	0.06088	17.14449	1028.66934	61720.16017	306.16495	8.76478	1624.9388
5	239	0.01	3	0.05752	17.14588	1028.75267	61725.16017	256.0279	8.03515	1511.665
5	240	0.01	3	0.05417	17.14727	1028.836	61730.16017	205.53467	7.29759	1397.5731
5	241	0.01	3	0.04059	17.15288	1029.17275	61750.36503	84.23499	7.32155	1180
5	242	0.01	3	0	17.15479	1029.28723	61757.23368	92.449	6.66	1180
5	243	0.01	3	0	17.32145	1039.28723	62357.23368	92.449	6.66	1180

Appendix C THE WATER EXPELLER DESIGN PATENT

(12) UK Patent (19) GB (11) 2531632 (13) B

(45) Date of B Publication 11.01.2017

(54) Title of the Invention: A mechanical device to suppress contrail formation

(51) INT CL: ***F01N 3/00*** (2006.01) ***F01D 25/30*** (2006.01)

(21) Application No: **1514047.8**

(22) Date of Filing: **10.08.2015**

(43) Date of A Publication **27.04.2016**

(56) Documents Cited:
JP 2006192348 A

(58) Field of Search:
As for published application 2531632 A viz:
INT CL **B01D, F01D, F01N, F02C**
Other: **EPODOC, WPI, TXTE, TXTT**
updated as appropriate

(72) Inventor(s):
Masood Latif Qureshi

(73) Proprietor(s):
Masood Latif Qureshi
House 12, Street 1, Block E,
Soan Gardens (P.O. Korang Town), Expressway,
Islamabad 44000, Zone 5, Pakistan

(74) Agent and/or Address for Service:
Masood Latif Qureshi
71 Beaks Hill Road, Kings Norton, BIRMINGHAM,
B38 8BL, United Kingdom

GB 2531632 B

Drawings

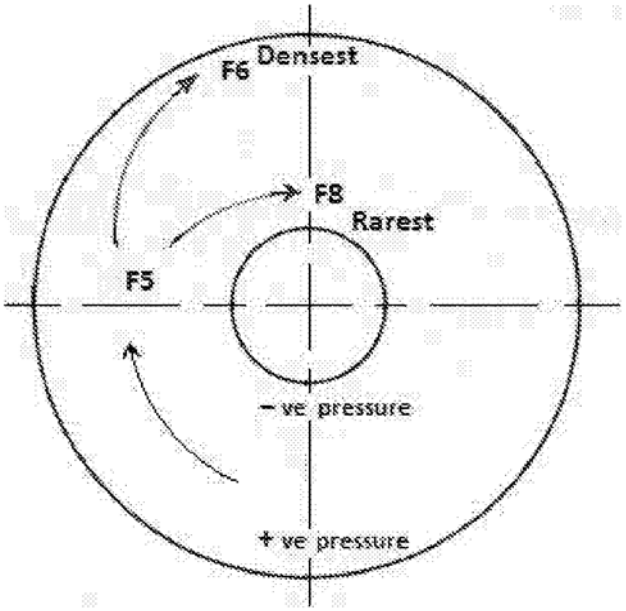

Figure 1

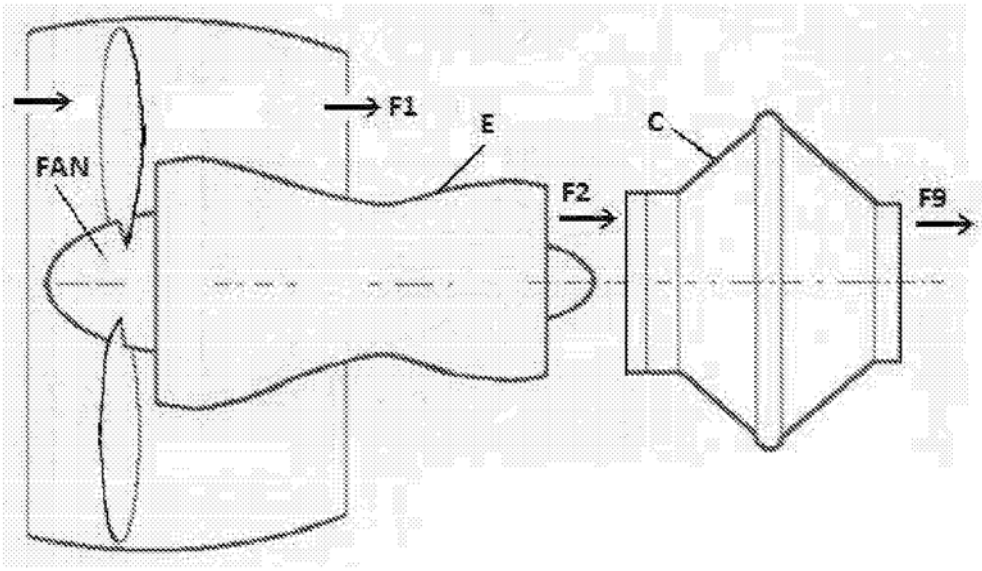

Figure 2

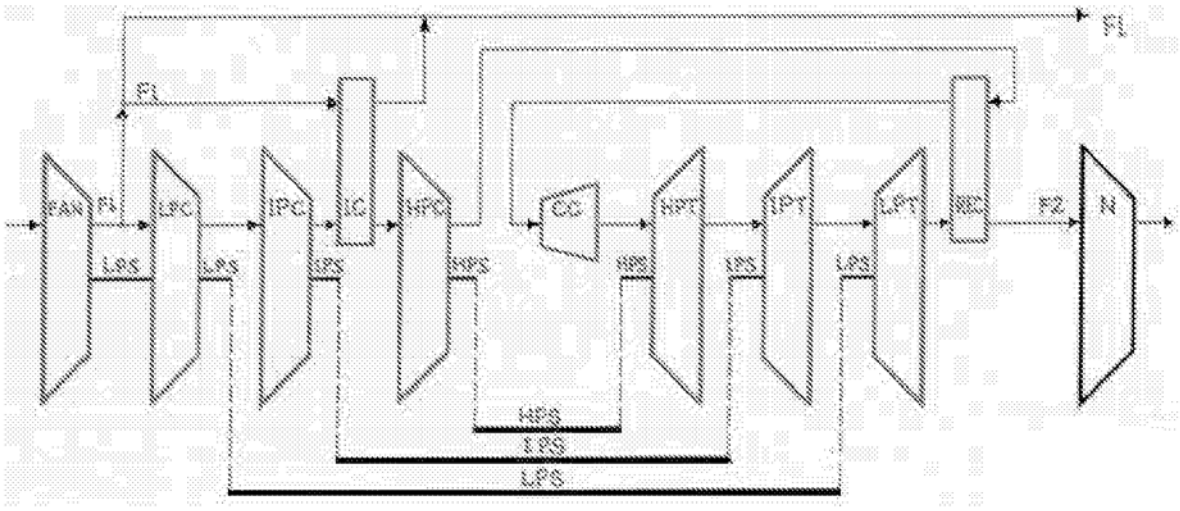

Figure 3

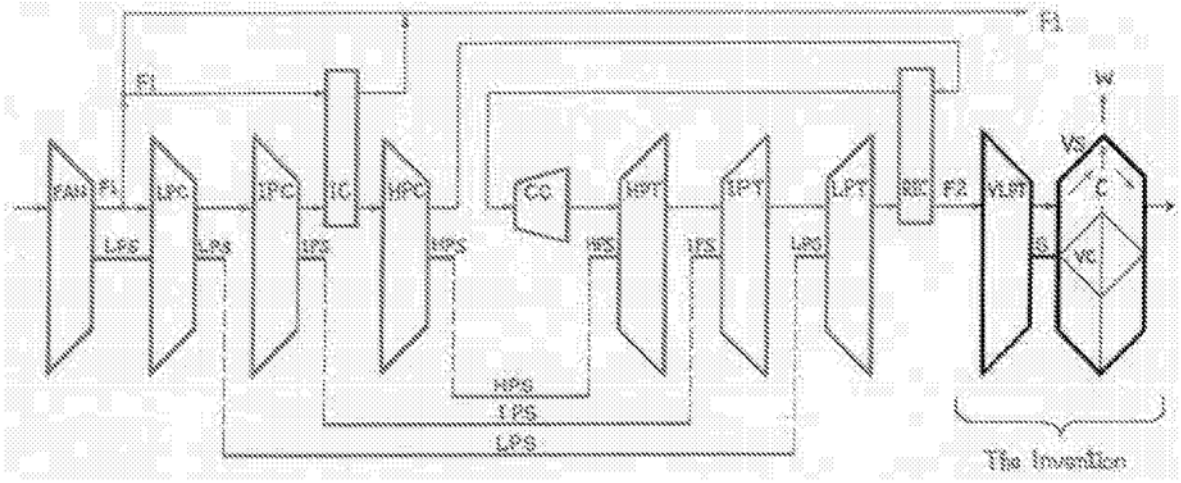

Figure 4

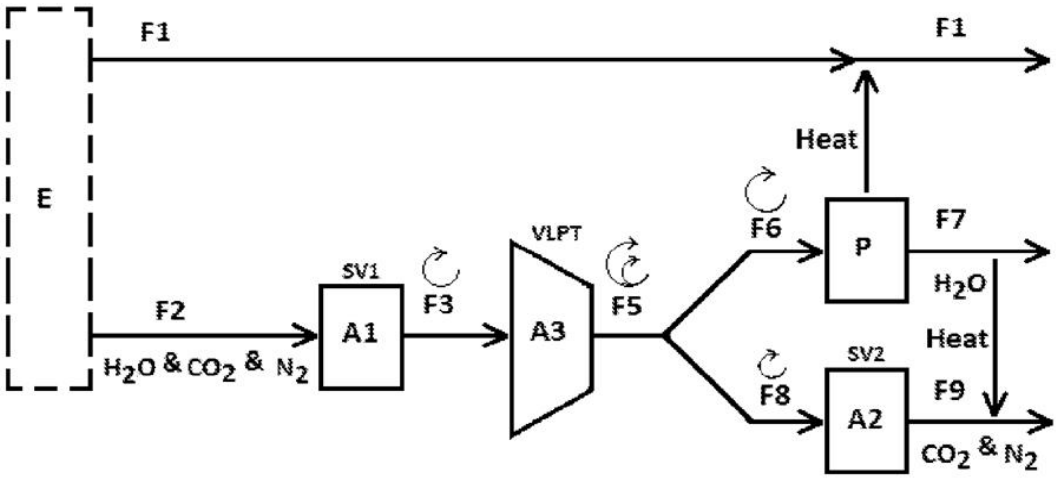

Figure 6

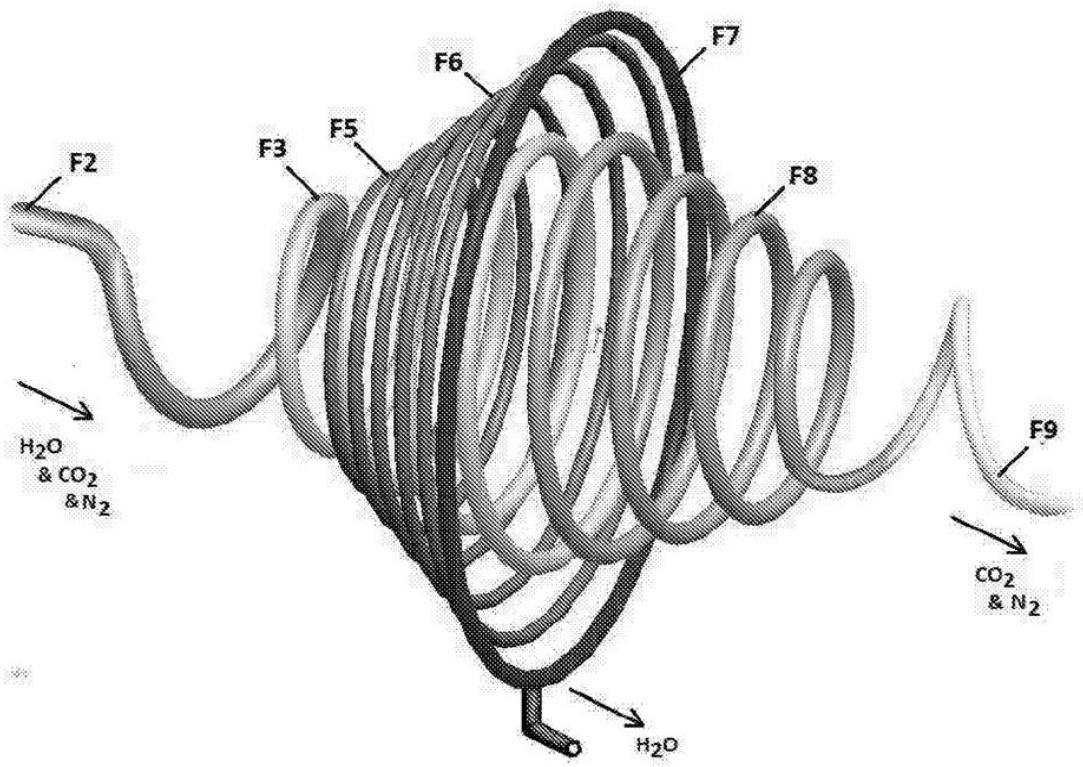

Figure 7

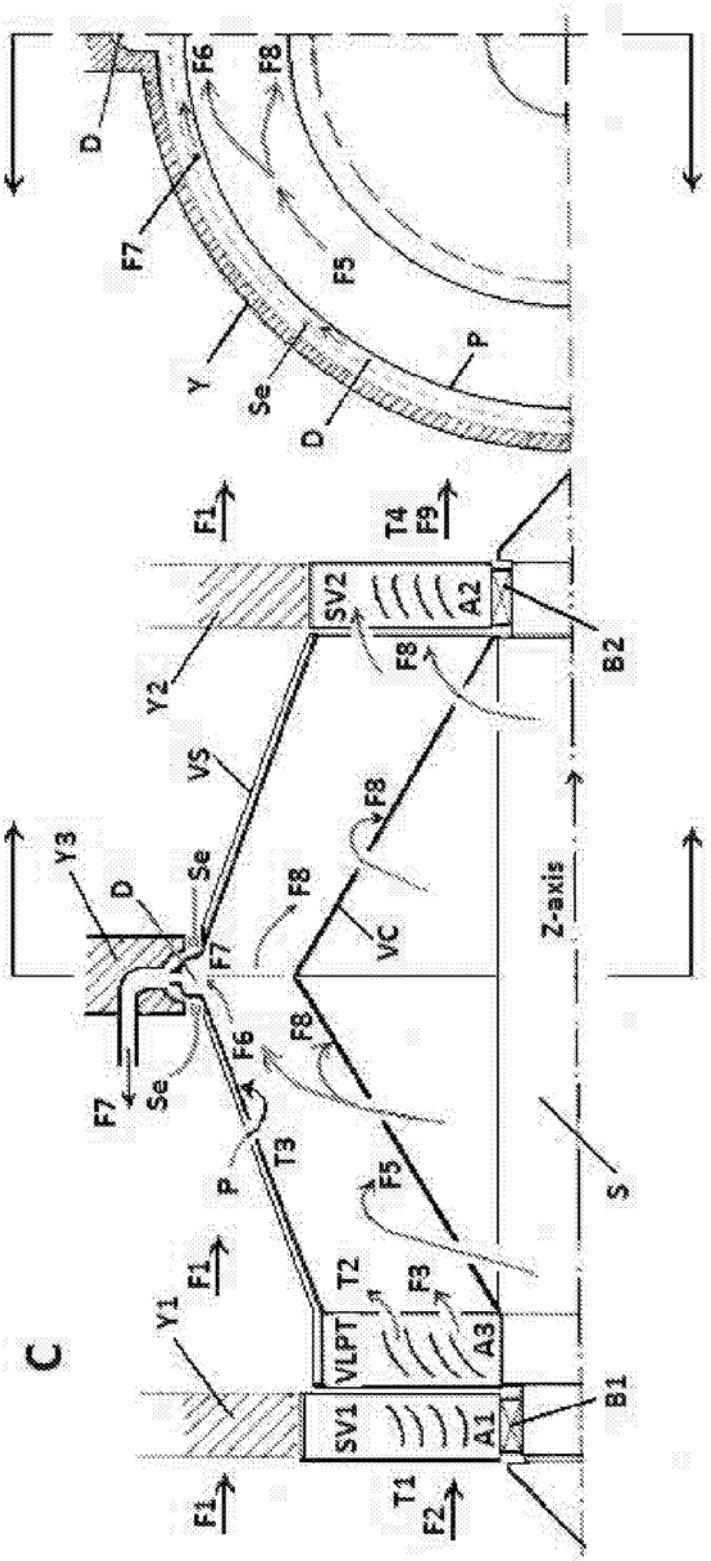
C
D
F6
F8
F7
F5
Y
Se
D
P
F1
T4
F9
SV2
A2
B2
Y2
F8
VS
F8
Y3
D
Se
F8
VC
Z-axis
F7
F6
F8
F7
Se
P
T3
F5
S
F1
T2
F3
Y1
VLPT
A3
B1
SV1
A1
F1
T1
F2

Figure 8

Description of Drawings:

[0006]. The present invention will be described by the accompanying drawings to illustrate the different aspects of design and workings.

Figure 1: Description of centrifugal forces shows a mixture of gases of different densities F5 rotating in a cylinder. The densest fluid F6 spins out towards the periphery, while, the rarest fluid F8 spins and converges in the centre. The centrifugal force also creates the maximum pressure on the peripheral wall.

Figure 2: Shows the invention of the centrifugal device C fitted to a typical high bypass turbine engine E. A feature of this invention is that no internal modification of any existing engine needs to be done, and the device is an external attachment C. The exhaust airflow F2 is utilized by the invention device C.

Figure 3: Description of a block diagram of a typical state of the art, high bypass 3-shaft turbine engine, with intercooler IC, recuperator REC, combustion chamber CC and Nozzle N. The shafts HPS, IPS and LPS are coaxial.

Figure 4: Description of a block diagram of a typical turbine engine as in figure 3, the Nozzle N replaced by the invention, co-axial to the shafts, shown here is the placement of the invention device C on the above turbine engine, where the invention containing a Very Low Pressure Turbine VLPT, Shell Vessel VS and Core Vessel VC.

Figure 6: The invention: Block diagram of the working of the device and the heat dissipation from H_2O to the other exhaust gases CO_2 and N_2 and partly to cold airflow F1.

Figure 7: The invention workings: Conceptual example of the path of a volume of flow F2 input to the device, its linear energy deflected into flow F3, the energy causing further deflection into rotational flow F5, its split into circular flows F6 and F8. The flow F6 condenses into a moisture laden flow F7 collecting into a rotating water ring and is drained out, while the residual rotational flow F8 is straightened out to exit as linear flow F9 with some residual thrust.

Figure 8: The invention: A simplified example of a cut-away drawing of the invention device showing the conceptually important parts. The assembly shown is supported by the rigid structural parts of the pylon Y1 and Y2 holding the stators SV1 and SV2 with aerofoils A1 and A2, the hub containing the bearings B1 and B2 respectively, to hold and freely allow rotation of the shaft S, the said shaft holding the rotor VLPT and the vessels VC and VS. The rotating drain D, part of VS, is placed within the rigid structure Y3, seals Se containing the rotating ring of water.

Claims

1. A mechanical Device C with a spinning vessel VS that can be externally attached to the exhaust port of an aircraft turbine engine wherein the combusted gases F2 are input into the said device, the thrust energy of the said gases forcing a set of turbine blades to create rotational force in spinning the attached vessel VS containing the said gases within, thus rotating the said gases in order to centrifugally generate pressure conducive to the condensation of water and using the same centrifugal effect to separate moisture from the combusted gases F2, allowing the other combustion products to exit the device without thermal dissipation.

2. The Device as claimed in claim 1 wherein rigid supports Y1 and Y2, holding co-axial stator turbines SV1 and SV2, containing aerofoils A1 and A2, the stator turbines centers fitted with bearings B1 and B2 respectively, whereas the Shaft S rotates between the said bearings, the vessels VS, VC and turbine VLPT fixed on S to thus rotate with the said shaft.

3. The Device as claimed in claim 1 wherein the shaft S of the centrifugal mechanism is coaxial with the Low Pressure Shaft of the said engine E, operates when the said engine is also operating, by the engine E forcing the exhaust gases F2 into the stator turbine SV1 containing the aero-foils A1 of the said device deflecting and training the exhaust linear airflow F2 such as to turn the turbine VLPT, the airflow emerging out of VLPT as helical airflow F3.

4. The Device as claimed in claim 1 and claim 3 wherein the Very Low Pressure Turbine VLPT aero-foils A3 co-axial to the vessel VS spins the said vessel thus rotating the said combusted gases contained within the vessel VS creating the radial air-flow F5 on the rotational Z-axis.

5. The Device as claimed in claim 1 and claim 4 wherein the radial air-flow F5, rotating with almost the same angular velocity as the turbine VLPT, the said airflow splits into a dense, moisture laden, circular air-flow F6 rotating circumferentially and the rarer moisture free helical airflow F8, rotating closer to the centre of the rotational axis.

6. The Device as claimed in claim 1 wherein the linear exhaust gas F2 from the core of the engine E exits the engine at a temperature T1, considered here as also the temperatures of the exhaust gases consisting mainly of H_2O, CO_2 and N_2, in the molecular state, in variations of some engines could be higher than the critical point for water vapour to form, possibly still contain a minor amount of H_2O below the critical point of water, the temperature would

drop to T2 when a part of mechanical energy of the linear exhaust F2 is utilized to drive the turbine VLPT, the pressure and temperature preferably in, or close to, the liquid phase.

7. The Device as claimed in claim 1 and claim 6 wherein the temperature and pressure of a small percentage of the molecular H_2O in air-flow F6 initially drops to a liquid phase, condenses on to the soot particles, the soot particles acting as nucleation centers for further precipitation.

8. The Device as claimed in claim 1 wherein the bypass airflow F1 is utilized, without let or hindrance, to absorb some thermal energy from the external surface of the spinning vessel VS.

9. The Device as claimed in claim 1 wherein the material of vessel VS is a thermally conducting material, however, the inner surface P is coated with any condensation initiating metal.

10. The Device as claimed in claim 1 wherein the spinning vessel containing the rotating exhaust gases, both having approximately similar angular velocities, prevent the boundary layer separation of the gas from the surface P, thus maintaining a close contact of the water with the said surface.

11. The Device as claimed in claim 1 and claim 7 wherein the outer surface of the centrifugal vessel V is subject to the cold bypass-airflow F1 from the engine E, cooling the inner surface P thus selectively dissipating thermal energy from the airflow F6 in close contact with P.

12. The Device as claimed in claim 1 and claim 10 wherein the H_2O component in the portion of the air-flow F6 in direct contact with the inner periphery P of the spinning vessel V is cooled sufficiently to condense into additional water droplets.

13. The Device as claimed in claim 1 and claim 12 wherein the centrifugal forces on the flow further forces the flow F6 against the cold inner surface P of the vessel VS, the pressure thus generated would tend to move the phase point on the water-phase plot of figure 5 to enter the liquid phase as flow F7, as a rotating conical sheet of water at temperature T3.

14. The Device as claimed in claim 1 and claim 12 wherein due to compression at the periphery of the vessel VS, the vapour would further experience coagulation, the Phase Point on the graph in Figure 7 would move down toward the liquid region furthering precipitation of water into a liquid state F7 collecting in the drain D as a rotating ring of water.

15. The Device as claimed in claim 1 wherein seals Se between the rigid support Y3 and the spinning vessel VS prevent the liquid in drain D from leaking out and thus loosing pressure.

16. The Device as claimed in claim 1 wherein the diameter of the centrifugal vessel V is enlarged to enhance the centrifugal effect created by the rotor turbine VLPT, finally converging back into the exit stator SV2 of reduced diameter creating back-pressure.

17. The device as claimed in claim 1 and in claim 16 wherein the stator turbine aero-foils A2 straighten the radial airflow F8 to exit the device C as linear air-flow F9 at temperature T4 into the atmosphere, the aperture of stator turbine SV2 acting as a nozzle preferably increasing exit speed.

18. The Device as claimed in claim 1 and claim 15 wherein the residual heat in the drained out water-flow F7 is partially recovered by the requirements of thermal energy, possibly by the utilities in the aircraft cabin, the leading edges, the engine, before the water-flow F7 is disposed off.

19. The Device as claimed in claim 1, and claim 16 wherein due to the condensation of water, the latent heat released by water is absorbed by the residual airflow F8 consisting mainly of CO_2 and N_2 such that the gases now contain the additional energy released by the water.

20. The Device as claimed in claim 1 and all the above claims wherein the exhaust air-flow F9 released into the atmosphere does not contain sufficient moisture to create contrails.